

# Pacific Northwest National Laboratory

Operated by Battelle for the  
U.S. Department of Energy

## In Situ Redox Manipulation Field Injection Test Report - Hanford 100-H Area

RECEIVED  
DEC 26 1996  
OSTI

J. S. Fruchter  
J. E. Amonette  
C. R. Cole  
Y. A. Gorby  
M. D. Humphrey  
J. D. Isok

F. A. Spane  
J. E. Szecsody  
S. S. Teel  
V. R. Vermeul  
M. D. Williams  
S. B. Yabusaki

December 1996

DISTRIBUTION OF THIS DOCUMENT IS UNLIMITED

MASTER

Prepared for the U.S. Department of Energy  
under Contract DE-AC06-76RLO1830

PNNL-11372

## DISCLAIMER

This report was prepared as an account of work sponsored by an agency of the United States Government. Neither the United States Government nor any agency thereof, nor Battelle Memorial Institute, nor any of their employees, makes any warranty, express or implied, or assumes any legal liability or responsibility for the accuracy, completeness, or usefulness of any information, apparatus, product, or process disclosed, or represents that its use would not infringe privately owned rights. Reference herein to any specific commercial product, process, or service by trade name, trademark, manufacturer, or otherwise does not necessarily constitute or imply its endorsement, recommendation, or favoring by the United States Government or any agency thereof, or Battelle Memorial Institute. The views and opinions of authors expressed herein do not necessarily state or reflect those of the United States Government or any agency thereof.

PACIFIC NORTHWEST NATIONAL LABORATORY

*operated by*

BATTELLE

*for the*

UNITED STATES DEPARTMENT OF ENERGY

*under Contract DE-AC06-76RLO 1830*

Printed in the United States of America

Available to DOE and DOE contractors from the  
Office of Scientific and Technical Information, P.O. Box 62, Oak Ridge, TN 37831;  
prices available from (615) 576-8401.

Available to the public from the National Technical Information Service,  
U.S. Department of Commerce, 5285 Port Royal Rd., Springfield, VA 22161



The document was printed on recycled paper.

# **In Situ Redox Manipulation Field Injection Test Report - Hanford 100-H Area**

J. S. Fruchter, Project Manager  
J. E. Amonette  
C. R. Cole  
Y. A. Gorby  
M. D. Humphrey  
J. D. Isok  
F. A. Spane  
J. E. Szecsody  
S. S. Teel  
V. R. Vermeul  
M. D. Williams  
S. B. Yabusaki

November 1996

Pacific Northwest National Laboratory  
Richland, WA 99352

Pacific Northwest National Laboratory  
is operated by Battelle  
for the U.S. Department of Energy  
under Contract DE-AC06-76RLO 1830.

This work is funded by the Office of Science and Technology, within the  
Department of Energy's Office of Environmental Management, under the  
Subsurface Contaminant Focus Area.

**DISCLAIMER**

**Portions of this document may be illegible  
in electronic image products. Images are  
produced from the best available original  
document.**

## DISCLAIMER

This report was prepared as an account of work sponsored by an agency of the United States Government. Neither the United States Government nor any agency thereof, nor any of their employees, make any warranty, express or implied, or assumes any legal liability or responsibility for the accuracy, completeness, or usefulness of any information, apparatus, product, or process disclosed, or represents that its use would not infringe privately owned rights. Reference herein to any specific commercial product, process, or service by trade name, trademark, manufacturer, or otherwise does not necessarily constitute or imply its endorsement, recommendation, or favoring by the United States Government or any agency thereof. The views and opinions of authors expressed herein do not necessarily state or reflect those of the United States Government or any agency thereof.

## Summary

This report presents results of an In Situ Redox Manipulation (ISRM) Field Injection Withdrawal Test performed at the 100-H Area of the U.S. Department of Energy's (DOE's) Hanford Site in Washington State in Fiscal Year 1996 by researchers at Pacific Northwest National Laboratory (PNNL). The test is part of the overall ISRM project, the purpose of which is to determine the potential for remediating contaminated groundwater with a technology based on in situ manipulation of subsurface reduction-oxidation (redox) conditions. The ISRM technology would be used to treat subsurface contaminants in groundwater zones at DOE sites.

Subsurface contaminants at DOE sites occur in both the vadose and its not the vadose-saturated zone. It's the vadose zone and GW-saturated zone. and groundwater-saturated zones. Some groundwater plumes at DOE sites are already dispersed over areas covering square miles and can be located hundreds of feet below the ground. This type of dispersed, inaccessible contamination is difficult to treat using excavation or pump-and-treat methods. Some contaminant plumes may be successfully treated by ISRM methods. Researchers are determining if these methods can be created by controlling the redox potential of the unconfined aquifers in which the contaminants reside. The concept requires creating a permeable treatment barrier in the subsurface by injecting reagents and/or microbial nutrients into the subsurface. The reagents and nutrients are selected to make the aquifer reducing, thereby destroying or immobilizing specific redox-sensitive contaminants.

The concept relies on the fact that unconfined aquifers are usually oxidizing environments; therefore, most of the mobile contaminants in these aquifers are mobile under oxidizing conditions. If the redox potential of the aquifer can be made reducing, then a variety of contaminants can be treated.

The goal of ISRM is to create a permeable treatment zone in the subsurface for remediating redox-sensitive contaminants in the groundwater. The permeable treatment zone must be created just downstream of the contaminant plume or contaminant source through the injection of reagents and/or microbial nutrients to alter the redox potential of the aquifer fluids and sediments. Contaminant plumes migrating through this manipulated zone will then be destroyed or immobilized.

Three field experiments have been conducted at the site: a full-scale bromide tracer experiment, a mini dithionite injection/withdrawal experiment, and a full-scale dithionite injection/withdrawal experiment. All the major objectives of the ISRM field test were achieved. These objectives included demonstrating the feasibility of reducing the aquifer sediments, determining how long the reducing conditions can be maintained, determining the nature and severity of any secondary effects, and developing a methodology for evaluating ISRM technologies in general.

Twenty-one thousand gallons of buffered sodium dithionite solution were successfully injected into the unconfined aquifer at the Hanford 100-H Area in September 1995. No significant plugging of the well screen or the formation was detected during any phase of the test. Dithionite was detected in monitoring wells at least 7.5 m (25 ft) from the injection point. Injection, drift, and withdrawal data were obtained from all three test phases.

Preliminary core data show that from 60 to 100% of the available reactive iron in the treated aquifer sediments was reduced by the injected dithionite. Reducing capacity measurements were obtained on cores recovered after the reagent injection by dissolved oxygen consumption measurements, and confirmed in some core samples using hexavalent chromium solutions.

Calculations show that these levels of reducing capacity within the treated sediments translate to a contaminant plume treatment capacity of 51 to 85 pore volumes (7 to 12 years). These estimates assume groundwater containing 1 ppm hexavalent chromium and 9 ppm dissolved oxygen. If additional treatment capacity were required to meet target cleanup levels, the treatment zone could be made wider during the initial emplacement or reinjected with dithionite once the available treatment capacity had been expended. The lifetime of the barrier at a specific site is determined by the accessible/reducible iron and the efficiency of the emplacement.

Ten months after the injection, groundwater in the injection zone remains anoxic. Hexavalent chromium levels remain below detection limits, and total chromium levels remain in the 1- to 8-ppb range and continue to decline. Concentrations of constituents in the water withdrawn for the test well met all applicable Hanford purgewater criteria, and the water was disposed to the ground.

Although the expected decreases in dissolved oxygen and chromate concentrations have appeared in monitoring well samples taken within the zone treated by dithionite, similar decreases have not yet appeared in the downgradient monitoring wells. Downgradient monitoring at the 100-H Area is complicated by the uncertainty in the gradient direction and edge effects from the small reduced zone. This uncertainty is thought to be due to historic high levels of the groundwater table in the 100-H Area wells caused by heavy precipitation during the winter and spring of 1996. These high levels have essentially flattened the groundwater gradient to the point where no net movement of the water is now occurring. We estimate that normal gradient conditions will reestablish themselves by the upcoming autumn.

The test conducted at 100-H has demonstrated so far that 1) sediments in the aquifer can be successfully reduced by treatment with a chemical reducing agent, 2) the reduced sediments can substantially lower the concentration of dissolved hexavalent chromium in the groundwater, and 3) the reducing conditions can be maintained in the aquifer for extended periods of time.

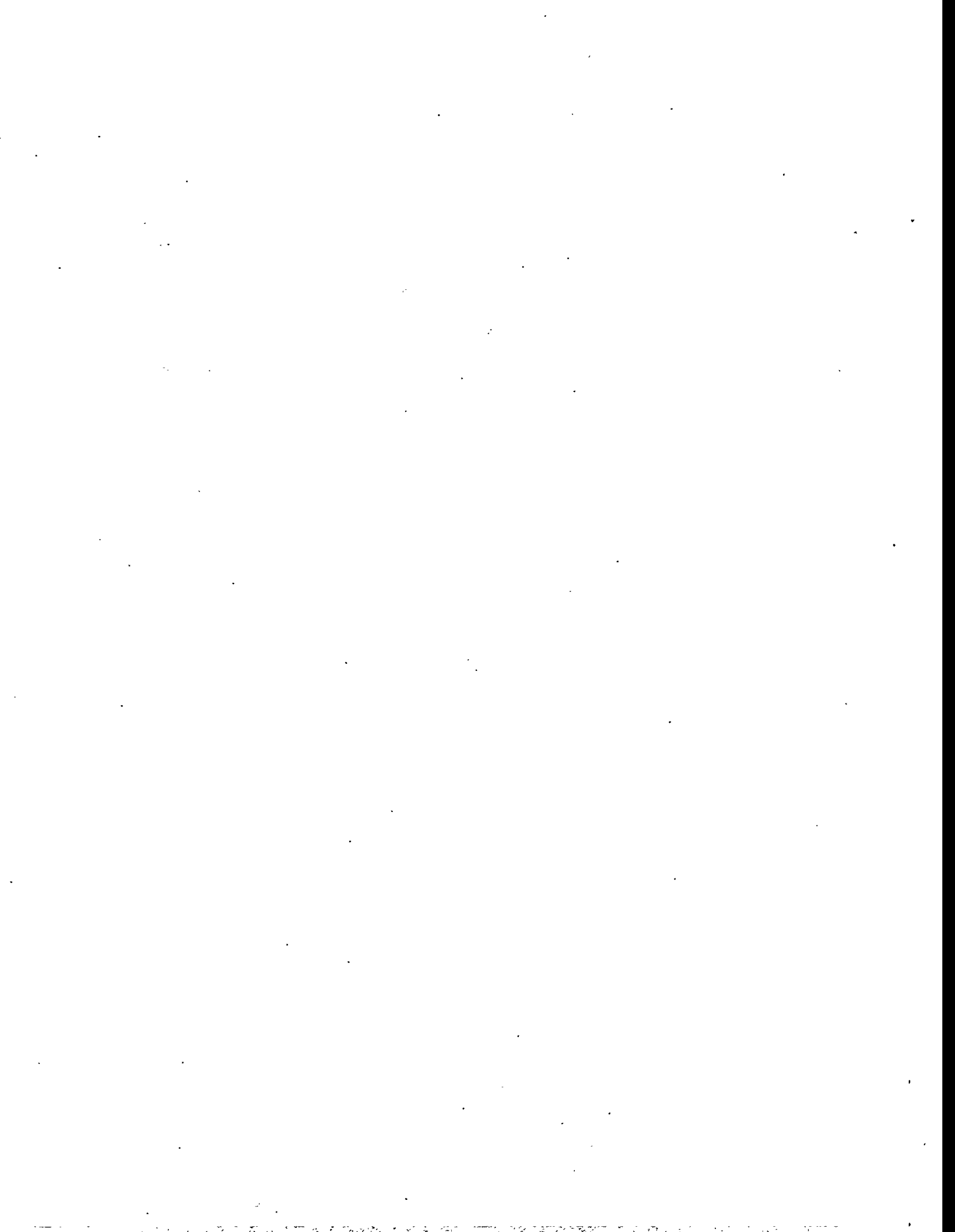
Several issues must still be resolved before ISRM can be routinely used to remediate contaminated groundwater. Scale-up issues include the logistics of handling large amounts of dithionite and disposing of the withdrawn water, methods of injecting the reductant to more efficiently use the dithionite, adequate downgradient monitoring, and the effects of a larger volume of reduced aquifer on the system's chemical behavior. Concerns involving long-term behavior and performance include reoxygenation of the water downgradient of the reduced zone, reoxidation of the zone itself with the resulting need to re-reduce the aquifer, reoxidation of precipitated metals within the zone, and downgradient precipitation of any metals which were mobilized during reduction.

Constructability issues include some of the scale-up issues, the ability to install fully overlapping reduced zones, and the costs associated with installing and maintaining the zone for decades. These issues should be resolved by a combination of larger-scale treatability tests and continued monitoring at the 100-H Area site. In addition, alternative methods of reducing the aquifer will be investigated.

## Acknowledgments

This work was prepared with the support of the following contributors:

Headquarters:	Office of Science and Technology Grover Chamberlain, HQ Program Lead
Focus Area/Program:	Subsurface Contaminant Focus Area Jim Wright, Program Lead
Operations Office:	Richland Operations Office Science and Technology Programs Division Jeffrey A. Frey, Technical Program Officer
Contractor:	Pacific Northwest National Laboratory Environmental Management Technology Development Program Steven C. Slate, Manager



# Contents

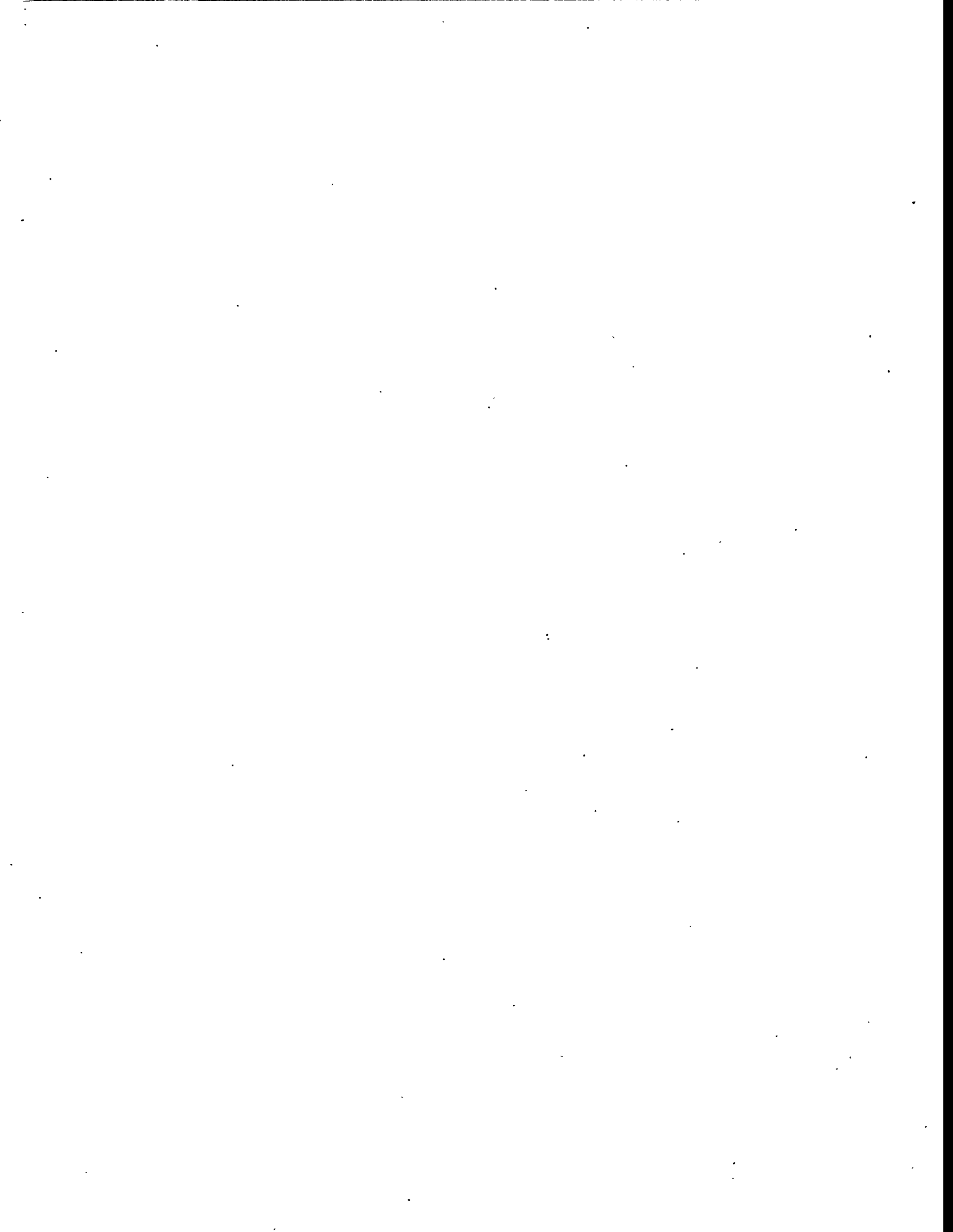
Summary .....	iii
1.0 Introduction .....	1.1
1.1 Description of Redox Concept .....	1.1
1.2 Applications and Benefits .....	1.2
1.3 Report Outline .....	1.2
2.0 Field Test Objectives .....	2.1
3.0 In Situ Redox Manipulation Approach .....	3.1
3.1 Basic Experimental Approach .....	3.2
3.2 Field Experiment Approach .....	3.2
3.2.1 Monitoring .....	3.3
3.2.2 Advantages .....	3.3
3.2.3 Limitations .....	3.3
3.3 Brief Description of Field Experiments .....	3.4
3.3.1 Full-Scale Bromide Tracer Field Experiment .....	3.4
3.3.2 Mini Dithionite Injection/Withdrawal Field Experiment .....	3.5
3.3.3 Main Dithionite Injection/Withdrawal Field Experiment .....	3.5
4.0 Background .....	4.1
4.1 Description of the Reagent and Reactions .....	4.3
4.1.1 Reduction Reactions .....	4.3
4.1.2 Disproportionation Reaction .....	4.4
4.1.3 Chromium Reduction, Groundwater Deoxygenation, Metals Mobilization .....	4.4
4.1.4 Reactions and Interactions During Various Phases of Field Experiment .....	4.5
5.0 Site Selection .....	5.1

5.1 Regulatory Criteria .....	5.1
5.2 Well Installation Costs .....	5.1
5.3 Hydrogeologic Criteria .....	5.1
5.4 Geochemical Criteria .....	5.2
5.5 Access Criteria .....	5.2
6.0 Site Characterization .....	6.1
6.1 Hydrogeologic Setting .....	6.1
6.2 Well and Corehole Installation .....	6.1
6.2.1 Drilling .....	6.1
6.2.2 Sampling .....	6.2
6.3 Hydrogeologic Characterization .....	6.3
6.4 Geochemical Characterization .....	6.4
6.5 Microbiologic Characterization .....	6.5
6.6 Groundwater Chemistry .....	6.6
6.7 Description and Operation of Field Site Test Facilities .....	6.7
6.7.1 Injection/Withdrawal Pump and Monitoring Equipment .....	6.8
6.7.2 Sampling Equipment .....	6.8
6.7.3 Argon System .....	6.9
6.7.4 Tanks .....	6.9
6.7.5 Mobile Laboratory .....	6.10
7.0 Pre-Injection Numerical Simulations .....	7.1
7.1 Tracer Experiment Modeling .....	7.2
7.2 Anoxic Water Plume Modeling .....	7.2

8.0 Tracer Test .....	8.1
8.1 Purpose .....	8.1
8.2 Description .....	8.1
8.3 Results .....	8.2
9.0 "Mini" Injection .....	9.1
9.1 Purpose .....	9.1
9.2 Description .....	9.1
9.3 Results .....	9.2
9.4 Interpretation .....	9.4
10.0 Main Dithionite Injection/Withdrawal Field Experiment .....	10.1
10.1 Purpose .....	10.1
10.2 Description .....	10.1
10.3 Monitoring and Analytical Equipment .....	10.2
10.4 Dithionite Injection/Withdrawal .....	10.2
10.4.1 Injection Solution Preparation .....	10.2
10.4.2 Injection Phase .....	10.3
10.4.3 Residence Phase .....	10.4
10.4.4 Withdrawal Phase .....	10.6
10.4.5 Mass Balance .....	10.7
10.4.6 Comparison with Bromide Tracer Test .....	10.6
10.5 Post-Experiment Reductive Capacity Measurements .....	10.7
10.5.1 Reductive Capacity by O <sub>2</sub> Reoxidation Method .....	10.8
10.5.2 Reductive Capacity by Chromium(VI) Reoxidation Method .....	10.11
10.6 Effect of Treatment on Microbial Populations .....	10.12
10.7 Comparison of Pre- and Post-Experiment Hydraulic Test .....	10.12
10.7.1 Discussion of Stress Well H5-2 Response .....	10.13

10.7.2 Discussion of Observation Well Response .....	10.14
10.8 Long-Term (Post Experiment) Monitoring of Wells .....	10.15
10.8.1 Dissolved Oxygen Monitoring .....	10.16
10.8.2 Chromium Monitoring .....	10.17
10.8.3 pH and Conductivity Monitoring .....	10.18
10.8.4 Trace Metals Analysis .....	10.18
11.0 Modeling of Results .....	11.1
11.1 Reactive Transport Modeling .....	11.1
11.1.1 Application to the Design Analysis .....	11.1
11.1.2 Analysis of the Intermediate-Scale Dithionite Injection/Withdrawal Experiment	11.3
11.2 Dissolved Oxygen Transport Modeling .....	11.3
12.0 Interpretation and Summary .....	12.1
12.1 Summary .....	12.1
12.2 Conclusions .....	12.1
13.0 Future Work .....	13.1
13.1 100-H Area ISRM Site Monitoring and Maintenance .....	13.1
13.2 Dissolved Oxygen Transport .....	13.1
13.3 Intermediate-Scale Test of Ultra-Micro Bacteria Injection .....	13.1
13.4 Intermediate-Scale Test of Zero-Valent Iron Colloid Injection .....	13.2
13.5 Reduced-Clay Colloid Studies .....	13.2
14.0 References .....	14.1

Appendix A - Analytical Methods .....	A.1
Appendix B - Well Diagrams .....	B.1
Appendix C - Geology and Hydrology of the 100-H Area .....	C.1
Appendix D - Hydrologic Tests .....	D.1
Appendix E - Background Chemistry of 100H Wells .....	E.1
Appendix F - Selected Chemical Data - "Mini" Injection .....	F.1
Appendix G - Monitoring Well Field Measurements for the Main Dithionite Injection/Withdrawal Experiment .....	G.1
Appendix H - Field Measurements from the Post-Experiment Monitoring of the 100-H Area ISRM Site .....	H.1



## Figures

1.1.	Location of the 100-H Area of DOE's Hanford Site in Washington State Where the Field Experiments Were Performed .....	1.4
1.2.	In Situ Permeable Treatment Zone Concept .....	1.5
1.3.	ISRM Reduction and Treatment .....	1.5
1.4	Advantage of an In Situ Permeable Treatment Zone .....	1.6
3.1.	Scales of Experiments Performed in Support of the In Situ Redox Manipulation Experiment Showing the Progression from Bench-scale Batch Studies Through the 100-H Area Field Experiment .....	3.6
3.2.	Location Map for the In Situ Redox Manipulation Field Test Site .....	3.7
3.3.	Photograph and Schematic Diagram of Intermediate-Scale Wedge Flow Cell at Oregon State University .....	3.8
4.1.	Injection Phase Interactions and Reactions During Creation of a Redox Treatment Zone .....	4.9
4.2.	Drift Phase Interactions and Reactions During Creation of a Redox Treatment Zone .....	4.10
4.3.	Withdrawal Phase Interactions and Reactions During Creation of a Redox Treatment Zone .....	4.11
4.4.	Interactions and Reactions Within and Downstream of the Redox Treatment Zone During the Remediation Phase .....	4.12
4.5.	Variation in Reagent Concentration as Percentage of Input Reagent Concentration Versus Radial Distance from the Injection Well at the Conclusion of Injection Phase .....	4.13
5.1.	Well Location Map for the In Situ Redox Manipulation Field Test Site .....	5.3
5.2.	Photographs of the ISRM Field Site at the 100-H Area. ....	5.4
6.1.	Schematic Well Construction Diagram for Wells Installed at the ISRM Site .....	6.11
6.2.	West-to-East Geologic Cross-Section of the Unconfined Aquifer .....	6.12
6.3.	A Comparison of Pre-Experiment Slug Interference Test Results From Well 199H5-5P with Normalized Constant-Rate Test Results .....	6.13
6.4.	Wells Sampled and Analyzed for Dissolved Oxygen Concentration Within and Upgradient from the 100H Area .....	6.14

6.5.	Schematic Drawing of the Sample Acquisition System Used at the ISRM Test Site . . .	6.15
7.1.	Preliminary Tracer Experiment Modeling Results . . . . .	7.4
7.2.	Simulation of Dispersion of Anoxic Plume Downgradient from the Test Site . . . . .	7.4
8.1.	Injection/Withdrawal Well (H5-2) Data including (a) Observed Bromide Tracer Concentrations During the Injection/Withdrawal Tracer Test and (b) Percent Recovery of the Br- Tracer During the Withdrawal Phase, indicating that 96% of the Injected Br- was Removed From the Aquifer . . . . .	8.3
8.2.	Observed Bromide Tracer Concentrations Along a Lower Zone Radial Transect During the Injection/Withdrawal Tracer Test . . . . .	8.4
8.3.	Observed Bromide Tracer Concentrations Along an Upper Zone Radial Transect During the Injection/Withdrawal Tracer Test. (a) H5-5o (5 ft), (b) H5-4o (12 ft), and (c) H5-30 (20 ft). . . . .	8.5
8.4.	Observed Bromide Tracer Concentrations Along a Lower Zone Radial Transect During the Injection/Withdrawal Tracer Test . . . . .	8.6
9.1.	Variation in the Selected Chemical Properties of the Withdrawal Waters (H5-2) During the Withdrawal Stage of the Mini Injection Experiment . . . . .	9.4
9.2.	Variation in the Trace Metals Content of Withdrawal Waters (H5-2) During the Withdrawal Stage of the Mini Injection Experiment . . . . .	9.4
10.1.	Photograph of Dithionite Delivery Truck and 7,000 Gallon Injection Tanks . . . . .	10.20
10.2.	Field Parameters Measured for the Injection/Withdrawal Well (H5-2) during all the phases of the 100-H. Area ISRM Field Experiment . . . . .	10.21
10.3.	Dithionite and Conductivity Measurements along the Transect with the Upper (o) and Lower (p) Monitoring Wells During the Injection, Residence, and Early Withdrawal Phases . . . . .	10.22
10.4.	Comparison of Bromide Concentrations from the Tracer Test with Conductivity Concentrations from the Main Dithionite Injection/Withdrawal Test for the Upper Zone Monitoring Wells . . . . .	10.23
10.5.	Comparison of Bromide Concentrations from the Tracer Test with Conductivity Concentrations from the Main Dithionite Injection/Withdrawal Test for the Lower Zone Monitoring Wells Corresponding to the Upper Zone Wells in Figure 10.2 . . . . .	10.24
10.6.	Comparison of the Observed Pre- and Post-Experiment Slug Test Response Exhibited at Stress Well H5-2 . . . . .	10.25

10.7.	Predicted Slug Test Response at the Stress Well (H5-2) for Decreasing Values of Hydraulic Conductivity .....	10.26
10.8.	Predicted Slug Test Response at the Stress Well (H5-2) for Various Low Permeability Skin Conditions .....	10.27
10.9.	Predicted Slug Test Response at the Stress Well (H5-2) for Varying Values of Storativity .....	10.28
10.10.	Predicted Slug Test Response at the Stress Well (H5-2) for Varying Values of Aquifer Vertical Anisotropy Ratio. ....	10.29
10.11.	Comparison of the Observed Pre- and Post Experiment Slug Interference Test Response Exhibited at Observation Well H5-4P .....	10.30
10.12.	Analysis Results for the Pre-Experiment Slug Interference Test Responses at Observation Well H5-4P Using a Homogeneous Formation Model .....	10.31
10.13.	Analysis Results for the Post-Experiment Slug Interference Test Responses at Observation Well H5-4P Using a Homogeneous Formation Model .....	10.32
10.14.	Analysis Results for the Post-Experiment Slug Interference Test Responses at Observation Well H5-4P Using a Finite-Skin (Composite Formation) Model .....	10.33
10.15.	Comparison of pH and Conductivity Measurements after the Injection/Withdrawal Experiment and in June, 1996 .....	10.34
10.16.	Location of Wells along Transect A .....	10.35
10.17.	Dissolved Oxygen Measurements along Transect A (as shown in Figure 10.16) Before (a) and After (b) the Injection/Withdrawal Experiment .....	10.36
10.18.	Dissolved Oxygen Measurements along Transect A (as shown in Figure 10.16) During the Post-Experiment Monitoring .....	10.37
10.19.	Total Chromium Along Transect A (as shown in Figure 10.16) Before (a) and After (b) the Injection/Withdrawal Experiment .....	10.38
10.20.	Hexavalent Chromium Measurements along Transect A (as shown in Figure 10.16) During the Post-Experiment Monitoring .....	10.39
11.1.	Example Dithionite Breakthrough Curves from Reactive Transport Model Showing Unreduced Fe(III) at Various Radial Distances .....	11.6

11.2.	Comparison of Reactive Transport Model Simulation Results to Dithionite and Conductivity Measurements at 150-cm Radial Distance in the Intermediate-Scale Wedge Experiment at Oregon State University .....	11.7
11.3.	Comparison of Reactive Transport Model Simulation Results to Dithionite and Conductivity Measurements at 250-cm Radial Distance in the Intermediate-Scale Wedge Experiment at Oregon State University .....	11.8

# Tables

6.1.	Well Construction Information for Wells Installed in 1995 at the ISRM Site .....	6.14
6.2.	Results of Hydrogeologic Characterization at the 100-H Area Site .....	6.15
6.3.	Available Fe(III) Analyses Results .....	6.16
6.4.	Microbiological Characterization Summary (after 28 days incubation) .....	6.17
6.5.	Baseline Trace Metals Analysis Results for the ISRM Test Site .....	6.18
6.6.	Baseline Field Parameter Measurement Results for the ISRM Test Site .....	6.19
6.7.	Results from Dissolved Oxygen Analysis of samples collected Within and Upgradient from the 100H Area .....	6.19
10.1	Summary of Peak Dithionite Concentrations and Conductivity During the Injection Phase of the 100-H Area ISRM Field Experiment .....	10.40
10.2	Final Modutank Concentrations Prior to Purging to Ground .....	10.41
10.3	Results from Reductive Capacity Analyses Using the O <sub>2</sub> reoxidation method for Core Samples Collected from the ISRM Treatment Zone .....	10.42
10.4.	Results from the Comparison of Field Experiment Achieved Reductive Capacity to Maximum Achievable Reductive Capacity .....	10.43
10.5.	Identification of Samples Used for Chromium Reduction Capacity Experiment .....	10.44
10.6.	Microbiological Characterization Summary (after 42 days incubation) .....	10.45
10.7.	Trace Metals for Wells within the Reduced Zone in January, 1996 measured by ICP/MS .....	10.46
10.8.	Trace Metals for Wells within the Reduced Zone in May, 1996 measured by ICP/MS .....	10.47
10.9.	Trace Metals for Wells within the Reduced Zone in August, 1996 measured by ICP/MS .....	10.48
10.10.	Trace Metals for Upgradient and Downgradient Wells in January, 1996 measured by ICP/MS .....	10.49
10.11.	Trace Metals for Upgradient and Downgradient Wells in May, 1996 measured by ICP/MS .....	10.50

10.12. Trace Metals for Upgradient and Downgradient Wells in August, 1996 measured by ICP/MS .....	10.51
11.1. Selected Parameters used in Intermediate Scale Wedge Modeling .....	11.9

# 1.0 Introduction

In Fiscal Year (FY) 1991, Pacific Northwest National Laboratory (PNNL)<sup>(a)</sup> researchers began work on a site remediation technology for the U.S. Department of Energy's (DOE's) Office of Health and Environmental Research's Subsurface Science Program. The purpose of the project was to determine the potential for remediating contaminated groundwater with a technology based on in situ manipulation of subsurface reduction-oxidation (redox) conditions. This technology, called In Situ Redox Manipulation (ISRM), would be used to treat subsurface contaminants in both vadose and groundwater-saturated zones at DOE sites. Initial work included laboratory proof-of-principle abiotic and biotic studies, conceptual design, and preliminary planning documents (Fruchter et al. 1994).

Attempts to control redox potential in an aquifer must overcome various scale-up complications arising from the interaction between contaminants, reducing agents, groundwater, and the natural variability of the subsurface. Therefore, in FY 1994, a site was selected for field-scale experiments of the ISRM technology. The site is located in the 100-H Area of DOE's Hanford Site in Washington State (Figure 1.1).

Three field experiments have since been conducted at the site: a full-scale bromide tracer experiment, a small-scale "mini" dithionite injection/withdrawal experiment, and a full-scale dithionite injection/withdrawal experiment. The "proof of principle" field experiment at the 100-H Area Site successfully achieved a significant reduction capacity in the aquifer. Laboratory measurements of sediment collected from the reduced zone show that the zone should remain reduced up to 12 years after emplacement. Monitoring of the site after the emplacement showed that chromate concentrations in the reduced zone have dropped below detection limits and remain below detection limits 1 year later. Dissolved oxygen measurement at the site had a similar trend as the chromate measurements. The data gathered from this series of experiments at the 100-H Area demonstrate that the ISRM method can be a viable approach to groundwater remediation and may have many advantages over traditional groundwater remediation methods (i.e., pump and treat). This work was supported by DOE's Office of Science and Technology (OST) in FY 1993 through FY 1995 and was funded by OST's Subsurface Contaminant (formerly Plumes) Focus Area in FY 1996.

This report describes ISRM, the approach taken by PNNL in developing the ISRM concept, site selection and characterization, and results of the three field experiments.

## 1.1 Description of Redox Concept

Subsurface contaminants at DOE sites occur in both the vadose and groundwater-saturated zones. Some groundwater plumes are already dispersed over large areas (square kilometers) and are located hundreds of meters below the ground. This type of dispersed, inaccessible contamination is more difficult to treat using excavation or pump-and-treat methods than other types of contamination; however, they may be treated successfully by ISRM methods, which immobilize inorganic contaminants and destroy organic contaminants. The concept requires creation of a permeable

---

(a) Pacific Northwest National Laboratory is operated for the U.S. Department of Energy by Battelle under Contract DE-AC06-76RLO 1830.

treatment barrier in the subsurface by injecting reagents and/or microbial nutrients into the subsurface. The types of reagents and nutrients injected are selected to reduce the aquifer, thereby destroying or immobilizing specific contaminants.

The concept relies on the fact that unconfined aquifers are usually oxidizing environments; therefore, most of the mobile contaminants in these aquifers are mobile under oxidizing conditions. If the redox potential of the aquifer can be reduced, then a variety of contaminants can be treated. The goal of ISRM is to create a permeable treatment zone in the subsurface to remediate redox-sensitive contaminants in the groundwater. As illustrated in Figure 1.2, the permeable treatment zone must be created just downgradient of the contaminant plume or contaminant source through the injection of reagents and/or microbial nutrients to alter the redox potential of the aquifer fluids and sediments. Contaminant plumes migrating through this manipulated zone will then be destroyed or immobilized.

As illustrated in Figure 1.3, the permeable treatment zone is created by reducing the ferric iron to ferrous iron within the clay minerals of the aquifer sediments. This reduction can be accomplished with chemical reducing agents such as sodium dithionite, by introducing small zerovalent or divalent iron particles, or by stimulating naturally occurring iron-reducing bacteria with nutrients (e.g., lactate). After the aquifer sediments are reduced, any soluble reagent or reaction products introduced into the subsurface are removed.

Redox-sensitive contaminants that migrate through the reduced zone in the aquifer become immobilized or degraded; for example, appropriate manipulation of the redox potential can result in the immobilization of inorganic (metals, inorganic ions, and radionuclides) and the destruction of organic (primarily chlorinated hydrocarbons) contaminants. Redox-sensitive contaminants that can be treated by this method include chromate, uranium, technetium and some chlorinated solvents (e.g., carbon tetrachloride and trichloroethylene). Chromate is immobilized by reduction to highly insoluble chromium hydroxide or iron-chromium hydroxide solid solution. This case is particularly favorable because chromium is not easily reoxidized under ambient environmental conditions at most locations.

## **1.2 Applications and Benefits**

Although the immediately proposed target of this technology is chromate contamination in the Hanford 100 Areas, the concept, as illustrated in Figure 1.1, is applicable to a range of other contaminants, including uranium, technetium, chlorinated solvents, and energetic compounds. The permeable treatment zone concept (Figure 1.4), is an improvement over baseline technology (e.g., pump and treat), because it places the treatment capacity in the most permeable regions of the subsurface, where the bulk of the contamination must migrate. In addition, the treatment capacity remains in the subsurface, where it is available to treat contaminants that seep slowly out of less-permeable regions (discussed in Section 3.2.2).

## **1.3 Report Outline**

Section 2.0 details the field test objectives, Section 3.0 describes the ISRM approach, and Section 4.0 provides background on the reagent and reactions. Site selection criteria and site characterization are outlined in Sections 5.0 and 6.0, and Section 7.0 describes numerical simulations. The tracer, mini-injection, and main dithionite injection/withdrawal tests are discussed in Sections 8.0, 9.0, and 10.0; and modeling results, interpretation and summary, and future work are described in Sections 11.0, 12.0, and 13.0. Section 14.0 provides references for this report.

The appendixes provide more technical data and details about the ISRM approach. Appendix A describes the analytical methods used; Appendix B the geology and hydrology of the 100-H Area. Appendix C contains as-built diagrams for wells installed at the ISRM, and Appendix D describes hydrologic tests conducted at the site. The background chemistry of site wells is given in Appendix E, and selected chemical data for the mini-injection tests are in Appendix F. Appendix G contains the monitoring well field measurements for the main dithionite experiment, and Appendix H has the measurements from post-experiment monitoring of the site.

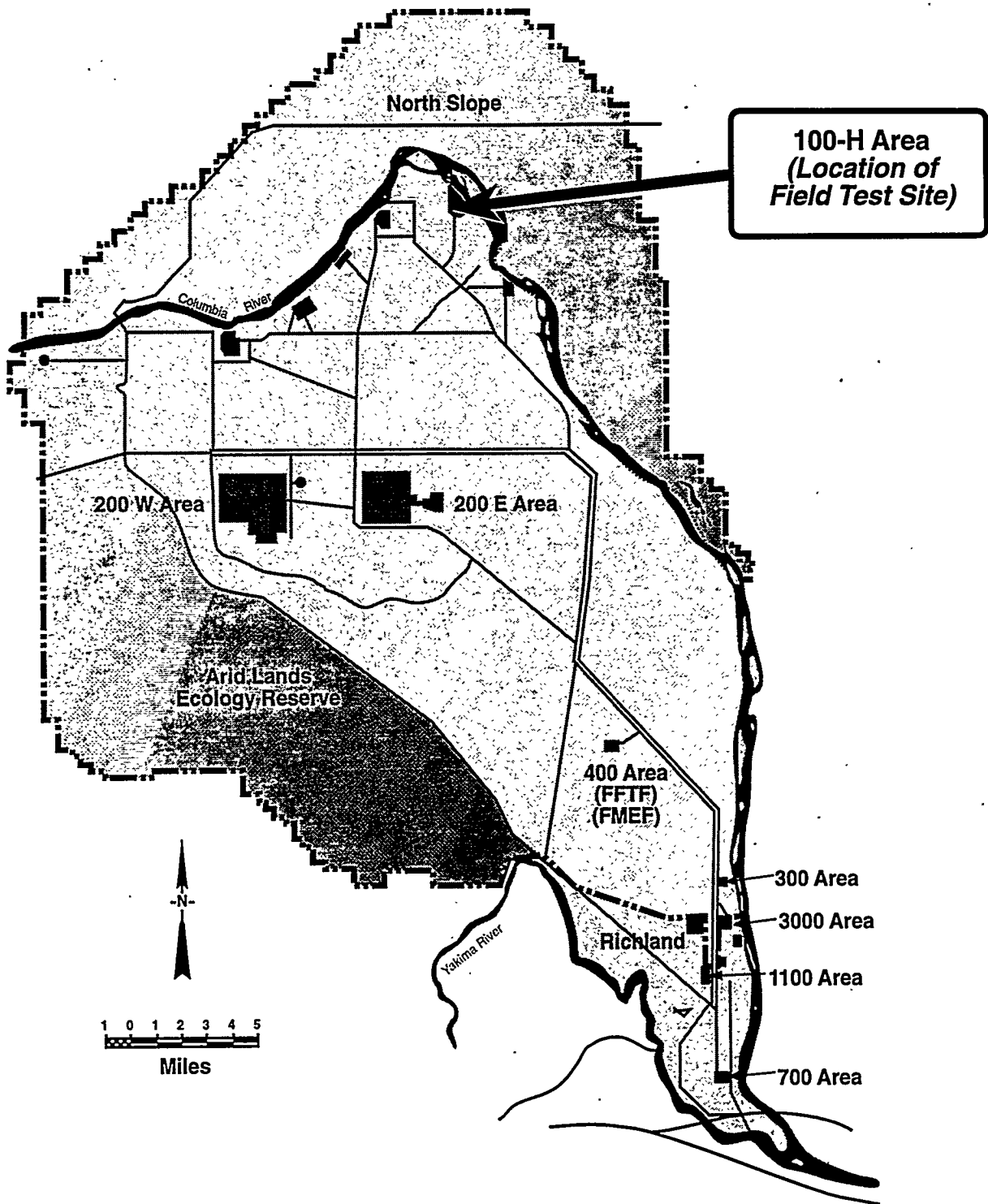


**Figure 1.1.** Location of the 100-H Area of DOE's Hanford Site in Washington State Where the Field Experiments were Performed

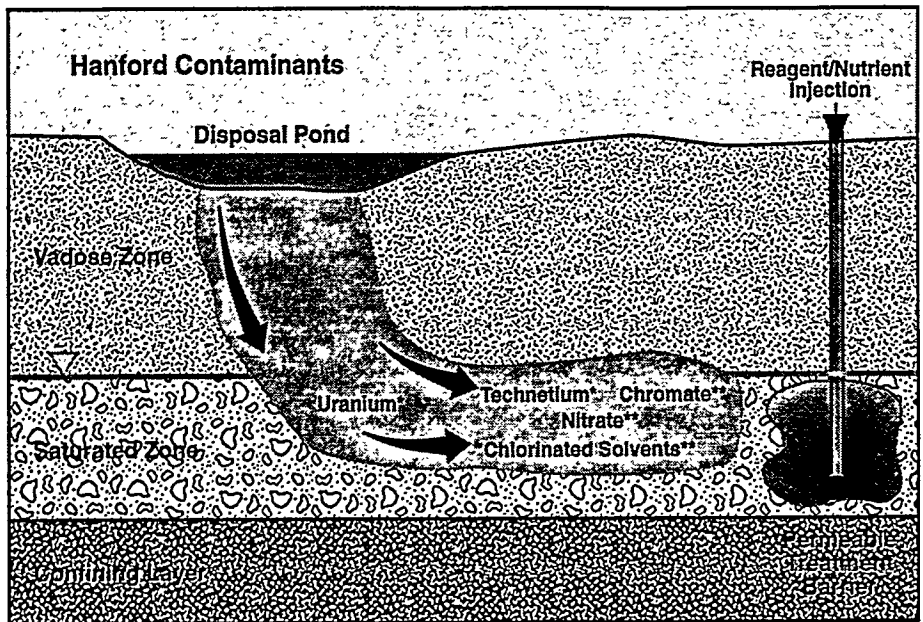


Figure 1.2. In Situ Permeable Treatment Zone Concept

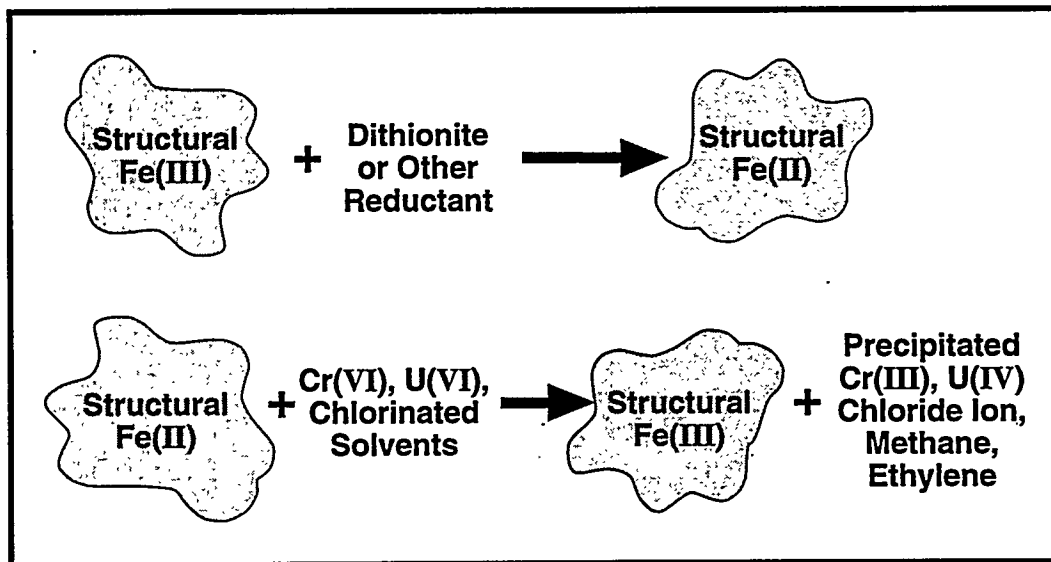
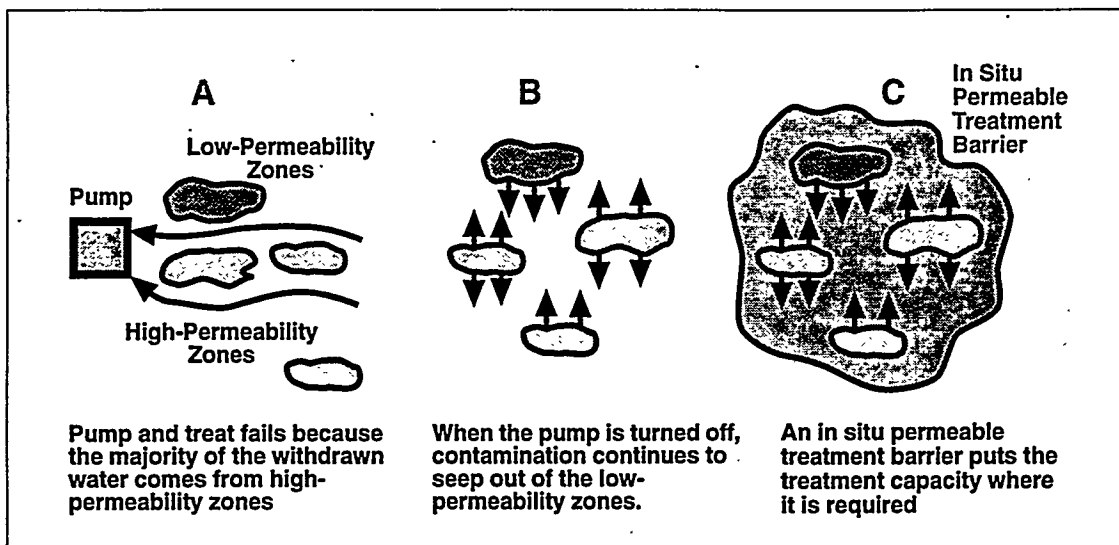


Figure 1.3. ISRM Reduction and Treatment



**Figure 1.4. Advantage of an In Situ Permeable Treatment Zone**

## 2.0 Field Test Objectives

The ISRM field test helps determine the feasibility of ISRM technologies for developing reduced sediment zones that can be used to lower contaminant concentration levels in the groundwater of the Hanford Site 100-H Area groundwater operable unit (OU) 100-HR-3.

The primary objective of the ISRM field test is to determine the feasibility of reducing the sediments in the aquifer. A second objective is to determine how long the reducing conditions can be maintained. Techniques include ISRM using either chemical reagents or microbial techniques. Initial efforts use a chemical reagent to manipulate the redox conditions in the aquifer in a proof-of-principle demonstration for future use in the selective removal of contaminants of concern at the 100-HR-3 groundwater OU. The target contaminant for this innovative technology at the 100 HR-3 OU is chromate; however, the results should also apply to other Hanford groundwater sites and other redox-sensitive contaminants.

The third objective is to determine whether any secondary environmental effects would be created by the ISRM process. Potential effects include mobilization of trace metals already present in the aquifer, aquifer plugging, the creation of an extended plume of anoxic groundwater, failure to remove the high concentrations of injected reagent and buffers, and removal of reagent degradation products (principally sulfates). Reagent recovery rates are expected to be in the range of 90% to 95%.

The final objective is to develop a methodology for evaluating other ISRM treatment technologies. This will include the development of experimental approaches (e.g., intermediate-scale wedge experiment) and computer models for designing and interpreting the results of an ISRM field experiment.



### **3.0 In Situ Redox Manipulation Approach**

The potential for a remediation technology based on in situ manipulation of subsurface redox conditions has been established through theory and laboratory experiments. The ISRM field experiments were undertaken to provide information on whether chemically induced reduction of solid mineral-phase ferric iron to a ferrous state can be controlled in an aquifer to the degree and for the times required for an effective ISRM treatment technology.

In an aquifer, attempts to control redox potential must overcome various scale-up complications from the interaction among contaminants, reducing agents, groundwater, and the natural variability of the subsurface. Field tests provide a way to evaluate the ability of the laboratory chemistry and microbiology studies to be scaled up and extrapolated under the less controlled (i.e., uncertain) conditions posed by the in situ environment.

Because a variety of reagents or types of microbial stimulation have the potential for favorably altering the redox conditions of the subsurface, a flexible and robust field testing method was sought by the ISRM team to be able to evaluate various reagents and microbial stimulation schemes. The field test design/approach must enable the semi-quantitative information to be derived in natural systems where complex interactions can lead to various scale-up and extrapolation issues. The information the approach must develop includes:

- the nature and kinetics of the reduction reaction
- the in situ efficiency of the reducing reagent/nutrient
- the rate of re-oxidation of the minerals in the reduced zone.

Field activities were scheduled in stages so that appropriate laboratory studies could be performed to supply additional information for the final design of each of the three field experiments. The major activities in the ISRM approach and their status follows:

- Bench- and Intermediate-Scale Experiments (ongoing)
- Well Construction and Configuration (completed)
- Pre-Experiment Site Characterization (completed)
- Design Analysis and Modeling (ongoing)
- Site Preparation (completed)
- Environmental, Safety, and Health (completed)
- Three Field Experiments
  - Full-Scale Bromide Tracer Experiment (completed)
  - Mini-Dithionite Injection/Withdrawal Experiment (completed)

- Full-Scale Dithionite Injection/Withdrawal Experiment (completed)
- Post-Experiment Site Characterization and Monitoring (ongoing)
- Final Analysis and Data Reporting
- Field Site Abandonment.

This section provides a description of the basic approach used to investigate the ISRM technology as well as a description of the approach used in the field tests and a brief summary of the three field experiments.

### 3.1 Basic Experimental Approach

Figure 3.1 illustrates the strategy used to prepare for the three ISRM field experiments (full scale bromide tracer test, mini-dithionite injection/withdrawal experiment, and full-scale dithionite injection/withdrawal experiment) conducted at the ISRM field test site (Figure 3.2).

The strategy consisted of a phased approach wherein successively larger-scale and more complex experiments were conducted. Experiments ranged from bench-scale batch and column experiments through a series of experiments conducted in an intermediate-scale flow cell at Oregon State University (Figure 3.3). The intermediate-scale flow cell (a 7-m 11° wedge) is nearly field-scale in the radial dimension. Each successively larger-scale experiment illustrated in Figure 3.1, permitted isolation of effects related to each scale of experiment and enabled better design of the next larger-scale experiment before conducting the full-scale field experiments at the ISRM test site.

These laboratory and field-scale experiments provided needed data and understanding for evaluating the suitability of using a chemical reagent (sodium dithionite) to manipulate aquifer reduction-oxidation (redox) conditions in situ for the purpose of groundwater remediation of hexavalent chromium.

Specifically, the three field experiments examined the feasibility of creating a 10-m-diameter reduced zone in a sandy gravel aquifer in the Hanford formation by injecting a chemical reagent (sodium dithionite buffered with potassium carbonate/bicarbonate). The reagent reduces the structural ferric iron in the clay minerals of these sediments to ferrous iron to create a permeable treatment barrier for remediation of redox-sensitive contaminants by either reductive precipitation (e.g., chromate) or reductive dechlorination for chlorinated solvents, as discussed in Section 1.0.

### 3.2 Field Experiment Approach

The approach used to evaluate the ISRM capability of a reagent involves performing a single-well, injection-withdrawal, reactive tracer test. The reagent, buffers, and tracers are pumped into the aquifer (injection phase), allowed to react for a period of time determined by the laboratory and bench-scale tests (the reaction/drift phase during which the injection plume drifts with natural groundwater gradients), and then pumped back out (the withdrawal phase). This approach, sometimes called a "push-pull" test, allows greater control over the travel of the reagent (i.e., reactive tracer) and involves a minimum volume of the aquifer.

A "push-pull" experiment is conducted using a single injection/withdrawal well to co-inject a reactive chemical reagent (sodium dithionite), buffers (potassium carbonate and bicarbonate), and a

non-reactive tracer (potassium bromide) into a small volume (a cylinder approximately 18.2 m [60 ft] in diameter and 1.5 to 3 m [5 to 10 ft] high) of the Hanford unconfined aquifer to induce reduction of the solid mineral-phase ferric iron. The reagent then reacts with the aquifer material for a time that is dependent on the reagent reaction rate (~18 h). Following the reaction/drift phase the unreacted reagent, buffers, non-reactive tracers, and any aqueous phase reaction products and byproducts are withdrawn from the aquifer through the central injection/withdrawal well.

### 3.2.1 Monitoring

Sixteen monitoring wells, including up and downgradient wells, are used to monitor the site. Within the reaction zone the wells are spaced along four transects emanating from the central injection/withdrawal well. These monitoring wells provide monitoring of the arrival of tracers, buffers, reagent, and various reaction products and other indicators (pH, conductivity dissolved oxygen) during the three stages of each of the three field experiments (injection, drift/reaction, and withdrawal). They are also used in the long-term monitoring phase of the project.

Because the solid-phase reactions need to be understood and the treatment capacity achieved needs to be assessed, core holes are drilled to obtain sediment samples at appropriate time intervals based on the laboratory and bench-scale studies. After reagent withdrawal, the re-equilibration rates are monitored using indicator species in the aqueous phase in the monitoring wells and through coring studies.

### 3.2.2 Advantages

The ISRM field experiment and reagent injection strategy of this type (i.e., "push-pull") was not chosen because it is necessarily the best way to inject reagent for manipulation of the subsurface redox conditions. It was chosen because it is considered to be the best field testing approach for evaluating the effectiveness of different reagents or microbial nutrients for predictably manipulating the redox potential of the Hanford unconfined aquifer.

The small scale of the ISRM experiment allows minimization of 1) the characterization difficulties, 2) the attendant dispersive transport uncertainty, 3) the amount of reagent and non-reactive tracers needed, and 4) the volume of withdrawn fluids (i.e., the waters containing unreacted reagents, non-reactive tracers, and any aqueous phase reaction products and byproducts) requiring special handling/disposal.

The single well injection/withdrawal method (or push-pull) was chosen for testing ISRM feasibility because this method's good recovery characteristics allow an integrated quantitative estimate to be made of the amount of solid mineral phase ferric iron that has been reduced. This estimate comes indirectly from the masses of non-reactive tracers, unreacted reagent, and aqueous phase reagent reaction and degradation byproducts recovered during the withdrawal phase and measurements made on the reacted cores recovered after ISRM treatment.

### 3.2.3 Limitations

The limited number of monitoring wells around the site, as was noted in the ISRM test plan, will not allow a quantitative interpretation (with any reasonable error bars) of the actual spatial distribution of the reagent and non-reactive tracers as a function of time. However, measurements of reagent and reaction product concentrations taken during the course of the experiment at these wells

do provide estimates of the transport rates and the relative extent of the reagent and non-reactive tracer plumes through time, and these measurements provide estimates of the completeness of the reaction at these points through time.

However, while aqueous groundwater chemistry measurements provide indirect evidence that the reagent has reacted or degraded, only a laboratory examination of a statistically significant number of sediment samples retrieved from core holes before and after the injection provides direct evidence for the effectiveness of dithionite reduction of solid-phase ferric iron. Consistency between these three monitoring data sets, the site characterization information and the smaller-scale laboratory data, is required to interpret the results of the ISRM field experiments. Consistency of this information is being tested with numerical models.

The chief complication in the ISRM field test is the natural variability of the subsurface, especially those scales of variability that cannot be tested in the laboratory. Physically, this variability can affect delivery and recovery of reagent and reaction products by allowing portions of the aquifer to be bypassed and, therefore, not reduced. Conversely, reduced zones may reoxidize prematurely along flow paths that permit more rapid re-invasion of dissolved oxygen. Chemically, the presence or absence of certain minerals along these preferential flow paths could diminish or prevent the reduction of ferric iron needed to alter the aquifer redox potential for the periods of time necessary for development of an effective permeable treatment zone.

The ISRM field experiment design methodology must overcome these uncertainties by integrating disparate information from laboratory and field characterization studies, then extrapolating this knowledge to the less certain environment of the aquifer. Mathematical modeling is one of the tools that can accomplish the required integration and extrapolation. Modeling permits an assessment of reagent behavior under a variety of conditions, which should add to the robustness of the experiment design.

### **3.3 Brief Description of Field Experiments**

Before conducting the three field experiments, intermediate-scale experiments that mimicked the field experiments in both the spatial and time scale were conducted at Oregon State University in the 7-m-long, 11-degree wedge-shaped flow cell (Figure 3.3) packed with sediments similar to the field site. This allowed the various operational difficulties to be identified, and the sampling and analysis plans to be amended as necessary.

#### **3.3.1 Full-Scale Bromide Tracer Field Experiment**

The first experiment, a three-stage bromide tracer experiment, was performed to determine design factors for the full-scale reagent injection experiment. This experiment provided hydrologic characterization data for the field site (e.g., volume of reagent required), and helped determine the sampling frequency required for each sampling location as well as test and improve operational effectiveness. The phases of the field tracer test (a 79,950-L [21,000-gal] injection phase lasting 17.5 h, a 24-h drift period, and a 68-h tracer withdrawal phase that retrieved ~4 injection volumes and contained ~96% of the injected tracer) mimicked the preliminary design for the full-scale reagent injection/withdrawal experiment.

### **3.3.2 Mini-Dithionite Injection/Withdrawal Field Experiment**

The second field experiment, a "mini" sodium dithionite injection/withdrawal, was conducted to obtain information on the behavior, handling, and analysis of dithionite and other analytes to fine-tune operations for the full-scale dithionite injection experiment. It was also conducted to determine if trace metals (e.g., Cu, As, Pb, Zn, Hg), above limits of regulatory concern, were mobilized by injected reagent/buffers and to provide information on the quality and quantity of purge waters so that an appropriate strategy for disposal of purgewater from the full-scale injection/withdrawal experiment could be developed. The mini-dithionite injection/withdrawal experiment involved a 1-h injection of 4,548 L (1,200 gal) of buffered reagent (this scale injection allowed reagent/buffers to reach the first observation well at 1.5 m), an 18-h drift/reaction phase, and a 5.5-h withdrawal phase in which a volume of water 5.5 times greater than the injection volume was removed.

### **3.3.3 Main Dithionite Injection/Withdrawal Field Experiment**

The final (full-scale) field experiment consisted of the injection of 79,950 L (21,000 gal) of reagent and buffer in 17.5-h, an 18-h drift/reaction phase, and a 379,000-L (100,000-gal) withdrawal phase. The volume of aquifer reduced, the reductive capacity emplaced, and the effectiveness of this reduced zone in removing chromate and oxygen from groundwater moving through the treated zone was measured by monitoring reagent and reagent reaction parameters during the experiment as well as groundwater quality parameters before, during, and after the experiment. These measurements are being carried out in wells located throughout the treatment zone as well as up- and downgradient to the zone. Additionally, measurements of the reductive capacity achieved and achievable was assessed from laboratory studies on sediment samples collected from core holes drilled before and after the experiment. These core samples were analyzed to determine the reductive capacity that was achieved as a result of the field-scale injection and the total reductive capacity that could have been achieved if the sediments were fully reduced. Long-term monitoring activities will continue at the site for several years.

# Multiple Scale Experimental Approach

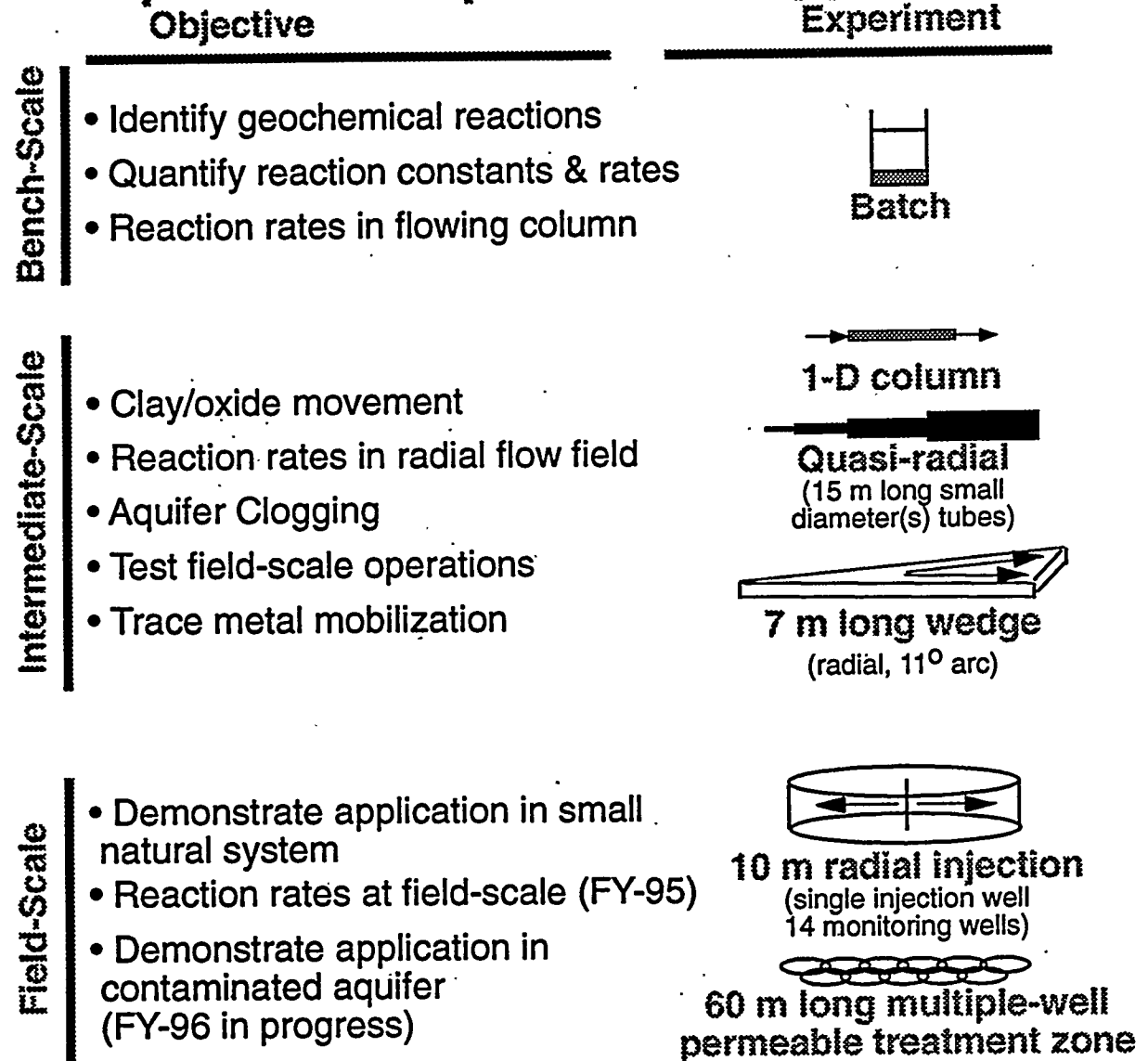
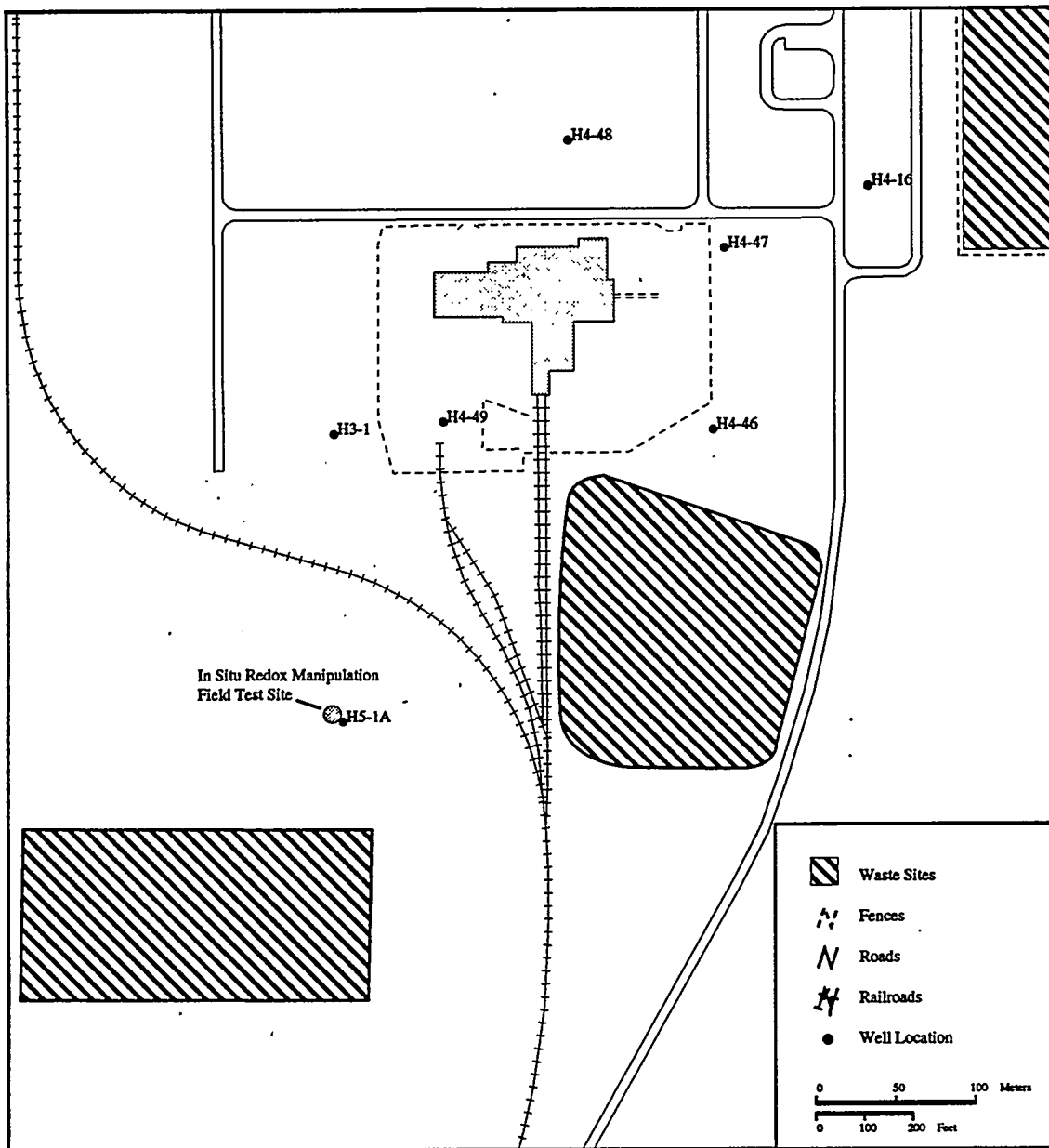
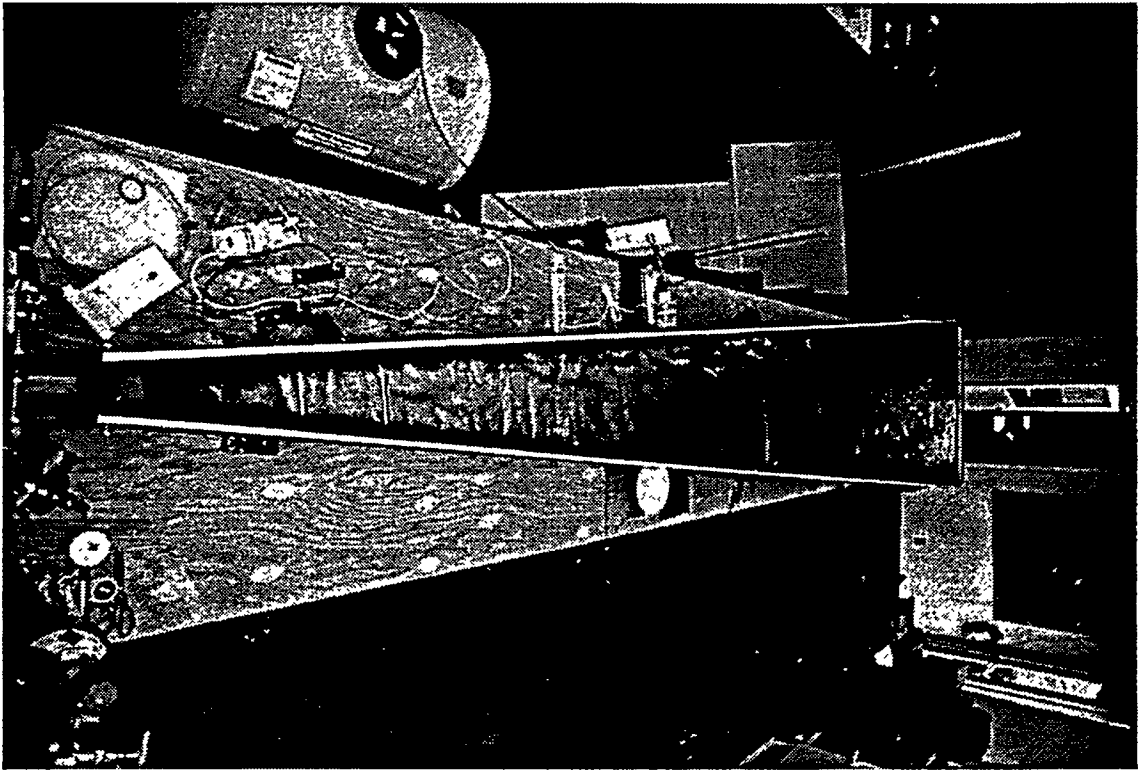


Figure 3.1. Scales of Experiments Performed in Support of the In Situ Redox Manipulation Experiment Showing the Progression from Bench-Scale Batch Studies Through the 100-H Area Field Experiment



**Figure 3.2.** Location Map for the In Situ Redox Manipulation Field Test Site. The location is near H Reactor in the 100-H Area of the 100-HR-3 Operable Unit

(a)



(b)

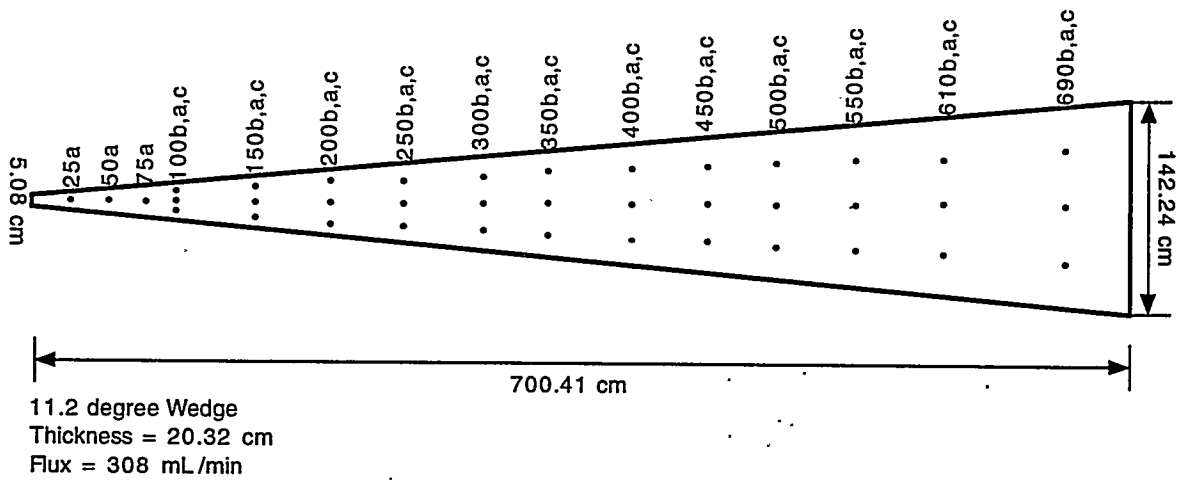


**Figure 3.3.** Photograph (a) and Schematic Diagram (b) of Intermediate-Scale Wedge Flow Cell at Oregon State University

## 4.0 Background

The ISRM Project began in FY 1991 with funding from DOE's Office of Health and Environmental Research's Subsurface Science Program. As part of this project, laboratory proof-of-principle abiotic and biotic studies, conceptual design, and preliminary planning documents were prepared (Fruchter et al. 1994). However, attempts to control redox potential in an aquifer must overcome various scale-up complications arising from the interaction between contaminants, reducing agents, groundwater, and the natural variability of the subsurface. Therefore, in FY 1993, the project was transferred to DOE's Office of Science and Technology (OST, EM-50), and a field site for the initial ISRM field test of the ISRM technology was selected in FY 1994. Laboratory bench-scale, intermediate-scale, and design studies, as well as the field tests described in this report, were funded through an OST EM-50 Integrated Program (IP) from FY 1993 through FY 1995, and through the Plumes and Subsurface Contaminants Focus Areas in FY 1996. This laboratory- and field-scale approach provided the means to evaluate the scale-up and extrapolation of the results of controlled laboratory-scale chemistry and microbiology studies to the less certain conditions encountered in the subsurface.

Because a variety of reagents or types of microbial stimulation have the potential for favorably altering the redox conditions of the subsurface, there was a need to evaluate various reagents and microbial stimulation schemes. As a result, a secondary focus of these OST-funded studies was on development of a field-testing approach for use in evaluating the ability of various reagents or microbial stimulation methods to control subsurface redox potential in the face of the complex interactions and heterogeneity expected in the subsurface.

Before going to the field, a series of experiments was performed at the bench and intermediate scales to test different reagents or microbial nutrients for their efficiency in manipulating the redox conditions of the Hanford unconfined aquifer. Bench-scale testing was used to determine the nature of the reactions that occur and the efficiency with which they are induced by the reagent or nutrient. The factors assessed include the kinetics of dithionite disproportionation, Fe(III) reduction, and the subsequent reoxidation of the reduced phases. The salient results from the bench- and intermediate-scale testing performed in support of the field experiment are outlined and discussed below. Details of the dithionite reagent chemistry and of the reactions and interactions during various phases of the experiment are presented in subsequent sections and in the appendices.

Comparative bench-scale batch studies with sulfite, thiosulfate, hydroxylamine, and dithionite under anoxic conditions established that dithionite was the most effective reductant for the structural ferric iron found in the silt and clay fractions of Hanford-Site sediments. These tests also confirmed that dithionite has a limited lifetime in these sediments due to 1) oxidation by Fe(III) present in the layer-silicate mineral structures or as oxyhydroxides and 2) a disproportionation reaction that was catalyzed by contact with mineral surfaces. Further experiments established that the longevity of the dithionite was prolonged by buffering the solution at neutral or higher pH. Using buffered solutions at room temperature, these experiments indicated that the half-life of the dithionite ion would be approximately 2 or 3 days under the conditions in the Hanford unconfined aquifer. This half-life allows enough time for reduction of structural iron in the aquifer solids, while ensuring that dithionite does not remain in the groundwater for extended periods of time.

Batch experiments with several different pH buffers (i.e., phosphate, carbonate, and bicarbonate) were conducted to identify the best buffer for use with dithionite. Based on these experiments, the pH-buffer selected for use in the dithionite experiments consisted of a 0.4 M  $K_2CO_3$ -0.04 M  $KHCO_3$

solution containing 0.1 M Na<sub>2</sub>S<sub>2</sub>O<sub>4</sub>. The initial pH of this solution was about 11.2 and decreased to about 8 as the dithionite was oxidized or disproportionated. Carbonate was selected because it had no microbial activity (unlike phosphate) or toxic properties and is the main pH buffer in groundwater at the Hanford Site. Potassium was used as the counter-ion to minimize the well-known dispersion and the associated mobilization of the clay-sized minerals when saturated with Na ion. Although bicarbonate could also have been used as the buffer, large volumes of CO<sub>2</sub> gas were released during the buffering process and it was unclear to what extent this would block access to mineral surfaces by the reagent or what impact the volumetric changes would have in a relatively confined subsurface system.

As the ability to quantitatively predict the rates of dithionite decomposition and Fe(III) reduction was needed to design field experiments, several batch experiments were performed to obtain overall rate equations describing the levels of dithionite in pH-buffered solutions contacting the sediments. These experiments showed that the rates of the dithionite disproportionation and Fe(III)-reduction reactions could each be described by pseudo-first-order kinetic rate laws. When these rate laws were combined into a single expression, the longevity of dithionite in the sediments over time could be predicted by the following expression:

$$C_t = \{C_0 - 2C_{Fe3(0)}[1 - \exp(-k_3t)]\}[\exp(-k_1t - k_2C_{surf}t)]$$

where  $C_t$  is the concentration of dithionite in solution at time  $t$ ,  $C_0$  is the initial concentration of dithionite,  $C_{Fe3(0)}$  is the initial concentration of available Fe(III) in the sediment,  $k_3$  is the pseudo-first-order rate constant for the reduction of sediment Fe(III) by dithionite,  $k_1$  and  $k_2$  are pseudo-first-order rate constants for the homogeneous and heterogeneous disproportionation of dithionite, respectively, and  $C_{surf}$  is a measure of the available surface area of the minerals in the sediment involved in the heterogeneous disproportionation reaction. In addition to surface area, the type of mineral surface encountered was shown to have a significant effect on the rate of disproportionation. For example, once the structural Fe(III) was reduced, the high-surface-area smectite clay minerals had no effect on dithionite disproportionation whereas the low-iron, low-surface-area feldspars rapidly catalyzed the decomposition of dithionite. Thus, in addition to the obvious need to assess available Fe(III) in sediment minerals, a determination of the mineralogy in the sediments of a prospective field site is an essential step in the design of an in situ dithionite-injection experiment because of its impact on dithionite stability.

Two types of intermediate-scale studies were performed. One-dimensional column studies using Hanford sediments were conducted to assess the optimum rates of dithionite injection and to establish whether diffusion was a significant factor in the overall process. On a larger scale, a wedge-shaped box, 7 m in length, 20 cm deep, and subtending a 11° angle, was constructed, packed with a sediment similar to that encountered on the Hanford Site, and used to simulate (in two dimensions) an actual injection without the associated risks of a field experiment. These experiments were successful in demonstrating the utility of dithionite as a reductant of aquifer materials using the pH-buffer solutions identified in the bench-scale experiments. They also served to define the injection procedure and develop the analytical methods later used in the field experiments.

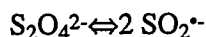
The injection procedure developed on the basis of the intermediate-scale experiments involved an injection phase during which the buffered dithionite solution was pumped into the sediment, a reaction phase during which no pumping occurred; the dithionite was allowed to continue to react with the sediment, and a withdrawal phase during which about 4 pore volumes of solution were pumped out of the sediment through the same well used to inject the reagent solution. The times for the injection stage were 24 h, for the reaction phase 48 h, and for the withdrawal phase 96 h. The

wedge-shaped box used in the experiment was plumbed with a series of sampling ports to allow withdrawal of small aliquots of solution for analysis of pH, and concentrations of oxygen, metals, and dithionite. Later, core samples of the material inside the box were taken and analyzed for reductive capacity using an automated column apparatus and flowing oxygenated groundwater as the oxidant (this approach was eventually adopted for determining of reductive capacity in core samples from the field experiment as well). The results of these determinations yielded reductive capacities as high as 85 meq kg<sup>-1</sup>, which, when emplaced in a 15-m (50-ft) wide zone and using the other assumptions detailed in Section 10.3.2, corresponds to a barrier lifetime of about 90 years. The sediment used in the intermediate-scale experiment contained substantially more available iron than the sediment in the actual field experiment, and as a result demonstrated the potential for very long-lived permeable redox barriers.

Lastly, the intermediate-scale experiments demonstrated the utility of the push-pull injection procedure for minimizing the impact of trace metals, such as arsenic, that were released upon dissolution of iron oxides, on the aquifer. Although the concentrations of these metals increased during the injection and reaction phases, they decreased to acceptable levels (i.e., below drinking water standards) as a result of reversing the pump flow direction and pumping out the treated zone with several pore volumes of groundwater from surrounding zones. For example, in the wedge experiment, arsenic levels in solution rose to an average of about 250 ng mL<sup>-1</sup> (maximum of about 500 ng mL<sup>-1</sup> in one portion of the box) at the end of the reaction phase, and decreased to about 50 ng mL<sup>-1</sup> (a maximum of 75 ng mL<sup>-1</sup> in one portion of the box) after only two pore volumes of withdrawal. On the basis of this experiment, we were able to design the field experiment to include collection and mixing of all the effluent during the withdrawal process to dilute the trace metals solubilized to acceptable purgewater levels.

#### 4.1 Description of the Reagent and Reactions

The redox altering reagent used in the field test is sodium dithionite (Na<sub>2</sub>S<sub>2</sub>O<sub>4</sub>). The dithionite ion (S<sub>2</sub>O<sub>4</sub><sup>2-</sup>), commonly known as hydrosulfite, is a strong reductant, particularly in strongly basic solutions (Amonette et al. 1994). This ion dissociates by the following reaction:



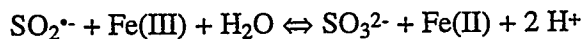
into sulfoxyl radicals (SO<sub>2</sub><sup>·-</sup>), which are strong and highly reactive reductants. According to Amonette et al. (1994) reduction reactions with the dithionite ion typically involve two steps:

1. dissociation of the ion to form the two SO<sub>2</sub><sup>·-</sup> radicals and
2. reaction of these radicals with the oxidized species [e.g., Fe(III) contained in layered silicate and oxide minerals] yields a reduced species [e.g., Fe(II) contained in layered silicate minerals or as a soluble species (Fe<sup>2+</sup>)] and sulfite (SO<sub>3</sub><sup>2-</sup>) or bisulfite (HSO<sub>3</sub><sup>-</sup>)

Because sulfoxyl radicals (SO<sub>2</sub><sup>·-</sup>) are highly reactive, the dissociation of the dithionite ion (S<sub>2</sub>O<sub>4</sub><sup>2-</sup>) is the slow or rate-limiting step in most reactions.

#### 4.1.1 Reduction Reactions

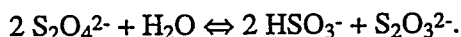
The desired reduction reaction with the dithionite ion takes place very quickly; with a reaction half-life, based on laboratory data, on the order of 1 to 3 h with Hanford sediments. The available ferric iron [Fe(III)] in the sediments of the aquifer are reduced to ferrous iron [Fe(II)] by the following reaction:



The most available/accessible forms of iron in the subsurface sediments occur in those mineral phases (i.e., iron oxyhydroxides and iron-bearing layer silicates) with the highest specific surface areas (Amonette et al. 1994). Since we wish the reduced iron species [i.e., Fe(II)] to remain in place, we are targeting the clay- and silt-sized iron-bearing layer silicates because the iron in this mineral phase is retained in the mineral structure regardless of its oxidation state (Stucki 1988; Scott and Amonette 1988). In contrast, the iron oxyhydroxide mineral phase dissolves when its iron is reduced, but this iron may reprecipitate as siderite ( $\text{FeCO}_3$ ) if sufficient carbonate is present (Amonette et al. 1994).

#### 4.1.2 Disproportionation Reaction

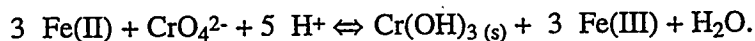
The dithionite ion is not stable in acidic or neutral pH aqueous solutions for long periods. In addition to the reduction reactions discussed above, the dithionite ion undergoes a disproportionation reaction that yields thiosulfate,  $\text{S}_2\text{O}_3^{2-}$ , and bisulfite,  $\text{HSO}_3^-$ :



This disproportionation reaction rate is slower than the reduction reaction rates discussed above and depends on the nature of the mineral surfaces encountered. Estimates of the disproportionation reaction half-life, based on laboratory experiments, are in the range of 12 to 16 h for the 100-H Area sediments and 18 h for the intermediate-scale wedge sediments. The byproducts of both the reduction and disproportionation reactions (i.e., sulfites, bisulfites, and thiosulfates) all eventually oxidize (at much slower rates) to yield sulfate.

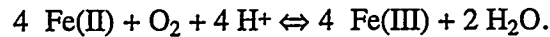
#### 4.1.3 Chromium Reduction and Groundwater Deoxygenation

The functioning of a redox treatment zone during the remediation phase is illustrated in Figure 4.1. Once a redox zone has been emplaced, the reduced iron in the sediments treated with dithionite will act to reduce the mobile Cr(VI) phase of chromium ( $\text{CrO}_4^{2-}$ ) in migrating groundwater at a chromium-contaminated site. The reduction reaction converts the mobile phase to a precipitated Cr(III) phase [ $\text{Cr(OH)}_3$ ] as follows:



It should be noted that there is not a chromium plume of concern at the 100-H Area experimental site, but there is enough chromium to demonstrate the effectiveness of the approach. The chromium reduction equation illustrates how the ISRM technology is capable of treating chromium.

Reduced sediments at the 100-H Area experimental site remove dissolved oxygen in the migrating groundwater by the following very fast reaction:



This oxygen reaction creates a deoxygenated plume of groundwater within the reduced zone and it is expected to migrate downgradient of the redox zone as is discussed in the next section and in Sections 7.0, 10.0, and 11.0.

#### 4.1.4 Reactions and Interactions During Various Phases of Field Experiment

Figures 4.1 through 4.4 illustrate the flow conditions, reactions, and interactions during each of the four phases of the 100-H Area field experiment. This includes the injection, drift, and withdrawal phase of the experiment that creates the reduced or redox treatment zone (Figures 4.1 through 4.3) and the remediation phase in which upgradient waters are altered as they flow through the redox treatment zone (Figure 4.4). Not illustrated in these figures is the disproportionation reaction (discussed in Section 4.1.2) that the dithionite ion undergoes. This process yields thiosulfate and bisulfite as byproducts that eventually oxidize (at much slower rates) to yield sulfate.

##### 4.1.4.1 Injection Phase

During the injection phase (Figure 4.1) a mixture consisting mostly of withdrawn groundwater mixed with the reagent (sodium dithionite) and buffers to maintain the injected fluid at a high pH (a mixture of mostly potassium carbonate with some potassium bicarbonate) is injected through a central injection well, as illustrated in Figure 4.1. During the injection phase, a diverging radial flow field and an injection mound are created by the injection process. During this phase the injection velocity field dominates ambient groundwater flow velocities. Because the reagent reacts with oxygen the injected fluid is depleted of oxygen. The reactions between the reagent and sediments illustrated in Figure 4.1 include the redox treatment zone creation reaction, whereby dithionite reduces the available ferric iron [Fe(III)] in the sediments of the aquifer to ferrous iron [Fe(II)]. Also as illustrated in Figure 4.1, other metals in the mineral phases of the sediments may be mobilized by reduction reactions with dithionite in the same way that some reduced iron mineral phases are mobilized by reduction reactions (see Section 4.1.1). Finally the change of the injection zone conditions to high pH, as a result of the injection, can alter adsorption properties of the sediment surfaces so that some sorbed metals may be released and some mobile metals may be sorbed.

It is important to understand how reagent reaction rates and reagent injection rates interact during the injection phase to determine the spatial distribution of reagent concentration that can be delivered to the sediments targeted for reduction, because the spatial distribution of reagent concentration and the spatial distribution of available, reactable iron in these sediments control the spatial distribution of treatment capacity that can be achieved. A simple spreadsheet model was developed to illustrate how the concentration of reagent that can be delivered to the sediments at the outer fringe of the zone targeted for reduction is controlled by the relationship between reaction half-times (e.g., for dithionite disproportionation and sediment reduction) and the time required for the injection front of reagent and buffers to reach the desired radius (e.g., 9 m [30 ft]). Figure 4.5 illustrates how the reagent concentration (as a percentage of input reagent concentration) varies with radial distance from the injection well for different reagent reaction rate half-lives and reagent/buffer injection rates. Results shown were calculated for the following ideal case:

- a zone 18.2 m [60 ft] in diameter of porosity 0.3 is targeted for reduction
- constant rate and concentration reagent/buffer injection
- rate for the disproportionation reaction is much greater than the Fe(III) reduction reaction and can be ignored
- no dispersion (i.e., plug flow)
- uniform aquifer sediments with sufficient reactable iron in the aquifer sediments that reagent reactions continue throughout the injection period.

Figure 4.5 illustrates 4 cases. Cases 1 through 3 are 20-gpm injection rate cases developed to illustrate the sensitivity of delivered reagent concentration to the reaction rate half-life. As indicated in the legend of the graph, the reagent concentration delivered to the outer limits of the zone targeted for reduction (i.e., a cylinder of radius of 9 m [30 ft]) varies from 0.2% of input for a reaction half-life of 2 h through 4.7% and 12.9% for 4- and 6-h reaction half-lives, respectively. Case 4 in Figure 4.5 was included for comparison with case 2 to illustrate that the delivered reagent concentration is actually dependent on the ratio of reaction half-life to time required for injection. For the 20- and 40-gpm injection rates the injection times are ~18h and ~9 h, respectively. The dependency on reaction half-life to injection time is documented by the jump in delivered reagent concentration (at a radius of 9 m [30 ft]) from 4.7% of input to 21.4% of input for the two 4-h reaction half-life cases (i.e., the 20-gpm case 2 and 40-gpm case 4).

#### 4.1.4.2 Drift Phase

This phase is illustrated in Figure 4.2. During the drift phase hydraulic conditions change. The radial flow field decays from the injection conditions of a strong radial flow field with an injection mound to nearly ambient groundwater flow conditions. Reactions during the drift phase are the same as discussed for the injection phase except that the dithionite concentration levels are steadily decreasing as it disproportionates (see Section 4.1.2) and is consumed by reduction reactions.

#### 4.1.4.3 Withdrawal Phase

The withdrawal phase pumping creates a converging radial flow field that forms a drawdown cone around the central injection/withdrawal well. The withdrawal velocity field dominates the ambient groundwater flow field during this phase. The purpose of the withdrawal phase is to remove the majority of the injected reagent and buffers as well as the any mobilized metals with the withdrawn groundwaters. The pH and other concentration conditions in the aquifer sediments and fluids initiate their return to near normal concentration levels of most constituents. As is discussed in Section 10, conductivity and pH are still above normal. In part, the elevated pH and conductivity as is related to the incomplete recovery (i.e., less than 100%) of the withdrawal phase. The redox conditions in the zone, however, will remain in the altered state because of the presence of the reduced iron [Fe(II)] in the structure of the clay- and silt-sized iron-bearing layer silicates of the aquifer sediments. Any mobilization of metals caused by reactions with the reagent or the altered conditions, other than the redox, should cease once the withdrawal stage is complete (i.e., when ~4 to 5 pore volumes of natural groundwater have been flushed through the reacted sediments) and these chemicals have been removed.

As will be discussed in Section 10, some trace metals within the reduced zone are still slightly elevated compared to their pre-experiment background levels. This could be in part due to the incomplete recovery or related to the elevated pH within the reduced zone altering the sorptive properties of the sediments as discussed in Section 4.1.4.1. Finally, as illustrated in Figure 4.3, the oxidation of the sediments in the reduced zone and the removal of redox sensitive contaminants is initiated during the withdrawal phase as the oxygenated groundwater and redox sensitive contaminants (e.g., chromium) are drawn into the reduced zone by the withdrawal phase pumping.

#### 4.1.4.4 Remediation Phase

During the remediation phase, as illustrated in Figure 4.4, the drawdown cone of the converging radial flow system is replaced with an ambient groundwater flow system, the system can be envisioned as consisting of an upstream zone, a reduced zone, and a downstream zone. Under ambient flow conditions oxygenated groundwater and redox-sensitive contaminants (e.g., chromium) enter the reduced zone and react as illustrated. The oxygen reoxidizes the structural Fe(II) of the sediments back to Fe(III). The redox-sensitive contaminants are treated (e.g., either immobilized or dechlorinated) by interactions with the structural Fe(II) of the reduced sediments that results in its oxidation to Fe(III). A deoxygenated, contaminant free, plume of groundwater forms downstream of the reduced zone. This plume of deoxygenated groundwater becomes reoxygenated by the hydrodynamic dispersion and diffusion as discussed in Sections 7.0, 10.0, and 11.0. Metals mobilized during the injection phase and not completely removed during the withdrawal phase or remaining elevated in the reduced zone because of the redox conditions or elevated pH levels are expected to precipitate as they move out of the reduced zone into the oxygenated sediments downgradient of the reduced zone.

ISRM is only applicable to groundwater systems that have sufficient, accessible (during the time frame of the treatment process), and appropriately distributed structural Fe(III) in the aquifer sediments downgradient of the contaminant plume to be treated to achieve the required treatment capacity within the zone to be reduced. Ignoring the effects of heterogeneity for the moment, the treatment capacity of the system is determined by the mass of structural Fe(II) created by the ISRM process, because the amount of contaminant that can be treated is related to the mass of the structural Fe(II) encountered along the contaminant flow path.

Oxygen, the targeted contaminant(s), and any other consumers of the structural Fe(II) in the reduced zone must be considered when estimating barrier longevity. It should also be noted that for many situations the levels of consumption of structural Fe(II) by the targeted contaminant(s) is small compared to the consumption by the oxygen in natural groundwater. For example, in treating a 1-ppm chromium plume, nearly all of the treatment capacity (i.e., the structural Fe(II)) is consumed by the 8 ppm of oxygen typically found in groundwater.

While there may be different ways to quantify treatment capacity, a convenient method is to express treatment capacity in terms of the number of pore volumes of oxygenated/contaminated groundwater that must pass through a unit volume of treated aquifer sediments before contaminant breakthrough at levels above those of regulatory concern occurs. Of course, the path through the treated aquifer sediments must be sufficiently long relative to the ambient flow rates and sediment/contaminant reaction rates. Treatment capacity quantified in this manner can be easily measured by studies on cores of treated sediments using natural oxygenated/contaminated groundwaters. Quantification in this manner also allows the lifetime of the redox barrier to be estimated directly from measure of the ambient groundwater flow rate at the site where the ISRM

treatment zone is to be emplaced. Barrier longevity ( $B_1$ ) in time units can be estimated from the treatment capacity ( $T_c$ ) in pore volumes, the barrier width ( $b_w$ ) in length units, and the expected groundwater velocity ( $v$ ) at the emplacement location by the following equation.

$$B_1 = T_c * b_w / v$$

For example, if a ISRM zone 18 m (60 ft) wide was emplaced with a treatment capacity of 50 pore volumes in an area where the groundwater flow rate was 18 m (60 ft)/y, then the estimated lifetime of the barrier would be ~50 years.

For groundwater systems with sufficient, reactable, structural Fe(III), as could be determined from tests on core samples, there are still heterogeneity concerns. The first is related to *accessibility* to sufficient, reactable, structural Fe(III). The second is related to the *scale* of the heterogeneity distribution in accessible, reactable, structural Fe(III); the concern being that if this scale is large with respect to the emplaced reduced zone contaminated water will break through prematurely via pathways with insufficient, reactable, structural Fe(III). With regard to the first concern, the time scale of the ISRM treatment-zone emplacement approach (order of days) assures that only reactable Fe(III) along the high conductivity pathways is reduced. The sufficiency part of this concern can be directly assessed by determining the amount of unreacted reagent recovered during the withdrawal phase of the ISRM emplacement approach. With regard to the scale concern, the width of the reduced zone needs to be adjusted to be large relative to the estimates of this "scale."

# Injection Phase

(ambient groundwater flow rate  $\ll$  radial flow rate)

Inject Dithionite and Buffers into Oxidized Aquifer

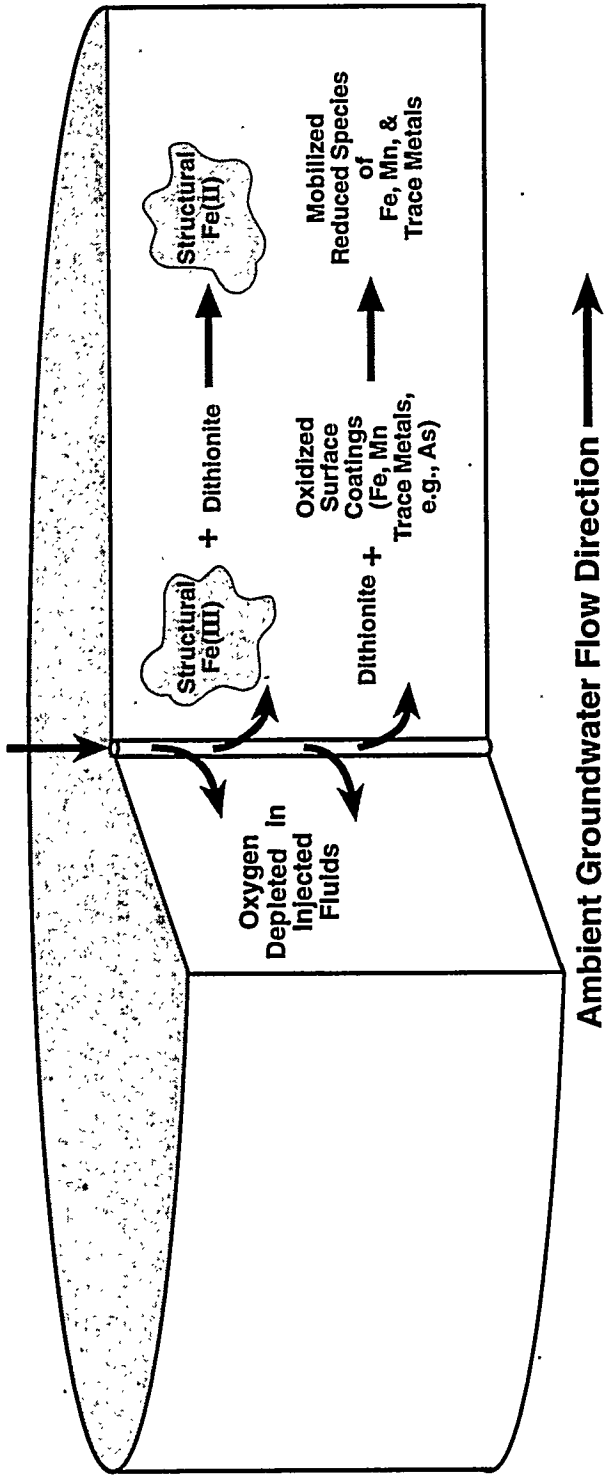


Figure 4.1. Injection Phase Interactions and Reactions During Creation of a Redox Treatment Zone

# Drift Phase

(only ambient groundwater flow)

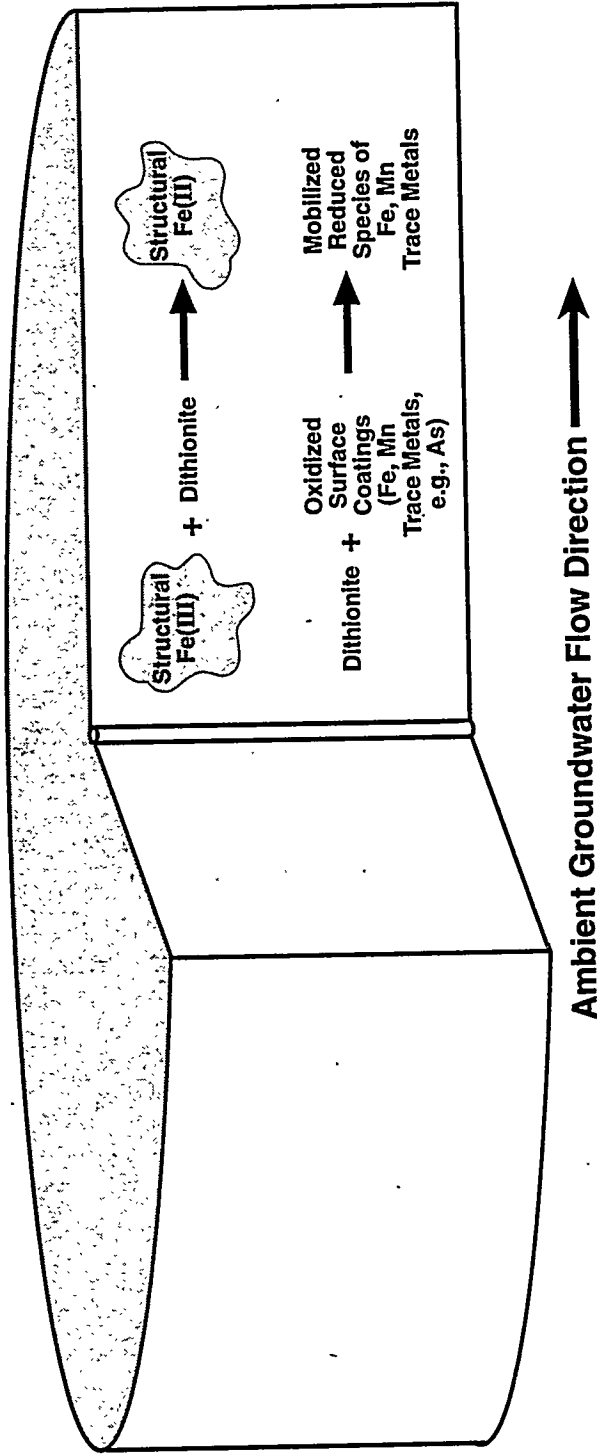


Figure 4.2. Drift Phase Interactions and Reactions During Creation of a Redox Treatment Zone

**Withdrawal Phase**  
(ambient groundwater flow rate  $\ll$  radial flow rate)

Withdraw Unreacted Dithionite, Reaction Products, Buffers and Mobilized Components

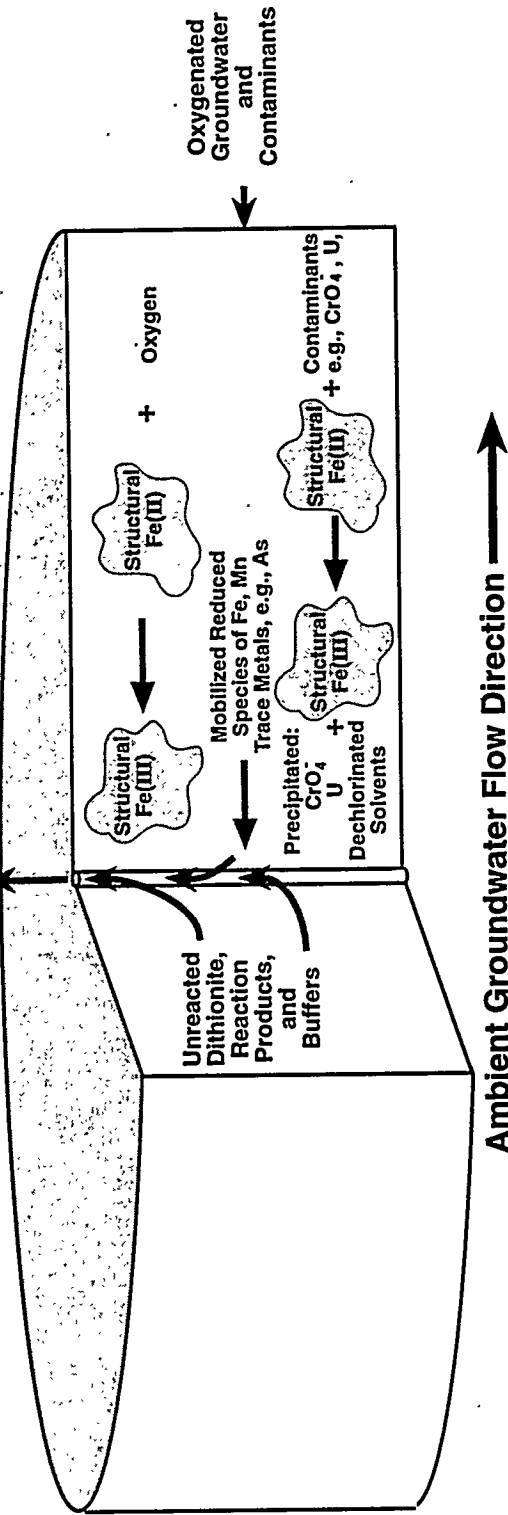


Figure 4.3. Withdrawal Phase Interactions and Reactions During Creation of a Redox Treatment Zone

# Remediation Phase

(only groundwater flow)

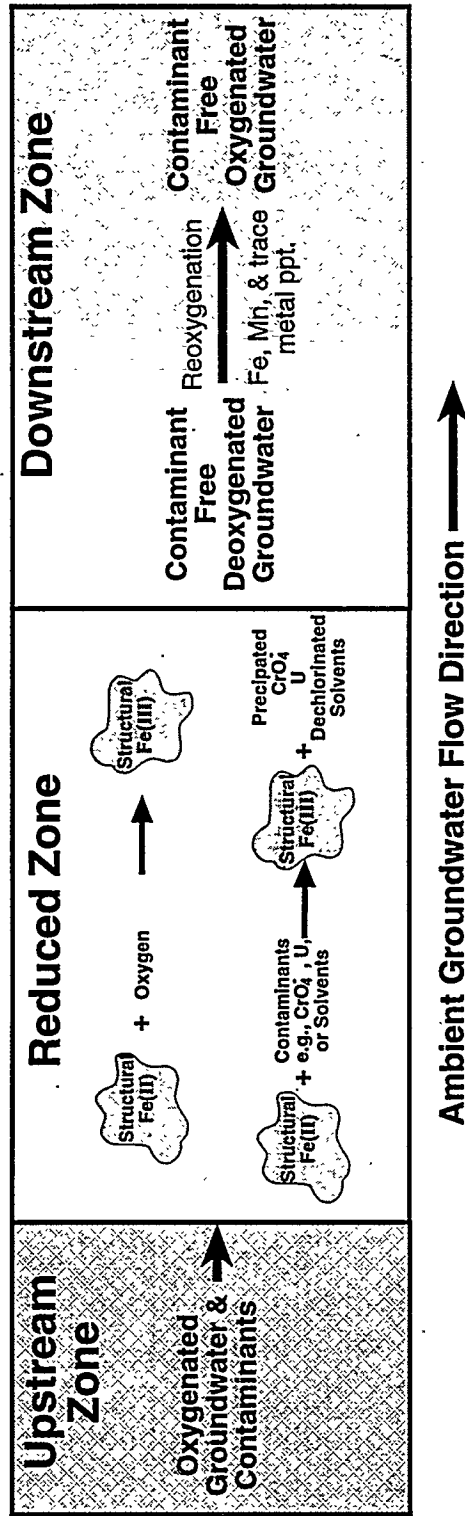
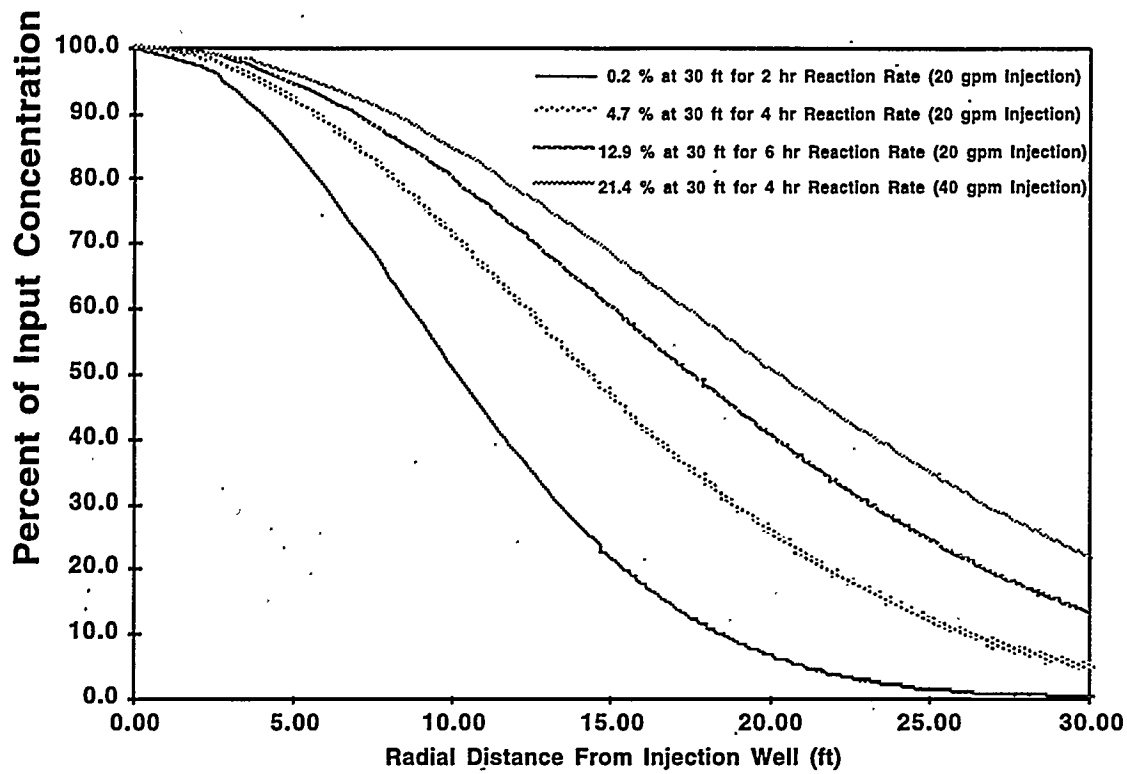
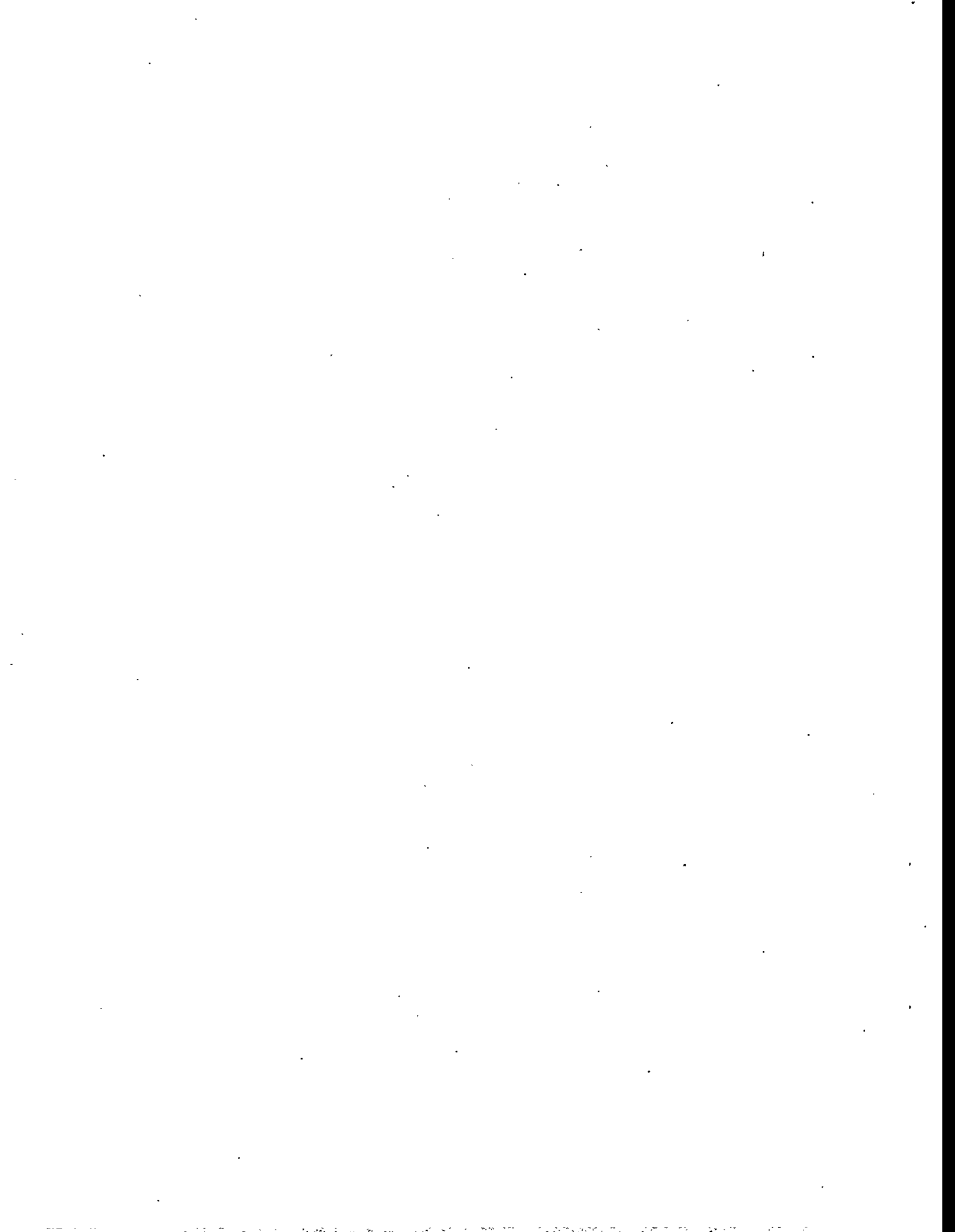


Figure 4.4. Interactions and Reactions Within and Downgradient of the Redox Treatment Zone During the Remediation Phase



**Figure 4.5.** Variation in Reagent Concentration as Percentage of Input Reagent Concentration Versus Radial Distance from the Injection Well at the Conclusion of Injection Phase. The legend indicates the actual percentage of input reagent concentration delivered at a radius of 9.1 m (30 ft) at the end of the injection phase for the different reaction half-life and injection rate cases.



## 5.0 Site Selection

During FY 1994, several locations on the Hanford Site were evaluated as potential sites for the ISRM field test site. During the site selection phase, various regulatory, cost, hydrogeologic, geochemical, and site access criteria were developed to provide a framework for the selection of a suitable demonstration site. A brief description of the site selection criteria used to locate the ISRM test site and a description of the selected site following the scope of our site selection was limited to the Hanford Site primarily because of logistics (e.g., staff and equipment onsite) and existing permits and approvals.

### 5.1 Regulatory Criteria

Because of the nature of the ISRM technology, regulatory/stakeholder participation during design and field deployment of the technology will help streamline approval procedures. Consequently, a site is required where there is likely to be administrative support from the agencies that control activities on the site. This would be the case for sites with contamination problems that might benefit from the technology being developed. In turn, those managing the site must be convinced that there will be minimal adverse impact to the site, especially where it might preclude future remediation options.

To encourage the development of cleanup alternatives, the U.S. Environmental Protection Agency established treatability studies in the Comprehensive Environmental Response, Compensation, and Liability Act (CERCLA) legislation to provide performance and cost data to aid in remedy selection and design. Treatability studies are performed to provide site-specific testing of innovative technologies for which general data are not readily available. Formal permitting of a cleanup activity is unnecessary for a treatability study, although the responsible administrative parties for the site must be agreeable to the designation. Treatability studies are a desirable alternative to formal permits because of the simplified approval procedure. For this reason, a site where a CERCLA treatability study is appropriate and desirable is required.

### 5.2 Well Installation Costs

The single largest cost associated with a field-scale ISRM experiment is well installation. The selected site should have features that minimize both the number of wells that must be installed and the installation cost per well/core hole. Sites with existing wells that can be used in the experiment array are especially desirable, not only for the savings in well installation costs but for the geologic and hydrologic characterization information accompanying these wells. Borehole construction costs are generally a function of the drilling depth. For this reason, a site with a relatively shallow depth (i.e., less than 30.3 m [100 ft]) to the water table would be desirable.

### 5.3 Hydrogeologic Criteria

Hydrogeologic conditions at the site affect the ability to control the emplacement of the treatment barrier. Sites with relatively slow groundwater velocities (i.e., less than 30.48 cm [1 ft] per day) in thin unconfined aquifers (i.e., less than 9.1 m [30 ft] thick) afford a higher degree of control over the extent of transport. This simplifies the monitoring requirements by reducing the sampling volume. Another control issue is the influence of fluctuations in the Columbia River stage on the experiment.

The site should be sufficiently distant from the Columbia River to limit the effect of diurnal changes in river stage to less than 1.27 cm (0.5 in.) at any of the wells. It is also desirable to provide long (i.e., greater than 10 years) travel times to the river to minimize any impacts associated with the treatment.

## 5.4 Geochemical Criteria

The permeable treatment zone is created by reducing the ferric iron to ferrous iron within the clay minerals of the aquifer sediments. Naturally occurring  $\text{Fe}^{3+}$  content should be 0.05% of total soil fraction, and should be associated with layer silicate clays. The selected site must meet this criteria. Analyses of clays from both the Ringold and Hanford formations indicate ferric iron contents averaging 3% to 6% iron by weight.

Contaminated groundwater requires special handling procedures depending on the type of contaminant and the concentration; exceptional procedures will incur significant costs to the project. Furthermore, the presence of additional constituents in the groundwater complicates the interpretation of the chemistry at the site. Although a site that minimizes these complications is desirable, the proximity of a target contaminant such as chromium is desirable from the standpoint that much of the knowledge and experience gained from the field experiment can be used in a subsequent treatability test.

## 5.5 Access Criteria

The selected site should provide unencumbered access for vehicles and heavy equipment. Level terrain is strongly preferred.

Using the above criteria, a search of potential locations on the Hanford Site resulted in selection of the 100-H Area for the ISRM field test site. The site is located in the vicinity of Hanford Site well 199-H5-1A (abbreviated H5-1A) and 199-H5-1B (H5-1B), approximately 260 m (850 ft) south of H Reactor (Figure 3.2) and is outside the main contamination plume for constituents of primary concern in the 100-H Area. The site, as configured for the redox manipulation experiment, consists of one 20-cm (8-in) diameter injection/withdrawal well and 16.5-cm-(2-in-) diameter monitoring wells, located at various radial distances from the injection/withdrawal well (Figures 5.1 and 5.2). Because H5-1A and H5-1B were not constructed to the same design specifications as wells installed for the field demonstration, they will not be used as primary monitoring wells.

⊗ H5-13

⊗ H5-14

⊗ H5-12

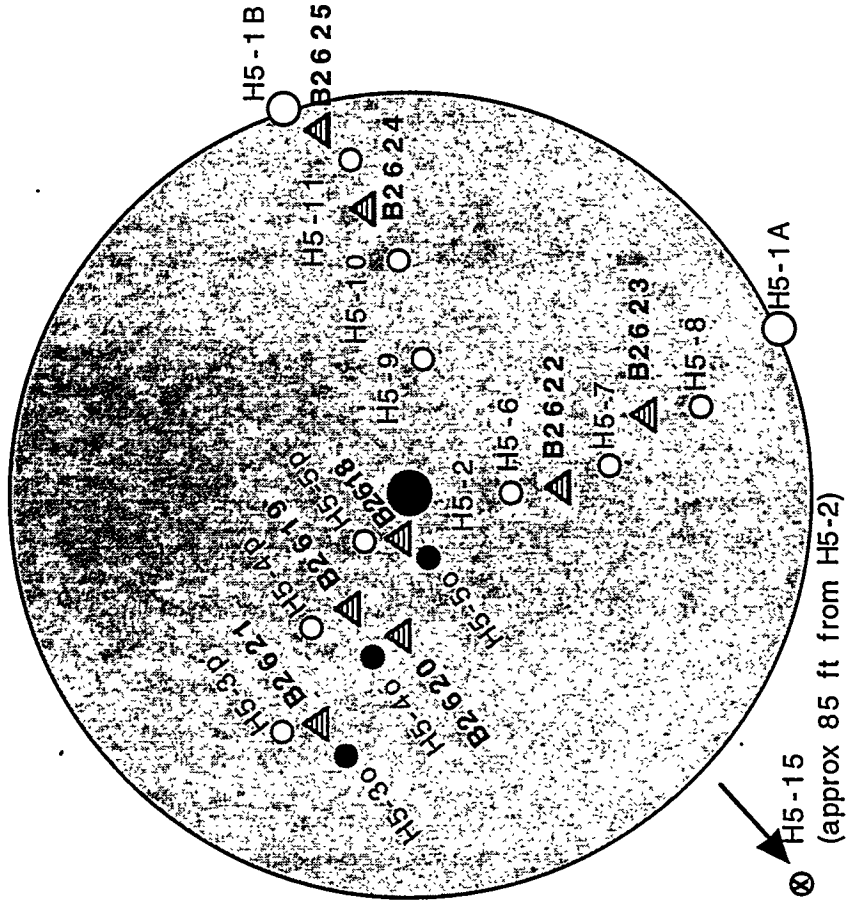


Figure 5.1. Well Location Map for the In Situ Redox Manipulation Field Test Site

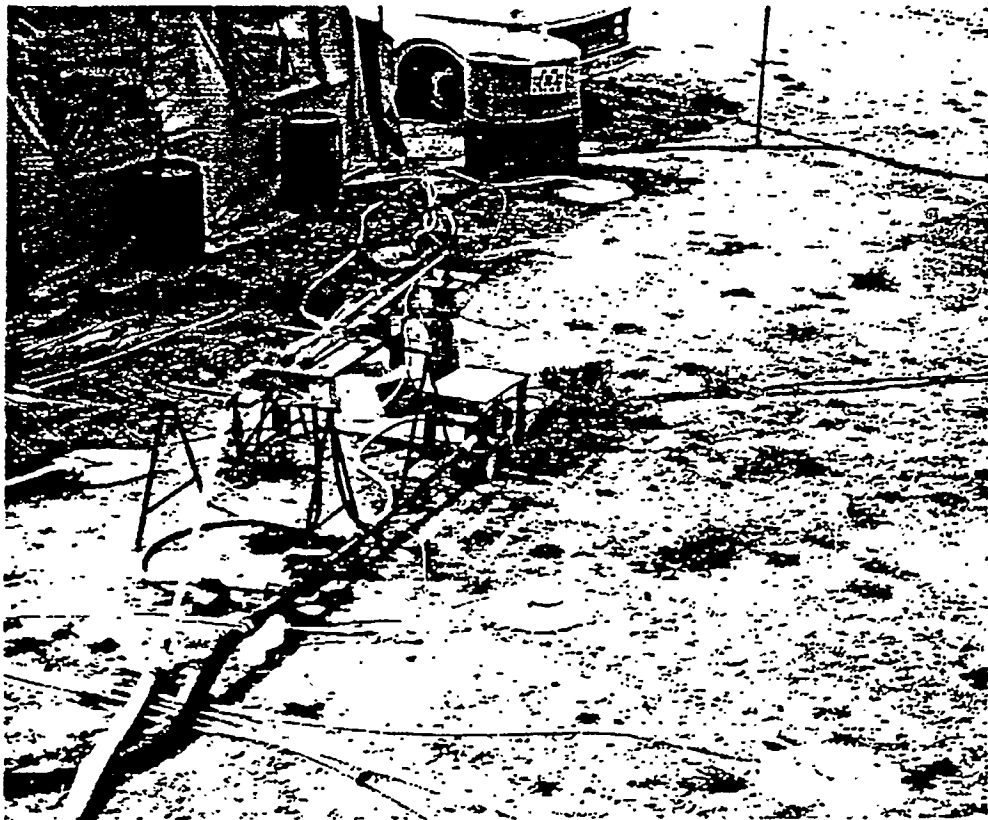


Figure 5.2. Photographs of the ISRM Field Site at the 100-H Area

## 6.0 Site Characterization

During FY 1995, site characterization activities began at the ISRM field test site. Information obtained during hydrogeologic characterization of the site included sediment physical, geochemical and aquifer hydraulic properties, and microbiologic population data. Obtaining this information improved the conceptual understanding of the hydrogeology beneath the ISRM test site and helped provide detailed, site-specific hydrogeologic parameter estimates. The resulting characterization data were incorporated into a numerical model developed to simulate the physical and chemical processes associated with the field experiment and aid in experiment design and interpretation. The following sections briefly describe and summarize results from site characterization activities at the ISRM test site; more detailed information is contained in a separate site characterization report (Vermeul et al. 1995).

### 6.1 Hydrogeologic Setting

In the 100-HR-3 OU, which encompasses the ISRM test site, the unconfined aquifer includes the unconsolidated sediments of the Hanford and Ringold formations and is underlain by the Columbia River Basalt Group (Lindsey and Jaeger 1993). The uppermost unconfined aquifer is approximately 3 m (9 ft) thick beneath the ISRM test site and is contained within the Hanford formation. The Hanford formation predominantly consists of sandy gravels; however, other lithologies that may be present include gravelly sand and sand. The uppermost unconfined aquifer is underlain by a fine-grained unit of the Ringold Formation, which is typically a sandy-clayey to clayey silt. The spatial continuity of this uppermost, fine-grained Ringold unit was observed during hydrogeologic characterization activities at the ISRM test site and is supported by hydrochemical data from across the 100-HR-3 OU that indicate contamination does not extend beyond the uppermost part of the unconfined aquifer (Peterson 1993).

The unconfined aquifer beneath the northern portion of the Hanford Site is laterally bounded by the basalt ridges surrounding the basin and the Columbia River to the north and east. The aquifer is recharged by the Cold Creek drainage to the west, by wastewater disposal in the 200 Areas, and by natural recharge (Fayer and Walters 1995). Groundwater generally flows from west to east across the Hanford Site and discharges to the Columbia River. In the 100-H Area, groundwater flow direction is generally in the northeast direction under a hydraulic gradient of  $\sim 0.0009$ . Groundwater velocity in the vicinity of the ISRM test site has been estimated at 0.3 m/d (0.9 ft/d), resulting in an approximate travel time of 4.5 years for the 730 m (2400 ft) between the site and the Columbia River.

### 6.2 Well and Core Hole Installation

During 1995, 17 wells and 8 core holes were drilled and/or installed at the ISRM field test site. Locations of these wells are shown in Figure 5.1. The wells consisted of one injection/withdrawal well (199-H5-2), three upper piezometers, nine lower piezometers, three downgradient monitoring wells, and one upgradient monitoring well. Core hole locations are also shown in Figure 5.1. Design and construction details of these wells and core holes are discussed below.

#### 6.2.1 Drilling

All of the wells and core holes were drilled using the resonant sonic drilling method by Water Development Hanford Company. It was crucial that the wells and piezometers be installed without the use of drilling fluids or muds so that minimally disturbed samples could be collected. The

resonant sonic drilling method satisfies all of these criteria. Both the conventional resonant sonic drilling method and the sonic push method were used. The drill method and total depth drilled for each well/core hole is shown in Table 6.1. Wells/core holes that were sampled were drilled exclusively with the conventional resonant sonic drilling method. The other 10 wells were generally drilled using a combination of the two methods. For these 10 wells, sonic push was generally used above a depth of 11.6 m (38 ft) and then conventional resonant sonic drilling was used from 11.6 m (38 ft) to total depth.

Safety monitoring during drilling consisted of periodic checks with a photoionization detector and a lower explosive limit/oxygen meter. No results above background were detected. Also, the drilling spoils were checked daily by a Radiation Control Technician; all spoils were below background values. In addition, samples of the drilling spoils and from the split-spoon sample intervals were submitted to the Westinghouse Hanford Company (WHC) 222-S Laboratory in the 200-West Area for total activity analyses. All results were below the laboratory's detection limit (50 pCi/g).

Table 6.1 shows well construction information for the 17 wells and 8 core holes installed at the ISRM site in 1995 including well diameter, radial distance from injection well, drill depth, and screened interval. Figure 6.1 shows a schematic illustration of the construction of each of the 4 types of wells. All of the wells were constructed of polyvinyl chloride casing and screen. The screen for the injection/withdrawal well was a 20-slot size, continuous wire wrap type. This screen is placed within the lower 1.5 m (5 ft) of the aquifer. The screen for all of the other wells was a 10-slot size, and they were also continuous wire wrap type. The screens for the upper and lower piezometers were 0.76 m (2.5 ft) in length and were placed to monitor the upper and lower portions of the aquifer, respectively. The downgradient monitoring wells have fully penetrating 3-m- (10-ft-) long screens that are placed just below the water-table surface.

All of the wells have an artificial filter pack placed around the well screen appropriate for the slot size of the well screen. Annular seal materials were placed above the filter pack and consist of bentonite crumbles, bentonite hole plug, cement grout, and a concrete pad. All wells meet Washington Administrative Code (WAC) 173-160 specifications. Detailed as-built diagrams for each well are shown in Appendix C.

Core holes were not completed as wells; these were abandoned upon reaching total depth. Abandonment was performed as per WAC 173-160 specifications.

## 6.2.2 Sampling

Sediment samples were collected from six wells during resonant sonic drilling and from the core holes (Table 6.1). Three types of samples were collected: 1) samples for sediment physical properties, 2) samples for sediment chemical characterization, and 3) samples for microbiologic characterization. Sediment samples were collected using a split-spoon sampler with lexan liners. The 1.5-m-(5-ft) on split-spoon sampler was advanced using resonant sonic energy. Microbiologic samples were collected using sterilized split-spoons, lexan liners, caps, and sample handling equipment. Care was taken not to contaminate the sampler and samples before or after sample recovery. Upon recovery from the borehole, samples for both chemical characterization and microbiologic characterization were immediately capped, placed in argon-filled bags, and placed in an ice-filled cooler. Following receipt of total activity analyses, the samples were transported to the laboratory and placed in a anaerobic glovebox for storage.

The quality of samples recovered and the percentage of sample recovery versus nonrecovery was generally very good. Significant heat can sometimes be generated during sonic drilling as a result of the drilling process. Heating of the core during sampling was generally not observed; however, one core sample was hot to the touch. This core was not used for microbiologic characterization.

### 6.3 Hydrogeologic Characterization

The primary focus of the sediment core sampling performed during well installation activities at the ISRM site was for detailed geologic characterization of the sediments within the unconfined aquifer. The unconfined aquifer is approximately 3-m (9-ft) thick beneath the ISRM test site and is contained within the sands and sandy gravels of the Hanford formation. The Lower Mud Unit of the Ringold formation, represented by a sandy clayey to clayey silt, forms the base of the upper unconfined aquifer.

The uppermost unconfined aquifer beneath the test site can be described as containing two hydrofacies: 1) a lower unit dominated by a sandy gravel (the lower 1.8 to 2.1 m [6 to 7 ft] of the aquifer), and 2) an upper unit dominated by sand (the upper 0.9 to 1.2 m [3 to 4 ft] of the aquifer). Figure 6.2 shows a west-to-east cross-section across the ISRM site illustrating the lithology of the unconfined aquifer. As shown on this cross-section, the lower 1.8 to 2.1 m (6 to 7 ft) of the aquifer is dominated by a sandy gravel. The upper 0.9 to 1.2 m (3 to 4 ft) of the aquifer is dominantly a sand lithology in most wells except 199-H5-2 and 199-H5-5P. In 199-H5-2, this sand lithology is present as only a thin layer. In well 199-H5-5P, this sandy interval contained noticeably more silt.

Sediment samples were collected from six wells during resonant sonic drilling for physical property analyses, which included moisture content, sieve, particle density, bulk density, hydrometer, and porosity. Average values obtained from selected sediment physical property analyses are shown in Table 6.2; complete analyses results are contained in Appendix B of the site characterization report (Vermeul et al. 1995).

Pre-experiment hydraulic tests conducted at the ISRM test site included several single-well slug displacement tests conducted during well installation, and a constant-rate discharge test and slug interference test that included pressure response monitoring at 15 locations across the site. Analysis of the constant-rate test response data indicate the following "best estimate" values for test site-scale hydraulic properties: transmissivity = 250 m<sup>2</sup>/d (2700 ft<sup>2</sup>/d); effective hydraulic conductivity = 90 m/d (300 ft/d); storativity = 0.0055; specific yield = 0.037; and vertical anisotropy ( $K_D = K_v/K_h$ ) = 0.06.

As noted in Vermeul et al. (1995), of the hydraulic properties determined from the constant-rate discharge test, only transmissivity exhibited any spatial dependence. A general dependence between transmissivity and well screen/aquifer depth was also suggested. A possible decreasing transmissivity with increasing depth relationship is consistent with geologic descriptions of well logs available for the ISRM test site. In addition, a general relationship of increasing transmissivity with increased distance from pumping well 199-H5-2 was indicated. This general association was exhibited irrespective of azimuth direction for observation wells at the ISRM test site. The cause for this distance correspondence is unknown. This distance dependence may be associated with changes in aquifer characteristics (e.g., increasing aquifer thickness or hydraulic conductivity with distance), presence of artificial pumping well conditions (i.e., well skin, well inefficiencies), or inherent deficiencies in the homogeneous aquifer analytical solution for analyzing tests conducted in heterogeneous unconfined aquifer formations.

As shown in Figure 6.3, a comparison of pre-experiment slug interference test data (when converted to an equivalent pumping test response following the procedures outlined in Peres et al. 1989 and Spane 1996) with normalized constant-rate test results indicate very similar test responses in most cases. Quantitative analysis of selected pre-experiment slug interference responses, however, indicate slightly lower estimates for transmissivity and hydraulic conductivity when compared to values derived from constant-rate test analysis. The divergence in property estimates is most prevalent for observation wells located in proximity to stress well 199-H5-2 (e.g., well 199-H5-5P; distance = 1.5 m [5.0 ft]), and becomes insignificant with distance (e.g., well 199-H5-3P; distance = 6.0 m [20.0 ft]).

The apparent difference in hydraulic property values for nearby observation wells is attributed to the fact that slug interference test analyses are dependent on early-time test results, which are primarily influenced by near-well aquifer conditions and artificial well effects (i.e., well skin, well inefficiencies). Pumping test analyses (especially analyses emphasizing later-test time results) are more significantly influenced by aquifer conditions at greater distance from the pumped well. The slight divergence in hydraulic property estimates derived by slug interference and pumping test analysis, therefore, is expected and is consistent with test comparison findings presented in Butler (1990).

Groundwater travel time from the proposed test site to the Columbia River was calculated using parameter estimates obtained from hydraulic characterization activities at the ISRM test site and slug test interpretations from two downgradient wells (DOE 1993). Hydraulic conductivities for wells 199-H6-1 and 199-H4-45 were estimated at 21 m/d (70 ft/d) and 30 m/d (100 ft/d) respectively. Travel time to the river was calculated by dividing the total pathline into two separate segments, one representative of conditions near the test site and the other representative of the higher hydraulic gradient and lower hydraulic conductivity near the river. Adding the first path travel time (550 m [1,800 ft] at 0.3 m/d [1.3 ft/d], see Table 6.2) and the second path travel time (180 m [600 ft] at 0.6 m/d [2 ft/d], hydraulic gradient of 0.0047, hydraulic conductivity of 26 m/d [85 ft/d], and a 20% effective porosity) resulted in a test site to the Columbia River travel time of 1,600 days (~4.5 years).

## 6.4 Geochemical Characterization

The redox status of the 100-H sediments is largely reflected in the redox state of the iron present in these sediments, but can also be inferred from the oxygen content of groundwater contacting the sediments. During the site-selection process, measurements were made of the total-Fe, total-Fe(II), and total-Fe(III) contents of selected sediments. These results, however, do not indicate how much of the iron is in contact with the groundwater and thus available to participate in the redox chemistry with dissolved species such as dithionite, oxygen, and contaminants. Methods used to determine "available" Fe(III) are described below. Dissolved oxygen data from monitoring wells located in the 100-D/100-H Areas (Section 6.6), in addition to available-Fe(III) data, suggest that the sediments and the aquifer beneath the ISRM test site were highly oxidized and that little or no Fe(II) was available for reaction with the groundwater constituents before treatment with a reductant such as dithionite.

The Fe(III) available for reduction to Fe(II) by dithionite (the reagent selected for the ISRM field experiment) in selected sediments was determined by either a colorimetric or a kinetic method. Both methods provided acceptable results. The kinetic method is advantageous because, in addition to measuring available Fe(III), it also yields rate constants for decomposition of dithionite and the reduction of Fe(III).

The colorimetric method, which was based on that of Komadel and Stucki (1988), measured the amount of Fe(II) in the silt- and clay-sized fractions of sediment samples before or after a 24-h

treatment with dithionite (and removal of the excess reductants by washing with an inert salt solution). With this method, samples were dissolved in acid in the presence of phenanthroline (an Fe[II] colorimetric reagent). The intensity of the color produced was used to calculate the amount of Fe(II) present. The difference in the Fe(II) measured for the samples before or after dithionite treatment was taken to be the amount of available Fe(III).

The kinetic method measured the decrease in dithionite concentration during treatment of the sediment samples under anoxic conditions at 15°C. Loss of dithionite was assumed to be due to a combination of two independent first-order reactions: 1) reduction of Fe(III), and 2) a surface-mediated decomposition reaction. Because the decomposition reaction occurred at the same rate throughout the treatment period, the loss of dithionite in the later portions of the treatment period (i.e., after ~24 h) was assumed to stem entirely from this reaction. Extrapolation of the rate law for this reaction to the starting time of the experiment yielded an initial dithionite concentration. The difference between this extrapolated value and the actual starting concentration represented the amount of dithionite consumed by reduction of Fe(III). Values for available Fe(III), therefore, were calculated from this value by assuming two moles of Fe(III) reduced for each mole of dithionite consumed.

Samples for geochemical analysis of ferrous/ferric iron [Fe(II)/Fe(III)] content were collected via split-spoon sampler and were analyzed using either the colorimetric or the kinetic method. Table 6.3 contains results from total-Fe, total-Fe(II), total-Fe(III), and available-Fe(III) analyses for sediment samples collected at the ISRM test site before the field experiment. Although total-Fe values ranged from about 3% to 6% by weight, the available-Fe(III) values were only a small fraction of these values, typically < 0.1% by weight. A wide range in available-Fe(III) values (0.01% to 0.10% by weight) was obtained for the Hanford formation sediments with an average value of 0.059 ( $\pm 0.035$ )% by weight. The two samples from the underlying Ringold Formation, which provides a lower boundary layer for the field experiment, yielded available-Fe(III) values of 0.73% by weight largely as a result of the higher clay and silt content of these samples relative to the Hanford formation.

## 6.5 Microbiologic Characterization

Microbiologic samples were collected using sterilized split-spoons, lexan liners, and sample handling equipment. Care was taken not to contaminate the sampler and samples before or following sample recovery. After the split-spoon sampler was recovered, the lexan liners were immediately capped, placed in an argon-filled plastic bag, and placed in an ice-filled cooler until the samples could be transported to PNNL.

For each analysis, about 10 g of sediment was added to a 0.1% sodium pyrophosphate (pH 7) solution for a total volume of 95 mL and mixed to aid in the release of microorganisms from the sediment. Serial dilutions of 1/10 were carried out using 90-mL blanks of phosphate buffered saline (pH 7). Duplicate plates were set up for each sample at five separate dilutions. Plates were incubated at room temperature and measured at two time points for colony forming units (CFUs) and colony types. The results of this analysis are summarized in Table 6.4.

Low microbiological populations are defined as having less than  $10^4$  CFU/g of sediment, medium populations are between  $10^4$  to  $10^7$  CFU/g, and high populations are above  $10^7$  CFU/g. Most of the sediment samples analyzed at the 100-H Area ISRM site have low (or no) microbiological populations. Although these populations are low, they are consistent with the results of other microbiological sampling on the Hanford Site.

## 6.6 Groundwater Chemistry

As part of the CERCLA process, a Limited Field Investigation was undertaken in the 100-HR-3 OU (DOE 1993). This investigation evaluated the groundwater chemistry of the 100-H Area and identified constituents of primary concern. These constituents were then evaluated further in a qualitative risk assessment (DOE 1993). Based on the qualitative risk assessment, the constituents of primary concern for human health risk in the groundwater beneath the 100-H Area are tritium,  $^{14}\text{C}$ ,  $^{90}\text{Sr}$ ,  $^{99}\text{Tc}$ ,  $^{238}\text{U}$ , chromium, and nitrate. The constituents of primary concern for ecological risk (contamination near the river) in the 100-H Area are chromium, iron, and lead. The human health risks for the occasional- and frequent-use scenarios are low to very low. The constituents identified for ecological risk exceed the chronic lowest observable effect level. DOE (1993) concluded that an interim remedial measure may be necessary based on the chromium and iron concentrations in the near river wells, springs, and/or the Columbia River. Appendix E contains background groundwater chemistry data for the 100-H Area wells.

Before the ISRM field experiment, samples were collected from site monitoring wells and submitted for trace metals analysis to determine baseline conditions at the site. Results of the ICP-MS trace metals analysis are reported in Table 6.5. Analysis results indicate that pre-experiment trace metals concentrations fall well below regulatory maximum contaminant levels. In addition to the baseline trace metals analysis, several field parameters were measured before the field experiment, including dissolved oxygen, conductivity, pH, and temperature. The following field parameter monitoring equipment was used:

- Dissolved oxygen. Orion model 810 dissolved oxygen meter. Range = 0 to 20 ppm, accuracy =  $\pm 1\%$  of full scale.
- Conductivity. Oakton WD-35607 series conductivity meter. Range = 0.0 to 199.9 mS, accuracy =  $\pm 1\%$  of full scale.
- pH. Oakton WD-35615 series pH meter. Range = -2.00 to 16.00, accuracy =  $\pm 0.01$  pH, calibration with up to 5 buffers, automatic temperature compensation.
- Temperature. Oakton WD-35615 series temperature meter. Range = 0.0 to 100.0°C, accuracy =  $\pm 0.5^\circ\text{C}$

Conductivity, pH, and temperature were relatively uniform across the site with average values of 452  $\mu\text{S}$ , 7.55, and 21.0°C, respectively (Table 6.6). Dissolved oxygen concentrations were highly variable across the site and in some cases, much lower than expected. Because of the suspect nature of the baseline dissolved oxygen concentrations observed at the ISRM test site, wells from across the 100-H Area were sampled and analyzed for dissolved oxygen concentration to determine local baseline conditions.

On June 11, 1996, an investigation of dissolved oxygen concentrations in wells across the 100-H Area was conducted (Figure 6.4). All wells were sampled using a variable speed electric submersible pump. Purge volumes were determined by monitoring dissolved oxygen and other standard field parameters (conductivity, pH, temperature) in a flow-through monitoring assembly; the flow-through assembly allows for parameter monitoring without the sample stream coming in contact with atmospheric oxygen. Field parameters were monitored using the equipment described above.

Following stabilization of the dissolved oxygen concentration (based on the dissolved oxygen probe readings) samples were collected for dissolved oxygen analysis using a Hach DR/2000

Spectrophotometer with high-range dissolved oxygen AccuVac Ampules (range = 0-13 mg/L). Samples were collected for analysis using the Hach AccuVac Sampler to minimize atmospheric oxygen contamination of the groundwater sample. Dissolved oxygen analysis results are reported in Table 6.7.

In most cases, dissolved oxygen concentrations across the 100-H Area fell within the expected range. Groundwater temperatures ranged from 16°C near the Columbia River (199-H4-4) to between 18°C and 21°C across the rest of the study area; this range in groundwater temperature results in theoretical air saturated dissolved oxygen concentrations, based on the solubility of oxygen in water at that temperature (Dean 1985), of 9.8 ppm, 9.4 ppm, and 8.9 ppm, respectively. However, there were three sampling locations (199-H3-2A, 199-H4-8, and 699-96-43) where dissolved oxygen concentrations greater than the theoretical air saturated concentration were observed. Possible explanations for these anomalously high dissolved oxygen concentrations include, but are not limited to, 1) agitation, and subsequent aeration of the sample by the sampling pump (however, it should be noted that all samples were collected using the same equipment and sampling procedure); 2) agitation, and subsequent aeration of the sample during sample collection; and 3) limitations of the analytical method near the upper end of its range.

As discussed previously, dissolved oxygen measurements at the ISRM test site before the field experiment were highly variable and in some cases much lower than expected. In addition, dissolved oxygen concentrations in the ISRM upgradient monitoring well (199-H5-15) continue to be lower than concentrations observed throughout the 100-H Area (Table 6.7). One possible explanation for these discrepancies in dissolved oxygen concentration observed in the newly constructed ISRM monitoring wells (i.e., compared with 100-H Area monitoring wells, which were installed in the mid 1980s to early 1990s) is that some finite quantity of reductive capacity, associated with the pulverization of formation materials during drilling, may have been generated within the sediments adjacent to the borehole during well installation. Similar reductions in dissolved oxygen concentration within newly constructed wells on the Hanford Site have been observed by others and have been associated with the interaction of groundwater and crushed basalt (Stevens and McKinley 1995) or basalt and steel filings (Bjornstad et al. 1994) generated during percussion drilling.

## 6.7 Description and Operation of Field Site Test Facilities

Equipment used as part of the field site test facility includes:

- injection/withdrawal pumps, piping, and flow control valves
- monitoring well sampling pumps and associated controllers, switch boxes, and sampling manifold
- pressure transducers
- argon gas and tubing
- flow-through assembly with geochemical field parameter monitoring probes
- transfer pump
- mixing tanks (26,900-L [7100-gal] and 9,475-L [2500-gal])

- Steel water storage tank (17,000-L [4500-gal])
- Sample purgewater collection tanks (950-L [250-gal])
- 100,000-gallon Modutank
- generator and lights
- mobile laboratory
- 12 m (40-ft) by 15.2-m (50-ft) enclosed tent.

### **6.7.1 Injection/Withdrawal Pump and Monitoring Equipment**

The well configuration for the test site is shown in Figure 5.1. The injection well was equipped with two sets of piping, one for injection and one for withdrawal. The injection piping extended to the approximate top of the screened interval and terminated with a flow restriction to keep the tubing full during injection. Flow rate monitoring equipment (Omega Engineering turbine flow meter), pressure monitoring equipment (Keller Series 173 pressure transducers) in both the injection/withdrawal well and selected monitoring wells, a flow control valve, and a sampling port were installed for use during both the injection and withdrawal phases of the experiment. Pressure and flow rate information was recorded using a Campbell Scientific datalogger (CR10x). The injection pump was located on the surface and consisted of an 1.5-hp electric centrifugal pump. The withdrawal pump consisted of a 3-hp electric submersible pump installed with the intake located at the approximate center of the screened interval. The piping connecting the injection and withdrawal pumps contained several diversion valves making it possible to direct flow to/from the mixing tanks or to storage in the Modutank (withdrawal water).

### **6.7.2 Sampling Equipment**

During each phase of the experiment, concentrations in monitoring wells were monitored via dedicated Grundfos Redi-Flo2 sampling pumps. The sampling pumps were controlled by four sampling pump controllers and sampling manifolds. Each sampling manifold was equipped with a flow-through assembly with geochemical field parameter monitoring probes for measurement of pH, dissolved oxygen, conductivity, and bromide (tracer test only). The pumps, controllers, manifolds, and probes used for obtaining groundwater samples are illustrated in Figure 6.5, and are described in detail below and in Appendix A.

The system included the following:

- Pump controller. This manufacturer supplied control box (Grundfos 115-VAC converter) converts standard 110-V single phase power into three-phase power, required by the pump switch box.
- Pump switch box. The pump switch box was developed to provide a multi-channel interface between a single pump controller and several pumps. Pumps connected to the single controller cannot be operated simultaneously. The desired pump is selected by turning the rotary switch to the indicated position (pump/monitoring well information will be clearly marked) and pulsing the reset switch. Once selected, the pump motor frequency, and subsequent flow rate, are adjusted with the pump controller.

- **Sampling manifold.** The sampling manifold was developed to direct the groundwater sample streams of each pump connected to the pump switch box to a common manifold. Once the sample stream is in the manifold, it can be directed to one of three places: 1) initially, to purgewater storage until a steady, low-turbidity sample stream is obtained, 2) once a steady sample stream was obtained, to the flow-through monitoring assembly and, 3) when the predetermined purge volume had been discharged and monitored parameters had stabilized and been recorded, to the sampling port, and samples were collected.

During the bromide tracer experiment and the mini-dithionite injection/withdrawal experiment, we determined that a two- to three-screened interval volume purge was sufficient to adequately flush the sampling equipment, allow probes to stabilize, and provide a representative groundwater sample. This sampling protocol resulted in the generation of approximately 11-L (3 gal) of purgewater during the collection of each sample; downgradient monitoring wells, which had longer screened intervals, required larger purge volumes. Pump flow rate and elapsed time were recorded to determine volume purged for each sample.

- **Flow-through monitoring assembly.** During the bromide tracer test, a Geotech multiprobe monitoring chamber was used. The monitoring chamber had a 1350-mL chamber volume and was capable of accommodating 5 probes simultaneously. During the mini and main dithionite injection/withdrawal experiments, a monitoring assembly was developed that utilized a series of Teflon swagelock "T" fittings; the reduced internal storage volume of this flow-through monitoring assembly provided significant improvement in probe performance over that realized with the Geotech chamber. Specifics of the geochemical field parameter monitoring probes, detection limits, and calibration information are contained in Appendix A.

The sampling equipment was housed in a 12-m (40-ft) by 15.2-m (50-ft) enclosed tent. Electricity was provided by a diesel generator.

### 6.7.3 Argon System

The injection/withdrawal well, monitoring wells, and mixing/injection tanks were plumbed so that a blanket of argon gas was maintained. This argon "blanket" minimized the exposure of both the groundwater within the wellbores and the reagent in the mixing tanks to atmospheric oxygen.

### 6.7.4 Tanks

Other equipment that was used at the field site included three 26,900-L (7100-gal) plastic mixing tanks equipped with 3/4-hp mixers, a 9,475-L (2500-gal) plastic tank equipped with a 3/4-hp mixer, and a 17,000-L (4500-gal) steel tank.

The three 26,900-L (7100-gal) plastic mixing tanks were plumbed so that they could either be individually isolated or interconnected as a group. This allowed the injection pump to pump liquid into the mixing tank(s) from an external source (e.g., groundwater supply or the refrigerated tank containing concentrated dithionite solution from the manufacturer).

A 379,000-L (100,000-gal) Modutank was also used for the onsite storage of the withdrawal water while testing was performed to determine the appropriate method of disposal. The Modutank was an open swimming pool-type tank with dimensions of 17.5 m (56.75 ft) by 17.5 (56.7 ft) by 1.47 m (4.75 ft) deep.

The mixing tanks and Modutank were connected to the injection/withdrawal well via a diversion valve and associated piping. Two 947-L (250-gal) plastic storage tanks were used to contain purgewater generated during the sampling of site monitoring wells. These tanks were periodically emptied into the Modutank using a trash pump.

### **6.7.5 Mobile Laboratory**

Onsite analytical equipment was housed in an Explorer 30 mobile laboratory. This equipment performed direct measurement of dithionite and dithionite degradation product concentrations and provided replicate groundwater geochemical property measurements using laboratory instruments (microelectrodes) for comparison with and verification of the geochemical field parameter monitoring probes. This instrumentation is discussed in more detail in Appendix A.

### In Situ Redox Well Schematics

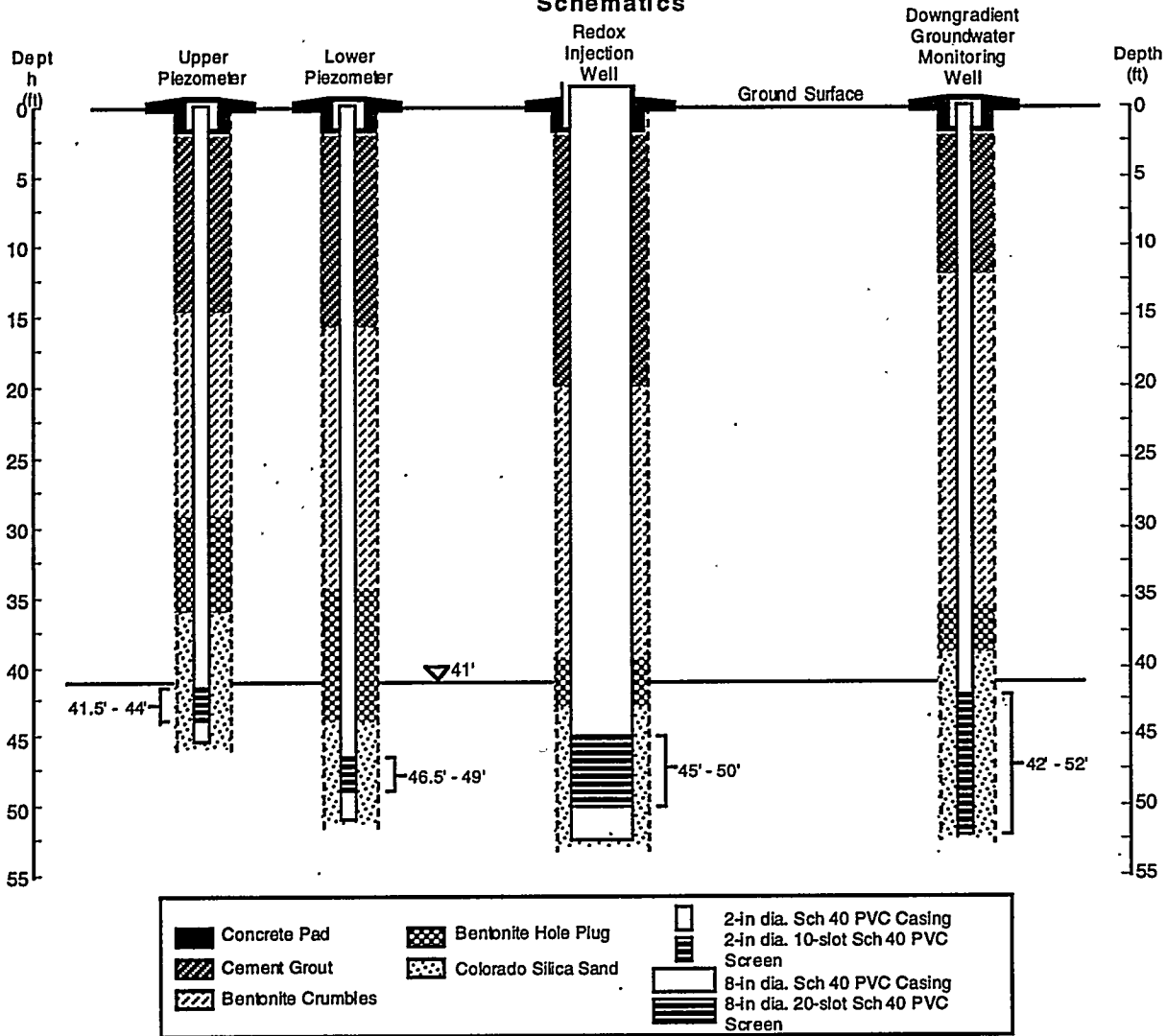


Figure 6.1. Schematic Well Construction Diagram for Wells Installed at the ISRM Site

**Generalized Geologic Cross-Section of the Upper Unconfined Aquifer Beneath the ISRM Test Site**

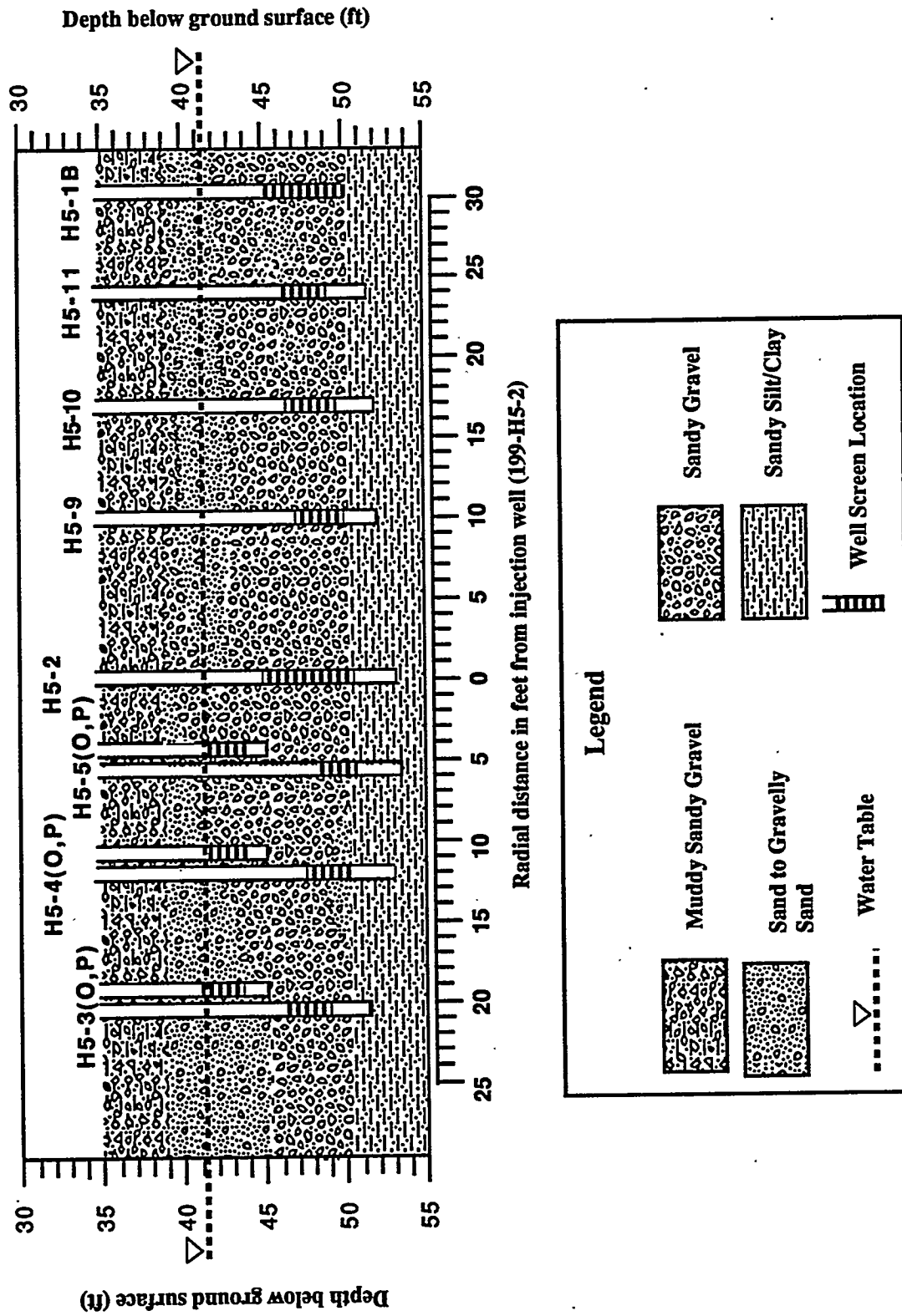


Figure 6.2. West-to-East Geologic Cross-Section of the Unconfined Aquifer

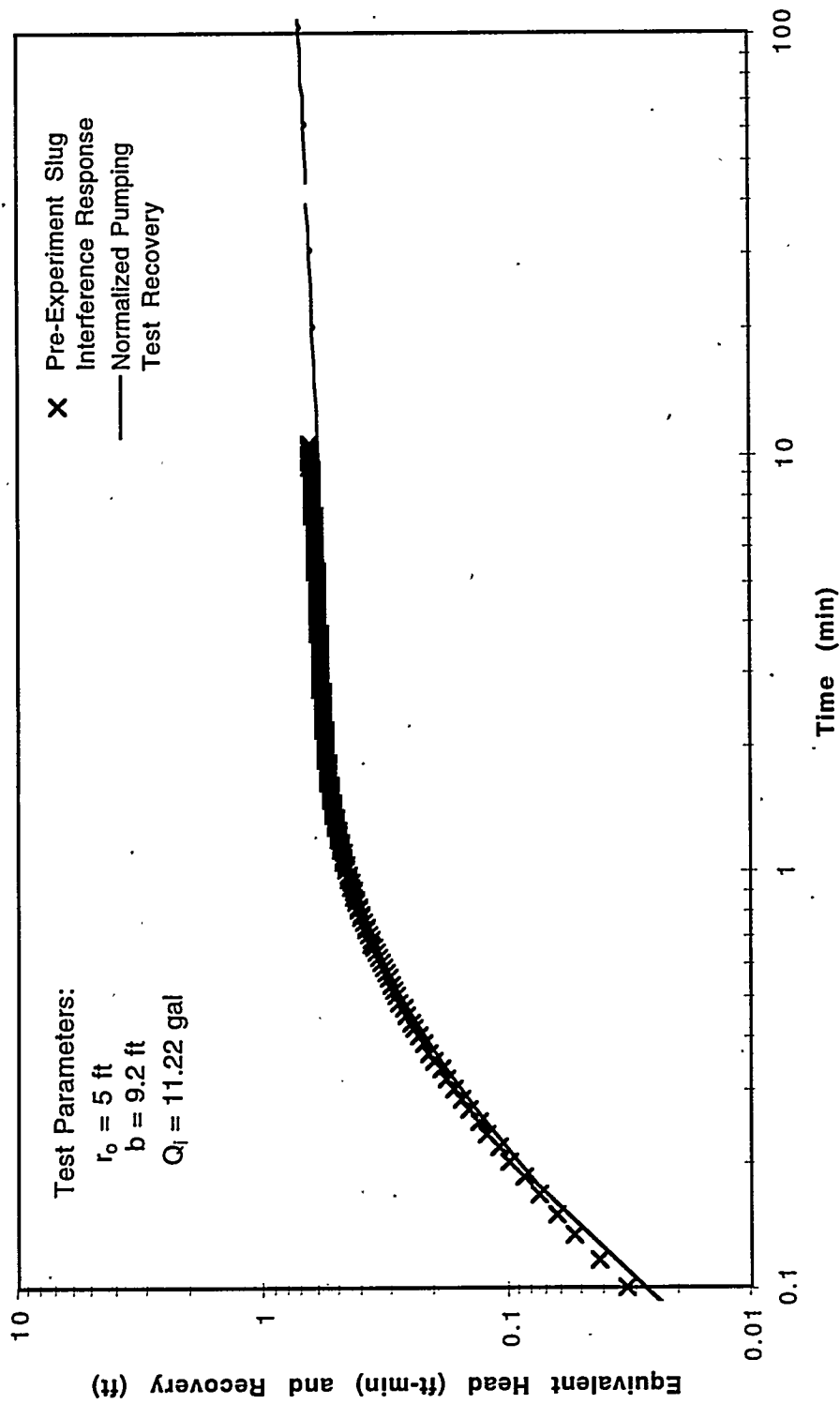


Figure 6.3. A Comparison of Pre-Experiment Slug Interference Test Results from Well 199-H5-5P with Normalized Constant-Rate Test Results

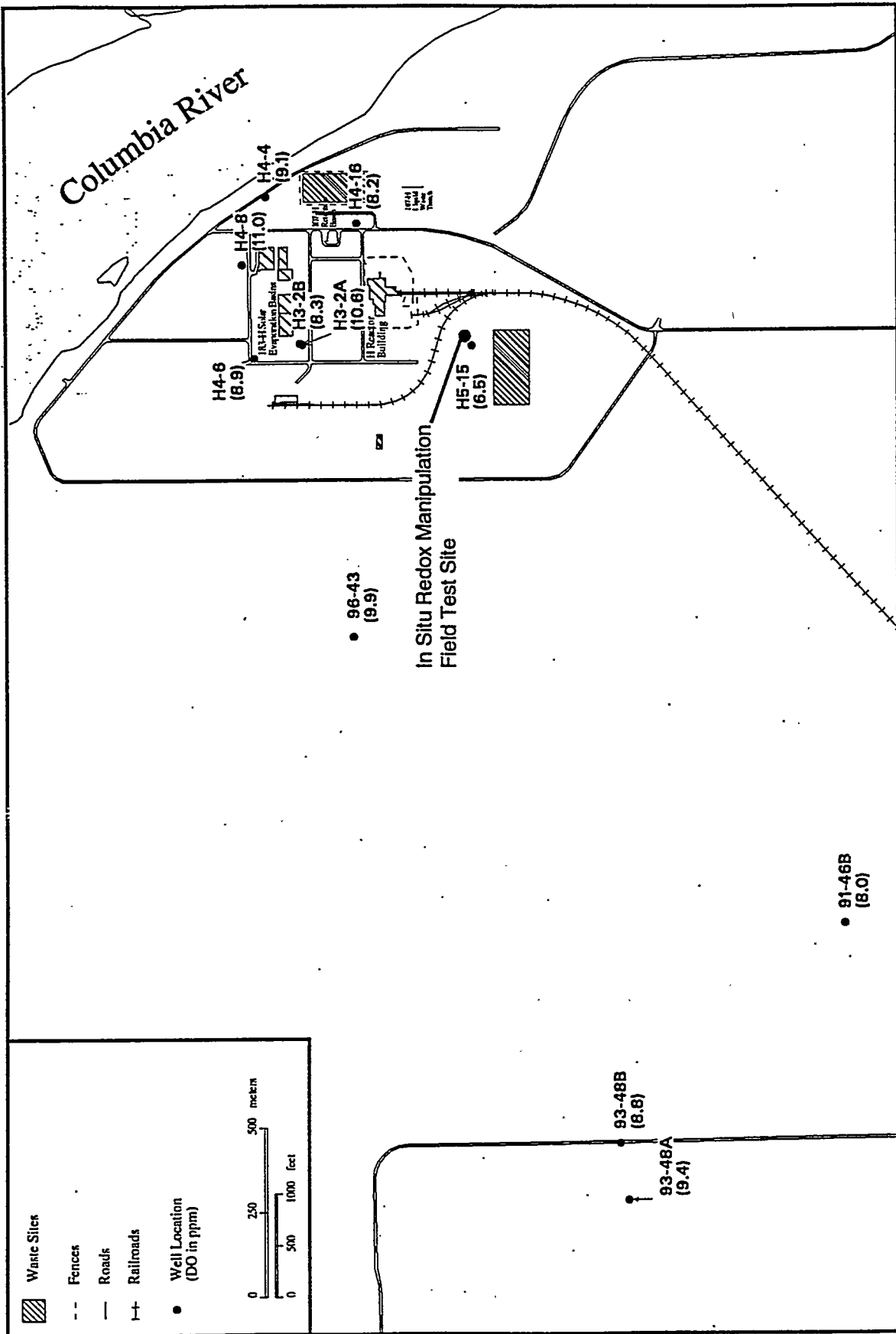


Figure 6.4. Wells Sampled and Analyzed for Dissolved Oxygen Concentration Within and Upgradient from the 100-H Area

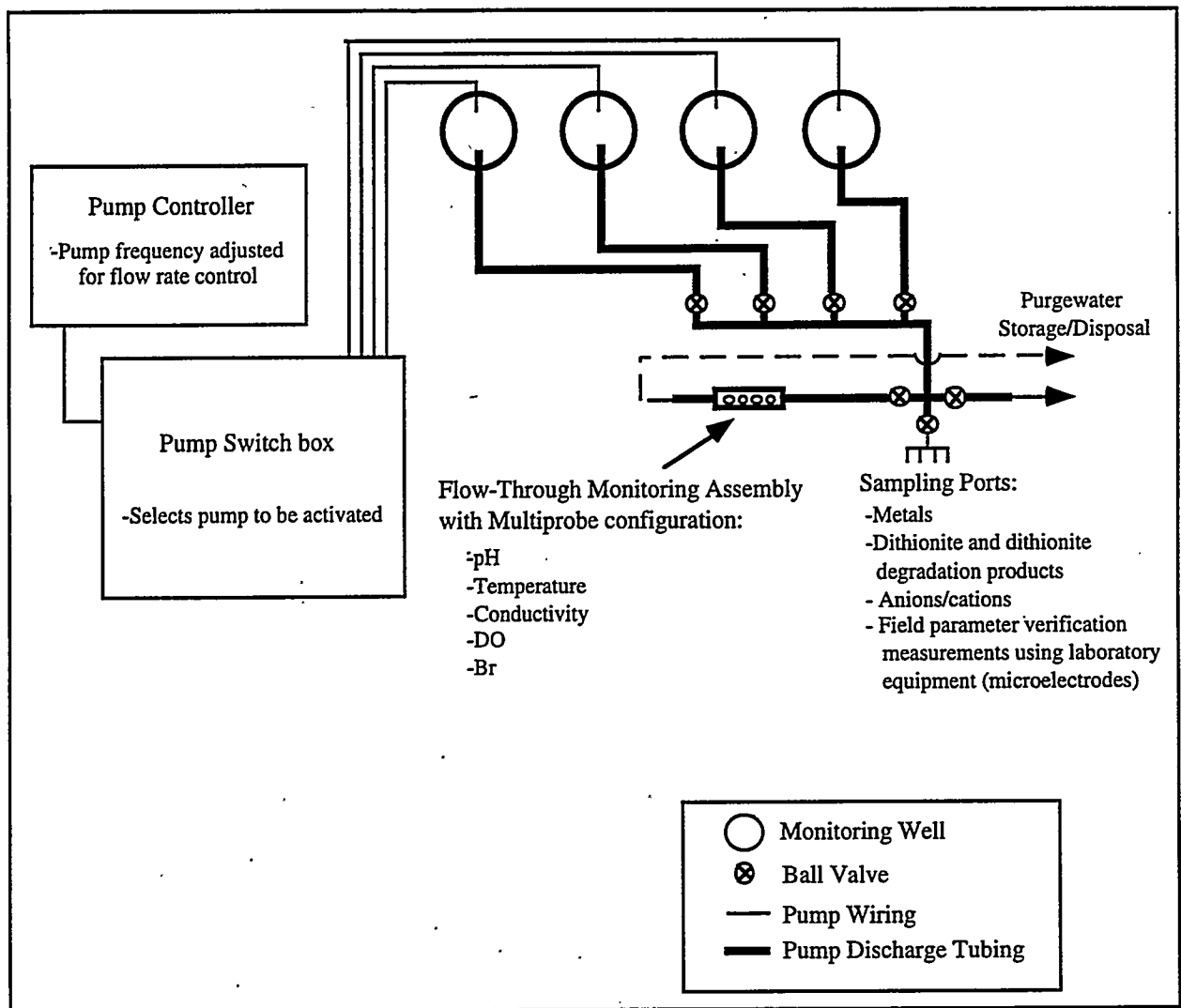


Figure 6.5. Schematic Drawing of the Sample Acquisition System Used at the ISRM Test Site

Table 6.1. Well Construction Information for Wells Installed in 1995 at the ISRM Site

Well Number	Well Diameter (cm)	Well Diameter (in.)	Radial Distance From Injection Well (ft)		Drill Depth (ft)	Screened Interval (m)	Screened Interval (ft)	Samples Collected?	Drill Method	Purpose
			(m)	(ft)						
199-H5-2	20	8	-	-	54.0	13.87 - 15.37	45.52 - 50.44	Yes	Sonic	Injection Well
199-H5-3 (O)	5	2	6.1	20.0	45.7	12.52 - 13.27	41.09 - 43.56	No	Sonic/Sonic Push	Upper Piezometer
199-H5-3 (P)	5	2	6.1	20.0	55.0	14.11 - 14.87	46.29 - 48.79	Yes	Sonic	Lower Piezometer
199-H5-4 (O)	5	2	3.8	12.5	46.9	12.70 - 13.46	41.69 - 44.16	No	Sonic/Sonic Push	Upper Piezometer
199-H5-4 (P)	5	2	3.8	12.4	54.0	14.55 - 15.29	47.72 - 50.18	Yes	Sonic	Lower Piezometer
199-H5-5 (O)	5	2	1.5	5.1	45.0	12.69 - 13.45	41.62 - 44.12	No	Sonic/Sonic Push	Upper Piezometer
199-H5-5 (P)	5	2	1.5	5.0	54.0	14.76 - 15.51	48.44 - 50.90	Yes	Sonic	Lower Piezometer
199-H5-6	5	2	2.3	7.6	53.7	13.99 - 14.75	45.91 - 48.38	No	Sonic/Sonic Push	Upper Piezometer
199-H5-7	5	2	4.6	15.2	53.2	14.23 - 14.98	46.69 - 49.16	No	Sonic/Sonic Push	Lower Piezometer
199-H5-8	5	2	6.9	22.7	52.0	14.26 - 15.01	46.80 - 49.26	Yes	Sonic	Lower Piezometer
199-H5-9	5	2	3.0	10.1	52.1	14.39 - 15.14	47.20 - 49.66	No	Sonic/Sonic Push	Lower Piezometer
199-H5-10	5	2	5.3	17.3	52.7	14.24 - 15.00	46.74 - 49.21	No	Sonic Push	Lower Piezometer
199-H5-11	5	2	7.6	24.6	53.0	14.12 - 14.9	46.33 - 48.8	Yes	Sonic	Lower Piezometer
199-H5-12	5	2	18.3	60.0	52.5	12.82 - 15.8	42.05 - 52.0	No	Sonic Push	Downgradient Monitoring
199-H5-13	5	2	27.4	90.6	52.6	12.81 - 15.84	42.03 - 51.97	No	Sonic/Sonic Push	Downgradient Monitoring
199-H5-14	5	2	27.4	89.9	52.0	12.88 - 15.91	42.26 - 52.21	No	Sonic	Downgradient Monitoring
199-H5-15	5	2	-26	-85	54.8	12.56 - 16.48	41.20 - 51.08	Yes	Sonic	Upgradient Monitoring
B2618	NA	NA	0.99	3.25	51.5	None	None	Yes	Sonic	Core hole
B2619	NA	NA	3.0	9.9	50.0	None	None	No	Sonic	Core hole
B2620	NA	NA	2.8	9.2	51.0	None	None	Yes	Sonic	Core hole
B2621	NA	NA	5.6	18.3	51.0	None	None	Yes	Sonic	Core hole
B2622	NA	NA	3.6	11.8	51.0	None	None	Yes	Sonic	Core hole
B2623	NA	NA	5.9	19.3	50.5	None	None	Yes	Sonic	Core hole
B2624	NA	NA	6.9	22.7	51.0	None	None	Yes	Sonic	Core hole
B2625	NA	NA	8.5	27.8	50.5	None	None	Yes	Sonic	Core hole

Notes: NA = not applicable (coreholes were abandoned after sampling was completed)

**Table 6.2.** Results of Hydrogeologic Characterization at the 100-H Area Site

<b>Parameter</b>	<b>Value</b>
Depth to Water Table	12.6 m (40.7 ft)
Aquifer Thickness	2.9 m (9.5 ft)
Aquifer Sediment	Sand and Sandy Gravel
Porosity	29 - 33%
Effective Porosity	≈20% (assumed)
Particle Density	2.7 g/cm <sup>3</sup>
Hydraulic Conductivity	93 m/d (300 ft/d)
Storativity	0.005
Specific Yield	>0.04
Anisotropy Ratio	0.06
Hydraulic Gradient	0.0009
Average Linear Velocity	39 cm/d (1.3 ft/d)
Note: Water-table elevation is based on data from well 199-H5-1A between May 1992 and December 1995.	

Table 6.3. Available Fe(III) Analyses Results

Well ID	Sample Interval (m)	Total Fe (% by weight)	Fe(II) (% by weight)	Fe(III) (% by weight)	Available Fe(III) (% by weight)
199-H5-1A	13.7-14.0 <sup>c</sup>	4.70	2.80	1.90	0.059 (±0.008)
	15.2-15.5 <sup>c</sup>	5.74	3.36	2.38	0.038 (±0.011)
	15.8-16.2 <sup>c</sup>	3.42	0.54	2.88	0.73 <sup>ab</sup>
	16.8-17.4 <sup>c</sup>	3.80	1.25	2.55	0.73 <sup>ab</sup>
199-H5-2	13.1-13.4 <sup>d</sup>	N/A	N/A	N/A	0.104 (±0.016)
	14.2-14.3 <sup>d</sup>	N/A	N/A	N/A	0.098 (±0.025)
199-H5-3P	12.8-13.1 <sup>d</sup>	N/A	N/A	N/A	0.019 <sup>b</sup>
	13.7-13.9 <sup>d</sup>	N/A	N/A	N/A	0.102 <sup>b</sup>
	14.6-14.8 <sup>d</sup>	N/A	N/A	N/A	0.013 <sup>b</sup>
199-H5-4P	12.5-12.8 <sup>d</sup>	N/A	N/A	N/A	0.025 (±0.007)
	14.3-14.6 <sup>d</sup>	N/A	N/A	N/A	0.025 (±0.000)
199-H5-5P	12.6-12.8 <sup>d</sup>	N/A	N/A	N/A	0.102 <sup>b</sup>
	13.6-13.7 <sup>d</sup>	N/A	N/A	N/A	0.043 (±0.003)
	14.6-14.9 <sup>d</sup>	N/A	N/A	N/A	0.030 (±0.000)
199-H5-8	12.8-13.1 <sup>d</sup>	N/A	N/A	N/A	0.091 (±0.009)
199-H5-11	13.6-13.7 <sup>d</sup>	N/A	N/A	N/A	0.043 <sup>b</sup>
	14.8-14.9 <sup>d</sup>	N/A	N/A	N/A	0.089 <sup>b</sup>

(a) Sample from lower confining layer (Ringold Formation).  
 (b) One replicate only.  
 (c) Colorimetric analysis method.  
 (d) Kinetic analysis method.

**Table 6.4. Microbiological Characterization Summary (after 28 days incubation)**

Well	Sample Interval		Lithology	CFU/g <sup>(a)</sup> sediment	# of Colony Types
	(m)	(ft)			
199-H5-2	13.4	44.0	Silty sandy gravel	$7.4 \times 10^3$	4
199-H5-2	14.3	47.0	Sandy gravel	$6.1 \times 10^3$	4
199-H5-2	14.5	47.5	Sandy gravel	$1 \times 10^2$	1
199-H5-2	15.5	51.0	Slightly clayey sandy silt	0	0
199-H5-2	15.8	52.0	Slightly clayey sandy silt	$1 \times 10^1$	1
199-H5-2	16.1	53.0	Slightly clayey sandy silt	0	0
199-H5-3	14.0-14.2	46.0 - 46.5	Sandy gravel	$1.5 \times 10^5$	4
199-H5-4	12.8-13.1	42.0 - 43.0	Sand	$1.3 \times 10^4$	6
199-H5-4	14.0-14.3	46.0 - 47.0	Sandy gravel	$2.2 \times 10^4$	2
199-H5-5	13.4-13.7	44.0 - 45.0	Sandy gravel	$1.6 \times 10^4$	3
199-H5-5	14.3-14.6	47.0 - 48.0	Sandy gravel	Suspect contamination	Suspect contamination
199-H5-8	13.1-13.4	43.0 - 44.0	Gravelly sand	$5.0 \times 10^1$	1
199-H5-8	14.9-15.2	49.0 - 50.0	Sandy gravel	0	0
199-H5-8	16.0-16.1	52.5 - 53.0	Silt/clay	0	0
199-H5-11	14.5-14.8	47.5 - 48.5	Sandy gravel	$9.0 \times 10^1$	1

a) CFU = colony forming unit.

Table 6.5. Baseline Trace Metals Analysis Results for the ISRM Test Site

Constituent		Sample Location														
		H5-3(P)	H5-3(O)	H5-4(P)	H5-4(O)	H5-5(P)	H5-5(O)	H5-6	H5-7	H5-8	H5-9	H5-9 Dup	H5-10	H5-11	H5-12	H5-13
Na	none	22.1	21.7	20.8	21.8	19.7	22.5	20.3	20.8	22.8	18.7	18.0	20.6	17.4	16.8	24.8
Mg	none	12.1	11.5	11.7	11.8	12.0	11.7	12.1	13.9	13.4	12.4	11.9	13.4	13.1	14.8	15.7
Si	none	13.0	13.8	11.3	14.7	13.3	14.8	14.2	15.1	13.1	15.5	12.6	13.8	13.1	10.1	11.9
K	none	4.93	4.52	4.58	4.89	7.16	5.09	4.70	5.28	4.86	5.11	4.56	5.56	4.74	5.43	5.84
Al	50 to 200*	16.6	46.8	27.3	20.2	20.5	20.1	17.6	19.6	18.9	35.3	35.7	22.1	51.1	16.3	27.4
Mn	50*	24.1	3.4±0.5	12.5	<1	<1	1.6±0.2	1.1	5.92	3.45	1±0.1	1.2±0.2	47.6	10	140	146
Fe	300*	<10	22±12	<10	<10	<10	<10	<10	<10	<10	<10	<10	<10	33±13	21±10	10±7
Ni	100	2.1±0.5	2.86	4.6±1.5	3.16	2.6±0.3	2.64	2.5±0.3	3.49	3.45	3.1±0.4	3.0±0.6	3.28	10.9	3.29	4.46
Cu	1000*	4.51	3.8±0.5	3.98	3.58	4.6±0.5	4.20	3.61	3.6±0.4	3.09	3.53	3.87	4.75	4.7	3.27	4.26
Zn	5000*	19.6	13.0	19.6	11.2	24.2	12.2	18.1	18.4	20±2	12.6	12.1	24.5	73.1	18.4	16.6
As	50	<1	<1	<1	<1	<1	<1	<1	<1	<1	<1	<1	<1	<1	<1	<1
Se	50	3.4±4.4	<1	<1	<1	<1	<1	<1	<1	<1	<1	<1	<1	<1	<1	<1
Ag	100*	<1	<1	<1	<1	<1	<1	<1	<1	<1	<1	<1	<1	<1	<1	<1
Cd	5	<1	<1	<1	<1	<1	<1	<1	<1	<1	<1	<1	<1	<1	<1	<1
Sn	none	1.1±0.2	<1	<1	<1	1.1±0.2	1.1±0.2	1.49	1.1±0.2	<1	<1	<1	<1	<1	<1	<1
Sb	6	<1	<1	<1	<1	<1	<1	<1	<1	<1	<1	<1	<1	<1	<1	<1
Ba	2000	34.6	42.9	40.5	37.8	57	36.6	36.6	51.1	76.1	35.4	36.3	41.7	38.1	61.5	76.5
Pb	50**	<1	<1	<1	<1	<1	<1	<1	<1	<1	<1	<1	<1	4.9±0.5	<1	<1
Cr	100	50.8	71.0	47.1	68.9	64.8	67.4	60.1	67.4	61.5	59.8	60.7	45.8	59.5	12.9	34.0

MCLs are from EPA 822-R-96-001, February 1996 unless otherwise indicated.

\* EPA Secondary Standard (in: EPA 822-R-96-001, February 1996)

\*\* CFR Part 265 Appendix III

Dup = duplicate sample

**Table 6.6. Baseline Field Parameter Measurement Results for the ISRM Test Site**

Well ID	Conductivity ( $\mu\text{S}$ )	Dissolved O <sub>2</sub> (ppm)	pH	Temperature ( $^{\circ}\text{C}$ )
H5-3o	447	5.7	7.44	20.5
H5-3p	460	4.4	7.53	20.8
H5-4o	437	6.1	7.46	20.4
H5-4p	345	2.4	7.53	22
H5-5o	439	6.0	7.45	20.9
H5-5p	463	4.3	7.57	20.8
H5-6	459	5.4	7.46	19.4
H5-7	455	5.1	7.51	19.8
H5-8	445	3.9	7.47	20.1
H5-9	445	6.9	7.55	20.5
H5-10	455	5.6	7.56	20.5
H5-11	460	6.6	7.52	20.3
H5-12	466	1.9	7.86	21.5
H5-13	553	3.5	7.72	26.3

**Table 6.7. Results from Dissolved Oxygen Analysis of Samples Collected Within and Upgradient from the 100-H Area**

Well ID	Screen Interval (ft bls*)	Screen Interval (ft bwt†)	DO Concentration (ppm)
199-H3-2A	36.0 - 51.0	0.0 - 14.6	10.6
199-H3-2B	50.0 - 55.0	13.3 - 18.3	8.3
199-H4-4	33.0 - 50.0	2.1 - 12.1	9.1
199-H4-6	39.0 - 49.0	0.6 - 10.6	8.9
199-H4-8	38.0 - 48.0	0.7 - 10.7	11.0
199-H4-16	42.5 - 57.5	0.0 - 14.9	8.2
199-H5-15	41.2 - 51.1	4.7 - 14.6	6.5
699-91-46A	23.0 - 43.8	0.0 - 13.5	7.3
699-91-46B	39.0 - 44.5	9.4 - 14.9	8.0
699-93-48A	41.2 - 62.3	0.0 - 11.7	9.4
699-93-48B	53.7 - 56.7	3.3 - 6.3	8.6
699-93-48B	66.7 - 70.7	16.3 - 20.3	9.0
699-96-43	32.4 - 48.5	0.0 - 9.7	9.9

\* bls = below land surface.  
† bwt = below water table (at time of sampling).



## 7.0 Pre-Injection Numerical Simulations

Pre-injection numerical simulation models aided design of the intermediate-scale and field experiments (see Figures 3.3, 5.1, and 5.2). These models, with updated parameters, are also being used to interpret the field- and intermediate-scale experiments (see Section 11). The models account for advection, dispersion, degradation, and chemical transformation processes. Design factors examined through pre-injection modeling included well and core hole placement, reagent concentration, injection and withdrawal rates, duration for each stage of the experiment (injection, reaction, and withdrawal), the effects of heterogeneity, and reagent reaction and dissociation rates. The models were used to examine and evaluate proposed field operations for delivering an effective concentration range of sodium dithionite in the desired aquifer volume for a period of time appropriate for the targeted ferric iron to be reduced.

The main limitation of these models is that the effect of heterogeneities on the extent and recovery of the injected plumes could not be factored into the simulations because of the limited characterization data. These effects can be important depending on the scale and type of heterogeneity involved, as shown in sensitivity studies using generic hydrologic data to model the injection/withdrawal experiment (Yabusaki and Cole 1993; Williams et al. 1994). These generic heterogeneity studies also illustrate other impacts of heterogeneities on the experiment and have identified important site characterization parameters (e.g., hydraulic conductivity anisotropy). The majority of the pre-injection numerical design simulations have been published in Williams et al. (1994) and include complete discussions of

- the experimental phases
- advantages/disadvantages of full versus partial penetrating wells
- the injection/withdrawal rates and aquifer drift interact to affect tracer recovery
- the effects of aquifer anisotropy
- heterogeneity.

Information from the bench-scale studies was used to develop a reactive chemistry model for the various dithionite groundwater/sediment interactions for a radial injection/withdrawal geometry. The initial model was subsequently modified to include the effects of hydrodynamic dispersion. This reactive transport model accounts for dithionite degradation, dithionite and ferric iron reduction reactions, pH buffer, sulfite, thiosulfate, and sulfate based on kinetic reaction data derived from the bench-scale experiments to design the intermediate-scale experiment. The rates were subsequently modified, based on modeling of the intermediate-scale experiments, to design the full-scale field injection experiment. This simple chemical model also tracks the amount of iron reduced in the sediment spatially and calculates the number of pore volumes of treatment capacity. The application of this model to the intermediate-scale experiment is discussed in Section 11.

Hydrologic models that account for density effects were developed for the intermediate-scale wedge experiment and for the 100-H Area site using preliminary site characterization data because the injection fluid (sodium dithionite with potassium carbonate and bicarbonate buffers) is nearly twice the density of seawater. These models provided estimates of both the radial extent the tracer and reagent plumes would attain during the injection and the required duration of the withdrawal

phase to recover the unreacted reagent (dithionite), buffers, and bromide tracer. These generic studies indicated that for the range of hydraulic conductivities found in the intermediate-scale wedge and at the field site that density effects should be minimal. Results from the full-scale injection/withdrawal experiment exhibit some density-dependent behavior (discussed in Section 10), which will be modeled.

The following two sections discuss the tracer experiment and anoxic plume modeling.

## 7.1 Tracer Experiment Modeling

A two-dimensional, radially symmetric hydrologic model of the field site was constructed using the preliminary 100-H Area site characterization information (i.e., 2.76-m-[9.1-ft-] thick sand and sandy gravel aquifer whose water table is 12.5 m (41.1 ft) below land surface, porosity 21%-25%, a hydraulic conductivity of 75.8 m (250 ft)/d, gradient of 0.0009). Table 6.2 contains the current estimates for the hydrologic parameters for the ISRM field site.

The system was modeled as homogeneous and anisotropic even though it was expected to be anisotropic (ratio 0.07). In the model the aquifer was partially screened with the injection well at the bottom 1.5 m (5 ft) of the 2.76-m-(9.1-ft-) thick aquifer. Steady-state heads were calculated during the injection and the withdrawal phases and the aquifer thickness was adjusted to account for the injection mound and pumping cone of depression. The results of the injection of conservative tracer after 1 and 24 h of injection at 7.58 L/min (20 gal/min [GPM]) are shown in Figures 7.1a and 7.1b. The tracer extends about 9.91 m (32 ft) from the injection well after 24 h of injection. Model results for the withdrawal phase indicate that almost all of the injected tracer will be recovered after 4 to 5 days of pumping at 75.8 L/min (20 gal/min). The actual recovery at the field site is dependent on sediment heterogeneities because tracer can be trapped in zones of low hydraulic conductivity and on the time it takes to drain any tracer that is trapped in the vadose zone due to the drop in the water table from the cone of depression caused by pumping during the withdrawal phase (see the heterogeneity discussions in Williams et al. 1994).

## 7.2 Anoxic Water Plume Modeling

The groundwater in the uppermost unconfined aquifer at the Hanford Site is nearly saturated with dissolved oxygen with most concentrations ranging from 7.4 to 9.5 ppm (Schreck 1992). Dissolved oxygen in the groundwater flowing through the reduced portion of the aquifer at the test site will be reduced, thus creating a plume of anoxic water flowing downgradient from the site. Column studies have shown that from 45 to 100 pore volumes of oxygenated water need to pass through the reduced zone to re-oxidize the sediment (depending on the amount of reducible iron in the sediment).

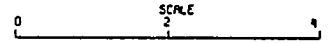
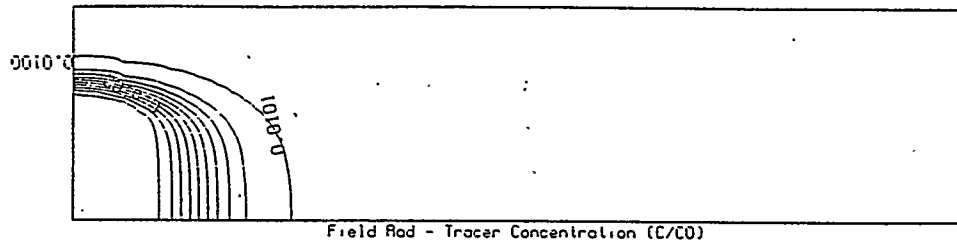
Numerical simulations were conducted to study how this anoxic plume will spread out as it moves away from the test site. The most important hydraulic parameter influencing the lateral spread of this plume is the transverse dispersivity. This quantity is not well known on the Hanford Site and is dependent on heterogeneities within the sediment and the distance the plume travels.

For a conservative estimate of the dispersion of the anoxic plume, values of longitudinal dispersivity of 3.03 m (10 ft) and transverse dispersivity of 1.0 m (3.3 ft) were used in simple transport simulations. This simulation (see Figure 7.2) shows the resulting anoxic plume from the 18.2-m-(60-ft-) diameter test site for a distance of 606.6 m (2000 ft). Concentrations are reported as the percent of dissolved oxygen depleted (e.g., 100 = no dissolved oxygen, 0 = saturated with dissolved oxygen). These results show that at a distance of 606.6 m (2000 ft) from the test site, close

to the distance to the Columbia River, 10% to 20% of the dissolved oxygen in the water will be depleted for a width of about 212.3 m (700 ft). This would yield a maximum reduction of 1.5 ppm dissolved oxygen at a distance from the test site similar to the distance to the Columbia River.

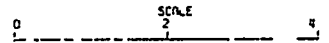
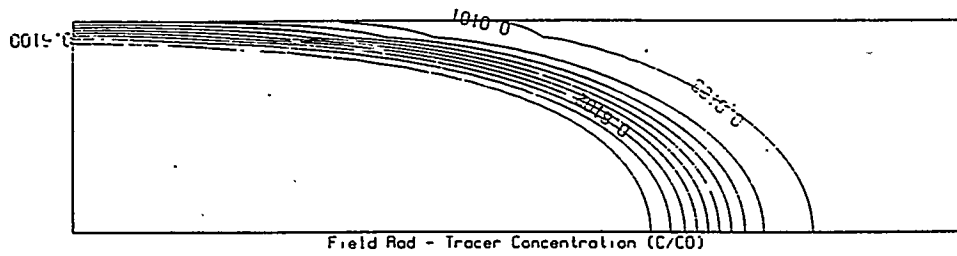
A rule of thumb often used in contaminant transport studies for screening purposes is that the longitudinal dispersivity is equal to 10% of the mean travel distance of the plume and the transverse dispersivity is equal to 33% of the longitudinal dispersivity (EPA 1985). Using this relationship, the longitudinal dispersivity would be 60.6 m (200 ft) for a 606.6-m (2000-ft) mean travel distance for the anoxic plume. The transverse dispersivity would be 20 m (33% of 60.6 m) in this case. This rule-of-thumb value for dispersivities was considered to be too high for the sediments at the Hanford Site. Actual values may be estimated as part of the long-term monitoring strategy of the ISRM experiment. Local dispersivity values will be estimated from the ongoing analysis of the field experiments. Higher values for dispersivity than were used in this simulation would result in more dispersion of the anoxic plume and result in higher dissolved oxygen concentrations along the centerline of the plume. These results also do not consider re-oxygenation of the water from soil gases or from vertical mixing of the groundwater. Initial modeling of this type has been undertaken and will be discussed in Section 11.

(a)



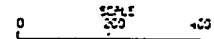
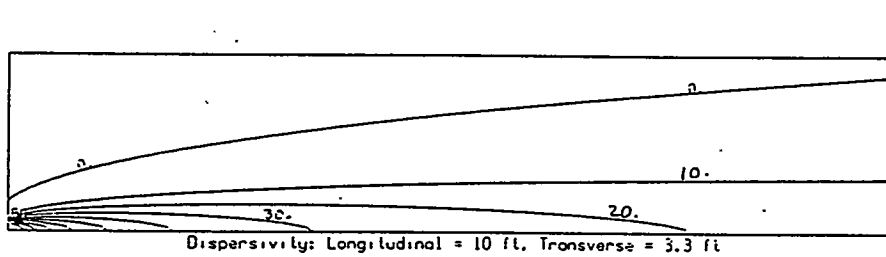
TOP SURFACE  
TIME 3600.00  
CONTOUR  
INTERVAL 0.10  
LOWEST 0.01  
HIGHEST 1.00

(b)



TOP SURFACE  
TIME 86400.00  
CONTOUR  
INTERVAL 0.10  
LOWEST 0.01  
HIGHEST 1.00

**Figure 7.1.** Preliminary Tracer Experiment Modeling Results. Radial cross-section showing tracer concentration contours from the injection/withdrawal well after (a) 1-h and (b) 24-h injection. Distances are in meters.



MATERIAL NUMBER :  
TOP SURFACE  
TIME 1.00  
CONTOUR  
INTERVAL 10.00  
LOWEST 0.10  
HIGHEST 100.00

**Figure 7.2.** Simulation of Dispersion of Anoxic Plume Downgradient from the Test Site. Only one half of the plume is shown. Concentrations are reported in percent depleted oxygen.

## 8.0 Tracer Test

### 8.1 Purpose

The single-well injection/withdrawal tracer test was performed to determine the volume of injection fluid required to create a 9.1-m (30-ft) radial plume, to estimate the withdrawal volume required to recover the injected conservative tracer and thus the injected reagent and reaction products from the full-scale dithionite injection experiment, and to determine aquifer transport properties at the ISRM test site (e.g., longitudinal dispersivity, effective porosity) for incorporation (along with other physical, chemical, and hydraulic properties) into numerical models developed to simulate site-specific transport processes for ISRM remedial design.

The tracer experiment provided information to fine-tune the sampling strategy, such as starting sampling time, sample volume, and sample frequency, required at each location. It also provided the means to troubleshoot systems (e.g., injection/withdrawal system equipment, sampling pumps, flow-through cells, bromide probes, mixing tank). Additionally, the experiment provided information on tracer recovery efficiency; for example, the recovery information was analyzed to determine the number of injection volumes required for nearly complete recovery (e.g., 96%) of the tracer.

### 8.2 Description

The conservative tracer injection/withdrawal experiment was completed the last week of June 1995. It consisted of a 17.5-h injection phase during which 79,600 L (21,000 gal) of potassium bromide solution (170 ppm) were injected into the aquifer at a rate of 75.8 L/min (20 gal) per minute (gpm) through the injection/withdrawal (199-H5-2) well (see Figure 5.1). The bromide tracer solution was prepared in three 26,500-L (7000-gal) tanks that were pre-filled with groundwater pumped from the site. Baseline samples from all the wells (Figure 5.1) were collected before injection started.

The second, or residence, phase lasted 27.5 h and was performed to simulate the reaction residence stage needed for the full-scale dithionite experiment. The third, or withdrawal, phase was 70 h and involved pumping four injection volumes (31,800 L [84,000 gal]) to recover as much of the injected tracer as possible. The withdrawn water, which met the Hanford purgewater criteria, was purged to the ground downgradient from the field site according to the procedure set forth in the test plan.

During the experiment, bromide concentration and temperature measurements were made on monitoring well and injection and withdrawal stream samples. Flowthrough cells, equipped with a bromide ion-selective electrode (ISE) and temperature probe, were used to measure these quantities in the monitoring wells, and samples were collected from the injection and withdrawal streams for bench analyses. The following probes were used to monitor bromide concentration and temperature during the experiment:

- Bromide - Cole Palmer ISE Br. Range = 0.4 to 79,900 ppm, reproducibility =  $\pm 2\%$  of full scale.
- Temperature - Oakton WD-35615 series temperature meter. Range = 0.0 to 100.0°C, accuracy =  $\pm 0.5^\circ\text{C}$ .

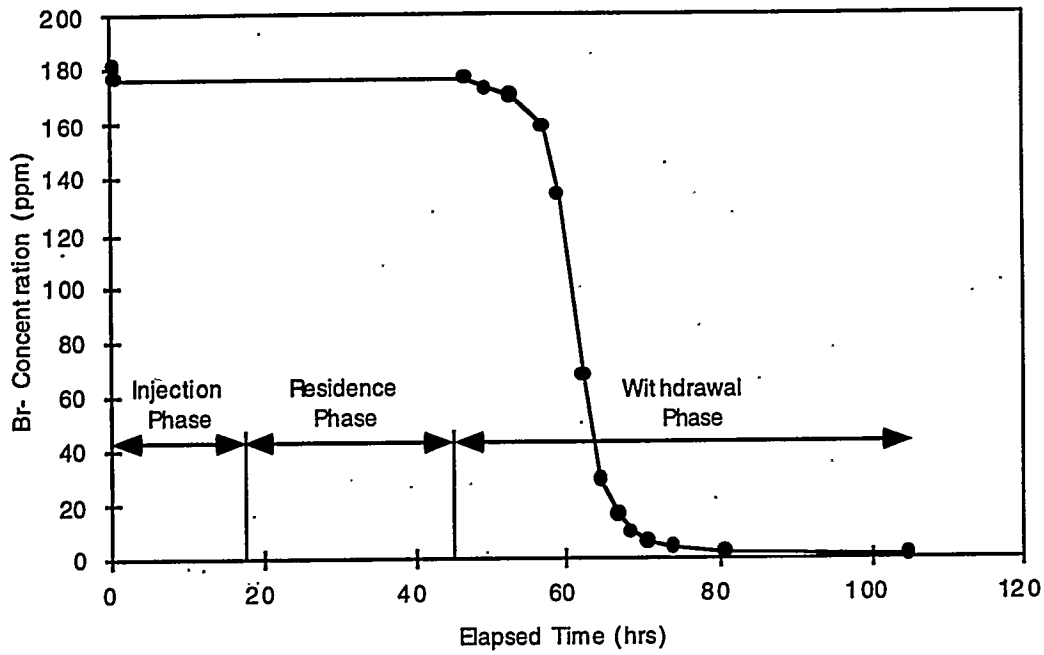
In addition to the bromide ISE data, approximately 100 samples were submitted for laboratory analysis of bromide concentration using ion chromatography (IC). Results of the laboratory analysis

were used to verify the calibration slope of the ion-selective electrodes and provide more reliable, if less frequent, bromide concentration data in cases where ISE data were suspect.

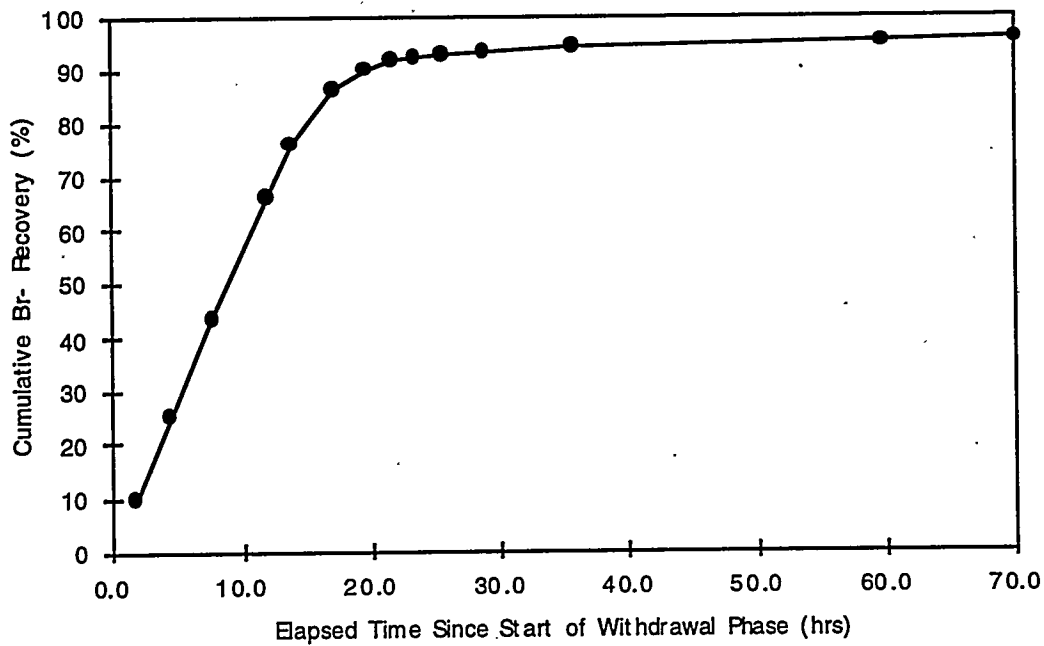
### 8.3 Results

Observed bromide tracer concentrations within the injection/withdrawal well (199-H5-2) during the three phases (i.e., injection-residence-withdrawal) of the tracer experiment are shown in Figure 8.1a. Analyses of the withdrawal stream bromide concentration and flow rate indicated that the withdrawal phase, which involved withdrawing four injection volumes, achieved a 96% recovery of the injected tracer mass (Figure 8.1b). It should be noted that only data obtained from laboratory analysis (i.e., IC) were used to characterize bromide concentration in the injection/withdrawal stream; the bromide ISE used to monitor this stream was poorly correlated with the IC data and, subsequently, provided suspect data.

Observed bromide tracer concentrations along three radial transects during the injection/withdrawal tracer test are shown in Figures 8.2, 8.3, and 8.4. Arrival distribution curves at the various monitoring wells were analyzed before the main dithionite injection/withdrawal experiment to improve the sampling strategy (i.e., number and sampling frequency of sampling needed at each observation well and in the injection and withdrawal streams) by providing information on the expected reagent arrival time at each monitoring location during the full-scale experiment. The bromide tracer data, once completely analyzed, will provide information on the porosity, dispersivity, anisotropy, and heterogeneity of the aquifer at the field site.

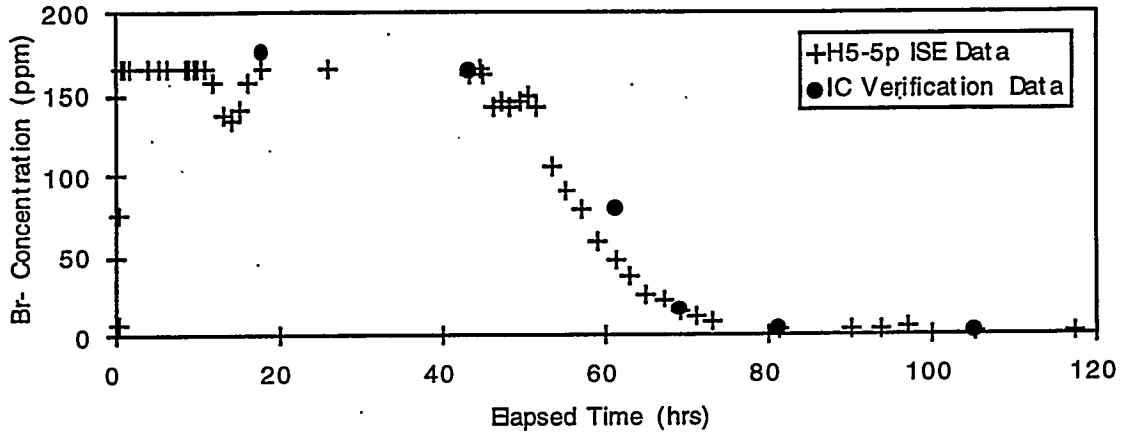


(a)

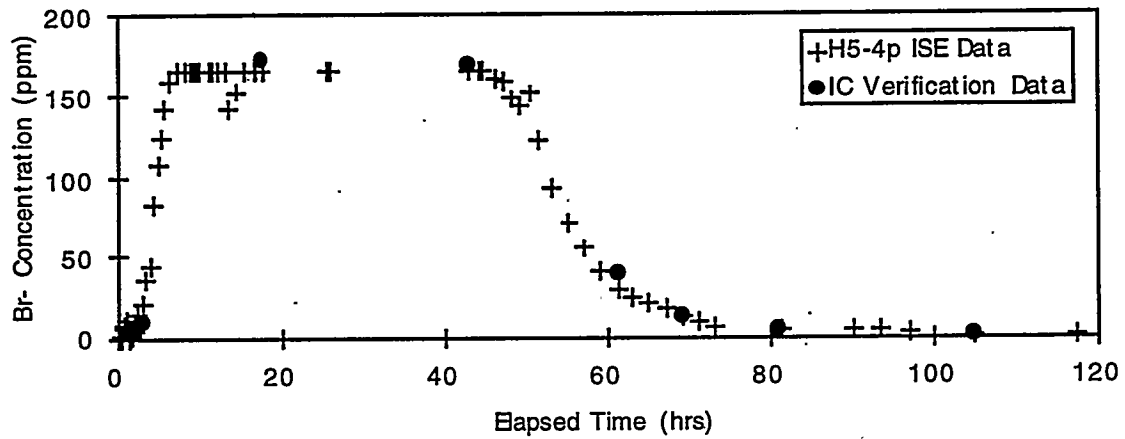


(b)

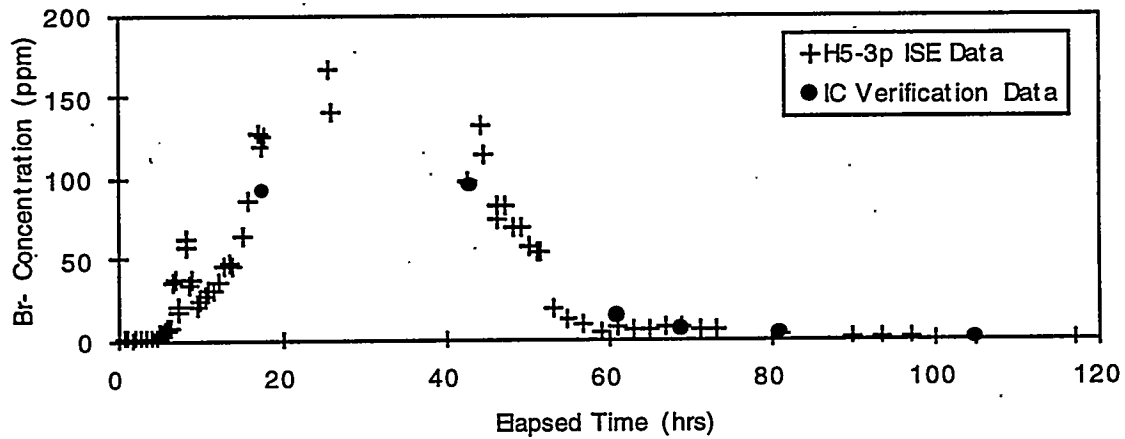
**Figure 8.1.** Injection/Withdrawal Well (H5-2) Data Including (a) Observed Bromide Tracer Concentrations During the Injection/Withdrawal Tracer Test and (b) Percent Recovery of the Br- Tracer During the Withdrawal Phase, Indicating That 96% of the Injected Br- was Removed from the Aquifer.



(a)

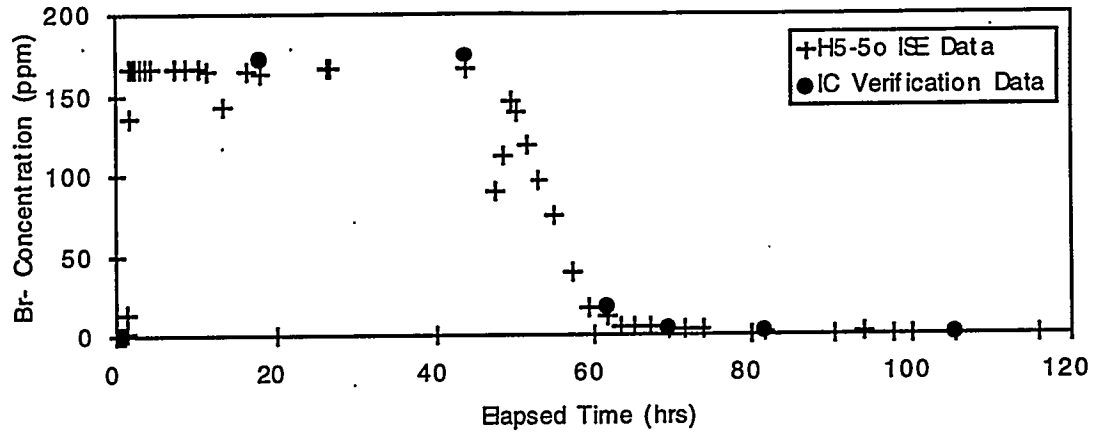


(b)

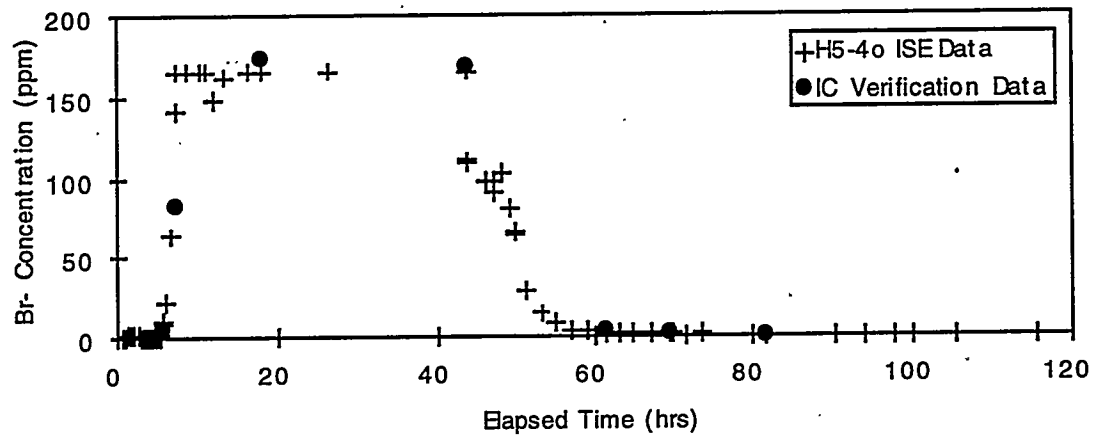


(c)

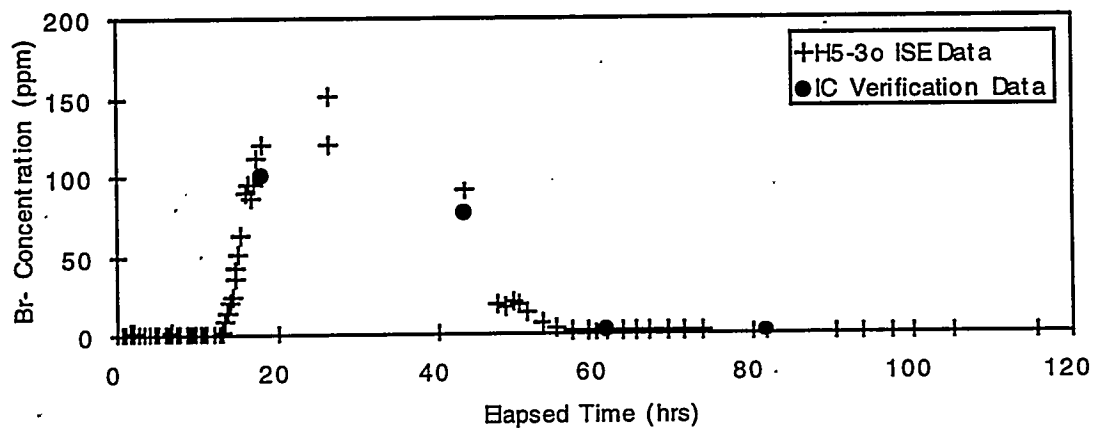
**Figure 8.2.** Observed Bromide Tracer Concentrations Along a Lower Zone Radial Transect During the Injection/Withdrawal Tracer Test. (a) H5-5p (5 ft), (b) H5-4p (12 ft), and (c) H5-3p (20 ft).



(a)

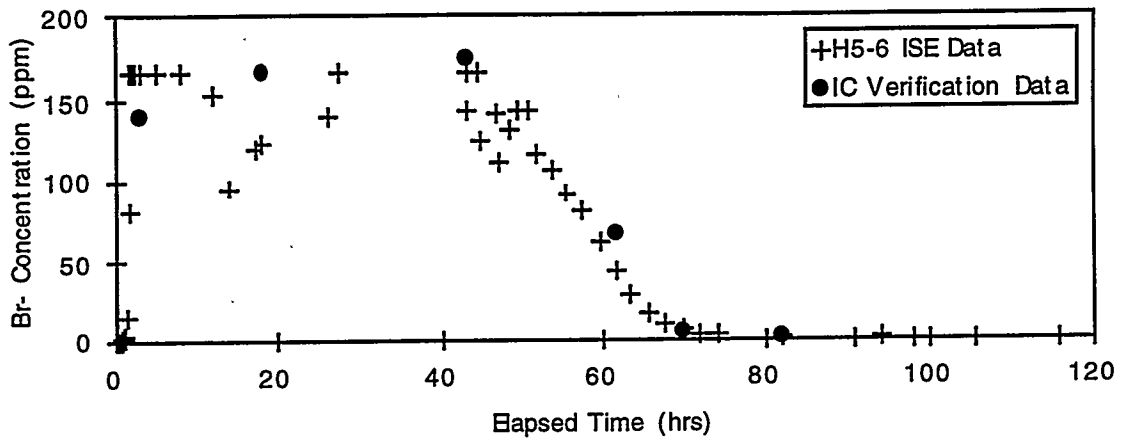


(b)

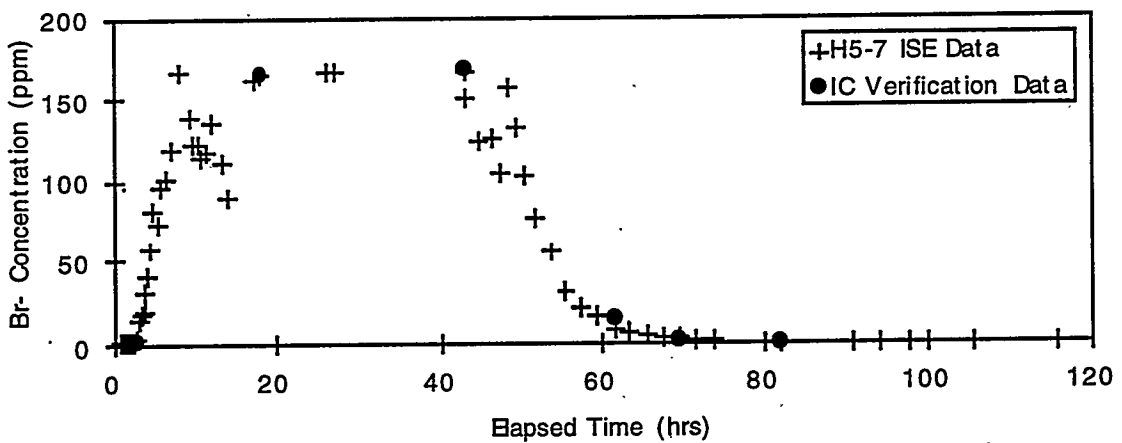


(c)

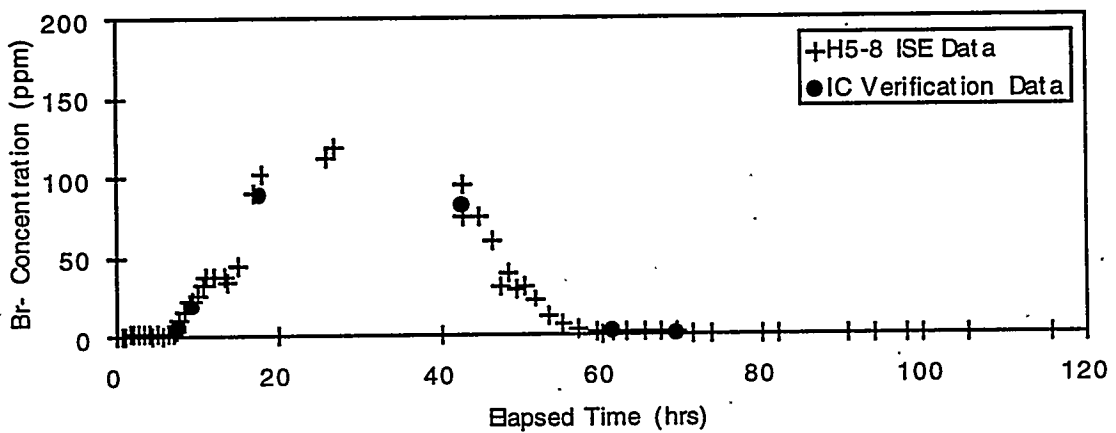
**Figure 8.3.** Observed Bromide Tracer Concentrations Along an Upper Zone Radial Transect During the Injection/Withdrawal Tracer Test. (a) H5-5o (5 ft), (b) H5-4o (12 ft), and (c) H5-3o (20 ft).



(a)



(b)



(c)

**Figure 8.4.** Observed Bromide Tracer Concentrations Along a Lower Zone Radial Transect During the Injection/Withdrawal Tracer Test. (a) H5-6 (8 ft), (b) H5-7 (15 ft), and (c) H5-8 (23 ft).

## 9.0 "Mini" Injection

This section describes the mini-dithionite injection/withdrawal field experiment, a small-scale injection/withdrawal test designed to reach the first two monitoring wells (H5-5p and H5-5o) located ~1.5 m (~5 ft) from the injection well (Figure 5.1).

### 9.1 Purpose

The primary objective of the mini-dithionite injection/withdrawal field experiment was to determine the behavior of dithionite in the aquifer at the field site before conducting the main (i.e., full-scale) dithionite injection/withdrawal experiment, but designed to reach the outer monitoring wells ~9 m (~30 ft) from the injection well. Specific objectives for this mini injection experiment included:

- Testing of dithionite handling procedures at field site and to examine its stability at field temperatures and under field conditions. This testing provided a means to check out procedures and setup for mixing the groundwater, reagent, and buffers in the field mixing tanks and to examine the effectiveness of the argon blanketing setup, which was designed to minimize dithionite degradation as a result of contact with atmospheric oxygen.
- Testing of the more complex dithionite sampling and analysis methodology at the field site under field conditions.
- Confirmation that trace metal mobilization from the actual subsurface sediments at the field site are generally the same as observed in the laboratory batch and intermediate scale (wedge) experiments so that sampling and purgewater strategies could be modified before the full-scale injection.
- Confirmation of withdrawal volume requirements determined from the bromide tracer experiment. This was particularly important because the dithionite and potassium carbonate buffer are denser than the fluid injected during the bromide tracer experiment. The mini injection/withdrawal test was used to confirm our modeling results that density-related effects would not cause the withdrawal volumes to be significantly greater than those estimated from the bromide tracer experiment.

### 9.2 Description

The mini-dithionite injection/withdrawal experiment was performed at the 100-H Area field site the second week in August 1995. The experiment consisted of the following four major activities:

- 1-h injection stage - During this stage a 4548-L (1200-gal) mixture of groundwater with a conservative tracer (bromide) and a reactive reagent along with the pH buffers (i.e., sodium dithionite with a potassium carbonate/bicarbonate buffer) were injected into the aquifer at a 76 L/min (20-gpm) rate through a single injection well (H5-2, Figure 5.1), which is screened only over the lower 1.5 m (5 ft) of the ~3-m (~10-ft)-thick aquifer. The experiment was designed to affect a cylinder of aquifer materials ~10 ft in diameter so that concentrations of the bromide tracer, the reagent, and buffers contained in the injection fluid could be observed at the two closest wells (i.e., H5-5p and H5-5o, Figure 5.1). Because of the small quantity of dithionite and

buffer solution required for this experiment it was not purchased as a concentrated premixed solution from the supplier. Instead it was prepared onsite by mixing dry chemicals with withdrawn groundwater to create the 4548 L (1200 gal) of injection fluid. This 4548 L of injection fluid contained 193 lb of 90% pure sodium dithionite (0.1 M), 550 lb of potassium carbonate (0.4 M), and 40 lb of potassium bicarbonate (0.04 M).

- 18-h reaction or drift stage - This stage provided the time required for the reactive reagent plume that was injected to react with aquifer fluids and solids. During this period the plume of injected fluids at first continued to move radially, although much more slowly, as the injection mound decayed. It also began to drift under natural gradients.
- ~5.5-h withdrawal or recovery stage - This stage involved withdrawal of the injected groundwater plume containing bromide tracer, aqueous reaction products, buffers, and any species that may have been mobilized by the reagent and buffers. The withdrawal rate was 76 L/min (20 gpm) through the same well used for injection (H5-2). The 25,240 L (6660 gal) of withdrawn waters were stored in an on-site tank for chemical analysis.
- analysis and disposal of the purgewater - This activity involved determining the quantity (relative to the injection volume) and quality of the withdrawn waters so appropriate plans for the disposal of purgewater from the full-scale injection/withdrawal experiment could be made. Following these water quantity/quality determinations the purgewater were disposed by trucking them to the Hanford purgewater disposal facility.

Bromide tracer and dithionite movement during the injection, drift, and recovery stages of the mini test was monitored using the four monitoring/sample collection stations at the field site described in Section 6.7. Geochemical properties of the injected fluid and withdrawn fluid as well as at various monitoring well locations were measured at different points in time and samples were archived for later analysis in the mobile field and permanent laboratory facility. Groundwater geochemical property measurement and sampling consisted of system purging, measurement of pH, dissolved oxygen, and electrical conductivity by in-line electrodes; the collection and preparation of samples for measurement of dithionite and dithionite degradation product concentrations using equipment in the mobile laboratory; and the collection and preparation of samples for measurement of trace metals at the permanent laboratory. The sampling procedure used for the mini injection was the same as used for the full injection and it is described more fully in Section 10.0 and Appendix A.

### 9.3 Results

Figure 9.1 shows a plot of the recovery curves from the field scale mini-dithionite injection/withdrawal experiment. Sampling of H5-5p, the closest well to the injection/withdrawal well (H5-2), was performed every ten minutes during the injection. These results indicated that the objective of having the injection plume reach well H5-5p was achieved. The conductivity and pH at this observation well began rising 20 minutes after the start of the injection and rose to injection fluid levels at the conclusion of the injection. Measurements indicated a jump from background conductivity (pH) levels of  $\sim 450 \mu\text{s}/\text{cm}^2$  ( $\sim 7.5$ ) to conductivity (pH) levels of  $8.02 \text{ ms}/\text{cm}^2$  (10.04) after 20 minutes. Measurements after 30 minutes had climbed to  $34 \text{ ms}/\text{cm}^2$  (10.29) and they continued to rise up to the end of the 1-h injection period where they reached injection fluid levels of  $74 \text{ ms}/\text{cm}^2$  (10.58). Figure 9.1 shows a plot of the recovery curves from the field scale mini-dithionite injection/withdrawal experiment and Figure 9.2 illustrates the time variation of trace metals concentrations in the withdrawn waters. Appendix F contains individual plots of metals concentrations with time.

## 9.4 Interpretation

Preliminary analyses of the field scale mini-dithionite injection/withdrawal experiment confirmed the Oregon State University (OSU) intermediate-scale wedge experiment results of an ~8-h reaction half-life for the dithionite/ferric iron reduction reaction. Results also indicate that while some trace metals are mobilized that they are removed by the withdrawal phase and that the trace metal compositions of the purgewater from the full-scale experiment would be below the purgewater criteria. It provided confirmatory information on the chemical composition of withdrawal fluids, dithionite reaction rates, and the number of pore volumes that must be recovered to achieve ~90% recovery. The information on metals, sulfate concentrations, and required withdrawal volumes allowed appropriate plans to be made for the disposal of the large volume of withdrawal fluids from the full-scale experiment. This test also provided information to make adjustments in the residence phase duration and sampling strategies.

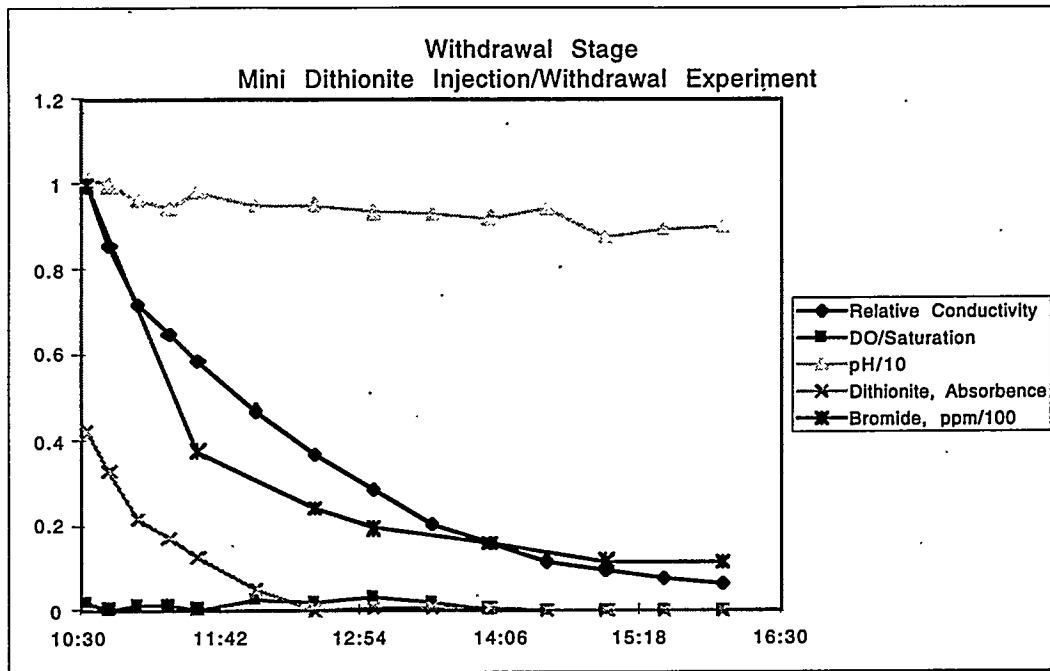


**Figure 9.1.** Variation in the Selected Chemical Properties of the Withdrawal Waters (H5-2) During the Withdrawal Stage of the Mini Injection Experiment. Illustrated values are normalized as indicated in the chart legend.

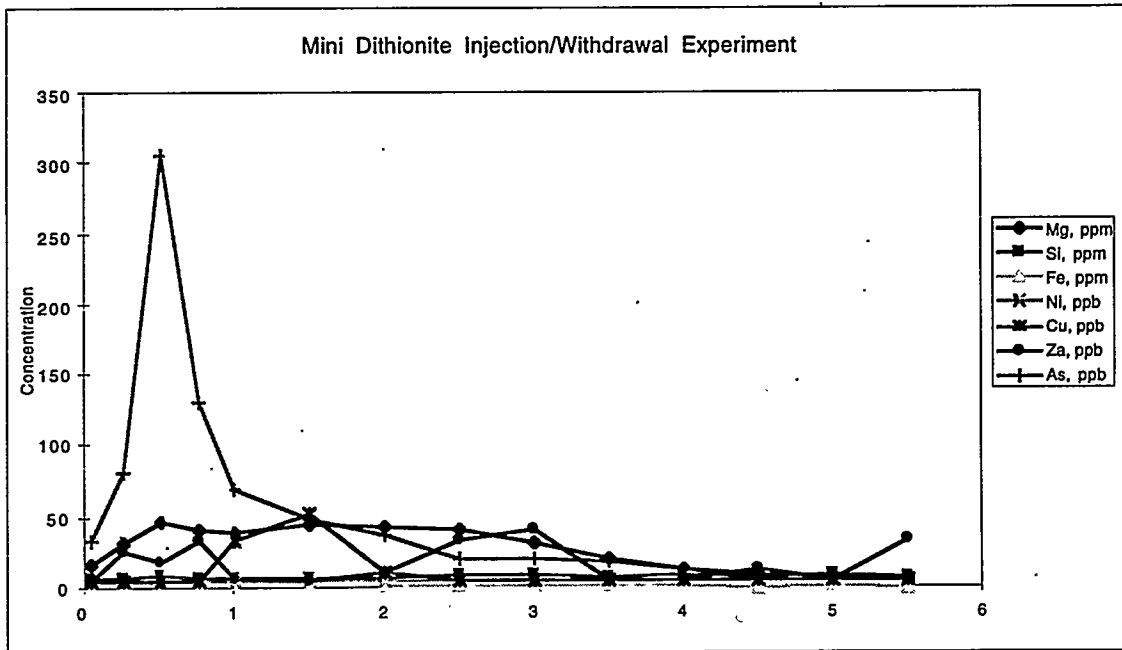


**Figure 9.2.** Variation in the Trace Metals Content of Withdrawal Waters (H5-2) During the Withdrawal Stage of the Mini Injection Experiment. Some values are in ppm while others are in ppb.

## 10.0 Main Dithionite Injection/Withdrawal Field Experiment

### 10.1 Purpose

The purpose of the full-scale dithionite injection/withdrawal experiment was to determine the feasibility of manipulating the redox potential (i.e., create reducing conditions) of a portion 15.2 to 18.3 m (50 to 60 ft) diameter of the unconfined aquifer within Hanford formation sediments at the 100-H Area ISRM field test site. The experiment was designed to 1) determine whether information obtained during the various experimental stages of the ISRM concept (i.e., bench-scale laboratory experiments, intermediate-scale laboratory experiments, mini-dithionite injection/withdrawal experiment) could be scaled to actual field-scale in situ conditions, 2) provide the site-scale hydrogeologic and geochemical data needed to determine the feasibility of creating a reduced zone and estimate the total reductive capacity of the reduced zone, and 3) provide information and gain experience with the emplacement and performance assessment monitoring of a field-scale implementation of the ISRM technology.

### 10.2 Description

The main dithionite injection/withdrawal experiment was similar to the mini-dithionite injection/withdrawal experiment described in the previous section except that the volume of reagent injected, and subsequently the volume of aquifer materials affected, was larger; the experiment was designed to produce a 15.2-m (50-ft)-diameter reduced zone. The full-scale dithionite injection/withdrawal experiment also differed from the mini-dithionite injection/withdrawal experiment in that the reagent and buffer were not mixed from powder but were delivered to the site in a concentrated liquid form which simplified preparation of the injection solution.

The 17.1-h injection phase of the experiment was followed by an 18.5-h reaction (or residence) phase to provide time for the reagent to react with the iron within the sediments. This phase was followed by an 83-h withdrawal phase in which approximately 4.8 injection volumes were withdrawn from the aquifer through the injection/withdrawal well (199-H5-2) to remove any unreacted reagent and buffer, reaction products, mobilized metals, and bromide tracer.

During the injection phase the reagent was injected from three 26,900-L (7,100-gal) mixer tanks. These tanks were pre-filled to an appropriate level with site groundwater (pumped from well 199-H5-2) followed by addition of the appropriate amount of concentrated liquid reagent, containing sodium dithionite and buffers, to achieve the desired injection concentration and volume in each of the tanks. Sodium dithionite and buffer concentrations were different in each of the three tanks to compensate for the longer residence time and reaction path length of the first 26,900 L (7,100 gal) of solution to be injected. This also compensated for some of the effects of hydrodynamic dispersion (the maximum tracer concentration observed in a monitoring well located 9.14 m (30 ft) from the injection well during the bromide tracer experiment was less than 30% of the injection concentration).

The concentration of sodium dithionite in the first tank injected was the highest in order to deliver adequate amounts of reagent to portions of the aquifer located furthest (radially) from the injection well. The concentration of sodium dithionite in the last tank injected was minimal because

the portion of aquifer that was influenced by this solution had already been in contact with the higher concentrations of reagent for 5 to 10 h. Overall, the average concentration of sodium dithionite injected was 0.065 M so that the sulfate concentrations in the anticipated 379,000 L (100,000 gal) of withdrawal water would be below the 2500-ppm purgewater collection criteria.

Following the residence phase, the reagent as well as any mobile reaction products and byproducts (e.g., mobilized metals) were withdrawn from the aquifer through the injection/withdrawal well. A larger withdrawal volume than injection volume was required to recover the reagent due to groundwater drift and dispersive effects. The withdrawal water from this experiment was stored in a 379,000-L (100,000-gal) Modutank installed at the site. Samples of the withdrawn water were collected and submitted for analyses; results from these analyses were used to perform a mass balance calculation on the amount of reagent, reaction products, buffer, and conservative tracer withdrawn during the 4.8 pore volume withdrawal phase. The withdrawn water was also analyzed to determine if concentrations of sulfate and trace metals were below the purgewater collection criteria. Results indicated that all Hanford purgewater collection criteria were met, and the stored withdrawal water was purged to the ground.

### **10.3 Monitoring and Analytical Equipment**

Dithionite movement and reactivity during the injection, residence, and withdrawal phases of the field test were characterized by monitoring geochemical changes in the groundwater (oxygen, pH, electrical conductivity) and by direct measurement of dithionite and dithionite degradation product concentrations. Groundwater geochemical measurements and samples were taken at sampling intervals ranging from 0.25 to 6.0 h from the injection/withdrawal well and 12 monitoring wells resulting in the collection of approximately 2500 water samples; collected samples were analyzed to characterize dithionite distribution and reactivity within the aquifer.

Monitoring and analytical equipment used during the main dithionite injection/withdrawal experiment are discussed in detail in Section 6.7 and Appendix A.

### **10.4 Dithionite Injection/Withdrawal**

This section describes the various aspects of the dithionite injection/withdrawal experiment, including injection solution preparation, conducting the injection, residence, and withdrawal phases of the experiment, mass balance calculations, and a comparison of the reagent/buffer breakthrough curves with bromide breakthrough responses observed during the bromide tracer experiment.

#### **10.4.1 Injection Solution Preparation**

A concentrated solution of sodium dithionite, potassium carbonate, and potassium bicarbonate was delivered to the site on September 6, 1995, in a refrigerated tanker truck (see Figure 10.1). The reagent/buffer chemicals (1800 lb of  $\text{Na}_2\text{S}_2\text{O}_4$ , 200 lb  $\text{Na}_2\text{SO}_3$ , 5700 lb of  $\text{K}_2\text{CO}_3$ , and 400 lb of  $\text{KHO}_3$ ) were mixed with water to produce a total volume of 4500 gallons for delivery in the tanker truck. The concentrated solution was mixed with groundwater in three 7100-gallon tanks at the site to three different injection concentrations on the morning of September 7, 1995. The concentrations of the tanks are shown below:

	Sodium Dithionite	Potassium Carbonate	Potassium Bicarbonate	Sodium Bromide
Tank A	0.1 M	0.4 M	0.04 M	90 ppm
Tank B	0.065 M	0.26 M	0.026 M	90 ppm
Tank C	0.033 M	0.13 M	0.013 M	90 ppm

Equal amounts of conservative tracer (3 kg NaBr) were added to each of the three tanks. The injection tanks were equipped with mixing blades driven by electric motors mounted on the top of the tanks. The reagent, once in the mixing tanks, was blanketed with argon gas to minimize exposure to atmospheric oxygen.

The injection of three different concentrations was selected to minimize cost, waste, and to permit the injection of higher concentrations without exceeding the Hanford Purgewater Collection Criteria (DOE 1990) for sulfate in the withdrawal water. Sensitivity studies using the one-dimensional radial reactive transport model developed as part of the design analysis showed that with a reaction half-life of from 5 to 10 h, the maximum concentration is only required for the early portion of an 18-h injection period. Toward the end of the experiment, the sediment closer to the injection well has already been in contact with a significant amount of dithionite for a sufficient period of time. Higher concentrations are also needed at the early part of the injection because the dithionite is consumed during the travel radially outward. Dispersion and diffusion also act to reduce the concentrations. A uniformly reduced zone is desired for emplacement. If the system is iron-limited (i.e., more dithionite than ferric iron), then the reagent injected in the later part of the experiment is not required and will only undergo disproportionation or be unreacted.

The experiment consisted of three phases: injection, residence, and withdrawal phase. Details of these phases and observations are discussed below.

#### 10.4.2 Injection Phase

Reagent injection began at 12:00 (noon) September 7, 1995, from Injection Tank A (highest concentration) at a constant rate of 20 gpm. The injection rate was monitored by an in-line turbine flow meter and manually corrected to maintain a constant injection rate. Each tank was injected in 5.7 h for a total duration of 17.1 h, resulting in the injection of 77,543 L (20,460 gal). Samples from the injection stream and monitoring wells were collected, archived, and monitored with geochemical field parameter monitoring probes (pH, temperature, electrical conductivity, dissolved oxygen); a secondary station for pH, dissolved oxygen, and conductivity measurements (laboratory microelectrodes); and with an UV-visible spectrophotometer for dithionite and degradation products. Groundwater samples were also filtered and preserved in nitric acid for trace metals analysis. Purgewater generated during sampling was added to the Modutank for the mass balance analysis.

The injection of three different concentrations can be seen by the stepped dithionite concentrations and conductivity curves shown for the injection well in Figure 10.2 and in the innermost wells (H5-5p, H5-6, H5-9) in Appendix G. Data for dithionite concentrations, conductivity, pH, and dissolved oxygen for all the monitoring wells during the field test are shown in Appendix G. Conductivity and dithionite concentrations for the wells screened in the lower and upper portion of the aquifer along the H5-5, H5-4, H5-3 transects are shown in Figure 10.3.

Peak dithionite concentrations reached at each monitoring well are shown in Table 10.1. The largest radial distance reached by dithionite (based on 1% of the averaged dithionite concentration of 0.065 M) was approximately 7.5 m (25 ft) from the injection/withdrawal well. This table also compares the peak conductivity measured at each well; 1% of the maximum conductivity extended beyond the monitoring well at the 9-m (30-ft) radial distance. The difference in the distances reached between the relative conductivity and relative dithionite concentrations is due to the reaction of dithionite with the aquifer sediments during the travel path outward from the injection/withdrawal well. Variations in the arrival times and peak concentrations of dithionite and conductivity with the radial distance (i.e., peak dithionite and conductivity measurements do not always decrease with increasing distance), as shown in Table 10.1, can be explained by hydrologic and geochemical heterogeneities in the sediment.

The pH of the injection solution was buffered to about 11 with the potassium carbonate/bicarbonate buffer. The pH was observed to dip by about 1 pH unit before the arrival of dithionite in the middle and outermost wells (see Appendix G). This effect may be from the arrival of reaction and degradation products at a well where the dithionite is used up at the leading edge of the injection plume. A white precipitate was also observed in the monitoring wells around the time of the first arrival of dithionite at the monitoring wells; the analysis of the precipitate by x-ray diffraction indicates the precipitate is a magnesian calcite. The dissolved oxygen concentrations measured zero coinciding with the arrival of the dithionite front at each well.

A comparison of conductivity and dithionite concentrations in the wells screened in the upper and lower portions of the aquifer at the same radial distance (see Figure 10.3) shows a delay in the arrival times in the wells screened in the upper wells. The injection/withdrawal well is screened in the lower 1.52 m (5 ft) of the 2.9-m (9.5-ft)-thick aquifer. Vertical spreading of the plume is controlled by the hydraulic conductivity anisotropy as shown by design analysis modeling as discussed in Williams et al. (1994).

### 10.4.3 Residence Phase

The duration of the residence phase was 18.5 h to provide time for the remaining dithionite to react with the aquifer sediments. Groundwater sampling and analysis was continued during the residence phase.

Some density effects were observed during the residence phase. The conductivity measured for the wells screened in the upper portion of the aquifer decreased during the residence phase and that for the wells screened in the lower portion of the aquifer increased, particularly for well H5-4o and H5-4p, as shown in Figure 10.3. Density effects are expected to be greatest where there is the largest contrast in density between the injection solution and the groundwater. The middle monitoring wells (i.e., H5-4p and H5-4o) showed the highest concentrations, and therefore highest densities, at the end of the injection phase due to the injection of the three different injection concentrations. The highest density injection solution (injected at the beginning the injection phase) was influenced the most by dilution from dispersion and mixing at the front of the plume and therefore had a reduced density by the end of the injection phase. The downward movement of reagent within the upper portion of the aquifer caused by density effects also significantly influenced the concentrations observed in the upper zone monitoring wells during the withdrawal stage (as discussed in Section 10.4.6).

Dithionite was still remaining in the innermost and middle wells at the end of the residence phase (see Appendix G). This could indicate that most of the iron in the sediments in this portion of the aquifer was reduced because there should have been sufficient time for the redox reaction of

dithionite and ferric iron to consume the dithionite given a sufficient amount of available iron. This is being investigated from the analysis of the sediment samples collected after the experiment and in reactive transport modeling.

#### 10.4.4 Withdrawal Phase

The withdrawal phase consisted of pumping from the injection/withdrawal well (H5-2) at a constant rate of 20 gpm for approximately 83 h. Pumping was started September 8 at 23:30 and completed September 12 at 10:28. The volume of water withdrawn during this phase was 375,370 L (99,570 gal), which is equivalent to 4.87 injection volumes 77,543 L (20,460 gal). The withdrawal water was stored in a 379,000 L (100,000-gal) Modutank for analysis to confirm that it met the purgewater criteria before purging to the ground, at a location downgradient from the site.

One effect of the injection of three different concentrations can be seen in the conductivity curves for the injection/withdrawal well as the concentration increases during the early part (~10 h) of the withdrawal as the higher concentration fluids are pulled back toward the injection/withdrawal well (see Figure 10.2).

The final Modutank concentrations for sulfur species and trace metals are shown in Table 10.2. The withdrawal water was below the Hanford Purgewater Collection Criteria (DOE 1990) and permission was obtained from the Washington State Department of Ecology to purge the water to the ground. The main constituent of the purgewater was sulfate at 2.11 g/L. The Modutank was purged to the ground starting on October 6, 1995. A total volume of 373,315 L (98,500 gal) was purged from the Modutank and the 15,160 L (4000-gal) steel tank at the site containing the last water withdrawn.

The total volume of water pumped to the Modutank and steel tank was 435,963 L (115,030 gal), which included the 375,370 L (99,570 gal) of withdrawal water, 7428 L (1960 gal) of purgewater from sampling, and 13,500 gallons of water that were put into the Modutank after it was erected at the site to prevent the tank liner from blowing in the wind. The difference between the total volume of water pumped to the Modutank and steel tank 435,963 L (115,030 gal) and the final volume purged to the ground from the Modutank and steel tank 373,315 L (98,500 gal) is 62,648 L (16,530 gal) of water; this represents the volume of water lost due to evaporation and a leak that was detected in the Modutank tank liner. Evidence of oxidation of the water in the Modutank was seen by a change in the water color, which originally was aquamarine in color but turned reddish in color by the time the Modutank was purged. A dark red precipitate was also found at the bottom of the Modutank after the water was purged; probably iron-hydroxides that formed after the mobile ferrous iron in the withdrawal water was oxidized to ferric iron.

At the end of the withdrawal phase, the pH in the aquifer dropped from the high range of up to 11 during the injection period but was still elevated above the ambient levels, which ranged from 8.10 to 9.66 with the higher pH levels observed in the innermost wells and the wells screened in the upper portion of the aquifer. At the end of the withdrawal period the conductivity returned to within 3 times the initial values, except for the wells screened in the upper portion of the aquifer (H5-5o, H5-4o, and H5-3o), which had 10 times the initial conductivity measurements. Both the high pH and conductivity observed in the wells screened in the uppermost part of the aquifer dropped to the levels seen in other wells one week after the withdrawal phase was completed (as discussed in Section 10.8). The outermost wells and the wells screened in the upper portion of the aquifer showed some reoxygenation during the withdrawal phase as oxygenated water was pulled back into the reduced zone (for examples, see wells H5-11, H5-1B, H5-3p, H5-4o in Appendix G).

## 10.4.5 Mass Balance

One objective of the study was to perform a mass balance to compare the mass of injection constituents with the mass of withdrawal constituents to calculate the percentage of recovery and as a measure of the effectiveness of treatment based on the amount of unreacted dithionite and reaction products. Using concentrations measured from the Modutank for performing the mass balance was complicated by leakage and evaporation losses from the Modutank that introduced uncertainty in the volume of water represented by the samples and the unknown loss of mass due to leakage. Early analysis of Modutank concentrations showed that there was incomplete mixing in the Modutank with the highest concentrations at the bottom of the tank. Once this was discovered, pumps were used to mix the water in the tank, and vertically discrete samples were collected from different locations in the tank. The concentrations of the final Modutank samples showed minimal variations due to sampling location (see Table 10.2).

Calculation of the percentage of bromide recovered, based on concentrations measured in the Modutank, provided a better recovery estimate than the same calculation for recovery of sulfur species because the amount of sulfur mass lost to leakage was larger and more difficult to quantify. Analysis of the earlier samples of density stratification within the Modutank showed that the more dense fluid at the bottom of the tank had a greater percentage of sulfur species than bromide due to the varying concentrations of dithionite and constant bromide concentration during the injection. Based on the known mass of bromide tracer injected and the recovery mass calculated from final modutank bromide concentrations, it was estimated that 98% of the injected bromide mass was recovered during the withdrawal phase.

Due to the complications discussed above regarding sulfur mass balance calculations using concentrations measured in the Modutank, a second approach was utilized to perform the mass balance on sulfur species. Samples collected from the extraction stream during the withdrawal phase of the experiment were analyzed for sulfate, sulfite, and bromide using ion chromatography (IC). Because the total sulfur species concentrations were much higher than bromide concentration in most of the samples, bromide recovery could not be accurately calculated without additional IC analyses; funding for these additional analyses was not available during FY 1996, and additional bromide analyses were not performed.

The total sulfur species recovery curve was well correlated with conductivity measurements made on the extraction stream during the withdrawal phase of the experiment (see the withdrawal phase conductivity and sulfur species data in Figure 10.2). A linear regression analysis of the total sulfur species concentration data and field measured conductivity data, using the method of least squares, resulted in an  $R^2$  value of 0.97. Based on integration of the extraction stream concentration data, it was estimated that 87% of the injected sulfur mass was recovered during the withdrawal phase.

The mass recovery estimate for total sulfur is considered to be a more credible estimate than the estimate for bromide recovery, which is based on concentrations measured in the modutank, because of the uncertainty introduced by the leakage and evaporative loss from the modutank. However, a higher percent recovery for bromide (i.e., 98%), when compared with sulfur species recovery (i.e., 87%), can be expected given the test conditions. The most difficult mass to recover from this type of a "push-pull" experiment is the mass constituting the leading edge of the injected reagent plume; because the highest reagent concentrations were injected first (as discussed in Section 10.4.1), the leading edge of the plume consisted of disproportionately higher sulfur species concentrations.

## 10.4.6 Comparison with Bromide Tracer Test

The bromide measurements from the bromide tracer test were compared to the conductivity measurements during the main injection/withdrawal experiment (see Figures 10.4 and 10.5). Although the main experiment involved the injection of three different solutions with varying conductivity values, the initial portion of the breakthrough curves during the injection match well. A comparison of the characteristics of the relative concentrations during the withdrawal is more complicated due to the injection of three different concentrations, but the bromide concentrations appear to decrease faster and to lower concentrations than the conductivity. This may be due to sorption of the injected cations (K, Na) during the main experiment.

A comparison of the relative concentrations measured during the withdrawal phase in the upper zone wells (see Figure 10.5) between the tracer test and the main dithionite injection/withdrawal test are significantly different, with the concentrations dropping much more rapidly in these wells in the main dithionite injection/withdrawal experiment. This is probably caused by the density settling of the reagent in the upper zone during the residence phase. Although some of these differences can be explained by the injection of three different concentrations, the differences between wells H5-5p and H5-4p in the lower zone during the withdrawal phase of the tracer test and main dithionite injection/withdrawal test were not as great (Figure 10.4). There was a large difference between the tests during the withdrawal phases in Well H5-3p, which also may be due to density effects. More analysis is needed to verify the role of density effects in these observations. Although some interesting density effects have been observed in the upper portion of the aquifer and outer portions of the reagent plume during the residence and withdrawal phases, no density-related effects have been observed that impacted the main objective of the experiment (i.e., the ability to create a reduced zone in the lower portion of the aquifer).

## 10.5 Post-Experiment Reductive Capacity Measurements

Although analysis of aqueous samples from the site provides indirect evidence of the reduction of aquifer sediments (dissolved oxygen and total chromium/hexavalent chromium concentrations), direct evidence of the reduction of the aquifer sediment is only possible through the analysis of sediment samples collected from core holes drilled at the site following the dithionite injection/withdrawal experiment.

Core samples were collected following the ISRM field experiment from seven core holes and during the installation of the upgradient monitoring well (H5-15). A total of 38 samples were collected; 22 of these 38 cores were cut and prepared for analysis. To date, 13 of the 22 samples (and one duplicate) have been analyzed for reductive capacity. The primary purpose for collecting the core samples was to determine the reductive capacity created during emplacement of the ISRM treatment zone. A limited number of microbiologic samples were also collected.

All sample preparation work was conducted in an anaerobic glovebox. Sample preparation consisted of 1) weighing the entire core before cutting, 2) cutting the core in half (lengthwise) using a Dremmel moto-tool with a circular blade, 3) photographing and describing the core lithology and texture, 4) sieving the sample through a 4.75-mm sieve, 5) weighing the <4.75-mm and >4.75-mm portions and the empty lexan liners and caps, and 6) homogenizing the <4.75-mm sample, weighing a portion approximately between 300 g to 500 g, and placing the sample into a labeled plastic container. Unused portions were weighed, labeled, and stored in the glovebox for archive purposes. Weights of all subsamples were recorded. To preserve sample integrity, the samples were transported to the analytical laboratory in an argon-filled bag.

A slightly different sample preparation procedure was followed for the 14.3 m to 14.6 m (47-ft to 48-ft sample from core hole B2624. This procedure consisted of steps 1 to 3, above, but then, instead of sieving the entire core sample through a sieve (homogenizing the sample), a selected subsample from the center of the core was collected for analysis, along with a selected subsample from the external portion of the core (adjacent to the lexan liner). The remaining portion of the core was homogenized and stored as archive. The purpose of this altered procedure was to test the degree of variability in reductive capacity within the core, specifically, whether the inner portion of the core was more reduced than the outer portion; reduced capacity of the outer portion of the sample would indicate the core was contaminated with atmospheric oxygen during sample collection.

Post-experiment core samples were analyzed for reductive capacity by two separate methods; these methods included reoxidation of the sample with oxygen-saturated water and reoxidation of the sample with hexavalent chromium. Following is a description of each of the methodologies, a summary of available results, and a preliminary estimate of the reductive capacity of the emplaced treatment zone.

### 10.5.1 Reductive Capacity by O<sub>2</sub> Reoxidation Method

The primary methodology for determining the reductive capacity of core samples collected from the treatment zone following the ISRM field experiment was reoxidation of the sample with oxygen-saturated water. The O<sub>2</sub> reoxidation method was selected as the primary methodology because the processes involved in the methodology were easily automated; automation of the process significantly increased the number of core samples that could be analyzed by reducing the labor costs associated with reductive capacity determination.

In the O<sub>2</sub> reoxidation method, selected sediment cores were first sieved to remove particles larger than 4.75 mm and then packed into polyvinyl chloride columns. A separate column was used for each core. The columns were 2.5 cm diameter, 20 cm long, and had a total internal volume of 108.7 cm<sup>3</sup>. The sediment was retained in the column using 200-mesh stainless-steel screening. During packing, a small amount of sediment was placed into a tared pan, weighed, oven dried (105°C for 24 h), and weighed again to determine the gravimetric water content of the sediment packed in each column. After packing, the columns were flooded with compressed argon to remove entrapped air, and then connected to the measurement system.

The measurement system consisted of

- a piston pump (Model QC 50, Fluid Metering Inc., Oyster Bay, NY) that delivered air-saturated synthetic groundwater to the column inlet
- a computer-controlled syringe pump (Model 50300, Kloehe, Las Vegas, NV) that alternatively delivered samples of the supply reservoir or the column effluent to the measurement cell
- the measurement cell consisting of a Plexiglas chamber (2 cm internal volume) containing a stir bar, a thermocouple, and an oxygen probe (Model 5331, Yellow Springs Instrument Corp., Yellow Springs, OH)
- an oxygen meter (Model 5300, Yellow Springs Instrument Corp.) that displayed probe potentials as a percentage of a preset value and converted probe potentials to a 5-V range that could be recorded by the datalogger

- an electronic datalogger (Model 21 X, Campbell Scientific Inc., Logan, UT)
- a computer.

The syringe pump was programmed to first collect a 10-mL water sample from the supply reservoir and deliver it to the measurement cell. After 90 seconds, the pump was programmed to first drain the cell and then to collect an additional 10-mL water sample from the column effluent and deliver it to the measurement cell. This process was repeated continuously for the duration of the experiment; the time required for one cycle was approximately 3 minutes. The datalogger was programmed to communicate with the syringe pump so that the source of the sample (supply reservoir or column effluent) and the time of its delivery to the measurement cell could be recorded. The datalogger also recorded voltage outputs supplied by the thermocouple in the measurement cell and the probe potential's output by the oxygen meter. Once the sample was delivered to the cell, the datalogger program recorded the time of measurement, the cell thermocouple potential (which was converted by the program to cell temperature in °C), and the oxygen probe potential every 15 to 20 seconds for 1 minute after the sample was delivered to the cell (previous experiments with the measurement cell indicated that oxygen probe readings stabilized approximately 30 seconds after the introduction of a sample).

Experiments continued until dissolved oxygen concentrations in the column effluent exceeded 85% of the dissolved oxygen concentration of the synthetic groundwater in the supply reservoir. Dissolved oxygen concentrations in the supply reservoir were assumed to be equal to the solubility of oxygen in water at the temperature of the measurement cell and at the partial pressure of oxygen in the standard atmosphere ( $P = 0.21$  bar). The dissolved oxygen concentration of the effluent sample was computed by multiplying the dissolved oxygen concentration of the preceding reservoir sample by the ratio (probe potential of the effluent sample)/(probe potential of the reservoir sample). A spreadsheet macro was written to reduce the experimental data, prepare plots of the reduced data, and compute summaries of various experimental conditions.

After an experiment, the inlet and outlet ports of each column were sealed with threaded plugs and the columns were stored in ambient laboratory conditions. The bulk density ( $\rho_b$ ) of the packed sediment was computed by dividing the dry weight of the sediment (computed using the wet weight of the sediment and the gravimetric water content of the sediment subsample collected while packing) by the internal column volume; the porosity ( $\phi$ ) was computed using the equation:  $\phi = 1 - (\rho_b/\rho_g)$  where the grain density ( $\rho_g$ ) was assumed to be equal to 2.9 g/cm<sup>3</sup>. The average flow rate was computed by dividing the total pumped volume (the volume of collected column effluent combined with the total sampled volume) by the duration of the experiment. The total mass of oxygen removed from the synthetic groundwater as it flowed through the sediment in the column was determined by subtracting the total mass of dissolved oxygen that entered the column (computed from the flow rate and the measured dissolved oxygen concentration in the supply reservoir) from the total mass of dissolved oxygen that exited the column (computed from the flow rate and the measured dissolved oxygen concentrations in the column effluent).

As discussed above, because of time constraints and the asymptotic nature of the oxygen breakthrough curves, the reoxidation experiments were continued until dissolved oxygen concentrations in the column effluent exceeded 85% of the dissolved oxygen concentration of the synthetic groundwater in the supply reservoir; total capacity was calculated by extrapolating the late-time slope to 100% breakthrough. The oxygen reducing capacity (ORC) was computed by dividing the total mass of oxygen removed by the sediment's dry weight and an assumed equivalent weight of 8 mg/meq for oxygen.

A summary of preliminary results obtained from the O<sub>2</sub> reoxidation method are contained in Table 10.3. As indicated, the reductive capacity, or in this case ORC, is highly variable. Sample ORC represents the reductive capacity of the less than 7.5-mm size fraction (i.e., the size fraction used in the reoxidation experiments); core ORC has been scaled to account for the removal of the coarse size fraction. The observed variability in reductive capacity measurements makes it difficult to interpret the data with respect to spatial trends. However, this type of variability would be expected among samples collected from a heterogeneous aquifer when the measurement is highly dependent upon the small size fraction.

Another method of measuring the effectiveness of the treatment zone emplacement, that better accounts for the heterogeneity in the system, is to compare the achieved reductive capacity of a sample with its maximum possible reductive capacity; this comparison provides an estimate of the percent of the available Fe(III) that was reduced by the dithionite injection.

To obtain this information, the sediments in the column were re-reduced by first pumping a prepared dithionite solution (synthetic groundwater + 0.1 M dithionite + 0.4 M K<sub>2</sub>CO<sub>3</sub> + 0.04 KHCO<sub>3</sub>) through the columns continuously for 24 h followed by a 24-h reaction period (no flow). Following the reaction period, three pore volumes of anoxic water were run through the column to flush out the dithionite solution. Then air-saturated synthetic groundwater was pumped through the column, dissolved oxygen concentrations in the column effluent were measured, and the total mass of oxygen removed from the synthetic groundwater as it flowed through the sediment and the oxygen-reducing capacity were determined using procedures described above. Preliminary results from the comparison of field experiment achieved reductive capacity to maximum achievable reductive capacity are summarized in Table 10.4.

As indicated in Table 10.4, spatial trends in the effectiveness of the treatment zone emplacement are evident when comparisons of the percentage of available Fe(III) that was reduced by the treatment are made between core samples. There is a general trend of increasing percent reduced with depth; this is consistent with the experiment design, which targeted the bottom 1.5 m (5 ft) of the aquifer. There is also a general trend of decreasing percent reduced with increasing distance from the injection/withdrawal well. However, it should be noted that comparison of samples collected from the interior portion of a core sample (B2624, 14.3 m to 14.6 m [47 ft to 48 ft] {int}) were significantly more reduced than the outer portion of the core, indicating that some of the cores may have been partially reoxidized during core sampling or during handling/storage of the core samples. Partial reoxidation of some of the core samples could account for some of the variability observed in the reductive capacity measurements.

One method used to estimate the total reductive capacity of the treatment zone was to apply the average reductive capacity measurement obtained from analysis of core samples collected from within the treatment zone (7.5 m [25 ft] radial distance) as shown in Table 10.3. The treatment capacity of the bottom five feet of the aquifer was estimated to be 70 pore volumes based on the average reductive capacity of the core samples, bulk density and effective porosity estimates of 1.9 g/cm<sup>3</sup> and 0.2, respectively, and assumed dissolved oxygen and hexavalent chromium concentrations of 9 ppm and 1 ppm, respectively. Assuming a 15.2-m (50-ft)-wide treatment zone and a groundwater velocity of 30.48 cm/d (1 ft/d), the emplaced treatment zone would have a life of approximately 10 years. Because there is evidence that some of the core samples were partially reoxidized during core sampling and/or during handling/storage, this estimate of barrier treatment capacity is considered to be a conservative estimate.

A second method used to estimate the total reductive capacity of the treatment zone involved using available Fe(III) data obtained from the analysis of core samples collected at the ISRM site (see

Table 6.3) and information on the percent total available Fe(III) that was reduced during the field experiment (Table 10.4). The available Fe(III) data reported in Table 6.3 indicates an average value of 0.059% by weight for Hanford formation sediments. The treatment capacity of the bottom 1.5 m (5 ft) of the aquifer was estimated to be between 51 and 85 pore volumes based on 1) the average available Fe(III), 2) bulk density and effective porosity estimates of 1.9 g/cm<sup>3</sup> and 0.2, respectively, and assumed dissolved oxygen and hexavalent chromium concentrations of 9 ppm and 1 ppm, respectively, and 3) core data that indicated that from 60% to 100% of the available reactive iron (from core samples collected up to a 7.5-m (25-ft) radial distance) was reduced during the dithionite injection/withdrawal experiment. Assuming a 15.2-m- (50-ft)-wide treatment zone and a groundwater velocity of 30.48 cm/d (1 ft/d), the emplaced treatment zone would have a life of between 7 and 12 years.

Current plans for FY 1997 performance assessment activities at the ISRM test site include additional coring to determine if there has been any loss of reductive capacity. During this second phase of post-experiment sediment coring, more rigorous procedures will be developed to reduce the potential for core samples being contaminated with atmospheric oxygen during collection.

### 10.5.2 Reductive Capacity by Chromium(VI) Reoxidation Method

The purpose of this experiment was to develop a test method to evaluate the reductive capacity of sediments collected from the ISRM treatment zone using chromium(VI) as the oxidant. These reductive capacity measurements, using the chromium(VI) reoxidation method, will then be compared to measurements made using the O<sub>2</sub> reoxidation method to verify the accuracy of the O<sub>2</sub> method; as discussed previously, the O<sub>2</sub> reoxidation method is less labor-intensive, and subsequently less expensive, than the chromium(VI) reoxidation method.

The reductive capacity of five core sample aliquots to chromium(VI) were measured during the course of this experiment. The core sample aliquots representing various borehole segments are listed in Table 10.5.

A ten gram aliquot of a core sample was removed from the cores stored in an argon filled glove box and placed into a 250-mL ground glass flask. A ground glass stopper was used to seal each flask and the flask and its contents were removed from the glove box. All samples, except sample 2, were used immediately after removal from the glove box. Sample 2 was used 72 h after removal from the glove box. Immediately after removal from the glove box, 100 mL (water-to-solid ratio of 10:1) of argon-purged unpreserved groundwater from the upgradient monitoring well (199-H5-15) were added to the sediment sample in the flask. For the first experiment no additional chromium(VI) was initially spiked into the groundwater. For the subsequent four experiments additional chromium(VI) was added to the groundwater at the start of the experiment. Spike additions were either 100 ppb, 500 ppb, 1000 ppb, or 10,000 ppb amounts. Immediately on addition of the groundwater (or spiked groundwater) a 1-mL aliquot of the groundwater was removed and a flowing blanket of argon was placed over the slurry throughout the experiment. The 1-mL aliquot of groundwater removed from the slurry was analyzed by adsorptive stripping voltammetry (AdSV) according to the method described below. This initial sample was defined as time 0. Subsequent samples of groundwater were removed from the reaction vessel from 30 minutes to 117.25 h after initial spike addition. When the concentration of chromium(VI) decreased to less than 10 ppb in the slurry solution additional chromium(VI) was spiked into the slurry sample. Immediately on addition of the spike a 1-mL aliquot of groundwater was removed and analyzed for chromium(VI). This sample result was again defined as time 0.

Adsorptive stripping voltammetry measurements of chromium(VI) were based on the procedure of Golimowski et al., where 9.9 mL of the supporting electrolyte solution, containing 0.05 M diethylenetriaminepenta-acetic acid (DTPA), were injected by pipette into the cell and purged with nitrogen for 4 minutes. An accumulation potential of -0.8 V was applied to a fresh mercury drop, while the solution was stirred (usually for 10 to 30 s). The stirring was then stopped, and the voltammogram was recorded by applying a negative-going differential pulse potential scan terminating at -1.65 V. A known volume of the leachate (usually 10 to 100  $\mu$ L) was then added, and the accumulation/stripping cycle was repeated with a new mercury drop. Subsequent standard additions (0.25 to 1.0  $\mu$ g/L chromium) were used for quantifying the original chromium level in each sample. In addition to the measurement of chromium(VI) this procedure is capable of measuring the concentrations of chromium(III). Several measurements for chromium(III) were conducted on selected samples.

The data collected from the above experiments is presently being analyzed and was not available for inclusion in this report. Chromium(VI) reoxidation method verification analyses are ongoing and results will be included in subsequent project reports and journal publications.

## 10.6 Effect of Treatment on Microbial Populations

Microbiological characterization results from wells 199-H5-2, -H5-3, -H5-4, -H5-5, -H5-8, and -H5-11 (pre-experiment) are shown in Table 6.4 and were reported in Vermeul et al. (1995). An additional 14 microbiologic samples were collected from the coreholes and from well 199-H5-15 in November 1995 (post-experiment). Of the 14 microbiologic samples collected, 7 were analyzed for microbiological population (expressed as colony forming units per gram). Analyses results are shown in Table 10.6. The analysis technique is discussed in Section 6.5.

Comparison of the microbiological population data previously collected before the experiment (see Table 6.4) and the corresponding corehole location (Table 10.6) suggests that in general, the presence of the dithionite tends to reduce populations by 1- to 2 orders of magnitude. This effect was noticed in 4 of the 7 samples. However, one of the samples showed relatively similar pre- and post values (B2618, 44-45), and two samples showed an increase of CFU/g of 2 and 4 orders of magnitude (B2623, 48.5-49.5; and B2624 49-50, respectively). One explanation for this increase is that these coreholes are located in an area that received low- to very low dithionite concentrations, and the increase reflects natural heterogeneity and/or a situation where the presence of the buffer solution acted to stimulate population growth.

## 10.7 Comparison of Pre- and Post-Experiment Hydraulic Tests

Pre- and post-experiment slug interference test responses were compared for selected observation well sites at the Redox Manipulation test facility to assess the impact of the applied field experiment on existing in situ hydraulic properties. As indicated in Spang (1996), slug interference response transmission (i.e., from the stress well to the point of observation) is highly dependent on the aquifer-interwell transmissivity (which is equal to hydraulic conductivity times aquifer thickness;  $T = K b$ ). The shape and amplitude characteristics of the slug interference response is primarily controlled by the elastic storage (S) and vertical anisotropy ( $K_v/K_h$ ) of the aquifer materials. A comparison of the pre- and post-experiment slug interference responses (for identical test conditions), therefore, should provide a direct means of evaluating any changes in in situ hydraulic properties induced by the experiment application.

Pre-experiment slug interference tests were conducted on May 23, 1995, while post-experiment testing was conducted on April 11, 1996. To eliminate any scale-dependence effects, identical stress levels were applied for the slug interference tests ( $H_o = 1.17$  ft and 4.298 ft for low- and high-level stress tests, respectively) conducted during the pre- and post-experiment phases. A comparison of normalized test responses indicated identical response behavior for low- and high-level stress tests conducted during each test phase. The high-level stress test responses were the focus of the pre- and post-experiment test evaluation, because of the greater radius of investigation afforded by the higher imposed stress.

It should be noted that a direct comparison of slug interference responses was not possible, however, because the aquifer thickness increased from 9.2 to 12.1 ft for the pre- and post-experiment tests, respectively. A visual comparison of the pre- and post experiment test responses, taking into account the existing aquifer thickness and well penetration/aspect conditions indicates the following:

- the post-experiment slug tests at stress well H5-2 exhibit a lagged (i.e., delayed) and steeper recovery response, in comparison to pre-experiment tests
- post-experiment slug interference tests for observation wells completed within the lower half of the aquifer (e.g., H5-3P, -4P, -5P) exhibit a lagged and damped (i.e., diminished) response, in comparison to pre-experiment tests

### 10.7.1 Discussion of Stress Well H5-2 Response

Figure 10.6 shows a direct comparison of the observed pre- and post-experiment slug test response exhibited at stress well H5-2. As indicated in the figure, the post-experiment test response exhibits a delayed and steepened recovery pattern, in comparison to the pre-experiment test. The delayed response or time shift exhibited can be attributed to a number of factors including: an overall reduction in aquifer hydraulic conductivity or development of a zone of significantly reduced permeability (i.e., "skin effect") immediately surrounding the stress well screen. Figures 10.7 and 10.8 show the predicted slug test response for decreasing aquifer hydraulic conductivity and presence of various low permeability skin conditions, respectively.

As indicated in Figure 10.7, decreasing aquifer hydraulic conductivity causes a proportional time lag or delay in the predicted slug test response. Figure 10.8 shows the predicted slug test response for selected skin values of reduced permeability over an affected distance of 0.5 ft surrounding the well ( $r_{sk} = 1.0$  ft). As shown in the figure, skin zones of progressively lower permeability (i.e., greater positive value) cause a similar time lag shift or delay, as indicated in Figure 10.7, for uniform decreases in aquifer hydraulic conductivity. This similarity in predicted responses makes it difficult to distinguish the factor responsible for the time lag exhibited in the post-experiment test, when only test responses at the stress well are available for analysis.

In addition to the presence of a low permeability skin, factors that can cause an overly steepened recovery test response include: a decrease in the aquifer's elastic storage ( $S$ ), and an increase in aquifer vertical anisotropy ratio ( $K_D = K_v/K_h$ ). Figures 10.9 and 10.10 illustrate the effect on predicted slug test response for varying values of  $S$  and  $K_D$ . Figure 10.9 indicates that slug test responses for varying storativity values are divergent in early test times and converge at late test times, with lower storativity aquifers exhibiting over-steepened responses during intermediate test times. In contrast, Figure 10.10 shows that slug test responses for varying vertical anisotropy values are convergent in early test times and display greater divergence with increasing test time. Tests with higher vertical anisotropy ratios (i.e., more isotropic conditions) exhibit oversteepened test responses

that recover more rapidly. The fact that the post-experiment test response displayed a lagged and oversteepened test response in comparison to pre-experiment results suggests that an increase in the vertical anisotropy cannot be solely responsible for the observed results (i.e., if only one factor is operative).

### 10.7.2 Discussion of Observation Well Response

To examine the areal effects of the field experiment on in situ aquifer properties, pre- and post-experiment slug interference responses at wells H5-3P, -4P, and -5P were evaluated. These wells are all located at varying distances from stress well H5-2, along a common northwest direction, and are all completed in the lower half of the aquifer (similar to the stress well). A comparison of the test results all indicated the same response patterns, with post experiment slug interference tests exhibiting a lagged and diminished response, in comparison to pre-experiment tests at each observation well location. Figure 10.11 shows an example of the pre- and post-interference patterns as recorded at observation well H5-4P. The divergence in slug interference responses indicates that the field experiment application imposed a change in the previously existing, pre-experiment in situ well/aquifer test conditions.

To assess whether post experiment response changes are associated with uniform aquifer changes or possibly induced hydraulic changes only in the vicinity of the stress well, two analysis approaches were applied. The first focused on the analysis of the pre- and post experiment slug interference responses using a homogeneous formation model to assess whether a quantitative analysis match could be obtained for both tests. If the first analysis approach was not successful (indicating more complex test/formation conditions), then a composite formation model was applied that accounts for changes in hydraulic properties in the vicinity of the stress well.

Figures 10.12 and 10.13 show the analysis results for the pre- and post experiment slug interference responses at observation well H5-4P, using the initial homogeneous formation model. As shown in Figure 10.12, the homogeneous formation model provides a reasonably good fit of the pre-experiment test response for the matched aquifer properties of  $K = 163$  ft/d,  $S = 0.0043$ , and  $K_D = 0.14$ . Efforts to match the post-experiment test response, however, were not as successful, and significant changes in aquifer properties ( $K = 105$  ft/d,  $S = 0.0092$ ,  $K_D = 0.3$ ) were required (in comparison to the pre-experiment determined values) to obtain a final best analysis fit (note: a predicted response based on pre-experiment analysis values is also shown in Figure 10.13).

The extremely poor match of post experiment early-time test behavior (i.e., 0 to 20 sec) suggests that other operative test/aquifer conditions were present, and that the homogeneous formation model approach may not be applicable for determining aquifer properties when used in the analysis of post experiment test responses. To examine whether better post experiment analysis results could be obtained, a finite-skin (composite formation) model was applied using the previously determined pre-experiment test aquifer properties as input. As indicated in Earlougher (1977), skin effect ( $sk$ ) is related to the ratio of the aquifer and skin hydraulic conductivity and radii by the following relationship:

$$sk = [(K_f/K_{sk}) - 1] \ln(r_{sk}/r_w) \quad (10.1)$$

where,  $sk$  = skin effect; dimensionless

$K_f$  = formation hydraulic conductivity; [L/T]

$K_{sk}$  = skin zone hydraulic conductivity; [L/T]

$r_{sk}$  = skin zone radius; [L]

$r_w$  = well radius; [L]

Equation 10-1 indicates that the skin value parameter is not unique, and various combinations of skin hydraulic conductivity and radial thickness can provide similar test responses.

For the analysis of the post experiment test response, a trial-and-error approach was applied. Skin properties were adjusted for various skin thickness,  $r_{sk}$ , and the skin hydraulic conductivity,  $K_{sk}$ , values. Figure 10.14 shows an example of a finite-skin solution for the post experiment slug interference results at well H5-4P. Although a complete match of the early-time test response was not attainable, the overall match and shape of the predicted post experiment slug interference response suggests that the finite-skin solution is better than the homogeneous model in matching post experiment test behavior. Preliminary analysis results indicate the presence of a small zone (e.g., 1 in. to 4 in.) of reduced permeability immediately outside the wellbore. The cause of this zone of reduced permeability is unknown, but may be attributed to entrapment of suspended or colloidal material in the sandpack zone immediately outside the well screen during the pumpback phase of the experiment. Analysis results using the homogeneous aquifer and finite-skin (composite formation) models for observation wells H5-3P, -4P, and -5P are presented in Appendix D.

As mentioned previously, a direct comparison of the pre- and post-experiment slug interference responses was not possible because of the change in aquifer thickness that occurred between the two test times. To eliminate the uncertainties associated with this change in aquifer thickness, additional slug interference tests will be conducted at the ISRM test site once water-levels have returned to their pre-experiment conditions. This second phase of hydraulic testing will provide a direct, and more definitive, comparison.

## 10.8 Long-Term (Post-Experiment) Monitoring of Wells

Monitoring of the groundwater at the ISRM site has been ongoing since the injection/withdrawal experiment, initially on a biweekly frequency and then, after approximately 6 months, on a monthly frequency. Water samples are collected from the wells at the site and measured for geochemical field parameters (pH, conductivity, DO, and hexavalent chromium). The pH, conductivity, and dissolved oxygen are measured with electrodes (see Section 6.7 and Appendix A for details). A portable Hach DR/2000 Spectrophotometer is used to measure hexavalent chromium (8-ppb detection limit) and for comparison of the dissolved oxygen concentrations measured with an electrode. Archive samples are also collected with one set of samples preserved in nitric acid for trace metal analysis (if needed). Three rounds of groundwater samples for all the wells at the site were analyzed for trace metals using an ICP/MS. In addition to the wells within the treatment zone, upgradient and downgradient monitoring wells are sampled and analyzed.

Field parameter measurements for each well are plotted in Appendix H. Figure 10.15 shows the pH and conductivity concentrations for the times immediately after the experiment and from the latest round of field sampling and analysis. The results of the three sets of trace metal analysis

(ICP/MS) are summarized in Tables 10.7 through 10.9 for the wells within the reduced zone and Tables 10.10 through 10.12 for the upgradient and downgradient wells. Table 6.5 shows the trace metals concentrations measured at the site before conducting the experiment. These analyses results are discussed in the sections below.

Although no negative impact on the aquifer have been observed downgradient from the reduced zone, a larger and longer reduced zone is needed to adequately monitor and address downgradient effects. The small scale of the ISRM treatment zone makes quantification of downgradient effects difficult because of edge effects and uncertainty in gradient direction at the smaller scale.

During post-experiment monitoring in December and January, an increase in dissolved oxygen was detected in some wells within the reduced zone and dark-colored (gray-black) water was occasionally observed as water from within the wellbore was removed during sampling. The anoxic water in the aquifer around the wells was re oxygenating from atmospheric oxygen in the boreholes and causing soluble ferrous iron to oxidize and precipitate in the well yielding the dark-color. This problem was remedied by blanketing the wells with argon gas that is continuously fed to the wells from liquid argon dewers stored at the site. A permanent solution would be to install mechanical or inflatable packers in the wells just above the screened interval to isolate the groundwater from direct contact with atmospheric gases in the well bore. Argon blanketing is currently being used to permit easy access to the wells during sampling and hydraulic testing. The concentration of oxygen in the well bore is checked with a hand-held oxygen meter before each sampling event. This method was effective in removing the oxygen from the well bore, resulting in a stabilization of the dissolved oxygen measurements in the groundwater, and elimination of the occurrence of dark gray-black colored water accumulation within the wellbore.

Very turbid, muddy water was observed in some of the wells during the first sampling event following the corehole drilling in November. This was from fines that were generated during the drilling and sampling of the coreholes.

### 10.8.1 Dissolved Oxygen Monitoring

Post experiment monitoring data is presented for wells along a transect in a generally upgradient to downgradient direction as shown in Figure 10.16. Dissolved oxygen concentrations at the site measured in the wells before the injection/withdrawal experiment ranged between 1.9 to 6.1 ppm (see Figure 10.17a). Following the experiment, the dissolved oxygen concentrations in most of the wells within the reduced zone were approximately 0.00 ppm as shown in Figures 10.17b and 10.18. The two wells on the upgradient portion of the reduced zone (H5-3p and H5-3o) have shown an increase in dissolved oxygen concentrations, with the monitoring well screened in the upper portion of the aquifer (H5-3o) showing higher concentrations. The upper portion of the aquifer was expected to reoxygenate before the lower portion because the dithionite was injected in the bottom of the aquifer resulting in less reagent contacting the upper portion of the aquifer with increasing distance from the injection/withdrawal well. The dissolved oxygen concentration in H5-3o has been climbing since November 1995 and H5-3p concentrations have been increasing since March 1996.

Well H5-1B, which is located on the downgradient edge of the reduced zone, and the downgradient monitoring wells had increased levels of dissolved oxygen from March, 1996 through June, 1996. These increases are most likely associated with historically high Columbia River stage caused by heavy precipitation during the winter and spring of 1996, and the subsequent rise in the water-table beneath the 100-H Area. These abnormally high water-levels have increased dissolved oxygen levels in the upper part of the aquifer and may have altered the direction of the hydraulic

gradient at the site. The dissolved oxygen concentrations in the downgradient monitoring wells (H5-12, H5-13, H5-14) are lower than the upgradient concentrations (H5-15), but the downgradient concentrations were also lower before the experiment.

The dissolved oxygen electrodes used to measure concentrations in the field have been significantly below saturation concentrations even before the injection/withdrawal experiment. Since April 1996, the concentrations measured with these probes were compared against dissolved oxygen concentrations measured with a Hach DR/2000 Spectrophotometer (both high and low range methods). This comparison showed that the electrodes yielded lower concentrations in the higher ranges (above 2 ppm) by a constant bias of 2 ppm than the Hach method, but the measurements were comparable in the low range (<1 ppm). New calibration procedures for the dissolved oxygen electrodes at saturation have yielded consistent measurements between the methods in the higher ranges of dissolved oxygen concentrations. Previous measurements of dissolved oxygen in the high ranges made with the electrodes have not been corrected. Other reasons for the low dissolved oxygen concentrations measured at the site may be due to effects from the relatively new wells at the site as was discussed in Section 6.6.

### 10.8.2 Chromium Monitoring

Total chromium concentrations before the experiment ranged from 46 to 71 ppb within the treatment zone (see Figure 10.19a and Table 6.5), but the downgradient monitoring wells had significantly lower concentrations (13 to 34 ppb). Following the injection/withdrawal experiment, total chromium concentrations have declined to below the detection limit of the analytical method (ICP/MS; 2 ppb) in wells located within the reduced zone (see Figure 10.19b and Tables 10.7 through 10.9). Hexavalent chromium concentrations within the reduced zone following the injection/withdrawal experiment are mostly below the detection limit of the field measurement method (8 ppb) as shown in Figure 10.20. The general trends seen in dissolved oxygen concentrations, as discussed in the previous section, are also seen in the chromium measurements at the site (compare Figures 10.17 and 10.18 with Figures 10.19 and 10.20). Hexavalent chromium was not analyzed in groundwater at the site before the field experiment, but the total chromium measurements after the experiment had similar concentrations and trends as the hexavalent chromium measurements. Chromium concentrations for two wells located on the upgradient edge of the reduced zone (H5-3p and H5-3o) have been increasing, with the well screened in the upper portion of the aquifer (H5-3o) in the range of the pre-experiment concentrations. These wells have shown similar trends in dissolved oxygen concentrations and are located within the portion of the aquifer expected to re-oxidize first. Well H5-3o has consistently had the highest chromium and hexavalent chromium concentrations at the site. This could be an indication of a higher chromium concentrations near the top of the aquifer because well H5-3o is screened only in the upper portion of the aquifer, while the upgradient and downgradient monitoring wells are screened across the entire aquifer thickness.

Hexavalent chromium concentrations in the upgradient monitoring well (H5-15) have been relatively constant during monitoring. Downgradient concentrations of hexavalent chromium are below the upgradient concentrations, but as noted above, the concentrations of total chromium in these wells were also lower before the experiment.

### 10.8.3 pH and Conductivity Monitoring

The pH and conductivity measured in the wells at the site are shown for the sampling events at the end of the injection/withdrawal experiment and for the latest sampling event in Figure 10.15. Appendix H contains plots of the pH and conductivity measurements for all site monitoring wells during post-experiment monitoring.

The pH before the experiment ranged from 7.4 to 7.8 at the 100-H Area ISRM site. At the end of the injection/withdrawal experiment (September 12, 1995) the pH ranged from 9.66 to 8.1 in the reduced zone. Some of the highest values observed at that time (e.g., 9.66) were in the wells screened in the upper portion of the aquifer. These values substantially decreased to levels observed in other wells within the reduced zone by the next sampling event one week later (overall pH range of 7.68 to 9.37). The pH ranged from 7.7 to 8.9 in the wells within the reduced zone on September 12, 1996.

Baseline conductivity at the site ranged from 345 to 553  $\mu\text{S}/\text{cm}$ . Following the experiment, conductivity increased up to four times the baseline values in lower zone monitoring wells located within the reduced zone. The conductivity in wells screened within the upper portion of the aquifer were 10 times greater than the baseline values. These values declined to the levels of the other wells in the reduced zone by the next sampling event one week later (similar to the pH trend) and had returned to near baseline levels by about 7 months after the experiment. Most of the remaining wells within the reduced zone are 2 to 3 times the baseline levels by the latest sampling event (September 1996).

### 10.8.4 Trace Metals Analysis

During the post-experiment monitoring, three sets of groundwater samples from all the wells were collected and analyzed for trace metals by ICP/MS (January 23, May 7, and August 14, 1996) as shown in Tables 10.7 through 10.12. These analyses can be compared to the baseline samples collected before the field experiment as shown in Table 6.5. These tables also show the relevant MCLs for each metal analyzed. The samples collected for trace metal analysis were filtered and preserved with nitric acid at the site at the time of collection.

Relative to the baseline data, manganese and zinc concentrations within the reduced zone, following the experiment, were significantly elevated; however, levels of both of these metals have continued to decrease since the January sampling events. The wells with the highest concentrations in January still had the highest concentrations in May, indicating the elevated values could be a local effect; available data indicate there is no evidence of migration. Manganese exceeded the secondary drinking water standards of 50 ppb (EPA 1985) in 8 of the wells within the reduced zone for the January samples and 6 of the wells for the August samples; the two wells that no longer exceeded the drinking water standard in August monitored the upper portion of the aquifer. The baseline sampling and analysis before the field experiments indicated that two of the downgradient wells also exceeded the secondary drinking water standards for Manganese.

Sodium, potassium, and barium were slightly elevated above the baseline values. High concentrations of sodium and potassium were in the injection fluid as discussed in Section 10.4.1. Chromium (total and hexavalent) levels were significantly reduced below the baseline values within the reduced zone as discussed in the previous section.

The post-experiment trace metals concentrations in the upgradient and downgradient wells (see Tables 10.10, 10.11, and 10.12) were similar to the baseline values. Copper, zinc, and barium were

slightly elevated and manganese concentrations were lower in May than the baseline data before the experiment. Two of the wells in the baseline analysis (H5-12 and H5-13) were elevated in manganese, which may be due to sediment disturbance during drilling (i.e., crushed basalt). Chromium levels in H5-12 were below the ambient concentrations in the area in May, but this cannot be attributed to a downgradient effect because the baseline concentration of chromium was also low in this well. Similarly, dissolved oxygen concentrations have been consistently below saturated values for H5-12 but the baseline dissolved oxygen concentrations in this well were also low. Thus, no downgradient effects, either positive or negative, from the reduced zone has been conclusively observed after nine months of monitoring.

In addition to trace metals, sulfate and sulfite were analyzed in groundwater samples by ion chromatography as shown in Tables 10.8, through 10.12. Sulfite concentrations were much lower than sulfate at the site. Sulfite concentrations within the reduced zone were at the low levels measured in the upgradient and downgradient wells. The range of sulfate concentrations in the reduced zone ranged from 54 to 556 ppm. Nine of the wells within the reduced zone exceeded the secondary drinking water standard of 250 ppm for sulfate. The highest concentrations of sulfate were located within the reduced zone along the downgradient direction (H5-10, H5-11, H5-1B). This provides some evidence of the migration of the residual sulfate plume (unrecovered from the withdrawal phase) in the estimated gradient direction at the site. Sulfate concentrations in the wells screened in the upper portion of the aquifer within the reduced zone were similar to the upgradient and downgradient monitoring well concentrations outside the zone.

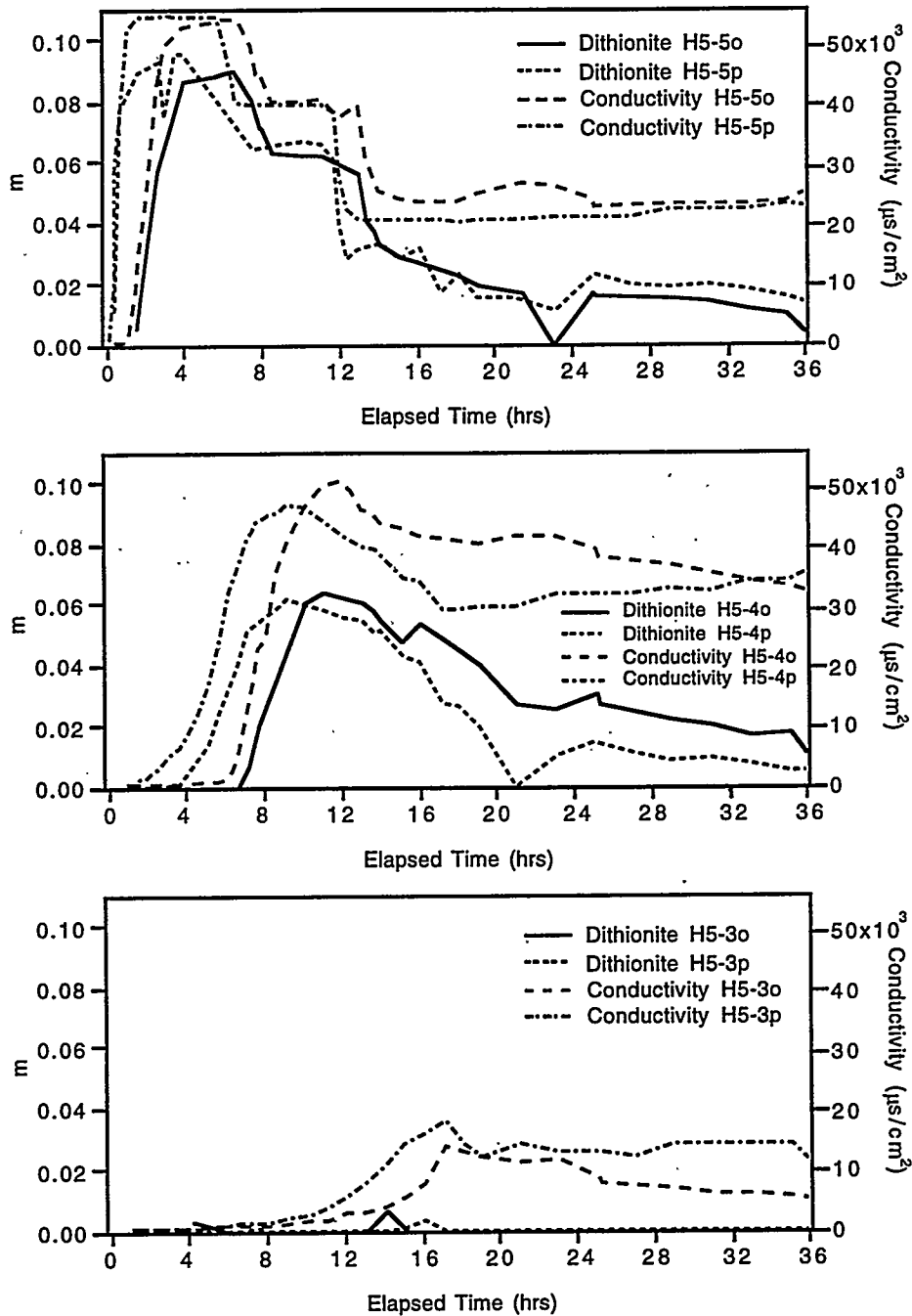
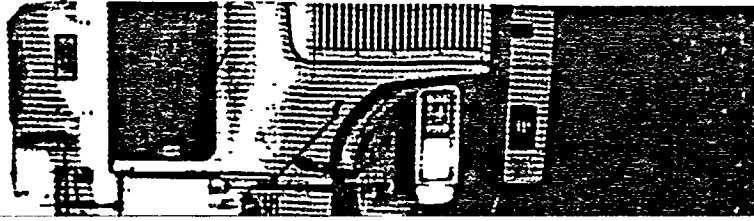
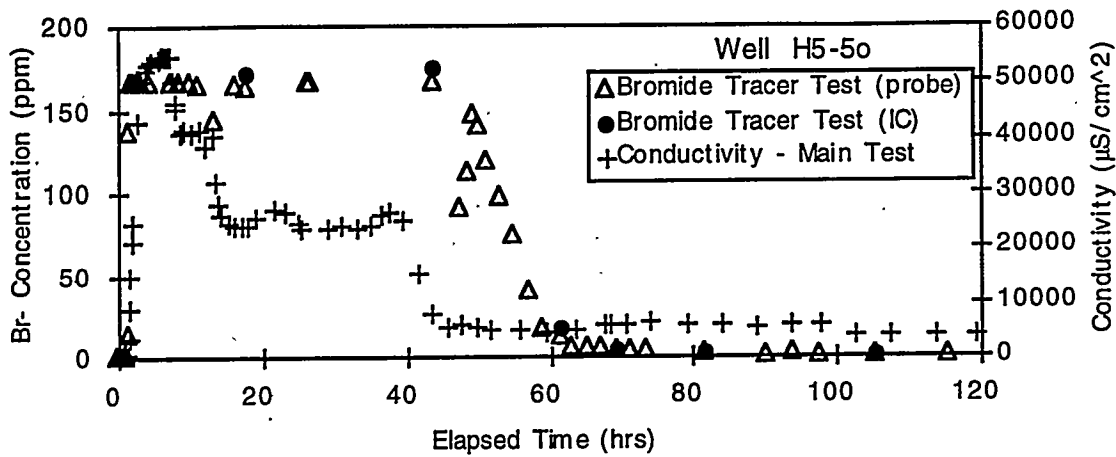
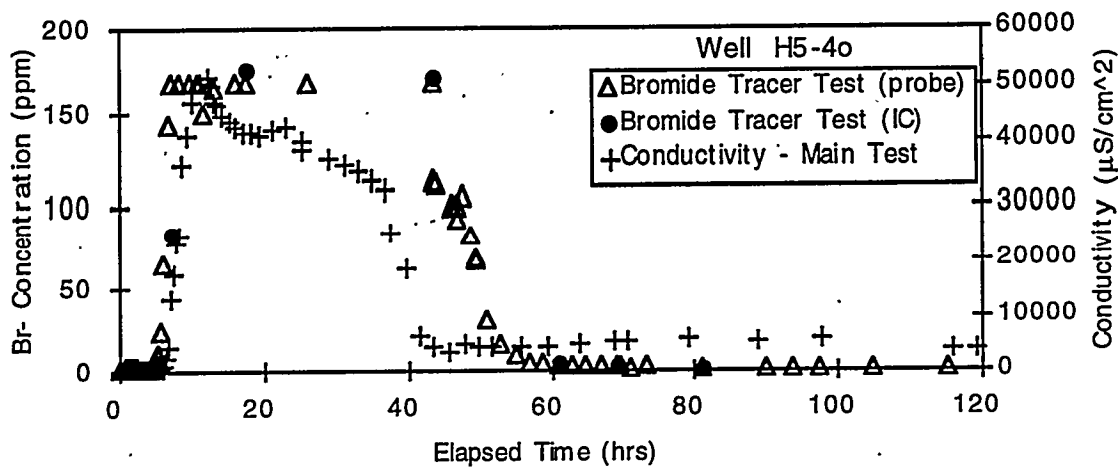


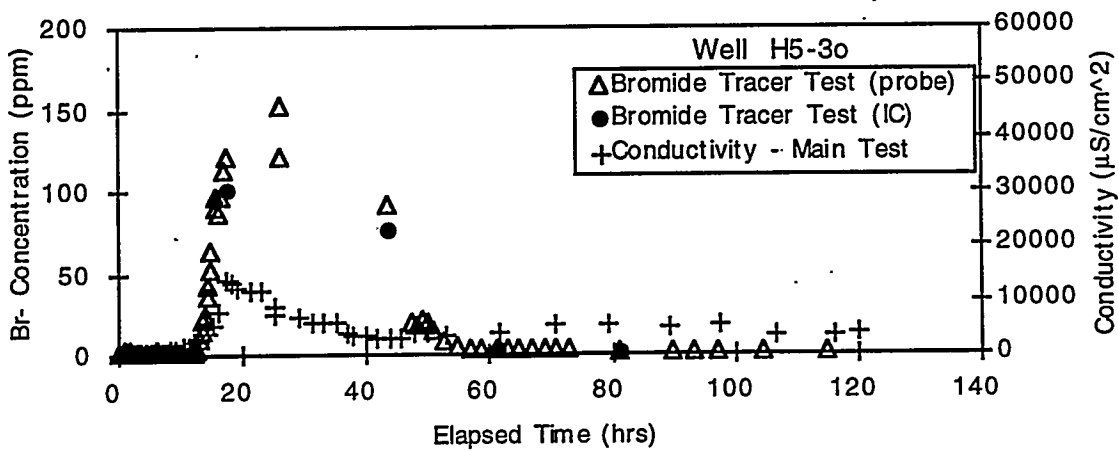
**Figure 10.3.** Dithionite and Conductivity Measurements along the Transect with the Upper (o) and Lower (p) Monitoring Wells During the Injection, Residence, and Early Withdrawal Phases.



(a)



(b)



(c)

Figure 10.4. Comparison of Bromide Concentrations from the Tracer Test with Conductivity Concentrations from the Main Dithionite Injection/Withdrawal Test for the Upper Zone Monitoring Wells

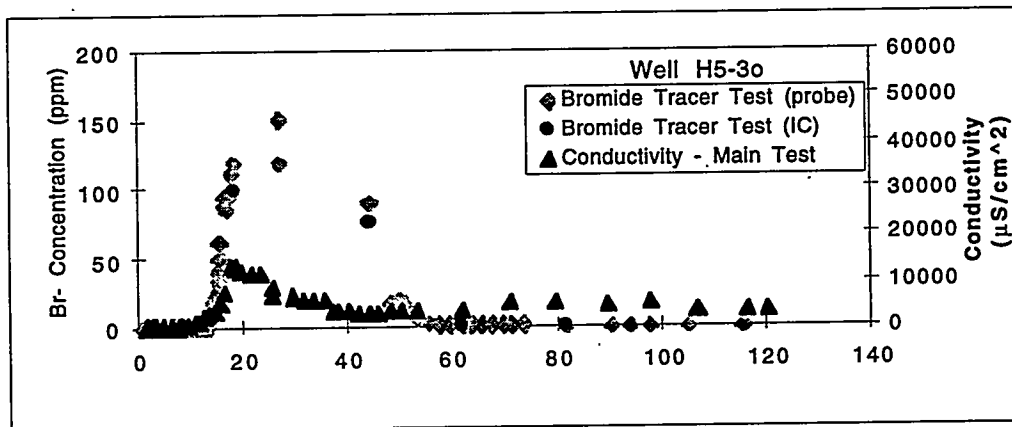
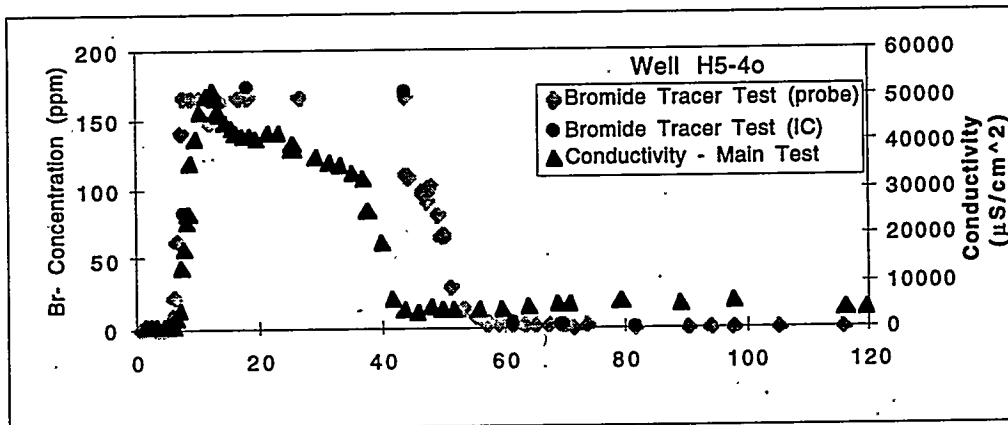
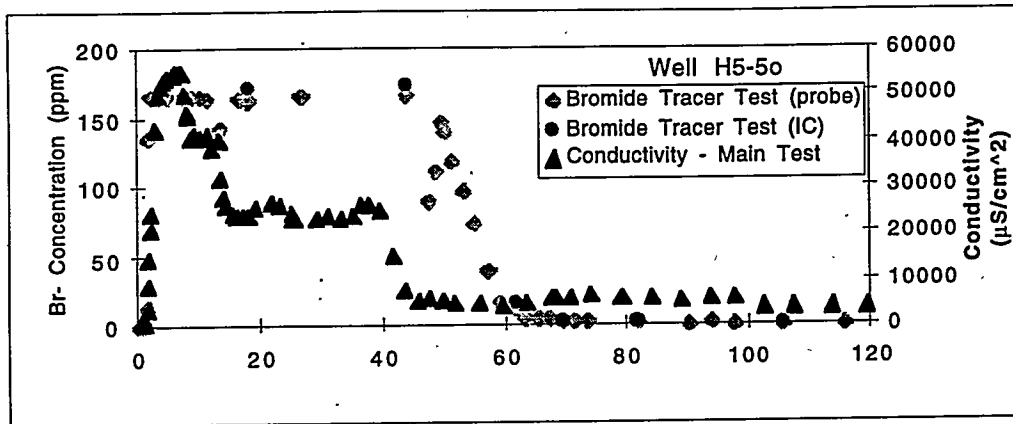


Figure 10.5. Comparison of Bromide Concentrations from the Tracer Test with Conductivity Concentrations from the Main Dithionite Injection/Withdrawal Test for the Lower Zone Monitoring Wells Corresponding to the Upper Zone Wells in Figure 10.

slightly elevated and manganese concentrations were lower in May than the baseline data before the experiment. Two of the wells in the baseline analysis (H5-12 and H5-13) were elevated in manganese, which may be due to sediment disturbance during drilling (i.e., crushed basalt). Chromium levels in H5-12 were below the ambient concentrations in the area in May, but this cannot be attributed to a downgradient effect because the baseline concentration of chromium was also low in this well. Similarly, dissolved oxygen concentrations have been consistently below saturated values for H5-12 but the baseline dissolved oxygen concentrations in this well were also low. Thus, no downgradient effects, either positive or negative, from the reduced zone has been conclusively observed after nine months of monitoring.

In addition to trace metals, sulfate and sulfite were analyzed in groundwater samples by ion chromatography as shown in Tables 10.8, through 10.12. Sulfite concentrations were much lower than sulfate at the site. Sulfite concentrations within the reduced zone were at the low levels measured in the upgradient and downgradient wells. The range of sulfate concentrations in the reduced zone ranged from 54 to 556 ppm. Nine of the wells within the reduced zone exceeded the secondary drinking water standard of 250 ppm for sulfate. The highest concentrations of sulfate were located within the reduced zone along the downgradient direction (H5-10, H5-11, H5-1B). This provides some evidence of the migration of the residual sulfate plume (unrecovered from the withdrawal phase) in the estimated gradient direction at the site. Sulfate concentrations in the wells screened in the upper portion of the aquifer within the reduced zone were similar to the upgradient and downgradient monitoring well concentrations outside the zone.

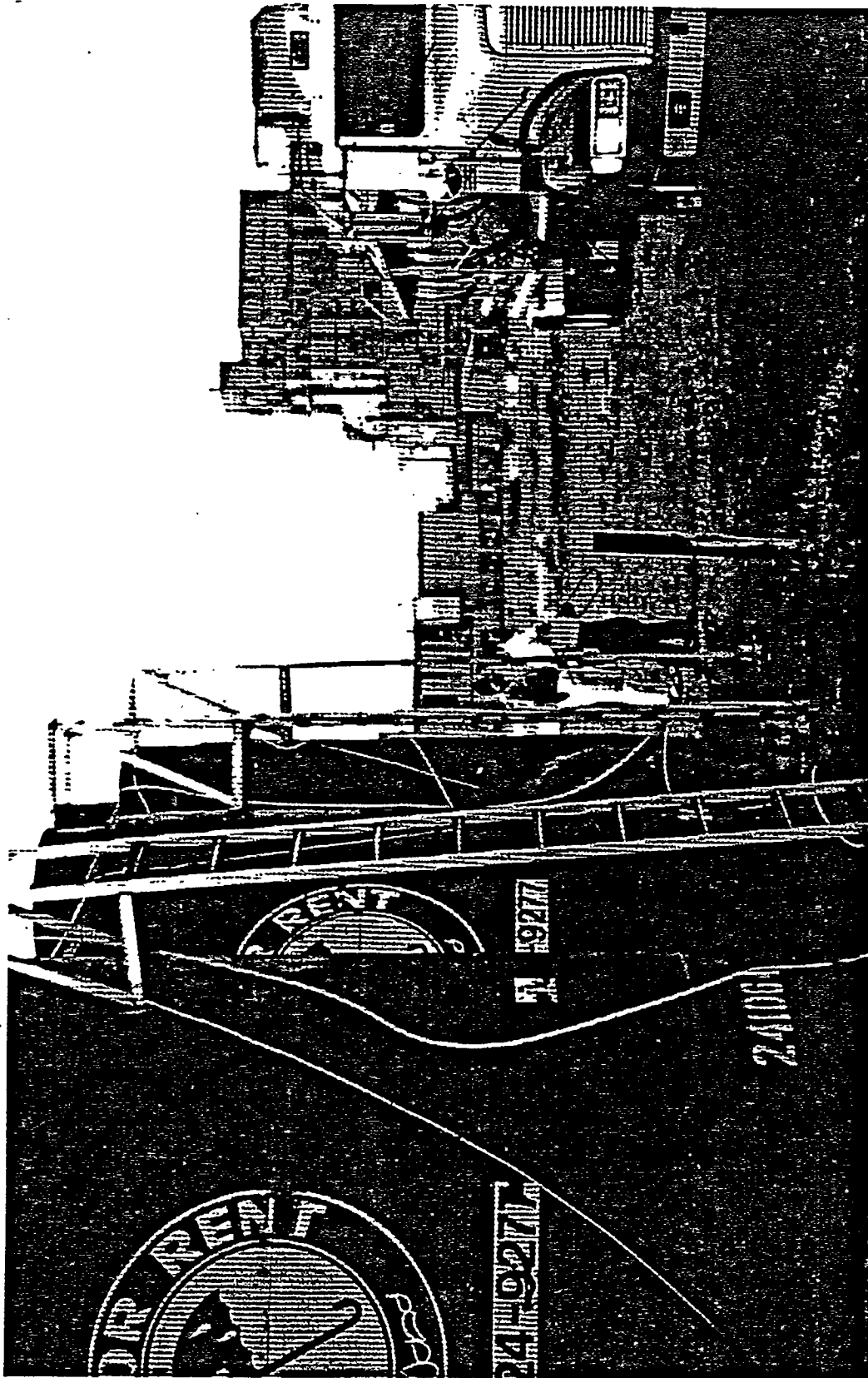


Figure 10.1. Photograph of Dithionite Delivery Truck and 7000-Gal Injection Tanks

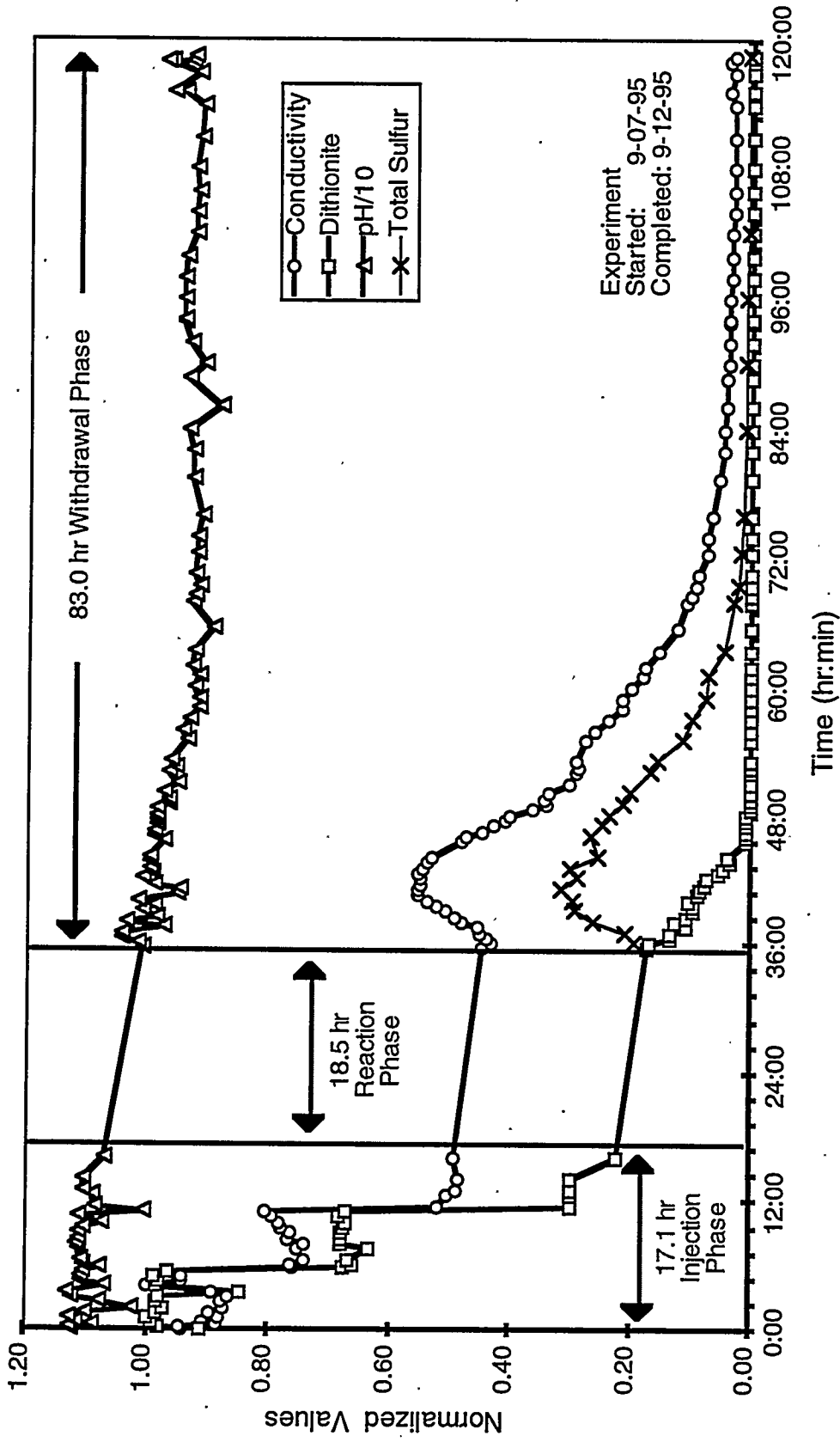
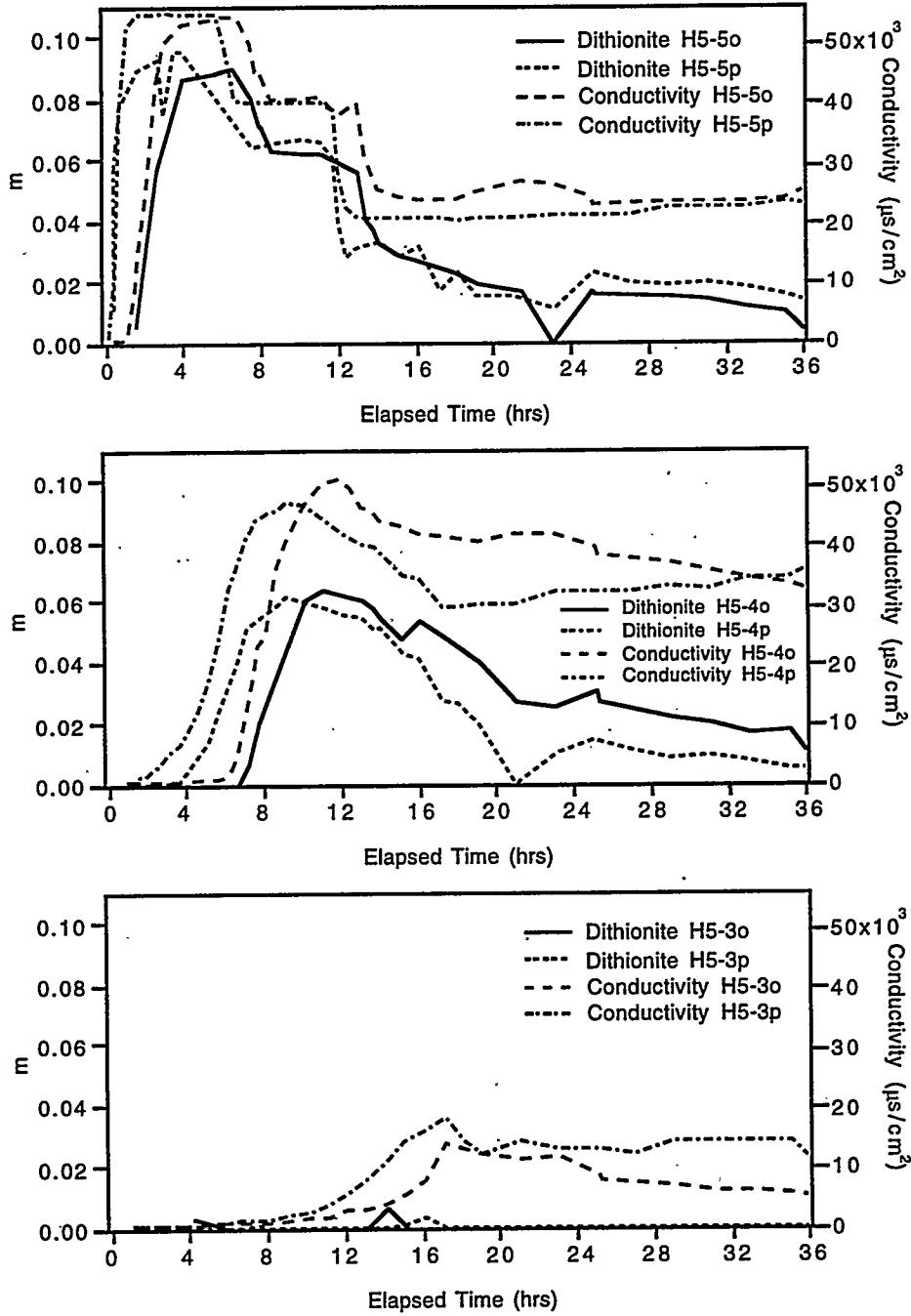
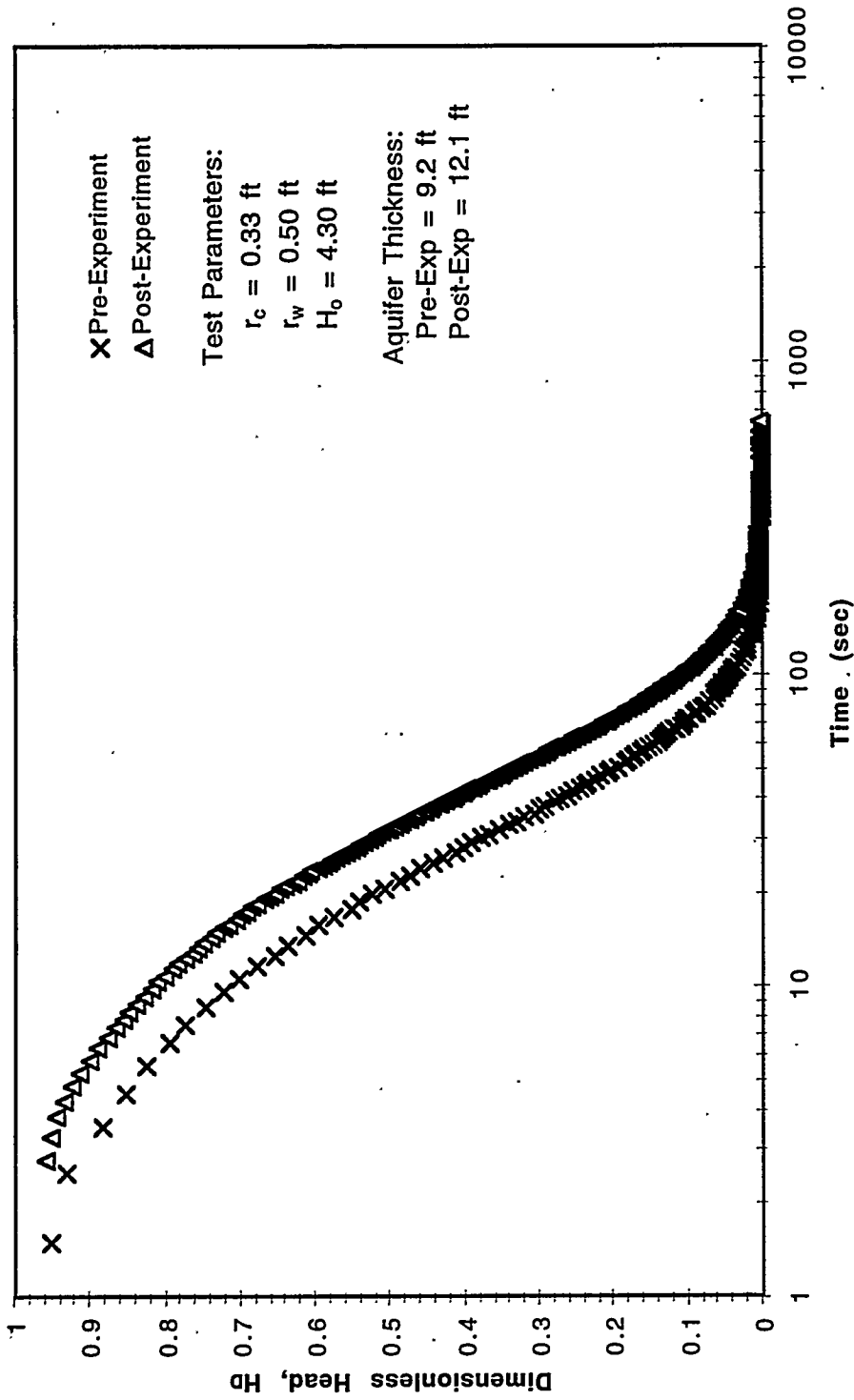


Figure 10.2. Field Parameters Measured for the Injection/Withdrawal Well (H5-2) during all the phases of the 100-H Area ISRM Field Experiment



**Figure 10.3.** Dithionite and Conductivity Measurements along the Transect with the Upper (o) and Lower (p) Monitoring Wells During the Injection, Residence, and Early Withdrawal Phases.



**Figure 10.6.** Comparison of the Observed Pre- and Post-Experiment Slug Test Response Exhibited at Stress Well H5-2

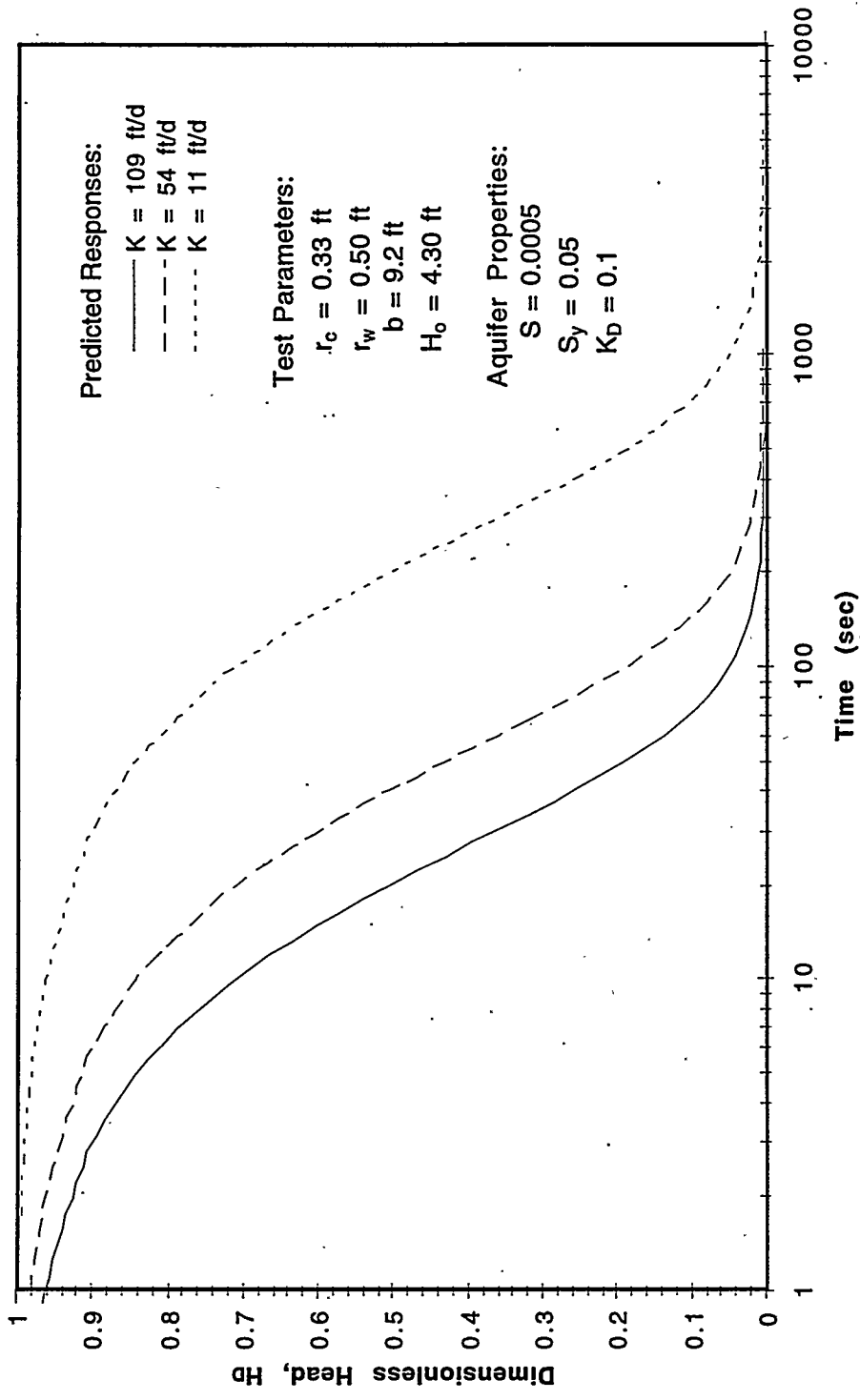


Figure 10.7. Predicted Slug Test Response at the Stress Well (H5-2) for Decreasing Values of Hydraulic Conductivity

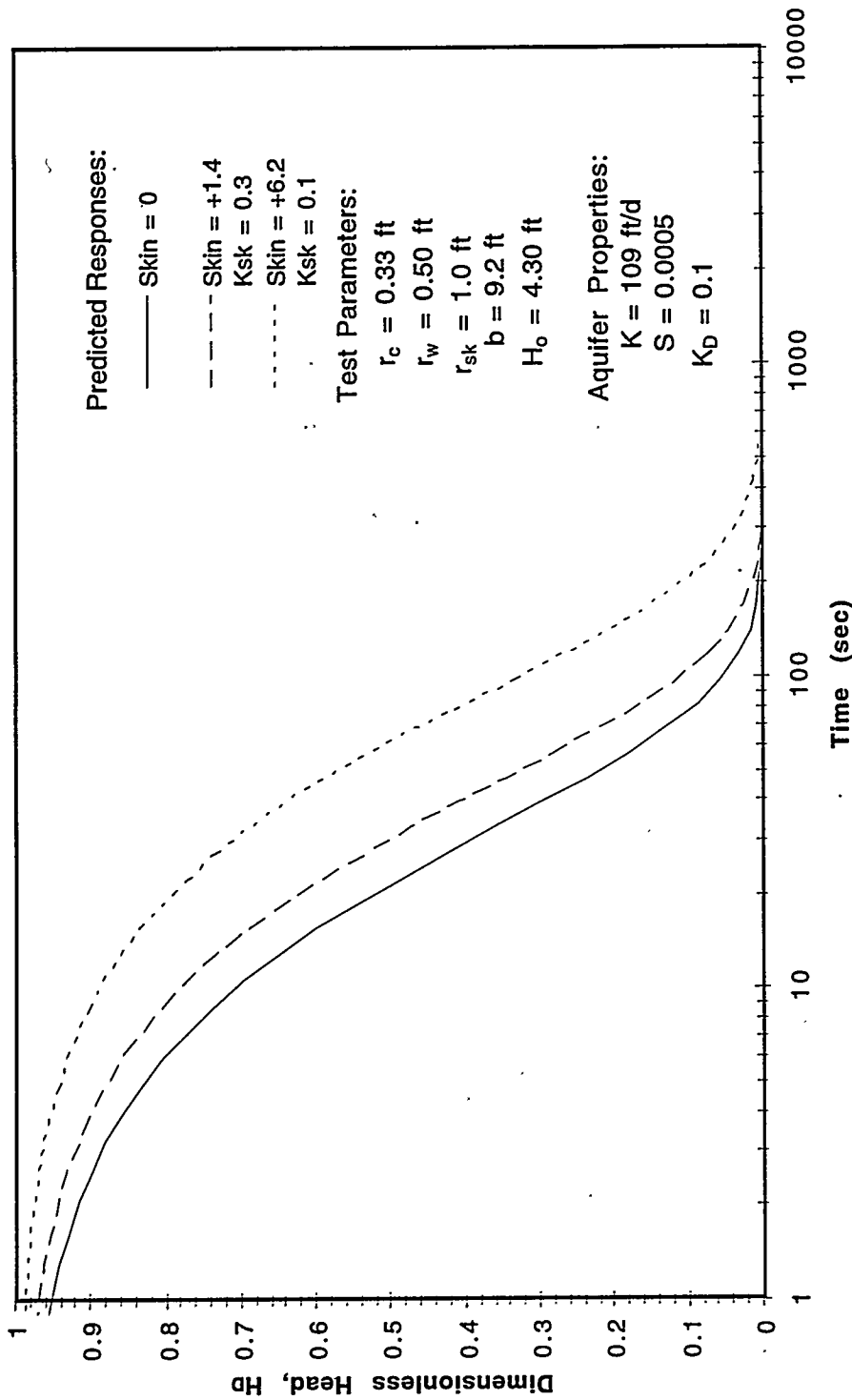


Figure 10.8. Predicted Slug Test Response at the Stress Well (H5-2) for Various Low-Permeability Skin Conditions

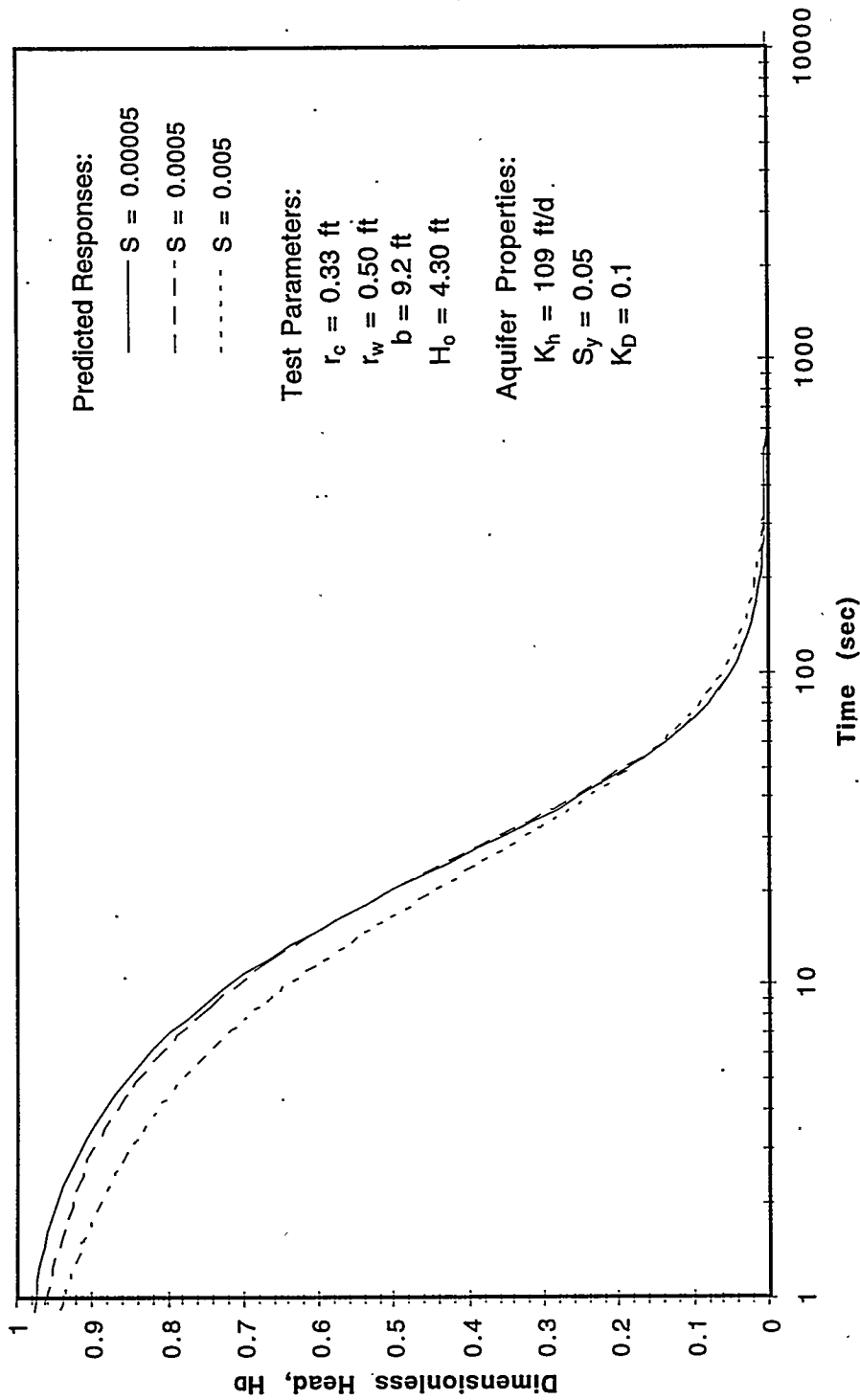


Figure 10.9. Predicted Slug Test Response at the Stress Well (H5-2) for Varying Values of Storativity

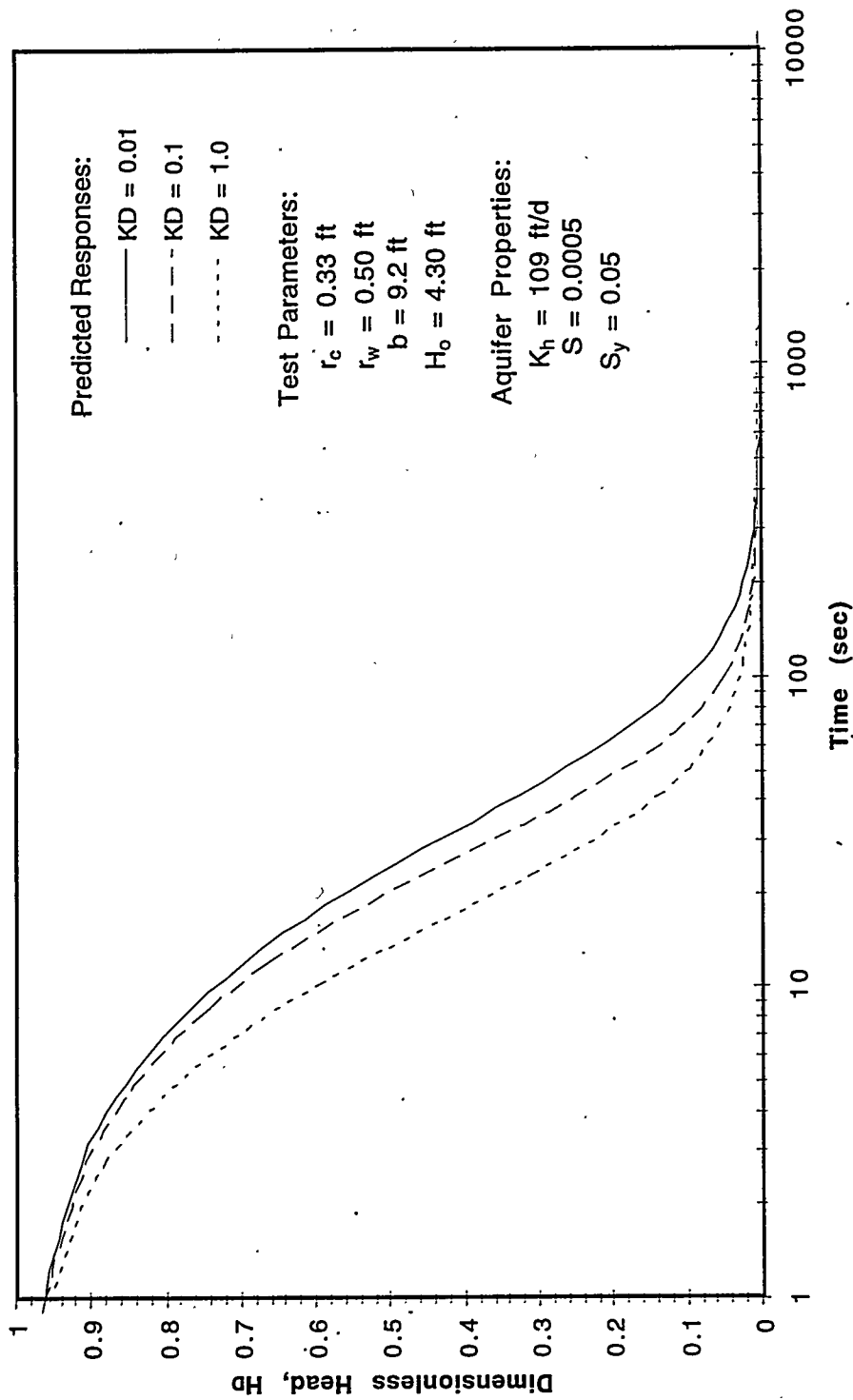


Figure 10.10. Predicted Slug Test Response at the Stress Well (H5-2) for Varying Values of Aquifer Vertical Anisotropy Ratio

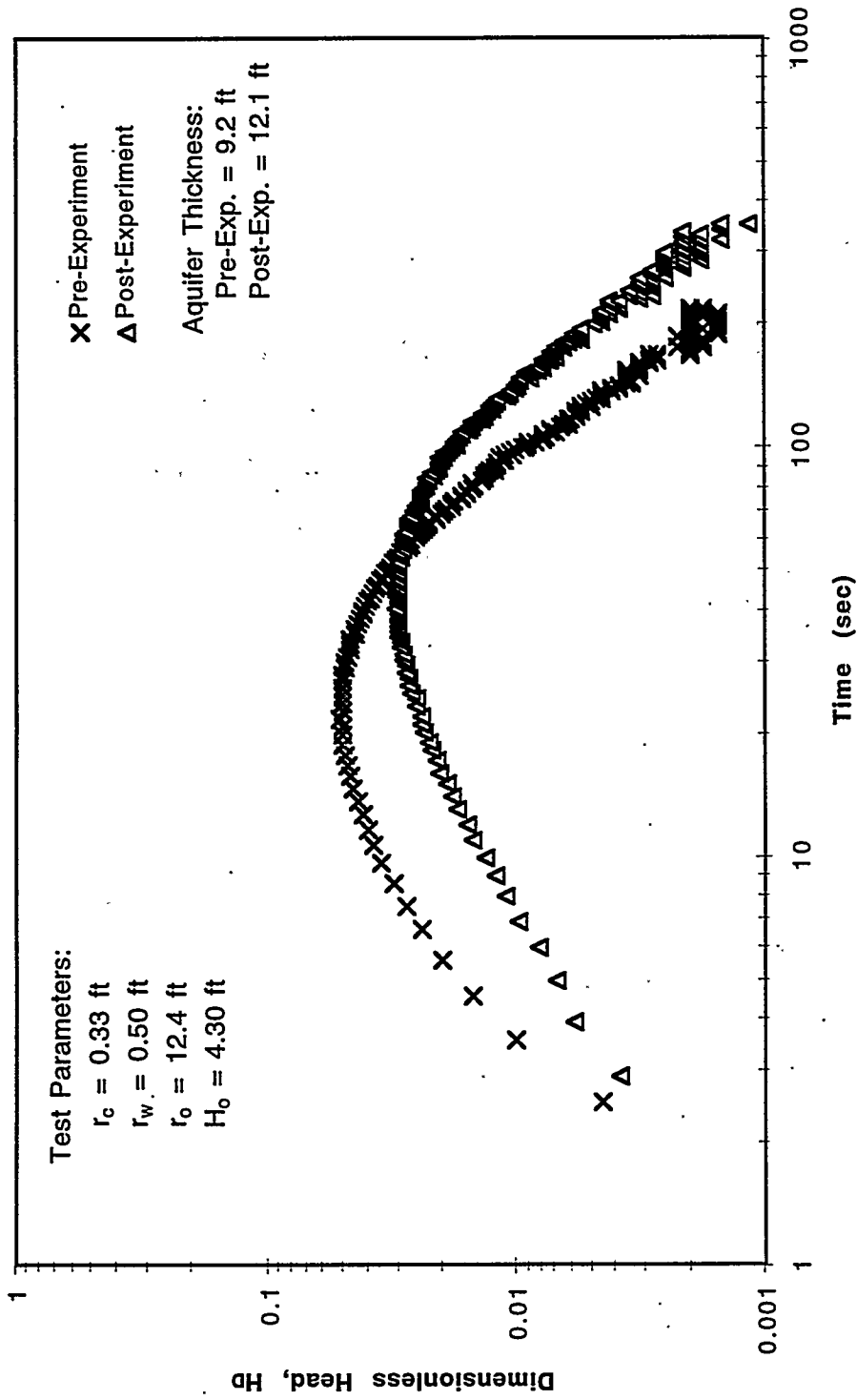


Figure 10.11. Comparison of the Observed Pre- and Post-Experiment Slug Interference Test Response Exhibited at Observation Well H5-4P

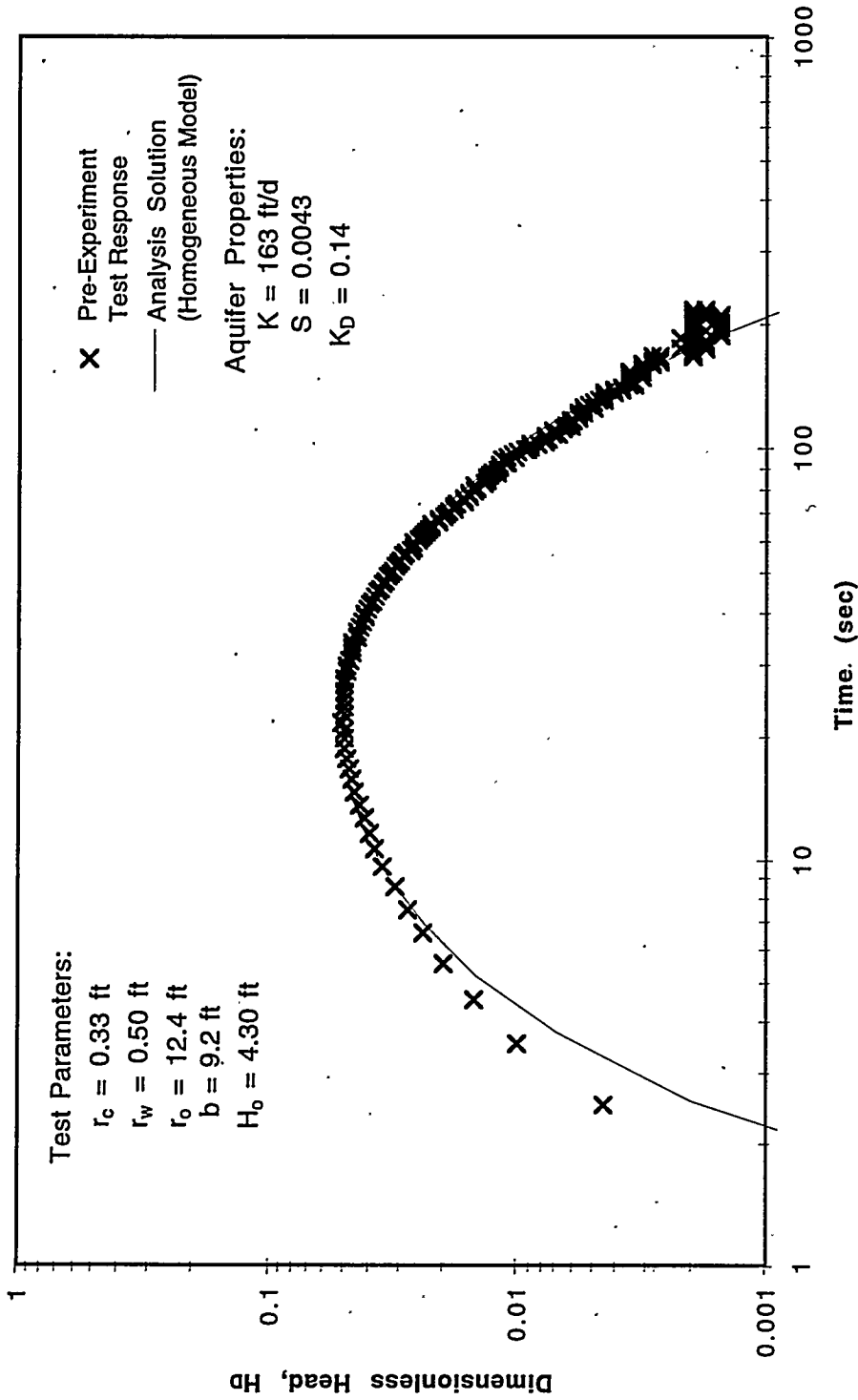


Figure 10.12. Analysis Results for the Pre-Experiment Slug Interference Test Responses at Observation Well H5-4P Using a Homogeneous Formation Model

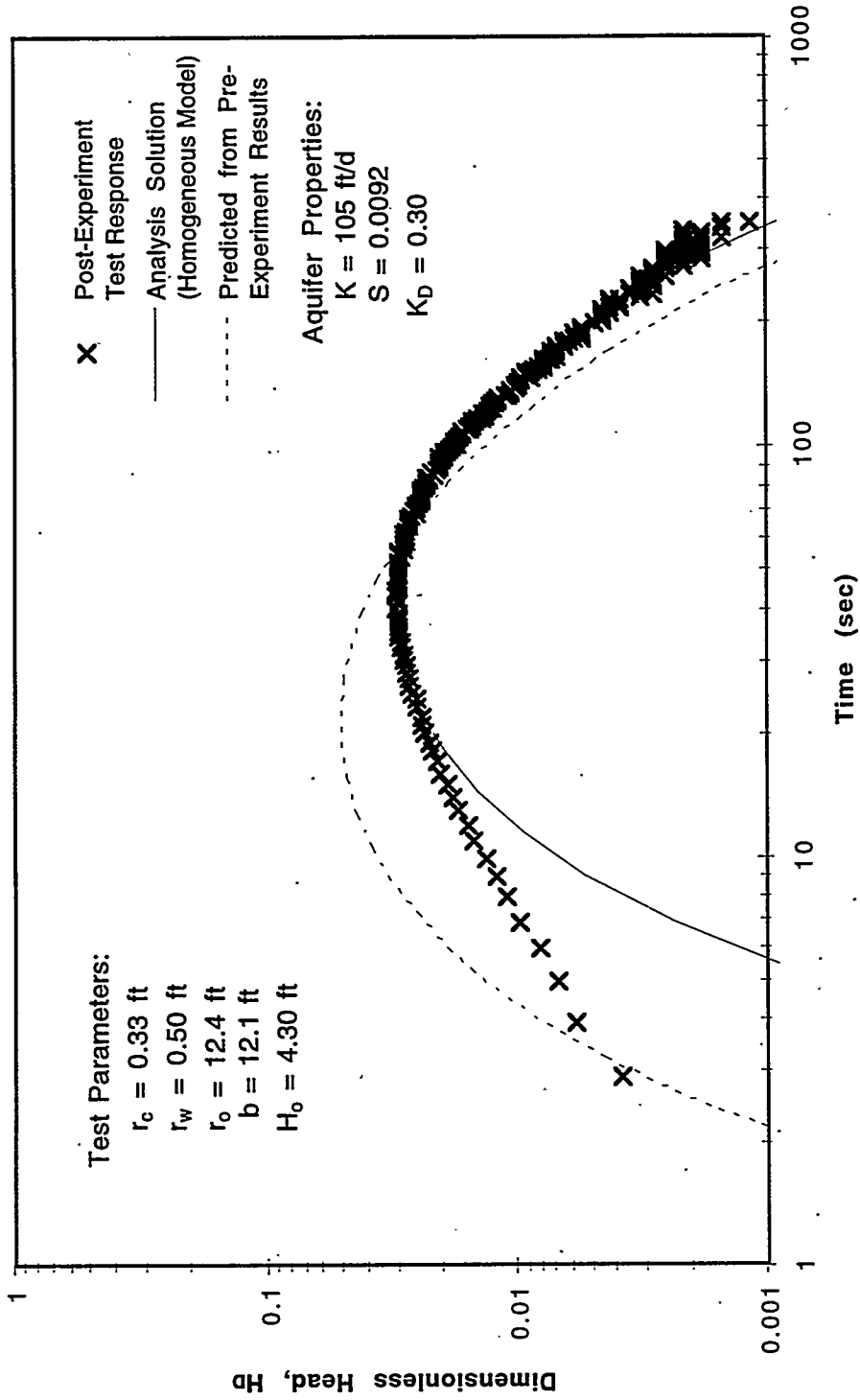
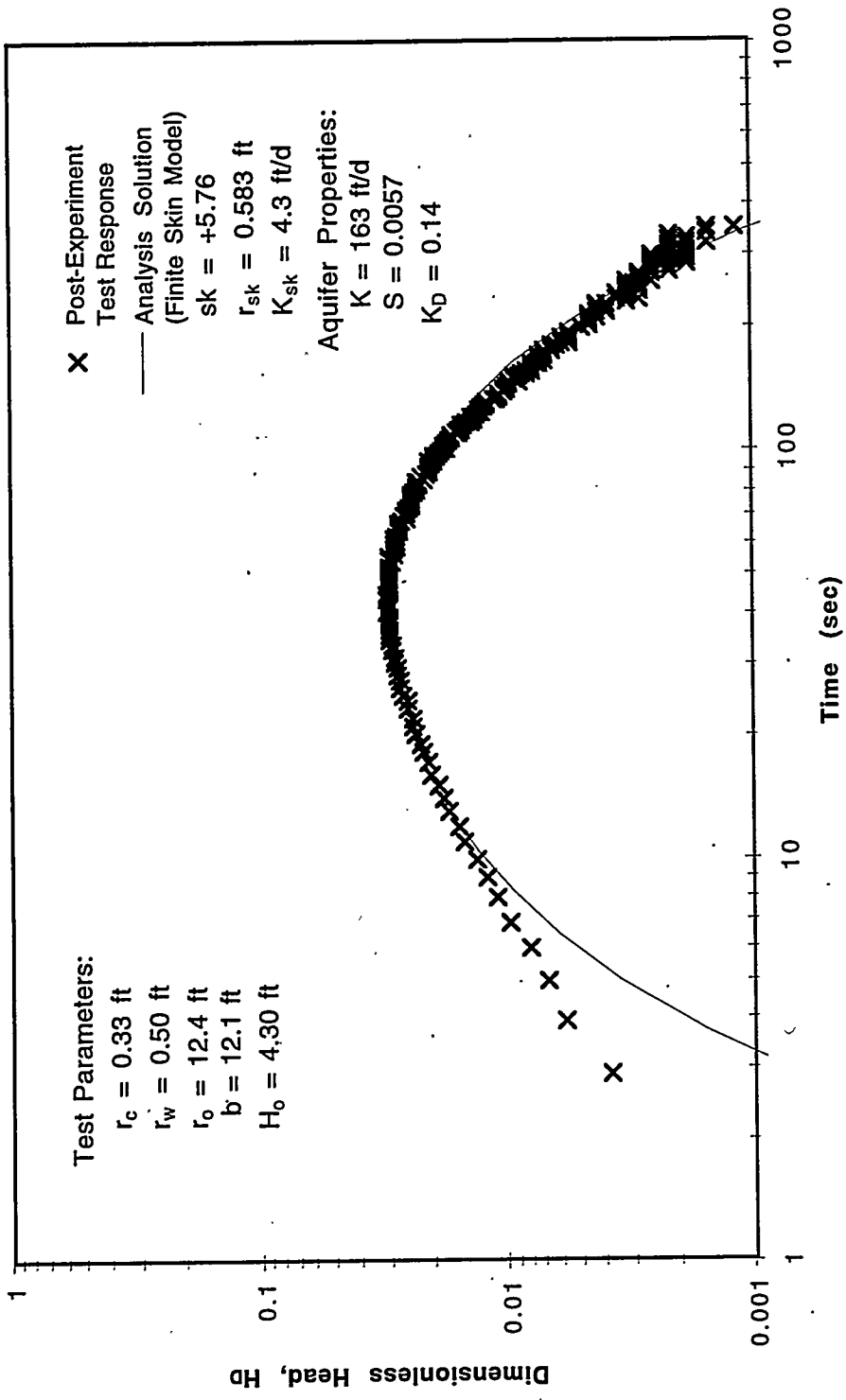
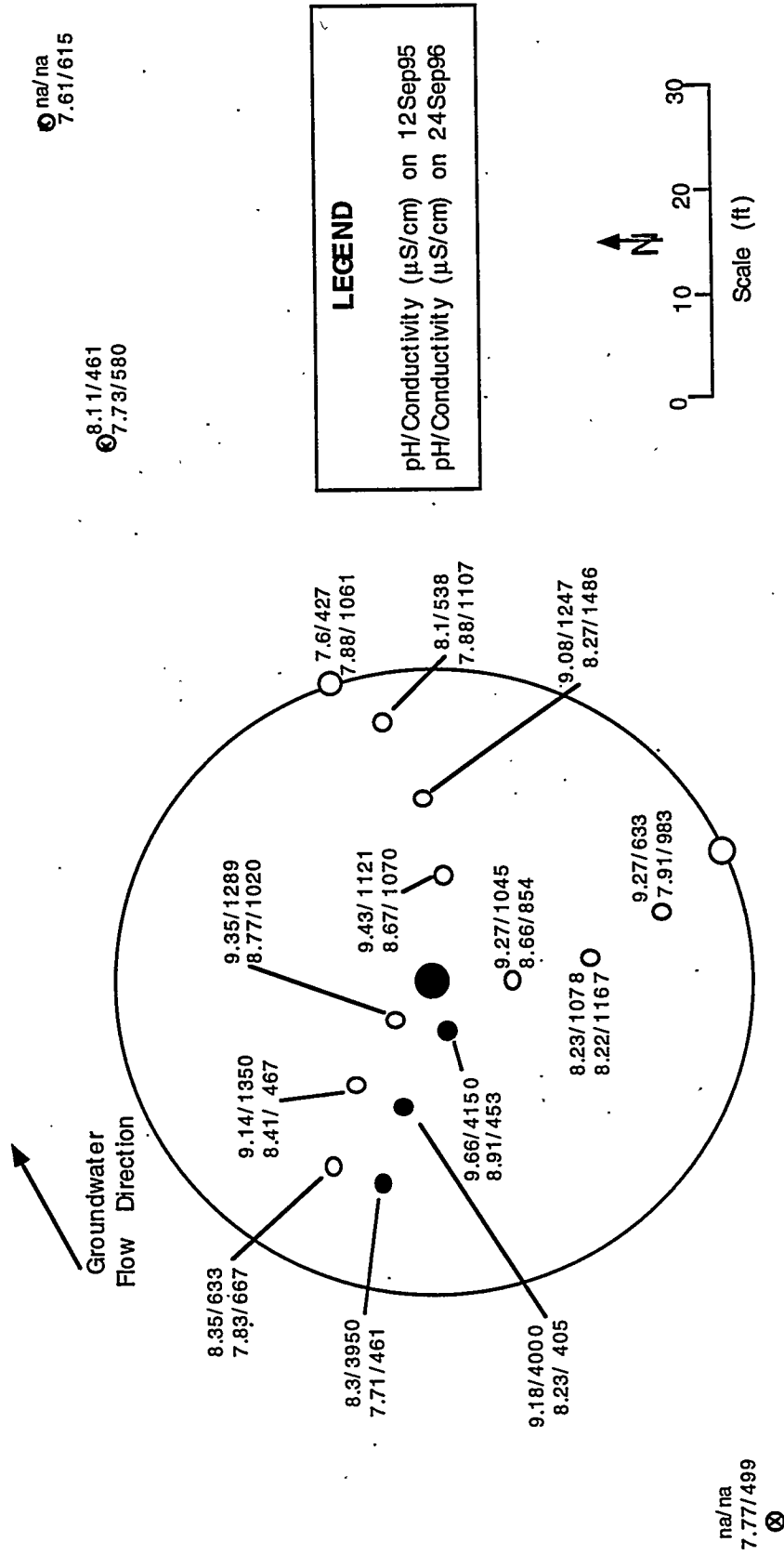


Figure 10.13. Analysis Results for the Post-Experiment Slug Interference Test Responses at Observation Well H5-4P Using a Homogeneous Formation Model



**Figure 10.14.** Analysis Results for the Post-Experiment Slug Interference Test Responses at Observation Well H5-4P Using a Finite-Skin (Composite Formation) Model

# In-Situ Redox Manipulation 100-H Area Site



**Figure 10.15.** Comparison of pH and Conductivity Measurements after the Injection/Withdrawal Experiment September 12, 1995 and June 5, 1996

# In-Situ Redox Manipulation 100-H Area Site

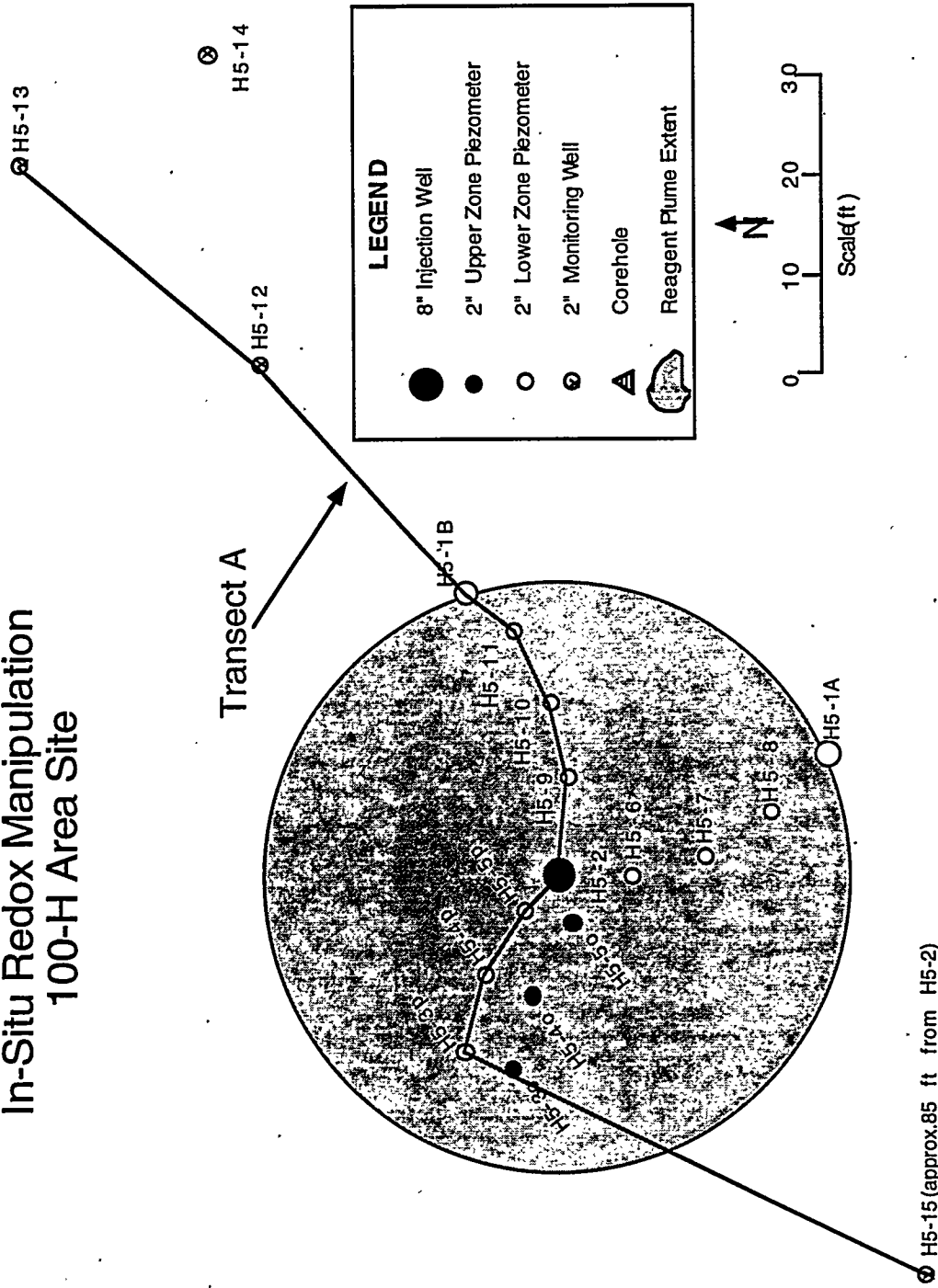
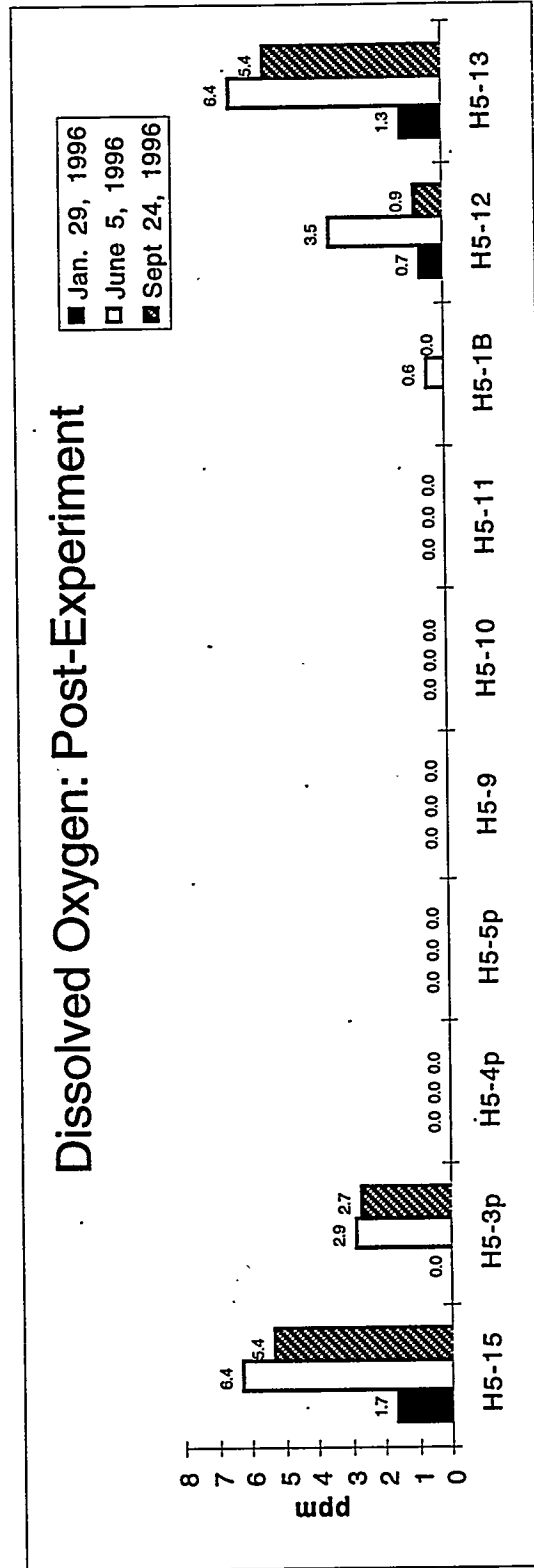
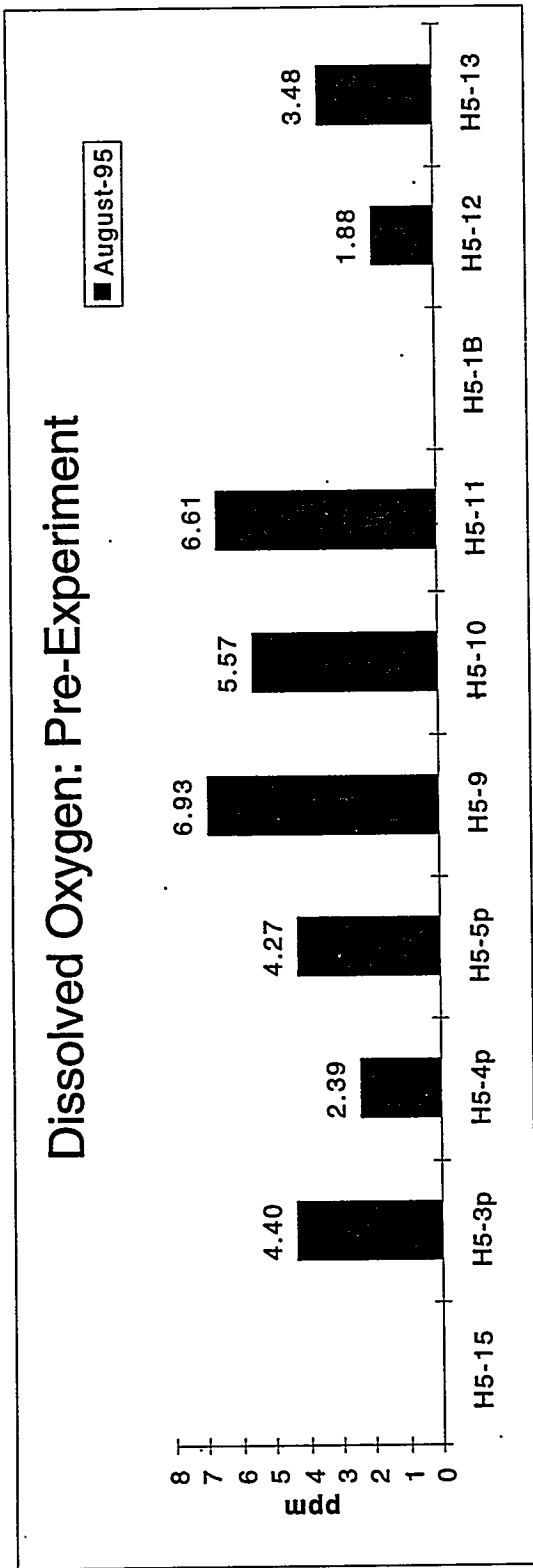


Figure 10.16. Locations of Wells along Transect A



**Figure 10.17.** Dissolved Oxygen Measurements along Transect A (as shown in Figure 10.16) Before (a) and After (b) the Injection/Withdrawal Experiment

# Dissolved Oxygen: Post-Experiment

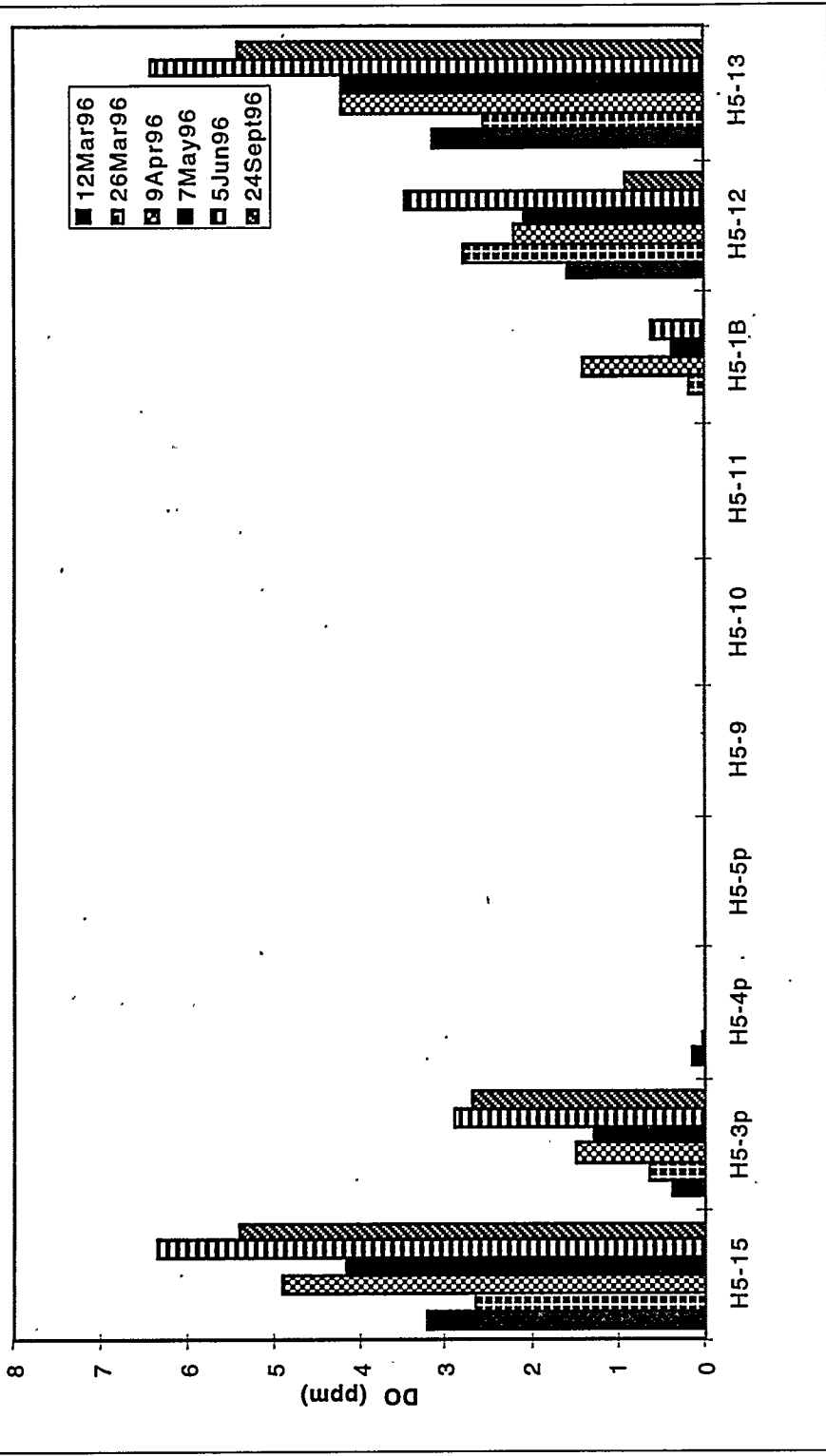
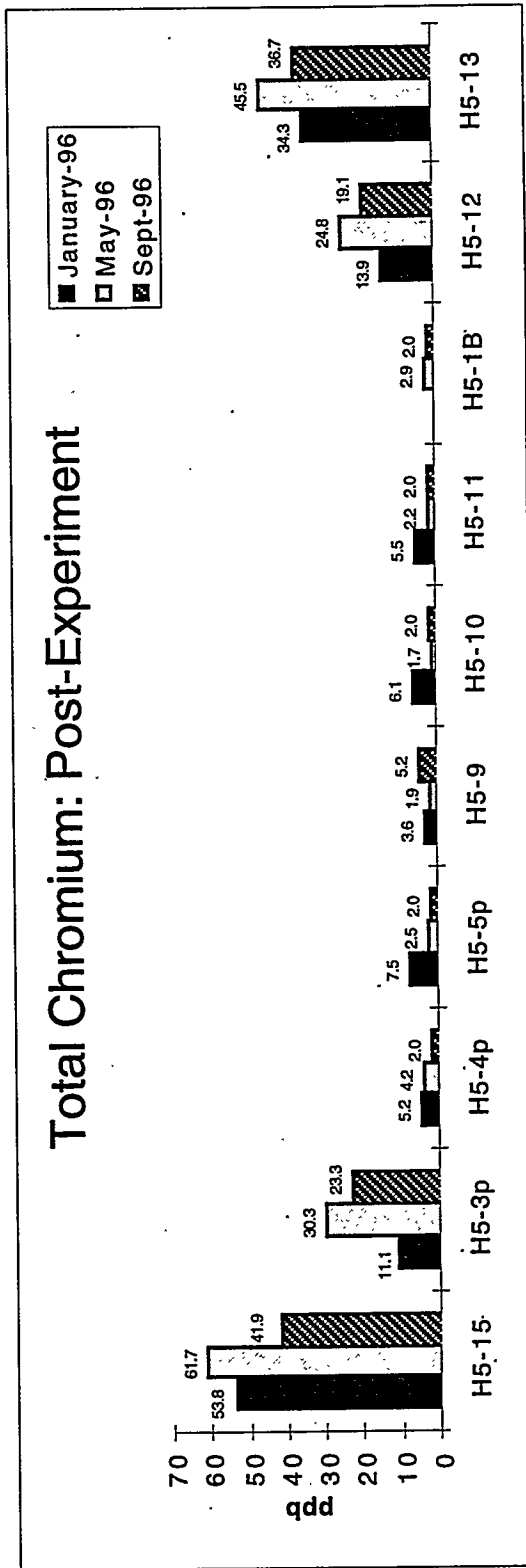
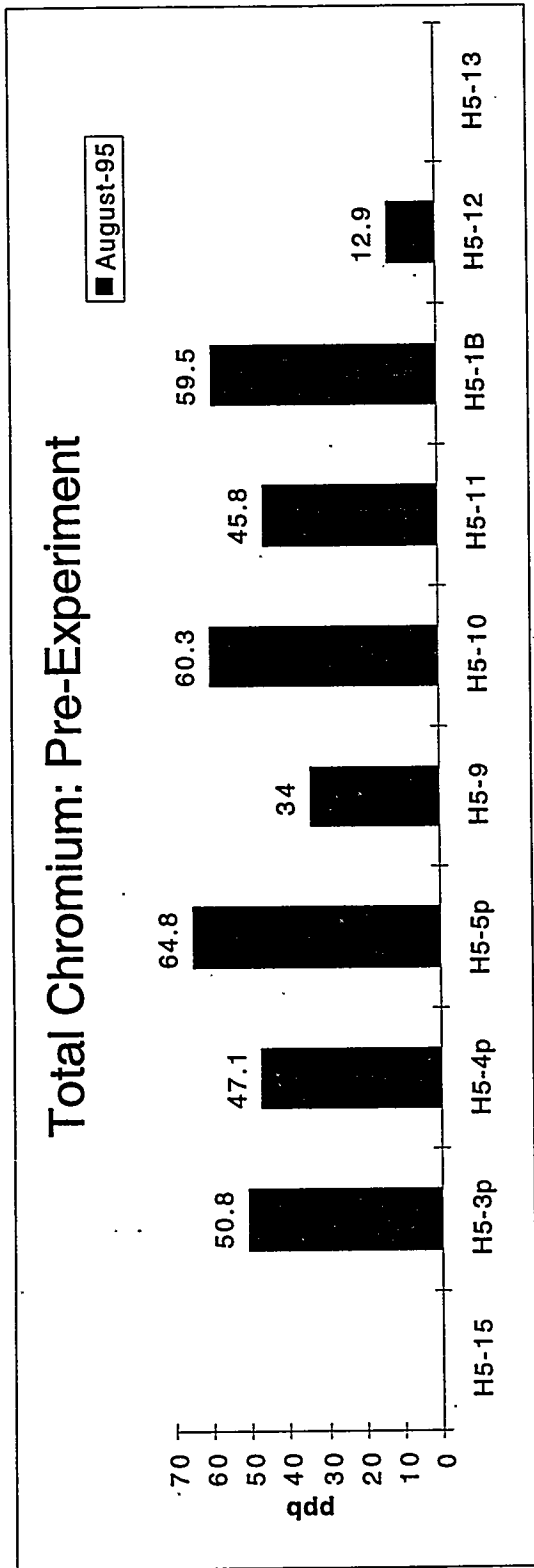


Figure 10.18. Dissolved Oxygen Measurements along Transect A (as shown in Figure 10-16) during the Post-Experiment Monitoring



**Figure 10.19.** Total Chromium along Transect A (as shown in Figure 10-16) Before (a) and After (b) the Injection/Withdrawal Experiment

# Hexavalent Chromium: Post-Experiment

Note: Detection limit = 8ppb.

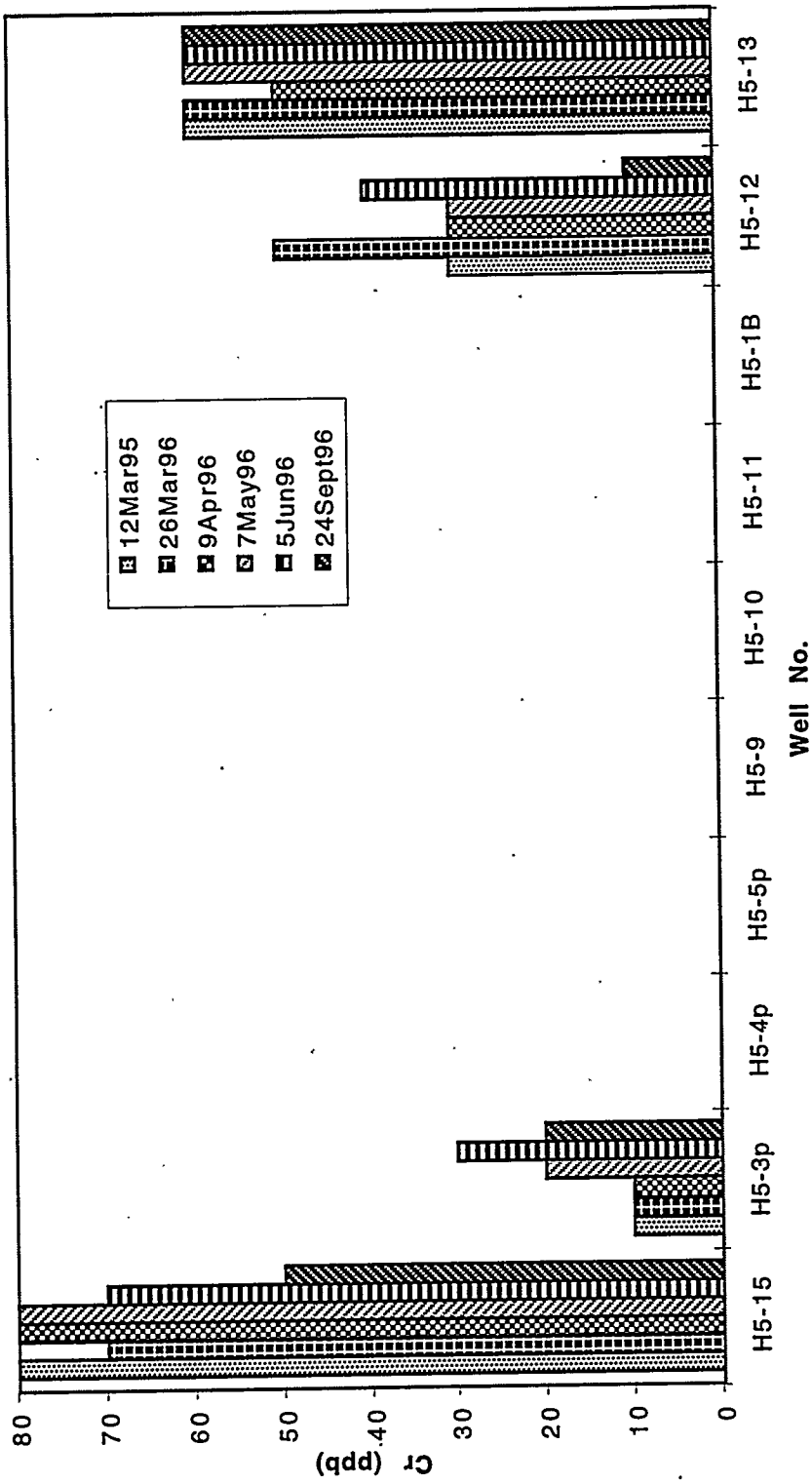


Figure 10.20. Hexavalent Chromium Measurements along Transect A (as shown in Figure 10-16) during the Post-Experiment Monitoring

**Table 10.1.** Summary of Peak Dithionite Concentrations and Conductivity During the Injection Phase of the 100-H Area ISRM Field Experiment

Well Number	Distance (ft)	Peak Dithionite(m)	% of Average	Peak Conductivity ( $\mu\text{s}/\text{cm}^2$ )	% of Maximum
H5-5p	5.0	0.10754	165.45	55400	100.00
H5-5o	5.0	0.10092	155.26	54500	98.38
H5-6	7.5	0.09342	143.73	53700	96.93
H5-9	10.0	0.10052	154.65	54900	99.10
H5-4p	12.5	0.06145	94.54	47600	85.92
H5-4o	12.5	0.06387	98.25	51400	92.78
H5-7	15.0	0.05904	90.83	42300	76.35
H5-10	17.5	0.02743	42.21	34000	61.37
H5-3p	20.0	0.00283	4.35	18300	33.03
H5-3o	20.0	0.00645	9.92	13700	24.73
H5-8	22.5	0.00770	11.84	23700	42.78
H5-11	25.0	0.00090	1.38	5150	9.30
H5-1B	30.0	0.00040	0.62	910	1.64

**Table 10.2. Final Modutank Concentrations Before to Purging to Ground**

Samples Collected on Tuesday, September 19, 1995

Sample #	Sulfite SO <sub>3</sub> ppm	Thiosulfate S <sub>2</sub> O <sub>3</sub> ppm	Sulfate SO <sub>4</sub> ppm	Total Sulfate (oxidized) ppm	Bromide Br ppm	Potassium K ppm	Chromium Cr ppb	Manganese Mn ppb	Zinc Zn ppb	Arsenic As ppb	Lead Pb ppb
1614 West Side	304	7.8	1760	2138	19	3020	88	13.9	293	76.1	3.8
1615 North Side	778	7.3	1150	2096	19	3000	54.5	14.1	194	84.7	2.29
1616 East Side	777	7.8	1160	2106	19.8	3280	57.8	13.9	240	73.4	2
1617 South Side	787	7.3	1160	2117	19.3	2750	58.3	14.6	196	79.2	1.48
Average	661.5	7.55	1307.5	2114	19.275	3012.5	64.65	14.125	230.75	78.35	2.3925
Purge Criteria	n/a	n/a	2500	2500 n/a	n/a	n/a	110	500	1100	480	32

**Table 10.3. Results from Reductive Capacity Analyses Using the O<sub>2</sub> Reoxidation Method for Core Samples Collected from the ISRM Treatment Zone**

Boring ID	Depth (ft)	Radial Distance (ft)	% of sample < 4.75 mm	Sample ORC (meq/kg)	Core ORC (meq/kg)	Pore Volumes of Treatment*	Barrier Life (years)**
B2618	39-40	4	79	9.9	7.8	63	9
B2618	42-43	4	37	12.6	4.7	38	5
B2618	46-47	4	51	42.7	21.9	176	24
B2618	48.5-49.5	4	43	6.5	2.8	22	3
B2620	42-43	10	79	1.0	0.8	6	1
B2620	47-48	10	34	10.0	3.4	28	4
B2620	49-50	10	30	32.5	9.8	78	11
B2621	49-50	19	29	10.7	3.1	25	3
B2624	41-42	21	79	13.9	11.0	88	12
B2624	44-45	21	42	25.1	10.6	85	12
B2624	48-49	21	38	21.0	8.0	64	9
B2624	47-48 (int)	21	60	17.9	10.7	86	12
B2624	47-48 (ext)	21	60	13.8	8.3	66	9
B2625	47.5-48.5	27	21	1.3	0.3	2	0

\* Assumes: bulk density = 1.9 g/cm<sup>3</sup>; eff. porosity = 20%; 9ppm dissolved oxygen; 1ppm hexavalent Cr

\*\* Assumes: 50 ft wide treatment zone; groundwater velocity = .1 ft/d

**Table 10.4. Results from the Comparison of Field Experiment Achieved Reductive Capacity to Maximum Achievable Reductive Capacity**

Boring ID	Depth (ft)	Radial Distance (ft)	% of sample < 4.75 mm	Sample ORC (meq/kg)	Max. Sample ORC (meq/kg)	% of Available Fe(III) Reduced
B2618	39-40	4	79	9.9	23.4	42
B2618	42-43	4	37	12.6	22.4	56
B2618	46-47	4	51	42.7	39.1	100
B2618	48.5-49.5	4	43	6.5	35.9	18
B2620	42-43	10	79	1.0	18.5	5
B2620	47-48	10	34	10.0	19.6	51
B2620	49-50	10	30	32.5	32.4	100
B2621	49-50	19	29	10.7	17.8	60
B2624	41-42	21	79	13.9	39.8	35
B2624	44-45	21	42	25.1	32.9	76
B2624	48-49	21	38	21.0	37.1	57
B2624	47-48 (int)	21	60	17.9	21.5	83
B2624	47-48 (ext)	21	60	13.8	35.9	38
B2625	47.5-48.5	27	21	1.3	16.5	8

**Table 10.5.** Identification of Samples Used for Chromium Reduction Capacity Experiment

<b>Sample Number</b>	<b>Borehole ID</b>	<b>Sample Depth (ft)</b>
Sample 1	B2618	48.5-49.5
Sample 2	B2618	42-43
Sample 4	B2618	46-47
Sample 4-2	B2620	49-50

**Table 10.6. Microbiological Characterization Summary (after 42 days incubation)**

Core hole ID	Sample Interval (m) (ft)		Lithology	CFU/g sediment
B2618	12.5 - 12.8	41 - 42	Sandy Gravel <sup>(a)</sup>	5.00 x 10 <sup>2</sup>
B2618	13.4 - 13.7	44 - 45	Sandy Gravel	5.40 x 10 <sup>3</sup> 3.50 x 10 <sup>3</sup>
B2621	14.3	47.0	Sand	2.65 x 10 <sup>3</sup> 2.00 x 10 <sup>3</sup>
B2621	14.6	48.0	Sandy Gravel	1.10 x 10 <sup>4</sup> 1.85 x 10 <sup>4</sup>
B2623	13.1 - 13.4	43 - 44	Sandy Gravel	0
B2623	14.8 - 15.1	48.5 - 49.5	Sandy Gravel	1.01 x 10 <sup>4</sup> 1.30 x 10 <sup>4</sup>
B2624	14.9 - 15.2	49 - 50	Sandy gravel	7.95 x 10 <sup>3</sup> 8.00 x 10 <sup>3</sup>
<p>CFU = colony forming unit.                      (a) *Core sediment grain sizes were not representative - probably are decreased due to drilling effects.</p>				

**Table 10.7. Trace Metals for Wells Within the Reduced Zone in January 1996 Measured by ICP/MS**

Constituent	MCL (ppb)	Sample Location													
		H5-2	H5-3"O"	H5-3"P"	H5-4"O"	H5-4P	H5-5"O"	H5-5"P"	H5-5"P" Dup	H5-6	H5-7	H5-8	H5-9	H5-10	H5-11
Na	none	49,800	21,300	38,600	25,700	34,300	28,500	71,600	70,300	65,800	64,400	45,700	64,100	82,300	38,500
Mg	none	2,300	10,500	17,500	8,580	7,460	2,660	6,200	6,140	6,000	15,100	23,800	7,120	13,000	26,400
Si	none	5,800	13,100	11,500	10,000	5,310	6,580	6,150	6,310	7,560	9,860	11,300	5,930	10,800	12,100
K	none	294,000	7,700	23,000	83,100	153,000	155,000	248,000	246,000	195,000	175,000	71,900	232,000	221,000	24,100
Al	50 to 200*	28.1	9.29	8.46	10±2	7.98	13.8	170	182	11.3	19.4	21.6	13.6	7.14	28.1
Mn	50*	6.80	118	*394	67.2	195	9.63	25.4	22.4	26.1	145	*542	21.0	95.0	*436
Fe	300*	<10	<10	<10	<10	<10	<10	<10	<10	22.7	25.0	36±7	15±4	<10	<10
Ni	100	6.23	11.2	19.6	7.46	6.15	4.61	5.04	4.67	33.4	21.1	16.2	18.4	7.05	14.3
Cu	1000*	7.74	5.23	8.40	6.26	6.37	5.63	19.0	17.2	5.41	7.32	10.4	6.21	6.83	8.85
Zn	5000*	*674	*608	*710	*863	*622	18±2	22.4	23.4	*610	*861	*878	*864	*575	*918
As	50	7.94	2.44	3.16	8.71	4.66	8.94	8.88	7.78	10.4	10.0	4.86	7.38	12.4	3.57
Se	50	<1	6.7±5.7	<1	<1	<1	<1	<1	<1	8.9±2.8	<1	30±9	13±7	<1	<1
Ag	100*	<1	<1	<1	<1	<1	<1	<1	<1	<1	<1	<1	<1	<1	<1
Cd	5	<1	<1	<1	<1	<1	<1	<1	<1	<1	3.05	<1	<1	<1	<1
Sn	none	2.18	1.3±0.2	2.26	<1	1.5±0.3	<1	<1	<1	1.6±0.2	3.3±1.0	2.82	1.8±0.3	2.5±0.3	1.6±0.3
Sb	6	2.06	2.6±0.8	<1	<1	<1	1.5±0.2	1.9±0.4	1.71	3.85	1.8±0.4	7±1.5	5.8±1.4	1.75	1.3±0.2
Ba	2000	26.2	63.7	97.8	30.6	183	24.9	63.9	68.2	51.7	158	193	52.6	140	92.8
Pb	50**	5.54	2.68	1.81	4.41	<1	<1	3.01	2.77	1.48	1.79	1.41	1.72	1.35	4.47
Cr	100	4.82	77.2	11.1	5.79	5.23	5.08	7.74	7.28	4.17	5.94	4.86	3.58	6.10	5.54

MCLs are from EPA 822-R-96-001, February 1996 unless otherwise indicated.

\* EPA Secondary Standard (in: EPA 822-R-96-001, February 1996)

\*\* CFR Part 265 Appendix III

NA = not analyzed

**Table 10.8. Trace Metals for Wells Within the Reduced Zone in May 1996 Measured by ICP/MS**

Post-experiment data for wells within the Redox zone, ng/ml (ppb). Sample date 5/7/96, analyses date 5/30/96.

Constituent	MCL (ppb)	Sample Location															
		HS-1B	HS-2	HS-3P	HS-3P Dup	HS-3VO	HS-4P	HS-4VO	HS-5P	HS-5VO	HS-6	HS-7	HS-8	HS-9	HS-9 Dup	HS-10	HS-11
SO3	<5000	17500	<2500	NA	<500	<500	<500	<500	4020	3860	3190	<5000	<2500	19600	NA	<12500	<5000
SO4	25000*	235,000	215,000	NA	54,400	295,000	66,600	273,000	273,000	62,400	280,000	397,000	346,000	332,000	NA	556,000	481,000
Na	none	55,400	35,300	NA	22,600	49,200	23,600	61,600	61,600	23,800	57,000	57,400	52,200	60,900	NA	75,200	63,500
Mg	none	2,650	16,900	NA	11,300	9,200	11,200	5,190	5,190	3,160	6,840	14,800	22,700	6,650	NA	17,400	27,800
Si	none	12,000	9,430	NA	15,700	10,400	8,820	6,660	6,660	9,300	5,600	10,800	10,800	9,050	NA	9,010	12,300
K	none	80,800	189,000	NA	7,180	152,000	45,500	180,000	180,000	102,000	172,000	170,000	67,200	193,000	NA	205,000	33,600
Al	50 to 200*	10±1	25.1	10.2	15.0	14.2	12.4	13.7	13.7	15±3	10.1	11±3	18±3	11.2	11.6	14.4	13.4
Mn	50*	253	7.08	196	17.6	102	57.5	18.8	18.8	8.27	37.8	161	499	21.6	21.0	161	780
Fe	300*	121	41.4	<10	<10	78.4	<10	26±6	26±6	16.4	36±6	240	67.4	70±11	45.6	39±5	60.4
Ni	100	4.4±0.9	<1	2.8±0.3	1.79	1.3±0.4	1.4±0.2	<1	<1	<1	<1	1.67	5.22	<1	<1	3.5±0.8	4.37
Cu	1000*	13.7	12.9	12.1	13.1	14.1	12.8	14.5	14.5	12.4	13.1	12.2	13.0	12.3	11.9	14±2	12.5
Zn	5000*	58.5	59.8	60.0	64.6	65.1	52.2	70.4	70.4	65.2	66.1	49.6	62.6	54.2	50.3	60.3	57.5
As	50	4.4±0.9	3.92	1.09	1.6±0.8	4.3±0.6	1.4±0.3	3.2±0.4	3.2±0.4	7.36	4.08	5.5±1.5	2.85	3.82	4.29	6.6±1.3	1.9±0.5
Se	50	<6	<6	<6	<6	<6	<6	<6	<6	<6	<6	<6	<6	<6	<6	<6	<6
Ag	100*	<1	<1	<1	<1	<1	<1	<1	<1	<1	<1	<1	<1	<1	<1	<1	<1
Cd	5	<1	<1	<1	<1	<1	<1	<1	<1	<1	<1	<1	<1	<1	<1	<1	<1
Sn	none	<1	<1	<1	<1	<1	<1	<1	<1	<1	<1	<1	<1	<1	<1	<1	<1
Sb	6	<1	<1	<1	<1	<1	<1	<1	<1	<1	<1	<1	<1	<1	<1	<1	<1
Ba	2000	117	32.6	78.4	80.5	109	31.2	54.1	54.1	21.9	63.3	111	92.0	60.9	62.0	93.7	112
Pb	50**	<1	1.05	1.00	1±0.2	<1	<1	<1	<1	<1	<1	<1	<1	1.32	1.31	1.09	<1
Cr	100	2.93	2.51	30.3	75.5	4.18	3.34	2.54	2.54	10.2	2.42	1.86	14.5	1.9±0.3	1.8±0.3	1.7±0.3	2.20

MCLs are from EPA 822-R-96-001, February 1996 unless otherwise indicated.

\* EPA Secondary Standard (in: EPA 822-R-96-001, February 1996)

\*\* CFR Part 265 Appendix III

SO<sub>3</sub> and SO<sub>4</sub> were analyzed 5/8/96-5/9/96; all other analyses were reported 5/30/96.

NA = not analyzed

Dup = duplicate sample

**Table 10.9. Trace Metals for Wells Within the Reduced Zone in August 1996 Measured by ICP/MS**

Constituent	MCL (ppb)	Sample Location														
		HS-1B	HS-2	HS-3P	HS-3"O"	HS-4P	HS-4"O	HS-5P	HS-5"O	HS-6	HS-7	HS-8	HS-9	HS-9 Dup	HS-10	HS-11
SO3	none	<10000	<10000	<10000	<10000	<10000	<10000	<10000	<10000	<10000	<10000	<10000	<10000	<10000	<10000	<10000
SO4	250000*	540,000	236,000	151,000	50,200	302,000	54,600	297,000	56,800	260,000	422,000	394,000	403,000	NA	710,000	659,000
Na	none	48,700	49,000	26,700	21,600	47,300	21,500	55,700	23,900	47,500	48,600	44,300	59,400	64,800	70,300	58,700
Mg	none	27,300	2,670	13,200	10,500	9,560	11,100	5,240	4,010	5,730	14,200	19,200	6,860	7,220	18,000	30,900
Si	none	7,790	2500±500	7,710	9,490	5600±600	7,630	3300±500	4,780	4,070	6,300	7,140	4,170	5,110	6,170	7,520
K	none	62,100	154,000	20,200	6,030	134,000	22,300	136,000	77,600	135,000	134,000	58,200	144,000	161,000	173,000	30,100
Al	50 to 200*	<10	<10	<10	<10	<10	<10	<10	<10	<10	<10	<10	<10	<10	<10	<10
Mn	50*	274	3.6±0.4	129	4.2	99.7	44.9	20.2	6.3	42.9	132	389	25.7	26.6	201	730
Fe	300*	268	28±14	<20	21±6	70±10	<20	37±15	<20	483	90±10	247	40±13	44±19	150±20	175
Ni	100	6.0±0.8	<2	4.6±0.9	2.5±0.4	2.2±0.3	2.4	<2	<2	<2	3.5	4.0±1.0	3.1±0.9	2.8±0.9	4.5±1.3	9.2
Cu	1000*	9.8±1.1	7.5±0.9	6.7±1.3	5.9±1.5	6.5±1.1	5.1	7.8±1.2	6.9±1.5	8.1±1.2	6.2±0.8	6.4±1.8	8.0	7.5±1.4	6.4±0.7	6.4
Zn	5000*	44.1	41.3	41±6	39.5	44±7	42.9	49±7	37±7	38±8	45±7	44±8	39.3	42±5	50.2	35±5
As	50	<2	<2	<2	<2	<2	<2	<2	<2	<2	<2	<2	<2	<2	<2	<2
Se	50	<20	<20	<20	<20	<20	<20	<20	<20	<20	<20	<20	<20	<20	<20	<20
Ag	100*	<2	<2	<2	<2	<2	<2	<2	<2	<2	<2	<2	<2	<2	<2	<2
Cd	5	<2	<2	<2	<2	<2	<2	<2	<2	<2	<2	<2	<2	<2	<2	<2
Sn	none	<2	<2	<2	<2	<2	<2	<2	<2	<2	<2	<2	<2	<2	<2	<2
Sb	6	<2	<2	<2	<2	<2	<2	<2	<2	<2	<2	<2	<2	<2	<2	<2
Ba	2000	78.8	24.9	49.7	37.1	90.0	25.8	45.7	23.5	44.3	84.6	66.2	59.3	59.1	55.4	90.7
Pb	50**	<2	<2	<2	<2	<2	<2	<2	<2	<2	<2	<2	<2	<2	<2	<2
Cr	100	<2	<2	23.3	66.2	<2	<2	<2	<2	<2	<2	<2	5.2±1.0	4.5±0.5	<2	<2

MCLs are from EPA 822-R-96-001, February 1996 unless otherwise indicated.

\* EPA Secondary Standard (in: EPA 822-R-96-001, February 1996)

\*\* CFR Part 265 Appendix III

SO<sub>3</sub> and SO<sub>4</sub> were reported 9/25/96; all other analyses were reported 9/17/96.

NA = not analyzed

Dup = duplicate sample

**Table 10.10. Trace Metals for Upgradient and Downgradient Wells in January 1996 Measured by ICP/MS**

Post-experiment data for upgradient and downgradient wells, ng/ml (ppb). Sample date 1/23/96, analyses report date 2/2/96.						
Constituent	MCL (ppb)	Upgradient Well	Downgradient Wells			
		H5-15	H5-12	H5-13	H5-13 (duplicate)	H5-14
SO3	none	NA	NA	NA	NA	NA(a)
SO4	250000*	NA	NA	NA	NA	NA(a)
Na	none	23,800	17,400	26,500	26,000	NA(a)
Mg	none	11,200	14,900	13,800	13,800	NA(a)
Si	none	12,400	8,910	10,800	11,200	NA(a)
K	none	5,010	5,750	5,530	5,670	NA(a)
Al	50 to 200*	6.30	8.39	8.32	8.51	NA(a)
Mn	50*	357	92.3	15.1	17.0	NA(a)
Fe	300*	<10	<10	<10	<10	NA(a)
Ni	100	3.00	2.3±0.5	2.3±0.4	2.5±0.4	NA(a)
Cu	1000*	1.5±0.2	1.9±0.4	2.11	2.5±0.3	NA(a)
Zn	5000*	775	*697	734	716	NA(a)
As	50	<1	<1	<1	<1	NA(a)
Se	50	<1	<1	<1	<1	NA(a)
Ag	100*	<1	<1	<1	<1	NA(a)
Cd	5	<1	<1	<1	<1	NA(a)
Sn	none	1.3±0.2	1.2±0.2	<1	1.02	NA(a)
Sb	6	<1	<1	<1	<1	NA(a)
Ba	2000	60.5	48.6	46.7	49.9	NA(a)
Pb	50**	<1	3.0±0.4	<1	<1	NA(a)
Cr	100	53.8	13.9	34.3	36.6	NA(a)

MCLs are from EPA 822-R-96-001, February 1996 unless otherwise indicated.  
 \* EPA Secondary Standard (in: EPA 822-R-96-001, February 1996)  
 \*\* CFR Part 265 Appendix III  
 NA = not analyzed  
 (a) Well pumped dry during sampling, therefore no samples collected.

**Table 10.11. Trace Metals for Upgradient and Downgradient Wells in May 1996 Measured by P/MS ICP/MS**

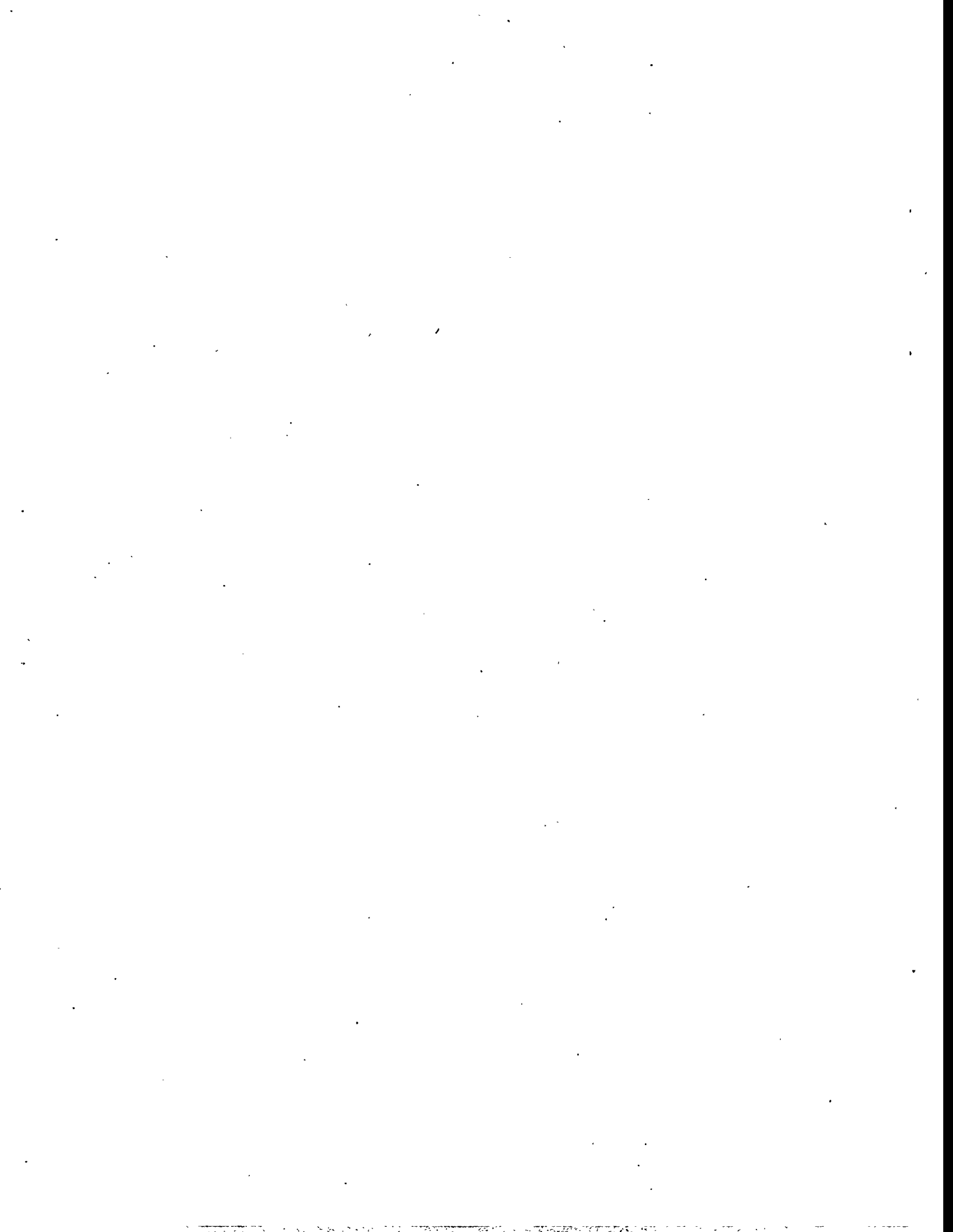
Post-experiment data for upgradient and downgradient wells, ng/ml (ppb).					
Sample date 5/7/96.					
Constituent	MCL (ppb)	Upgradient Well	Downgradient Wells		
		H5-15	H5-12	H5-13	H5-14
SO <sub>3</sub>	none	4240	3110	<2500	3090
SO <sub>4</sub>	250000*	72,600	82,200	84,500	89,200
Na	none	34,800	18,000	28,000	36,300
Mg	none	11,900	16,600	14,700	14,100
Si	none	13,800	10,800	13,200	12,800
K	none	6,340	6,680	6,520	7,450
Al	50 to 200*	11.4	9.87	9.16	12.8
Mn	50*	34.5	41.3	4.40	44.5
Fe	300*	29±4	<10	<10	<10
Ni	100	2.1±0.4	2.19	2.17	1.9±0.9
Cu	1000*	11.3	12.3	13.2	12.3
Zn	5000*	53.1	56.5	62.5	57.6
As	50	1.2±0.7	<1	1.1±0.6	<1
Se	50	(<6)	<6	7.6±3.9	<6
Ag	100*	<1	<1	<1	<1
Cd	5	<1	<1	<1	<1
Sn	none	<1	<1	<1	<1
Sb	6	<1	<1	<1	<1
Ba	2000	68.9	53.8	49.7	56.5
Pb	50**	<1	<1	1±0.2	<1
Cr	100	61.7	24.8	45.5	42.1

MCLs are from EPA 822-R-96-001, February 1996 unless otherwise indicated.  
 \* EPA Secondary Standard (in: EPA 822-R-96-001, February 1996)  
 \*\* CFR Part 265 Appendix III  
 SO<sub>3</sub> and SO<sub>4</sub> were analyzed 5/8/96-5/9/96; all other analyses were reported 5/30/96.

Table 10.12. Trace Metals for Upgradient and Downgradient Wells in August 1996 Measured by ICP/MS

Post-experiment data for upgradient and downgradient wells, ng/ml (ppb).					
Sample date 8/14/96.					
Constituent	MCL (ppb)	Upgradient Well	Downgradient Wells		
		H5-15	H5-12	H5-13	H5-14
SO3	none	<10,000	<10,000	<10,000	<10,000
SO4	250000*	96,200	115,000	69,700	101,000
Na	none	35,000	26,300	25,000	35,900
Mg	none	10,400	15,800	12,700	12,600
Si	none	8,180	7300±1000	7,730	8,040
K	none	5,210	5,720	6,200	6,340
Al	50 to 200*	<10	<10	<10	<10
Mn	50*	8.6	16±2	<2	18.2
Fe	300*	34±5	49	<20	<20
Ni	100	4.0±0.8	4.9±1.3	3.6±1.4	3.3±1.2
Cu	1000*	8.8±0.9	9.6	7.5±1.3	6.0±0.8
Zn	5000*	42.7	56±6	41±7	39±4
As	50	<2	<2	<2	<2
Se	50	<20	<20	<20	<20
Ag	100*	<2	<2	<2	<2
Cd	5	<2	<2	<2	<2
Sn	none	<2	<2	<2	<2
Sb	6	<2	<2	<2	<2
Ba	2000	51.7	52.2	39.6	44.7
Pb	50**	<2	<2	<2	<2
Cr	100	41.9	19.1	36.7	34.7

MCL's are from EPA 822-R-96-001, February 1996 unless otherwise indicated.  
 \* EPA Secondary Standard (in: EPA 822-R-96-001, February 1996)  
 \*\* CFR Part 265 Appendix III  
 SO<sub>3</sub> and SO<sub>4</sub> were reported 9/25/96; all other analyses were reported 9/17/96.



## 11.0 Modeling of Results

Numerical modeling was used in both the design analysis for the ISRM experiment and to interpret the experimental results. If the important reactions and hydrologic processes can be adequately characterized and modeled, then the ability to optimize the design for the deployment of this technology at future sites will be greatly enhanced. Optimization of the emplacement of a reduced zone could lead to lower reagent costs and minimization of the concentrations within the withdrawal water. These modeling studies will also allow us to explore other approaches to emplacement, address stakeholder and regulatory concerns, and identify important parameters for future field activities.

This section contains a description of the preliminary modeling studies of the reactive transport modeling of the intermediate-scale wedge experiment and a second modeling effort to investigate molecular diffusion and dispersion processes that influence the reoxidation of anoxic zones within an aquifer. Hydrologic and geochemical modeling of the 100-H Area field site have not been completed, these results will be presented in subsequent project reports and journal publications.

### 11.1 Reactive Transport Modeling

A one-dimensional, radial, reactive transport code was developed as part of the design analysis and interpretation of the intermediate-scale and field experiments. Chemical reactions are modeled using pseudo-first-order kinetics based on the bench-scale studies (Amonette et al. 1995) of the redox and disproportionation reactions of dithionite and sediment as described in Section 4.1. Pseudo-first-order kinetics are first-order exponential decay rates, the same as radioactive decay, so the rates are commonly expressed in terms of half-life.

The model simulates both advective and dispersive transport. The current version assumes a confined aquifer with a fully penetrating well. Hydraulic properties are homogeneous and isotropic. The flow is non-density dependent, steady state with transient multiple species transport and reactions. Aqueous species are assumed to be non-sorbing. In addition to dithionite, thiosulfate, and sulfite, the carbonate pH buffer concentrations are also modeled. Ferric and ferrous iron concentrations in the sediment are tracked from the redox reactions and the initial iron valence state is set to all ferric iron.

The assumptions and limitations used in the model result in very fast execution times (less than 5 minutes on a Sun Workstation), which permits numerous simulations to be run for sensitivity analysis and parameter changes for curve matching. Many of these limitations will need to be removed to use this code for the initial geochemical modeling of the field experiment results. Otherwise, an existing, more robust geochemical reactive transport model will be used (e.g., RAFT).

#### 11.1.1 Application to the Design Analysis

The reactive transport model was used as part of the design analysis to investigate the influence of different dithionite and ferric iron redox reaction rates on the extent of injection of a dithionite plume and the resulting distribution of reduced iron. These studies resulted in the selection of injecting decreasing concentrations of dithionite during the field experiment, as discussed in Section 10.4.1. The simulations showed that based on ferric iron measured in the sediments at the site and using the range of redox reaction rates measured from the bench-scale and intermediate-scale experiments, most of the ferric iron within the sediments near the injection well would already be reduced before the injection phase was over. Therefore the concentrations of dithionite used in

the later part of the injection is less than that required at the early part of the injection. The main importance of the later stage of the injection phase is to push the front of the dithionite plume radially outwards. Dispersion and the mixing of oxygen at the front of the plume also increases the need for greater dithionite concentrations in the early part of the injection.

A thorough understanding of the field-scale iron content and redox reaction rates would permit, through modeling, even more optimization of the time-varying dithionite concentrations resulting in less mass of reagent and producing a more uniform, reduced zone. The selection of the concentrations used in the field experiment were conservative because of the uncertainty in the parameters involved.

Generic simulations using this model showed some interesting features observed in the dithionite concentration versus time plots at fixed points in this system. As shown in an example in Figure 11.1, dithionite concentrations at a point increased and then leveled off to a constant concentration for a period of time and then begin increasing again to a new concentration plateau for the remainder of the injection stage. The concentration at which these plateaus appeared decreased with increasing radial distance. The first dithionite concentration plateau was due to the amount of ferric iron in the system limiting the dithionite concentrations until all the ferric iron was reduced to ferrous iron between the injection well and the monitoring location. The dithionite/ferric iron reaction rate is much greater than the dithionite disproportionation rate. Thus, the dithionite was being consumed at a fast rate until all the ferric iron between the injection well and the monitoring location was reduced to ferrous iron. Afterwards, the dithionite concentrations would climb again to a new level that was controlled by the much slower disproportionation reaction rate. The concentrations where these plateaus appear is a function of the travel time to the point and the reaction rates of the dithionite-ferric iron reaction and the dithionite disproportionation reaction.

The maximum distance that dithionite can be injected, based on the travel time, is limited by the dithionite-ferric iron reaction rate until all the iron along the pathway has been reduced. Then the maximum distance is limited by the slower disproportionation rate. The maximum distance can be increased by using a faster injection rate. Simulations showed that the initial selection of a 20-gpm injection rate should be adequate to inject dithionite out to at least 7.5 m (25 ft) based on estimates of these reaction rates from laboratory experiments and the preliminary ferric iron measurements from sediment from the site.

At greater radial distances, where the dithionite concentrations and contact time has not exceeded the amount of ferric iron in the sediment, the behavior of the dithionite concentrations during the residence stage is similar to that observed in batch studies (see Figure 11.1). The rate of decrease in the dithionite concentrations are controlled by the dithionite ferric iron reaction rate and these curves can be fitted to an exponential decay to estimate the reaction rate. If the initial concentration of dithionite at the beginning of the residence stage is sufficient to reduce the remaining ferric iron, then rate of decay in the dithionite concentration will be controlled by the disproportion rate (which is much slower ~18 h).

The simulated arrival of dithionite was earlier than measured during the experiment at larger radial distances, but the peak concentrations reached at these distances were similar to the simulation results. Measurements during the experiment showed that the arrival was earlier on one side of the wedge than the middle and opposite side of the wedge at the same radial distance. The modeling also does not account for significant volume of water removed during sampling. The amount of ferric iron used in the model to match the dithionite curves was very similar to the ferric iron required to

product the reductive capacity measurements in post-experiment sediment samples (0.30% versus 0.324%); the reductive capacity analyses were conducted after these predictive simulations were completed.

### **11.1.2 Analysis of the Intermediate-Scale Dithionite Injection/Withdrawal Experiment**

The reactive transport code is being used to analyze the results of the intermediate-scale and field experiments to back out redox reaction rates, iron content, and predict the reductive capacity achieved. This is accomplished by varying the parameters to match the breakthrough curves of dithionite, conductivity, and tracers measured at various radial distances (sampling ports and monitoring wells) from the injection well. The results of the modeling can be checked and compared against the analytical measurements of the iron content and reduction capacity of the sediments made before and after the experiments.

The preliminary results of the modeling for the intermediate-scale dithionite injection/withdrawal experiment conducted at OSU (see Section 7.0) are described below. The model is more appropriate for this experiment because of the confined conditions of the flow cell and model. The modeling results for one case at two different locations are shown in Figures 11.2 and 11.3, compared against conductivity and dithionite measurements made during the experiment. Selected parameters used in this simulation are shown in Table 11.1. This simulation was the result of systematically varying parameters and comparing the results to the measured values. The conductivity curves help to match the dispersivity using a simulated conservative tracer. This case had a better match of the dithionite breakthrough curves at smaller radial distances (Figure 11.2) than the farther radial distances (Figure 11.3).

The simulated arrival of dithionite was earlier than measured during the experiment at larger radial distances, but the peak concentrations reached at these distances were similar to the simulation results. Measurements during the experiments showed that the arrival was earlier on one side of the wedge than the middle and opposite side of the wedge at the same radial distance. The modeling also does not account for the significant volume of water removed during sampling. The amount of ferric iron used in the model to match the dithionite curves was very similar to the ferric iron required to produce the reductive capacity measurements in post-experiment sediment samples (0.30% versus 0.324%); the reductive capacity analyses were conducted after these predictive simulations were completed.

## **11.2 Dissolved Oxygen Transport Modeling**

A second numerical modeling effort was undertaken to quantify the mass fluxes of dissolved oxygen into an anoxic aquifer to estimate the natural attenuation of an anoxic plume that migrates from a reduced zone and other mechanisms, in addition to the advection of oxygenated water from upgradient, that could accelerate the re-oxidation of the reduced zone.

Many of the factors that could attenuate the anoxic plume are complex and poorly understood, with some important parameters not well characterized. Downgradient monitoring data from the 100-H Area study is not adequate to quantify reoxygenation rates due to edge effects from the limited extent of the reduced zone and the uncertainties in the gradient direction (particularly during the winter and spring of 1996 with the elevated water table at the site from the high stage of the Columbia River). Potential migration of the anoxic plume from the 100-H Area site was addressed in the test plan using a simple dispersion model, which showed a 10 to 20% decrease in the dissolved

oxygen from ambient levels by the time the 18.28-m (60-ft)-wide plume traveled the approximate 609-m (2000-ft) distance to the Columbia River (see discussion in Section 7). One of the objectives of the proposed larger-scale Treatability Study is to collect the required data to address this issue. The length of the proposed ISRM barrier and downgradient monitoring network planned for the proposed study are adequate to reduce the influence of edge effects and uncertainty in the gradient.

In addition to the factors mentioned above that influence reoxygenation rates, other mechanisms that complicate the analysis include the composition of the air within the vadose zone, concentration and variation of dissolved oxygen within the aquifer, and water table fluctuations. Recent field and laboratory studies by Dr. J. D. Istok at OSU have discovered the importance of trapped air bubbles below the water table in controlling dissolved gas concentrations and transport due to the partitioning of the gases between these trapped air bubbles and the aqueous phase. Depletion of the dissolved gas will drive the gas from the air bubbles into the aqueous phase, thus increasing the dissolved gas content. The volume of trapped air bubbles and magnitude of this effect in the upper unconfined aquifer at the Hanford Site is unknown, but can be determined through a tracer injection test using multiple gases.

Simulations were conducted that take into account molecular diffusion and dispersion within the aquifer to estimate a conservative limit to the magnitude of the anoxic plume. Taking into account additional processes that are not part of the model (e.g., trapped air bubbles, water table fluctuations) would act to increase the reoxygenation rates above the simulated results. The geometry and hydraulic properties used in these simulations were taken from the 100-H Area ISRM site. The unconfined aquifer (Hanford formation gravels) is approximately 3 m thick with a clay unit forming the base (Ringold formation mud). The domain was 100 m long with a porewater velocity in the unconfined aquifer of 30.48 cm/d (1 ft/d). Simulations were conducted in which anoxic water entered the system in the lower 1.5 m of the aquifer. Additional simulations were conducted with the anoxic water entering the upper 1.5 m of the aquifer. The diffusion coefficient (in free solution) for dissolved oxygen in the model was  $2.29 \times 10^{-5}$  cm<sup>2</sup>/s, and the dispersivities used in the model were 0.1 m for longitudinal and 0.01 m for transverse (these values are very conservative for gravels and cobbles).

For the case where the anoxic plume is in the lower 1.5 m of the aquifer (similar to the 100-H Area Test), the anoxic plume is reoxygenated to more than 10% of the ambient value starting at about 25 m downgradient. The plume has reoxygenated to 33% of the ambient value at a 100-m distance downgradient. In the simulation where the anoxic plume is in the upper 1.5 m of the aquifer, the plume has reoxygenated to 10% of the ambient value at about 7.5 m distance downgradient, 30% at a 20-m distance, and 75% at an 85-m distance. The upper anoxic plume case reoxygenates faster and in a shorter distance than the lower zone anoxic case due to the proximity of the upper zone to the vadose zone (results of this simulation are more sensitive to assumptions of flux through the vadose zone). The reoxygenation of the lower anoxic plume is limited by the aqueous diffusion and transverse dispersion rates.

The aqueous diffusion rate of dissolved oxygen is a limiting factor compared to the much greater gaseous diffusion rates in the vadose zone. Fluctuations in the water table elevation would help to increase the flux of dissolved oxygen into the aquifer. The magnitude of the reoxygenation in the simulations with the anoxic plume in the lower 1.5 m of the aquifer is not very sensitive to the flux of oxygen through the vadose zone, although it does influence the dissolved oxygen depletion of the upper portion of the aquifer. Two-phase (air and water) transport simulations of the saturated and unsaturated zone are planned to bracket the boundary conditions used in the 1.5-m upper zone anoxic plume simulation. Additional studies to quantify reoxygenation rates are ongoing, and

similar modeling is planned for the proposed large-scale Treatability Study once the pre-design characterization is completed at the site and the depth interval that will be targeted for reduction is determined.

**Example Dithionite Breakthrough Curves  
(with amount of Fe(III) unreduced)**

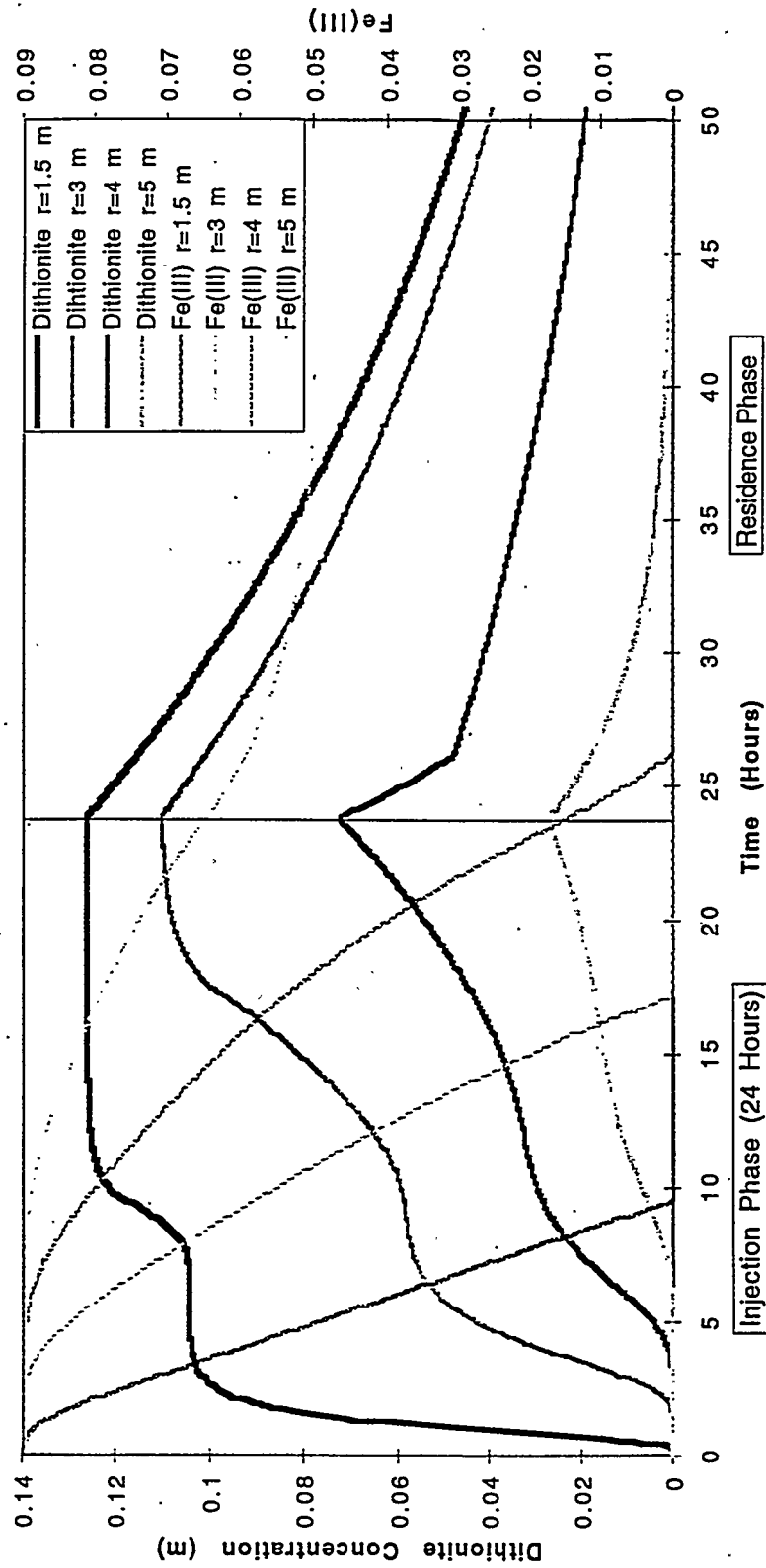


**Figure 11.1. Example Dithionite Breakthrough Curves from Reactive Transport Model Showing Unreduced Fe(III) at Various Radial Distances**

### Modeling Results From Intermediate-Scale Dithionite Experiment 150 cm from Inlet

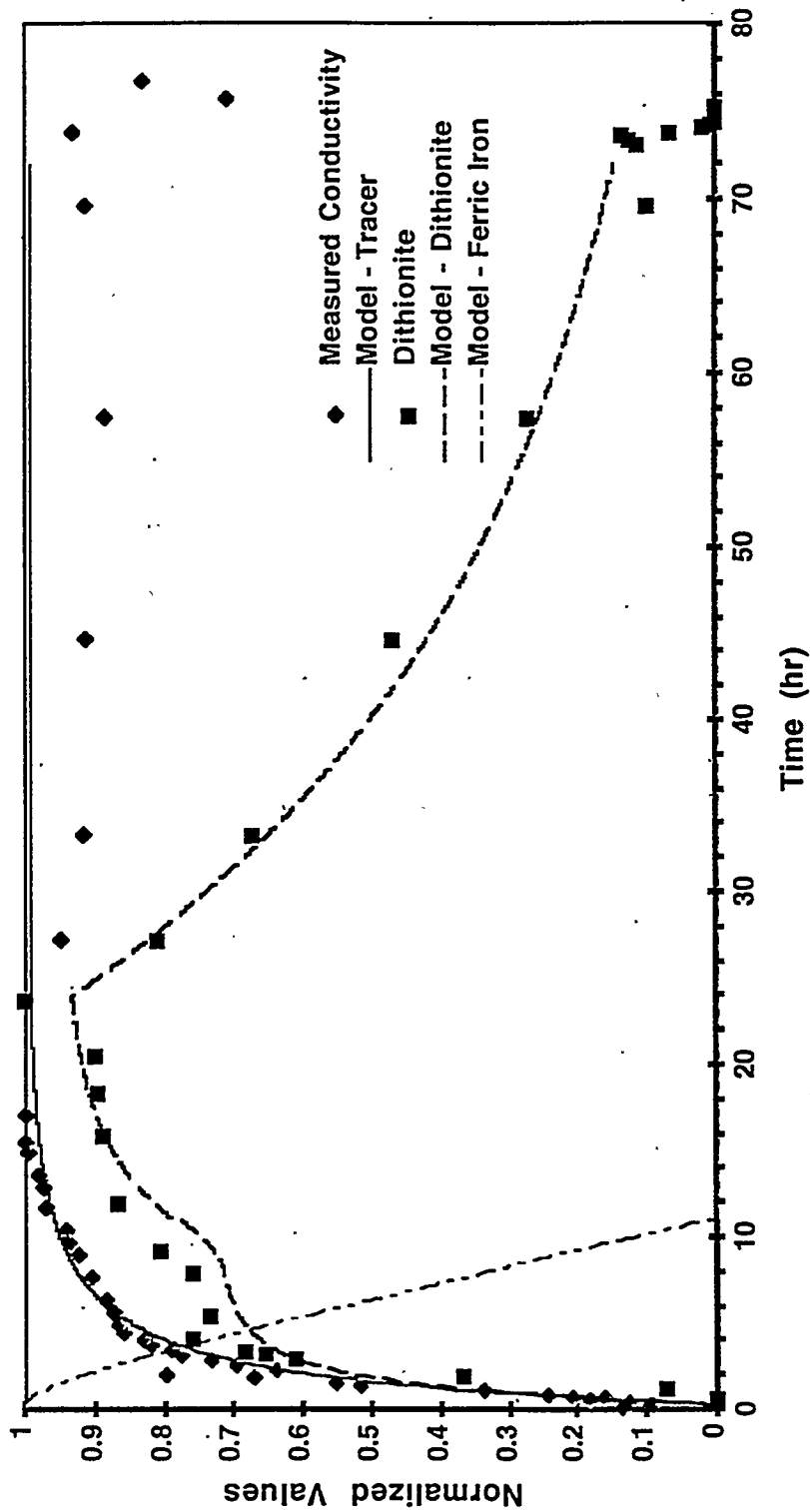


**Figure 11.2.** Comparison of Reactive Transport Model Simulation Results to Dithionite and Conductivity Measurements at 150-cm Radial Distance in the Intermediate-Scale Wedge Experiment at Oregon State University

Modeling Results From Intermediate Scale Dithionite Experiment  
250 cm from Inlet

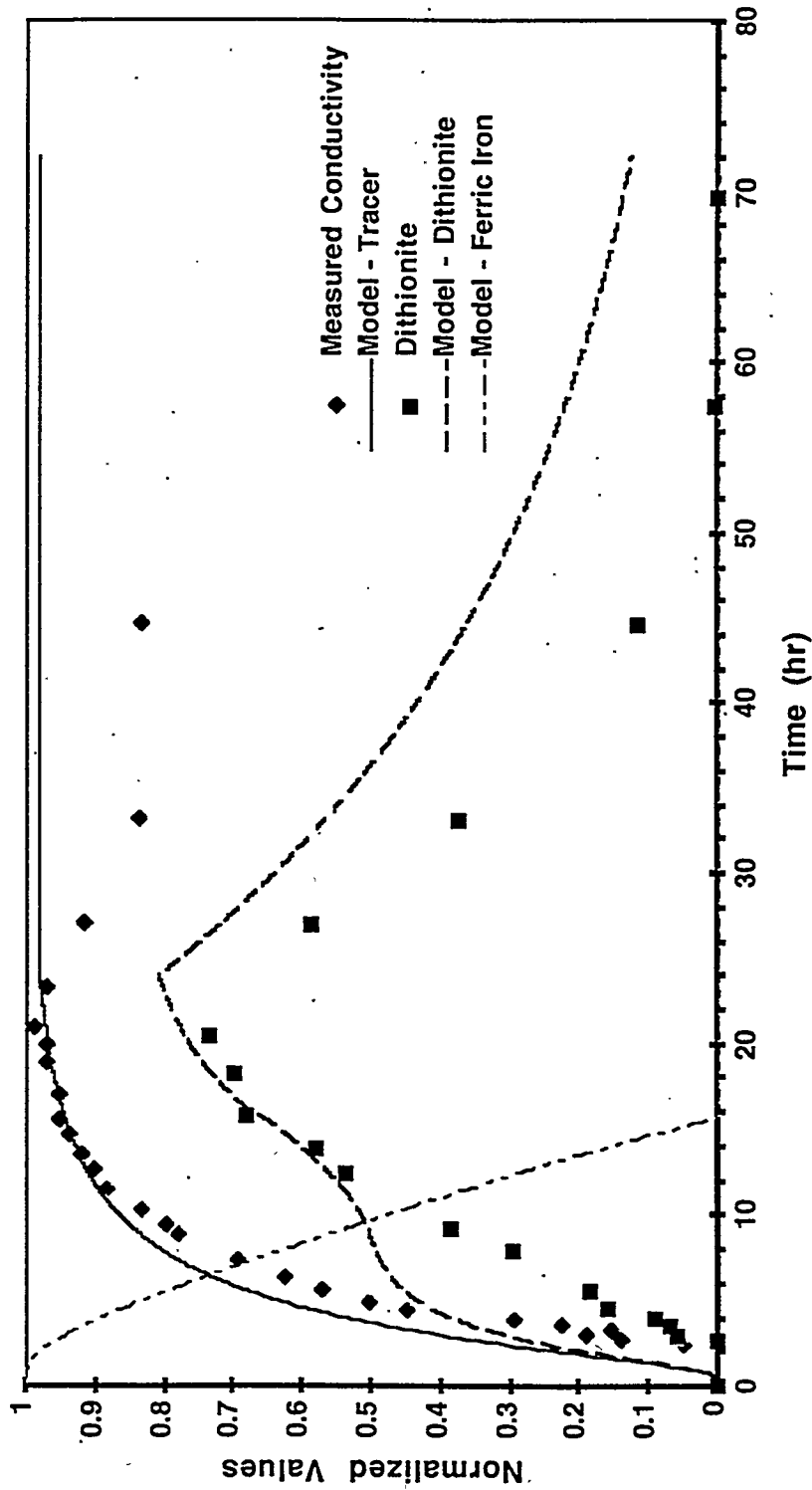
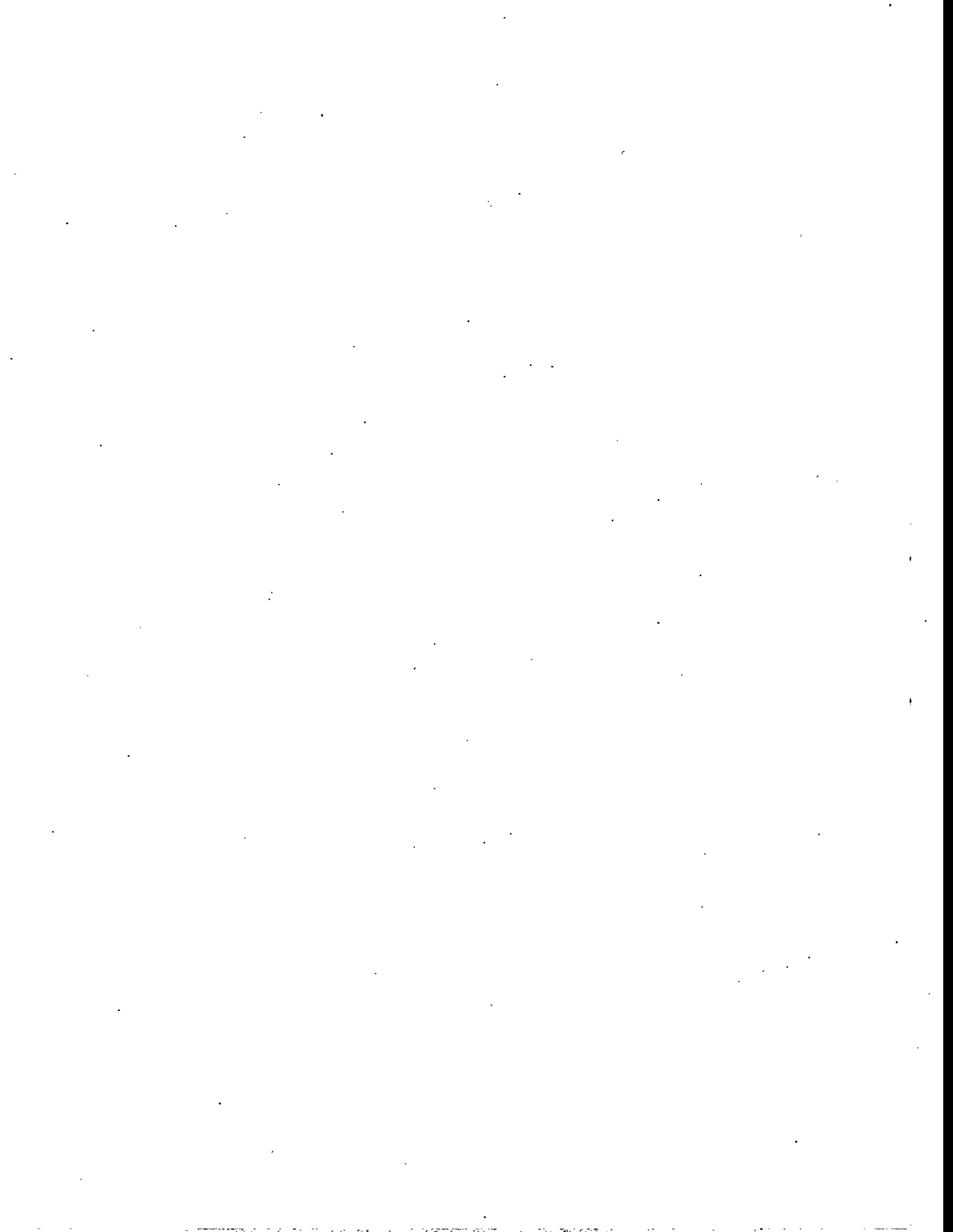


Figure 11.3. Comparison of Reactive Transport Model Simulation Results to Dithionite and Conductivity Measurements at 250-cm Radial Distance in the Intermediate-Scale Wedge Experiment at Oregon State University

**Table 11.1.** Selected Parameters Used in Intermediate-Scale Wedge Modeling.

<b>Values of Fitted Parameters in Model</b>	
<b>Parameter</b>	<b>Value</b>
Dithionite/ferric iron reduction rate (half-life)	5 h
Dithionite disproportionation rate (half-life)	18 h
Wt% of ferric iron in sediments (initial)	0.30
Dispersivity	2.5 ft



## 12.0 Interpretation and Summary

### 12.1 Summary

All the major objectives of the ISRM field test, as described in the Test Plan (Fruchter et al. 1994) were achieved. These objectives included demonstrating the feasibility of reducing the aquifer sediments, determining how long the reducing conditions can be maintained, determining the nature and severity of any secondary effects, and developing a methodology for evaluating ISRM technologies in general.

Seventy nine thousand five hundred ninety liters (21,000 gal) of buffered sodium dithionite solution were successfully injected into the unconfined aquifer at the Hanford 100-H Area in September 1995. No significant plugging of the well screen or the formation was detected during any phase of the test. Dithionite was detected in monitoring wells at least 7.5 m (25 ft) from the injection point.

Preliminary core data show that 60% to 100% of the available reactive iron in the treated aquifer sediments was reduced by the injected dithionite. PNNL staff obtained reducing capacity measurements on cores recovered after the reagent injection using dissolved oxygen consumption measurements, and confirmed these measurements in some core samples using hexavalent chromium solutions. Calculations show that these levels of reducing capacity within the treated sediments translate to a contaminant plume treatment capacity of from 51 to 85 pore volumes (7 to 12 years). These estimates assume groundwater containing 1 ppm hexavalent chromium and 9 ppm dissolved oxygen. If additional treatment capacity were required to meet target cleanup levels, the treatment zone could be made wider during the initial emplacement or re-injected with dithionite once the available treatment capacity had been expended.

Twelve months after the injection, groundwater in the injection zone remains anoxic. Hexavalent chromium levels remain below detection limits, and total chromium levels remain in the 1 to 8 ppb range, and continue to decline. Other trace metals (e.g., arsenic, lead) mobilized into the groundwater during the reduction phase remain below drinking water maximum contaminant levels, and are also decreasing with time, as are conductivity and pH values. Concentrations of constituents in the water withdrawn for the test well met all applicable Hanford purgewater criteria and was disposed to the ground.

Although the expected decreases in dissolved oxygen and chromate concentrations have appeared in monitoring well samples taken within the zone treated by dithionite, similar decreases have not yet appeared in the downgradient monitoring wells. This is thought to be due to historic high levels of the groundwater table in the 100-H Area wells caused by heavy precipitation during the winter and spring of 1996. These high levels have essentially flattened the groundwater gradient to the point where no net movement of the water is now occurring. We estimate that normal gradient conditions will reestablish themselves in 1997.

### 12.2 Conclusions

The "proof-of-principle" test conducted at the 100-H Area has demonstrated so far that 1) sediments in the aquifer can be successfully reduced by treatment with a chemical reducing agent, 2) the

reduced sediments can substantially lower the concentration of dissolved hexavalent chromium in the groundwater, and 3) the reducing conditions can be maintained in the aquifer for extended periods of time.

Several issues must still be resolved before ISRM can be used routinely to remediate contaminated groundwater. These issues are grouped into three major categories: 1) scale-up, 2) long-term behavior and performance of the reduced zone, and 3) cost and constructability. Scale-up issues include the logistics of handling large amounts of dithionite and disposing of the withdrawn water, methods of injecting the reductant to more efficiently use the dithionite, and the effects of a larger volume of reduced aquifer on the system's chemical behavior. Concerns involving long-term behavior and performance include reoxygenation of the water downgradient of the reduced zone, reoxidation of the zone itself, with the resulting need to re-reduce the aquifer, reoxidation of precipitated metals within the zone, and downgradient precipitation of any metals that were mobilized during reduction.

Constructability issues include some of the scale-up issues, the ability to install fully overlapping reduced zones, and the costs associated with installing and maintaining the zone for decades. These issues should be resolved by a combination of larger-scale treatability tests and continued monitoring at the 100-H Area site. In addition, alternative methods of reducing the aquifer will be investigated. This work is discussed in Section 13.0.

## 13.0 Future Work

Future work in ISRM revolves around four issues: 1) long-term effects, 2) constructability and cost, 3) scale-up issues, and 4) additional methods for manipulating the redox potential of the subsurface. Specific areas for future research identified at the time of this report are briefly described in the following sections.

### 13.1 100-H Area ISRM Site Monitoring and Maintenance

Continued monitoring of the 100-H Area site will be conducted to determine longevity of the reduced zone and any impact on the water quality downgradient from the site. Additional core holes will be drilled at the site to collect and analyze sediment samples more than one year after emplacement for comparison with the samples collected immediately following the emplacement. These data will permit the analysis of the reoxidation of the reduced zone both vertically and from upgradient. Quarterly monitoring of dissolved oxygen and chromate concentrations at the site will continue along with semi-annual analysis of trace metals.

### 13.2 Dissolved Oxygen Transport

An important question for the implementation of ISRM technology involves the reoxidation of the reduced zone and the fate of the anoxic plume downgradient from the reduced zone. A comprehensive understanding is needed of the mechanisms controlling the transport of dissolved oxygen in the aquifer. Current knowledge in this field is limited, and important controlling parameters are unknown or poorly characterized at the Hanford Site.

Recent studies have identified the importance of trapped air bubbles below the water table in controlling the transport behavior and concentrations of dissolved gas in the aqueous phase. A tracer injection test using multiple dissolved gas tracers will be conducted to determine the amount of trapped air bubbles in the saturated zone and the impact on dissolved gas transport. Three pairs of wells will be installed with each pair screened at the same depth interval. Gas tracer tests will be conducted between each pair to determine the variation in trapped air bubbles with depth. These wells will be drilled downgradient of the 100-H Area reduced zone to supplement the downgradient monitoring of the experiment. Data gathered from this study will be integrated into an existing model of two-phase (gas, water) saturated and unsaturated code to quantify the impact of these processes on reoxygenation.

### 13.3 Intermediate-Scale Test of Ultra-Micro Bacteria Injection

Another method for reducing the iron-containing minerals in an aquifer involves the injection and stimulation of iron-reducing bacteria into the aquifer. Work will be conducted to show whether these bacteria can be distributed throughout porous, saturated subsurface media. Flow experiments will be conducted in an intermediate-scale, radial flow box containing porous media. Following injection and distribution of the bacteria in simulated aquifers, cells will be resuscitated by adding sodium lactate as an organic electron donor. Distribution of cells, reduction of Fe(III) minerals, degradation of chlorinated solvents, and immobilization of Cr(VI) will be used as measures of success. Information obtained from intermediate-scale experiments will be used to design a field-scale demonstration.

## 13.4 Intermediate-Scale Test of Zero-Valent Iron Colloid Injection

Bench-scale tests have shown that iron colloids can be injected in columns for up to 3 m (10 ft) using viscosity enhancers. The next step will be to show that reasonable distributions of these colloids will be obtained in a field-scale radial injection. Flow experiments will be conducted in an intermediate-scale, radial flow box at OSU containing porous media. Distribution of the colloids, degradation of chlorinated solvents, and immobilization of Cr(VI) will be used as measures of success. Information obtained from intermediate-scale experiments will be used to design a field-scale demonstration.

## 13.5 Reduced-Clay Colloid Studies

In addition to the direct injection of a soluble reagent such as dithionite to react with iron-bearing clays already present in the sediment, a permeable reducing barrier can be created in high-porosity sediments by the injection of a colloidal suspension of Fe(II)-bearing clay minerals. This approach avoids some of the difficulties of chemical injection in that no pull-back of the reagent solution is needed and the materials injected occur naturally and thus are of little or no regulatory concern. Preliminary experiments conducted at PNNL (in collaboration with Heritage College) using laboratory-directed research and development (LDRD) and Permeable Barrier Project funds have shown that both  $\text{CCl}_4$  and TCE are degraded by Fe(II)-bearing clays with minimal amounts of hazardous degradation products. Further research is needed to assess and understand the reaction mechanisms, identify and test other clay substrates and contaminants, and to develop and demonstrate the injection techniques.

## 14.0 References

- Amonette JE, LSM Garnett, HT Schaef, JD Istok, MD Humphrey, JE Szecsody, MD Williams, E Camacho, E Parker, H Divanfar, and JS Fruchter. 1995. *Removal of Oxidized Contaminant by Abiotically Reduced Sediments: Laboratory Experiments in FY 1995*, Pacific Northwest National Laboratory, Richland, Washington.
- Amonette J E, J E Szecsody, JC Templeton, YA Gorby, and J S Fruchter. 1994. "Abiotic Reduction of Aquifer Materials by Dithionite: The Promise for In Situ Remediation." *Thirty-Third Hanford Symposium on Health and the Environment*, November 7-11, 1994, Pasco, Washington.
- Bjornstad BN, JP Mckinley, TO Stevens, SA Rawson, J K Fredrickson, and PE Long. Fall 1994. "Generation of Hydrogen Gas as a Result of Drilling Within the Saturated Zone." *Ground Water Monitoring and Remediation*.
- Butler JJ Jr. 1990. "The Role of Pumping Tests in Site Characterization: Some Theoretical Considerations." *Ground Water*, Vol. 28, No. 3, pp. 394-402.
- Dean JA (Ed). 1985. *Lange's Handbook of Chemistry*. Thirteenth Edition. McGraw-Hill Book Company, New York.
- Earlougher RC Jr. 1977. *Advances in Well Test Analysis*. Soc. of Petroleum Engineers, Monograph Vol. 5, Henry L. Doherty Series.
- Fayer MJ, and TB Walters. 1995. *Estimated Recharge Rates at the Hanford Site*. PNL-10285, Pacific Northwest Laboratory, Richland, Washington.
- Fruchter JS, FA Spane, JE Amonette, JK Fredrickson, CR Cole, JC Templeton, TO Stevens, DJ Holford, LE Eary, JM Zachara, BN Bjornstad, GD Black, VR Vermeul, and CS Simmons. 1994. *Interim Report Manipulation of Natural Subsurface Processes: Field Research and Validation*. PNL-10123, Pacific Northwest Laboratory, Richland, Washington.
- Komadell P, and J W Stucki. 1988. "The quantitative assay of minerals for Fe<sup>2+</sup> and Fe<sup>3+</sup> using 1,10-phenanthroline. III. A rapid photochemical method." *Clays and Clay Minerals*, 36:379-381.
- Lindsey KA, and GK Jaeger. 1993. *Geologic Setting of the 100-HR-3 Operable Unit, Hanford Site, South-Central Washington*. WHC-SD-EN-TI-132, Rev. 0, Westinghouse Hanford Company, Richland, Washington.
- Peres AM, M Onur, and AC Reynolds. 1989. "A New Analysis Procedure for Determining Aquifer Properties From Slug Test Data." *Water Resources Research*, Vol. 25, No. 7, pp. 1591-1602.
- Peterson RE. 1993. "183-H Solar Evaporation Basins," in Geosciences, *Annual Report for RCRA Groundwater Monitoring Projects at Hanford Site Facilities for 1991*. DOE/RL-93-09, Rev. 0, U.S. Department of Energy, Richland Field Office, Richland, Washington.
- Schreck RI. 1992. *Hanford Environmental Information System (HEIS) Operator's Manual*, WHC-SP-0660, vol. 1, Westinghouse Hanford Company, Richland, Washington.

Scott AD, and JE Amonette. 1988. "Role of iron in mica weathering" In J. W. Stucki, B. A. Goodman, and U. Schwertmann (eds.) *Iron in Soils and Clay Minerals*, pp. 537-623, Reidel, Dordrecht.

Spane FA, Jr. 1996. "Applicability of Slug Interference Tests for Hydraulic Characterization of Unconfined Aquifers: (1) Analytical Assessment." *Ground Water*, Vol. 34, No. 1, pp. 66-74.

Stevens TO, and JP Mckinley. 1995. "Lithoautotrophic Microbial Ecosystems in Deep Basalt Aquifers." *Science*, Vol. 270, pp. 450-454.

Stucki JW. 1988. "Structural Iron in Smectites," pp. 625-675. In: *Iron in Soils and Clay Minerals*. BA Goodman, and U Schwertmann, eds. D Reidel publishers Dordrecht, The Netherlands.

U. S. Department of Energy, Richland Field Office (DOE-RL). 1990. *Strategy for Handling and Disposal of Purgewater at the Hanford Site*, Washington, U.S. Department of Energy, Richland Field Office, Richland, Washington.

U. S. Department of Energy, Richland Field Office (DOE-RL). 1993. *Limited Field Investigation Report for the 100-HR-3 Operable Unit*. DOE/RL-93-34, U.S. Department of Energy, Richland Field Office, Richland, Washington.

U.S. Environmental Protection Agency, 1985, Water Quality Assessment: A Screening Procedure for Toxic and Conventional Pollutants in Surface and Ground Water - Part II (Revised 1985), EPA/600/6-85/002b, U.S. Environmental Protection Agency, Athens, Georgia.

Vermeul VR, SS Teel, JE Amonette, CR Cole, JS Fruchter, YA Gorby, FA Spane, JE Szecsody, MD Williams, and SB Yabusaki. 1995. *Geologic, Geochemical, Microbiologic, and Hydrologic Characterization at the In Situ Redox Manipulation Test Site*, PNL-10633, Pacific Northwest Laboratory, Richland, Washington.

Washington Administrative Code (WAC). 1992. Minimum Standards for Construction and Maintenance of Wells, as amended. WAC 173-160, Olympia, Washington.

Williams MD, SB Yabusaki, CR Cole, and VR Vermeul. 1994 "In Situ Redox Manipulation Field Experiment: Design Analysis." *Thirty-Third Hanford Symposium on Health and the Environment*, November 7-11, 1994, Richland, Washington.

Yabusaki SB and CR Cole. 1993 "Investigation of Tracer Behavior in Heterogeneous Porous Media," AGU 1993 Spring Meeting, May 17-21, 1993, Baltimore, Maryland.

**Appendix A**  
**Analytical Methods**

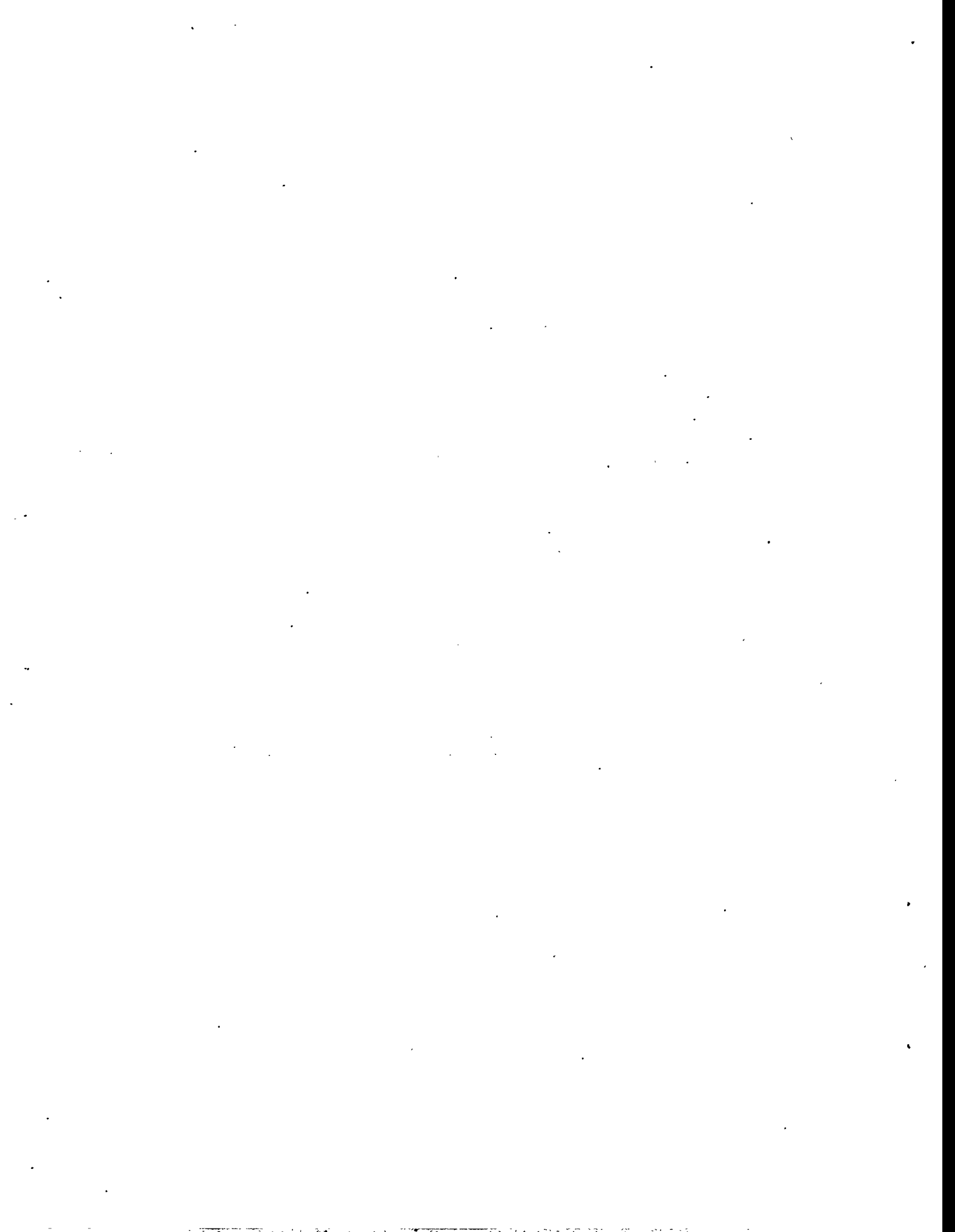


## Table of Contents

A.1 Geochemical Field Parameter Monitoring Probes .....	1
A.2 On-site Laboratory Equipment .....	2
A.2.1 Groundwater Geochemical Analyses .....	2
A.2.2 Dithionite Analyses .....	2
A.3 Metals Analyses .....	3
A.4 Ion Chromatography Analyses .....	3

## List of Figures

Figure A-1. Diagram of Dilution System for Fast (within 30 seconds) 150x to 600x Dilution. ....	4
---	---

## Appendix A

### Analytical Methods

In this appendix, analytical methodologies are discussed. These methodologies include those used in field, on-site laboratory, and analytical laboratory measurements.

Field measurements of groundwater chemistry were made using two different systems: 1) a flow-through assembly at each sampling station with geochemical field parameter-monitoring probes for measuring pH, dissolved oxygen, conductivity, and bromide (tracer test only), and 2) on-site laboratory equipment that measured groundwater geochemical parameters and dithionite concentrations. On-site analytical equipment was housed in an Explorer 30 mobile laboratory.

Samples were collected and submitted to analytical laboratories for trace metals analyses (ICP-MS) and sulfate/sulfite and bromide analyses (ion chromatography).

The sampling procedure for collecting the samples for laboratory analyses was as follows: Well pump effluent was routed to a sample manifold that simultaneously filled four 20-mL plastic vials. These four samples were taken for 1) additional oxygen, pH, and electrical conductivity measurements (on-site laboratory); 2) dithionite and dithionite degradation product measurement (on-site laboratory); 3) metals (analytical laboratory); and 4) bromide and sulfate/sulfite (analytical laboratory). All vials were immediately capped after collection. Samples for metals analyses were filtered through 0.45  $\mu\text{m}$ -diameter (pore size) membranes into a separate vial and acidified with 0.5 mL of 6 N nitric acid.

#### A.1 Geochemical Field Parameter Monitoring Probes

The geochemical field parameter probes had the following specifications:

- pH. Oakton WD-35615 series pH meter. Range = -2.00 to 16.00, accuracy =  $\pm 0.05$  pH, calibration with up to five buffers, automatic temperature compensation.
- Temperature. Oakton WD-35615 series temperature meter. Range = 0.0 to 100.0  $^{\circ}\text{C}$ , accuracy =  $\pm 0.5$   $^{\circ}\text{C}$ .
- Conductivity. Oakton WD-35607 series conductivity meter. Range = 0.0 to 199.9 mS, accuracy =  $\pm 50$   $\mu\text{S}$ .
- Dissolved oxygen. Orion model 810 dissolved oxygen meter. Range = 0 to 20 ppm, accuracy =  $\pm 0.1$  ppm.
- Bromide. Cole Palmer ISE Br. Range = 0.4 to 79,900 ppm, reproducibility =  $\pm 2\%$  of full scale. (Used during the tracer test only).

A flow-through monitoring assembly equipped with the above probes was located at each of the four sampling stations. The pumps, controllers, and manifolds used for obtaining groundwater samples at these sampling stations are discussed in Section 6.7.2 and are illustrated in Figure 6.5.

## A.2 On-site Laboratory Equipment

The following sections provide a description of on-site laboratory equipment and analytical methods used for field analysis of geochemical parameters, dithionite concentration, and verification of the presence of dithionite degradation products.

### A.2.1 Groundwater Geochemical Analyses

On-site laboratory instruments (microelectrodes) were used for duplicate pH, dissolved oxygen, and electrical conductivity measurements of all samples. This in-line electrode system was designed for much smaller volumes (0.02-in.-diameter flow path), so only a small amount of water was needed for accurate measurements (1 to 2 mL). Flow through instrumentation consisted of an oxygen electrode (Microelectrodes Inc., Londonery, NH), pH electrode (Fisher Scientific, Chicago, IL), and electrical conductivity electrode (Dionix Instruments, Sunnyvale, CA).

Laboratory electrodes were calibrated several times a day injecting calibration standards through the in-line system. Water temperature, as measured by each instrument was also recorded for calibration purposes. Three pH calibration standards used (4.0, 7.0, and 10.0). Calibration of the laboratory instruments indicated that the pH electrodes were very stable over the course of the field experiment. Accuracy of pH was  $\pm 0.02$ . Two electrical conductivity standards used (1000 and 10,000  $\mu\text{S}$ ) also indicated little recalibration of the conductivity electrodes was necessary. Accuracy of electrical conductivity measurement was  $\pm 1 \mu\text{S}$ . Oxygen electrode calibration consisted of two solutions: an oxygen-saturated sample (8.2 mg/L) and an oxygen-free sample (0.0 mg/L, dithionite-treated water). Oxygen electrode recalibration indicated a fair amount of drift as electrodes aged. Several oxygen electrodes were replaced during the course of the field experiment. Oxygen readings took a  $>1$  minute to stabilize if current and previous sample differed considerably in amount of dissolved oxygen. Accuracy of dissolved oxygen measurement was  $\pm 0.1 \text{ mg/L}$ .

### A.2.2 Dithionite Analyses

Dithionite concentrations and verification of the presence of dithionite degradation products were obtained on well samples and dithionite injection solution samples using laboratory equipment housed in the on-site mobile laboratory. Two separate dilution/UV absorbance systems were used to handle the sample load. Dithionite was measured on one system by UV absorbance at 315 nm with a fixed-wavelength UV detector (HP 1050 series, Hewlett Packard, Corvallis, OR). Dithionite was measured and the presence of dithionite degradation products (sulfite, thiosulfate) was verified on the second system with a scan from 200 to 450 nm using a diode array UV detector (Hewlett Packard, Corvallis, OR).

Two to three dithionite measurements were taken on each sample to insure accurate results. Measurements were extremely reproducible if sequential samples had similar concentrations of dithionite, but additional measurements were necessary, for example, to accurately measure a high concentration of dithionite directly after a sample of oxygenated water. Blanks (oxygen-free dilution water) were frequently injected to insure the dilution system was operating correctly. Dithionite standards were periodically made up and immediately analyzed. The highest sodium dithionite concentration used in the injection experiment (0.1 mol/L) was diluted 600x and measured within  $\pm 10^{-5} \text{ mol/L}$ . Samples with lower dithionite concentrations were diluted less or not at all, giving detection limits of  $10^{-7} \text{ mol/L}$  dithionite for undiluted samples. All blanks and standards were injected through both dilution/UV absorbance systems for cross calibration.

Dithionite and dithionite degradation product samples needed to be anaerobically diluted and measured quickly to insure accuracy. Accurate dithionite measurements were extremely sensitive to even small amounts of oxygen, so several in-line oxygen traps and other precautions were used in the dilution system. The dilution system allowed for fast (within 30 seconds) 150x to 600x dilution (Figure A-1) and consisted of an injection valve, a syringe pump for dilution, and a mixing system. A liquid sample (1 to 5 mL) is first 0.1- $\mu$ m filter injected into a 6-way high-performance liquid chromatography (HPLC) injection valve (Valco Industries, Houston, TX) with a 20- $\mu$ L sample loop. This accurately ( $\pm 0.5\%$ ) separated 20  $\mu$ L which, with the syringe pump, was mixed with 3.0 to 12.0 mL of degassed, oxygen-free water, depending on the amount of dilution desired. Dilution water was degassed with helium sparging and oxygen removed from the helium gas stream with dithionite solution sparging. The diluted sample was then manually mixed between two in-line syringes then injected into one of two flow-through UV absorbance detectors. Stainless steel tubing was used on the dilution system to minimize oxygen diffusion.

### A.3 Metals Analyses

Samples were collected and submitted to a PNNL laboratory for trace metals analyses. These samples included ground water and injection water. The samples were 0.45- $\mu$ m filtered and acidified with 0.5 mL of 6 N nitric acid in the field. Metals samples were analyzed by inductively coupled plasma - mass spectrometry (ICP-MS) using PNNL procedure PNL-ALO-280 from the PNL-599 procedure manual ("Analytical Chemistry Laboratory (ACL) Procedure Compendium"). The results included the following constituents: manganese, iron, nickel, copper zinc, arsenic, selenium, silver, cadmium, tin, antimony, barium, lead, and chromium. Metals analyses results are discussed in Section 10.8.4.

### A.4 Ion Chromatography Analyses

Samples were analyzed by ion chromatography by PNNL for bromide and sulfate/sulfite using a modified version of procedure IC-1 ("IC-1 PNL Test Method for Anions in Water by Ion-Chromatography"). The equipment used consisted of a Dionex 4000i ion chromatograph, a SpectraPhysics SP 8875 autosampler, a Waters WISP Model 710B Sample Changer, and the Nelson Analytical 3000 Series Chromatography System. Bromide analyses were performed in support of the Tracer Test; results are discussed in Section 8.0. Sulfate/sulfite samples submitted for analysis included those from the Modutank (Section 10.4.4) and the monitoring wells (Section 10.8).

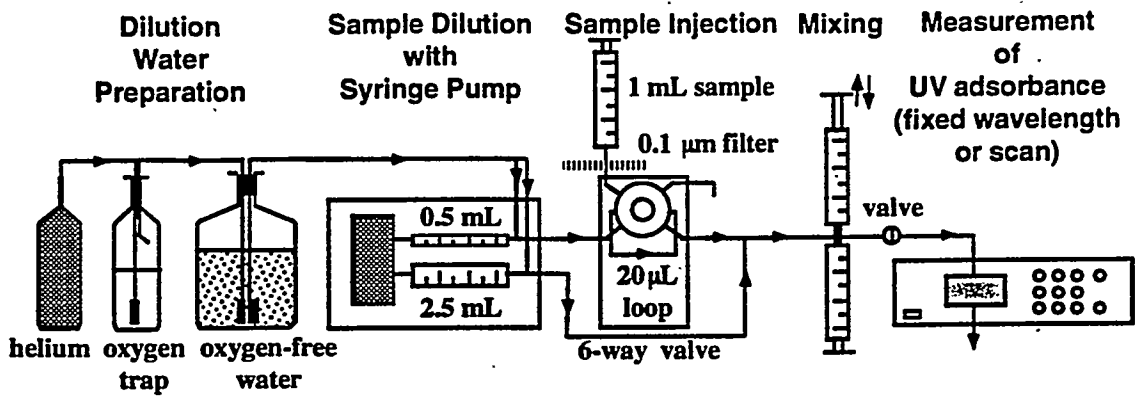
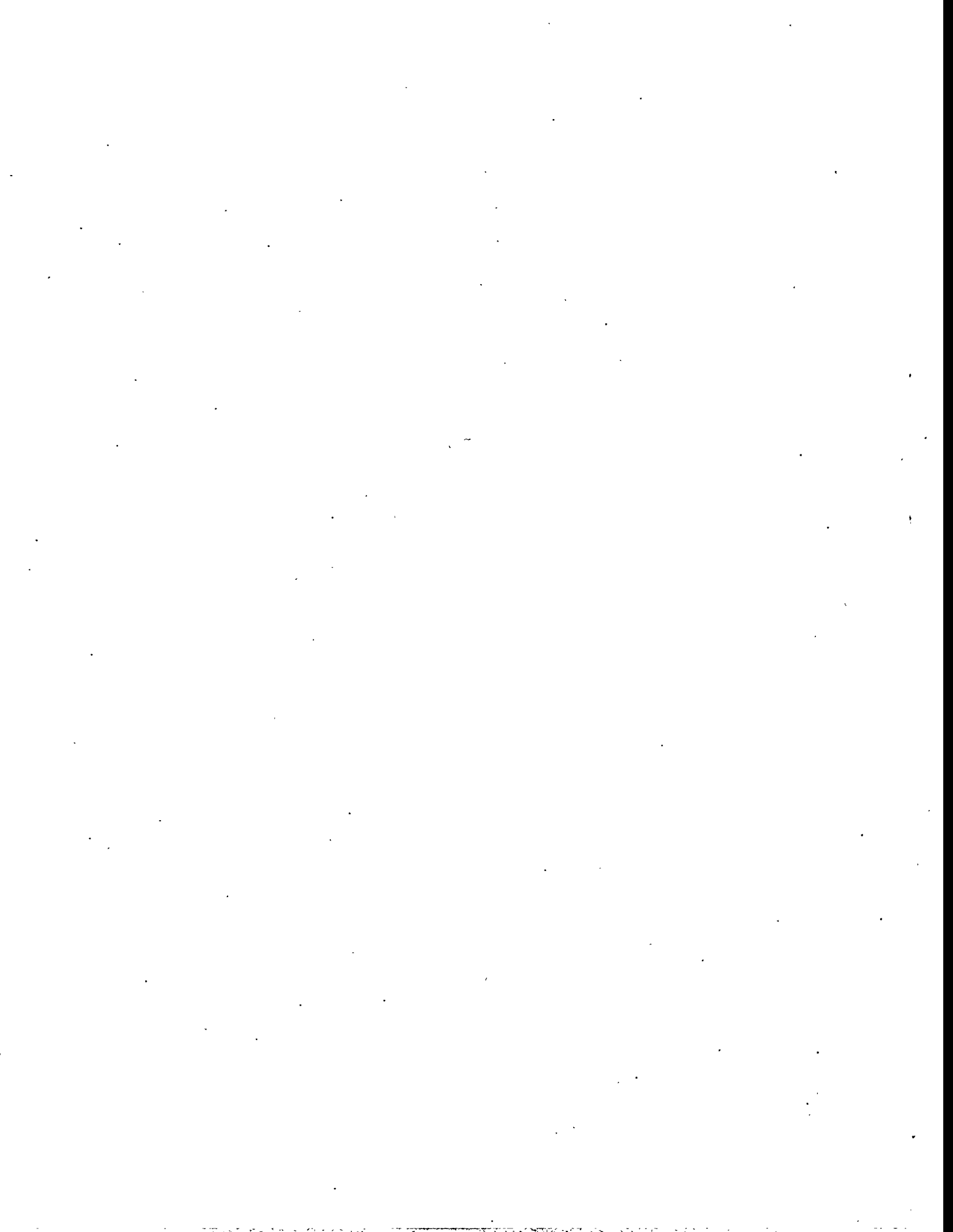


Figure A-1. Diagram of Dilution System for Fast (within 30 seconds) 150x to 600x Dilution.

**APPENDIX B**

**WELL DIAGRAMS**



# Table of Contents

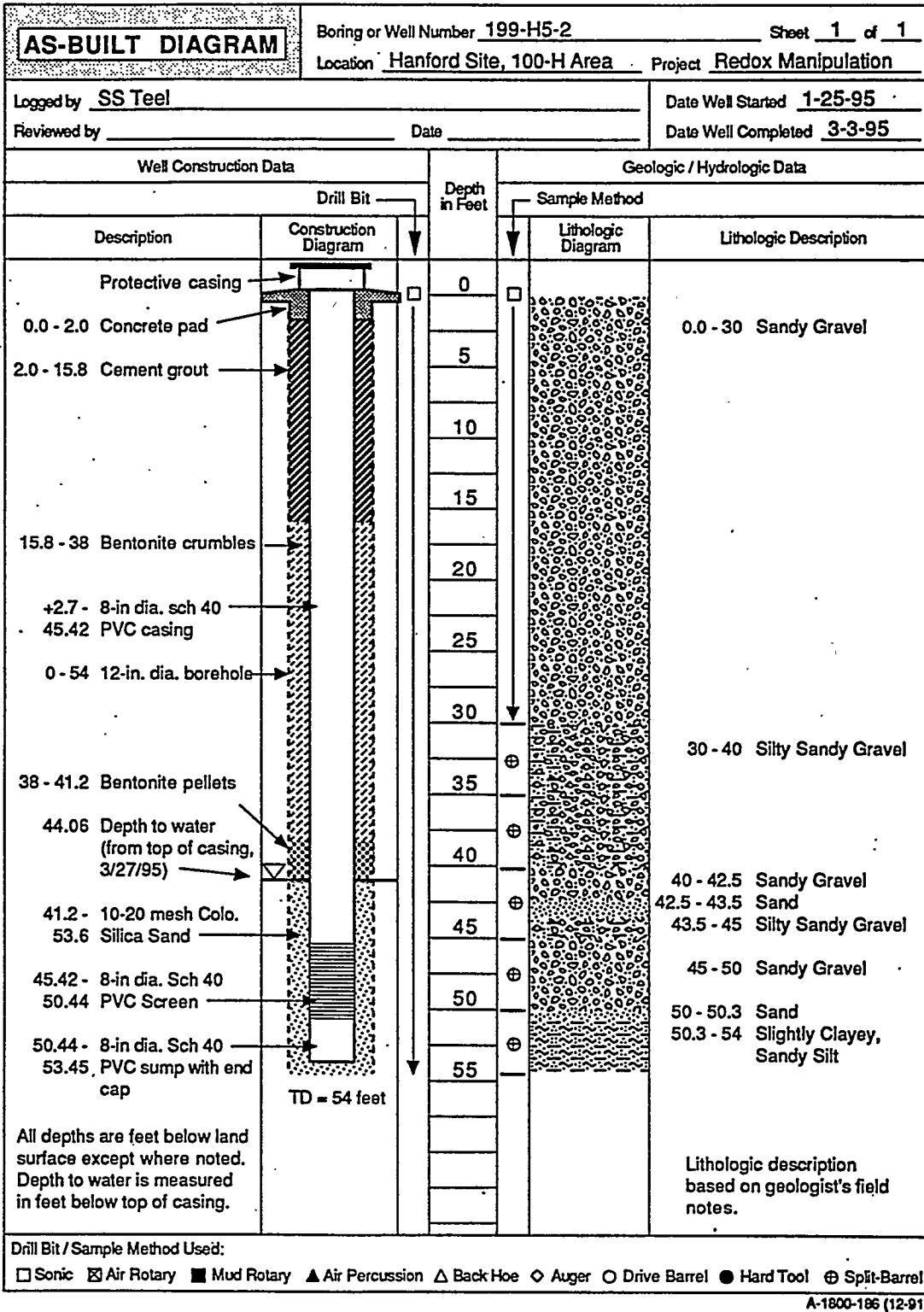
Appendix B. Well Diagrams .....	B.1
---------------------------------	-----

## List of Figures

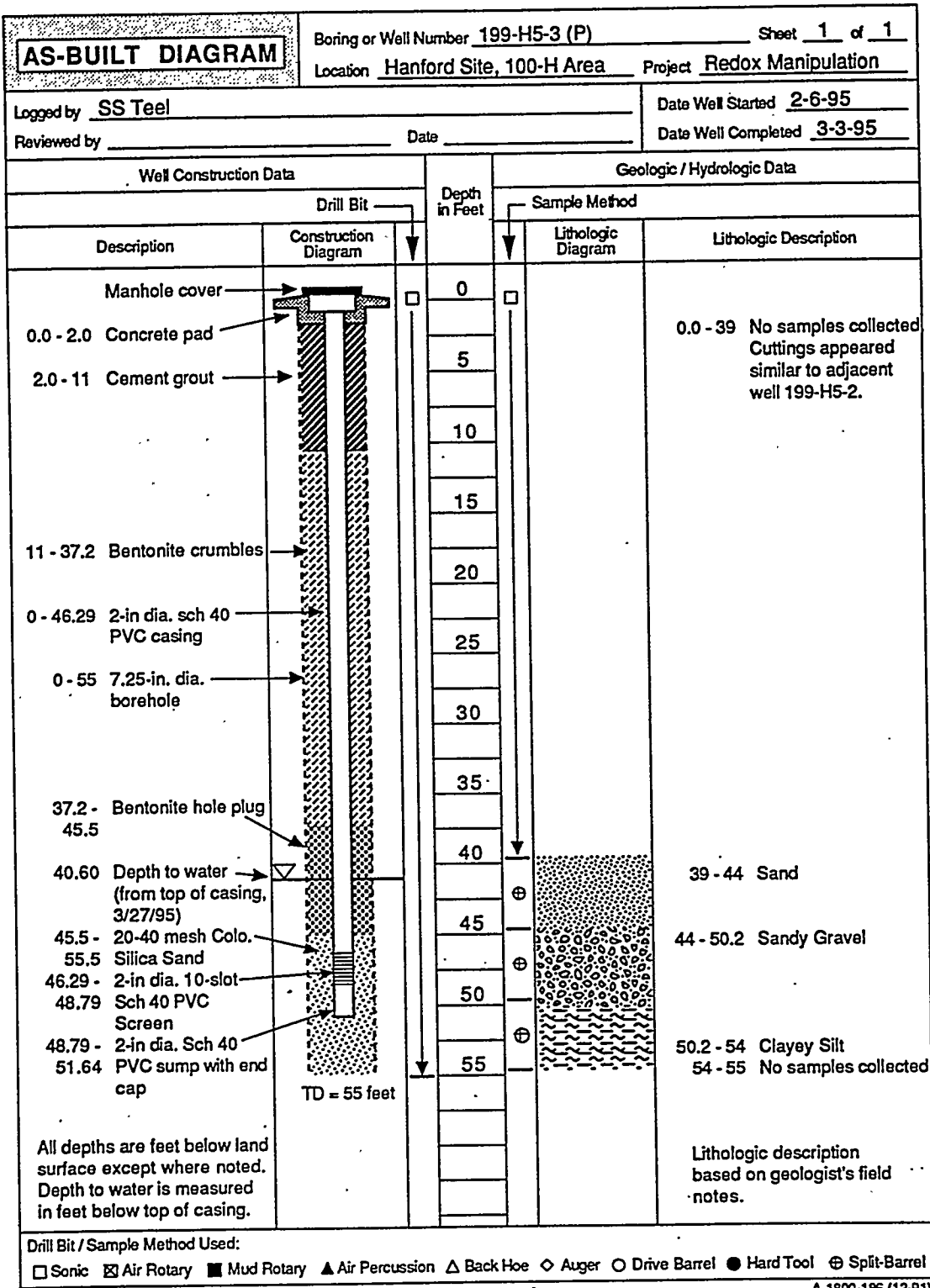
199-H5-2 .....	B.2
199-H5-3(P) .....	B.3
199-H5-4(P) .....	B.4
199-H5-5(P) .....	B.5
199-H5-3(O) .....	B.6
199-H5-4(O) .....	B.7
199-H5-5(O) .....	B.8
199-H5-6 .....	B.9
199-H5-7 .....	B.10
199-H5-8 .....	B.11
199-H5-9 .....	B.12
199-H5-10 .....	B.13
199-H5-11 .....	B.14
199-H5-12 .....	B.15
199-H5-13 .....	B.16
199-H5-14 .....	B.17
199-H5-15 .....	B.18
B2618 .....	B.19
B2619 .....	B.20
B2620 .....	B.21
B2621 .....	B.22
B2622 .....	B.23
B2623 .....	B.24
B2624 .....	B.25
B2625 .....	B.26

## **Appendix B. Well Diagrams**

**This Appendix contains as-built diagrams for the 17 wells and 8 coreholes installed during FY 1995-96 at the In-Situ Redox Manipulation Test Site in the 100-H Area. Information contained on these diagrams include well construction details, sampling intervals, and lithology.**



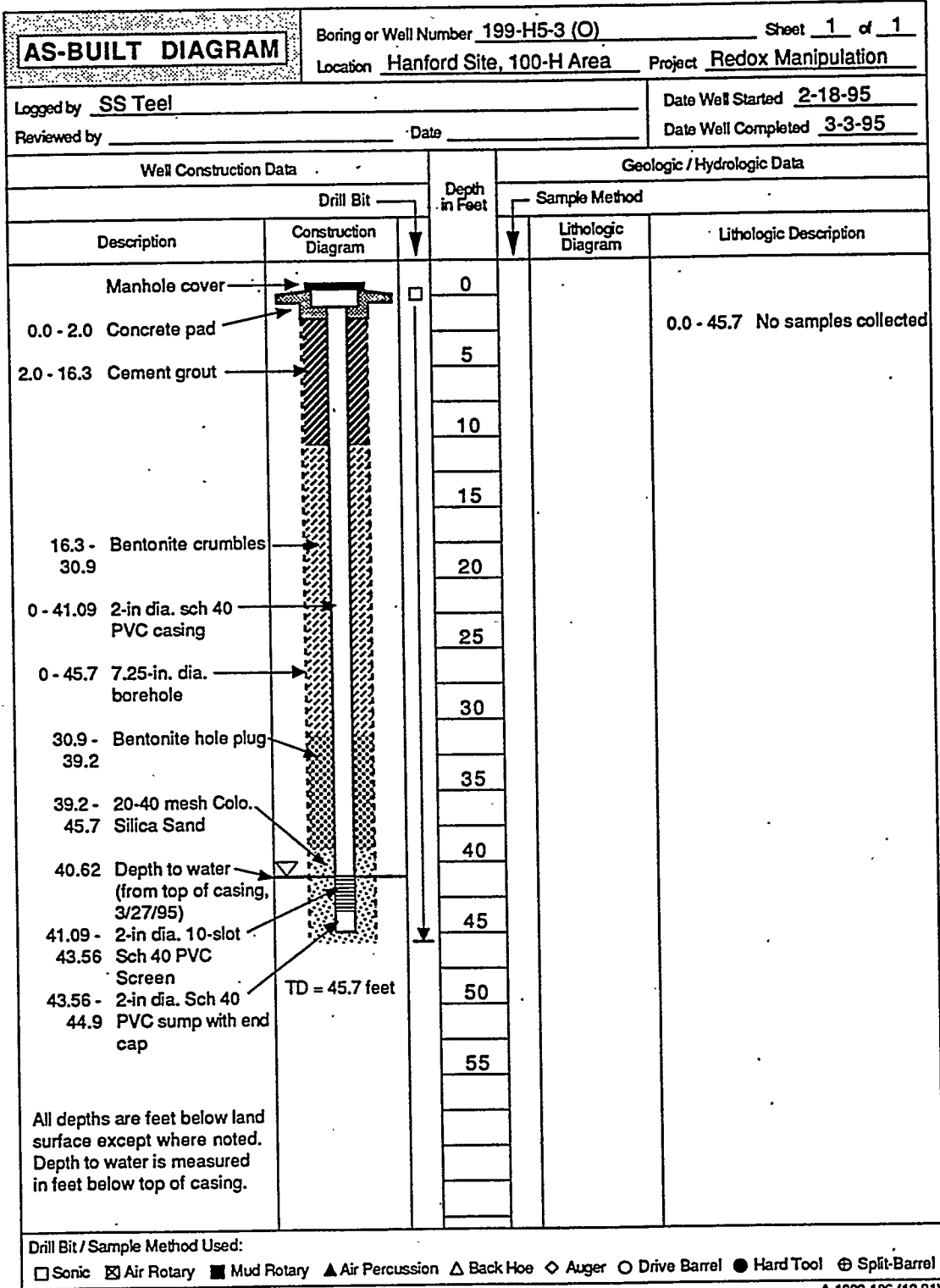
A-1800-186 (12-91)



A-1800-186 (12-91)







A-1800-186 (12-91)

# AS-BUILT DIAGRAM

Boring or Well Number 199-H5-4 (O) Sheet 1 of 1

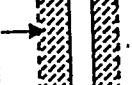
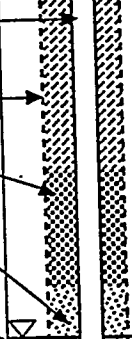
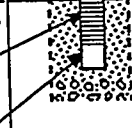
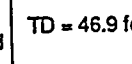
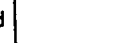
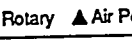
Location Hanford Site, 100-H Area Project Redox Manipulation

Logged by SS Teel

Date Well Started 2-17-95

Reviewed by \_\_\_\_\_ Date \_\_\_\_\_

Date Well Completed 3-3-95

Well Construction Data		Depth in Feet	Geologic / Hydrologic Data	
Description	Construction Diagram		Sample Method	Lithologic Description
Manhole cover		0		0 - 46.9 No samples collected
0.0 - 2.0 Concrete pad		5		
2.0 - 12.5 Cement grout		10		
		15		
12.5 - Bentonite crumbles		20		
30.8		25		
0 - 41.69 2-in dia. sch 40 PVC casing		30		
0 - 46.9 7.25-in. dia. borehole		35		
30.8 - Bentonite hole plug		40		
38.2		45		
38.2 - 20-40 mesh Colo. Silica Sand		50		
40.62 Depth to water (from top of casing, 3/27/95)		55		
41.69 - 2-in dia. 10-slot Sch 40 PVC Screen				
44.16 - 2-in dia. Sch 40 PVC sump with end cap				
45.5 - Slough				
46.9				

TD = 46.9 feet

All depths are feet below land surface except where noted. Depth to water is measured in feet below top of casing.

Drill Bit / Sample Method Used:  
 Sonic  Air Rotary  Mud Rotary  Air Percussion  Back Hoe  Auger  Drive Barrel  Hard Tool  Split-Barrel

A-1800-186 (12-91)



# AS-BUILT DIAGRAM

Boring or Well Number 199-H5-6 Sheet 1 of 1

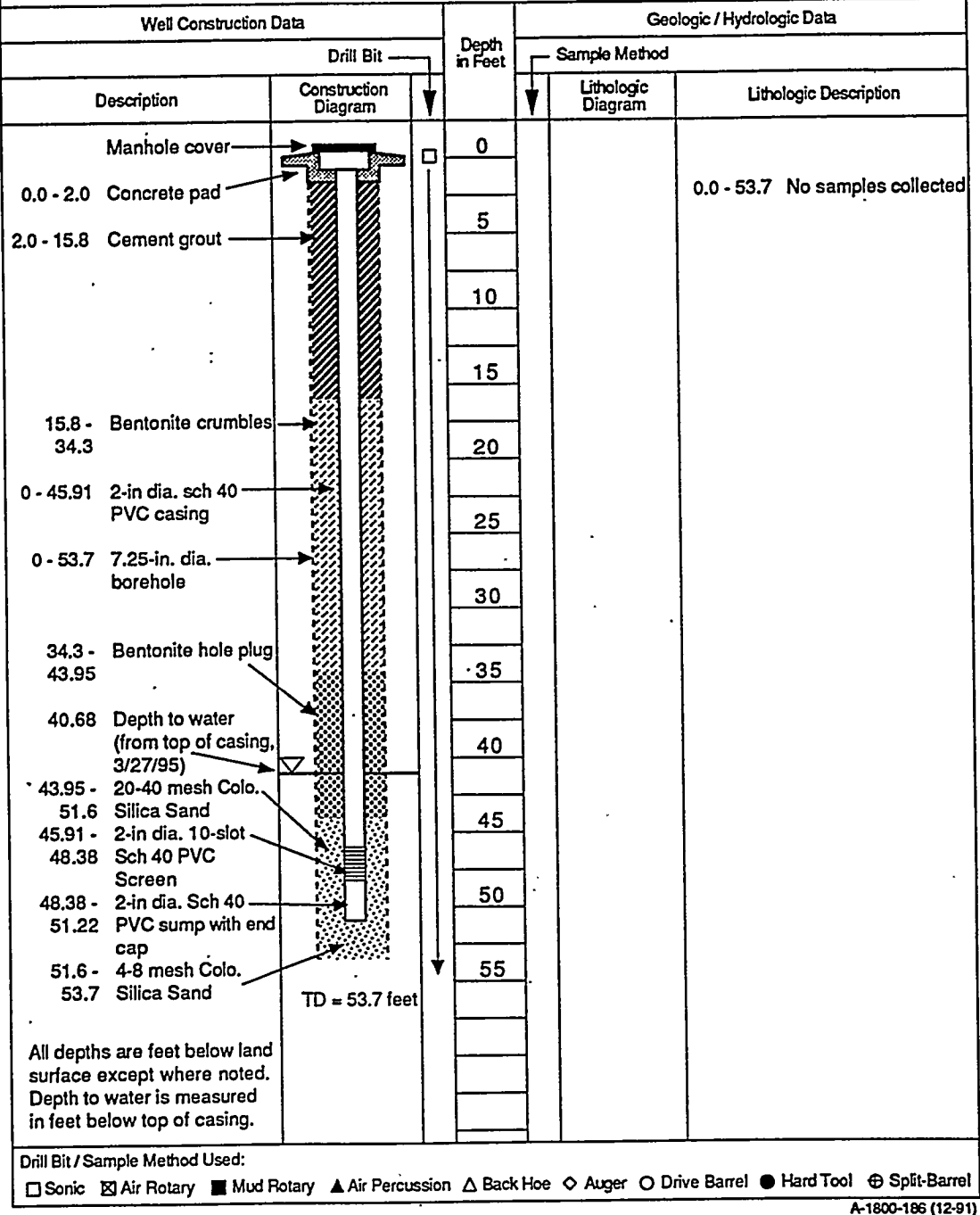
Location Hanford Site, 100-H Area Project Redox Manipulation

Logged by SS Teel

Date Well Started 2-20-95

Reviewed by \_\_\_\_\_ Date \_\_\_\_\_

Date Well Completed 3-3-95



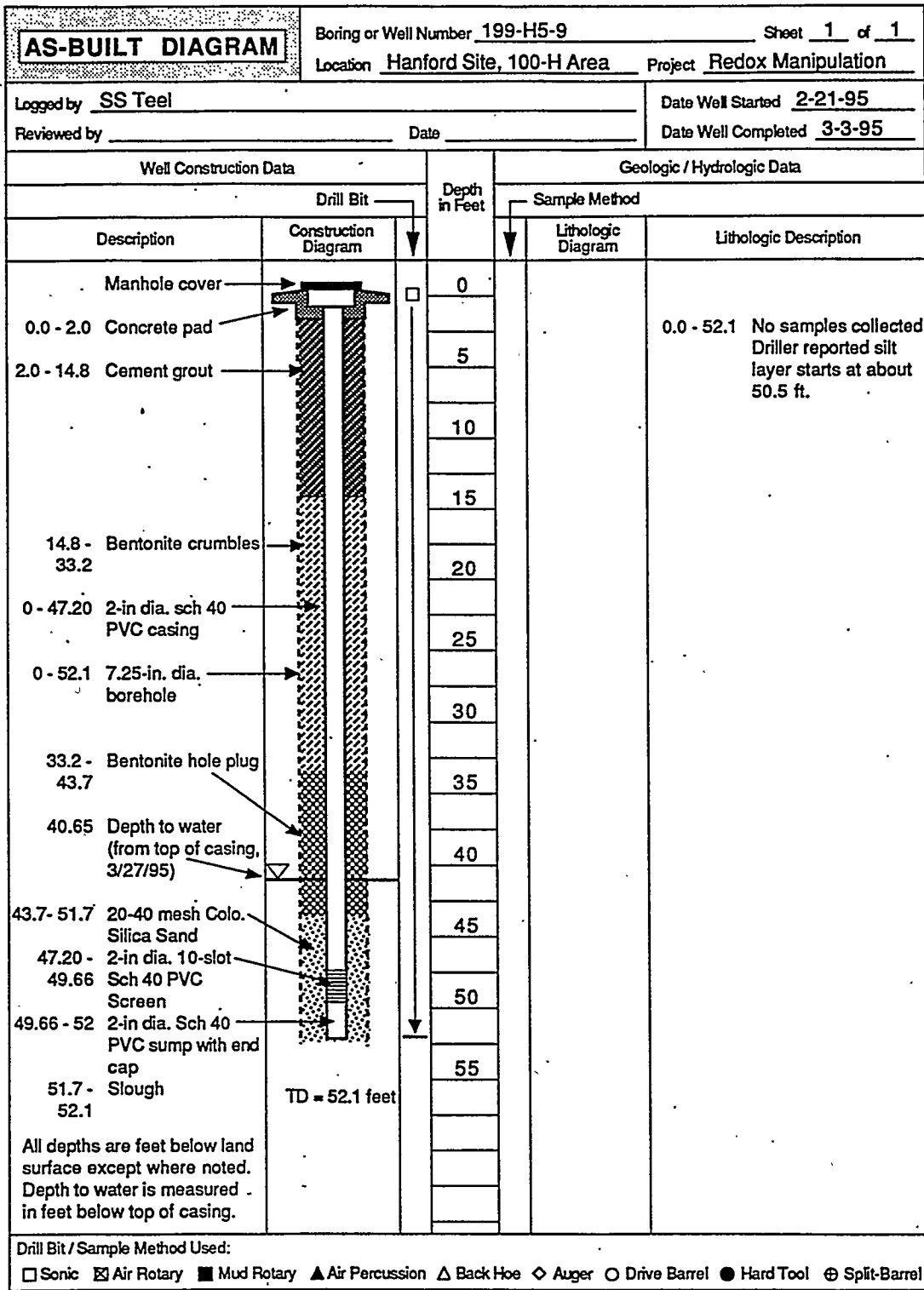
Drill Bit / Sample Method Used:

Sonic  
  Air Rotary  
  Mud Rotary  
  Air Percussion  
  Back Hoe  
  Auger  
  Drive Barrel  
  Hard Tool  
  Split-Barrel

A-1800-186 (12-91)



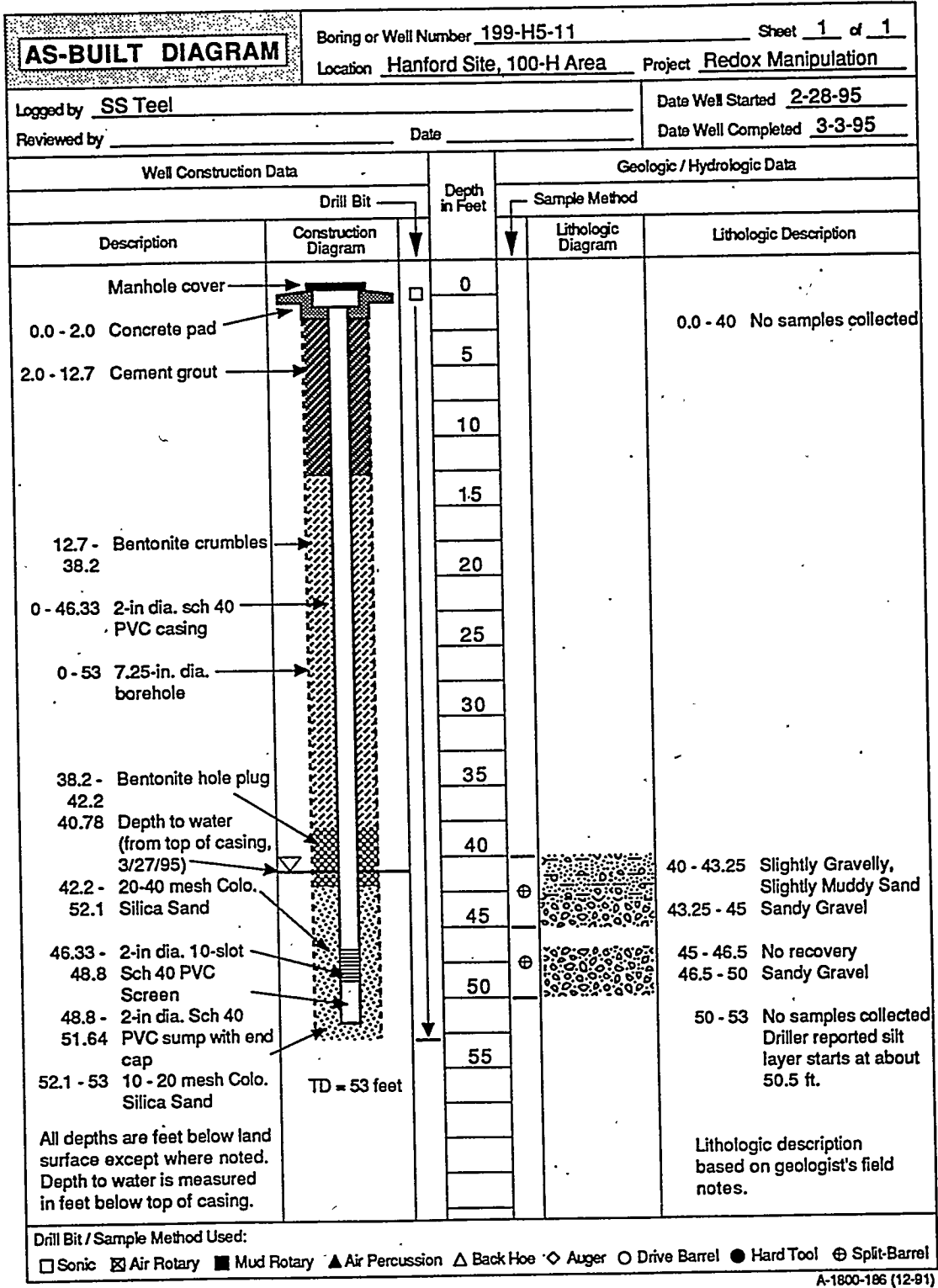




Drill Bit / Sample Method Used:  
 Sonic     Air Rotary     Mud Rotary     Air Percussion     Back Hoe     Auger     Drive Barrel     Hard Tool     Split-Barrel

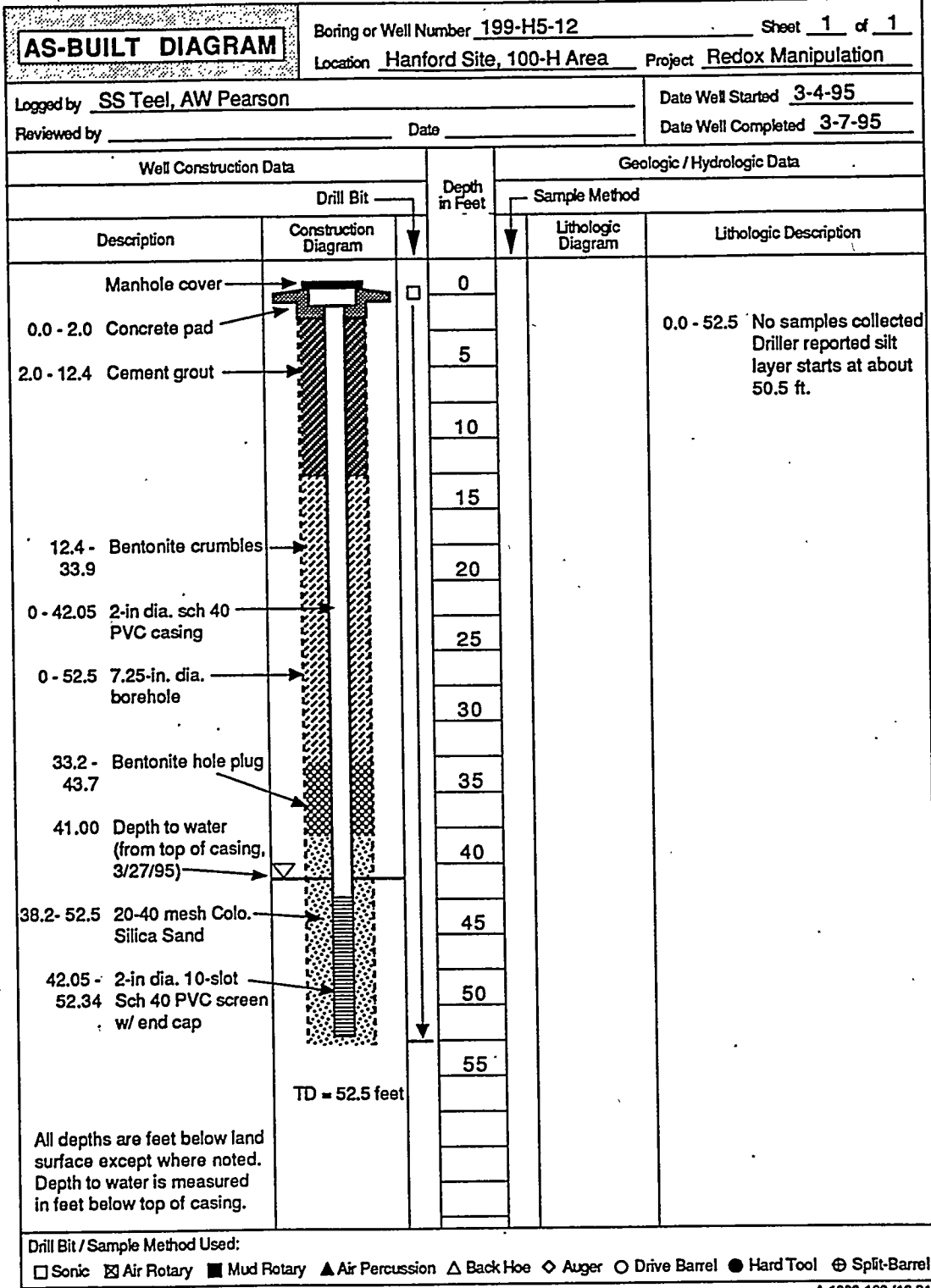
A-1800-186 (12-91)





Drill Bit / Sample Method Used:  
 Sonic  Air Rotary  Mud Rotary  Air Percussion  Back Hoe  Auger  Drive Barrel  Hard Tool  Split-Barrel

A-1800-186 (12-91)



Drill Bit / Sample Method Used:  
 Sonic    Air Rotary    Mud Rotary    Air Percussion    Back Hoe    Auger    Drive Barrel    Hard Tool    Split-Barrel

A-1800-186 (12-91)



# AS-BUILT DIAGRAM

Boring or Well Number 199-H5-14 Sheet 1 of 1

Location Hanford Site, 100-H Area Project Redox Manipulation

Logged by AW Pearson

Date Well Started 3-6-95

Reviewed by \_\_\_\_\_ Date \_\_\_\_\_

Date Well Completed 3-7-95

Well Construction Data		Depth in Feet	Geologic / Hydrologic Data	
Description	Construction Diagram		Lithologic Diagram	Lithologic Description
Manhole cover		0		0.0 - 52.0 No samples collected
0.0 - 2.0 Concrete pad		5		
2.0 - 13.2 Cement grout		10		
		15		
13.2 - Bentonite crumbles		20		
35.7		25		
0 - 42.26 2-in dia. sch 40 PVC casing		30		
0 - 52.0 7.25-in. dia. borehole		35		
35.7 - Bentonite hole plug		39.0		
41.66 Depth to water (from top of casing, 3/27/95)		40		
39.0 - 52.0 20-40 mesh Colo. Silica Sand		45		
42.26 - 2-in dia. 10-slot Sch 40 PVC screen w/ end cap		50		
		55		
TD = 52 feet				

All depths are feet below land surface except where noted. Depth to water is measured in feet below top of casing.

Drill Bit / Sample Method Used:

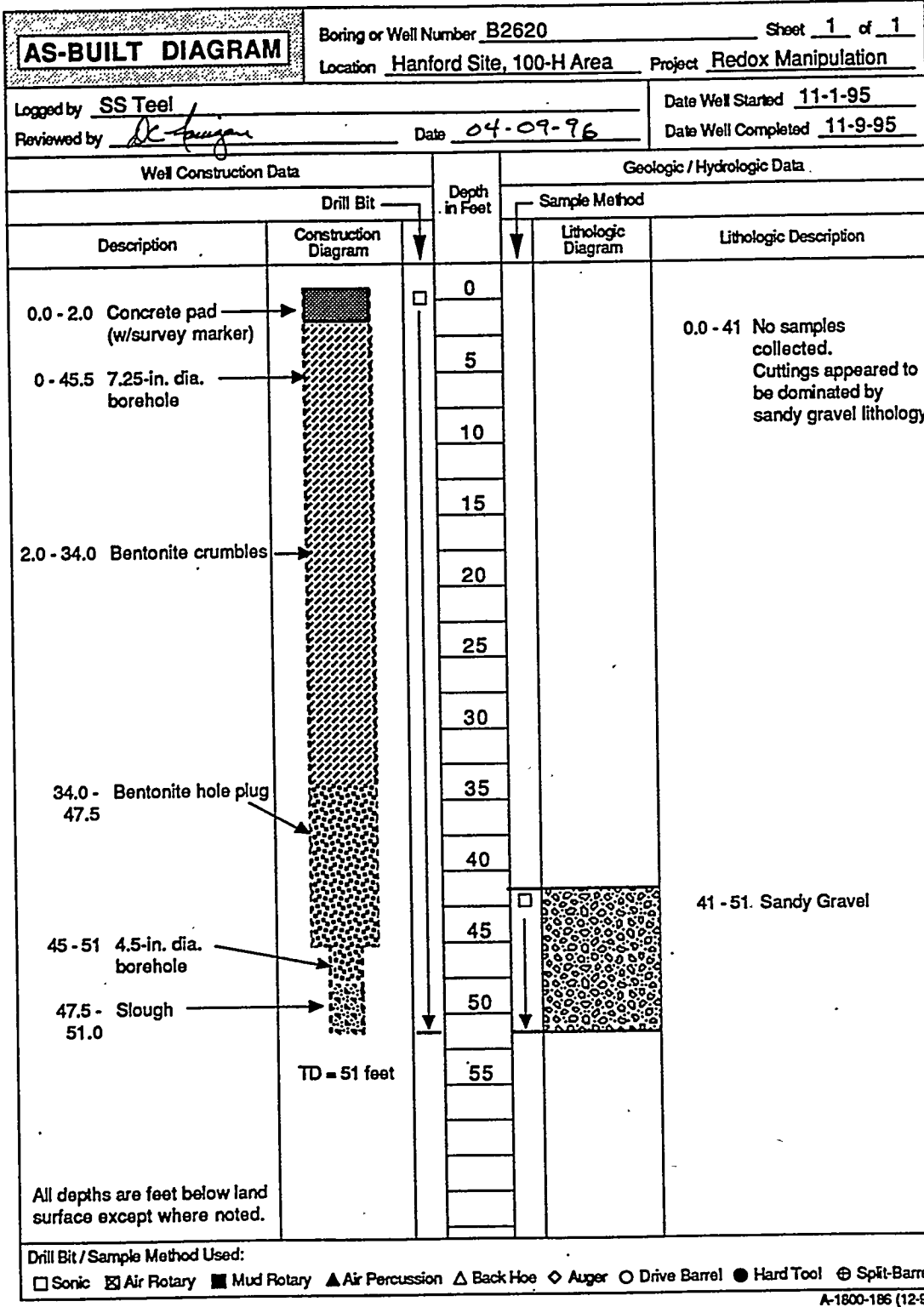
Sonic  
  Air Rotary  
  Mud Rotary  
  Air Percussion  
  Back Hoe  
  Auger  
  Drive Barrel  
  Hard Tool  
  Split-Barrel

A-1800-186 (12-91)



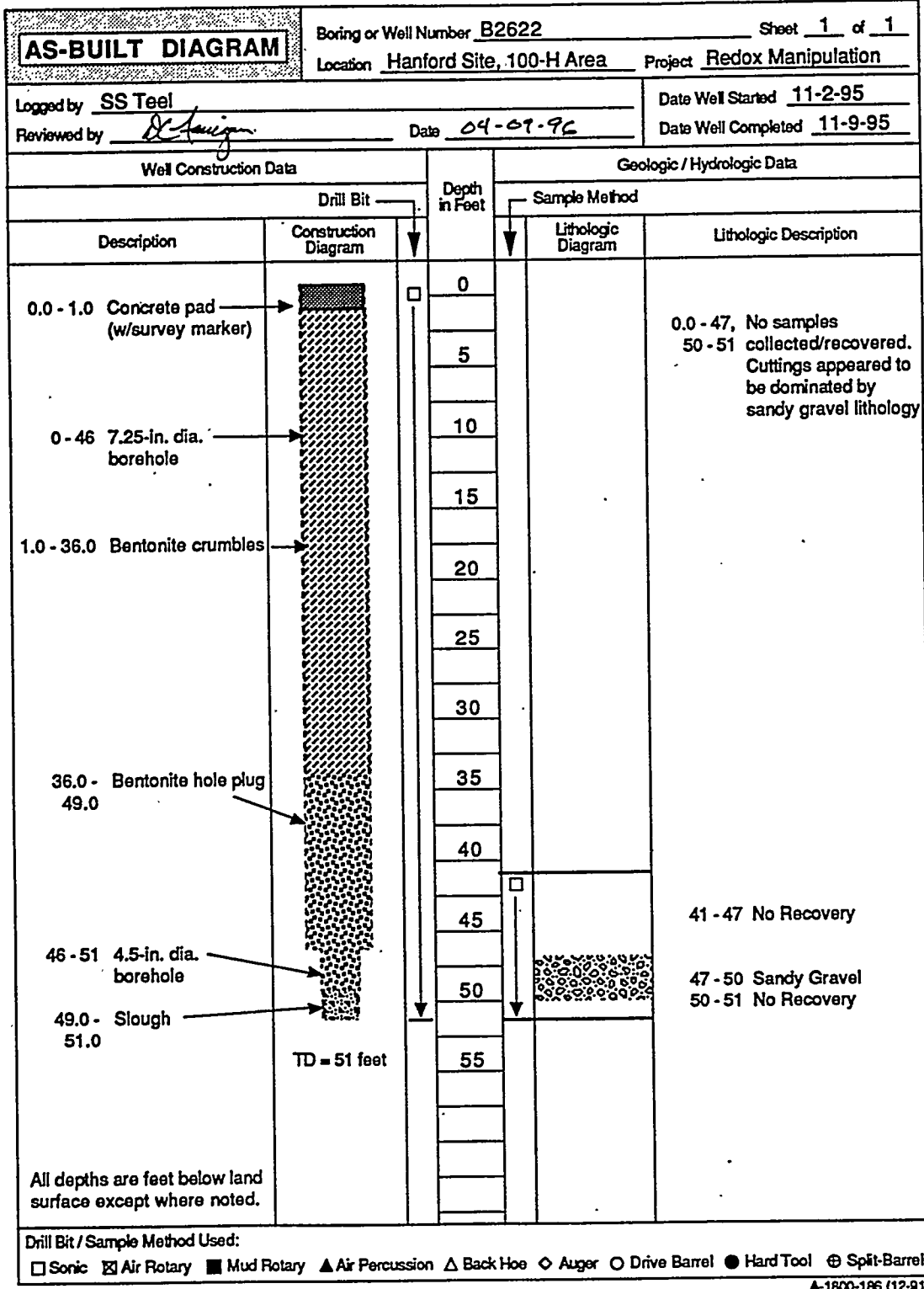


<b>AS-BUILT DIAGRAM</b>		Boring or Well Number <u>B2619</u> Sheet <u>1</u> of <u>1</u>	
Location <u>Hanford Site, 100-H Area</u> Project <u>Redox Manipulation</u>		Date Well Started <u>10-30-95</u>	
Logged by <u>SS Teel</u>		Date Well Completed <u>11-9-95</u>	
Reviewed by <u>DC Lanyon</u> Date <u>04-09-96</u>			
Well Construction Data		Geologic / Hydrologic Data	
Description	Construction Diagram	Depth in Feet	Sample Method / Lithologic Description
0.0 - 1.5 Concrete pad (w/survey marker)		0	0.0 - 50 No samples collected/recovered. Cuttings appeared to be dominated by sandy gravel lithology
		5	
		10	
		15	
1.5 - 35.0 Bentonite crumbles		20	
		25	
0 - 45 7.25-in. dia. borehole		30	
		35	
35.0 - Bentonite hole plug		40	
47.0		45	
45 - 50 4.5-in. dia. borehole		50	
47.0 - Slough		50	
50.0		55	
		60	
		65	
		70	
		75	
		80	
		85	
		90	
		95	
		100	
		105	
		110	
		115	
		120	
		125	
		130	
		135	
		140	
		145	
		150	
		155	
		160	
		165	
		170	
		175	
		180	
		185	
		190	
		195	
		200	
		205	
		210	
		215	
		220	
		225	
		230	
		235	
		240	
		245	
		250	
		255	
		260	
		265	
		270	
		275	
		280	
		285	
		290	
		295	
		300	
		305	
		310	
		315	
		320	
		325	
		330	
		335	
		340	
		345	
		350	
		355	
		360	
		365	
		370	
		375	
		380	
		385	
		390	
		395	
		400	
		405	
		410	
		415	
		420	
		425	
		430	
		435	
		440	
		445	
		450	
		455	
		460	
		465	
		470	
		475	
		480	
		485	
		490	
		495	
		500	
		505	
		510	
		515	
		520	
		525	
		530	
		535	
		540	
		545	
		550	
		555	
		560	
		565	
		570	
		575	
		580	
		585	
		590	
		595	
		600	
		605	
		610	
		615	
		620	
		625	
		630	
		635	
		640	
		645	
		650	
		655	
		660	
		665	
		670	
		675	
		680	
		685	
		690	
		695	
		700	
		705	
		710	
		715	
		720	
		725	
		730	
		735	
		740	
		745	
		750	
		755	
		760	
		765	
		770	
		775	
		780	
		785	
		790	
		795	
		800	
		805	
		810	
		815	
		820	
		825	
		830	
		835	
		840	
		845	
		850	
		855	
		860	
		865	
		870	
		875	
		880	
		885	
		890	
		895	
		900	
		905	
		910	
		915	
		920	
		925	
		930	
		935	
		940	
		945	
		950	
		955	
		960	
		965	
		970	
		975	
		980	
		985	
		990	
		995	
		1000	
		1005	
		1010	
		1015	
		1020	
		1025	
		1030	
		1035	
		1040	
		1045	
		1050	
		1055	
		1060	
		1065	
		1070	
		1075	
		1080	
		1085	
		1090	
		1095	
		1100	
		1105	
		1110	
		1115	
		1120	
		1125	
		1130	
		1135	
		1140	
		1145	
		1150	
		1155	
		1160	
		1165	
		1170	
		1175	
		1180	
		1185	
		1190	
		1195	
		1200	
		1205	
		1210	
		1215	
		1220	
		1225	
		1230	
		1235	
		1240	
		1245	
		1250	
		1255	
		1260	
		1265	
		1270	
		1275	
		1280	
		1285	
		1290	
		1295	
		1300	
		1305	
		1310	
		1315	
		1320	
		1325	
		1330	
		1335	
		1340	
		1345	
		1350	
		1355	
		1360	
		1365	
		1370	
		1375	
		1380	
		1385	
		1390	
		1395	
		1400	
		1405	
		1410	
		1415	
		1420	
		1425	
		1430	
		1435	
		1440	
		1445	
		1450	
		1455	
		1460	
		1465	
		1470	
		1475	
		1480	
		1485	
		1490	
		1495	
		1500	
		1505	
		1510	
		1515	
		1520	
		1525	
		1530	
		1535	
		1540	
		1545	
		1550	
		1555	
		1560	
		1565	
		1570	
		1575	
		1580	
		1585	
		1590	
		1595	
		1600	
		1605	
		1610	
		1615	
		1620	
		1625	
		1630	
		1635	
		1640	
		1645	
		1650	
		1655	
		1660	
		1665	
		1670	
		1675	
		1680	
		1685	
		1690	
		1695	
		1700	
		1705	
		1710	
		1715	
		1720	
		1725	
		1730	
		1735	
		1740	
		1745	
		1750	
		1755	
		1760	
		1765	
		1770	
		1775	
		1780	
		1785	
		1790	
		1795	
		1800	
		1805	
		1810	
		1815	
		1820	
		1825	
		1830	
		1835	
		1840	
		1845	
		1850	
		1855	
		1860	
		1865	
		1870	
		1875	
		1880	
		1885	
		1890	
		1895	
		1900	
		1905	
		1910	
		1915	
		1920	
		1925	
		1930	
		1935	
		1940	
		1945	
		1950	
		1955	
		1960	
		1965	
		1970	
		1975	
		1980	
		1985	
		1990	
		1995	
		2000	
		2005	
		2010	
		2015	
		2020	
		2025	
		2030	
		2035	
		2040	
		2045	
		2050	
		2055	
		2060	
		2065	
		2070	
		2075	
		2080	
		2085	
		2090	
		2095	
		2100	
		2105	
		2110	
		2115	



A-1800-186 (12-91)

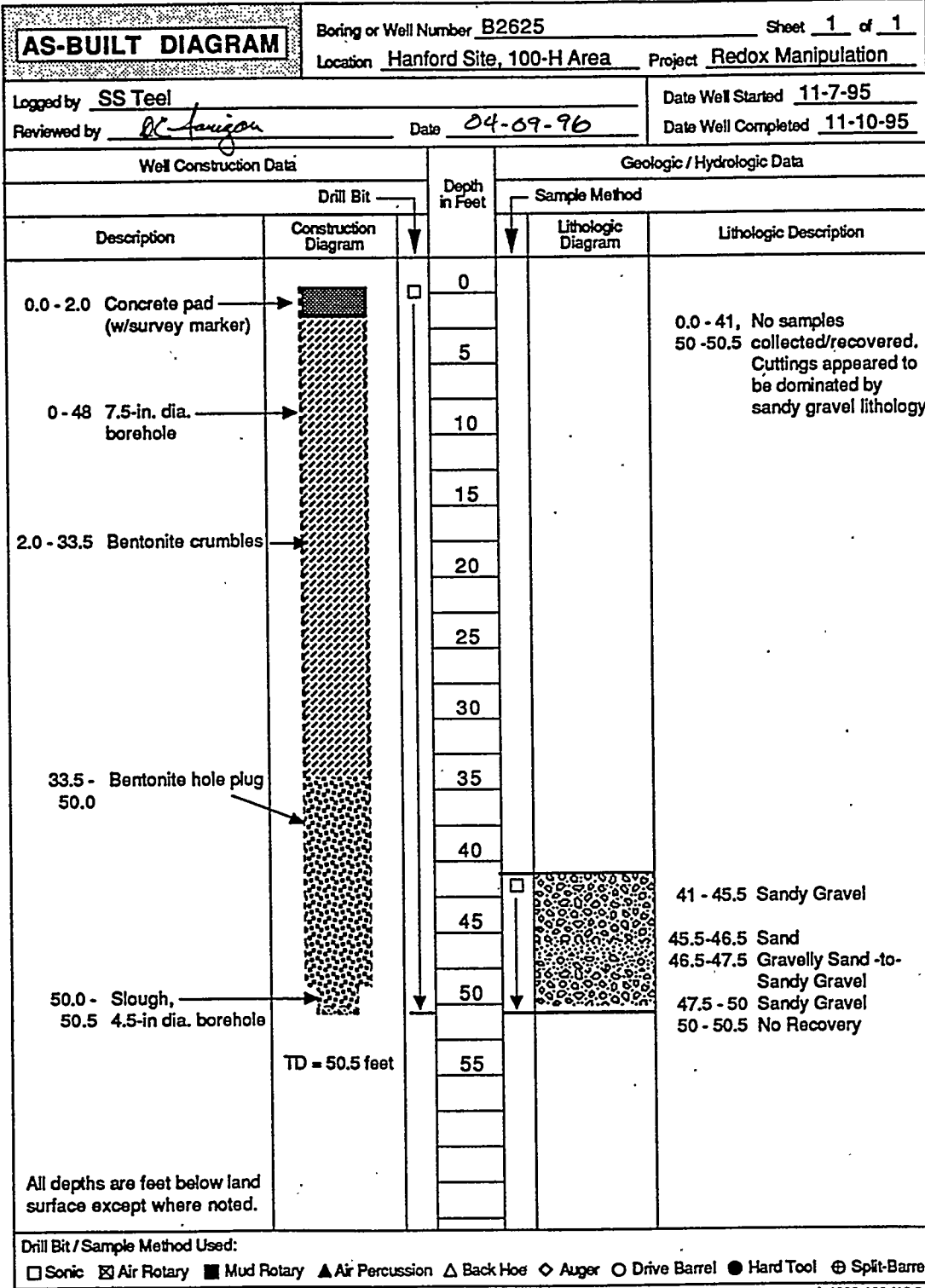




A-1800-186 (12-91)







**APPENDIX C**

**GEOLOGY AND HYDROLOGY OF THE 100-H AREA**

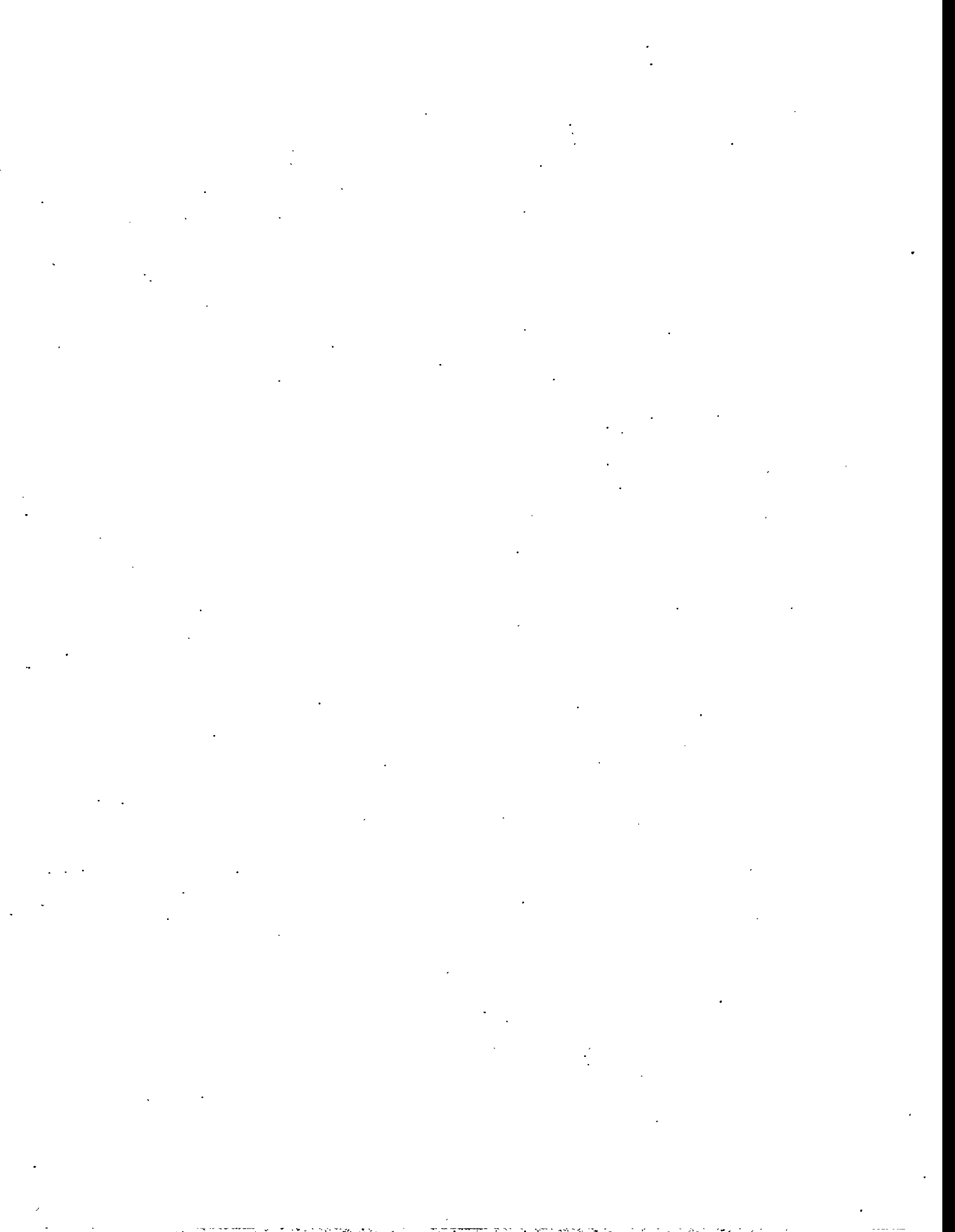


## Table of Contents

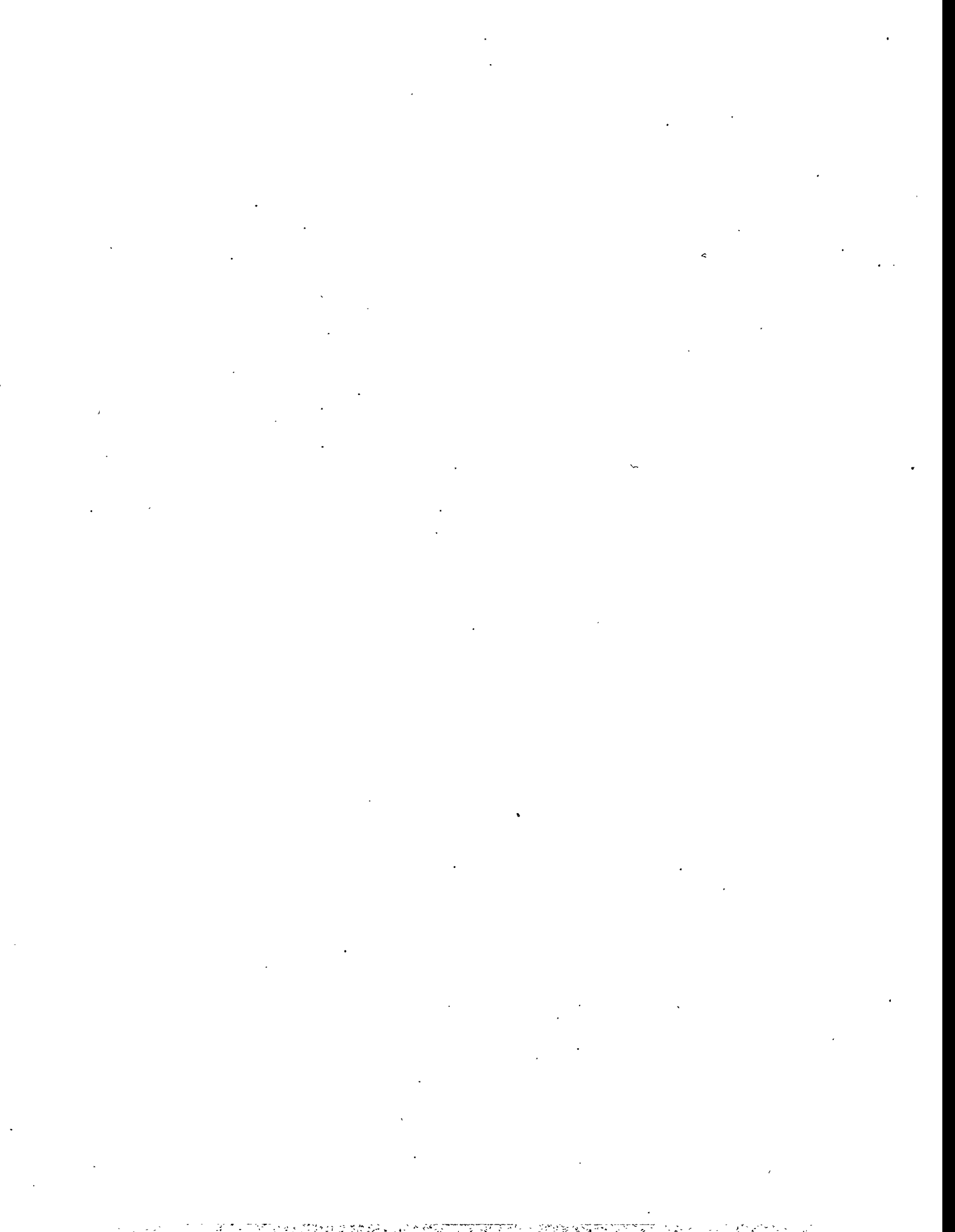
Appendix C. Geology and Hydrology of the 100H Area .....	C.1
C.1 Geology of the 100-H Area .....	C.1
C.1.1 Ringold Formation .....	C.1
C.1.2 Hanford Formation .....	C.2
C.2 Hydrology of the 100-H Area .....	C.4

## List of Figures

Figure C-1	Generalized Stratigraphy of the Suprabasalt Sediments in the Pasco Basin (from Lindsey and Jaeger 1993). .....	C.3
Figure C-2	Water Table at the 100-H Area during High Columbia River Stage (DOE-RL 1993). .....	C.5
Figure C-3	Water Table at the 100-H Area during Low Columbia River Stage (DOE-RL 1993) .....	C.6

## List of Tables

Table C-1. Hydrometer Analyses Results from the Ringold Formation. ....	C.2
---	-----



## Appendix C. Geology and Hydrology of the 100H Area

This Appendix briefly describes the geology and hydrology of the 100-H area, specifically the hydrogeologic setting in the vicinity of the ISRM test site. A more detailed discussion of the geology and hydrology of the area, incorporating recent characterization data, is presented in Sections 6.0 and Appendix D.

### C.1 Geology of the 100-H Area

The Hanford Site is underlain by the following units (oldest to youngest): 1) pre-Miocene sedimentary and crystalline rocks, 2) Miocene basalts of the Columbia River Basalt Group, 3) Ellensburg Formation, which occurs as sedimentary interbeds between the Columbia River Basalt Group flows, 4) late Miocene to Holocene sedimentary deposits including the Ringold Formation and the Hanford formation. Numerous reports have been written discussing the geology of the Pasco Basin and the Hanford Site (see Lindsey and Jaeger 1993). This section discusses the geology of the 100-H Area as it pertains to the ISRM test site.

#### C.1.1 Ringold Formation

The main units of interest for this report are the suprabasalt sediments that consist of the Hanford formation and the Ringold Formation. A generalized diagram showing the stratigraphy of these sediments is shown in Figure C-1. The Ringold Formation directly overlies the Columbia River Basalt Group. Lindsey et al. (1992) subdivided the Ringold Formation on the basis of sediment facies associations. The Ringold Formation, then can be described as containing intervals dominated by fluvial gravel units (designated as A, B, C, D, and E). These gravel units may be separated from each other by basin-wide intervals containing overbank and lacustrine facies deposits. The lowest of these overbank/lacustrine facies deposits is the Lower Mud Unit, which overlies the Unit A gravel (Lindsey et al. 1992).

In the 100-H Area and the ISRM site, the gravel facies of the Ringold Formation are not present. Instead, the Ringold Formation is typically expressed as a reddish brown, sandy clayey silt to clayey silt which corresponds to the Lower Mud Unit. The Lower Mud Unit is 23 to 30.5 m (75 to 100 ft) thick beneath the 100-H Area (Lindsey and Jaeger 1993). The unit appears to be continuous across the site, as observed in the wells installed at the ISRM site in 1995-96. It also appears to continuously extend westward from the 100-H Area to the 100-N Area (Lindsey and Jaeger 1993).

The Lower Mud Unit was encountered at a depth of approximately 15.3 m (50.3 ft) below ground surface beneath the ISRM site. This unit is typically a moderately consolidated, light brownish gray to light yellowish brown and reddish brown (2.5Y6/3) to brown (10YR5/3), sandy clayey silt to clayey silt. Colors are from the Munsell soil color chart (Munsell 1988). Hydrometer analyses of this unit are summarized in Table C-1 and show that it contains 12.7 to 27.5% sand, 46.8 to 67.9% silt, and 19.4 to 33.9% clay.

Table C-1. Hydrometer Analyses Results from the Ringold Formation.

Well Number	Depth Interval m (ft)	% Sand	% Silt	% Clay
199-H5-3P	15.4-15.5 (50.5-51)	12.7	67.9	19.4
199-H5-3P	15.8-16 (52-52.5)	19.1	46.8	33.9
199-H5-3P	16.2-16.3 (53-53.5)	27.5	49.4	23.1

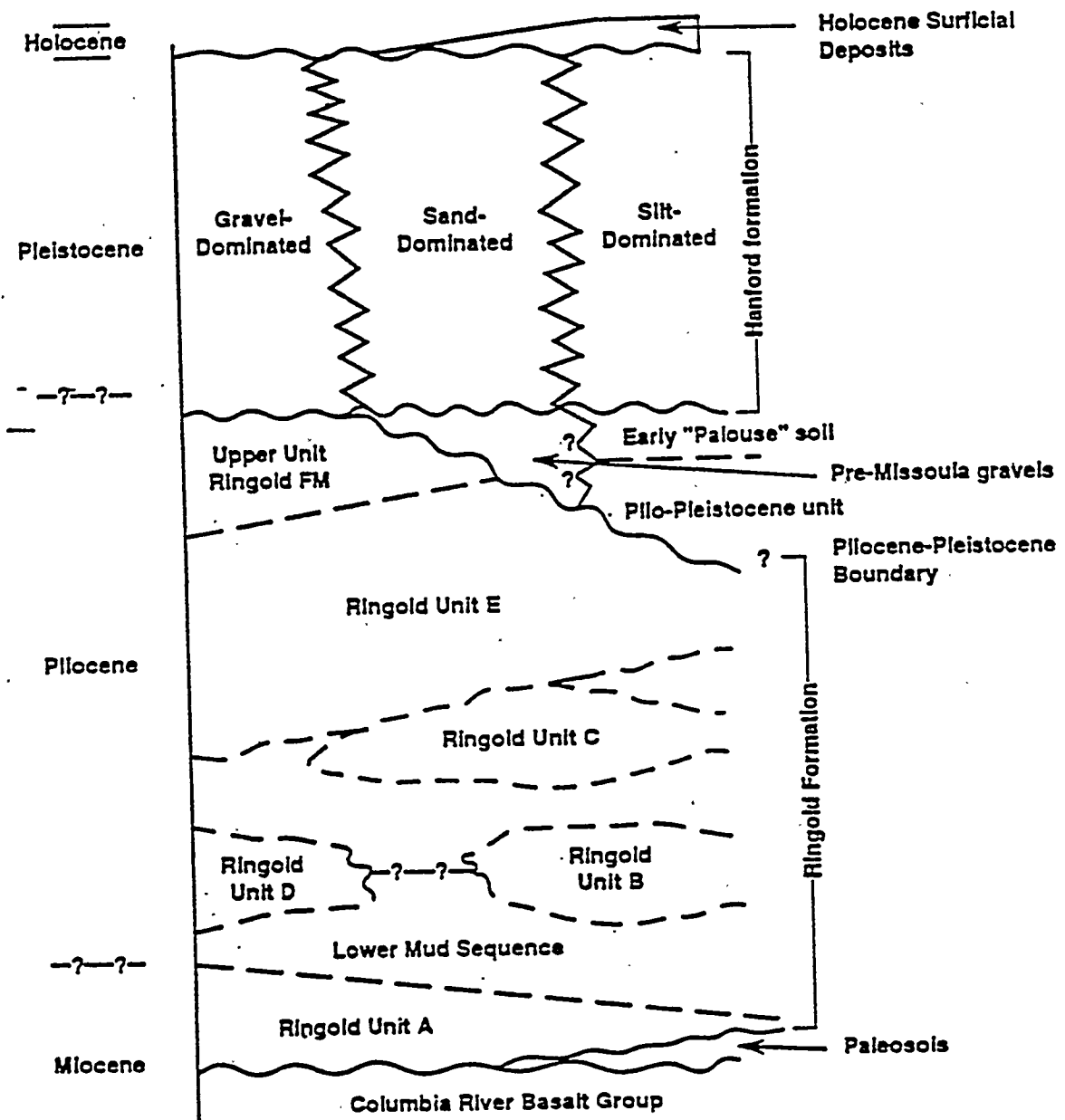
### C.1.2 Hanford Formation

The Hanford formation directly overlies the Ringold Formation. Lithologically, the Hanford formation is dominantly a sandy gravel but also may contain some significant sand layers and some minor silt/clay fractions. The contact with the underlying Ringold Formation in the 100-H Area is sharp and easily recognizable because of the much larger median grain size of the Hanford formation. The Hanford formation is approximately 19.8 m (65 ft) thick in the 100-H Area (Liikala et. al. 1988).

From the surface to a depth of approximately 11.9 m (39 ft), the Hanford formation consists of a light gray (10YR7/1) sandy gravel consisting of 50 to 65% gravel, 35 to 50% sand, and trace silt and clay. The gravel portion is typical of other Hanford formation deposits on the Hanford Site and is subangular to rounded, 60% felsic/40% mafic, and ranges from very fine pebble (2 to 4-mm diameter) to small cobble (64 to 128-mm diameter) size.

From approximately 11.9 to 13.7 m (39 to 45 ft) the formation lithology is variable and may consist of a sand, gravelly sand, sandy gravel (pebble size max.), or a sandy gravel (cobble size max.). Below 13.7 m (45 ft) the unit is dominated by a sandy gravel (cobble size max.) but may include pebble-size gravels and minor sand or gravelly sand lenses.

The contact with the underlying Ringold Formation (Lower Mud Unit) occurs at approximately 15.3 m (50.3 ft). Well locations are shown in Figure 5-1. The static water table is located at a depth of 12.5 m (41.1 ft) below ground surface.



HS21001&L1a

Figure C-1 Generalized Stratigraphy of the Suprabasalt Sediments in the Pasco Basin (from Lindsey and Jaeger 1993).

## C.2 Hydrology of the 100-H Area

As was discussed in Section 6.1, the unconfined aquifer is approximately 3-m (9-ft) thick beneath the ISRM test site and is contained within the sands and sandy gravels of the Hanford formation. The Lower Mud Unit of the Ringold Formation, represented by a sandy clayey silt to clayey silt, forms the base of the upper unconfined aquifer. The spatial continuity of this uppermost, fine-grained Ringold unit was observed during hydrogeologic characterization activities at the ISRM test site and is supported by hydrochemical data from across the 100-HR-3 Operable Unit that indicates contamination does not extend beyond the uppermost part of the unconfined aquifer (Peterson 1993).

The unconfined aquifer beneath the northern portion of the Hanford Site is laterally bounded by the basalt ridges that surround the basin and the Columbia River to the north and east. The aquifer is recharged by the Cold Creek drainage to the west, by waste water disposal in the 200-Areas, and by natural recharge (Fayer and Walters 1995). Groundwater generally flows from west to east across the Hanford Site and discharges to the Columbia River. In the 100-H Area, groundwater flow direction is generally in the northeast direction under a hydraulic gradient of approximately 0.0009. Water table contour maps of the 100-H Area at high and low Columbia River stage are shown in Figures C-2 and C-3, respectively (DOE-RL 1993). Data available from a continuous river stage monitoring station on the Columbia River near the old Hanford Townsite indicate diurnal variations in river stage of up to 2.5 m (8 ft) and seasonal variations of up to 3.5 m (12 ft).

As shown in the site water table contour maps, the effects of seasonal variability in Columbia River stage on the unconfined aquifer have dissipated at distances from the river comparable to that of the ISRM test site. The test site is located approximately 730 m (2400 ft) from the Columbia River. Water-level measurements made at Hanford Site well 199-H5-1A between July 1992, and June 1993, indicated seasonal variations in water-level of approximately 0.37 m (1.2 ft). Prior to hydrologic characterization activities at the ISRM test site, a continuous water-level monitoring system was installed to monitor diurnal water-level variations in 11 of the site monitoring wells. Water-level data collected on a 30-min interval over four days indicated that diurnal water-level fluctuation was less than 0.006 m (0.02 ft).

Previous hydrologic characterization of the uppermost unconfined aquifer in the vicinity of the ISRM test site is limited. Swanson (1994) reported results from a single-well slug test at Hanford Site well 199-H5-1A. Analysis of test response data resulted in a hydraulic conductivity estimate of 34 m/d (110 ft/d). Results from detailed hydrologic characterization, conducted in support of the ISRM field experiment, are presented in Section 6.3 and Appendix D.

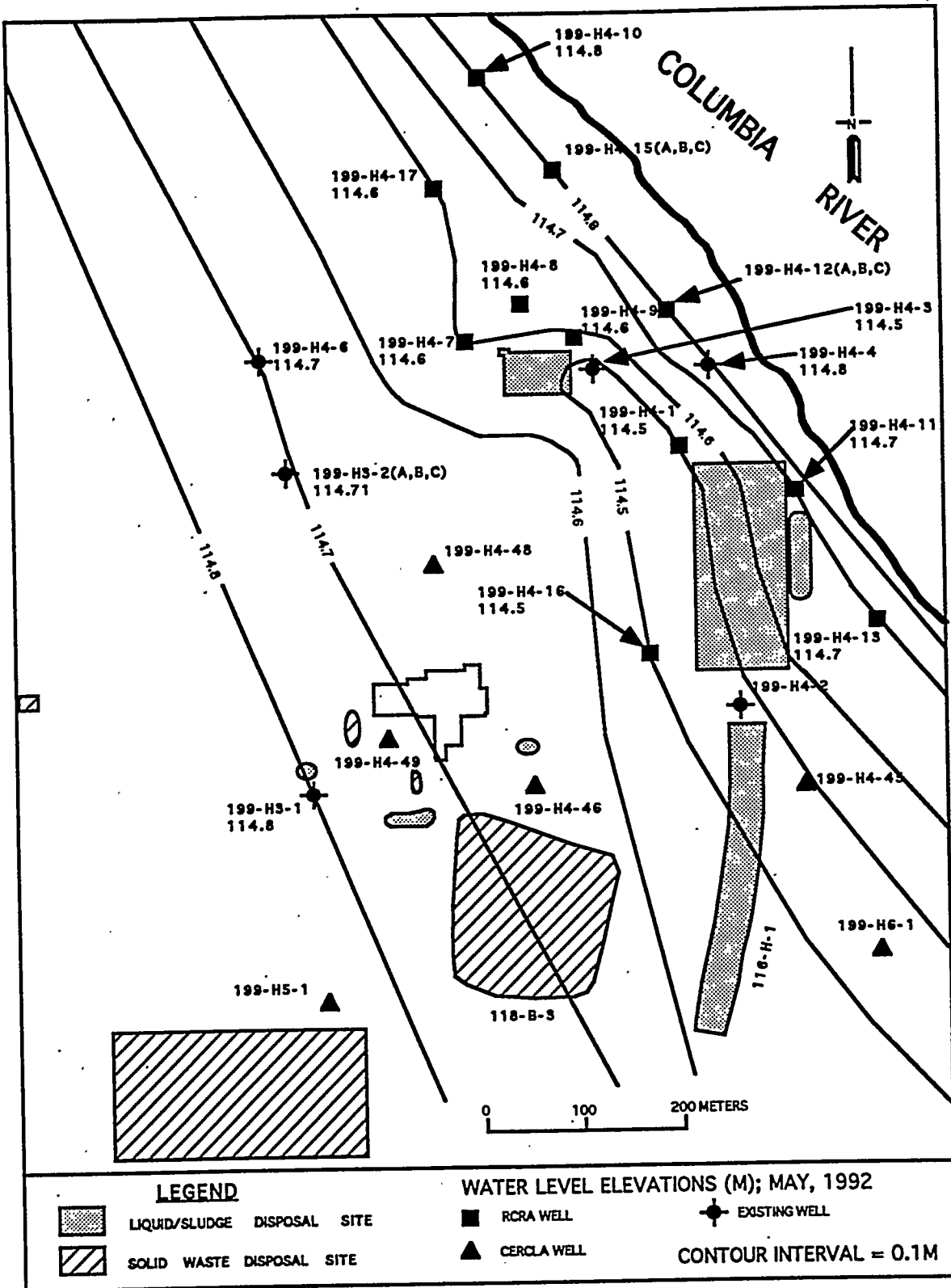


Figure C-2 Water Table at the 100-H Area during High Columbia River Stage (DOE-RL 1993).

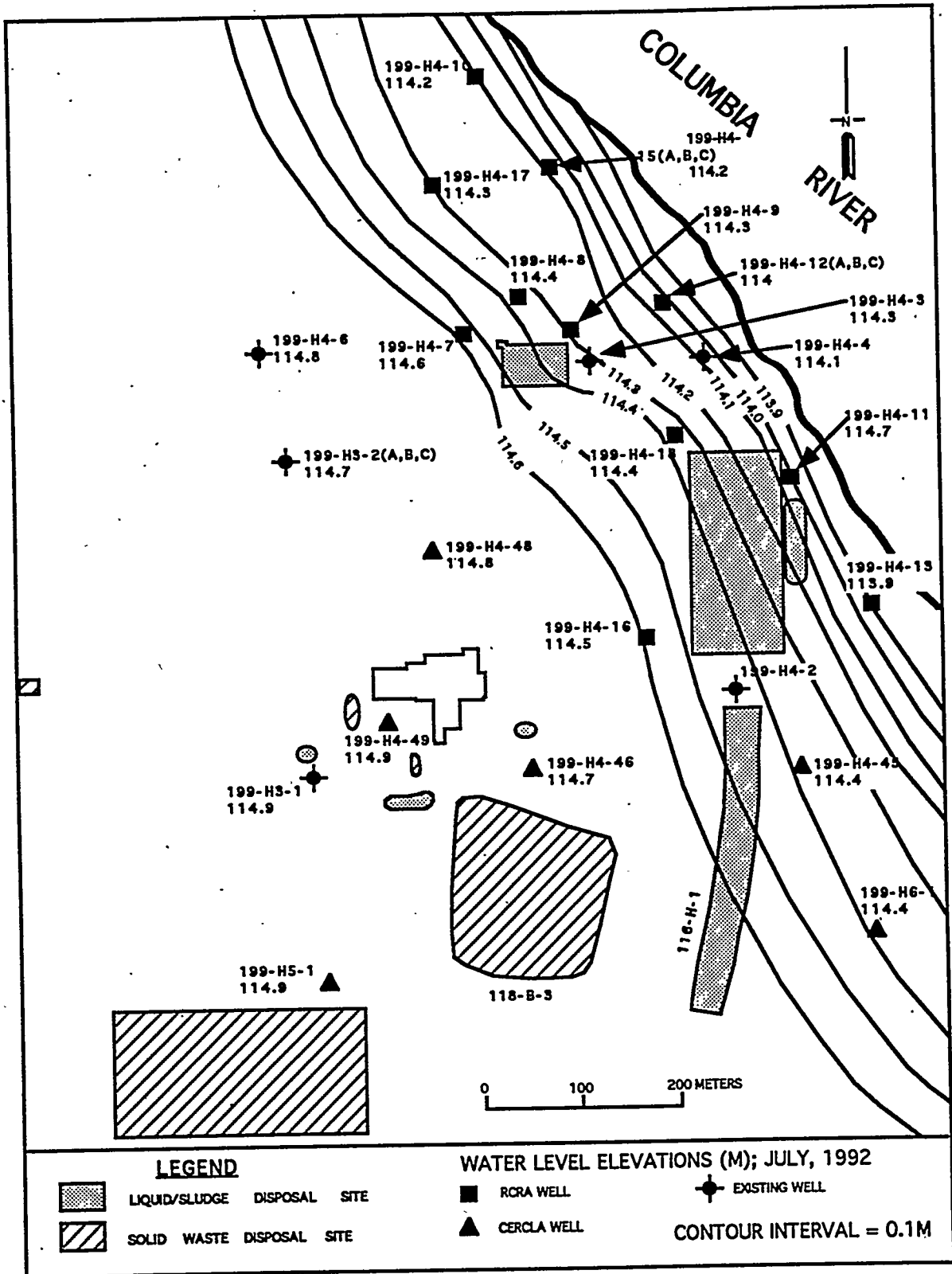
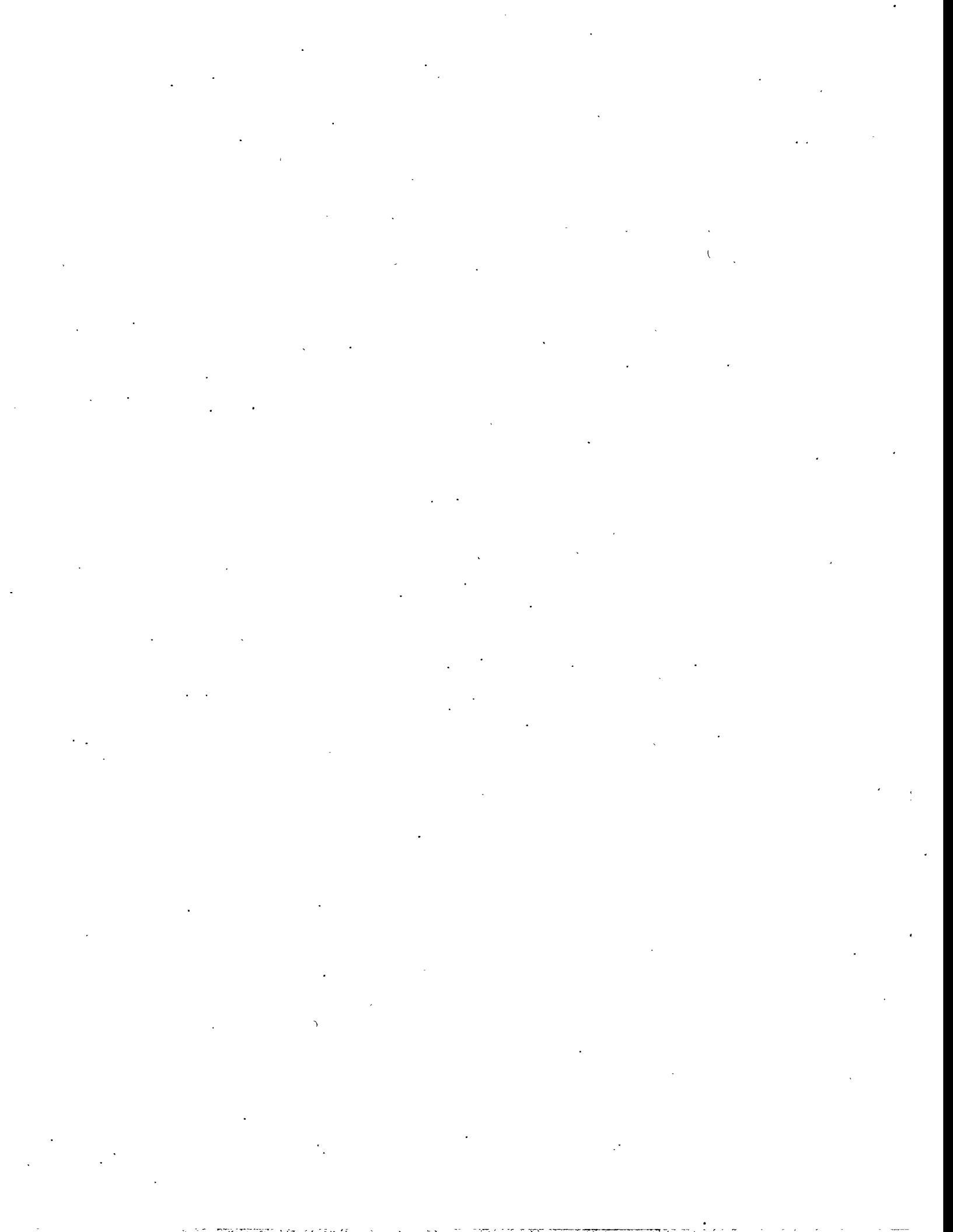


Figure C-3 Water Table at the 100-H Area during Low Columbia River Stage (DOE-RL 1993)

**APPENDIX D**

**HYDRAULIC TEST ANALYSES**



## Table of Contents

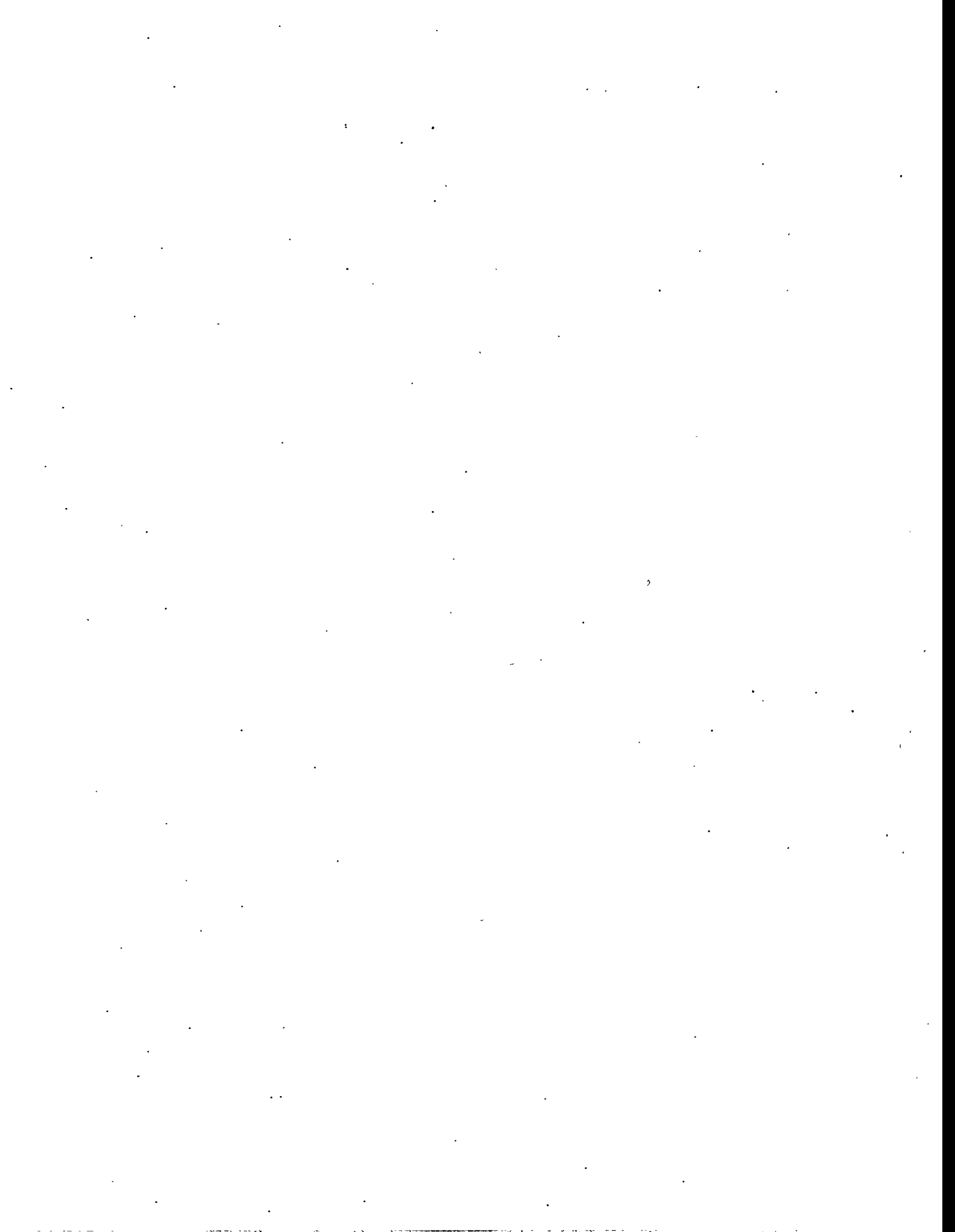
Appendix D. Hydraulic Test Analyses .....	D.1
---	-----

### List of Figures

- D.1 Well Location Map for the In-Situ Redox Manipulation Field Test Site.
- D.2 Comparison of Predicted Slug Test Response Based on Liu and Butler (1995) and Spane (1996) Analytical Methods.
- D.3 Comparison of Predicted Slug Interference Response Based on Liu and Butler (1995) and Spane (1996) Analytical Methods.
- D.4 Comparison of Pre- and Post Experiment Slug Test Responses for Stress Well H5-2.
- D.5 Pre-Experiment Slug Test Analysis for Well H5-2: Homogeneous Aquifer Model Solution.
- D.6 Post-Experiment Slug Test Analysis for Well H5-2: Homogeneous Aquifer Model Solution.
- D.7 Post-Experiment Slug Test Analysis for Well H5-2: Infinitesimal Thickness Skin Model Solution.
- D.8 Comparison of Pre- and Post Experiment Slug Interference Responses for Observation Well H5-5P.
- D.9 Pre-Experiment Slug Interference Response Analysis for Well H5-5P: Homogeneous Aquifer Model Solution.
- D.10 Post-Experiment Slug Interference Response Analysis for Well H5-5P: Homogeneous Aquifer Model Solution.
- D.11 Post-Experiment Slug Interference Response Analysis for Well H5-5P: Finite-Thickness Skin Model Solution.
- D.12 Comparison of Pre- and Post Experiment Slug Interference Responses for Observation Well H5-4P.
- D.13 Pre-Experiment Slug Interference Response Analysis for Well H5-4P: Homogeneous Aquifer Model Solution.
- D.14 Post-Experiment Slug Interference Response Analysis for Well H5-4P: Homogeneous Aquifer Model Solution.
- D.15 Post-Experiment Slug Interference Response Analysis for Well H5-4P: Finite-Thickness Skin Model Solution.
- D.16 Comparison of Pre- and Post Experiment Slug Interference Responses for Observation Well H5-3P.
- D.17 Pre-Experiment Slug Interference Response Analysis for Well H5-3P: Homogeneous Aquifer Model Solution.
- D.18 Post-Experiment Slug Interference Response Analysis for Well H5-3P: Homogeneous Aquifer Model Solution.
- D.19 Post-Experiment Slug Interference Response Analysis for Well H5-3P: Finite-Thickness Skin Model Solution.

### List of Tables

- D.1 Analysis Summary for Pre- and Post Experiment Tests.



## APPENDIX D

### HYDRAULIC TEST ANALYSES

This appendix provides a detailed description of the hydraulic tests conducted at the ISRM test site, the analytical techniques used to analyze the test response data, and a comparison of results from pre- and post-experiment hydraulic tests designed to assess the impact of the ISRM field experiment on existing in situ hydraulic properties.

#### D.1 HYDROLOGIC TESTING PROGRAM

To assess whether the applied field experiment had effects on the existing hydraulic properties at the Redox Manipulation test facility, pre- and post experiment slug interference test responses were compared for selected observation well sites. Slug interference testing requires a multi-well arrangement that includes: a stress well and surrounding observation wells. The general test procedure requires application of an instantaneous head increase or decrease at the stress well, and monitoring of the associated formation response (the slug interference) at the neighboring observation well locations. Figure D.1 shows the location of the stress well (H5-2) and surrounding observation wells within the test facility.

Analysis of the observation well test response can provide an estimate of aquifer transmissivity,  $T$ , storativity,  $S$ , and, under favorable conditions, estimates of vertical anisotropy,  $K_D$ . A detailed description of the performance and analysis of slug interference tests conducted within unconfined aquifers is contained in Spane (1992, 1996), and Spane et al. (1995). As discussed in Section 10.3.4, the shape, amplitude, and transmission of the slug interference response is highly dependent (i.e., in varying degrees) on the hydrologic properties ( $T$ ,  $S$ ,  $K_D$ ) of the aquifer-interwell region. A comparison of the pre- and post experiment slug interference responses, therefore, provides a direct means of evaluating any changes in in-situ hydraulic properties induced by the experiment application.

Pre-experiment slug interference tests were conducted on May 23, 1995, while post experiment testing was conducted on April 11, 1996. To eliminate any scale-dependence effects, identical stress levels were applied for the slug interference tests ( $H_0 = 1.17$  ft and 4.298 ft for low- and high-level stress tests, respectively) conducted during the pre- and post experiment phases. The stress levels were calculated based on the displacement volumes of the two different slugging rods used to initiated the low- and high-level stress tests. A comparison of the test responses for slug tests conducted at different stress levels provides information pertaining to possible hydraulic property scale dependence, well installation effects (e.g., groundwater flow turbulence), and lateral variation of hydraulic properties in the immediate well site vicinity. A comparison of normalized test responses indicated identical response behavior for low- and high-level stress tests conducted during each test phase. The high-level stress test responses were the focus of the pre- and post experiment test evaluation, because of the greater radius of investigation afforded by the higher imposed stress.

To examine the areal effects of the field experiment on in-situ aquifer properties, pre- and post experiment slug interference responses at wells H5-3P, -4P, and -5P were evaluated. These wells are all located at varying distances from stress well H5-2, along a common northwest direction, and are all completed in the lower half of the aquifer (similar to the stress well). It should be noted that a direct comparison of slug interference responses was not possible, however, since the

aquifer thickness increased from 9.2 to 12.1 ft for the pre- and post experiment tests, respectively. A visual comparison of the pre- and post experiment test responses, taking into account the existing aquifer thickness and well penetration/aspect conditions, indicates the following:

- post experiment slug tests at stress well H5-2 exhibit a lagged (i.e., delayed) and steeper recovery response, in comparison to pre-experiment tests
- post experiment slug interference tests for observation wells completed within the lower half of the aquifer (e.g., H5-3P, -4P, -5P) exhibit a lagged and damped (i.e., diminished) response, in comparison to pre-experiment tests

## **D.2 HYDROLOGIC TEST ANALYSIS METHODS**

In the following sections, the preferred analytical methods for slug and slug interference tests are discussed. Inherent with almost all hydrologic analysis methods is the fact that laminar, i.e., nonturbulent flow (Bouwer 1996) and homogeneous test formation conditions exist. For the pre- and post experiment hydrologic tests performed, turbulent/laminar flow conditions were assessed by calculating the Reynolds Number based on flow velocity calculations within the stress well casing/fluid column. Analysis of the test data indicates that laminar flow conditions (i.e., Reynolds Number  $\leq 2000$ ) were maintained for nearly all test times (i.e.,  $t > 2$  sec) for low stress level tests and after approximately 30 sec for high-level stress tests. The nearly identical normalized test responses observed for slug and slug interference tests indicates that turbulent flow condition effects were not significant for either pre- or post experiment slug tests performed.

The homogeneous aquifer assumption implies that the formation that the test wells penetrate (either fully or partially) is uniform throughout (i.e., vertically and laterally). The net effect that individual layer characteristics have within an actual test formation are, therefore, "averaged" and an "equivalent" hydraulic property value assigned for the entire formation thickness. It should be recognized, however, that layers of higher and lower hydraulic conductivity exist within the test formation; but taken as a whole, the test formation would have the indicated equivalent hydraulic conductivity based on the observed test response characteristics.

A homogeneous aquifer approach was used initially for analysis of pre- and post experiment tests. As will be discussed, many of the post experiment tests exhibited responses atypical of homogeneous aquifer behavior. For these tests a heterogeneous or composite aquifer analysis method was used.

Results of the pre- and post experiment stress well H5-2 slug tests and selected observation well slug interference responses are provided in the following sections of the appendix A.

### **D.2.1. Slug Test Analysis Methods**

Analytical methods used in the analysis of the slug test responses include the type-curve matching method for unconfined and confined aquifers, as discussed in Hyder et al. (1994), Hyder and Butler (1995), Liu and Butler (1995), and Spane (1996), together with the combined type-curve and derivative analysis method described in Ostrowski and Kloska (1989) and Spane and Wurstner (1993). Because these analytical methods can use all or any part of the slug test response in the analysis procedure, they are particularly useful in the analysis of unconfined aquifer tests. They

also do not have any of the inherent analytical weaknesses of the commonly used Bouwer and Rice method (e.g., assumption of steady-state flow, isotropic conditions, etc.), as originally described in Bouwer and Rice, 1976 and Bouwer, 1989 for unconfined aquifer slug tests. These analytical limitations are discussed in Hyder and Butler (1995), Brown et al. (1995), and Bouwer (1996).

Because of the ease of application, the analytical method described in Spane (1996) was used to analyze slug tests conducted at well H5-2. The method presented in Spane (1996) pertains to the analysis of slug interference tests; however, the general procedure of converting available pumping test type curves to an equivalent slug test response also applies. Figure D.2 shows a comparison of predicted slug test responses for the analytical methods presented in Spane (1996) and Liu and Butler (1995). As indicated, for the given test/aquifer conditions examined, similar results were obtained for both methods. It should be noted that both type-curve analysis methods account for the effects of well partial penetration, anisotropy, wellbore storage, and aquifer elasticity effects (storativity).

Several analytical assumptions were made to facilitate analysis of the pre- and post experiment slug test results. These assumptions include:

- a vertical anisotropy ( $K_D$ ) value of 0.1 was assumed
- a storativity value of 0.0001 was used initially
- the well screen interval was assumed to be equivalent to the test interval section.

To standardize the slug test type-curve matching analysis for all overdamped slug test responses, a vertical anisotropy ( $K_D$ ) of 0.1 was assumed. As shown in text figures presented in Section 10.3.4, only a slight variation and offset in test response is indicated for the range of vertical anisotropy ( $K_D = 0.01 - 1.0$ ) that encompasses the commonly reported values in stratified alluvial formations (e.g., Weeks 1969). The predicted responses shown are for the existing well completion conditions at well H5-2. The effect of  $K_D$ , would be expected to increase slightly with smaller aquifer penetration ratios, and to become barely perceptible with full aquifer penetration. Because of the relative insensitivity of slug test response to vertical anisotropy, the use of an assumed (constant) value of 0.1 is not expected to have a significant impact in the determination of aquifer transmissivity ( $T$ ) and hydraulic conductivity ( $K$ ) from the type-curve matching analysis.

Figures presented in Section 10.3.4 also show the effects of varying storativity on slug test response. As shown, for the range of storativity commonly exhibited by shallow unconfined aquifers (i.e.,  $S = 0.005$  to  $0.00005$ ), aquifers having higher storativity values are associated with "flatter" test recovery curves. This characteristic of storativity allows for better type-curve matches through slight modifications of the storativity input. It should be noted, however, that other factors influence the shape of the slug test curve (e.g., skin effects, vertical anisotropy). For this reason, storativity values used in the final slug test analyses are considered to be of qualitative value, and should not be used (as in the case for transmissivity) for quantitative applications. To facilitate the unconfined aquifer slug-test type-curve analysis, an elastic storage value of 0.0001 was utilized for all initial pre- and post experiment analysis runs. Slight adjustments were made to this input storativity value to improve the final analysis match.

For stress well H5-2, the well screen section (rather than the sandpack interval) was used to represent the test interval for the analyses. This was based on the assumption that the formation

materials within the aquifer have a higher permeability than the sandpack; and, therefore, test response transmission is expected to propagate faster laterally from the stress well screen to the surrounding test formation, than vertically within the sandpack zone.

### **D.2.2 Slug Interference Test Analysis Methods**

Analytical methods used in the analysis of the slug interference responses include the type-curve matching method for unconfined aquifers, as presented in Liu and Butler (1995) and Spane (1996). It should be noted that Liu and Butler (1995) state that the software program described in their paper only predicts slug test response, and that slug interference test capabilities would be added later. This model addition was subsequently provided by Butler (1996, personal communication).

Because of the ease of application, the analytical method described in Spane (1996) was used to initially analyze slug interference tests conducted at the test facility. After preliminary slug interference test matches were obtained, final analyses were completed using the analytical model described in Liu and Butler (1995). Figure D.3 shows a comparison of predicted-slug interference responses for the analytical methods presented in Spane (1996) and Liu and Butler (1995). As indicated, for the given test/aquifer conditions examined, similar results were obtained using both methods. It should be noted that both analysis methods account for the effects of well partial penetration, anisotropy, wellbore storage, and aquifer elasticity effects (storativity). The Liu and Butler (1995) model, however, also has the capability of analyzing slug interference tests affected by the presence of skin effects at the stress well. This analytical method was used for those post experiment tests exhibiting possible finite-skin behavior.

Several analytical assumptions were made to facilitate analysis of the pre- and post experiment slug interference tests. These assumptions are identical to previously cited assumptions for the analysis of slug tests described in Section D.2.1. Quantitative analysis of the slug interference responses utilized the trial and error curve-fitting procedure outlined in Spane et al. (1995). Briefly stated, the slug interference amplitude and initial rising limb segments were approximately matched first by assuming values for  $K_D$  (e.g., 0.1) and  $S/S_y$  (e.g., 0.01); and by adjusting the predicted aquifer  $S$  and  $T$ . The descending limb segment match was then be approximately matched by adjusting predicted values for  $K_D$  and  $S/S_y$ . Repetitive minor adjustments for the four hydrologic input parameters were continued until a final match was obtained.

To assess whether post experiment response changes are associated with uniform aquifer changes or possibly induced hydraulic changes only in the vicinity of the stress well, two analysis models were applied. The first focused on the analysis of the slug interference responses using a homogeneous formation model to assess whether a quantitative analysis match could be obtained for both tests. If the first analysis approach was not successful (indicating more complex test/formation conditions), then a composite formation model was applied that accounts for changes in hydraulic properties in the vicinity of the stress well.

## **D.3 TEST ANALYSIS RESULTS**

In this section analysis results for pre- and post experiment slug tests conducted at stress well H5-2, and associated slug interference responses at observation wells H5-3P, -4P, and -5P are presented. As noted previously, tests were analyzed using both a homogeneous formation and finite-skin analytical model approach. Results for the pre- and post experiment test analyses are

summarized in Table D.1.

### D.3.1 Stress Well H5-2

Figure D.4 shows a direct comparison of the observed pre- and post experiment slug test response exhibited at stress well H5-2. As indicated in the figure, the post experiment test response exhibits a delayed and slightly steepened recovery pattern, in comparison to the pre-experiment test. As noted in Section 10.3.4 and D.2.1, the delayed response or time shift exhibited can be attributed to a number of factors including: an overall reduction in aquifer hydraulic conductivity or development of a zone of significantly reduced permeability (i.e., "skin effect") immediately surrounding the stress well screen. This similarity in predicted responses makes it difficult in distinguishing the causative factor responsible for the time lag exhibited by the post experiment test, when only test responses at the stress well are available for analysis. For this reason, analyses based on both homogeneous aquifer and skin effects are provided for the post experiment tests results.

#### Pre-Experiment Test Analysis

Figure D.5 shows the combined type-curve and derivative analysis for the pre-experiment test response observed at stress well H5-2. As indicated, a good test response and derivative match was obtained using the homogeneous model solution. Aquifer properties used in the final analysis included:

$K = 109$  ft/d;  $S = 0.0005$ , using an assumed value for  $K_D = 0.1$ . The analysis results compare favorably with slug test results of  $K = 121$  and  $132$  ft/d previously reported in Vermeul et al. (1995) for earlier slug tests conducted at well H5-2, prior to well screen installation and final well completion.

#### Post-Experiment Test Analysis

Figure D.6 shows the combined type-curve and derivative analysis for the post experiment test response. As shown, considerable modifications to the previously determined pre-experiment aquifer properties were required to match the post experiment response, using the homogeneous model solution. Of particular significance  $K$  was decreased to  $60$  ft/d (i.e., a decrease of 45% from the pre-experiment derived value), while  $K_D$  was increased to  $0.3$ . This post-experiment analysis was based on the assumption that the specific storage,  $S_s$ , was equal to the pre-experiment value (Note:  $S_s = S/b$ ; where  $b =$  aquifer thickness). If valid, results from the homogeneous model solution of the post experiment slug test response suggest that aquifer hydraulic properties were altered through administering of the field experiment.

To examine if the observed post experiment slug test response could be related to a thin zone of reduced permeability (i.e., skin) immediately surrounding the stress well, a heterogeneous aquifer model solution was applied. For this analysis approach, the effect of a zone of reduced permeability or skin can be predicted through use of an apparent wellbore radius,  $r_{wa}$ , as indicated in Earlougher (1977):

$$r_{wa} = r_w e^{-s}$$

This test solution approach is referred to as the infinitesimal-thickness skin solution, and assumes that the skin zone of reduced permeability has no storage capacity; and, hence, no skin thickness (see Agarwal et al., 1970, Ramey et al., 1975 for pertinent discussions). The infinitesimal skin

solution is shown by Earlougher (1977) to be related to the finite-thickness skin solution, which is a function of the ratio of the aquifer and skin zone hydraulic conductivity and radii, by the following relationship:

$$sk = [(K_f/K_{sk}) - 1] \ln(r_{sk}/r_w)$$

where,

$sk$  = skin effect; dimensionless

$K_f$  = formation hydraulic conductivity; [L/T]

$K_{sk}$  = skin zone hydraulic conductivity; [L/T]

$r_{sk}$  = skin zone radius; [L]

$r_w$  = wellbore radius; [L]

The finite-thickness skin solution listed in Equation 2 indicates that the  $sk$  parameter value is not unique, and various combinations of skin hydraulic conductivity and radial thickness can provide similar test responses. For this reason, the infinitesimal skin thickness solution (Equation 1) was used in the analysis of the post-experiment slug test response.

For this analysis of the post experiment test response, a trial-and-error approach was applied. The pre-experiment derived hydraulic properties were held constant and the apparent wellbore radius,  $r_{wa}$ , adjusted until a match was obtained. Figure D.7 shows the results of the combined type-curve and derivative analysis for the post experiment test response using the infinitesimal thickness skin solution. As indicated, a reasonable test response and derivative match were obtained using the pre-experiment analysis derived aquifer properties (Figure D.5) and a  $sk$  value of +1.47 ( $r_{wa} = 0.115$  ft). Comparable finite-thickness skin matches could be developed using the  $sk$  value of +1.47, and various  $K_{sk}$  and  $r_{sk}$  combinations in Equation 2. For example, for a finite skin zone having a hydraulic conductivity one tenth the aquifer value (i.e.,  $K_{sk} = 0.1K$ ), a skin thickness of approximately 1 in. ( $r_{sk} = 0.583$  ft) beyond the wellbore would produce a similar response as shown in Figure D.7. The results of the various skin analyses suggest that the observed post experiment slug test response may be attributed to a near-well reduction in permeability and not associated with an aquifer-wide reduction in hydraulic conductivity.

### D.3.2 Observation Well H5-5P

Figure D.8 shows a direct comparison of the observed pre- and post experiment slug interference test response exhibited at observation well H5-5P, which is located 5 ft from stress well H5-2. As indicated in the figure, the post experiment test response exhibits a delayed and damped (diminished) amplitude, in comparison to the pre-experiment test. As previously noted, the delayed response or time shift exhibited can be attributed to a number of factors including an overall reduction in aquifer hydraulic conductivity or development of a zone of significantly reduced permeability (i.e., skin effect) immediately surrounding the stress well screen. A decrease in slug interference amplitude may also be attributed to a number of factors including increases in

elastic storage (S) or the vertical anisotropy ratio.

In this section, slug interference analysis results for the pre-experiment response using a homogeneous aquifer solution are presented. For comparison purposes, analysis results for solutions based on both homogeneous aquifer and skin effects are provided for the post experiment test response.

### Pre-Experiment Test Analysis

Figure D.9 shows the pre-experiment slug interference response observed at well H5-5P and associated test analysis solution. As indicated, a good match for the test response was obtained using the homogeneous model solution. Aquifer properties used in the final analysis included:  $K = 117$  ft/d;  $S = 0.006$ , and  $K_D = 0.3$ . The hydraulic conductivity estimate compares favorably with pre-experiment slug test results obtained at stress well H5-2.

### Post-Experiment Test Analysis

Figure D.10 shows the post-experiment slug interference response observed at well H5-5P and associated test analysis solution. As shown, considerable modifications to the previously determined pre-experiment aquifer properties were required to match the post experiment response, using the homogeneous model solution. Of particular significance,  $K$  was decreased to 74 ft/d (i.e., a decrease of 35% from the pre-experiment derived value), while  $S$  was increased to 0.017 and  $K_D$  was increased to an unrealistic value of 1.0 to achieve a reasonable match. These significant changes in hydrologic properties to provide a reasonable match in post-experiment response behavior suggests that the homogeneous model solution may not adequately describe actual post-experiment test conditions.

To examine if the observed post experiment slug test response could be better predicted by the presence of a thin zone of reduced permeability (i.e., skin) immediately surrounding the stress well, a heterogeneous, finite-thickness skin model solution was applied. For this analysis, a trial-and-error approach was utilized. The pre-experiment derived hydraulic properties were held constant and various  $K_{sk}$  and  $r_{sk}$  combinations were used. Figure D.11 shows the results of one  $K_{sk}$  and  $r_{sk}$  analysis combination. As indicated, a reasonable match for the observed post-experiment response was obtained, using the finite-thickness skin solution and pre-experiment derived aquifer properties.

### **D.3.3 Observation Well H5-4P**

Figure D.12 shows a direct comparison of the observed pre- and post experiment slug interference test response exhibited at observation well H5-4P, which is located 12.4 ft from stress well H5-2. As previously observed at well H5-5P, the post experiment test response exhibits a delayed and damped (diminished) amplitude, in comparison to the pre-experiment test. In this section, slug interference analysis results for the pre-experiment response using a homogeneous aquifer solution are presented. For comparison purposes, analysis results for solutions based on both homogeneous aquifer and skin effects are provided for the post experiment test response.

### Pre-Experiment Test Analysis

Figure D.13 shows the pre-experiment slug interference response observed at well H5-4P and associated test analysis solution. As shown in the figure, the homogeneous formation model provides a reasonably good fit of the pre-experiment test response for test times greater than about 8 sec. Matched aquifer properties used in the homogeneous model include:  $K = 163$  ft/d,  $S = 0.0043$ , and  $K_D = 0.14$ . The cause for the poor early-time pre-experiment test response prediction is unknown; however, it may be attributed to the presence of a zone of lower permeability (skin) near the stress well. This effect may become more evident for slug interference responses for observation wells located at greater distance from the stress well.

### Post-Experiment Test Analysis

Figure D.14 shows the post-experiment slug interference response observed at well H5-4P and associated test analysis solution. Efforts to match the post-experiment test response were not as successful as for the pre-experiment analysis, and significant changes in aquifer properties ( $K = 105$  ft/d,  $S = 0.0092$ ;  $K_D = 0.3$ ) were required (in comparison to the pre-experiment determined values) to obtain a final best analysis fit (note: a predicted response based on pre-experiment analysis values is also shown in Figure 14).

The poor match of post experiment early-time test behavior (i.e., 0 to 20 sec) and significant changes in hydrologic properties required to provide a reasonable match in post-experiment response behavior suggests that the homogeneous model solution may not adequately describe actual post-experiment test conditions.

To examine if the observed post experiment slug test response could be better predicted by the presence of a thin zone of reduced permeability immediately surrounding the stress well, a heterogeneous, finite-thickness skin model solution was applied. For this analysis, a trial-and-error approach was used. The pre-experiment derived hydraulic properties were held constant and various  $K_{sk}$  and  $r_{sk}$  combinations were utilized. Figure D.15 shows the results of one  $K_{sk}$  and  $r_{sk}$  analysis combination. Although a complete match of the early-time test response was not attainable, the overall match and shape of the predicted post experiment slug interference response suggests that the finite-skin solution is better than the homogeneous model in matching post experiment test behavior. An improved early-time match using the finite-skin model is also likely if the aquifer properties were also adjusted (i.e., not set to pre-experiment analysis derived values) for the trial-and-error solutions.

#### **D.3.4 Observation Well H5-3P**

Figure D.16 shows a direct comparison of the observed pre- and post experiment slug interference test response exhibited at observation well H5-3P, which is located 20.0 ft from stress well H5-2. As previously observed at wells H5-4P and -5P, the post experiment test response exhibits a delayed and damped (diminished) amplitude, in comparison to the pre-experiment test. In this section, slug interference analysis results for the pre-experiment response using a homogeneous aquifer solution are presented. For comparison purposes, analysis results for solutions based on both homogeneous aquifer and skin effects are provided for the post experiment test response.

### Pre-Experiment Test Analysis

Figure D.17 shows the pre-experiment slug interference response observed at well H5-3P and associated test analysis solution. As shown in the figure, the homogeneous formation model only provides a reasonably good fit of the pre-experiment test response for test times greater than about 18 sec. Matched aquifer properties used in the homogeneous model include:  $K = 283$  ft/d,  $S = 0.006$ , and  $K_D = 0.07$ . The slug interference analysis results are almost identical to values determined for well H5-3P from the analysis of pre-experiment pumping test results ( $K = 286$  ft/d,  $K_D = 0.07$ ,  $S = 0.0055$ ) previously reported in Vermeul et al. (1995)

The cause for the poor early-time slug interference test response prediction shown in Figure D.17 is unknown; however, it may be attributed to the presence of a zone of lower permeability (skin) near the stress well. This effect becomes more evident for slug interference responses for observation wells located at greater distances (e.g., H5-3P) from the stress well.

### Post-Experiment Test Analysis

Figure D.18 shows the post-experiment slug interference response observed at well H5-3P and associated test analysis solution. Efforts to match the entire post experiment test response were not successful, and changes in aquifer properties ( $K = 260$  ft/d,  $S = 0.014$ ) were required (in comparison to the pre-experiment determined values) to obtain a final best analysis fit. The poor match of post experiment early-time test behavior (i.e., 0 to 25 sec) and significant changes in hydrologic properties required to provide a reasonable match in post-experiment response behavior suggests that the homogeneous model solution may not adequately describe actual post-experiment test conditions.

To examine if the observed post experiment slug test response could be better predicted by the presence of a thin zone of reduced permeability immediately surrounding the stress well, a heterogeneous, finite-thickness skin model solution was applied. For this analysis, a trial-and-error approach was utilized. The pre-experiment derived hydraulic properties were held constant and various  $K_{sk}$  and  $r_{sk}$  combinations were used. Figure D.19 shows the results of one  $K_{sk}$  and  $r_{sk}$  analysis combination. Although a complete match of the entire test response was not attainable, the overall match and shape of the post experiment slug interference response suggests that the finite-skin solution is better than the homogeneous model in matching post experiment test behavior. A slightly improved early-time match using the finite-skin model is also likely if the aquifer properties were also adjusted (i.e., not set to pre-experiment analysis derived values) for the trial-and-error solutions.

## D.4 SUMMARY

Table D.1 summarizes the results of the pre- and post experiment slug and slug interference test analyses. Salient observations obtained from the pre- and post experiment test analyses include:

- post experiment test responses indicated a change from pre-experiment test/aquifer conditions
- a distance scale-dependence for hydraulic conductivity was exhibited
- the finite-thickness skin analysis model provided better matches for post experiment slug interference test responses than did the homogeneous aquifer solution model.

Post experiment slug interference responses exhibit a delayed and damped (diminished) amplitude, in comparison to the pre-experiment test. As noted previously, the delayed response or time shift exhibited can be attributed to a number of factors including an overall reduction in aquifer hydraulic conductivity or development of a zone of significantly reduced permeability (i.e., skin effect) immediately surrounding the stress well screen. A decrease in slug interference amplitude may also be attributed to a number of factors including increases in elastic storage (S) or the vertical anisotropy ratio.

Based on a comparison of post experiment analysis results obtained using both homogeneous aquifer and finite-thickness skin model solutions, the response change observed for post experiment tests is best explained by the presence of a small zone (e.g., 1 in. to 4 in.) of reduced permeability immediately outside the wellbore. The cause of this zone of reduced permeability is unknown, but may be attributed to entrapment of suspended or colloidal material in the sandpack zone immediately outside the well screen during the pumpback phase of the chemical reagent solution used in the field experiment.

Hydraulic conductivity estimates obtained from the pre- and post experiment test analyses indicate an increasing trend, with increased radial distance from the stress well. A similar pattern was reported by Vermeul et al. (1995) for results obtained from the pre-experiment pumping test. The cause for this distance dependence relationship is currently unknown, but may be associated with changes in aquifer characteristics (e.g., increasing aquifer thickness or hydraulic conductivity with distance), presence of artificial stress well conditions (i.e., well skin, well inefficiencies), or inherent deficiencies in the homogeneous aquifer analytical solution for analyzing tests conducted in heterogeneous unconfined aquifer formations.

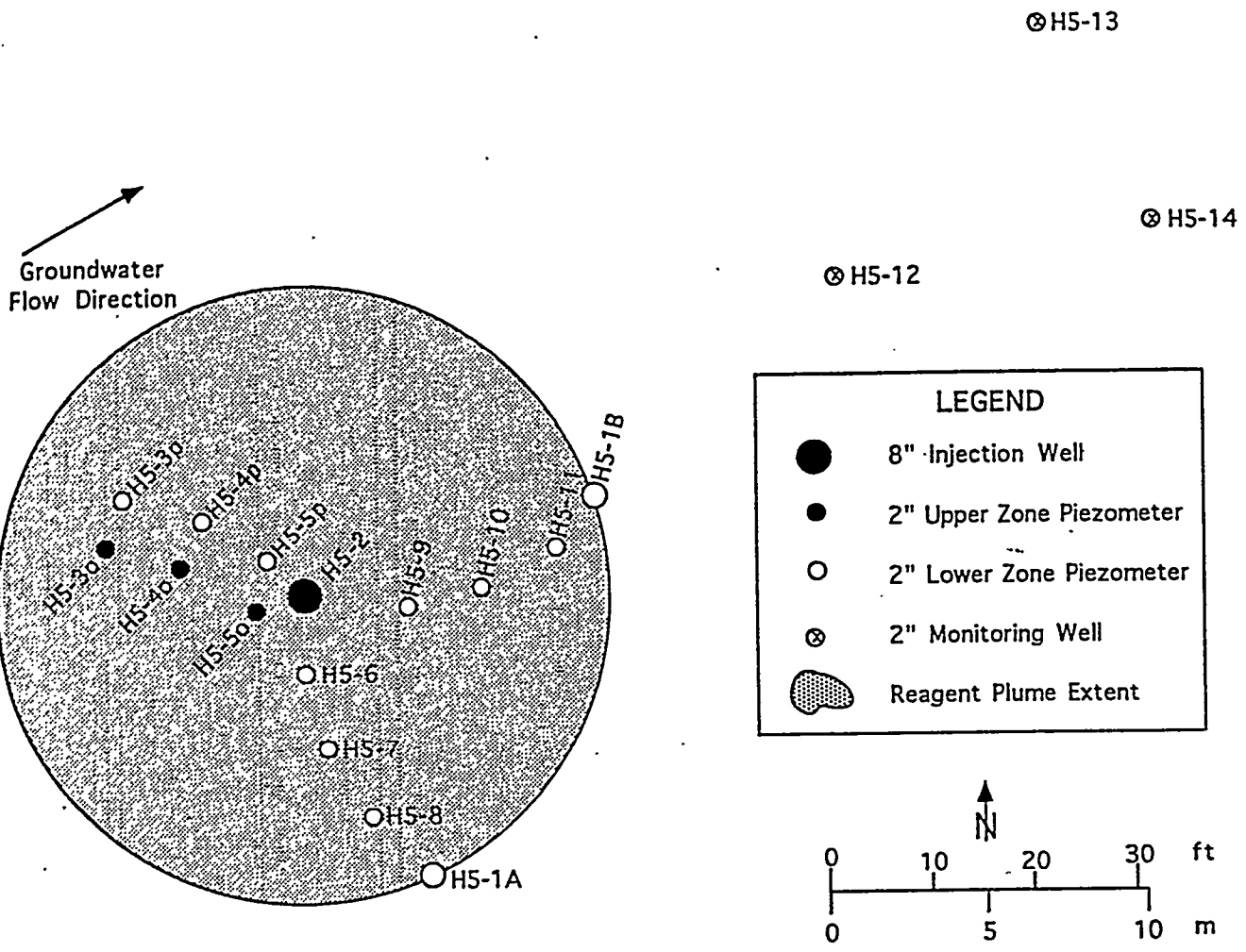
As noted above, the finite-thickness skin solution provided better early-time and overall matches for observed post experiment slug interference responses. The finite-thickness skin solutions used were based on using pre-experiment analysis derived aquifer properties as input to the solution. An improvement in the early-time match (using the finite-skin model) may be possible by slight adjustments of aquifer properties (i.e., not set to pre-experiment analysis derived values) for the trial-and-error solutions. Final quantitative analysis of the pre- and post experiment slug interference responses using the finite-skin model is continuing, and will be documented in a subsequent report.

## D.5 REFERENCES

- Agarwal, R.G., A. Rafi, and H.J. Ramey, Jr. 1970. An Investigation of Wellbore Storage and Skin Effect in Unsteady Liquid Flow: I. Analytical Treatment. Society Petroleum Engineers Journal, (Sept. 1970) pp. 279-290.
- Bouwer, H. 1989. The Bouwer and Rice Slug Test - An Update. Ground Water, Vol. 27, No. 3, pp. 304-309.
- Bouwer, H. 1996. Discussion of Bouwer and Rice Slug Test Review Articles. Ground Water, Readers' Forum, Vol. 34, No. 1, p. 171.
- Bouwer, H. and R.C. Rice. 1976. A Slug Test for Determining Hydraulic Conductivity of Unconfined Aquifers With Completely or Partially Penetrating Wells. Water Resources Research, Vol. 12, pp. 423-428.
- Brown, D.L., T.N. Narasimhan, and Z. Demir. 1995. An Evaluation of the Bouwer and Rice Method of Slug Test Analysis. Water Resources Research, Vol. 31, No. 5, pp. 1239-1246.
- Earlougher, R. C., Jr. 1977. Advances in Well Test Analysis. Soc. of Petroleum Engineers, Monograph Vol. 5, Henry L. Doherty Series.
- Hyder, Z., J.J. Butler, Jr., C.D. McElwee, and W. Liu. 1994. Slug Tests in Partially Penetrating Wells. Water Resources Research, Vol. 31, No. 5, pp: 1239-1246.
- Hyder, Z. and J.J. Butler, Jr. 1995. Slug Tests in Unconfined Formations: An Assessment of the Bouwer and Rice Technique. Ground Water, Vol. 33, No. 1, pp. 16-22.
- Liu, W. and J.J. Butler, Jr. 1995. The KGS Model for Slug Tests in Partially Penetrating Wells. Kansas Geological Survey, Computer Series Report. 95-1, Lawrence, Kansas.
- Ostrowski, L.P. and M.B. Kloska. 1989. Use of Pressure Derivatives in Analysis of Slug Test or DST Flow Period Data. Society of Petroleum Engineers, SPE Paper 18595.
- Ramey, H.J., Jr., R.G. Agarwal, and I. Martin. 1975. Analysis of "Slug Test" or DST Flow Period Data. Journal of Canadian Petroleum Technology, (July-Sept. 1975) pp. 37-47.
- Spane, F.A., Jr. 1992. Applicability of Slug Interference Tests Under Hanford Site Conditions: Analytical Assessment and Field Test Evaluation. Pacific Northwest Laboratory, PNL-8070, Richland, Washington.
- Spane, F.A., Jr., 1996. Applicability of Slug Interference Tests for Hydraulic Characterization of Unconfined Aquifers: (1) Analytical Assessment. Ground Water, Vol. 34, No. 1, pp. 66-74; also published as Pacific Northwest Laboratory, PNL-SA-24283, Richland, Washington.
- Spane, F.A., Jr. and S.K. Wurstner. 1993. DERIV: A Program for Calculating Pressure Derivatives for Use in Hydraulic Test Analysis. Ground Water, Vol. 31, No. 5, pp. 814-822.
- Spane, F.A., Jr., P.D. Thorne, and L.C. Swanson. 1995. Applicability of Slug Interference Tests for Hydraulic Characterization of Unconfined Aquifers: (2) Field Test Examples. Pacific Northwest Laboratory, PNL-SA-26011; accepted for publication in Ground Water sometime in

1996.

Weeks, E.P. 1969. Determining the Ratio of Horizontal to Vertical Permeability by Aquifer-Test Analysis. Water Resources Research, Vol. 5, No. 1, pp. 196-213.



Well Location Map for the In Situ Redox Manipulation Field Test Site

Figure D.1

# Unconfined Aquifer Slug Test Example

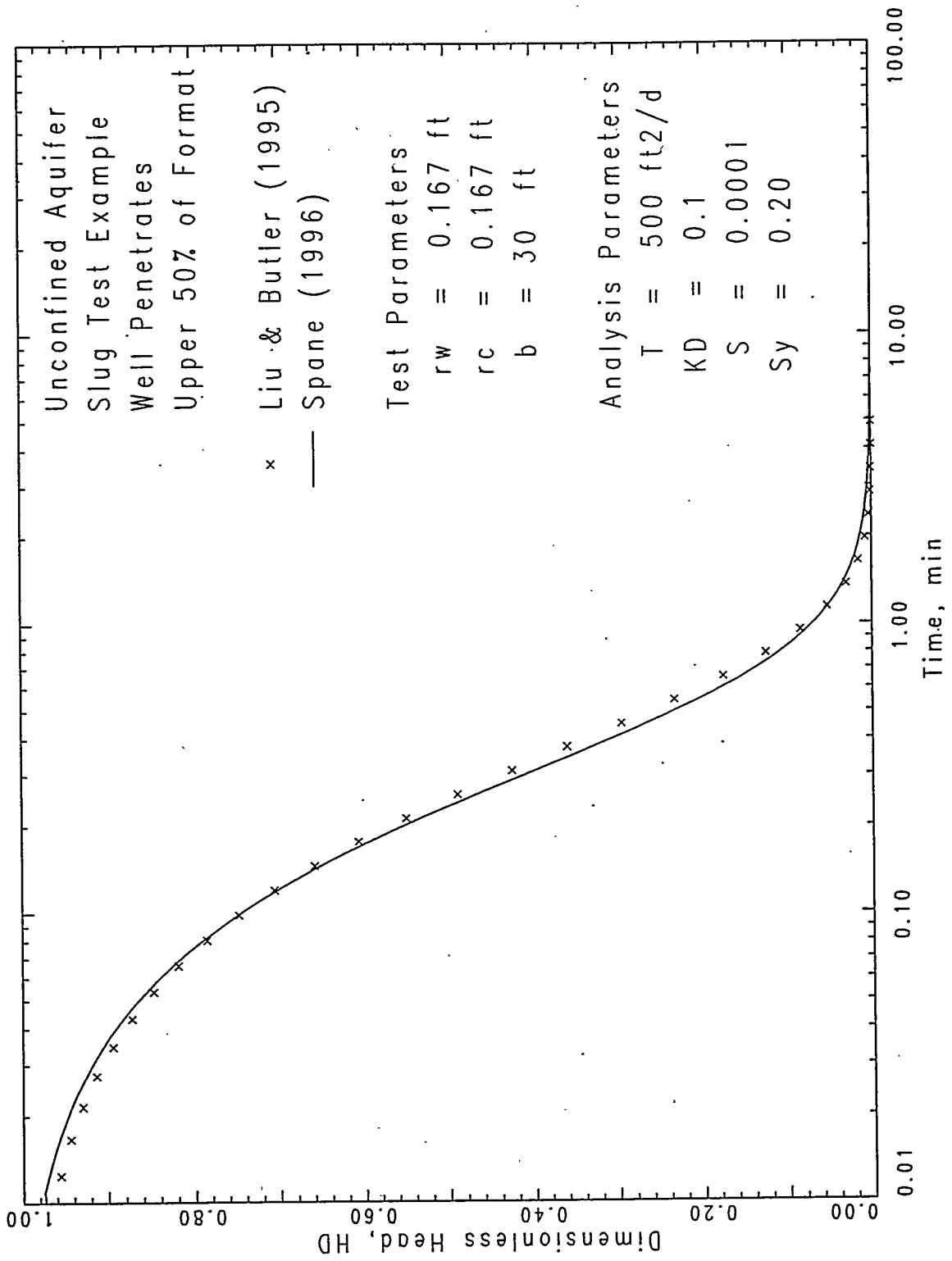


Figure D.2

# Unconfined Aquifer Slug Interf. E.G.

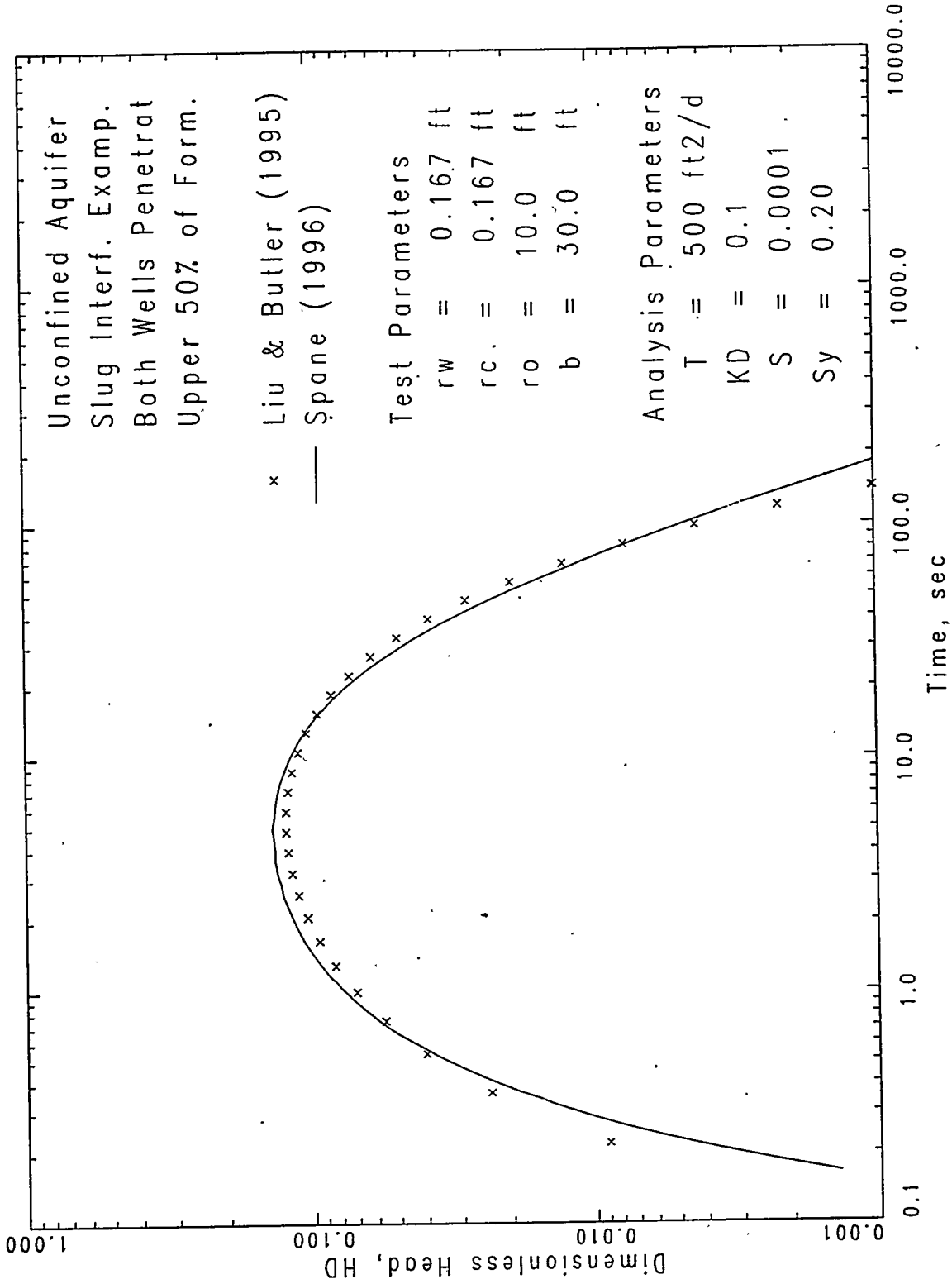


Figure D.3

# Pre- & Post Experiment Slug Test Comp.

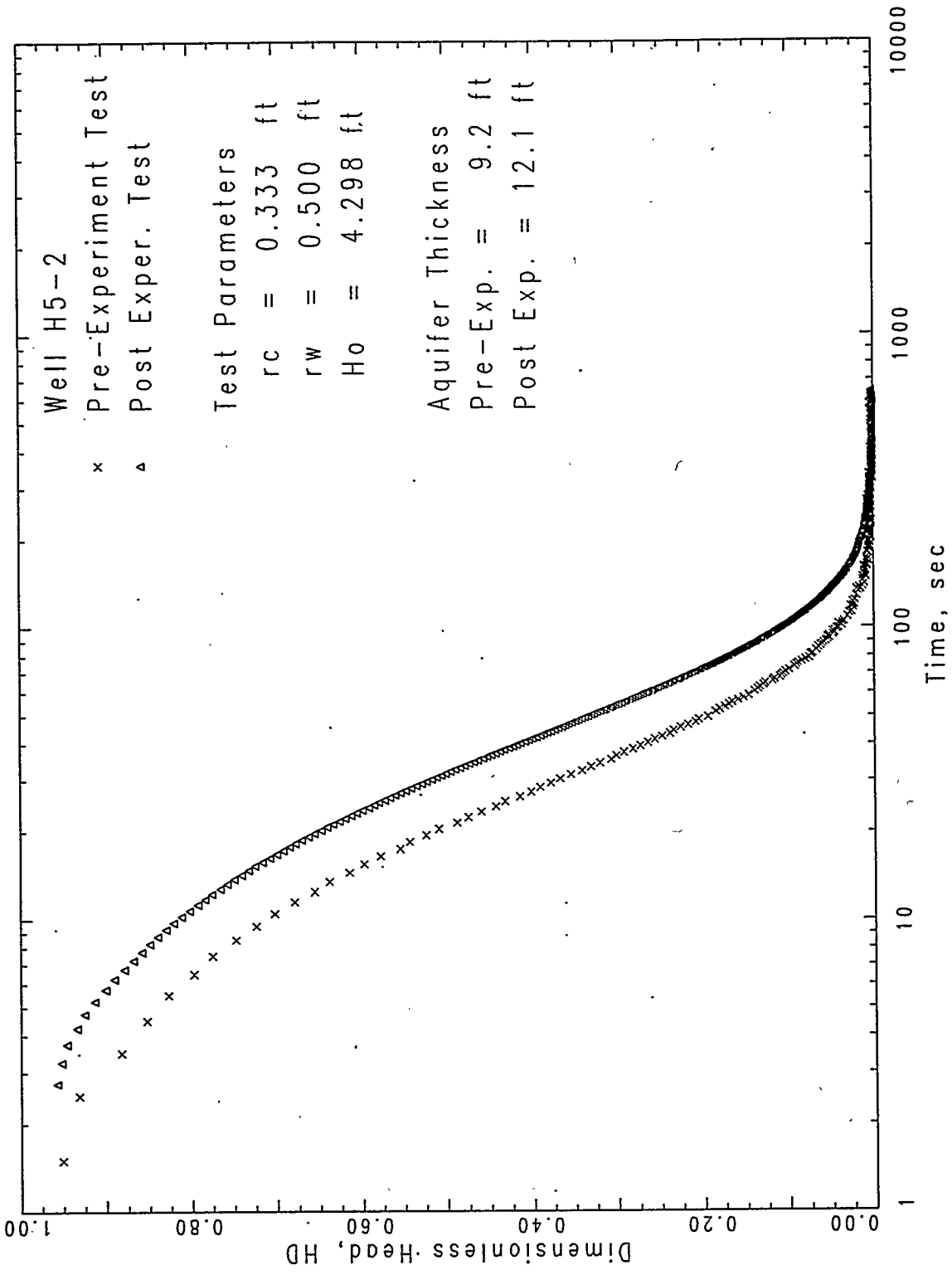


Figure D.4.

# Pre-Experiment Slug Test Analysis

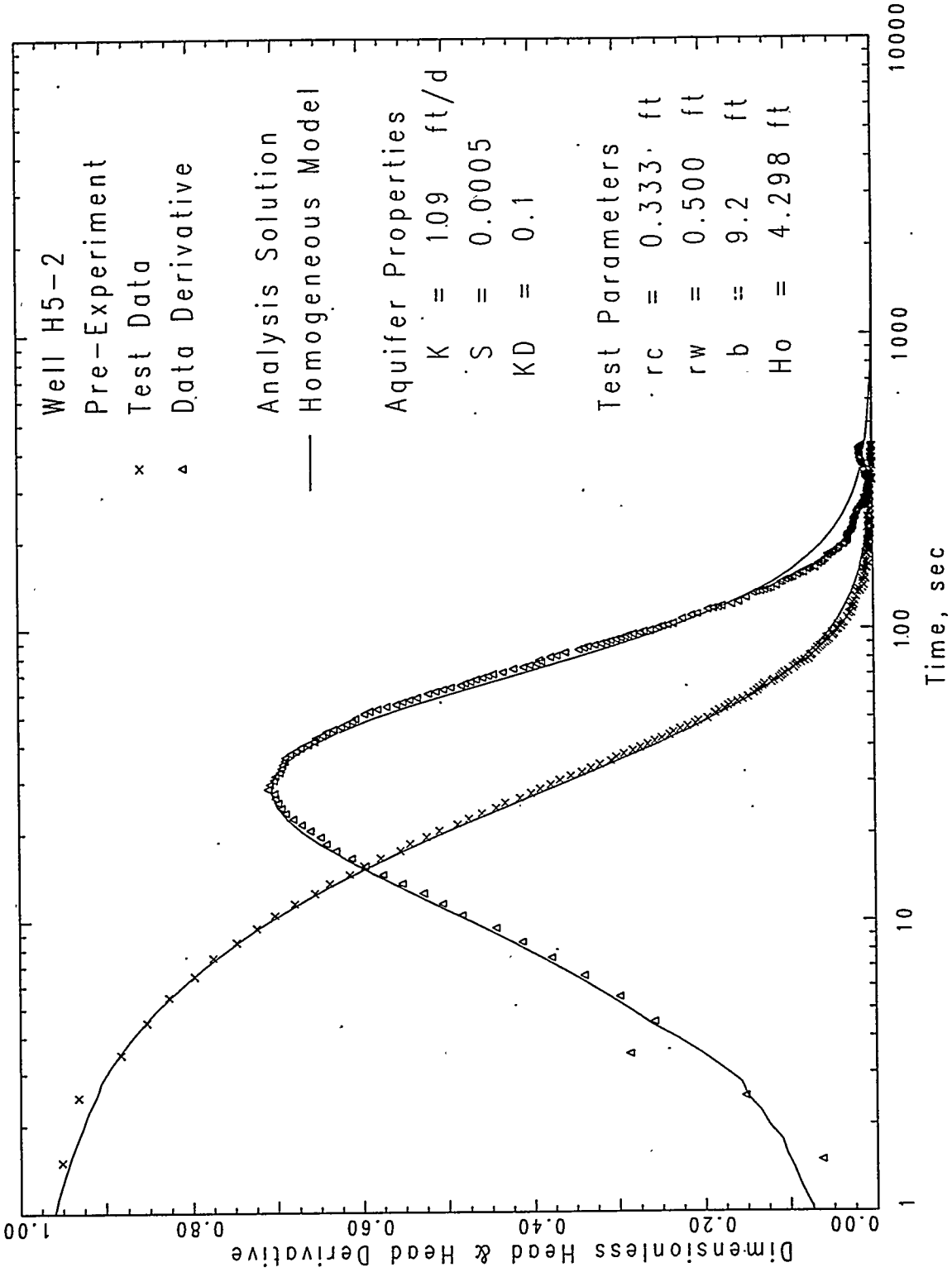


Figure D.5

# Post Experiment Slug Test Analysis

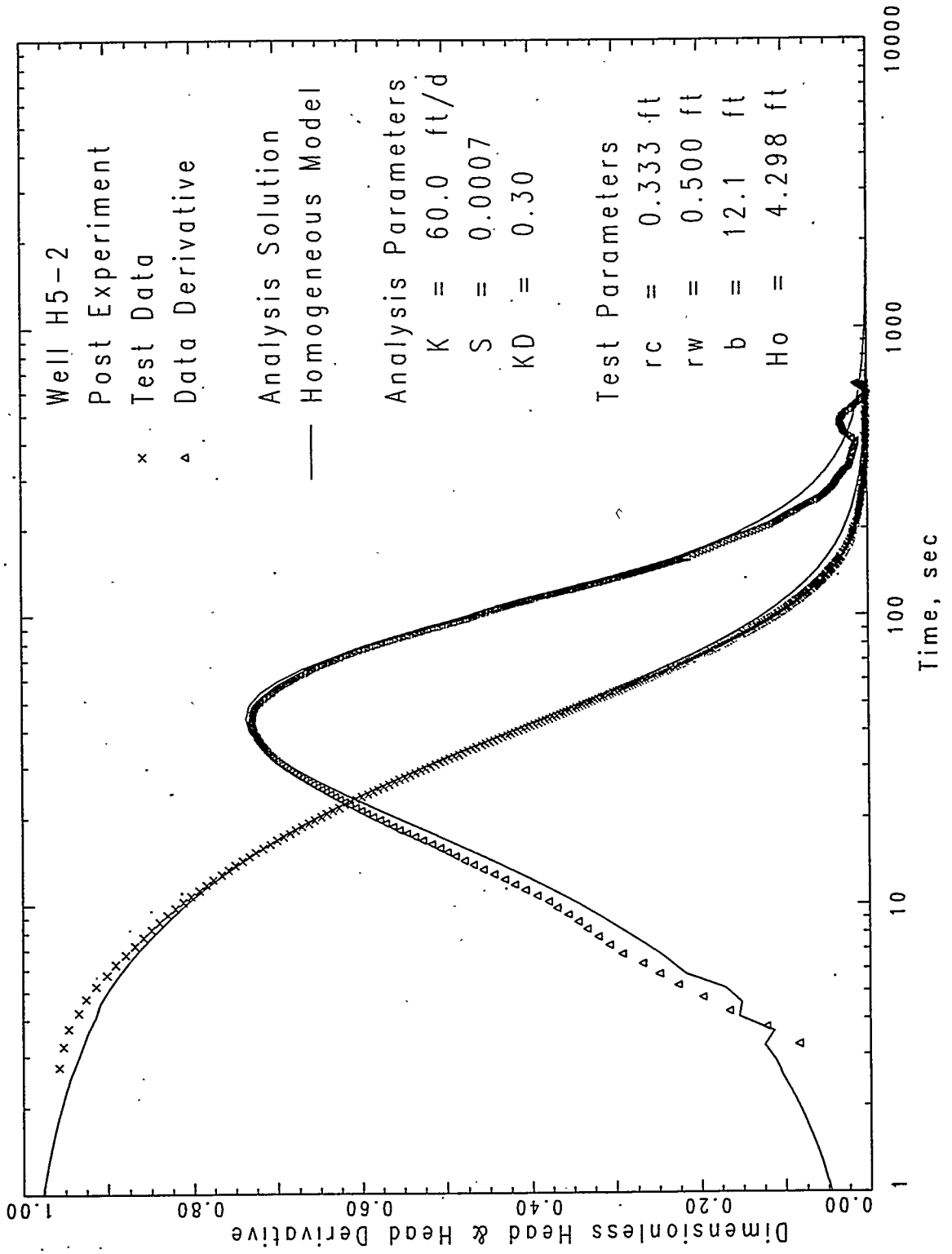


Figure D.6

# Post Experiment Slug Test Analysis

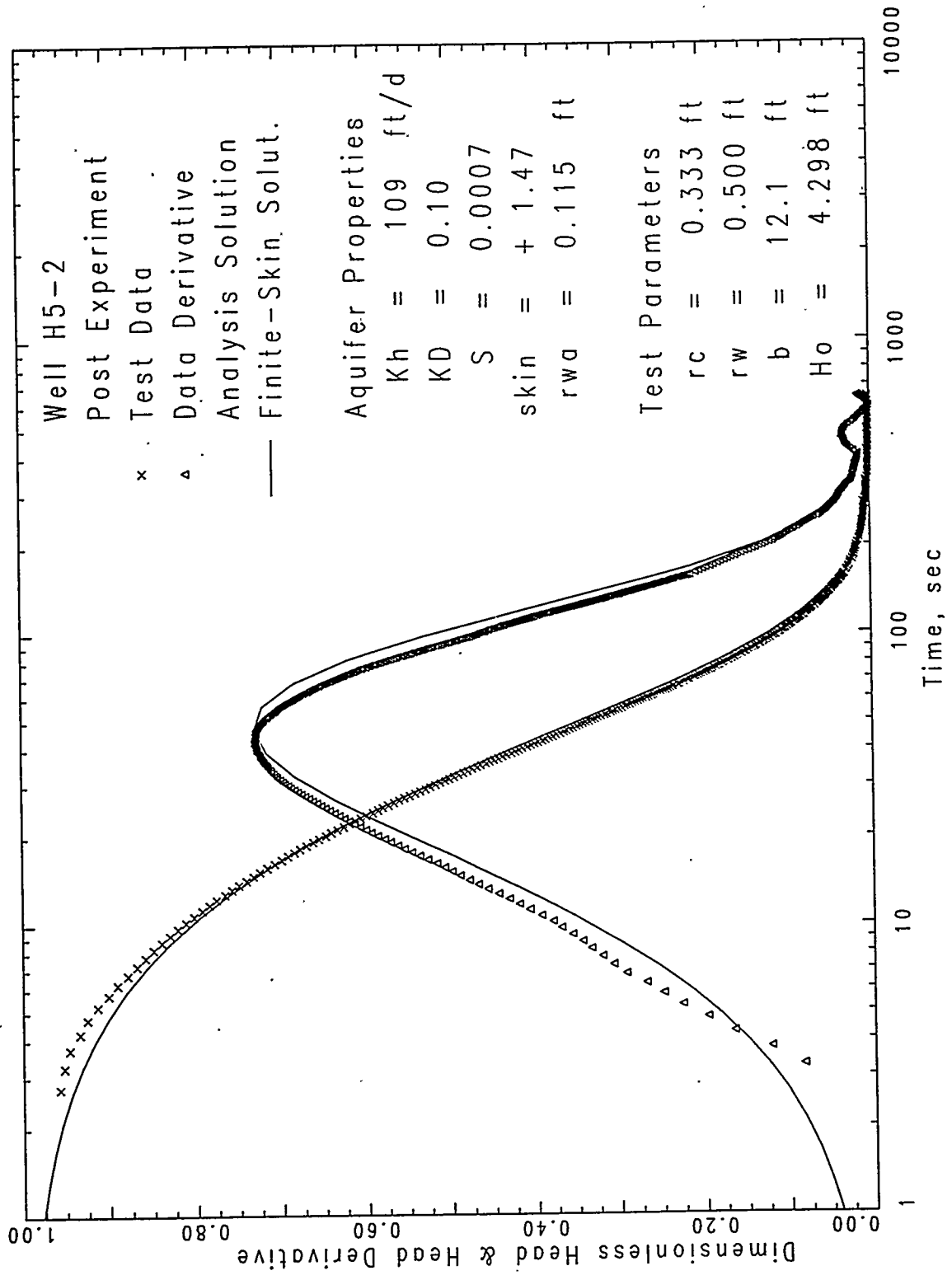


Figure D.7

# Slug Interference Response Comparison

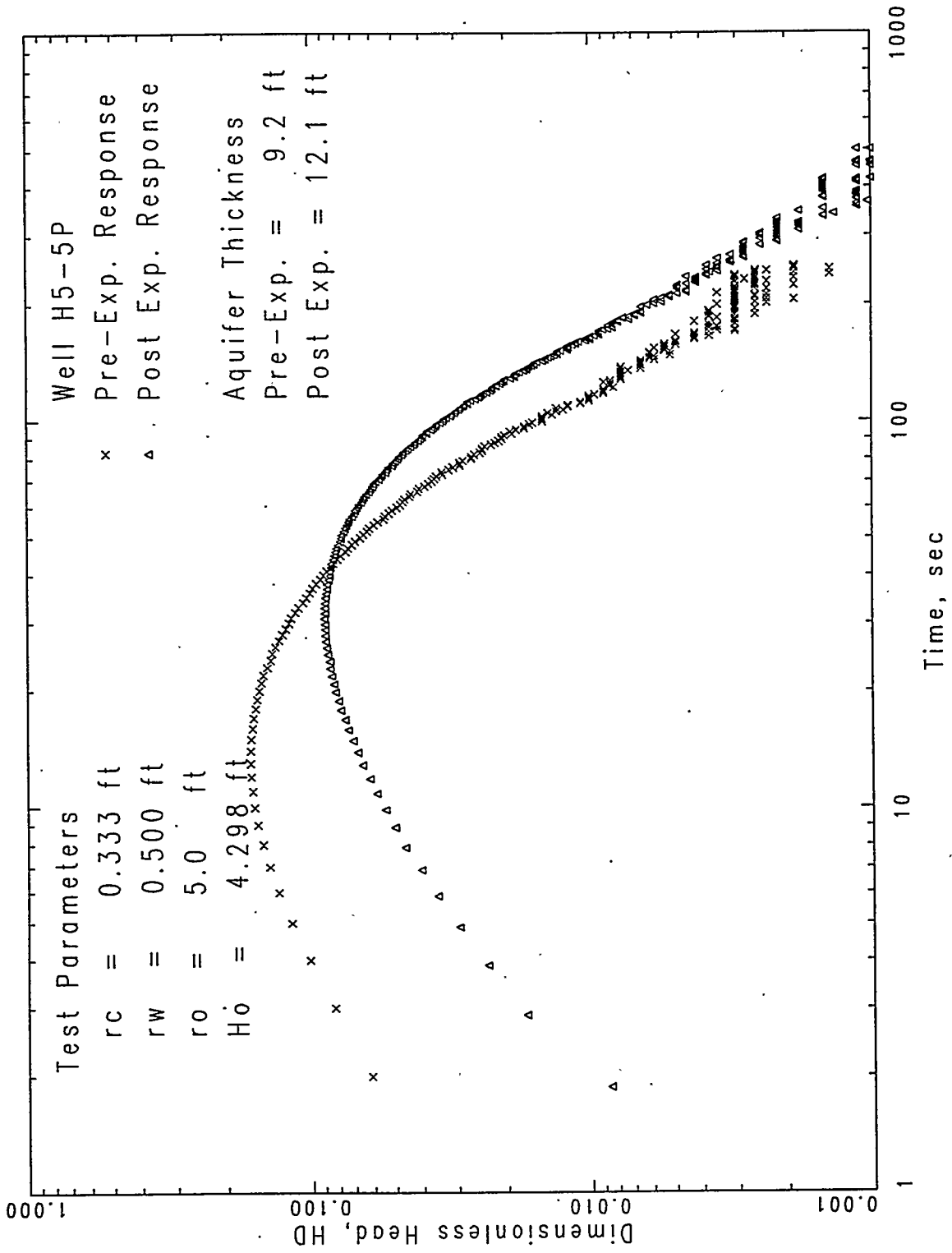


Figure D.8

# Pre-Exper. Slug Intert. Iest Analysis

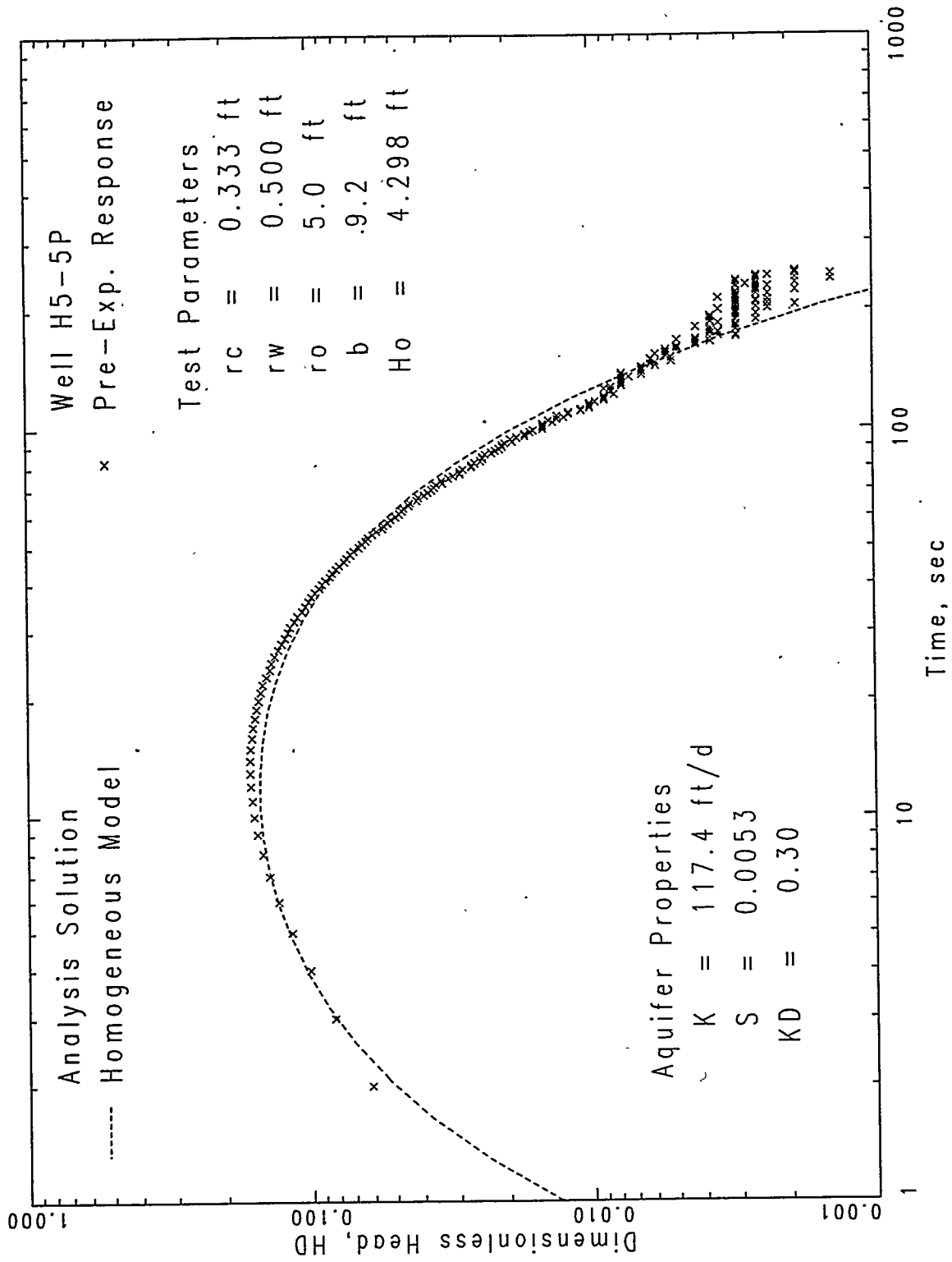


Figure D.9

# Post Exper. Slug Interf. Test Analysis

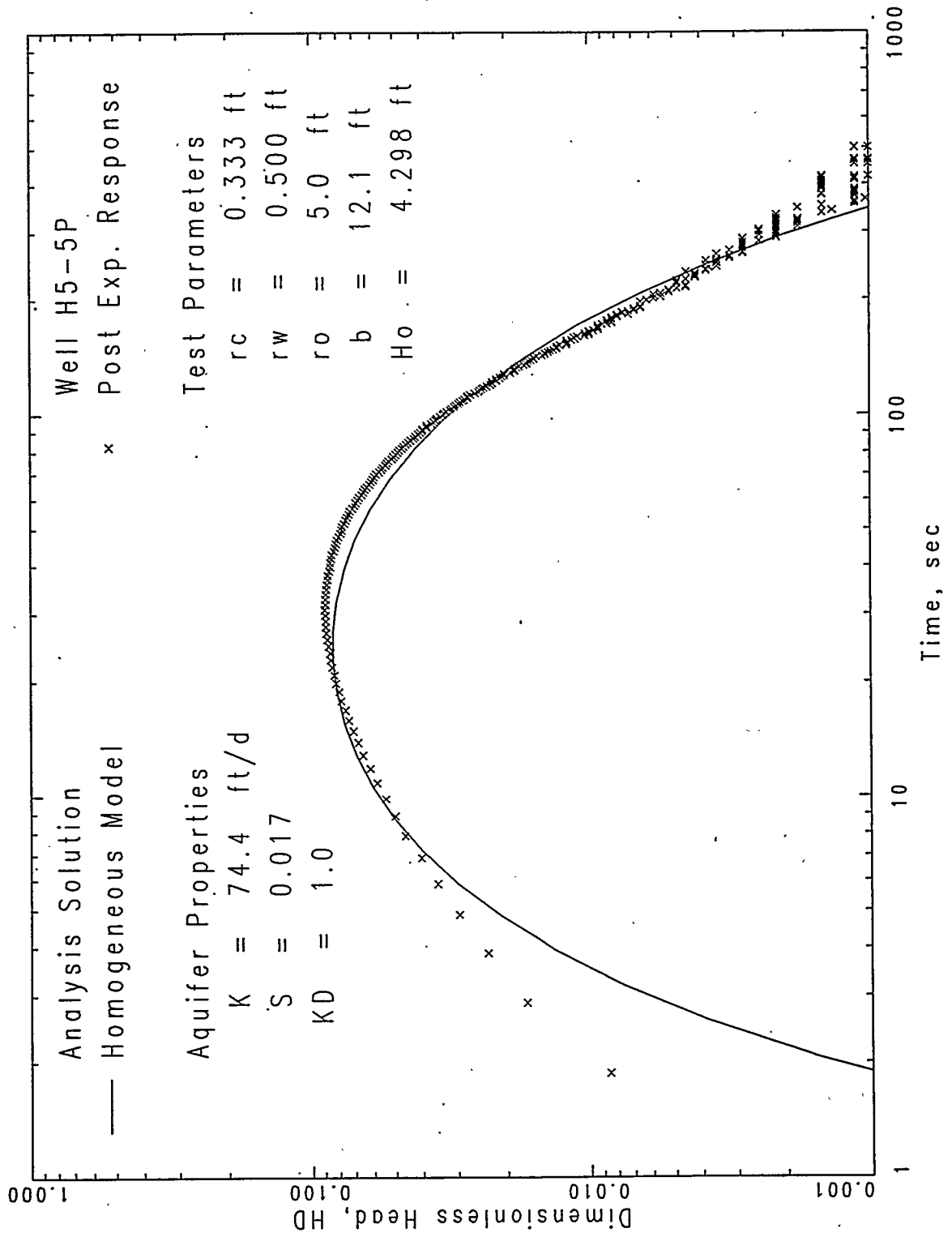


Figure D.10

# Post Exper. Slug Interf. Iest Analysis

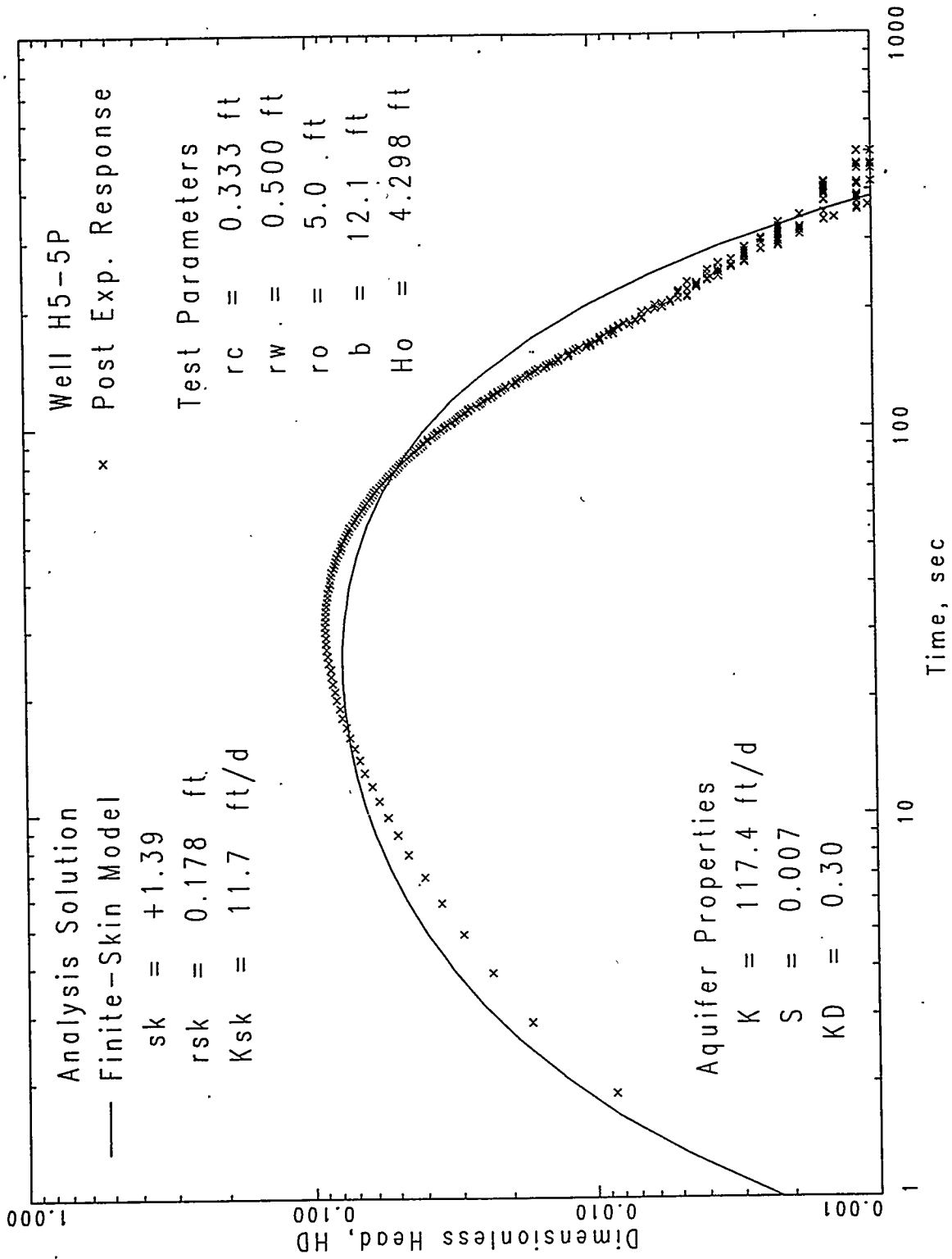


Figure D.11

# Slug Interference Response Comparison

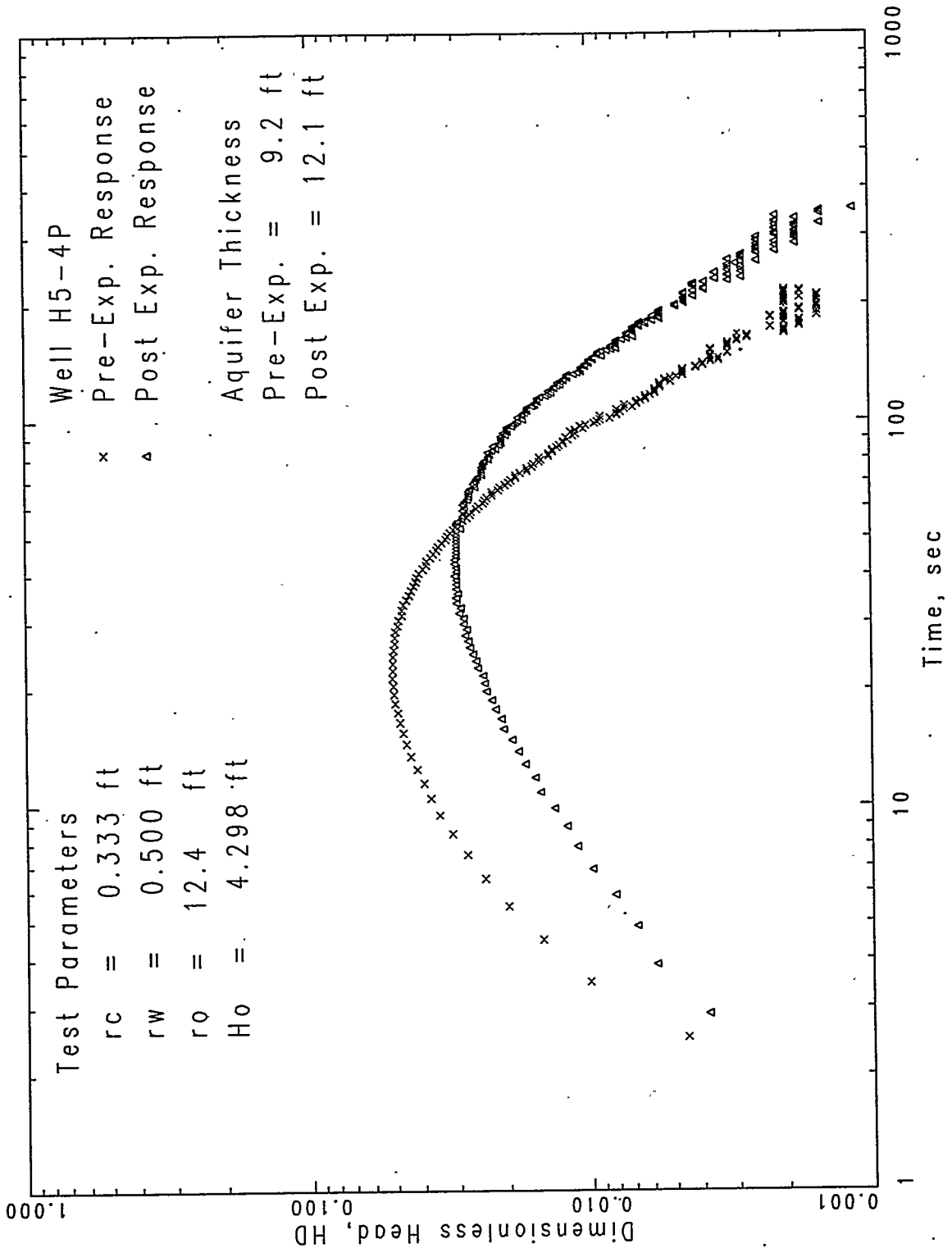


Figure D.12

# Pre-Exper. Slug Interf. Test Analysis

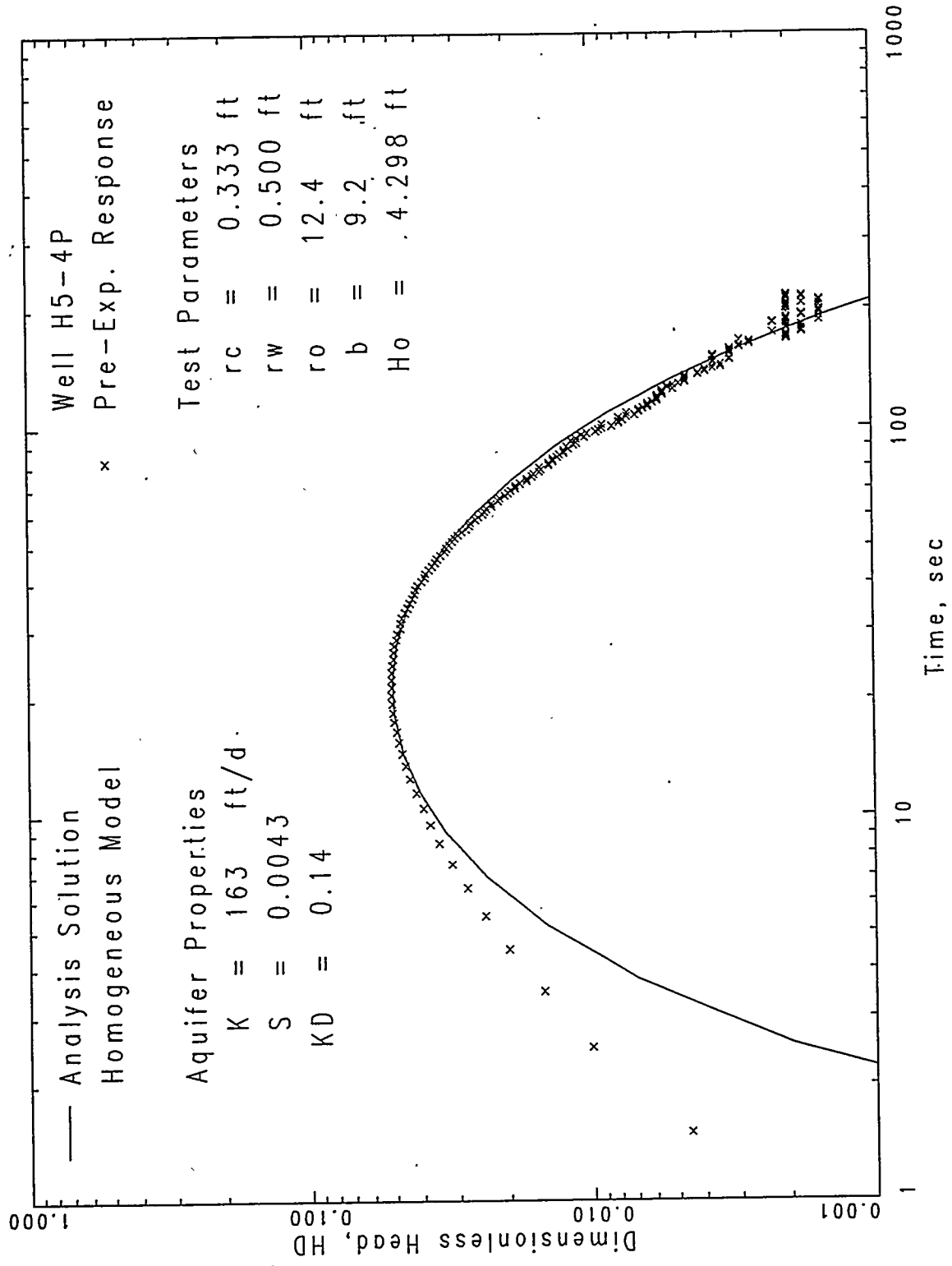


Figure D.13

# Post Exper. Slug Interf. Test Analysis

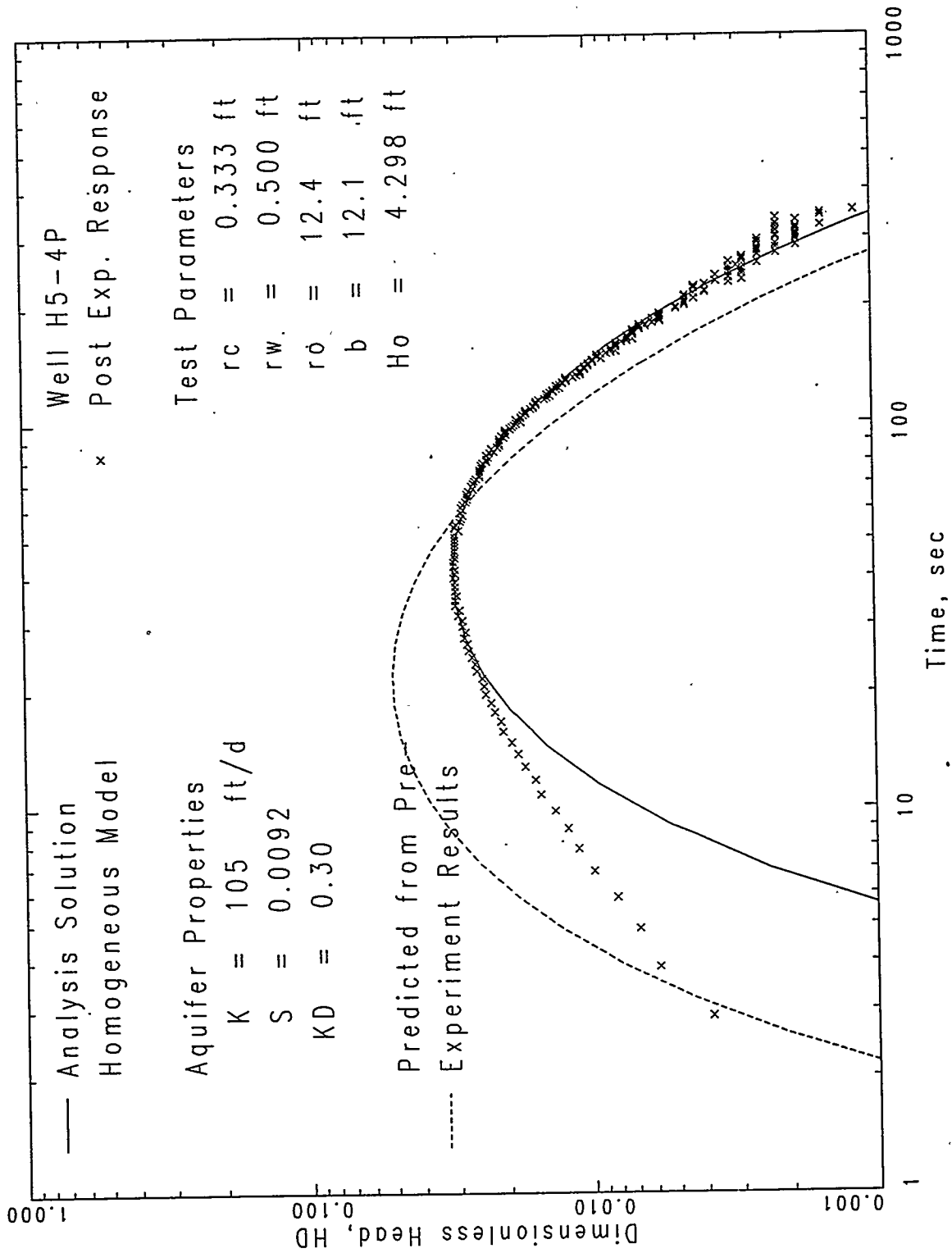


Figure D.14

# Post Exper. Slug Interf. Test Analysis

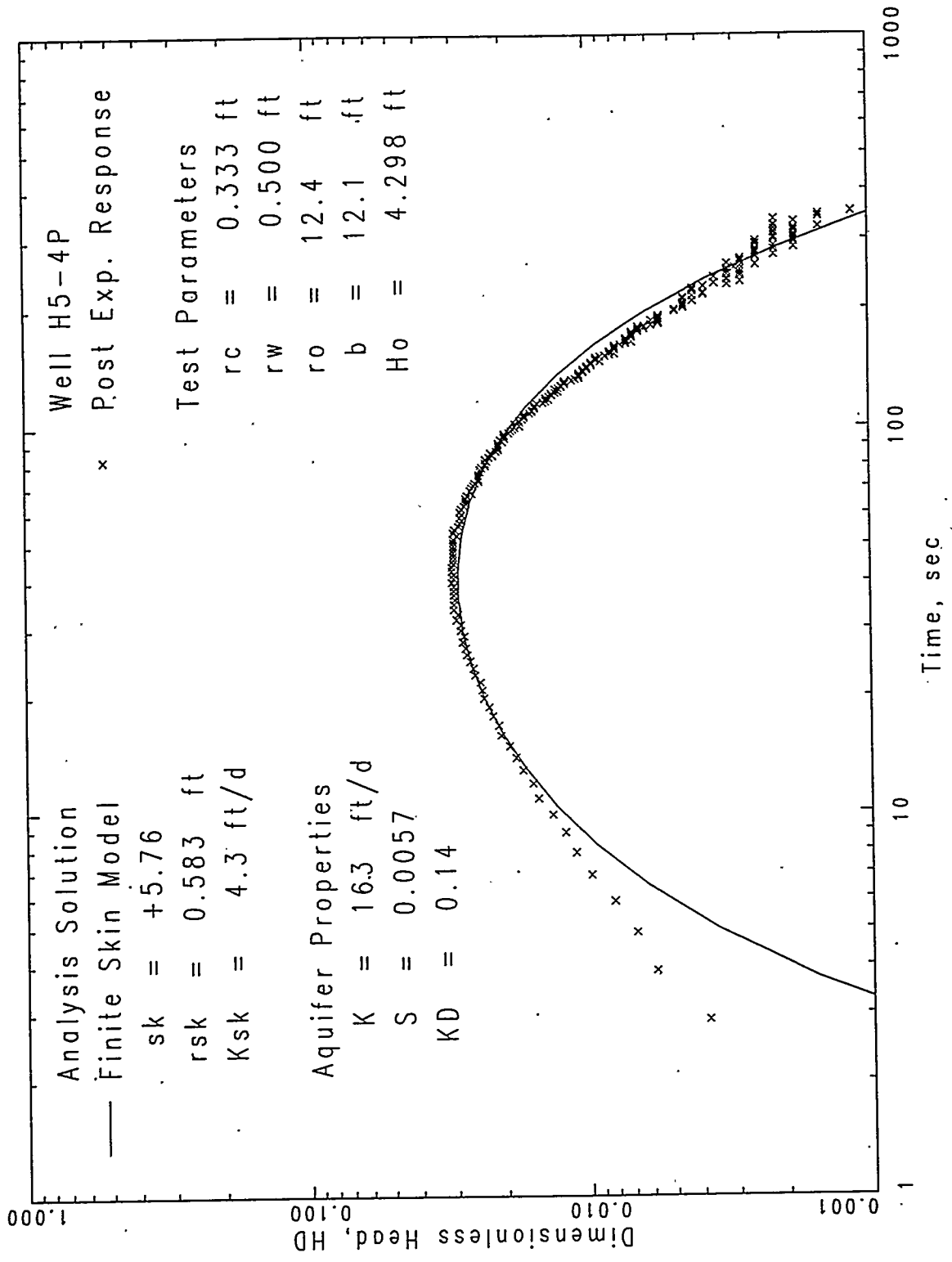


Figure D.15

# Slug Interference Response Comparison

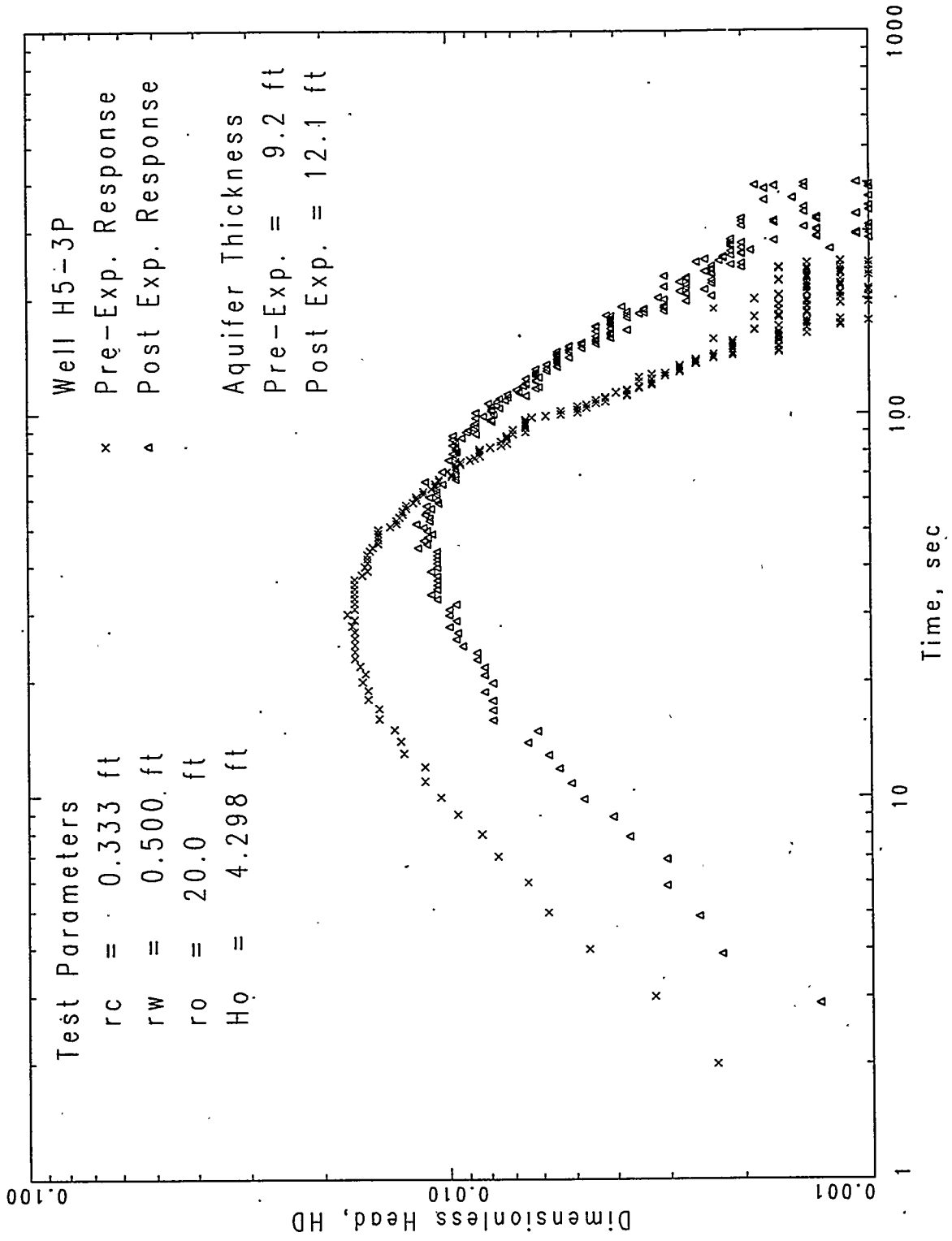


Figure D.16

# Pre-Experiment Slug Inert: Analysis

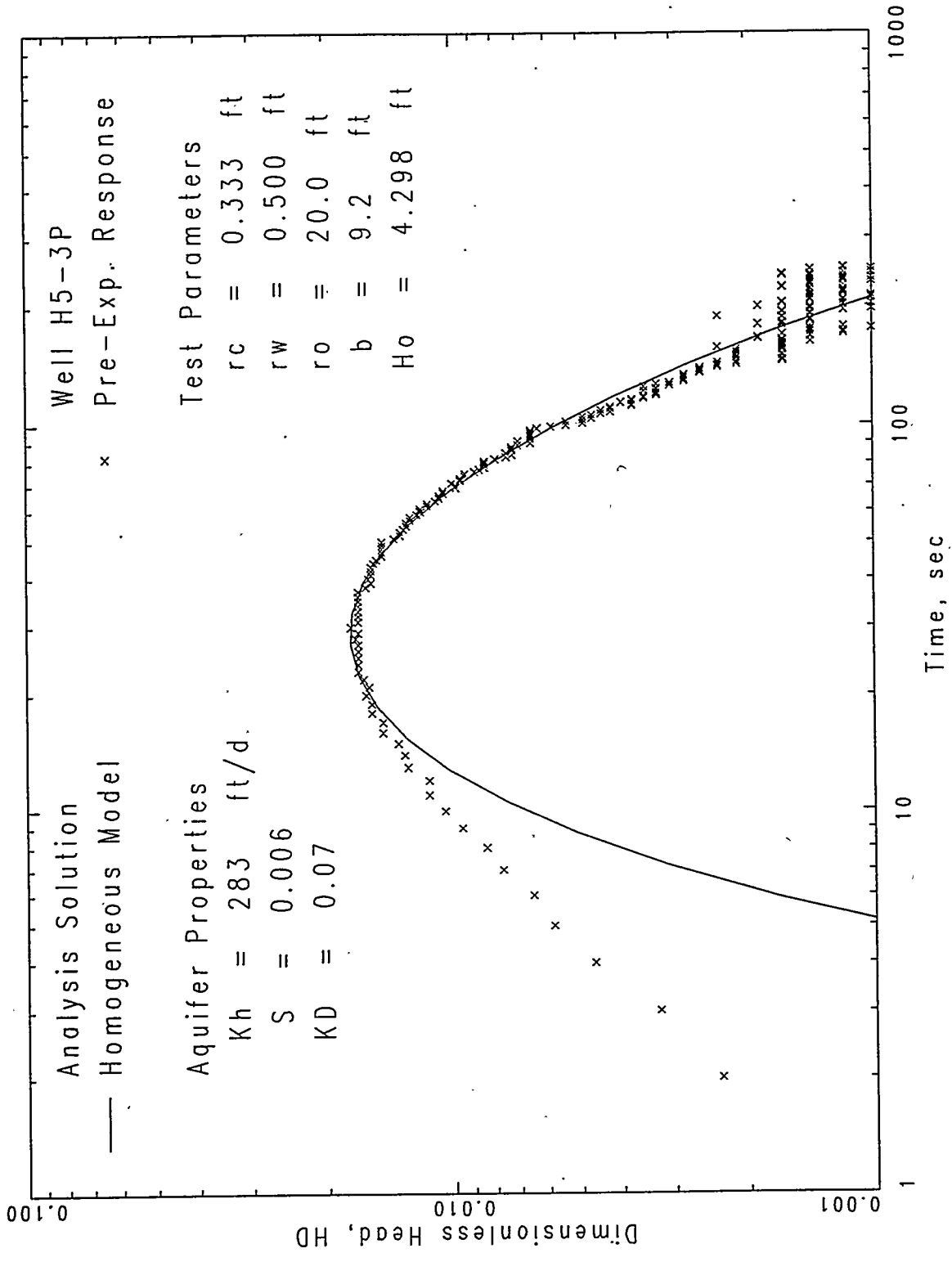


Figure D.17

# Post Experiment Slug Interf. Analysis

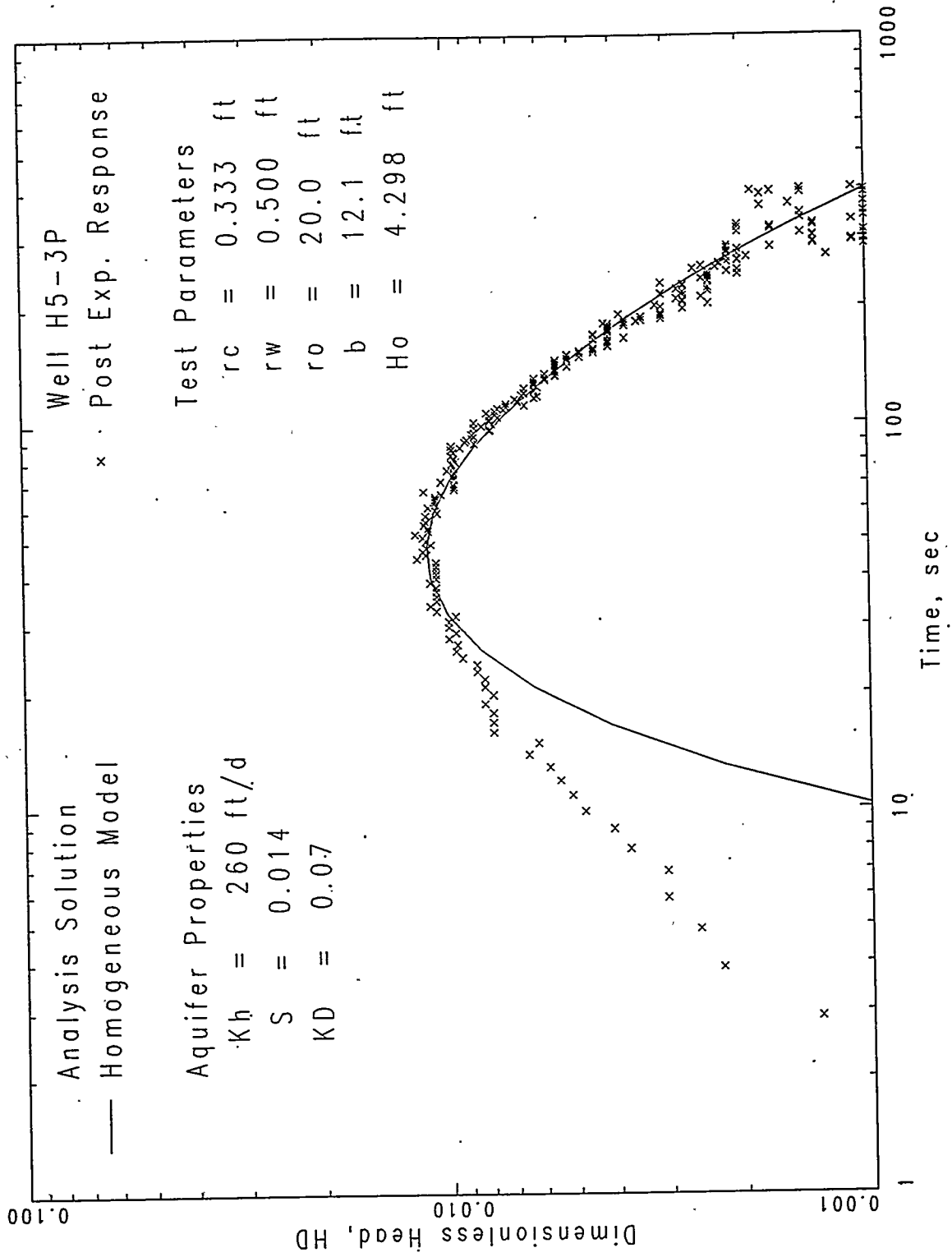


Figure D.18

# Post Experiment Slug Interf. Analysis

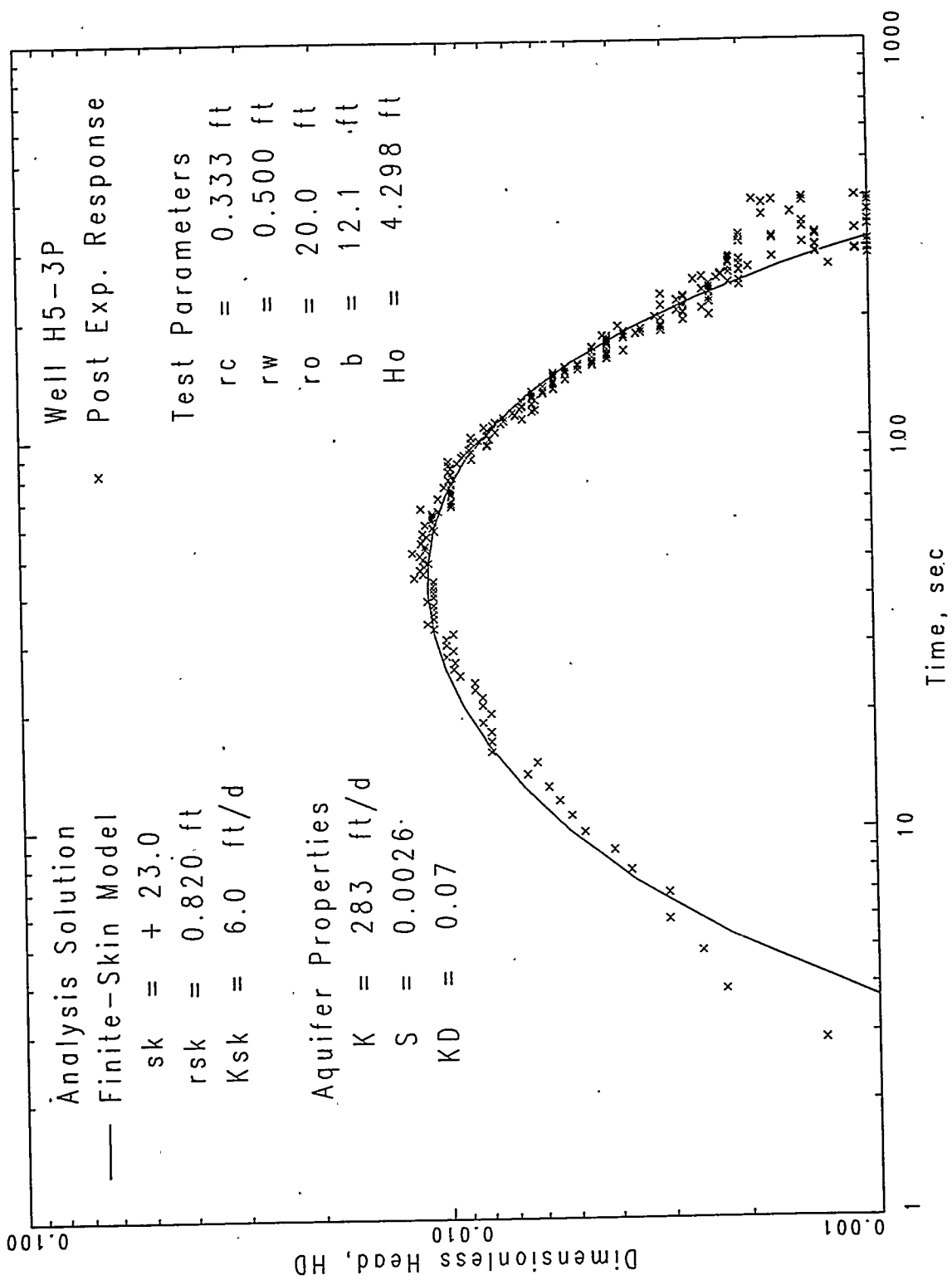


Figure D.19

**TABLE D.1 Analysis Summary for Pre- and Post Experiment Tests.**

WELL SITE	PRE-EXPERIMENT HOMOGENEOUS FORMATION SOLUTION	POST EXPERIMENT HOMOGENEOUS FORMATION SOLUTION	POST EXPERIMENT FINITE-THICKNESS SKIN SOLUTION
H5-2 (r = 0 ft)	$K_h$ : 109 ft/d $K_D$ : 0.10 $S_s$ : 5.4E-5 ft <sup>-1</sup> S: 5.0E-4	$K_h$ : 60.0 ft/d $K_D$ : 0.3 $S_s$ : 5.4E-5 ft <sup>-1</sup> S: 7.0E-4	$K_h$ : 109 ft/d $K_D$ : 0.1 $S_s$ : 5.4E-5 ft <sup>-1</sup> S: 6.6E-4  $r_{sk}$ : 0.58 ft* $K_{sk}$ : 10.3 ft/d
H5-3P (r = 20 ft)	$K_h$ : 283 ft/d $K_D$ : 0.07 $S_s$ : 6.5E-4 ft <sup>-1</sup> S: 6.0E-3	$K_h$ : 260 ft/d $K_D$ : 0.07 $S_s$ : 1.2E-3 ft <sup>-1</sup> S: 1.4E-2	$K_h$ : 283 ft/d $K_D$ : 0.07 $S_s$ : 1.7E-4 S: 2.0E-3  $r_{sk}$ : 0.82 ft $K_{sk}$ : 14.5 ft/d
H5-4P (r = 12.4 ft)	$K_h$ : 163 ft/d $K_D$ : 0.14 $S_s$ : 4.7E-4 ft <sup>-1</sup> S: 4.3E-3	$K_h$ : 105 ft/d $K_D$ : 0.30 $S_s$ : 7.6E-4 ft <sup>-1</sup> S: 9.2E-3	$K_h$ : 163 ft/d $K_D$ : 0.14 $S_s$ : 4.7E-4 S: 5.7E-3  $r_{sk}$ : 0.58 ft $K_{sk}$ : 4.3 ft/d
H5-5P (r = 5.0 ft)	$K_h$ : 117 ft/d $K_D$ : 0.3 $S_s$ : 5.8E-4 ft <sup>-1</sup> S: 5.3E-3	$K_h$ : 74.4 ft/d $K_D$ : 1.0 $S_s$ : 1.7E-3 ft <sup>-1</sup> S: 2.0E-2	$K_h$ : 117 ft/d $K_D$ : 0.3 $S_s$ : 5.8E-4 ft <sup>-1</sup> S: 0.007  $r_{sk}$ : 0.178 ft $K_{sk}$ : 11.7 ft/d

\* The finite-thickness skin values derived from a skin factor value of +1.47, which was previously determined from an infinitesimal-thickness skin solution

**APPENDIX E**

**BACKGROUND CHEMISTRY OF 100-H WELLS**

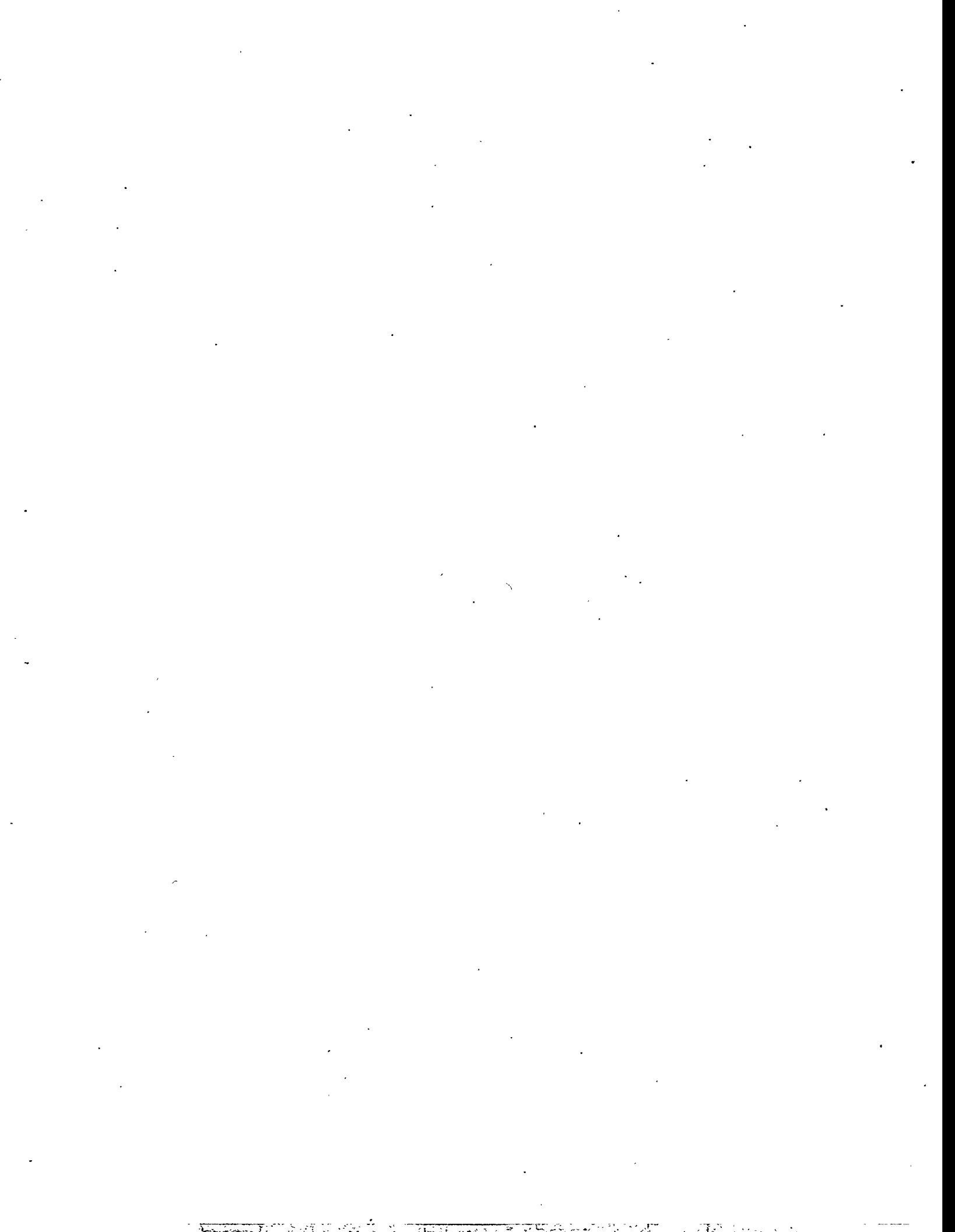
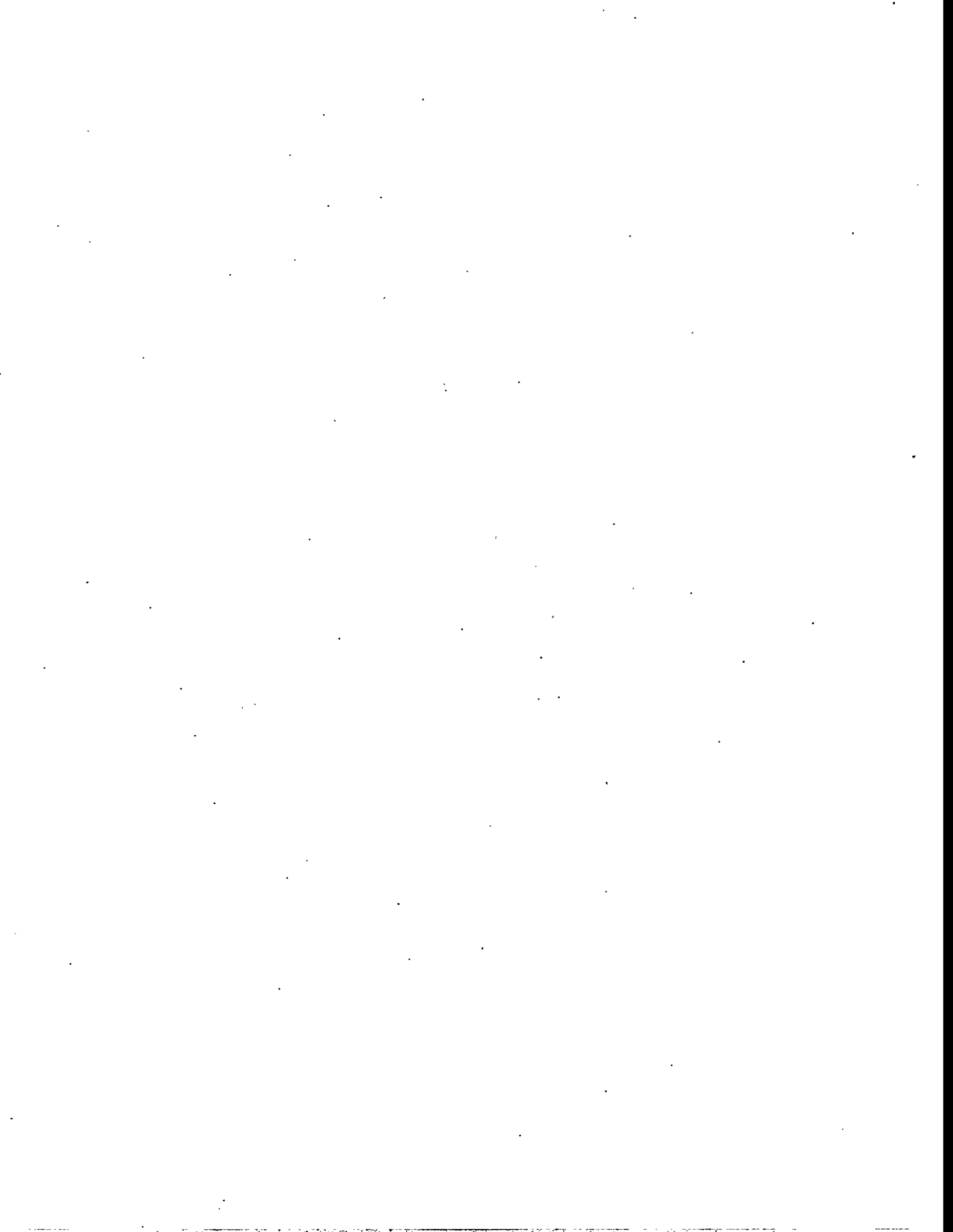


## Table of Contents

Appendix E. Background Chemistry of 100H Wells .....	E.1
--	-----

### List of Tables

Table E-1. Baseline Trace Metals Analysis Results for the ISRM Test Site .....	E.2
Table E-2. Ground-water Chemistry Data for Well 199-H5-1A .....	E.3
Table E-3. Dissolved Oxygen Data for Hanford Site Wells .....	E.34



## APPENDIX E

### BACKGROUND CHEMISTRY OF 100-H WELLS

The purpose of this Appendix is to present available background groundwater chemistry data for wells at the 100-H In-situ Redox Manipulation Experiment Site. Groundwater samples were collected from 14 of the monitoring wells at the 100-H site in August 1995, prior to the "Mini" Injection. These samples were analyzed for metals by PNNL using the ICP-MS (inductively coupled plasma - mass spectrometry) method. These results are provided in Table E-1.

Data are also available from well 199-H5-1A. This well was installed in 1992 as a monitoring well for the 100-HR-3 CERCLA Operable Unit. Groundwater data from well 199-H5-1A is presented in Table E-2. These data were obtained from the Hanford Environmental Information System (HEIS) database.

In addition, dissolved oxygen data for Hanford Site wells are presented in Table E-3. These data were also obtained from the Hanford Environmental Information System (HEIS) database.

Table E-1. Baseline Trace Metals Analysis Results for the ISRM Test Site.

Constituent	MCL (ppb)	Sample Location														
		H5-3(P)	H5-3(O)	H5-4(P)	H5-4(O)	H5-5(P)	H5-5(O)	H5-6	H5-7	H5-8	H5-9	H5-9 dup	H5-10	H5-11	H5-12	H5-13
Na	none	22.1	21.7	20.8	21.8	19.7	22.5	20.3	20.8	22.8	18.7	18.0	20.6	17.4	16.8	24.8
Mg	none	12.1	11.5	11.7	11.8	12.0	11.7	12.1	13.9	13.4	12.4	11.9	13.4	13.1	14.8	15.7
Si	none	13.0	13.8	11.3	14.7	13.3	14.8	14.2	15.1	13.1	15.5	12.6	13.8	13.1	10.1	11.9
K	none	4.93	4.52	4.58	4.89	7.16	5.08	4.70	5.28	4.86	5.11	4.56	5.56	4.74	5.43	5.84
Al	50 to 200*	16.6	46.8	27.3	20.2	20.5	20.1	17.6	18.6	18.9	35.3	35.7	22.1	51.1	16.3	27.4
Mn	50*	24.1	3.4±0.5	12.5	<1	<1	1.6±0.2	1.1	5.92	3.45	1±0.1	1.2±0.2	47.6	10	140	146
Fe	300*	<10	22±12	<10	<10	<10	<10	<10	<10	<10	<10	<10	<10	33±13	21±10	10±7
Ni	100	2.1±0.5	2.86	4.6±1.5	3.16	2.6±0.3	2.64	2.5±0.3	3.49	3.45	3.1±0.4	3.0±0.6	3.28	10.9	3.29	4.48
Cu	1000*	4.51	3.8±0.5	3.98	3.58	4.6±0.5	4.20	3.61	3.6±0.4	3.09	3.53	3.87	4.75	4.7	3.27	4.26
Zn	5000*	19.6	13.0	19.6	11.2	24.2	12.2	18.1	18.4	20±2	12.6	12.1	24.5	73.1	18.4	16.6
As	50	<1	<1	<1	<1	<1	<1	<1	<1	<1	<1	<1	<1	<1	<1	<1
Se	50	3.4±4.4	<1	<1	<1	<1	<1	<1	<1	<1	<1	<1	<1	<1	<1	<1
Ag	100*	<1	<1	<1	<1	<1	<1	<1	<1	<1	<1	<1	<1	<1	<1	<1
Cd	5	<1	<1	<1	<1	<1	<1	<1	<1	<1	<1	<1	<1	<1	<1	<1
Sn	none	1.1±0.2	<1	<1	<1	1.1±0.2	1.1±0.2	1.49	1.1±0.2	<1	<1	<1	<1	<1	<1	<1
Sb	6	<1	<1	<1	<1	<1	<1	<1	<1	<1	<1	<1	<1	<1	<1	<1
Ba	2000	34.6	42.9	40.5	37.8	57	36.6	36.6	51.1	76.1	35.4	36.3	41.7	38.1	61.5	76.5
Pb	50**	<1	<1	<1	<1	<1	<1	<1	<1	<1	<1	<1	<1	<1	<1	<1
Cr	100	50.8	71.0	47.1	68.9	64.8	67.4	60.1	67.4	61.5	59.8	60.7	45.8	59.5	12.9	34.0

MCL's are from EPA 822-R-96-001, February 1996 unless otherwise indicated.

\* EPA Secondary Standard (In: EPA 822-R-96-001, February 1996)

\*\* CFR Part 265 Appendix III

Dup = duplicate sample

Table E-2. Ground-water Chemistry for Well 199-H5-1A

Constituent	Sample Date	Filtered	Qualifier	Value	Units
1,1,1-T	01-AUG-92	N	U	10	ug/L
1,1,1-T	01-AUG-92	N	U	10	ug/L
1,1,1-T	18-MAY-92	N	U	10	ug/L
1,1,1-T	18-MAY-92	N	U	10	ug/L
1,1,1-T	01-NOV-92	N	U	10	ug/L
1,1,2-T	01-AUG-92	N	U	10	ug/L
1,1,2-T	01-AUG-92	N	U	10	ug/L
1,1,2-T	18-MAY-92	N	U	10	ug/L
1,1,2-T	01-NOV-92	N	U	10	ug/L
1,1,2-T	18-MAY-92	N	U	10	ug/L
1,1-DCL	01-AUG-92	N	U	10	ug/L
1,1-DCL	18-MAY-92	N	U	10	ug/L
1,1-DCL	18-MAY-92	N	U	10	ug/L
1,1-DCL	01-NOV-92	N	U	10	ug/L
1,1-DCL	01-AUG-92	N	U	10	ug/L
1,2-DCL	01-AUG-92	N	U	10	ug/L
1,2-DCL	01-AUG-92	N	U	10	ug/L
1,2-DCL	18-MAY-92	N	U	10	ug/L
1,2-DCL	18-MAY-92	N	U	10	ug/L
1,2-DCL	01-NOV-92	N	U	10	ug/L
1122-TCE	01-AUG-92	N	U	10	ug/L
1122-TCE	18-MAY-92	N	U	10	ug/L
1122-TCE	01-NOV-92	N	U	10	ug/L
1122-TCE	18-MAY-92	N	U	10	ug/L
1122-TCE	01-AUG-92	N	U	10	ug/L
12DICHL	01-AUG-92	N	U	10	ug/L
12DICHL	18-MAY-92	N	U	10	ug/L
12DICHL	01-NOV-92	N	U	10	ug/L
12DICHL	18-MAY-92	N	U	10	ug/L
12DICHL	01-AUG-92	N	U	10	ug/L
12DICLBENZ	18-MAY-92	N	U	10	ug/L

Table E-2. Ground-water Chemistry for Well 199-H5-1A

Constituent	Sample Date	Filtered	Qualifier	Value	Units
12DICLBENZ	01-AUG-92	N	U	10	ug/L
12DICLBENZ	01-NOV-92	N	U	10	ug/L
13DICLBENZ	18-MAY-92	N	U	10	ug/L
13DICLBENZ	01-AUG-92	N	U	10	ug/L
13DICLBENZ	01-NOV-92	N	U	10	ug/L
14DICLBENZ	18-MAY-92	N	U	10	ug/L
14DICLBENZ	01-AUG-92	N	U	10	ug/L
14DICLBENZ	01-NOV-92	N	U	10	ug/L
245TRCLPHN	18-MAY-92	N	U	25	ug/L
245TRCLPHN	01-AUG-92	N	U	25	ug/L
245TRCLPHN	01-NOV-92	N	U	25	ug/L
246TRCLPHN	18-MAY-92	N	U	10	ug/L
246TRCLPHN	01-AUG-92	N	U	10	ug/L
246TRCLPHN	01-NOV-92	N	U	10	ug/L
24DICLPHEN	18-MAY-92	N	U	10	ug/L
24DICLPHEN	01-AUG-92	N	U	10	ug/L
24DICLPHEN	01-NOV-92	N	U	10	ug/L
24DIMET	18-MAY-92	N	U	10	ug/L
24DIMET	01-AUG-92	N	U	10	ug/L
24DIMET	01-NOV-92	N	U	10	ug/L
24DINITOLU	18-MAY-92	N	U	10	ug/L
24DINITOLU	01-AUG-92	N	U	10	ug/L
24DINITOLU	01-NOV-92	N	U	10	ug/L
26DINITOLU	18-MAY-92	N	U	10	ug/L
26DINITOLU	01-NOV-92	N	U	10	ug/L
26DINITOLU	01-AUG-92	N	U	10	ug/L
2HEXANONE	01-AUG-92	N	U	10	ug/L
2HEXANONE	01-AUG-92	N	U	10	ug/L
2HEXANONE	01-NOV-92	N	U	10	ug/L
2HEXANONE	18-MAY-92	N	U	10	ug/L
2HEXANONE	18-MAY-92	N	U	10	ug/L

Table E-2. Ground-water Chemistry for Well 199-H5-1A

Constituent	Sample Date	Filtered	Qualifier	Value	Units
2MENAPH	18-MAY-92	N	U	10	ug/L
2MENAPH	01-NOV-92	N	U	10	ug/L
2MENAPH	01-AUG-92	N	U	10	ug/L
2METHPH	18-MAY-92	N	U	10	ug/L
2METHPH	01-AUG-92	N	U	10	ug/L
2METHPH	01-NOV-92	N	U	10	ug/L
2NITRAN	18-MAY-92	N	U	25	ug/L
2NITRAN	01-AUG-92	N	U	25	ug/L
2NITRAN	01-NOV-92	N	U	25	ug/L
2NITRPH	18-MAY-92	N	U	10	ug/L
2NITRPH	01-NOV-92	N	U	10	ug/L
2NITRPH	01-AUG-92	N	U	10	ug/L
3NITRAN	18-MAY-92	N	U	25	ug/L
3NITRAN	01-NOV-92	N	U	25	ug/L
3NITRAN	01-AUG-92	N	U	25	ug/L
46DINIT	18-MAY-92	N	U	25	ug/L
46DINIT	01-AUG-92	N	U	25	ug/L
46DINIT	01-NOV-92	N	U	25	ug/L
4CHLOET	18-MAY-92	N	U	10	ug/L
4CHLOET	01-NOV-92	N	U	10	ug/L
4CHLOET	01-AUG-92	N	U	10	ug/L
4METHPH	18-MAY-92	N	U	10	ug/L
4METHPH	01-AUG-92	N	U	10	ug/L
4METHPH	01-NOV-92	N	U	10	ug/L
9H-CARB	18-MAY-92	N	U	10	ug/L
9H-CARB	01-AUG-92	N	U	10	ug/L
9H-CARB	01-NOV-92	N	U	10	ug/L
A-BHC	18-MAY-92	N	UJ	0.05	ug/L
A-BHC	01-NOV-92	N	U	0.05	ug/L
A-BHC	01-AUG-92	N	UJ	0.05	ug/L
ACENAPH	18-MAY-92	N	U	10	ug/L

Table E-2. Ground-water Chemistry for Well 199-H5-1A

Constituent	Sample Date	Filtered	Qualifier	Value	Units
ACENAPH	01-AUG-92	N	U	10	ug/L
ACENAPH	01-NOV-92	N	U	10	ug/L
ACENATL	18-MAY-92	N	U	10	ug/L
ACENATL	01-AUG-92	N	U	10	ug/L
ACENATL	01-NOV-92	N	U	10	ug/L
ACETONE	01-AUG-92	N	JN	7	ug/L
ACETONE	01-AUG-92	N	U	10	ug/L
ACETONE	18-MAY-92	N	U	10	ug/L
ACETONE	01-NOV-92	N	U	10	ug/L
ACETONE	18-MAY-92	N	U	10	ug/L
ALDRIN	18-MAY-92	N	U	0.05	ug/L
ALDRIN	01-AUG-92	N	UJ	0.05	ug/L
ALDRIN	01-NOV-92	N	U	0.05	ug/L
ALKALINITY	01-AUG-92	N		176	mg/L
ALKALINITY	01-NOV-92	N		171	mg/L
ALPHA	18-MAY-92	N	R	4	pCi/L
ALPHA	17-AUG-93	N	R	5.9	pCi/L
ALPHA	31-JAN-94	N		3.4	pCi/L
ALPHA	26-JUL-94	N		3.65	pCi/L
ALPHA	01-AUG-92	N	R	3.5	pCi/L
ALPHA	18-FEB-93	N	J	3.1	pCi/L
ALPHA	01-NOV-92	N	R	3.3	pCi/L
ALPHCHL	18-MAY-92	N	U	0.05	ug/L
ALPHCHL	01-NOV-92	N	U	0.05	ug/L
ALPHCHL	01-AUG-92	N	U	0.05	ug/L
ALUMINUM	18-MAY-92	Y		22	ug/L
ALUMINUM	18-MAY-92	N		1140	ug/L
ALUMINUM	01-AUG-92	Y		36.8	ug/L
ALUMINUM	18-FEB-93	N		44.2	ug/L
ALUMINUM	01-NOV-92	N		34.2	ug/L
ALUMINUM	31-JAN-94	Y		15	ug/L

Table E-2. Ground-water Chemistry for Well 199-H5-1A

Constituent	Sample Date	Filtered	Qualifier	Value	Units
ALUMINUM	31-JAN-94	N		38.2	ug/L
ALUMINUM	18-FEB-93	Y		21.2	ug/L
ALUMINUM	01-NOV-92	Y		14.7	ug/L
ALUMINUM	17-AUG-93	Y		20.9	ug/L
ALUMINUM	26-JUL-94	Y		34.5	UG/L
ALUMINUM	26-JUL-94	N		205	UG/L
ALUMINUM	01-AUG-92	N		32.8	ug/L
AM-241	18-MAY-92	N	UJ	0	pCi/L
AM-241	01-NOV-92	N	U	0	pCi/L
AM-241	01-AUG-92	N	UJ	-0.01	pCi/L
AMM-ABS	01-AUG-92	N	J	0.1	mg/L
AMM-ABS	31-JAN-94	N	U	-0.05	mg/L
AMM-ABS	17-AUG-93	N	U	0.05	mg/L
ANTHRACENE	18-MAY-92	N	U	10	ug/L
ANTHRACENE	01-NOV-92	N	U	10	ug/L
ANTHRACENE	01-AUG-92	N	U	10	ug/L
ANTIMONY	18-MAY-92	Y		16	ug/L
ANTIMONY	18-MAY-92	N		16	ug/L
ANTIMONY	01-AUG-92	Y		16.3	ug/L
ANTIMONY	26-JUL-94	N		46.2	UG/L
ANTIMONY	17-AUG-93	Y		15.7	ug/L
ANTIMONY	18-FEB-93	Y		19	ug/L
ANTIMONY	31-JAN-94	Y		12.2	ug/L
ANTIMONY	31-JAN-94	N		15.1	ug/L
ANTIMONY	01-NOV-92	Y		14.8	ug/L
ANTIMONY	18-FEB-93	N		18.4	ug/L
ANTIMONY	01-NOV-92	N		16.9	ug/L
ANTIMONY	01-AUG-92	N		16.5	ug/L
ANTIMONY	26-JUL-94	Y		46.2	UG/L
AR1016	18-MAY-92	N	U	1	ug/L
AR1016	01-AUG-92	N	U	1	ug/L

Table E-2. Ground-water Chemistry for Well 199-H5-1A

Constituent	Sample Date	Filtered	Qualifier	Value	Units
AR1016	01-NOV-92	N	U	1	ug/L
AR1221	18-MAY-92	N	U	2	ug/L
AR1221	01-NOV-92	N	U	2	ug/L
AR1221	01-AUG-92	N	U	2	ug/L
AR1232	18-MAY-92	N	U	1	ug/L
AR1232	01-AUG-92	N	U	1	ug/L
AR1232	01-NOV-92	N	U	1	ug/L
AR1242	18-MAY-92	N	U	1	ug/L
AR1242	01-NOV-92	N	U	1	ug/L
AR1242	01-AUG-92	N	U	1	ug/L
AR1248	18-MAY-92	N	U	1	ug/L
AR1248	01-NOV-92	N	U	1	ug/L
AR1248	01-AUG-92	N	U	1	ug/L
AR1254	18-MAY-92	N	U	1	ug/L
AR1254	01-NOV-92	N	U	1	ug/L
AR1254	01-AUG-92	N	U	1	ug/L
AR1260	18-MAY-92	N	U	1	ug/L
AR1260	01-AUG-92	N	U	1	ug/L
AR1260	01-NOV-92	N	U	1	ug/L
ARSENIC	18-MAY-92	Y		5	ug/L
ARSENIC	18-MAY-92	N		4.3	ug/L
ARSENIC	18-FEB-93	N		2	ug/L
ARSENIC	01-NOV-92	Y		2.5	ug/L
ARSENIC	31-JAN-94	N		3	ug/L
ARSENIC	31-JAN-94	Y		3	ug/L
ARSENIC	18-FEB-93	Y		3.9	ug/L
ARSENIC	17-AUG-93	Y		9.8	ug/L
ARSENIC	01-NOV-92	N	W	2.9	ug/L
ARSENIC	01-AUG-92	Y		2.6	ug/L
ARSENIC	01-AUG-92	N		2.6	ug/L
B-BHC	18-MAY-92	N	U	0.05	ug/L

Table E-2. Ground-water Chemistry for Well 199-H5-1A

Constituent	Sample Date	Filtered	Qualifier	Value	Units
B-BHC	01-NOV-92	N	U	0.05	ug/L
B-BHC	01-AUG-92	N	U	0.05	ug/L
BARIUM	18-MAY-92	Y		77.5	ug/L
BARIUM	18-MAY-92	N		87.8	ug/L
BARIUM	01-AUG-92	N		62.3	ug/L
BARIUM	01-AUG-92	Y		59	ug/L
BARIUM	18-FEB-93	N		57.5	ug/L
BARIUM	26-JUL-94	Y		57.5	UG/L
BARIUM	26-JUL-94	N		57.5	UG/L
BARIUM	31-JAN-94	Y		49.6	ug/L
BARIUM	31-JAN-94	N		51.2	ug/L
BARIUM	18-FEB-93	Y		56.4	ug/L
BARIUM	01-NOV-92	Y		58.7	ug/L
BARIUM	17-AUG-93	Y		49.8	ug/L
BARIUM	01-NOV-92	N		56.5	ug/L
BDCM	01-AUG-92	N	U	10	ug/L
BDCM	18-MAY-92	N	U	10	ug/L
BDCM	18-MAY-92	N	U	10	ug/L
BDCM	01-NOV-92	N	U	10	ug/L
BDCM	01-AUG-92	N	U	10	ug/L
BENZAAN	18-MAY-92	N	U	10	ug/L
BENZAAN	01-AUG-92	N	U	10	ug/L
BENZAAN	01-NOV-92	N	U	10	ug/L
BENZBFL	18-MAY-92	N	U	10	ug/L
BENZBFL	01-NOV-92	N	U	10	ug/L
BENZBFL	01-AUG-92	N	U	10	ug/L
BENZENE	01-AUG-92	N	U	10	ug/L
BENZENE	01-AUG-92	N	U	10	ug/L
BENZENE	18-MAY-92	N	U	10	ug/L
BENZENE	01-NOV-92	N	U	10	ug/L
BENZENE	18-MAY-92	N	U	10	ug/L

Table E-2. Ground-water Chemistry for Well 199-H5-1A

Constituent	Sample Date	Filtered	Qualifier	Value	Units
BENZOPE	18-MAY-92	N	U	10	ug/L
BENZOPE	01-AUG-92	N	U	10	ug/L
BENZOPE	01-NOV-92	N	U	10	ug/L
BENZOPY	18-MAY-92	N	U	10	ug/L
BENZOPY	01-NOV-92	N	U	10	ug/L
BENZOPY	01-AUG-92	N	U	10	ug/L
BERYLLIUM	18-MAY-92	Y		1	ug/L
BERYLLIUM	01-NOV-92	N		0.4	ug/L
BERYLLIUM	26-JUL-94	N		0.31	UG/L
BERYLLIUM	17-AUG-93	Y		1.2	ug/L
BERYLLIUM	18-FEB-93	Y		0.9	ug/L
BERYLLIUM	01-NOV-92	Y		0.3	ug/L
BERYLLIUM	31-JAN-94	Y		0.3	ug/L
BERYLLIUM	31-JAN-94	N		0.3	ug/L
BERYLLIUM	26-JUL-94	Y		0.3	UG/L
BERYLLIUM	18-FEB-93	N		0.5	ug/L
BERYLLIUM	01-AUG-92	Y		0.81	ug/L
BERYLLIUM	18-MAY-92	N		1	ug/L
BERYLLIUM	01-AUG-92	N		0.4	ug/L
BETA	18-MAY-92	N	J	7.3	pCi/L
BETA	01-NOV-92	N		8.4	pCi/L
BETA	18-FEB-93	N	J	7.9	pCi/L
BETA	26-JUL-94	N		8.23	pCi/L
BETA	31-JAN-94	N		5	pCi/L
BETA	17-AUG-93	N	R	4.2	pCi/L
BETA	01-AUG-92	N		6.9	pCi/L
BIS2CHE	18-MAY-92	N	U	10	ug/L
BIS2CHE	01-NOV-92	N	U	10	ug/L
BIS2CHE	01-AUG-92	N	U	10	ug/L
BIS2CHM	18-MAY-92	N	U	10	ug/L
BIS2CHM	01-AUG-92	N	U	10	ug/L

Table E-2. Ground-water Chemistry for Well 199-H5-1A

Constituent	Sample Date	Filtered	Qualifier	Value	Units
BIS2CHM	01-NOV-92	N	U	10	ug/L
BIS2EPH	18-MAY-92	N	U	10	ug/L
BIS2EPH	01-NOV-92	N	U	10	ug/L
BIS2EPH	01-AUG-92	N	U	10	ug/L
BIS2ETH	18-MAY-92	N	U	10	ug/L
BIS2ETH	01-AUG-92	N	U	10	ug/L
BIS2ETH	01-NOV-92	N	U	10	ug/L
BNZKFLU	18-MAY-92	N	U	10	ug/L
BNZKFLU	01-AUG-92	N	U	10	ug/L
BNZKFLU	01-NOV-92	N	U	10	ug/L
BROMOFORM	01-AUG-92	N	U	10	ug/L
BROMOFORM	18-MAY-92	N	U	10	ug/L
BROMOFORM	01-NOV-92	N	U	10	ug/L
BROMOFORM	18-MAY-92	N	U	10	ug/L
BROMOFORM	01-AUG-92	N	U	10	ug/L
BROPHEN	18-MAY-92	N	U	10	ug/L
BROPHEN	01-AUG-92	N	U	10	ug/L
BROPHEN	01-NOV-92	N	U	10	ug/L
BUTBENP	18-MAY-92	N	U	10	ug/L
BUTBENP	01-AUG-92	N	U	10	ug/L
BUTBENP	01-NOV-92	N	U	10	ug/L
C-14	18-MAY-92	N	J	66	pCi/L
C-14	01-AUG-92	N	UX	14	pCi/L
C-14	01-NOV-92	N	UJ	23	pCi/L
CADMIUM	18-MAY-92	Y		2	ug/L
CADMIUM	18-MAY-92	N		3.4	ug/L
CADMIUM	01-AUG-92	N		1.4	ug/L
CADMIUM	01-NOV-92	N		2.2	ug/L
CADMIUM	26-JUL-94	N		3.7	UG/L
CADMIUM	17-AUG-93	Y		1.5	ug/L
CADMIUM	18-FEB-93	Y		1.4	ug/L

Table E-2. Ground-water Chemistry for Well 199-H5-1A

Constituent	Sample Date	Filtered	Qualifier	Value	Units
CADMIUM	01-NOV-92	Y		1.5	ug/L
CADMIUM	31-JAN-94	Y		1.7	ug/L
CADMIUM	31-JAN-94	N		1.7	ug/L
CADMIUM	26-JUL-94	Y		3.7	UG/L
CADMIUM	18-FEB-93	N		1.6	ug/L
CADMIUM	01-AUG-92	Y		1.5	ug/L
CALCIUM	18-MAY-92	Y		60200	ug/L
CALCIUM	01-NOV-92	N		61600	ug/L
CALCIUM	26-JUL-94	N		67300	UG/L
CALCIUM	18-FEB-93	N		62800	ug/L
CALCIUM	31-JAN-94	Y		60300	ug/L
CALCIUM	31-JAN-94	N		61900	ug/L
CALCIUM	18-FEB-93	Y		61200	ug/L
CALCIUM	01-NOV-92	Y		59300	ug/L
CALCIUM	17-AUG-93	Y		59400	ug/L
CALCIUM	26-JUL-94	Y		70100	UG/L
CALCIUM	01-AUG-92	Y		59500	ug/L
CALCIUM	18-MAY-92	N		59800	ug/L
CALCIUM	01-AUG-92	N		60800	ug/L
CARBIDE	01-AUG-92	N	U	10	ug/L
CARBIDE	01-AUG-92	N	U	10	ug/L
CARBIDE	18-MAY-92	N	U	10	ug/L
CARBIDE	01-NOV-92	N	U	10	ug/L
CARBIDE	18-MAY-92	N	U	10	ug/L
CARBTET	01-AUG-92	N	U	10	ug/L
CARBTET	18-MAY-92	N	U	10	ug/L
CARBTET	01-NOV-92	N	U	10	ug/L
CARBTET	18-MAY-92	N	U	10	ug/L
CARBTET	01-AUG-92	N	U	10	ug/L
CDBM	01-AUG-92	N	U	10	ug/L
CDBM	01-AUG-92	N	U	10	ug/L

Table E-2. Ground-water Chemistry for Well 199-H5-1A

Constituent	Sample Date	Filtered	Qualifier	Value	Units
CDBM	18-MAY-92	N	U	10	ug/L
CDBM	01-NOV-92	N	U	10	ug/L
CDBM	18-MAY-92	N	U	10	ug/L
CHLANIL	18-MAY-92	N	U	10	ug/L
CHLANIL	01-NOV-92	N	U	10	ug/L
CHLANIL	01-AUG-92	N	U	10	ug/L
CHLCRES	18-MAY-92	N	U	10	ug/L
CHLCRES	01-NOV-92	N	U	10	ug/L
CHLCRES	01-AUG-92	N	U	10	ug/L
CHLNAPH	18-MAY-92	N	U	10	ug/L
CHLNAPH	01-AUG-92	N	U	10	ug/L
CHLNAPH	01-NOV-92	N	U	10	ug/L
CHLORIDE	18-MAY-92	N		17.2	mg/L
CHLORIDE	01-NOV-92	N		12.9	mg/L
CHLORIDE	31-JAN-94	N		11.5	mg/L
CHLORIDE	17-AUG-93	N		11.9	mg/L
CHLORIDE	01-AUG-92	N		13.1	mg/L
CHLOROBENZ	01-AUG-92	N	U	10	ug/L
CHLOROBENZ	01-AUG-92	N	U	10	ug/L
CHLOROBENZ	18-MAY-92	N	U	10	ug/L
CHLOROBENZ	01-NOV-92	N	U	10	ug/L
CHLOROBENZ	18-MAY-92	N	U	10	ug/L
CHLOROFORM	01-AUG-92	N	U	10	ug/L
CHLOROFORM	01-AUG-92	N	J	2	ug/L
CHLOROFORM	18-MAY-92	N	U	10	ug/L
CHLOROFORM	01-NOV-92	N	J	1	ug/L
CHLOROFORM	18-MAY-92	N	U	10	ug/L
CHLPHEN	18-MAY-92	N	U	10	ug/L
CHLPHEN	01-AUG-92	N	U	10	ug/L
CHLPHEN	01-NOV-92	N	U	10	ug/L
CHROMIUM	18-MAY-92	Y		44.8	ug/L

Table E-2. Ground-water Chemistry for Well 199-H5-1A

Constituent	Sample Date	Filtered	Qualifier	Value	Units
CHROMIUM	18-MAY-92	N		127	ug/L
CHROMIUM	01-NOV-92	N		84.4	ug/L
CHROMIUM	01-AUG-92	Y		66.3	ug/L
CHROMIUM	01-AUG-92	N		74.9	ug/L
CHROMIUM	18-FEB-93	N		99.9	ug/L
CHROMIUM	26-JUL-94	Y		91.5	UG/L
CHROMIUM	01-NOV-92	Y		72.2	ug/L
CHROMIUM	17-AUG-93	Y		5.1	ug/L
CHROMIUM	31-JAN-94	Y		76	ug/L
CHROMIUM	31-JAN-94	N		94	ug/L
CHROMIUM	18-FEB-93	Y		71	ug/L
CHROMIUM	26-JUL-94	N		177	UG/L
CHRYSENE	18-MAY-92	N	U	10	ug/L
CHRYSENE	01-NOV-92	N	U	10	ug/L
CHRYSENE	01-AUG-92	N	U	10	ug/L
CIS13DI	01-AUG-92	N	U	10	ug/L
CIS13DI	01-AUG-92	N	U	10	ug/L
CIS13DI	18-MAY-92	N	U	10	ug/L
CIS13DI	18-MAY-92	N	U	10	ug/L
CIS13DI	01-NOV-92	N	U	10	ug/L
CLETHAN	01-AUG-92	N	U	10	ug/L
CLETHAN	18-MAY-92	N	U	10	ug/L
CLETHAN	01-AUG-92	N	U	10	ug/L
CLETHAN	18-MAY-92	N	U	10	ug/L
CLETHAN	01-NOV-92	N	U	10	ug/L
CO-60	18-MAY-92	N	UJ	16	pCi/L
CO-60	01-AUG-92	N	U	13	pCi/L
CO-60	01-NOV-92	N	U	20	pCi/L
COBALT	18-MAY-92	Y		3	ug/L
COBALT	26-JUL-94	Y		3.4	UG/L
COBALT	01-NOV-92	Y		1.3	ug/L

Table E-2. Ground-water Chemistry for Well 199-H5-1A

Constituent	Sample Date	Filtered	Qualifier	Value	Units
COBALT	17-AUG-93	Y		2.5	ug/L
COBALT	31-JAN-94	Y		2.9	ug/L
COBALT	31-JAN-94	N		3.2	ug/L
COBALT	18-FEB-93	Y		3.2	ug/L
COBALT	26-JUL-94	N		3.4	UG/L
COBALT	01-AUG-92	N		2.3	ug/L
COBALT	01-AUG-92	Y		3.5	ug/L
COBALT	18-FEB-93	N		2.5	ug/L
COBALT	01-NOV-92	N		2.7	ug/L
COBALT	18-MAY-92	N		4.3	ug/L
COD	01-AUG-92	N	UJ	30	mg/L
CONDUCT	26-JUL-94	Y		527	umhos/cm
CONDUCT	18-MAY-92	N		452	umhos/cm
CONDUCT	01-AUG-92	N		451	umhos/cm
CONDUCT	01-NOV-92	N		494	umhos/cm
CONDUCT	26-JUL-94	N		527	umhos/cm
CONDUCT	06-APR-94	N		567	umhos/cm
CONDUCT	18-FEB-93	N		509	umhos/cm
COPPER	18-MAY-92	Y		2	ug/L
COPPER	01-AUG-92	Y		3.8	ug/L
COPPER	18-FEB-93	N		5.4	ug/L
COPPER	26-JUL-94	Y		7.6	UG/L
COPPER	01-NOV-92	Y		1.9	ug/L
COPPER	31-JAN-94	N		2.1	ug/L
COPPER	31-JAN-94	Y		1.6	ug/L
COPPER	18-FEB-93	Y		4.9	ug/L
COPPER	17-AUG-93	Y		4	ug/L
COPPER	26-JUL-94	N		13.7	UG/L
COPPER	01-NOV-92	N		3.5	ug/L
COPPER	18-MAY-92	N		10.6	ug/L
COPPER	01-AUG-92	N		2.4	ug/L

Table E-2. Ground-water Chemistry for Well 199-H5-1A

Constituent	Sample Date	Filtered.	Qualifier	Value	Units
CR-51	18-MAY-92	N	UJ	380	pCi/L
CR-51	01-NOV-92	N	U	700	pCi/L
CR-51	01-AUG-92	N	U	340	pCi/L
CS-134	18-MAY-92	N	UJ	15	pCi/L
CS-134	01-AUG-92	N	U	11	pCi/L
CS-134	01-NOV-92	N	U	10	pCi/L
CS-137	18-MAY-92	N	UJ	15	pCi/L
CS-137	01-AUG-92	N	U	13	pCi/L
CS-137	01-NOV-92	N	U	20	pCi/L
CYANIDE	18-MAY-92	N		10	ug/L
CYANIDE	01-NOV-92	N		10	ug/L
CYANIDE	01-AUG-92	N		10	ug/L
CYANIDE	31-JAN-94	Y			ug/L
D-BHC	18-MAY-92	N	UJ	0.05	ug/L
D-BHC	01-AUG-92	N	UJ	0.05	ug/L
D-BHC	01-NOV-92	N	U	0.05	ug/L
DDD	18-MAY-92	N	UJ	0.1	ug/L
DDD	01-AUG-92	N	U	0.1	ug/L
DDD	01-NOV-92	N	U	0.1	ug/L
DDE	18-MAY-92	N	UJ	0.1	ug/L
DDE	01-NOV-92	N	U	0.1	ug/L
DDE	01-AUG-92	N	U	0.1	ug/L
DDT	18-MAY-92	N	U	0.1	ug/L
DDT	01-AUG-92	N	U	0.1	ug/L
DDT	01-NOV-92	N	U	0.1	ug/L
DIBAHAN	18-MAY-92	N	U	10	ug/L
DIBAHAN	01-AUG-92	N	U	10	ug/L
DIBAHAN	01-NOV-92	N	U	10	ug/L
DIBENFR	18-MAY-92	N	U	10	ug/L
DIBENFR	01-AUG-92	N	U	10	ug/L
DIBENFR	01-NOV-92	N	U	10	ug/L

Table E-2. Ground-water Chemistry for Well 199-H5-1A

Constituent	Sample Date	Filtered	Qualifier	Value	Units
DIBPHTH	18-MAY-92	N	U	10	ug/L
DIBPHTH	01-NOV-92	N	U	10	ug/L
DIBPHTH	01-AUG-92	N	U	10	ug/L
DICETHY	01-AUG-92	N	U	10	ug/L
DICETHY	01-AUG-92	N	U	10	ug/L
DICETHY	18-MAY-92	N	U	10	ug/L
DICETHY	01-NOV-92	N	U	10	ug/L
DICETHY	18-MAY-92	N	U	10	ug/L
DICHBEN	18-MAY-92	N	U	10	ug/L
DICHBEN	01-NOV-92	N	U	10	ug/L
DICHBEN	01-AUG-92	N	U	10	ug/L
DICPANE	01-AUG-92	N	U	10	ug/L
DICPANE	01-NOV-92	N	U	10	ug/L
DICPANE	01-AUG-92	N	U	10	ug/L
DICPANE	18-MAY-92	N	U	10	ug/L
DICPANE	18-MAY-92	N	U	10	ug/L
DIELDRIN	18-MAY-92	N	U	0.1	ug/L
DIELDRIN	01-AUG-92	N	U	0.1	ug/L
DIELDRIN	01-NOV-92	N	U	0.1	ug/L
DIEPHTH	18-MAY-92	N	U	10	ug/L
DIEPHTH	01-NOV-92	N	U	10	ug/L
DIEPHTH	01-AUG-92	N	U	10	ug/L
DIMPHTH	18-MAY-92	N	U	10	ug/L
DIMPHTH	01-NOV-92	N	U	10	ug/L
DIMPHTH	01-AUG-92	N	U	10	ug/L
DINPHEN	18-MAY-92	N	U	25	ug/L
DINPHEN	01-AUG-92	N	U	25	ug/L
DINPHEN	01-NOV-92	N	U	25	ug/L
DIOPHTH	18-MAY-92	N	U	10	ug/L
DIOPHTH	01-AUG-92	N	U	10	ug/L
DIOPHTH	01-NOV-92	N	U	10	ug/L

Table E-2. Ground-water Chemistry for Well 199-H5-1A

Constituent	Sample Date	Filtered	Qualifier	Value	Units
DIPRNT	18-MAY-92	N	U	10	ug/L
DIPRNT	01-AUG-92	N	U	10	ug/L
DIPRNT	01-NOV-92	N	U	10	ug/L
ENDHYDE	18-MAY-92	N	U	0.1	ug/L
ENDHYDE	01-AUG-92	N	U	0.1	ug/L
ENDHYDE	01-NOV-92	N	U	0.1	ug/L
ENDO1	18-MAY-92	N	U	0.05	ug/L
ENDO1	01-NOV-92	N	U	0.05	ug/L
ENDO1	01-AUG-92	N	U	0.05	ug/L
ENDOS2	18-MAY-92	N	U	0.1	ug/L
ENDOS2	01-AUG-92	N	U	0.1	ug/L
ENDOS2	01-NOV-92	N	U	0.1	ug/L
ENDRIN	18-MAY-92	N	U	0.1	ug/L
ENDRIN	01-AUG-92	N	U	0.1	ug/L
ENDRIN	01-NOV-92	N	U	0.1	ug/L
ENDRKETONE	18-MAY-92	N	U	0.1	ug/L
ENDRKETONE	01-AUG-92	N	U	0.1	ug/L
ENDRKETONE	01-NOV-92	N	U	0.1	ug/L
ENDSFAN	18-MAY-92	N	U	0.1	ug/L
ENDSFAN	01-NOV-92	N	U	0.1	ug/L
ENDSFAN	01-AUG-92	N	U	0.1	ug/L
ETHBENZENE	01-AUG-92	N	U	10	ug/L
ETHBENZENE	01-AUG-92	N	U	10	ug/L
ETHBENZENE	18-MAY-92	N	U	10	ug/L
ETHBENZENE	01-NOV-92	N	U	10	ug/L
ETHBENZENE	18-MAY-92	N	U	10	ug/L
EU-152	01-AUG-92	N	U	23	pCi/L
EU-152	01-NOV-92	N	U	30	pCi/L
EU-154	01-AUG-92	N	U	15	pCi/L
EU-154	01-NOV-92	N	U	20	pCi/L
FE-59	01-AUG-92	N	U	71	pCi/L

Table E-2. Ground-water Chemistry for Well 199-H5-1A

Constituent	Sample Date	Filtered	Qualifier	Value	Units
FE-59	01-NOV-92	N	U	90	pCi/L
FLDCOND	18-MAY-92	N		514	umhos/cm
FLDCOND	01-NOV-92	N		460	umhos/cm
FLDCOND	01-NOV-92	N		460	umhos/cm
FLDCOND	18-MAY-92	Y		514	umhos/cm
FLDCOND	01-NOV-92	Y		460	umhos/cm
FLDCOND	01-AUG-92	Y		561	umhos/cm
FLDCOND	18-FEB-93	Y		530	umhos/cm
FLDCOND	18-FEB-93	N		530	umhos/cm
FLDCOND	01-NOV-92	N		460	umhos/cm
FLDCOND	01-AUG-92	N		561	umhos/cm
FLDCOND	01-AUG-92	N		561	umhos/cm
FLDCOND	01-AUG-92	N		561	umhos/cm
FLDCOND	01-AUG-92	N		561	umhos/cm
FLDTEMP	18-MAY-92	N		18.5	Deg C
FLDTEMP	01-NOV-92	N		17.3	Deg C
FLDTEMP	01-NOV-92	N		17.3	Deg C
FLDTEMP	18-MAY-92	Y		18.5	Deg C
FLDTEMP	01-NOV-92	Y		17.3	Deg C
FLDTEMP	01-AUG-92	Y		18.1	Deg C
FLDTEMP	18-FEB-93	Y		17.3	Deg C
FLDTEMP	18-FEB-93	N		17.3	Deg C
FLDTEMP	01-AUG-92	N		18.1	Deg C
FLDTEMP	01-AUG-92	N		18.1	Deg C
FLDTEMP	01-AUG-92	N		18.1	Deg C
FLDTEMP	01-NOV-92	N		17.3	Deg C
FLDTEMP	01-AUG-92	N		18.1	Deg C
FLUORAN	18-MAY-92	N	U	10	ug/L
FLUORAN	01-NOV-92	N	U	10	ug/L
FLUORAN	01-AUG-92	N	U	10	ug/L
FLUORENE	18-MAY-92	N	U	10	ug/L

Table E-2. Ground-water Chemistry for Well 199-H5-1A

Constituent	Sample Date	Filtered	Qualifier	Value	Units
FLUORENE	01-NOV-92	N	U	10	ug/L
FLUORENE	01-AUG-92	N	U	10	ug/L
FLUORIDE	18-MAY-92	N		0.5	mg/L
FLUORIDE	01-NOV-92	N		0.4	mg/L
FLUORIDE	31-JAN-94	N		0.2	mg/L
FLUORIDE	17-AUG-93	N		0.3	mg/L
FLUORIDE	01-AUG-92	N		0.3	mg/L
GAM-BHC	18-MAY-92	N	UJ	0.05	ug/L
GAM-BHC	01-AUG-92	N	UJ	0.05	ug/L
GAM-BHC	01-NOV-92	N	U	0.05	ug/L
GAMMCHL	18-MAY-92	N	U	0.05	ug/L
GAMMCHL	01-NOV-92	N	U	0.05	ug/L
GAMMCHL	01-AUG-92	N	U	0.05	ug/L
HEPTACHLOR	18-MAY-92	N	U	0.05	ug/L
HEPTACHLOR	01-NOV-92	N	U	0.05	ug/L
HEPTACHLOR	01-AUG-92	N	U	0.05	ug/L
HEPTIDE	18-MAY-92	N	U	0.05	ug/L
HEPTIDE	01-AUG-92	N	U	0.05	ug/L
HEPTIDE	01-NOV-92	N	U	0.05	ug/L
HEXCBEN	18-MAY-92	N	U	10	ug/L
HEXCBEN	01-NOV-92	N	U	10	ug/L
HEXCBEN	01-AUG-92	N	U	10	ug/L
HEXCBUT	18-MAY-92	N	U	10	ug/L
HEXCBUT	01-NOV-92	N	U	10	ug/L
HEXCBUT	01-AUG-92	N	U	10	ug/L
HEXCCYC	18-MAY-92	N	U	10	ug/L
HEXCCYC	01-NOV-92	N	U	10	ug/L
HEXCCYC	01-AUG-92	N	U	10	ug/L
HEXCETH	18-MAY-92	N	U	10	ug/L
HEXCETH	01-AUG-92	N	U	10	ug/L
HEXCETH	01-NOV-92	N	U	10	ug/L

Table E-2. Ground-water Chemistry for Well 199-H5-1A

Constituent	Sample Date	Filtered	Qualifier	Value	Units
HEXONE	01-AUG-92	N	U	10	ug/L
HEXONE	18-MAY-92	N	U	10	ug/L
HEXONE	01-NOV-92	N	U	10	ug/L
HEXONE	18-MAY-92	N	U	10	ug/L
HEXONE	01-AUG-92	N	U	10	ug/L
HYDRAZINE	01-NOV-92	N	U	3	ug/L
HYDRAZINE	01-AUG-92	Y	R	3	ug/L
I-129	06-APR-94	N		-0.26	pCi/L
INDENOP	18-MAY-92	N	U	10	ug/L
INDENOP	01-AUG-92	N	U	10	ug/L
INDENOP	01-NOV-92	N	U	10	ug/L
IRON	18-MAY-92	Y		35.7	ug/L
IRON	18-FEB-93	Y		6	ug/L
IRON	01-NOV-92	Y		11.4	ug/L
IRON	17-AUG-93	Y		15.5	ug/L
IRON	26-JUL-94	Y		70.2	UG/L
IRON	26-JUL-94	N		612	UG/L
IRON	18-FEB-93	N		173	ug/L
IRON	01-NOV-92	N		91.2	ug/L
IRON	01-AUG-92	Y		20.3	ug/L
IRON	31-JAN-94	Y		13.4	ug/L
IRON	31-JAN-94	N		74.4	ug/L
IRON	18-MAY-92	N		2070	ug/L
IRON	01-AUG-92	N		33.2	ug/L
ISOPHORONE	18-MAY-92	N	U	10	ug/L
ISOPHORONE	01-NOV-92	N	U	10	ug/L
ISOPHORONE	01-AUG-92	N	U	10	ug/L
K-40	18-MAY-92	N	UJ	250	pCi/L
K-40	01-NOV-92	N	U	300	pCi/L
K-40	01-AUG-92	N	U	160	pCi/L
LEAD	18-MAY-92	Y		1	ug/L

Table E-2. Ground-water Chemistry for Well 199-H5-1A

Constituent	Sample Date	Filtered	Qualifier	Value	Units
LEAD	31-JAN-94	Y		1.8	ug/L
LEAD	31-JAN-94	N		1.8	ug/L
LEAD	18-FEB-93	Y	W	1.2	ug/L
LEAD	01-NOV-92	Y		2	ug/L
LEAD	17-AUG-93	Y		3.4	ug/L
LEAD	18-MAY-92	N		5.1	ug/L
LEAD	01-AUG-92	N		6.9	ug/L
LEAD	01-AUG-92	Y		2.3	ug/L
LEAD	18-FEB-93	N		1.8	ug/L
LEAD	01-NOV-92	N	*	2.9	ug/L
LPHENOL	18-MAY-92	N	U	10	ug/L
LPHENOL	01-AUG-92	N	U	10	ug/L
LPHENOL	01-NOV-92	N	U	10	ug/L
M-XYLE	01-AUG-92	N	U	10	ug/L
M-XYLE	01-NOV-92	N	U	10	ug/L
M-XYLE	01-AUG-92	N	U	10	ug/L
M-XYLE	18-MAY-92	N	U	10	ug/L
M-XYLE	18-MAY-92	N	U	10	ug/L
MAGNESIUM	18-MAY-92	Y		15800	ug/L
MAGNESIUM	01-NOV-92	N	E	16600	ug/L
MAGNESIUM	26-JUL-94	N		17600	UG/L
MAGNESIUM	18-FEB-93	N		16700	ug/L
MAGNESIUM	31-JAN-94	Y		15600	ug/L
MAGNESIUM	31-JAN-94	N		15700	ug/L
MAGNESIUM	18-FEB-93	Y		16200	ug/L
MAGNESIUM	01-NOV-92	Y		15900	ug/L
MAGNESIUM	17-AUG-93	Y		18900	ug/L
MAGNESIUM	26-JUL-94	Y		18100	UG/L
MAGNESIUM	01-AUG-92	Y		16000	ug/L
MAGNESIUM	18-MAY-92	N		15900	ug/L
MAGNESIUM	01-AUG-92	N		16300	ug/L

Table E-2. Ground-water Chemistry for Well 199-H5-1A

Constituent	Sample Date	Filtered	Qualifier	Value	Units
MANGANESE	18-MAY-92	Y		175	ug/L
MANGANESE	18-MAY-92	N		206	ug/L
MANGANESE	01-AUG-92	N		56.2	ug/L
MANGANESE	01-NOV-92	N		18	ug/L
MANGANESE	26-JUL-94	N		17.3	UG/L
MANGANESE	17-AUG-93	Y		1.6	ug/L
MANGANESE	18-FEB-93	Y		9.1	ug/L
MANGANESE	01-NOV-92	Y		20	ug/L
MANGANESE	31-JAN-94	Y		1.8	ug/L
MANGANESE	31-JAN-94	N		4.2	ug/L
MANGANESE	26-JUL-94	Y		3.5	UG/L
MANGANESE	18-FEB-93	N		18.3	ug/L
MANGANESE	01-AUG-92	Y		53	ug/L
MERCURY	18-MAY-92	Y		0.2	ug/L
MERCURY	01-NOV-92	N		0.1	ug/L
MERCURY	17-AUG-93	Y		0.2	ug/L
MERCURY	18-FEB-93	N		0.1	ug/L
MERCURY	16-JUN-94	N	U		ug/L
MERCURY	31-JAN-94	Y		0.2	ug/L
MERCURY	31-JAN-94	N		0.2	ug/L
MERCURY	18-FEB-93	Y		0.1	ug/L
MERCURY	01-NOV-92	Y		0.1	ug/L
MERCURY	01-AUG-92	Y		0.2	ug/L
MERCURY	18-MAY-92	N		0.2	ug/L
MERCURY	01-AUG-92	N		0.2	ug/L
METHBRO	01-AUG-92	N	U	10	ug/L
METHBRO	18-MAY-92	N	U	10	ug/L
METHBRO	01-NOV-92	N	U	10	ug/L
METHBRO	18-MAY-92	N	U	10	ug/L
METHBRO	01-AUG-92	N	U	10	ug/L
METHCHL	01-AUG-92	N	U	10	ug/L

Table E-2. Ground-water Chemistry for Well 199-H5-1A

Constituent	Sample Date	Filtered	Qualifier	Value	Units
METHCHL	18-MAY-92	N	U	10	ug/L
METHCHL	18-MAY-92	N	U	10	ug/L
METHCHL	01-AUG-92	N	U	10	ug/L
METHCHL	01-NOV-92	N	U	10	ug/L
METHLOR	18-MAY-92	N	U	0.5	ug/L
METHLOR	01-AUG-92	N	UJ	0.5	ug/L
METHLOR	01-NOV-92	N	U	0.5	ug/L
METHONE	01-AUG-92	N	U	10	ug/L
METHONE	18-MAY-92	N	U	10	ug/L
METHONE	01-AUG-92	N	U	10	ug/L
METHONE	18-MAY-92	N	U	10	ug/L
METHONE	01-NOV-92	N	U	10	ug/L
METHYCH	01-AUG-92	N	U	10	ug/L
METHYCH	18-MAY-92	N	U	10	ug/L
METHYCH	01-NOV-92	N	J	4	ug/L
METHYCH	18-MAY-92	N	BJ	3	ug/L
METHYCH	01-AUG-92	N	U	10	ug/L
NAPHTHA	18-MAY-92	N	U	10	ug/L
NAPHTHA	01-AUG-92	N	U	10	ug/L
NAPHTHA	01-NOV-92	N	U	10	ug/L
NICKEL	18-MAY-92	Y		9.3	ug/L
NICKEL	18-MAY-92	N		56.1	ug/L
NICKEL	01-AUG-92	Y		3.9	ug/L
NICKEL	18-FEB-93	N		14.3	ug/L
NICKEL	26-JUL-94	Y		15.5	UG/L
NICKEL	01-NOV-92	Y		2.6	ug/L
NICKEL	31-JAN-94	N		9.9	ug/L
NICKEL	18-FEB-93	Y		5.4	ug/L
NICKEL	31-JAN-94	Y		4.4	ug/L
NICKEL	17-AUG-93	Y		4.7	ug/L
NICKEL	26-JUL-94	N		40	UG/L

Table E-2. Ground-water Chemistry for Well 199-H5-1A

Constituent	Sample Date	Filtered	Qualifier	Value	Units
NICKEL	01-NOV-92	N		5.9	ug/L
NICKEL	01-AUG-92	N		6	ug/L
NITBENZ	18-MAY-92	N	U	10	ug/L
NITBENZ	01-AUG-92	N	U	10	ug/L
NITBENZ	01-NOV-92	N	U	10	ug/L
NITPHENOL	18-MAY-92	N	U	25	ug/L
NITPHENOL	01-AUG-92	N	U	25	ug/L
NITPHENOL	01-NOV-92	N	U	25	ug/L
NITRANILIN	18-MAY-92	N	U	25	ug/L
NITRANILIN	01-AUG-92	N	U	25	ug/L
NITRANILIN	01-NOV-92	N	U	25	ug/L
NITRATE	18-MAY-92	N		8.4	mg/L
NITRATE	31-JAN-94	N		6.4	mg/L
NITRITE	18-MAY-92	N	U	0.1	mg/L
NITRITE	31-JAN-94	N	U	-0.1	mg/L
NNDIPHA	18-MAY-92	N	U	10	ug/L
NNDIPHA	01-AUG-92	N	U	10	ug/L
NNDIPHA	01-NOV-92	N	U	10	ug/L
NO2+NO3	01-AUG-92	N	J	6.32	mgN/L
NO2+NO3	31-JAN-94	N		7.76	mg/L
NO2+NO3	17-AUG-93	N		5.68	mg/L
NO2+NO3	18-FEB-93	N		6.89	mg/L
NO2+NO3	01-NOV-92	N		4.82	mg/L
NO2-N	17-AUG-93	N	R	0.1	mg/L
NO3-N	17-AUG-93	N	R	6.4	mg/L
PENTCHP	18-MAY-92	N	U	25	ug/L
PENTCHP	01-AUG-92	N	U	25	ug/L
PENTCHP	01-NOV-92	N	U	25	ug/L
PERCENE	01-AUG-92	N	U	10	ug/L
PERCENE	18-MAY-92	N	U	10	ug/L
PERCENE	01-NOV-92	N	U	10	ug/L

Table E-2. Ground-water Chemistry for Well 199-H5-1A

Constituent	Sample Date	Filtered	Qualifier	Value	Units
PERCENE	18-MAY-92	N	U	10	ug/L
PERCENE	01-AUG-92	N	U	10	ug/L
PH	26-JUL-94	Y		7.58	pH
PH	01-AUG-92	N	R	7.8	pH
PH	18-MAY-92	N		8.2	pH
PH	01-NOV-92	N		7.7	pH
PH	26-JUL-94	N		7.58	pH
PH	06-APR-94	N		7.53	pH
PH	18-FEB-93	N		7.86	pH
PHENANT	18-MAY-92	N	U	10	ug/L
PHENANT	01-AUG-92	N	U	10	ug/L
PHENANT	01-NOV-92	N	U	10	ug/L
PHFIELD	18-MAY-92	N		7.61	pH
PHFIELD	01-AUG-92	N		7.69	pH
PHFIELD	01-AUG-92	N		7.69	pH
PHFIELD	01-AUG-92	N		7.69	pH
PHFIELD	01-NOV-92	N		7.6	pH
PHFIELD	01-NOV-92	N		7.6	pH
PHFIELD	18-FEB-93	Y		8.19	pH
PHFIELD	01-NOV-92	Y		7.6	pH
PHFIELD	01-AUG-92	Y		7.69	pH
PHFIELD	18-MAY-92	Y		7.61	pH
PHFIELD	18-FEB-93	N		8.19	pH
PHFIELD	01-NOV-92	N		7.6	pH
PHFIELD	01-AUG-92	N		7.69	pH
PHOSPHATE	18-MAY-92	N	U	0.4	mg/L
PHOSPHATE	01-AUG-92	N	R	0.4	mg/L
PHOSPHATE	31-JAN-94	N	U	-0.4	mg/L
PHOSPHATE	17-AUG-93	N	R	0.4	mg/L
PHOSPHATE	01-NOV-92	N	U	0.4	mg/L
POTASSIUM	18-MAY-92	Y		6550	ug/L

Table E-2. Ground-water Chemistry for Well 199-H5-1A

Constituent	Sample Date	Filtered	Qualifier	Value	Units
POTASSIUM	01-AUG-92	Y		6250	ug/L
POTASSIUM	01-NOV-92	N		6480	ug/L
POTASSIUM	01-AUG-92	N		6360	ug/L
POTASSIUM	18-MAY-92	N		6510	ug/L
POTASSIUM	18-FEB-93	N		6430	ug/L
POTASSIUM	26-JUL-94	Y		7060	UG/L
POTASSIUM	26-JUL-94	N		6910	UG/L
POTASSIUM	31-JAN-94	Y		5910	ug/L
POTASSIUM	31-JAN-94	N		6070	ug/L
POTASSIUM	18-FEB-93	Y		6250	ug/L
POTASSIUM	01-NOV-92	Y		6170	ug/L
POTASSIUM	17-AUG-93	Y		6960	ug/L
PU-238	18-MAY-92	N	UJ	0.01	pCi/L
PU-238	01-AUG-92	N	U	0.01	pCi/L
PU-238	01-NOV-92	N	U	-0.01	pCi/L
PU39-40	18-MAY-92	N	UJ	-0.01	pCi/L
PU39-40	01-NOV-92	N	U	0.01	pCi/L
PU39-40	01-AUG-92	N	U	0	pCi/L
PYRENE	18-MAY-92	N	U	10	ug/L
PYRENE	01-NOV-92	N	U	10	ug/L
PYRENE	01-AUG-92	N	U	10	ug/L
RA-226	18-MAY-92	N	UJ	26	pCi/L
RA-226	01-NOV-92	N	U	30	pCi/L
RA-226	01-AUG-92	N	U	35	pCi/L
RU-106	01-AUG-92	N	U	100	pCi/L
RU-106	01-NOV-92	N	U	100	pCi/L
SELENIUM	18-MAY-92	Y		4	ug/L
SELENIUM	01-AUG-92	N	WN	2.8	ug/L
SELENIUM	01-NOV-92	N	WN	19	ug/L
SELENIUM	17-AUG-93	Y		3.4	ug/L
SELENIUM	18-FEB-93	N	WN	3.8	ug/L

Table E-2. Ground-water Chemistry for Well 199-H5-1A

Constituent	Sample Date	Filtered	Qualifier	Value	Units
SELENIUM	31-JAN-94	Y		2.8	ug/L
SELENIUM	31-JAN-94	N		2.8	ug/L
SELENIUM	18-FEB-93	Y	WN	3.1	ug/L
SELENIUM	01-NOV-92	Y	WN	3.6	ug/L
SELENIUM	01-AUG-92	Y		3.7	ug/L
SELENIUM	18-MAY-92	N		4	ug/L
SILVER	18-MAY-92	Y		2	ug/L
SILVER	01-AUG-92	Y		4.8	ug/L
SILVER	18-FEB-93	N		3.9	ug/L
SILVER	26-JUL-94	Y		3.8	UG/L
SILVER	26-JUL-94	N		3.8	UG/L
SILVER	31-JAN-94	Y		2.1	ug/L
SILVER	31-JAN-94	N		2.1	ug/L
SILVER	18-FEB-93	Y		4.6	ug/L
SILVER	01-NOV-92	Y		3.6	ug/L
SILVER	17-AUG-93	Y	N	5	ug/L
SILVER	01-NOV-92	N		2.5	ug/L
SILVER	01-AUG-92	N		2.3	ug/L
SILVER	18-MAY-92	N		2	ug/L
SODIUM	18-MAY-92	Y		27600	ug/L
SODIUM	01-AUG-92	N		26200	ug/L
SODIUM	18-MAY-92	N		27000	ug/L
SODIUM	01-AUG-92	Y		25500	ug/L
SODIUM	18-FEB-93	N		26900	ug/L
SODIUM	26-JUL-94	Y		28600	UG/L
SODIUM	01-NOV-92	Y		26100	ug/L
SODIUM	31-JAN-94	N		26100	ug/L
SODIUM	18-FEB-93	Y		26800	ug/L
SODIUM	31-JAN-94	Y		25600	ug/L
SODIUM	17-AUG-93	Y		55900	ug/L
SODIUM	26-JUL-94	N		28000	UG/L

Table E-2. Ground-water Chemistry for Well 199-H5-1A

Constituent	Sample Date	Filtered	Qualifier	Value	Units
SODIUM	01-NOV-92	N		27300	ug/L
SR-90	18-MAY-92	N	UJ	0.5	pCi/L
SR-90	01-AUG-92	N	U	-0.16	pCi/L
SR-90	18-FEB-93	N	UJ	-0.01	pCi/L
SR-90	17-AUG-93	N	R	0.1	pCi/L
SR-90	31-JAN-94	N	U	0.09	pCi/L
SR-90	26-JUL-94	N		-0.04	pCi/L
SR-90	01-NOV-92	N	R	1.4	pCi/L
STYRENE	01-AUG-92	N	U	10	ug/L
STYRENE	01-AUG-92	N	U	10	ug/L
STYRENE	18-MAY-92	N	U	10	ug/L
STYRENE	18-MAY-92	N	U	10	ug/L
STYRENE	01-NOV-92	N	U	10	ug/L
SULFATE	18-MAY-92	N		88	mg/L
SULFATE	01-AUG-92	N		68	mg/L
SULFATE	31-JAN-94	N		64	mg/L
SULFATE	17-AUG-93	N		66	mg/L
SULFATE	01-NOV-92	N		68	mg/L
SULFIDE	01-AUG-92	N	R	1	mg/L
SULFIDE	17-AUG-93	N	U	1	mg/L
SULFIDE	31-JAN-94	N	U	-1	mg/L
SULFIDE	01-NOV-92	N	U	1	mg/L
TC-99	18-MAY-92	N	UJ	0.14	pCi/L
TC-99	01-AUG-92	N	U	3.4	pCi/L
TC-99	01-NOV-92	N	U	0.3	pCi/L
TDS	01-AUG-92	N		375	mg/L
TDS	01-NOV-92	N		356	mg/L
TEMPERATUR	26-JUL-94	Y		18.7	Deg C
TEMPERATUR	26-JUL-94	N		18.7	Deg C
TEMPERATUR	06-APR-94	N		17.2	Deg C
TH-228	18-MAY-92	N	UJ	24	pCi/L

Table E-2. Ground-water Chemistry for Well 199-H5-1A

Constituent	Sample Date	Filtered	Qualifier	Value	Units
TH-228	01-AUG-92	N	U	23	pCi/L
TH-228	01-NOV-92	N	U	20	pCi/L
TH-232	18-MAY-92	N	UJ	67	pCi/L
TH-232	01-NOV-92	N	U	60	pCi/L
TH-232	01-AUG-92	N	U	55	pCi/L
THALLIUM	18-MAY-92	Y		1	ug/L
THALLIUM	18-MAY-92	N		4	ug/L
THALLIUM	01-AUG-92	Y	WN	0.9	ug/L
THALLIUM	17-AUG-93	Y		1.1	ug/L
THALLIUM	18-FEB-93	Y	W	2.6	ug/L
THALLIUM	31-JAN-94	Y		3.7	ug/L
THALLIUM	31-JAN-94	N		3.7	ug/L
THALLIUM	18-FEB-93	N	WN	1.9	ug/L
THALLIUM	01-NOV-92	N	WN	1.3	ug/L
THALLIUM	01-AUG-92	N	WN	1.3	ug/L
THALLIUM	01-NOV-92	Y		3.8	ug/L
TOC	01-AUG-92	N		1.2	mg/L
TOC	01-NOV-92	N		2.8	mg/L
TOLUENE	18-MAY-92	N	BJ	28	ug/L
TOLUENE	01-AUG-92	N	U	10	ug/L
TOLUENE	18-MAY-92	N	U	10	ug/L
TOLUENE	18-MAY-92	N	U	10	ug/L
TOLUENE	01-AUG-92	N	U	10	ug/L
TOLUENE	01-NOV-92	N	U	10	ug/L
TOLUENE	18-MAY-92	N	BJ	28	ug/L
TOX	01-AUG-92	N	R	35.8	ug/L
TOX	01-NOV-92	N		45	ug/L
TOXAPHENE	18-MAY-92	N	U	5	ug/L
TOXAPHENE	01-NOV-92	N	U	5	ug/L
TOXAPHENE	01-AUG-92	N	U	5	ug/L
TRANS13	01-AUG-92	N	U	10	ug/L

Table E-2. Ground-water Chemistry for Well 199-H5-1A

Constituent	Sample Date	Filtered	Qualifier	Value	Units
TRANS13	01-AUG-92	N	U	10	ug/L
TRANS13	18-MAY-92	N	U	10	ug/L
TRANS13	01-NOV-92	N	U	10	ug/L
TRANS13	18-MAY-92	N	U	10	ug/L
TRICELN	01-AUG-92	N	U	10	ug/L
TRICELN	18-MAY-92	N	U	10	ug/L
TRICELN	01-NOV-92	N	U	10	ug/L
TRICELN	18-MAY-92	N	U	10	ug/L
TRICELN	01-AUG-92	N	U	10	ug/L
TRICHLB	18-MAY-92	N	U	10	ug/L
TRICHLB	01-NOV-92	N	U	10	ug/L
TRICHLB	01-AUG-92	N	U	10	ug/L
TRITIUM	18-MAY-92	N	J	9900	pCi/L
TRITIUM	01-AUG-92	N		9300	pCi/L
TRITIUM	01-NOV-92	N		9100	pCi/L
TRITIUM	18-FEB-93	N		9300	pCi/L
TRITIUM	26-JUL-94	N		8900	pCi/L
TRITIUM	17-AUG-93	N	R	7500	pCi/L
TRITIUM	31-JAN-94	N		8500	pCi/L
TRITIUM	06-APR-94	N		7880	pCi/L
U-233/4	18-MAY-92	N	J	1.8	pCi/L
U-233/4	01-NOV-92	N		1.9	pCi/L
U-233/4	01-AUG-92	N		2	pCi/L
U-235	18-MAY-92	N	J	0.13	pCi/L
U-235	01-NOV-92	N	U	0.08	pCi/L
U-235	01-AUG-92	N	U	0.08	pCi/L
U-238	18-MAY-92	N	J	1.6	pCi/L
U-238	01-AUG-92	N		1.6	pCi/L
U-238	01-NOV-92	N		2.2	pCi/L
URANIUM	06-APR-94	N		7.15	ug/L
VANADIUM	18-MAY-92	Y		2	ug/L

Table E-2. Ground-water Chemistry for Well 199-H5-1A

Constituent	Sample Date	Filtered	Qualifier	Value	Units
VANADIUM	01-AUG-92	N		4.6	ug/L
VANADIUM	01-NOV-92	N		6.7	ug/L
VANADIUM	26-JUL-94	N		25.8	UG/L
VANADIUM	17-AUG-93	Y		17.2	ug/L
VANADIUM	26-JUL-94	Y		22.5	UG/L
VANADIUM	31-JAN-94	Y		6.3	ug/L
VANADIUM	31-JAN-94	N		4.7	ug/L
VANADIUM	18-FEB-93	Y		4.9	ug/L
VANADIUM	01-NOV-92	Y		2.5	ug/L
VANADIUM	18-FEB-93	N		5.2	ug/L
VANADIUM	01-AUG-92	Y		4.2	ug/L
VANADIUM	18-MAY-92	N		6.8	ug/L
VINYIDE	01-AUG-92	N	U	10	ug/L
VINYIDE	18-MAY-92	N	U	10	ug/L
VINYIDE	01-NOV-92	N	U	10	ug/L
VINYIDE	18-MAY-92	N	U	10	ug/L
VINYIDE	01-AUG-92	N	U	10	ug/L
ZINC	18-MAY-92	Y		123	ug/L
ZINC	31-JAN-94	Y		49.3	ug/L
ZINC	31-JAN-94	N		175	ug/L
ZINC	18-FEB-93	Y		97.7	ug/L
ZINC	01-NOV-92	Y		98.8	ug/L
ZINC	17-AUG-93	Y		3.7	ug/L
ZINC	26-JUL-94	Y		128	UG/L
ZINC	26-JUL-94	N		231	UG/L
ZINC	18-FEB-93	N		184	ug/L
ZINC	01-AUG-92	N		137	ug/L
ZINC	01-AUG-92	Y		51.9	ug/L
ZINC	18-MAY-92	N		684	ug/L
ZINC	01-NOV-92	N		195	ug/L
ZN-65	18-MAY-92	N	UJ	33	pCi/L

Table E-2. Ground-water Chemistry for Well 199-H5-1A

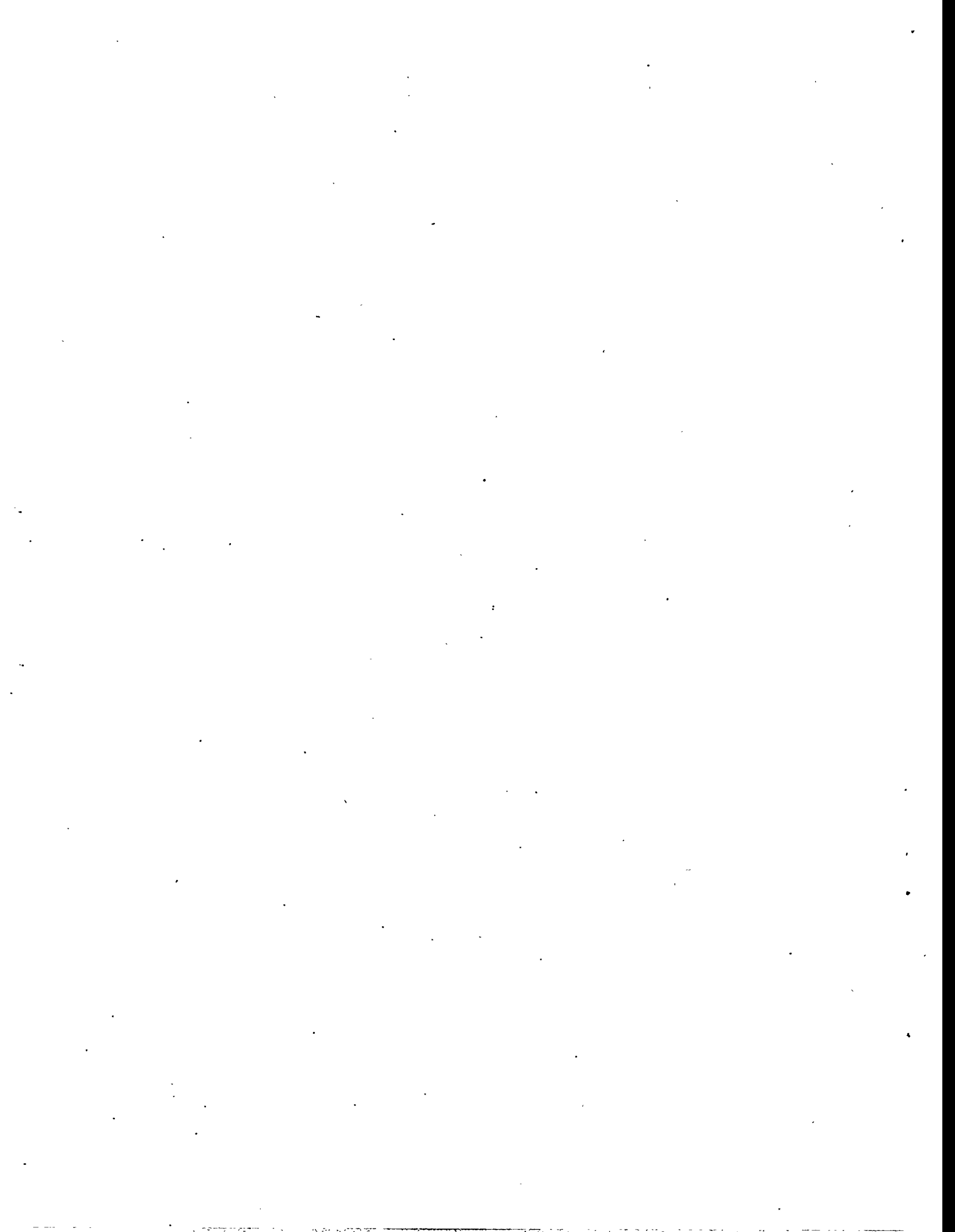
Constituent	Sample Date	Filtered	Qualifier	Value	Units
ZN-65	01-AUG-92	N	U	30	pCi/L
ZN-65	01-NOV-92	N	U	40	pCi/L

Table E-3. Dissolved Oxygen Data for Hanford Site Wells

Well Name	Constituent	Sample Date	Filtered	Qualifier	Value	Units
199-B5-1	DISS O2	03-JUN-87	N		7.74	ppm
199-B5-1	DISS O2	03-JUN-87	N		7.75	ppm
199-B5-1	DISS O2	03-JUN-87	N		7.44	ppm
199-B5-1	DISS O2	03-JUN-87	N		7.78	ppm
299-E25-7	DISS O2	17-JUN-87	N		8.71	ppm
299-E25-7	DISS O2	17-JUN-87	N		8.75	ppm
299-E25-7	DISS O2	17-JUN-87	N		8.82	ppm
299-E25-7	DISS O2	17-JUN-87	N		8.85	ppm
299-E26-1	DISS O2	16-JUN-87	N		5.5	ppm
299-E26-1	DISS O2	16-JUN-87	N		0.67	ppm
299-E26-1	DISS O2	16-JUN-87	N		1.32	ppm
299-E26-1	DISS O2	16-JUN-87	N		0.47	ppm
299-E26-3	DISS O2	16-JUN-87	N		8.83	ppm
299-E26-3	DISS O2	16-JUN-87	N		8.85	ppm
299-E26-3	DISS O2	16-JUN-87	N		8.84	ppm
299-E26-3	DISS O2	16-JUN-87	N		8.88	ppm
299-E28-17	DISS O2	23-JUN-87	N		7.52	ppm
299-E28-17	DISS O2	23-JUN-87	N		7.57	ppm
299-E28-17	DISS O2	23-JUN-87	N		7.51	ppm
299-E28-17	DISS O2	23-JUN-87	N		7.58	ppm
299-E28-7	DISS O2	22-JUN-87	N		8.23	ppm
299-E28-7	DISS O2	22-JUN-87	N		8.23	ppm
299-E28-7	DISS O2	22-JUN-87	N		8.23	ppm
299-E28-7	DISS O2	22-JUN-87	N		8.25	ppm
299-E33-2	DISS O2	23-JUN-87	N		7.95	ppm
299-E33-2	DISS O2	23-JUN-87	N		7.81	ppm
299-E33-2	DISS O2	23-JUN-87	N		7.81	ppm
299-E33-2	DISS O2	23-JUN-87	N		7.95	ppm
299-W12-1	DISS O2	04-JUN-87	N		9.19	ppm
299-W12-1	DISS O2	04-JUN-87	N		9.37	ppm
299-W12-1	DISS O2	04-JUN-87	N		9.45	ppm

Table E-3. Dissolved Oxygen Data for Hanford Site Wells

Well Name	Constituent	Sample Date	Filtered	Qualifier	Value	Units
299-W12-1	DISS O2	04-JUN-87	N		9.3	ppm
299-W19-1	DISS O2	10-JUN-87	N		6.42	ppm
299-W19-1	DISS O2	10-JUN-87	N		5.44	ppm
299-W19-1	DISS O2	10-JUN-87	N		6.65	ppm
299-W19-1	DISS O2	10-JUN-87	N		6.4	ppm
299-W23-1	DISS O2	09-JUN-87	N		6.31	ppm
299-W23-1	DISS O2	09-JUN-87	N		5.78	ppm
299-W23-1	DISS O2	09-JUN-87	N		5.32	ppm
299-W23-1	DISS O2	09-JUN-87	N		6.11	ppm
299-W23-11	DISS O2	04-JUN-87	N		7.42	ppm
299-W23-11	DISS O2	04-JUN-87	N		7.42	ppm
299-W23-11	DISS O2	04-JUN-87	N		7.41	ppm
299-W23-11	DISS O2	04-JUN-87	N		7.38	ppm
299-W23-7	DISS O2	09-JUN-86	N		6.86	ppm
299-W23-7	DISS O2	09-JUN-86	N		6.67	ppm
299-W23-7	DISS O2	09-JUN-86	N		7.15	ppm
299-W23-7	DISS O2	09-JUN-86	N		6.7	ppm
299-W6-1	DISS O2	10-JUN-87	N		10.01	ppm
299-W6-1	DISS O2	10-JUN-87	N		8.25	ppm
299-W6-1	DISS O2	10-JUN-87	N		9.92	ppm
299-W6-1	DISS O2	10-JUN-87	N		8.95	ppm



**APPENDIX F**

**SELECTED CHEMICAL DATA - "MINI" INJECTION**

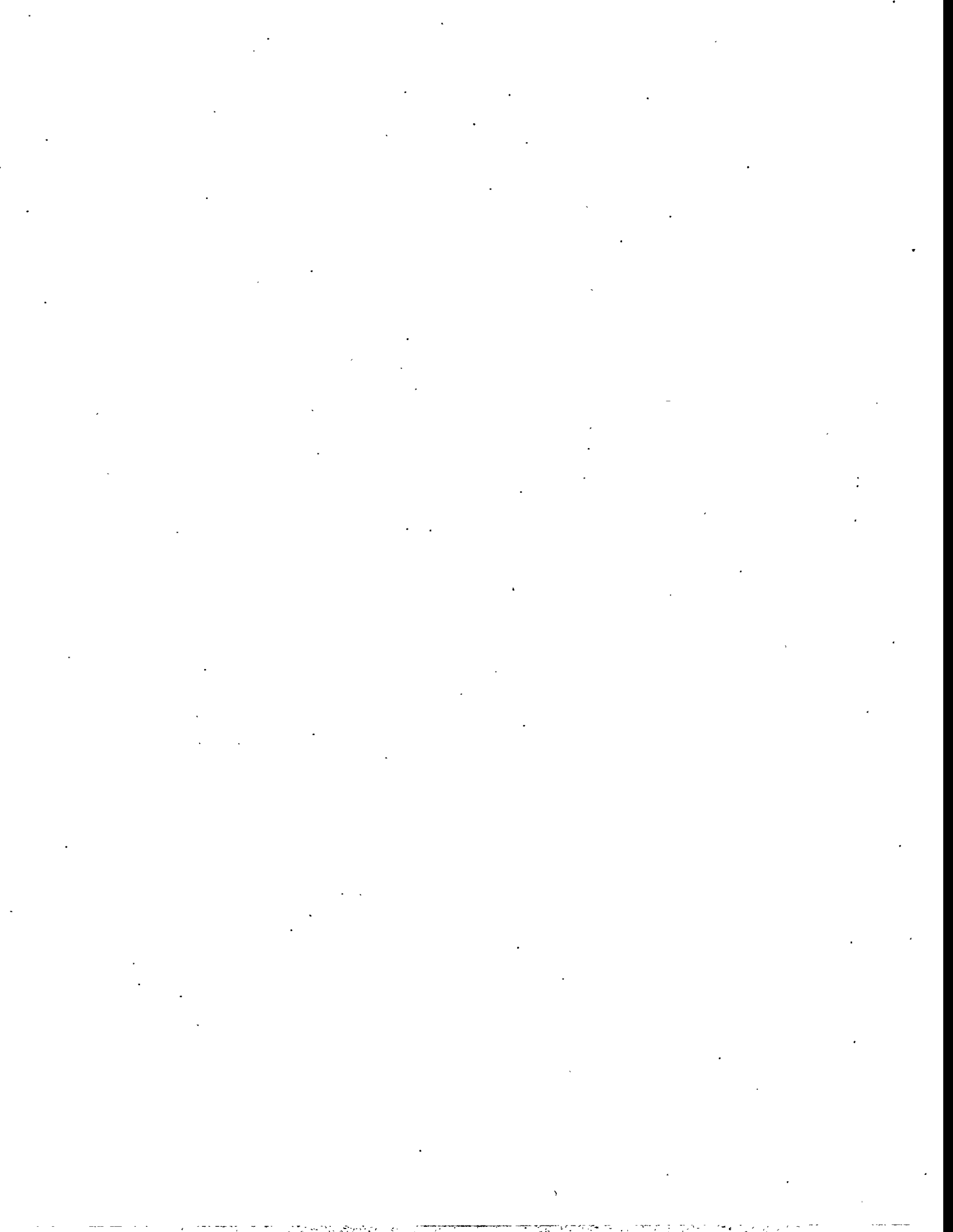
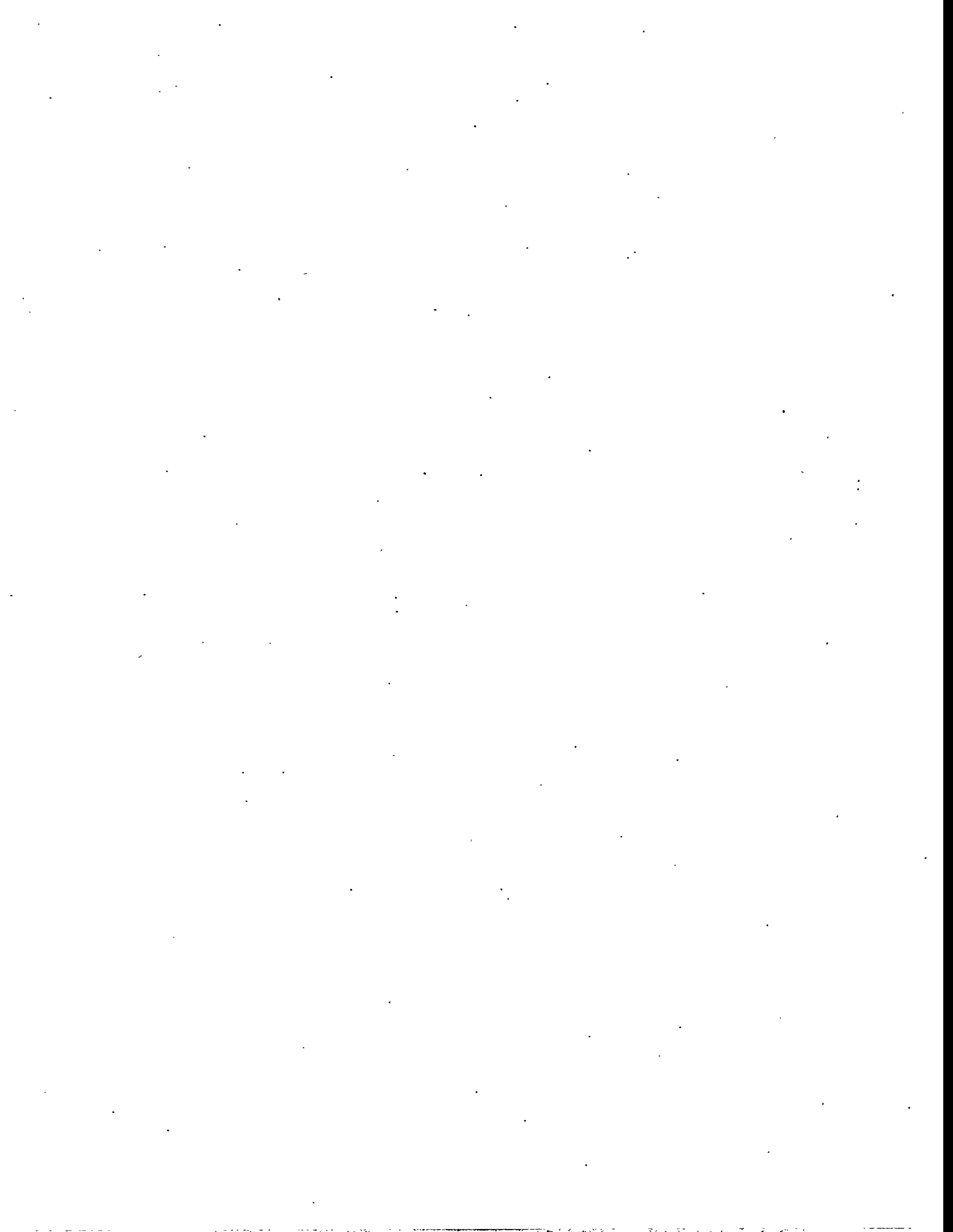


## Table of Contents

Appendix F. Selected Chemical Data - "Mini" Injection .....	F.1
---	-----

### List of Figures

Figure F-1. Variation in the Fe Trace Metals Content of Withdrawal Waters (H5-2) During the Withdrawal Phase of the Mini Injection Experiment .....	F.2
Figure F-2. Variation in the Cr Trace Metals Content of Withdrawal Waters (H5-2) During the Withdrawal Phase of the Mini Injection Experiment .....	F.3
Figure F-3. Variation in the Cu Trace Metals Content of Withdrawal Waters (H5-2) During the Withdrawal Phase of the Mini Injection Experiment .....	F.4
Figure F-4. Variation in the Zn Trace Metals Content of Withdrawal Waters (H5-2) During the Withdrawal Phase of the Mini Injection Experiment .....	F.5
Figure F-5. Variation in the As Trace Metals Content of Withdrawal Waters (H5-2) During the Withdrawal Phase of the Mini Injection Experiment. ....	F.6



## APPENDIX F

### SELECTED CHEMICAL DATA - "MINI" INJECTION

This appendix contains figures of trace metal variation in the withdrawn fluids as a function of time during the 5.5 hour withdrawal phase of the mini injection experiment

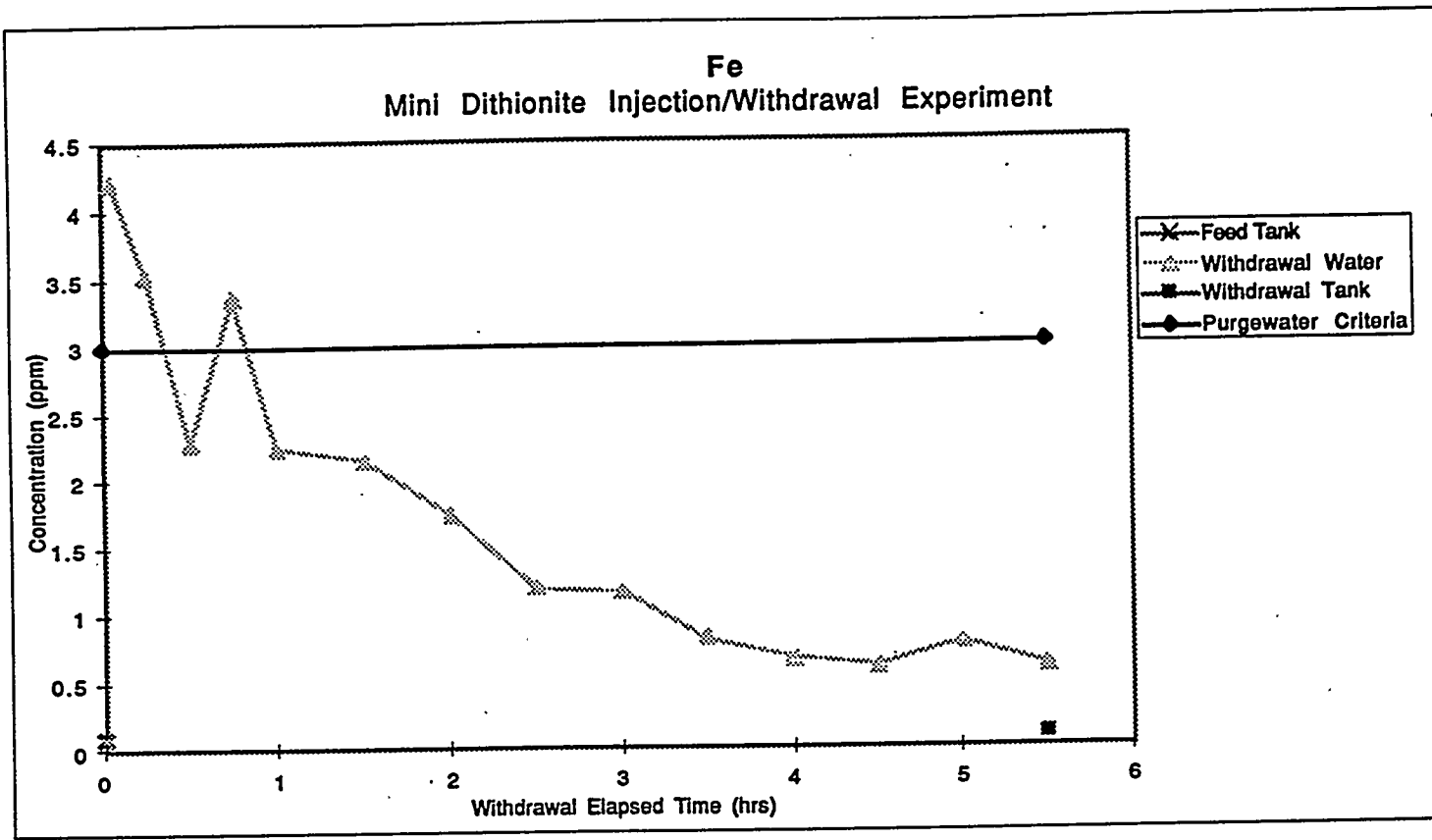


Figure F-1. Variation in the Fe Trace Metals Content of Withdrawal Waters (H5-2) During the Withdrawal Phase of the Mini Injection Experiment.

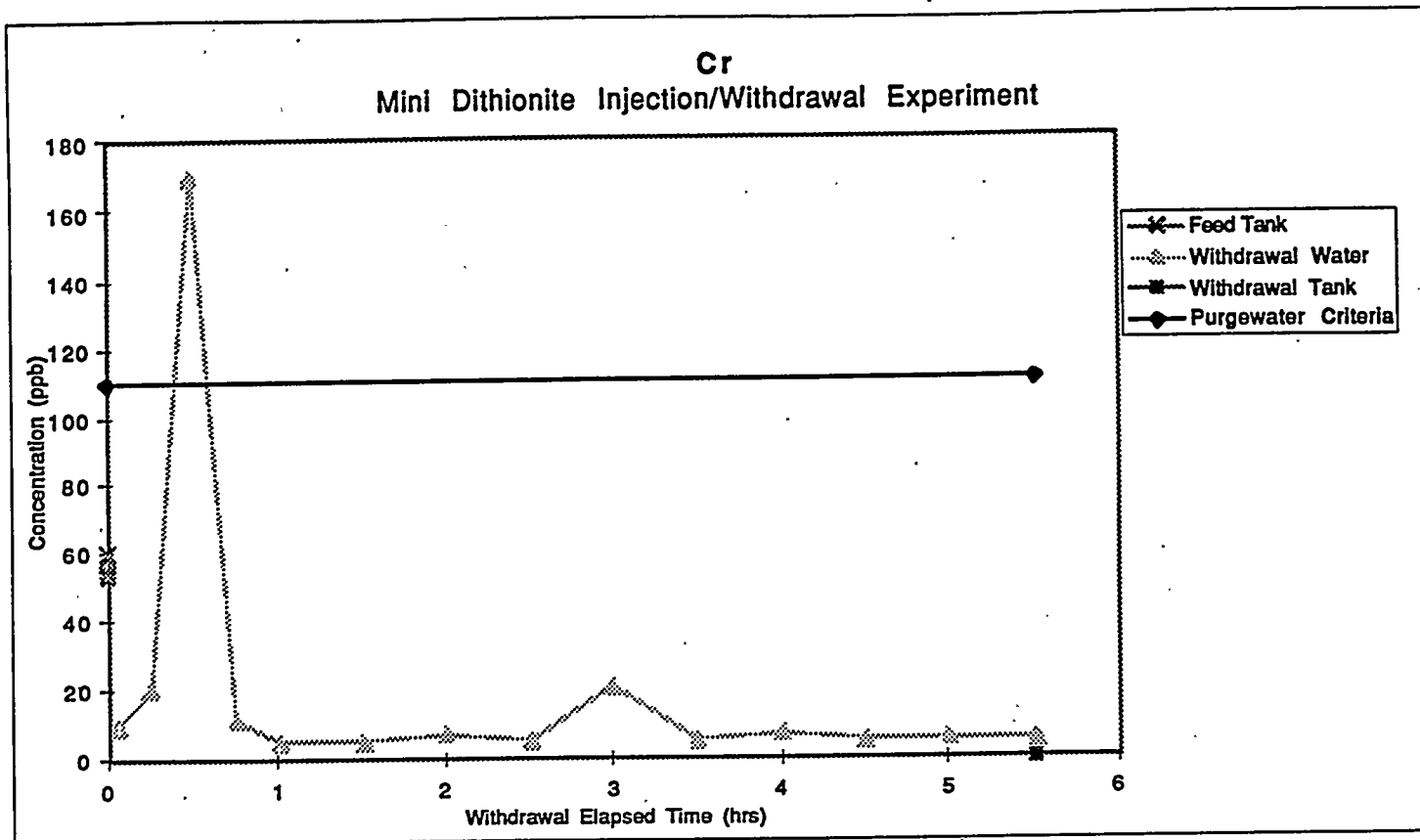


Figure F-2. Variation in the Cr Trace Metals Content of Withdrawal Waters (H5-2) During the Withdrawal Phase of the Mini Injection Experiment.

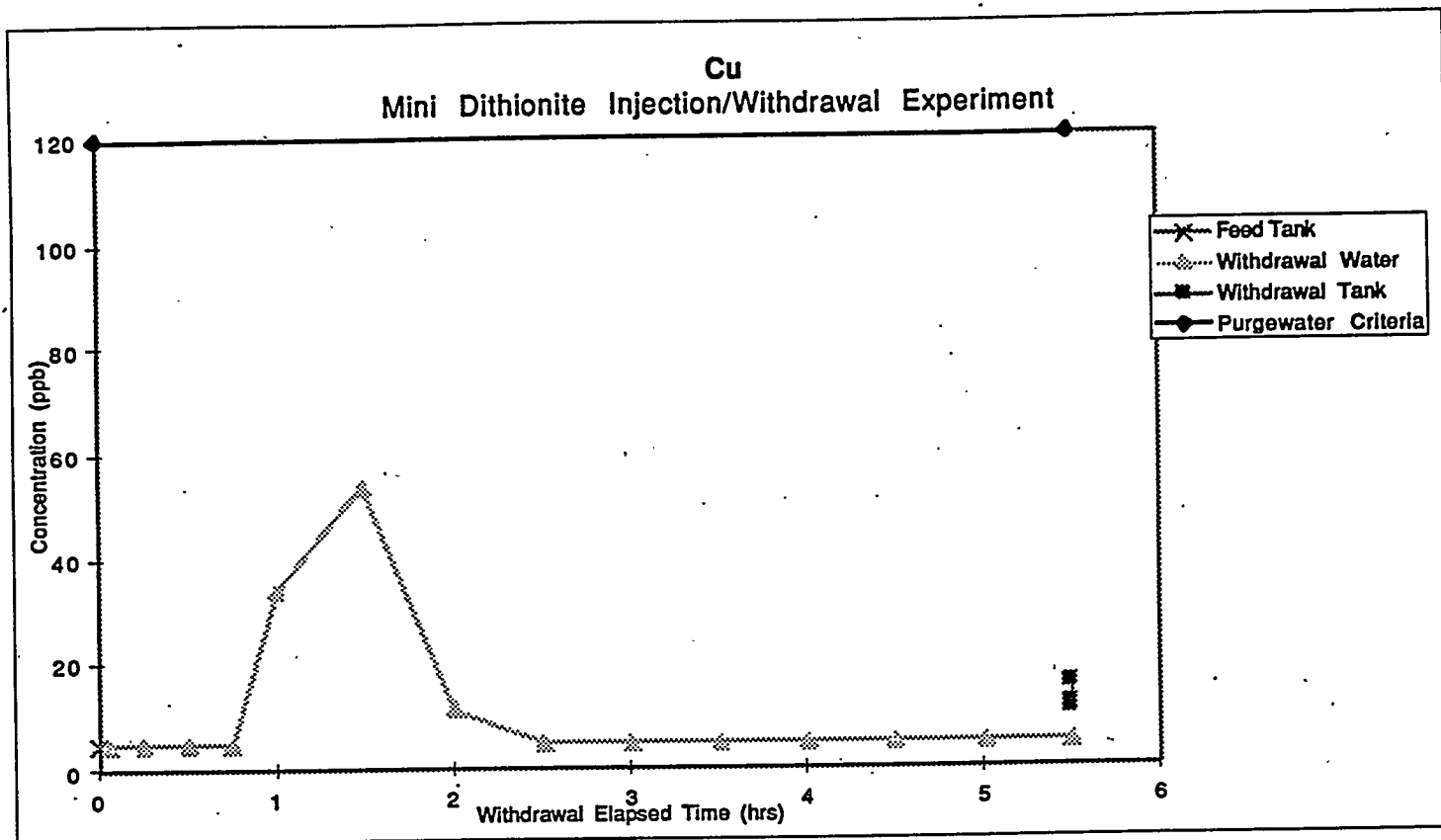


Figure F-3. Variation in the Cu Trace Metals Content of Withdrawal Waters (H5-2) During the Withdrawal Phase of the Mini Injection Experiment.

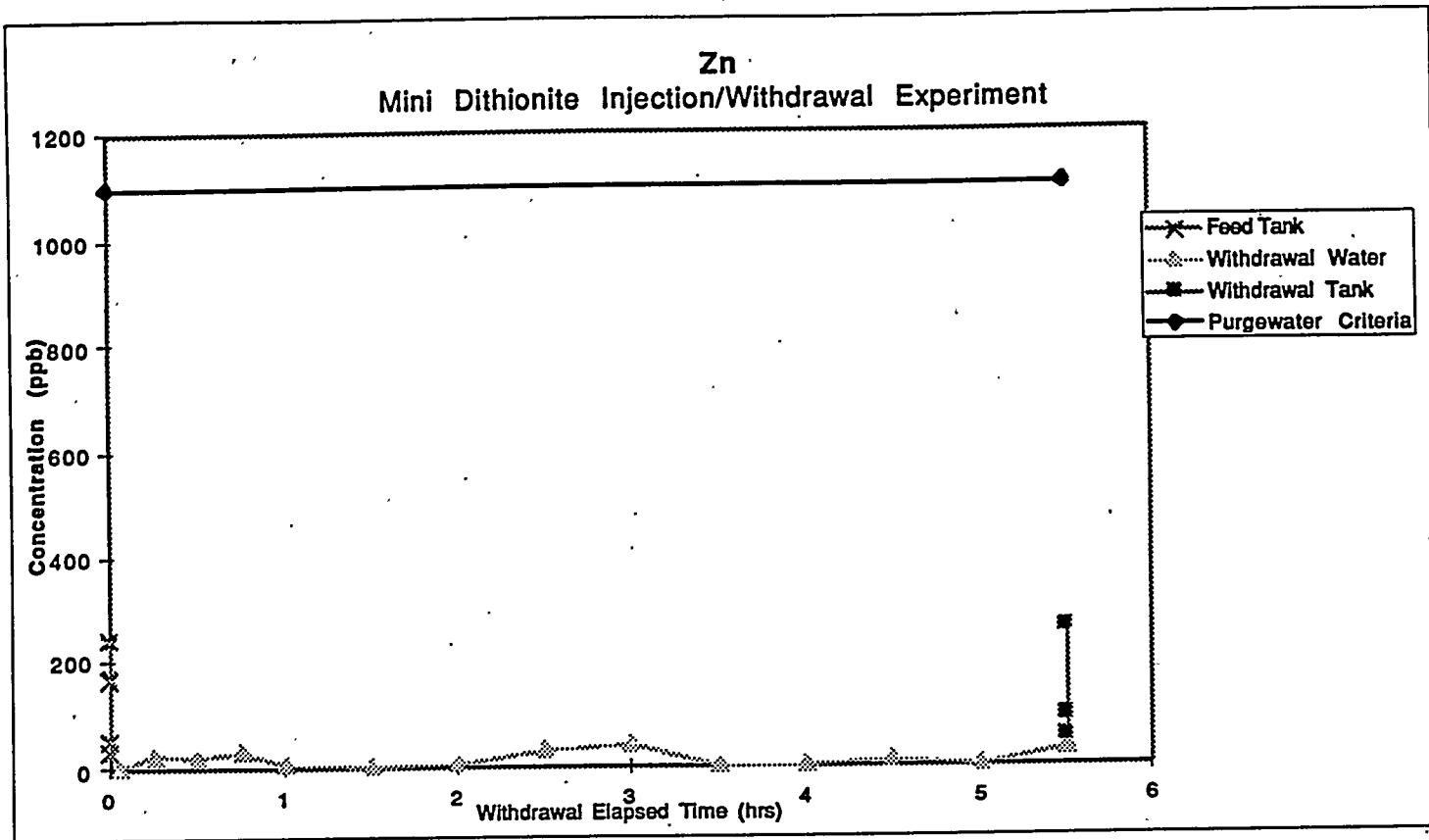


Figure F-4. Variation in the Zn Trace Metals Content of Withdrawal Waters (H5-2) During the Withdrawal Phase of the Mini Injection Experiment.

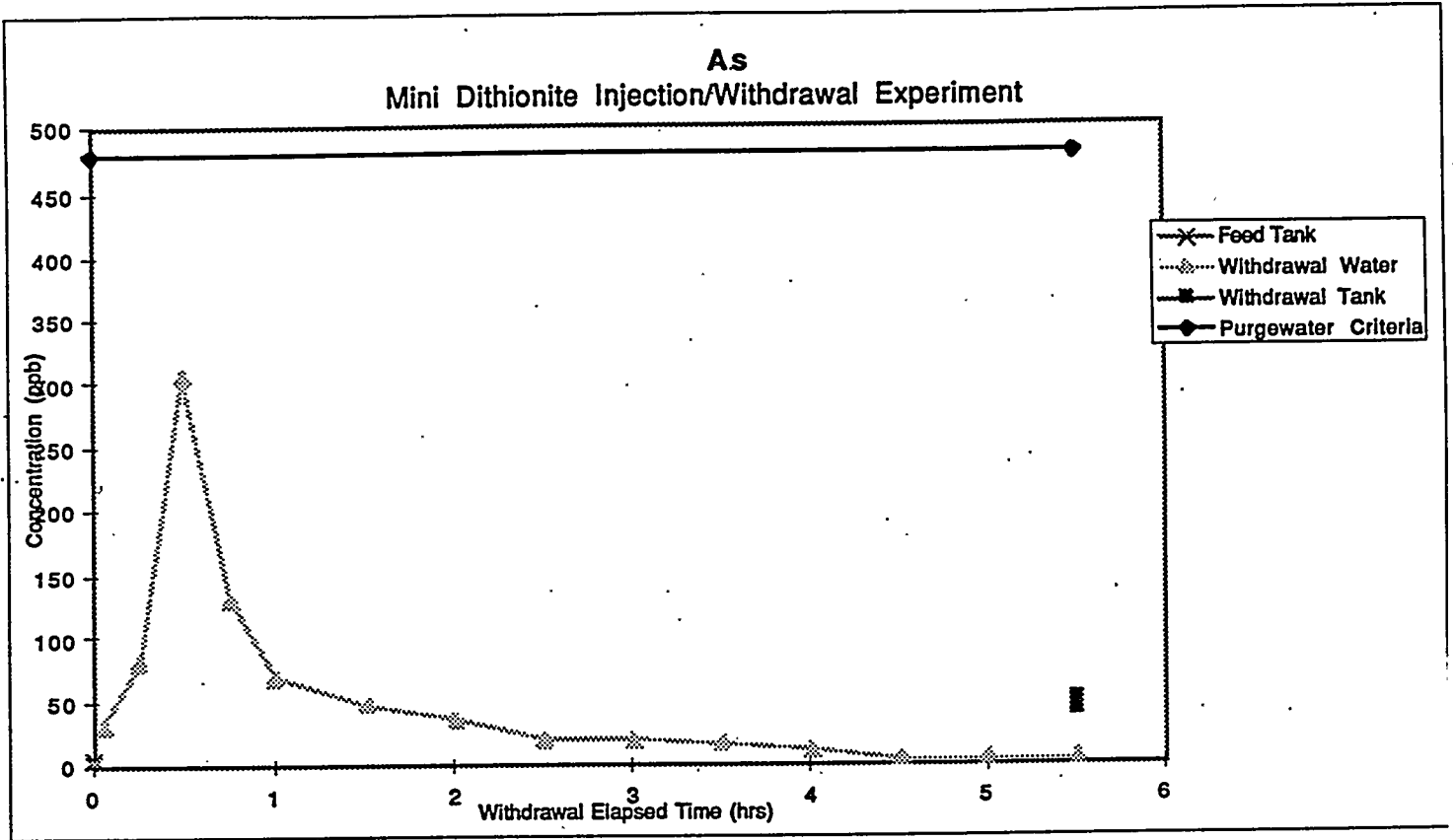
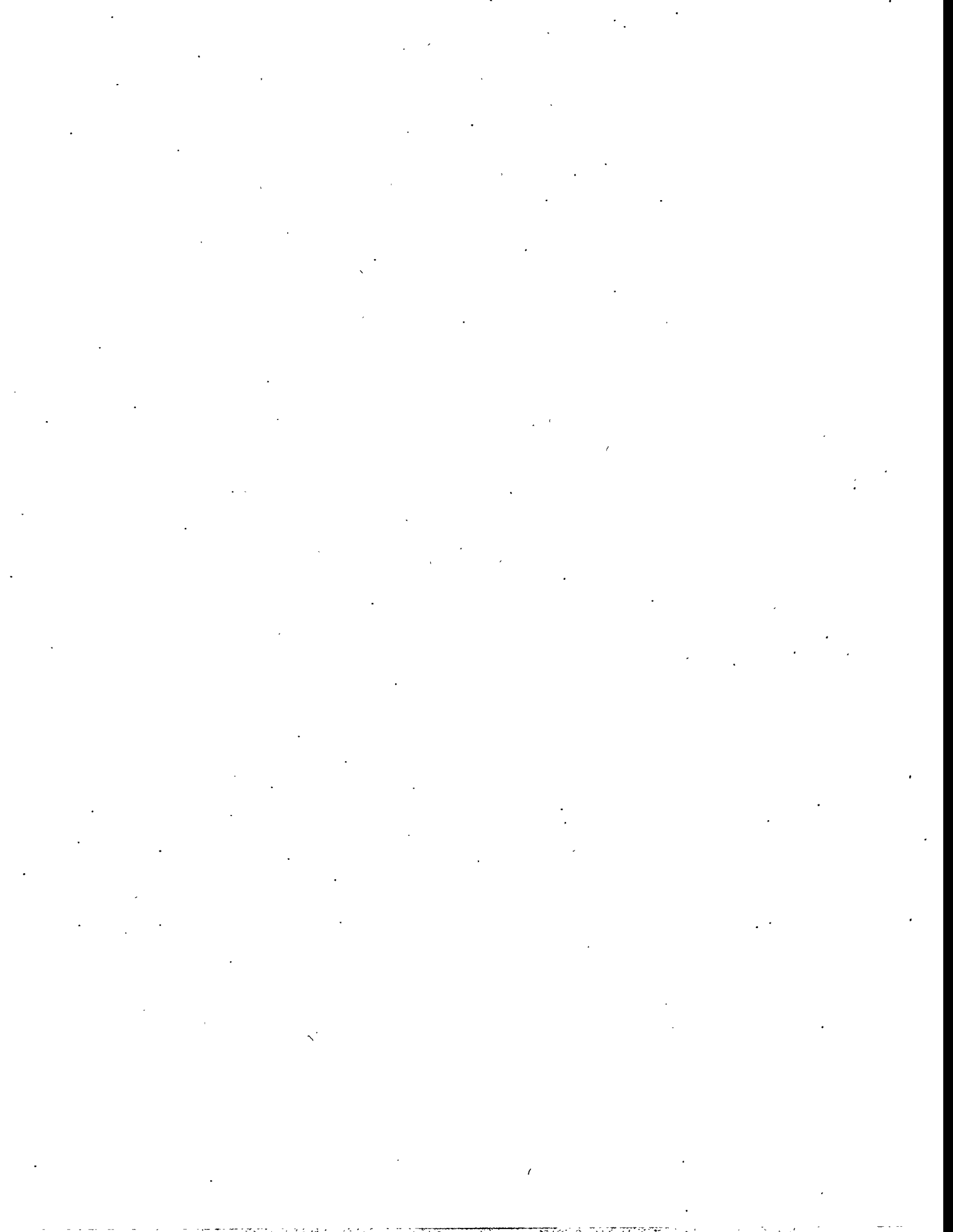


Figure F-5. Variation in the As Trace Metals Content of Withdrawal Waters (H5-2) During the Withdrawal Phase of the Mini Injection Experiment.

**APPENDIX G**

**MONITORING WELL FIELD MEASUREMENTS  
FOR THE MAIN DITHIONITE INJECTION/WITHDRAWAL  
EXPERIMENT**

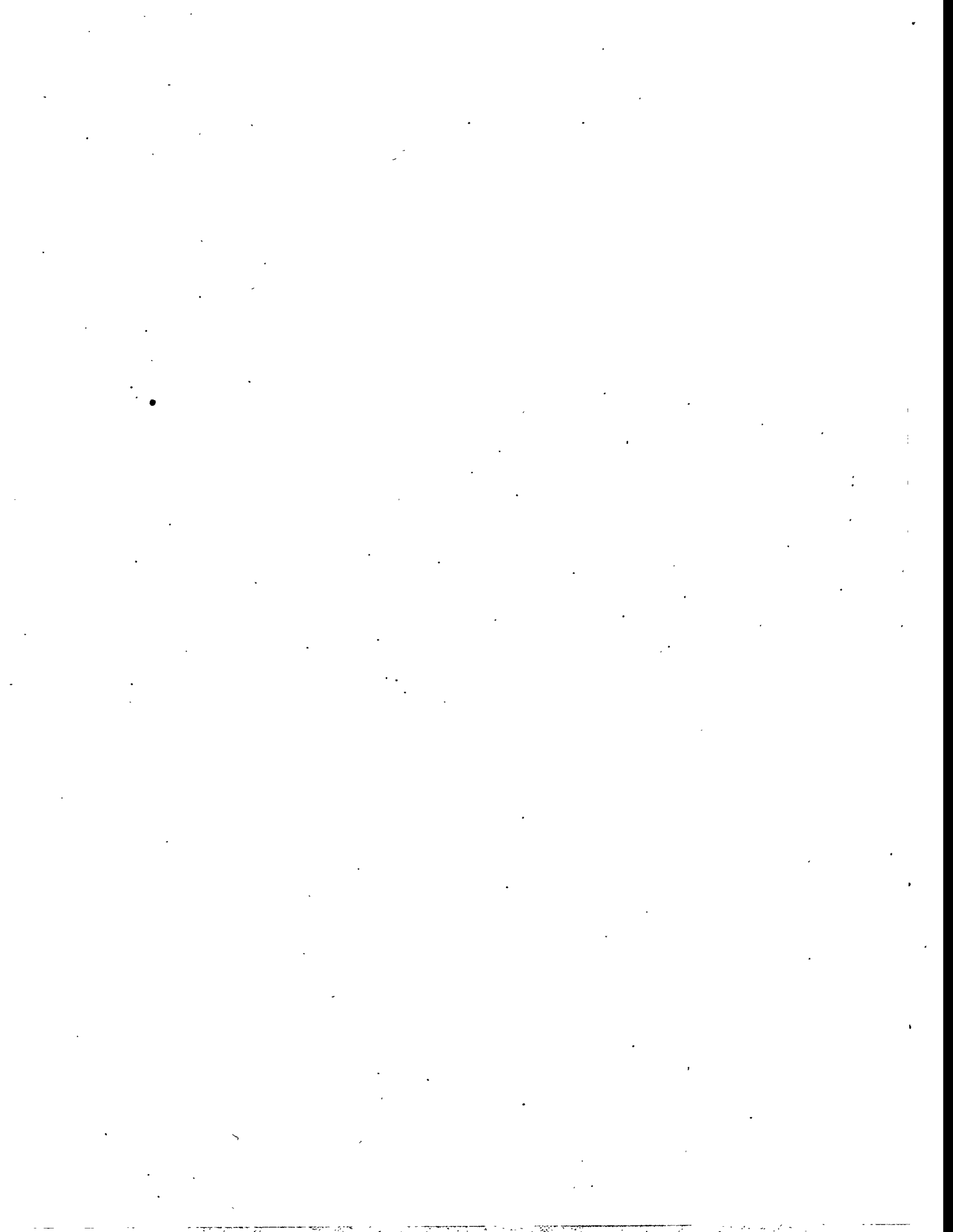


## Table of Contents

Appendix G. Monitoring Well Field Measurements for the Main Dithionite Injection/Withdrawal Experiment .....	G.1
--	-----

### List of Figures

Figure G-1. Measurements for well H5-5p during the ISRM 100-H area injection/withdrawal experiment. ....	G.2
Figure G-2. Measurements for well H5-5o during the ISRM 100-H area injection/withdrawal experiment. ....	G.3
Figure G-3. Measurements for well H5-6 during the ISRM 100-H area injection/withdrawal experiment. ....	G.4
Figure G-4. Measurements for well H5-9 during the ISRM 100-H area injection/withdrawal experiment. ....	G.5
Figure G-5. Measurements for well H5-4p during the ISRM 100-H area injection/withdrawal experiment. ....	G.6
Figure G-6. Measurements for well H5-4o during the ISRM 100-H area injection/withdrawal experiment. ....	G.7
Figure G-7. Measurements for well H5-7 during the ISRM 100-H area injection/withdrawal experiment. ....	G.8
Figure G-8. Measurements for well H5-10 during the ISRM 100-H area injection/withdrawal experiment. ....	G.9
Figure G-9. Measurements for well H5-3p during the ISRM 100-H area injection/withdrawal experiment. ....	G.10
Figure G-10. Measurements for well H5-3o during the ISRM 100-H area injection/withdrawal experiment. ....	G.11
Figure G-11. Measurements for well H5-8 during the ISRM 100-H area injection/withdrawal experiment. ....	G.12
Figure G-12. Measurements for well H5-11 during the ISRM 100-H area injection/withdrawal experiment. ....	G.13
Figure G-13. Measurements for well H5-1B during the ISRM 100-H area injection/withdrawal experiment. ....	G.14



## APPENDIX G

### MONITORING WELL FIELD MEASUREMENTS FOR THE MAIN DITHIONITE INJECTION/WITHDRAWAL EXPERIMENT

This appendix contains the pH, dissolved oxygen, conductivity, and dithionite field measurements from each monitoring well within the targeted treatment zone during the main dithionite injection/withdrawal experiment at the 100-H Area ISRM site conducted from September 7, 1995 to September 12, 1995.

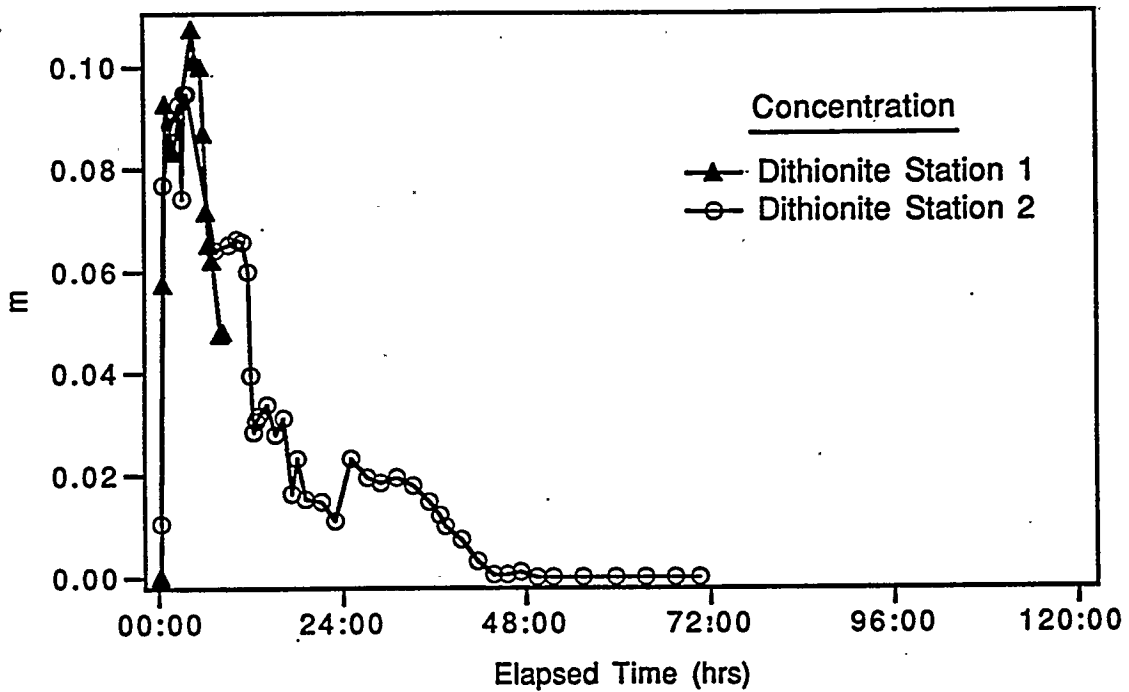
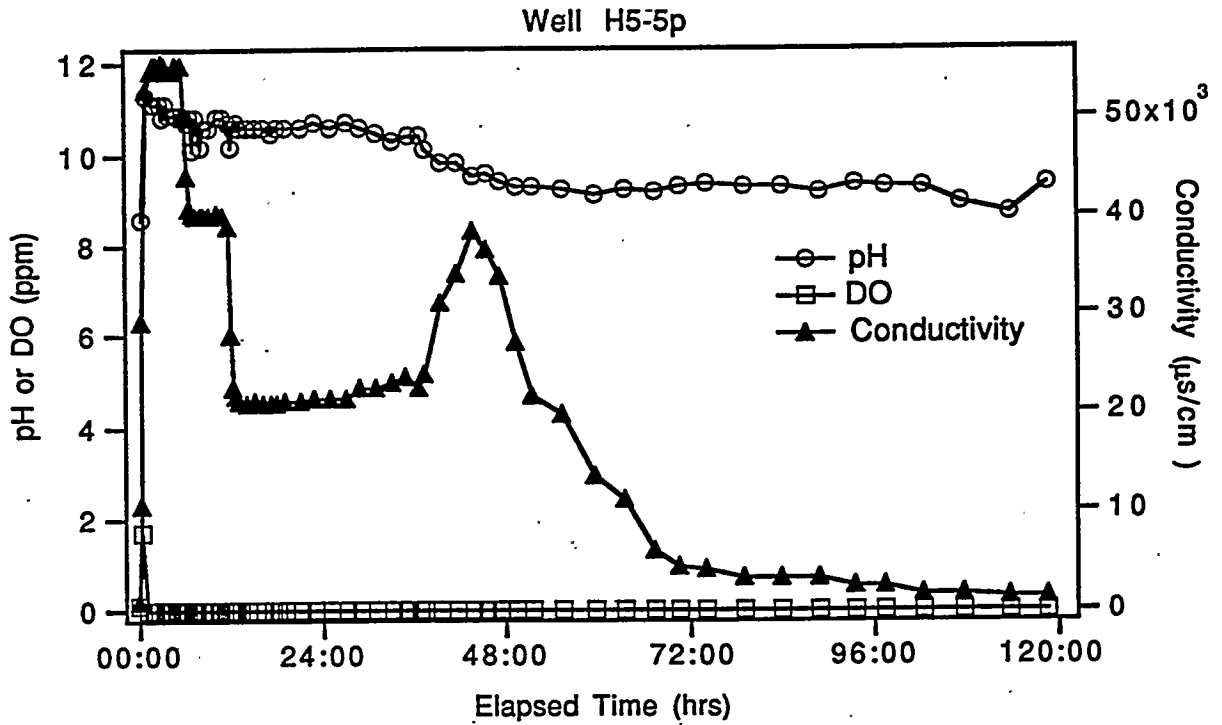


Figure G-1. Measurements for well H5-5p during the ISRM 100-H area injection/withdrawal experiment.

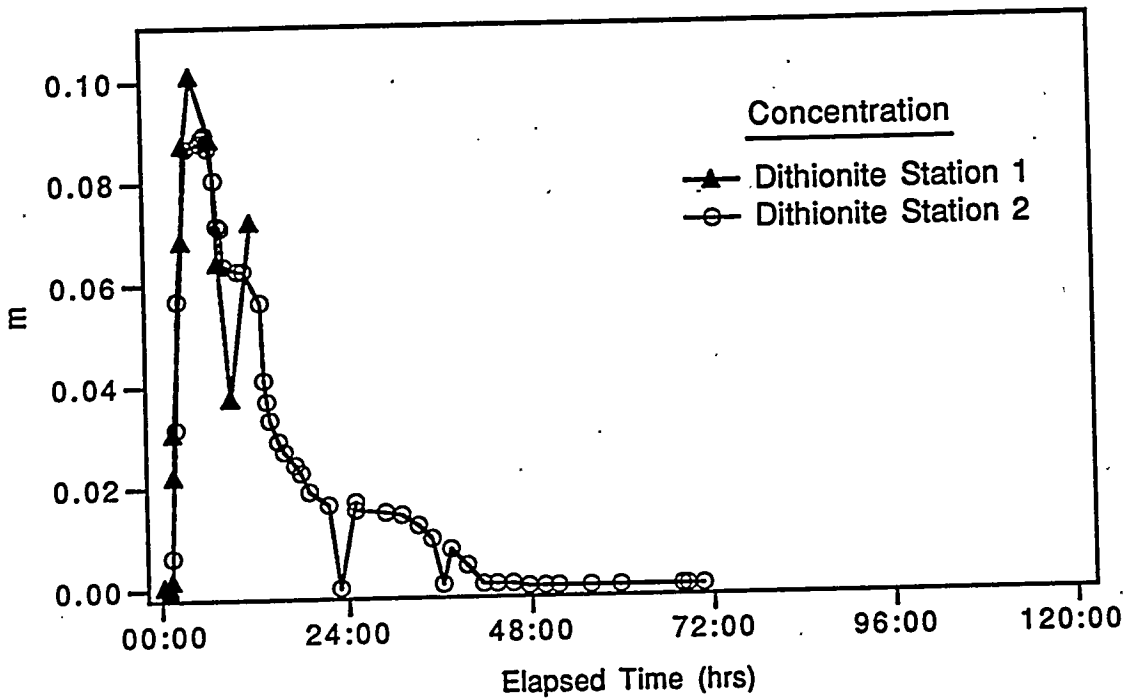
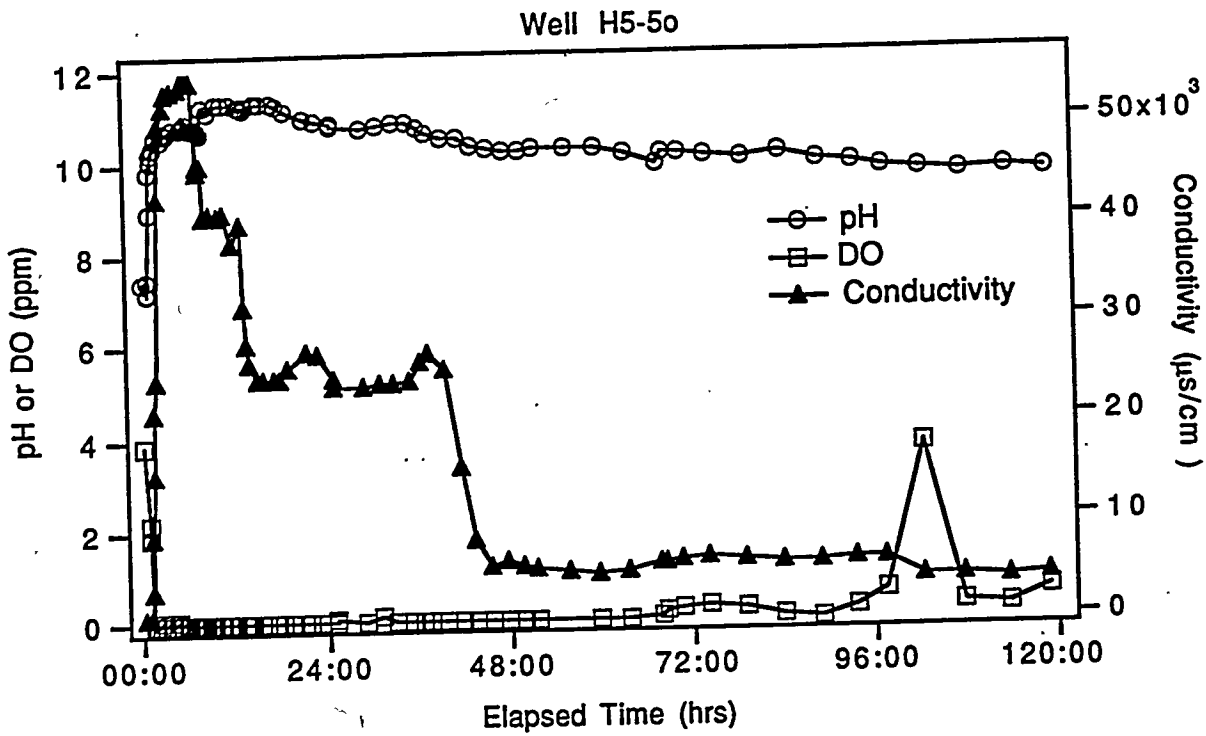


Figure G-2. Measurements for well H5-50 during the ISRM 100-H area injection/withdrawal experiment.

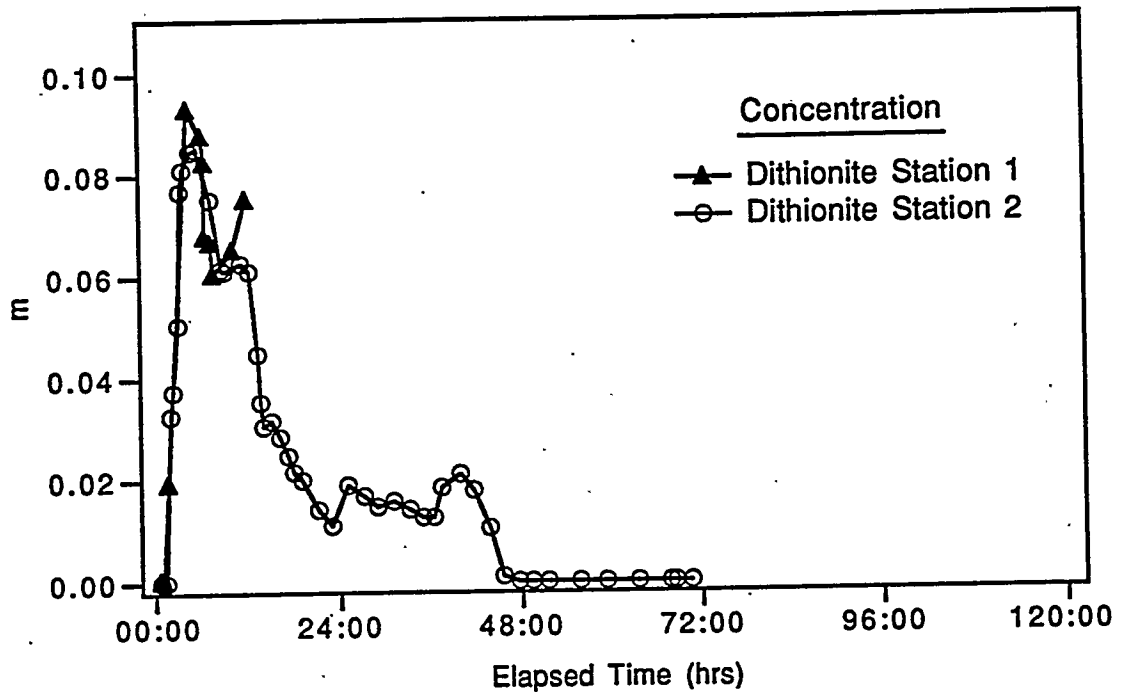
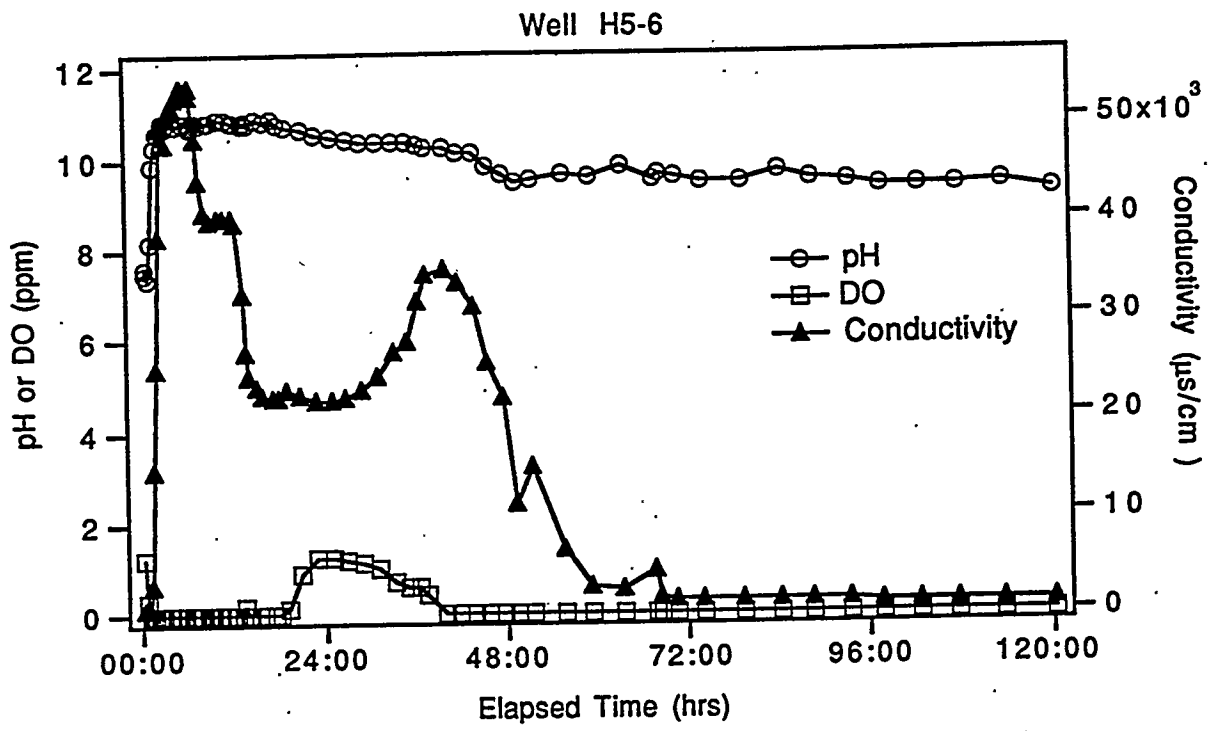


Figure G-3. Measurements for well H5-6 during the ISRM 100-H area injection/withdrawal experiment.

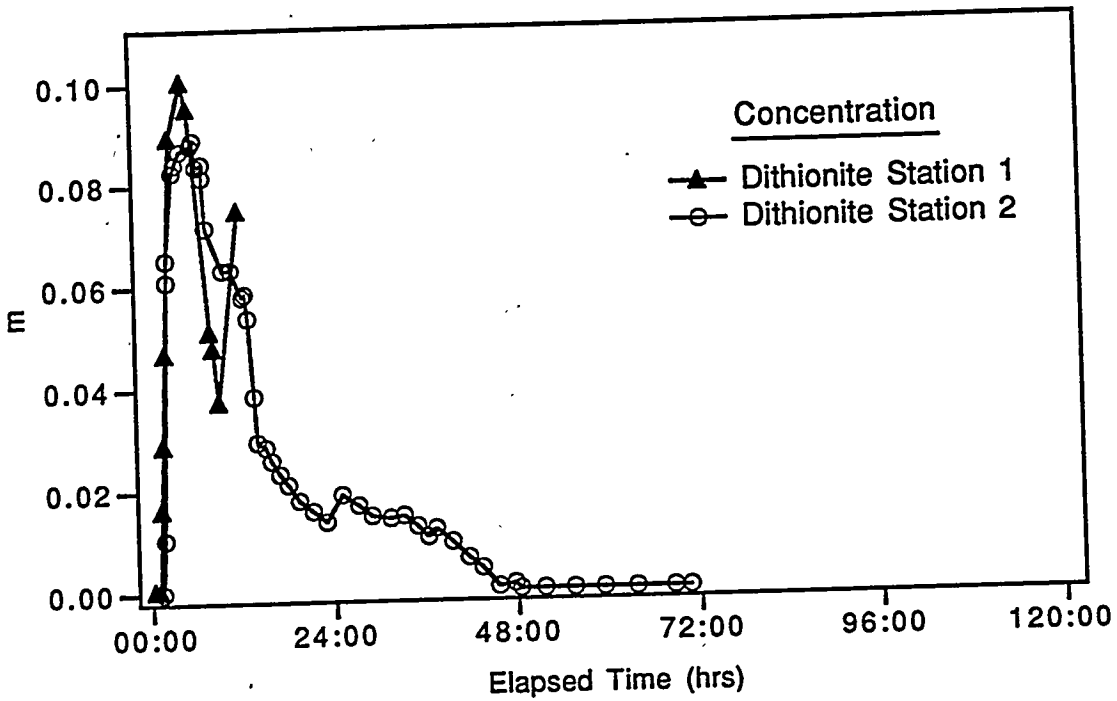
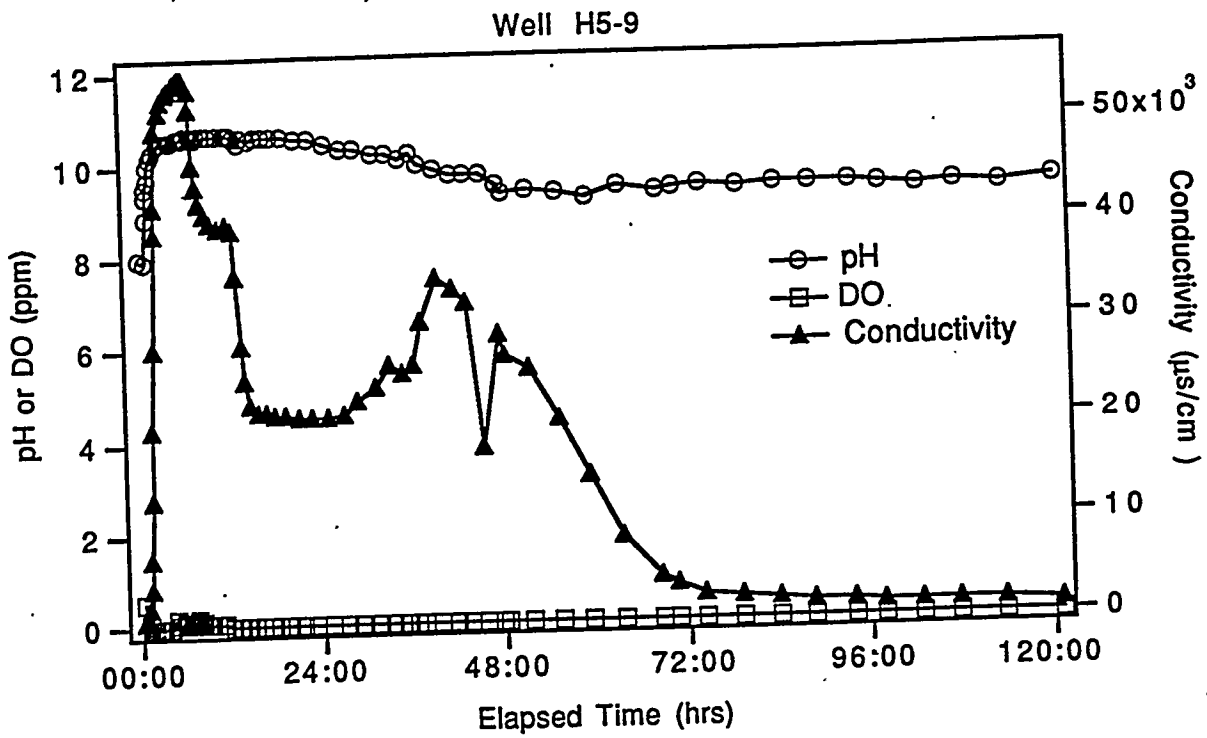


Figure G-4. Measurements for well H5-9 during the ISRM 100-H area injection/withdrawal experiment.

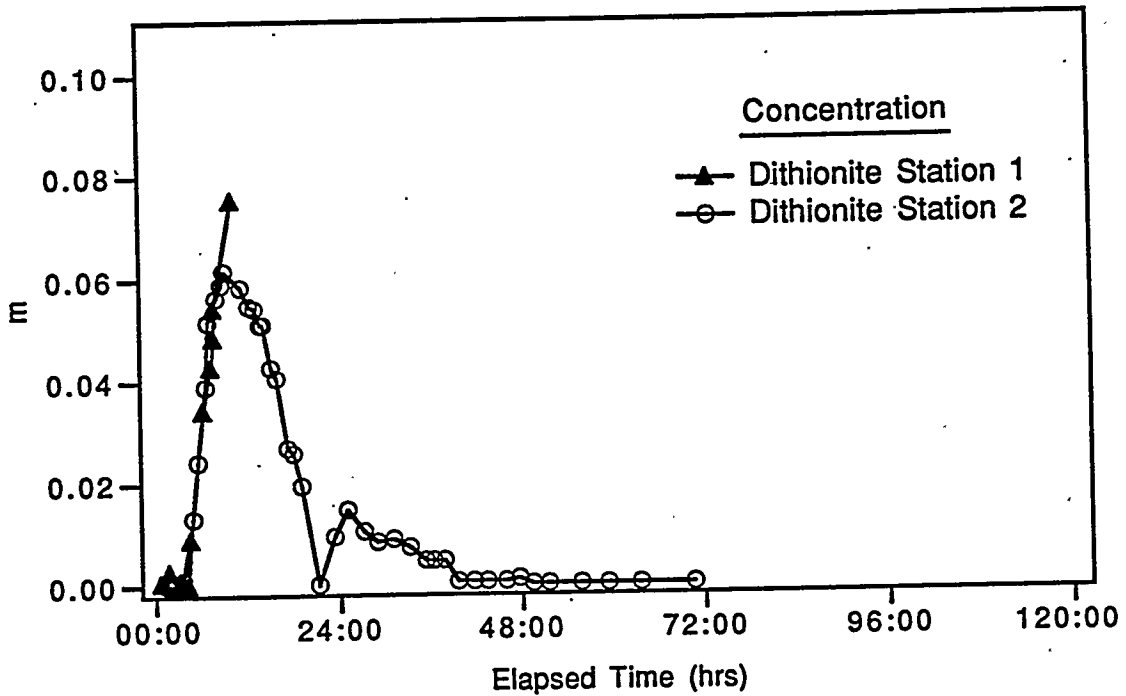
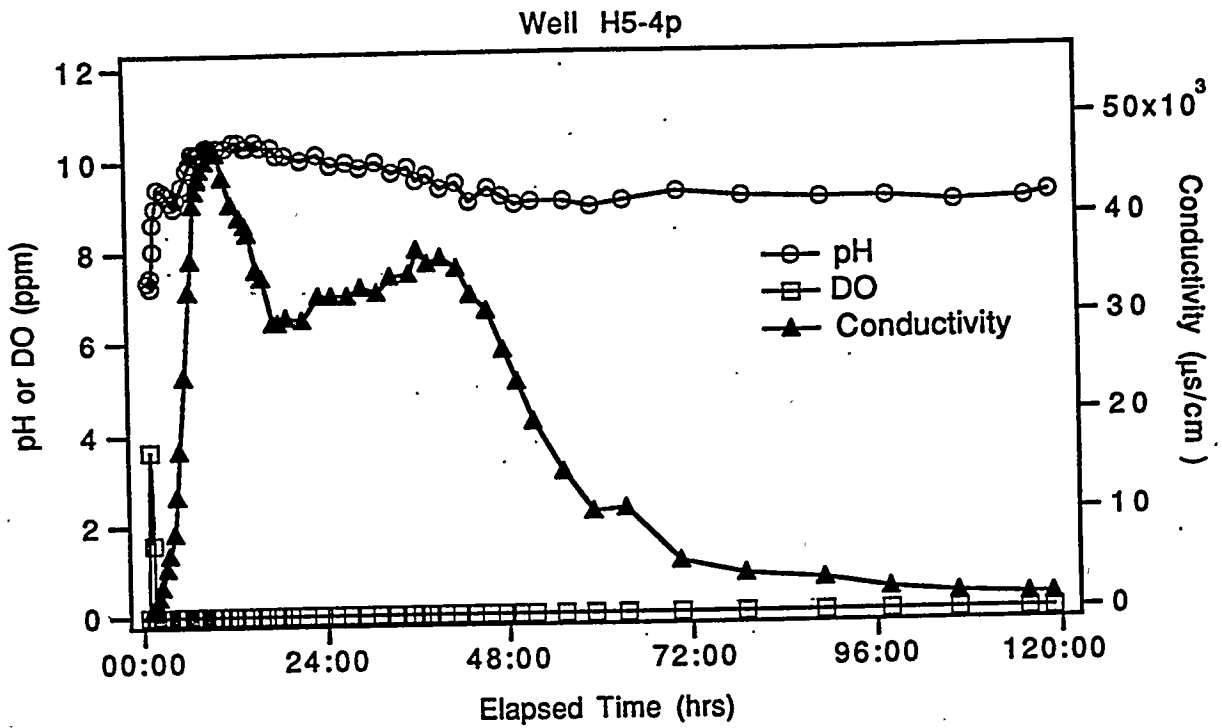


Figure G-5. Measurements for well H5-4p during the ISRM 100-H area injection/withdrawal experiment.

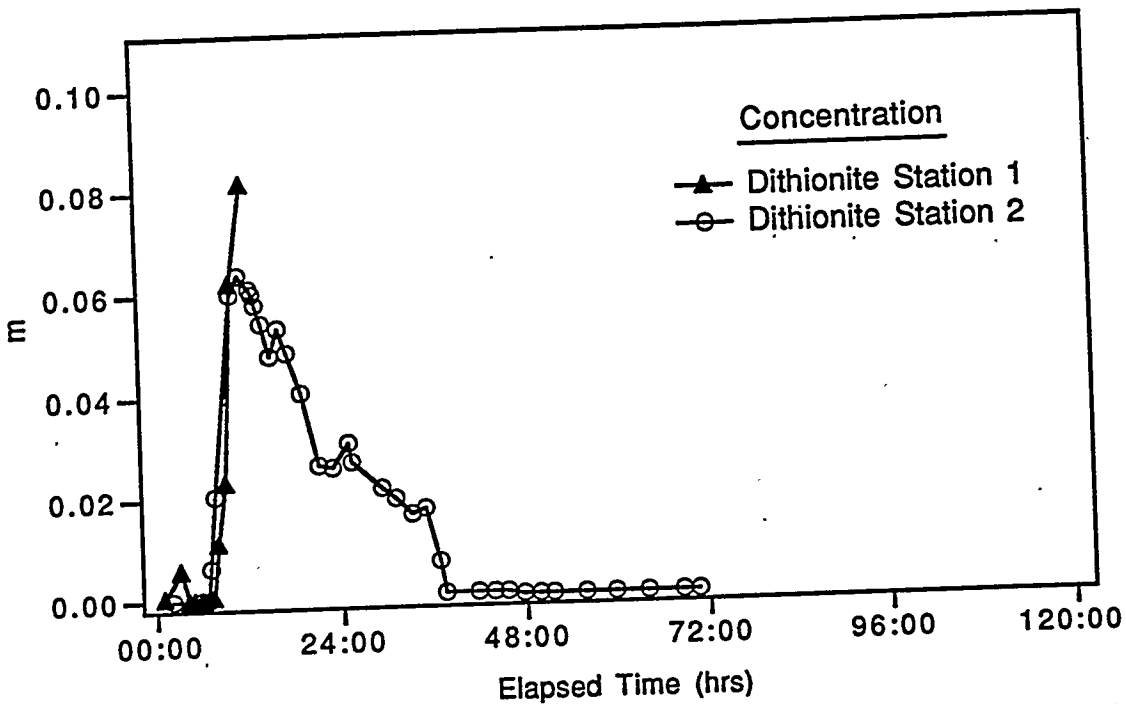
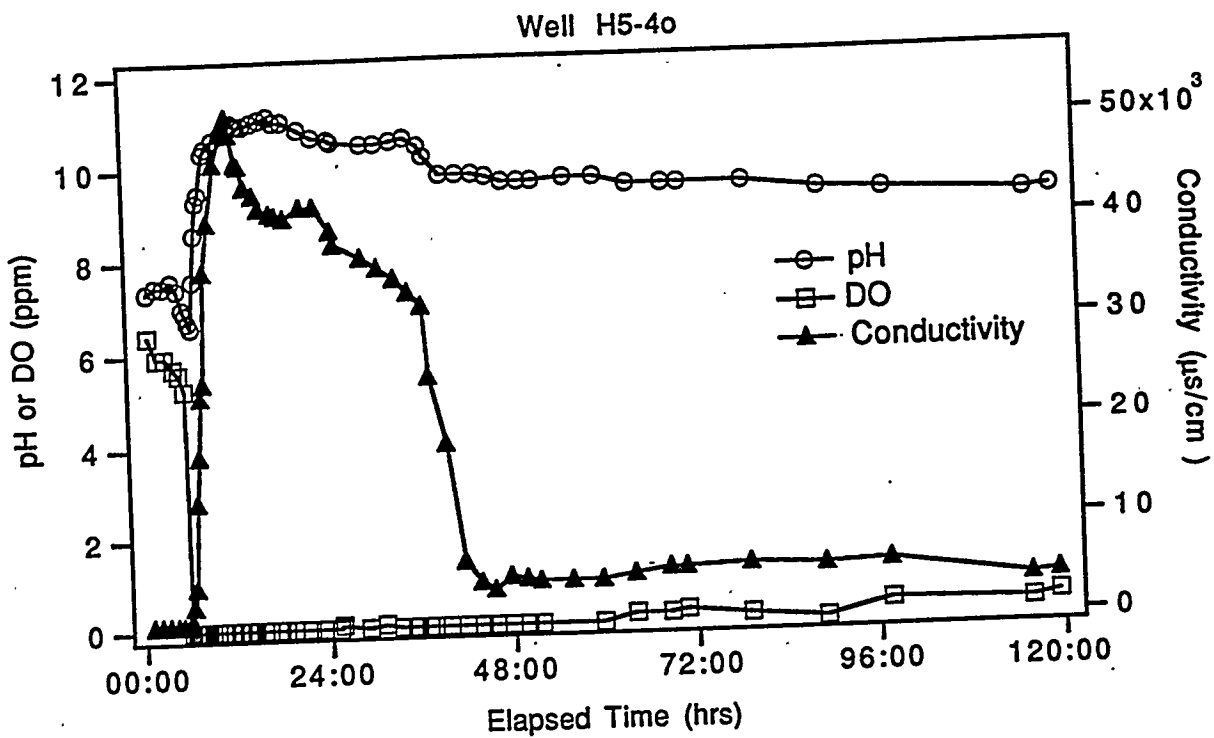


Figure G-6. Measurements for well H5-4o during the ISRM 100-H area injection/withdrawal experiment.

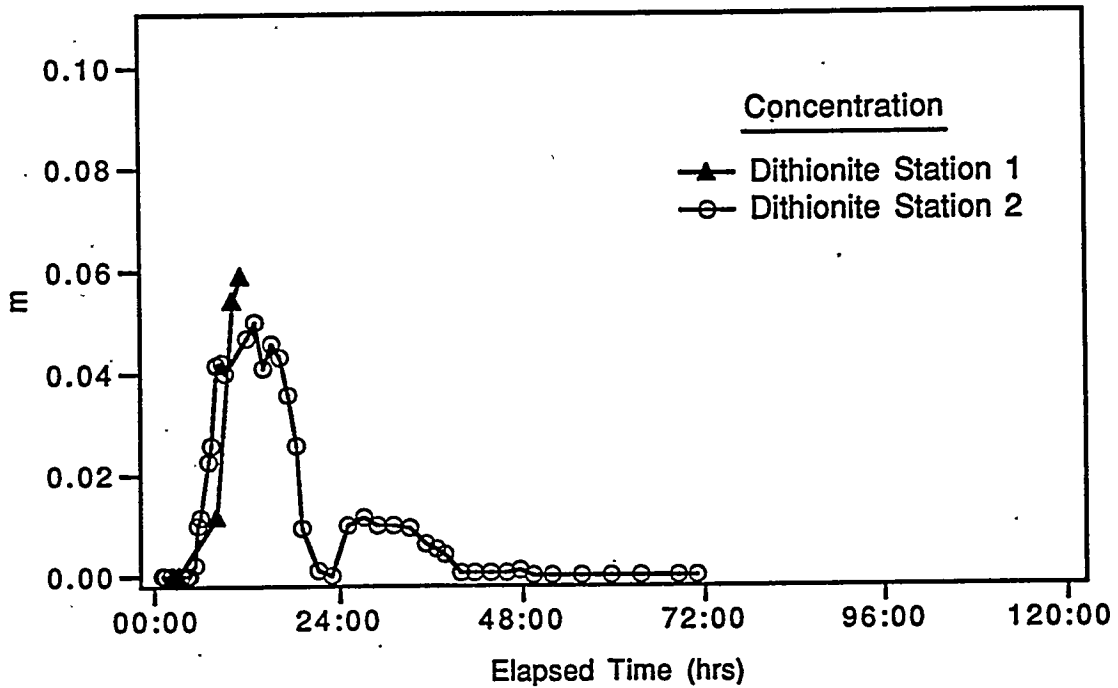
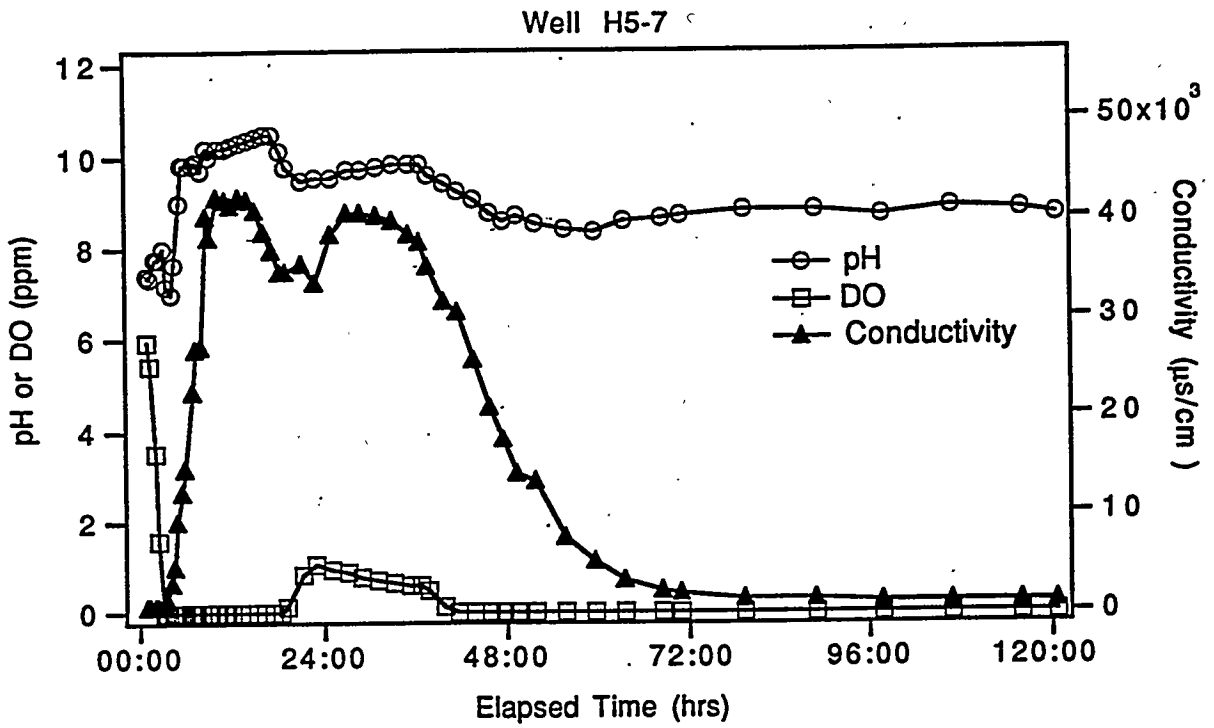


Figure G-7. Measurements for well H5-7 during the ISRM 100-H area injection/withdrawal experiment.

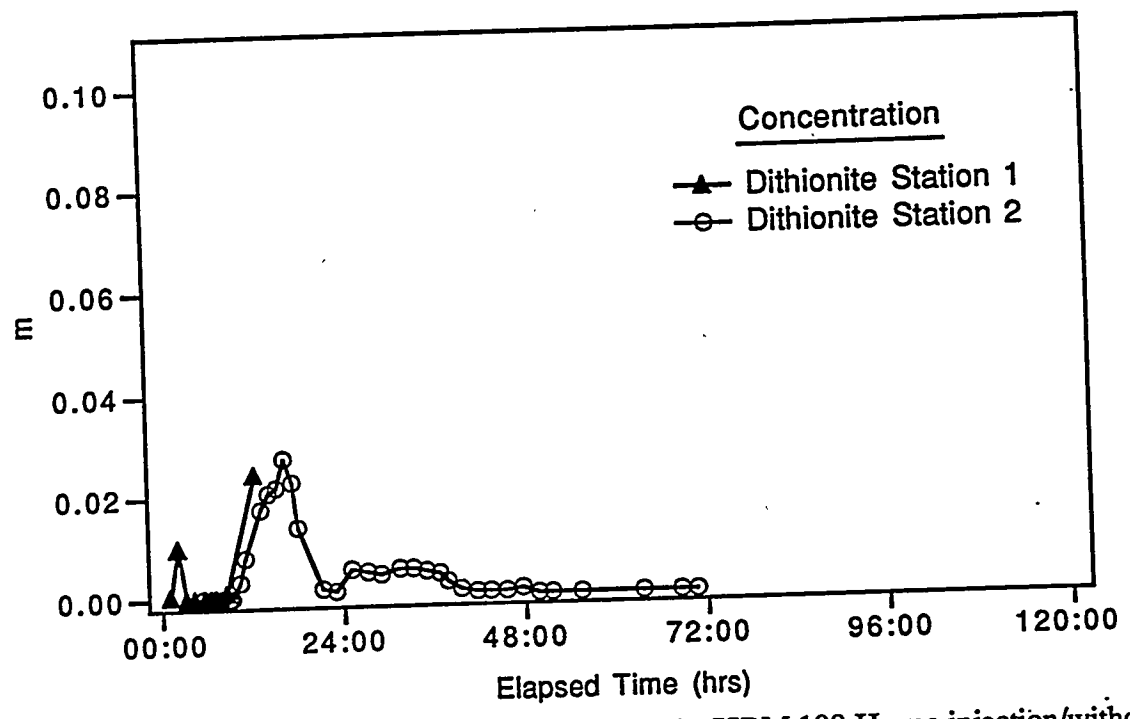
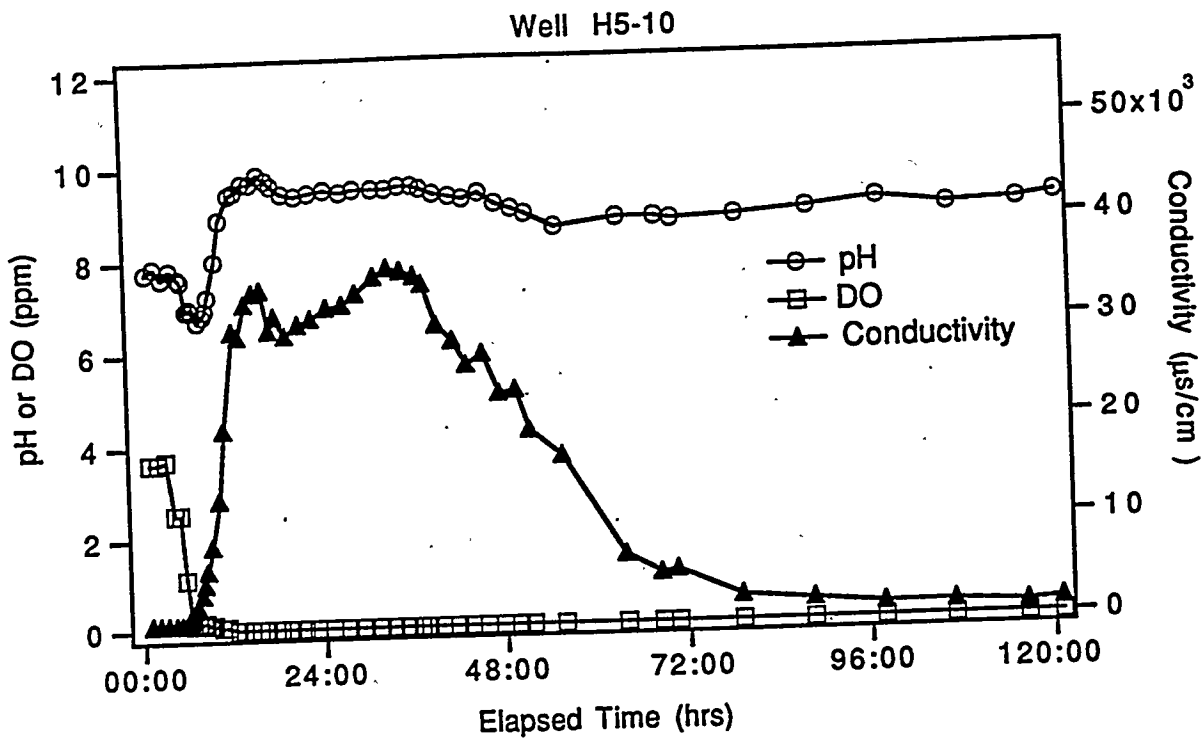


Figure G-8. Measurements for well H5-10 during the ISRM 100-H area injection/withdrawal experiment.

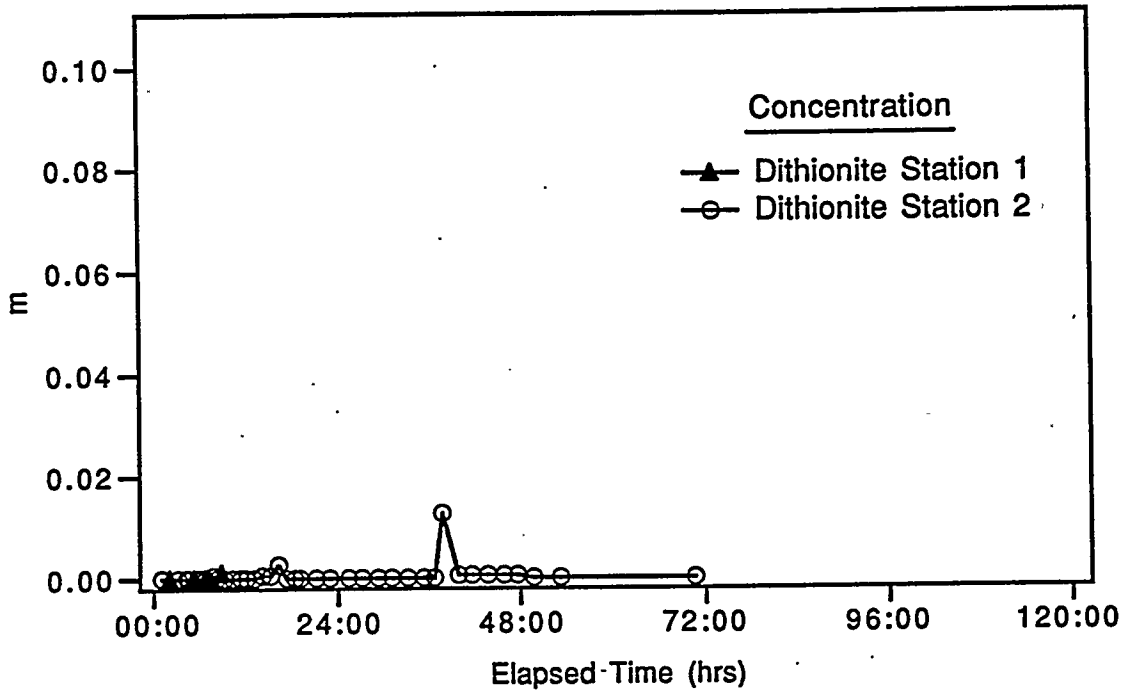
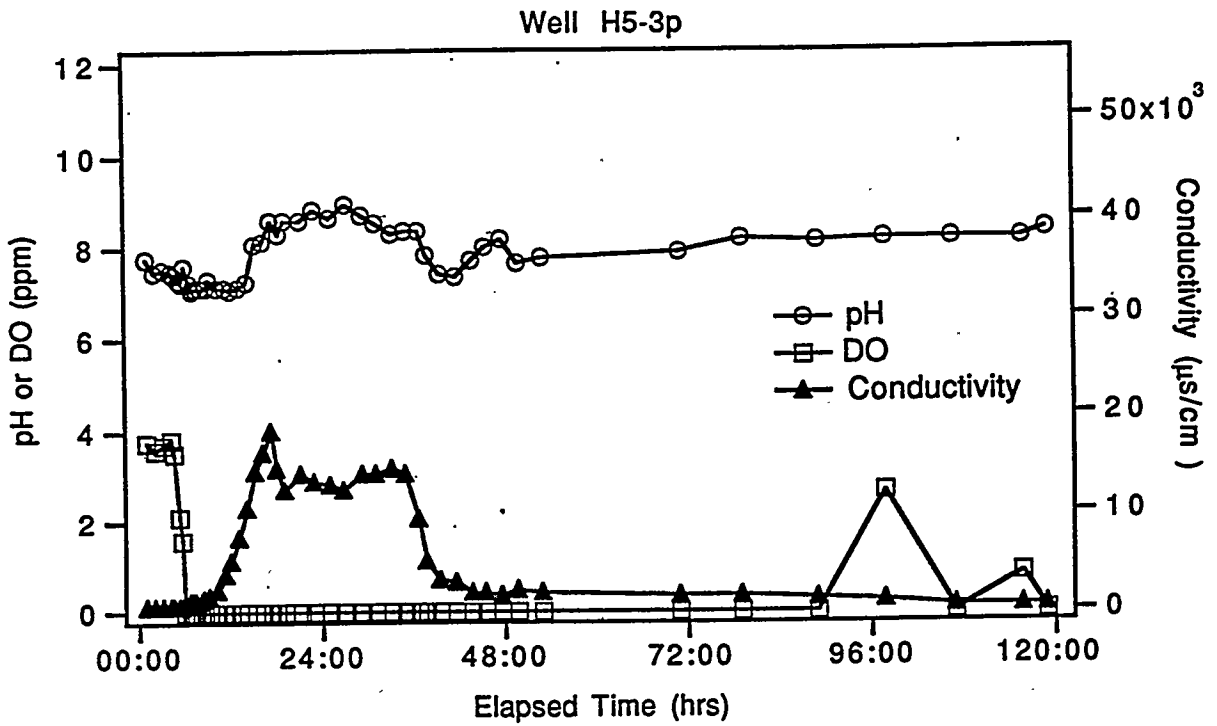


Figure G-9. Measurements for well H5-3p during the ISRM 100-H area injection/withdrawal experiment.

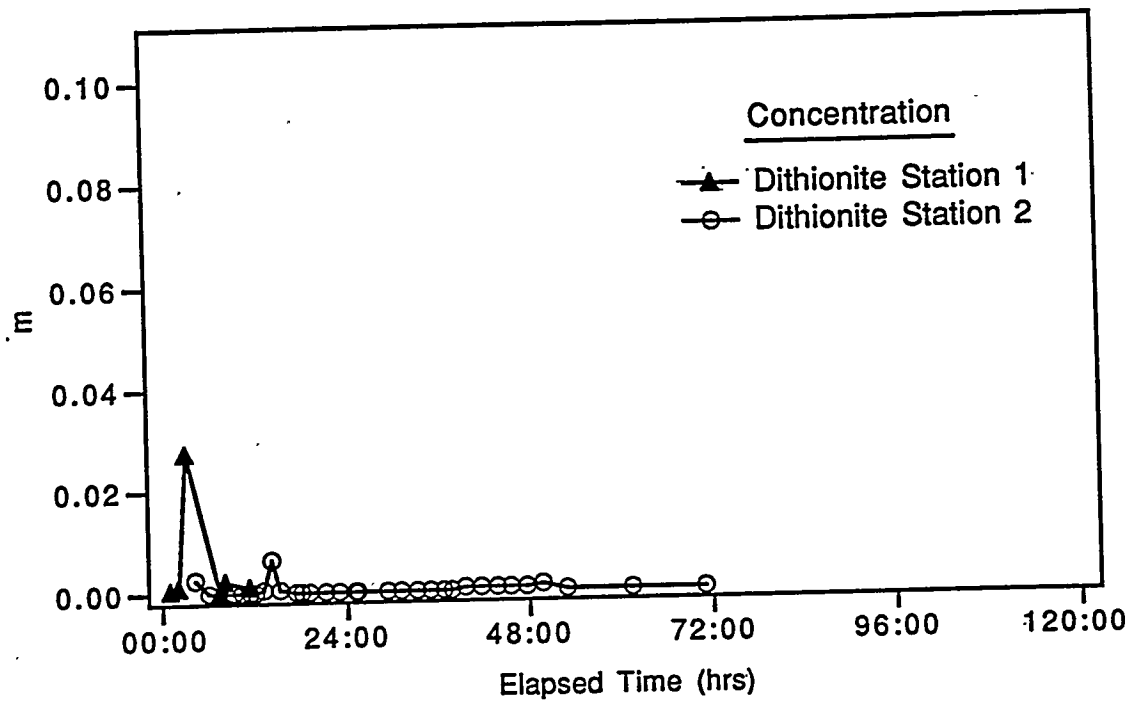
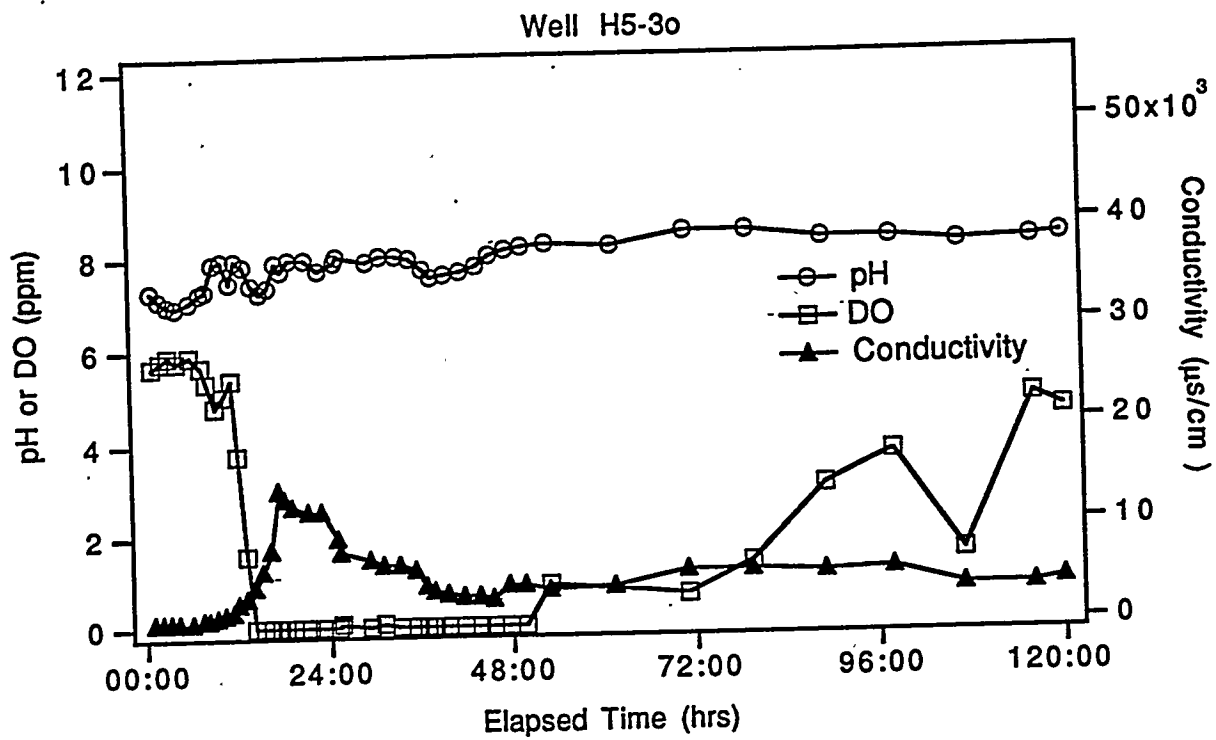


Figure G-10. Measurements for well H5-3o during the ISRM 100-H area injection/withdrawal experiment.

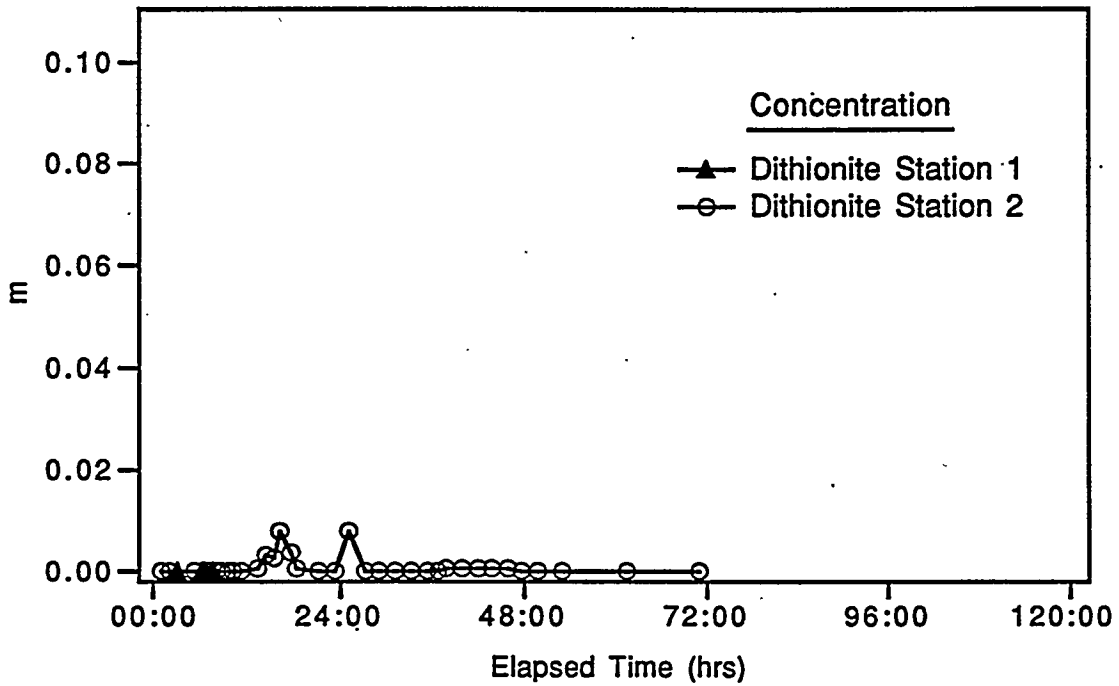
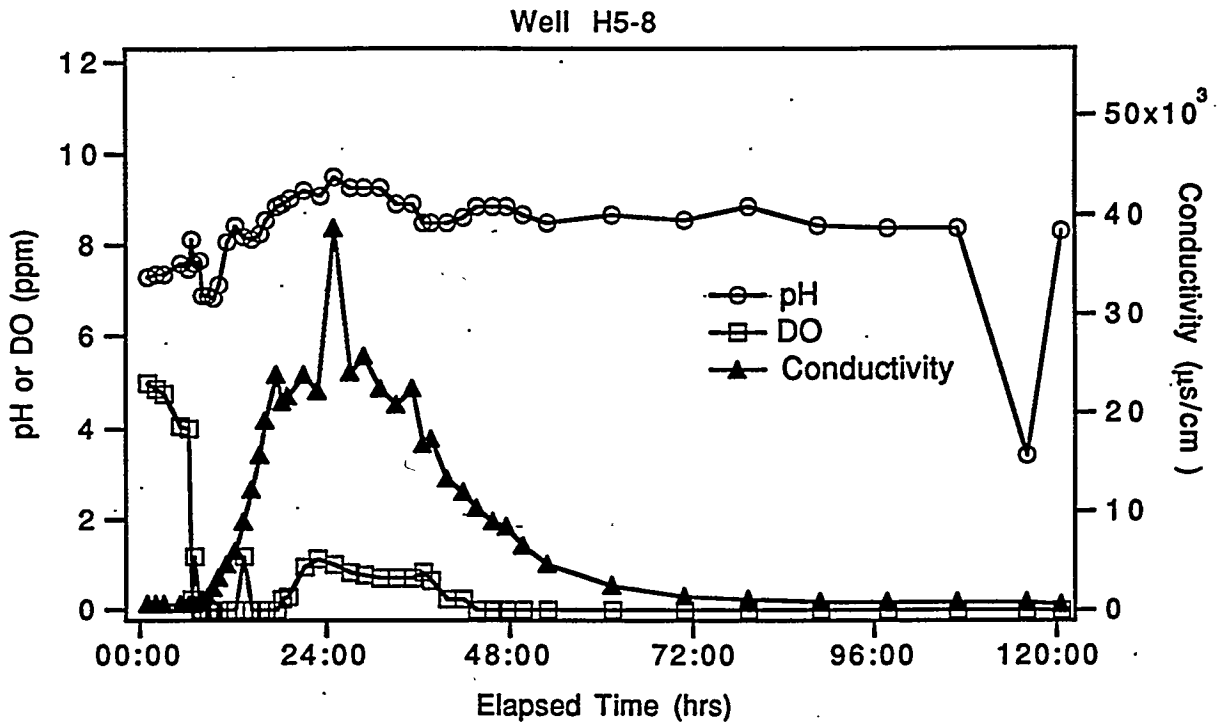


Figure G-11. Measurements for well H5-8 during the ISRM 100-H area injection/withdrawal experiment.

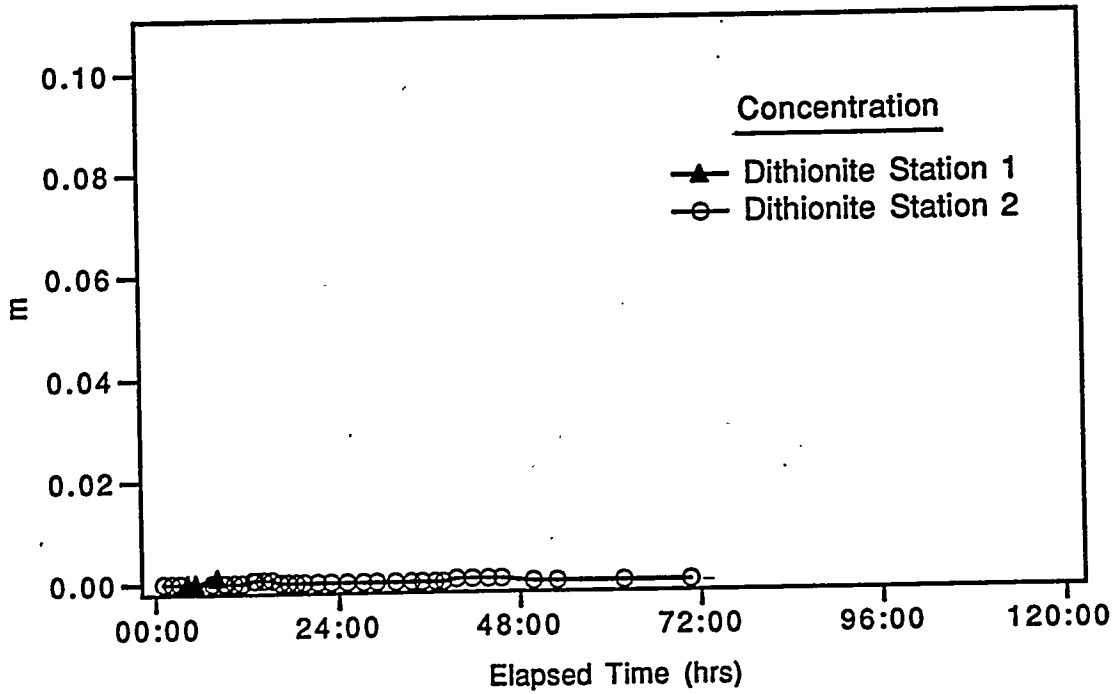
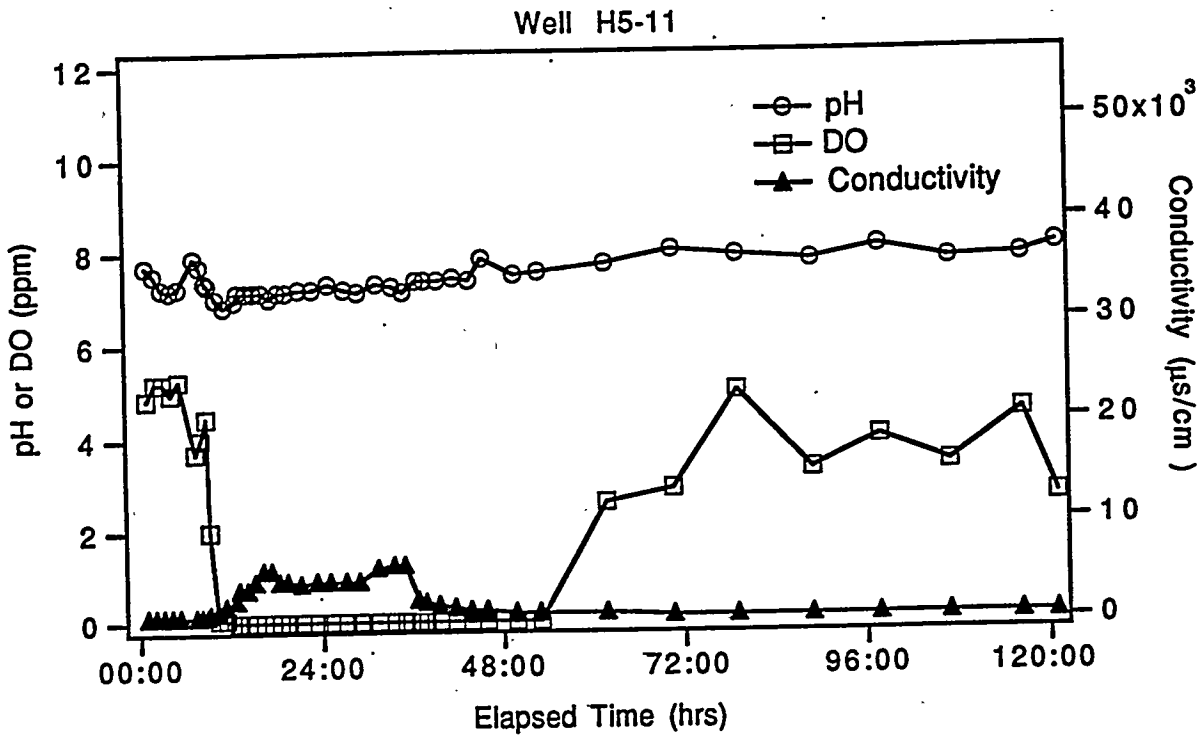


Figure G-12: Measurements for well H5-11 during the ISRM 100-H area injection/withdrawal experiment.

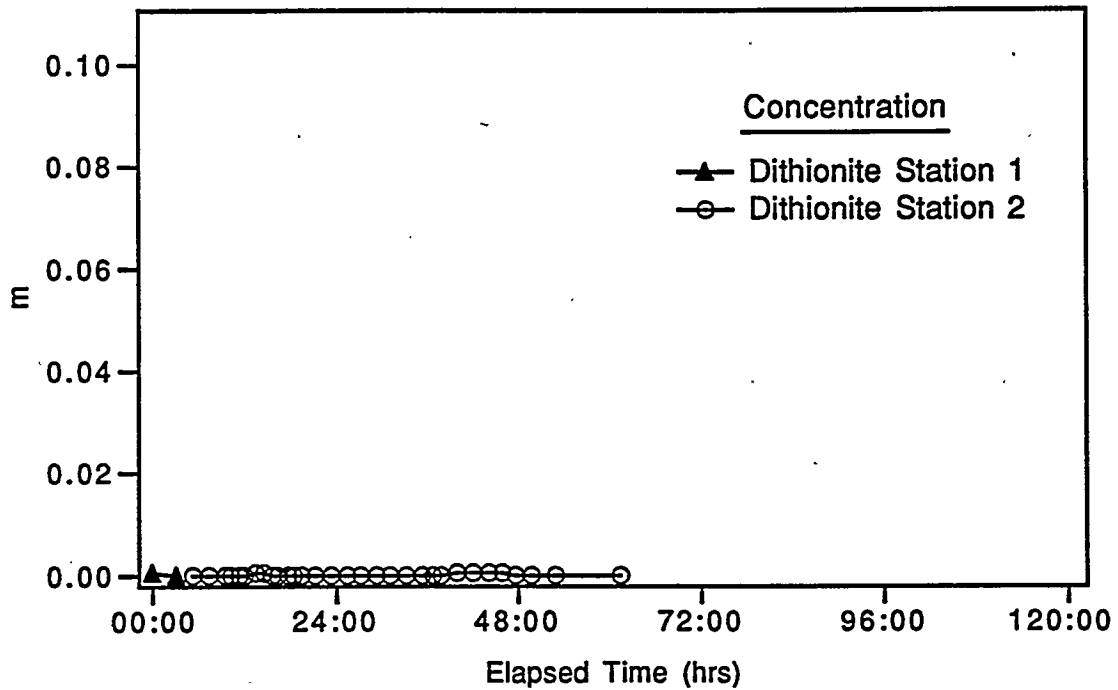
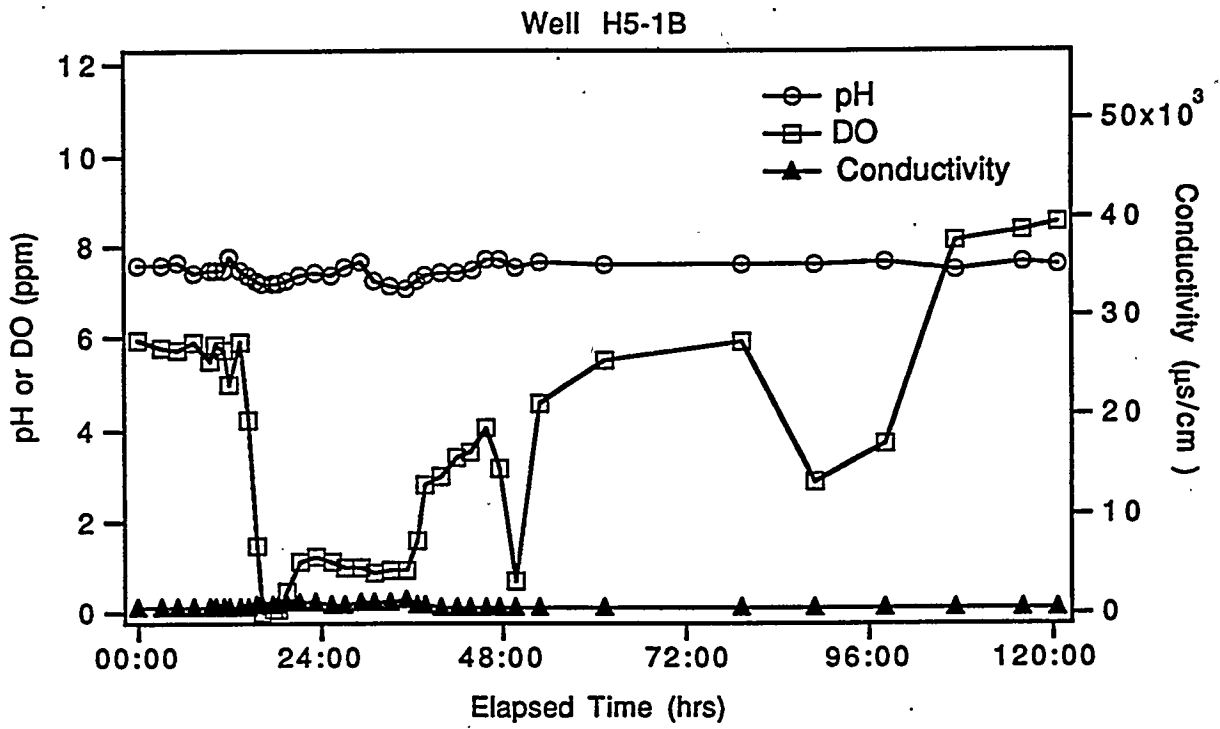
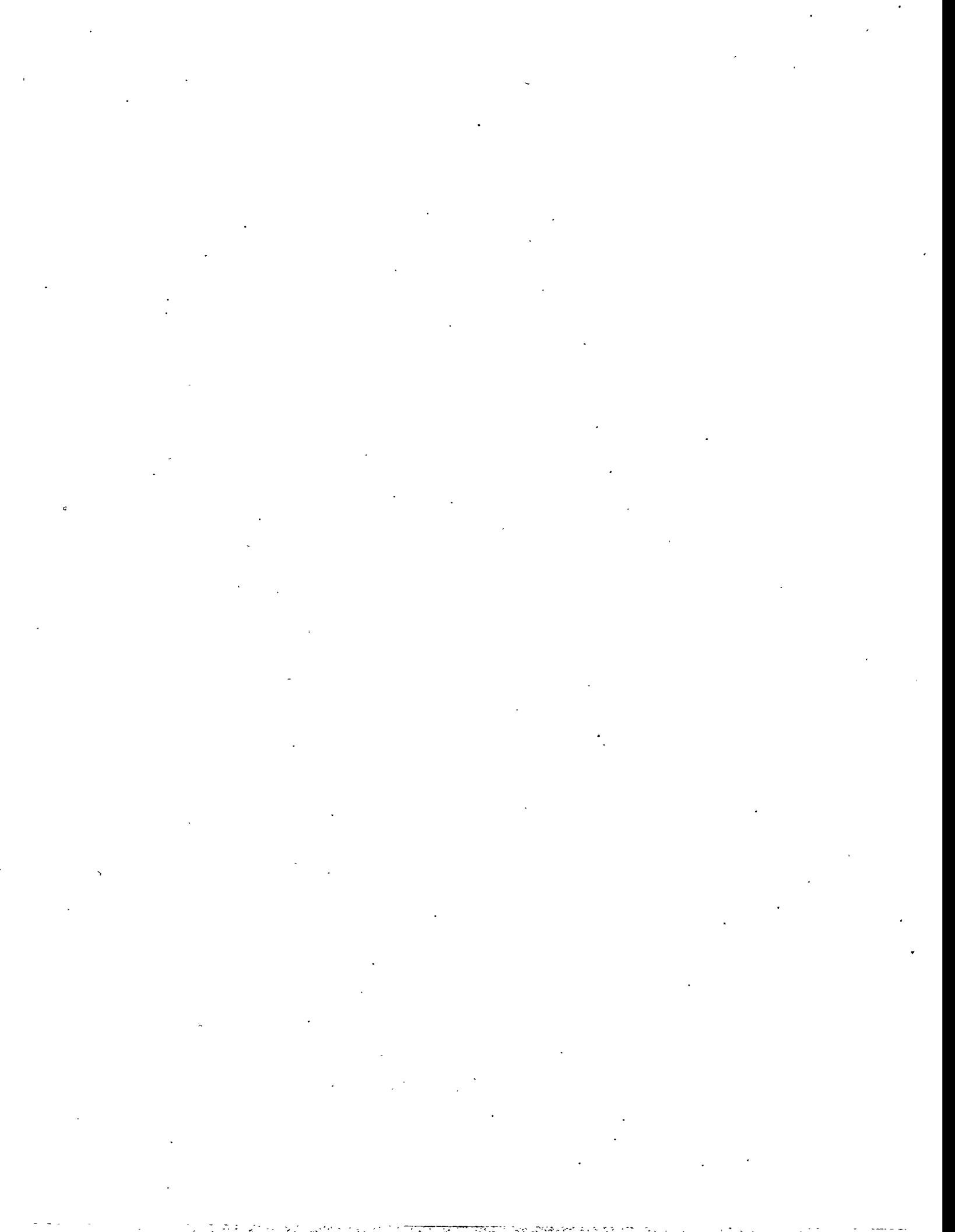


Figure G-13. Measurements for well H5-1B during the ISRM 100-H area injection/withdrawal experiment.

**APPENDIX H**

**FIELD MEASUREMENTS FROM THE POST-EXPERIMENT  
MONITORING OF THE 100-H AREA ISRM SITE**

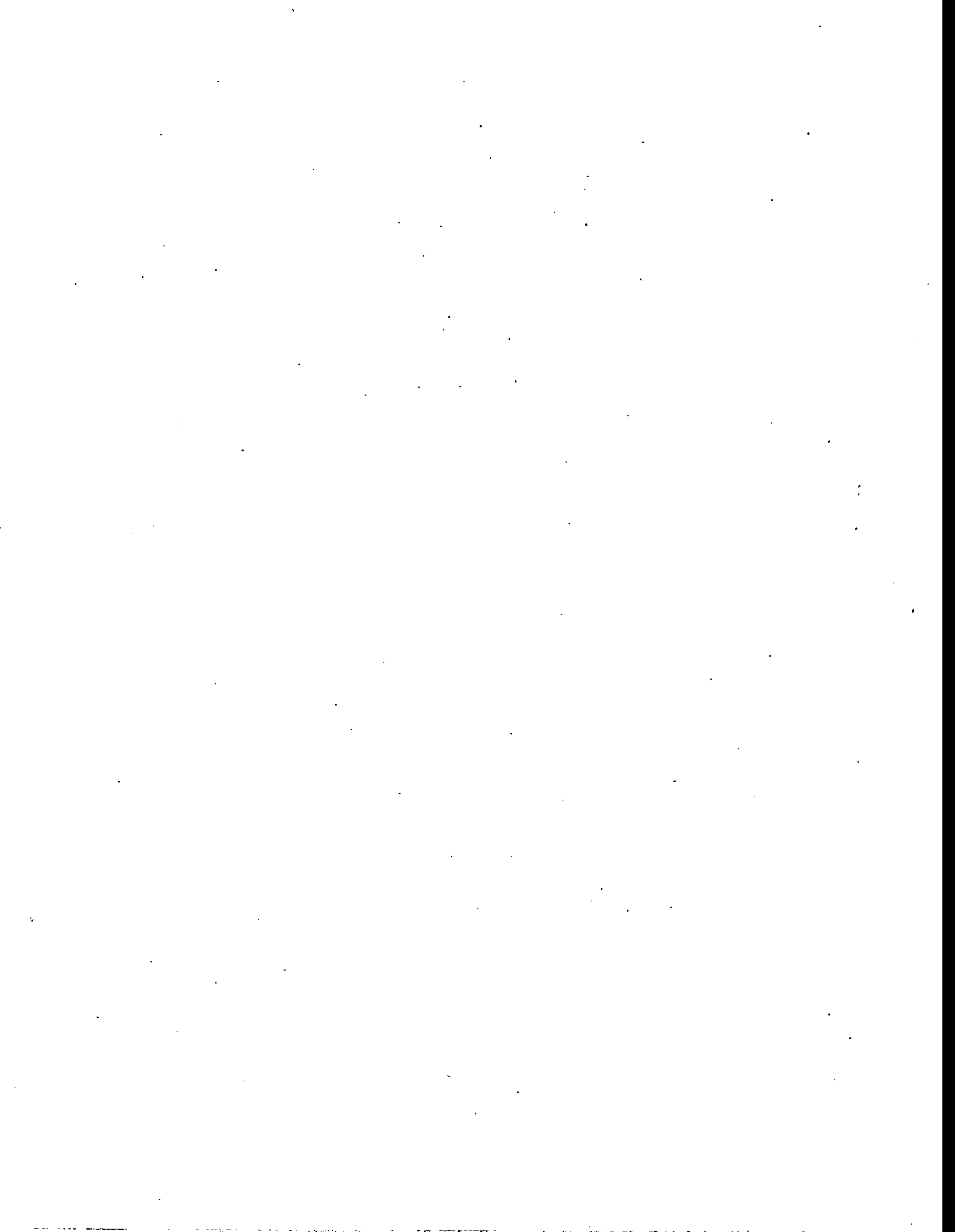


## Table of Contents

Appendix H	Field Measurements from the Post-Experiment Monitoring of the 100-H Area ISRM Site. ....	H.1
------------	--	-----

### List of Figures

Figure H-1.	Field measurements for Well H5-3p during post-experiment monitoring of 100-H area ISRM site. ....	H.2
Figure H-2.	Field measurements for Well H5-3o during post-experiment monitoring of 100-H area ISRM site. ....	H.3
Figure H-3.	Field measurements for Well H5-4p during post-experiment monitoring of 100-H area ISRM site. ....	H.4
Figure H-4.	Field measurements for Well H5-4o during post-experiment monitoring of 100-H area ISRM site. ....	H.5
Figure H-5.	Field Measurements for Well H5-5p during post-experiment monitoring of 100-H area ISRM site. ....	H.6
Figure H-6.	Field Measurements for Well H5-5o during post-experiment monitoring of 100-H area ISRM site. ....	H.7
Figure H-7.	Field Measurements for Well H5-6 during post-experiment monitoring of 100-H area ISRM site. ....	H.8
Figure H-8.	Field Measurements for Well H5-7 during post-experiment monitoring of 100-H area ISRM site. ....	H.9
Figure H-9.	Field Measurements for Well H5-8 during post-experiment monitoring of 100-H area ISRM site. ....	H.10
Figure H-10.	Field Measurements for Well H5-9 during post-experiment monitoring of 100-H area ISRM site. ....	H.11
Figure H-11.	Field Measurements for Well H5-10 during post-experiment monitoring of 100-H area ISRM site. ....	H.12
Figure H-12.	Field Measurements for Well H5-11 during post-experiment monitoring of 100-H area ISRM site. ....	H.13
Figure H-13.	Field Measurements for Well H5-1B during post-experiment monitoring of 100-H area ISRM site. ....	H.14
Figure H-14.	Field Measurements for Well H5-12 during post-experiment monitoring of 100-H area ISRM site. ....	H.15
Figure H-15.	Field Measurements for Well H5-13 during post-experiment monitoring of 100-H area ISRM site. ....	H.16
Figure H-16.	Field Measurements for Well H5-14 during post-experiment monitoring of 100-H area ISRM site. ....	H.17
Figure H-17.	Field Measurements for Well H5-15 during post-experiment monitoring of 100-H area ISRM site. ....	H.18
Figure H-18.	Field Measurements for Well H5-2 during post-experiment monitoring of 100-H area ISRM site. ....	H.19



## **Appendix H. Field Measurements from the Post-Experiment Monitoring of the 100-H Area ISRM Site**

This appendix contains the post-experiment monitoring field measurements (ph, Conductivity, dissolved oxygen, and hexavalent chromium) for all the monitoring wells of the 100-H Area ISRM Site. Note: Hexavalent chromium measurements for the date 1/9/96 are actually total chromium measured from ICP/MS.

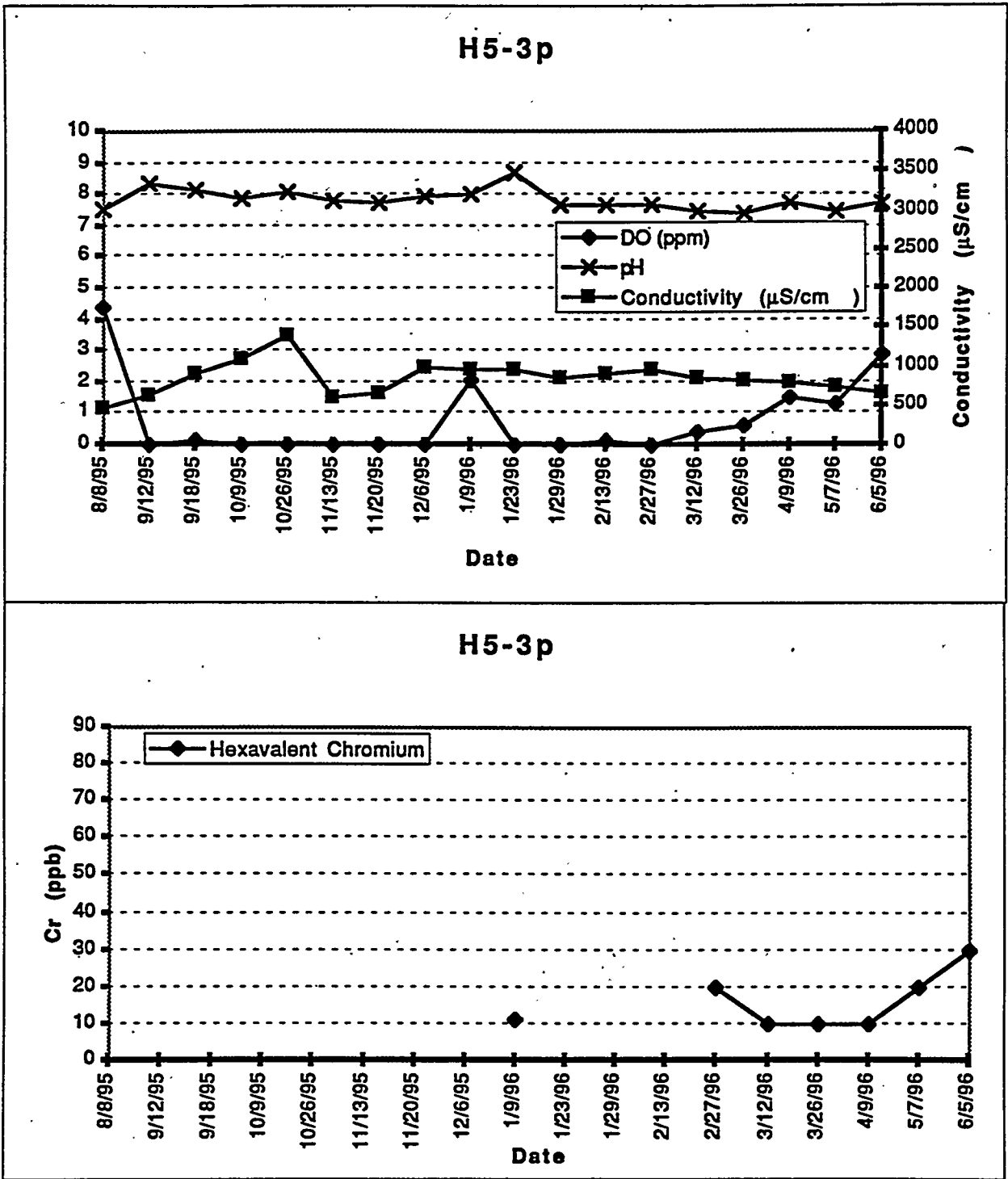


Figure H-1. Field measurements for Well H5-3p during post-experiment monitoring of 100-H area ISRM site.

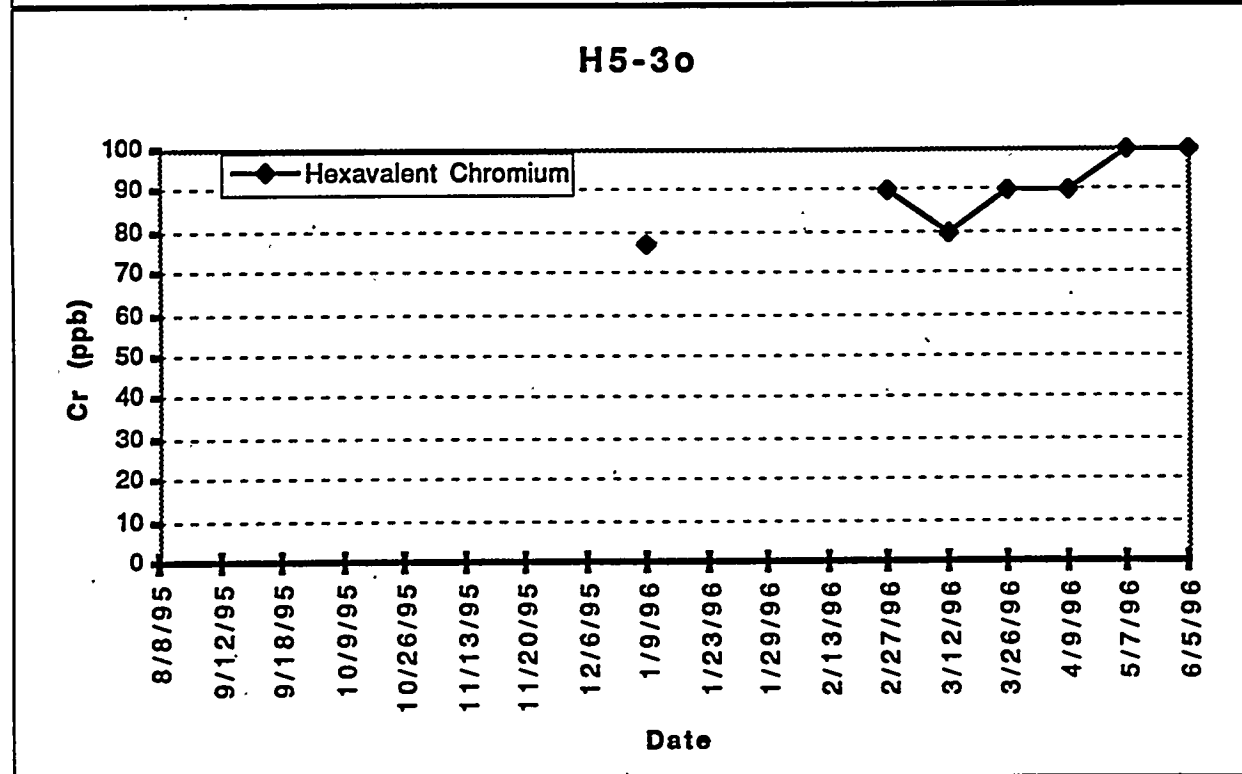
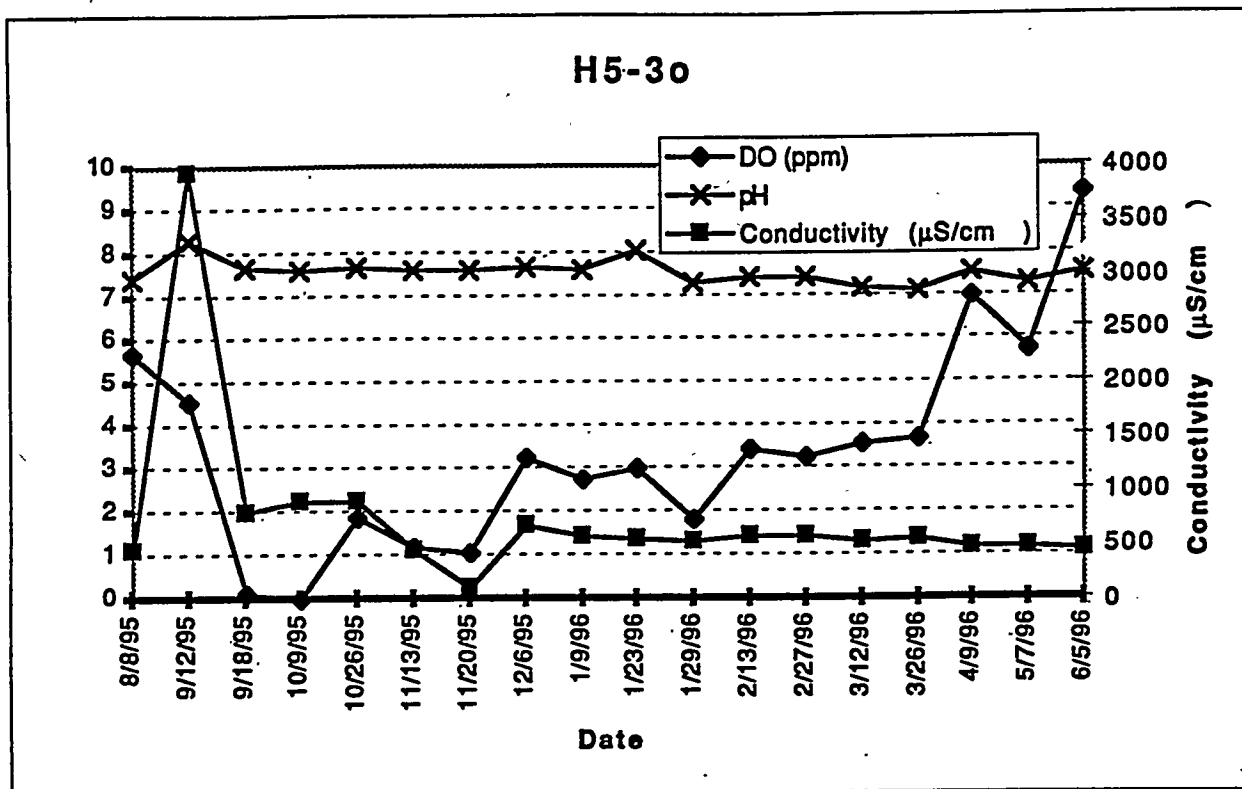


Figure H-2. Field measurements for Well H5-3o during post-experiment monitoring of 100-H area ISRM site.

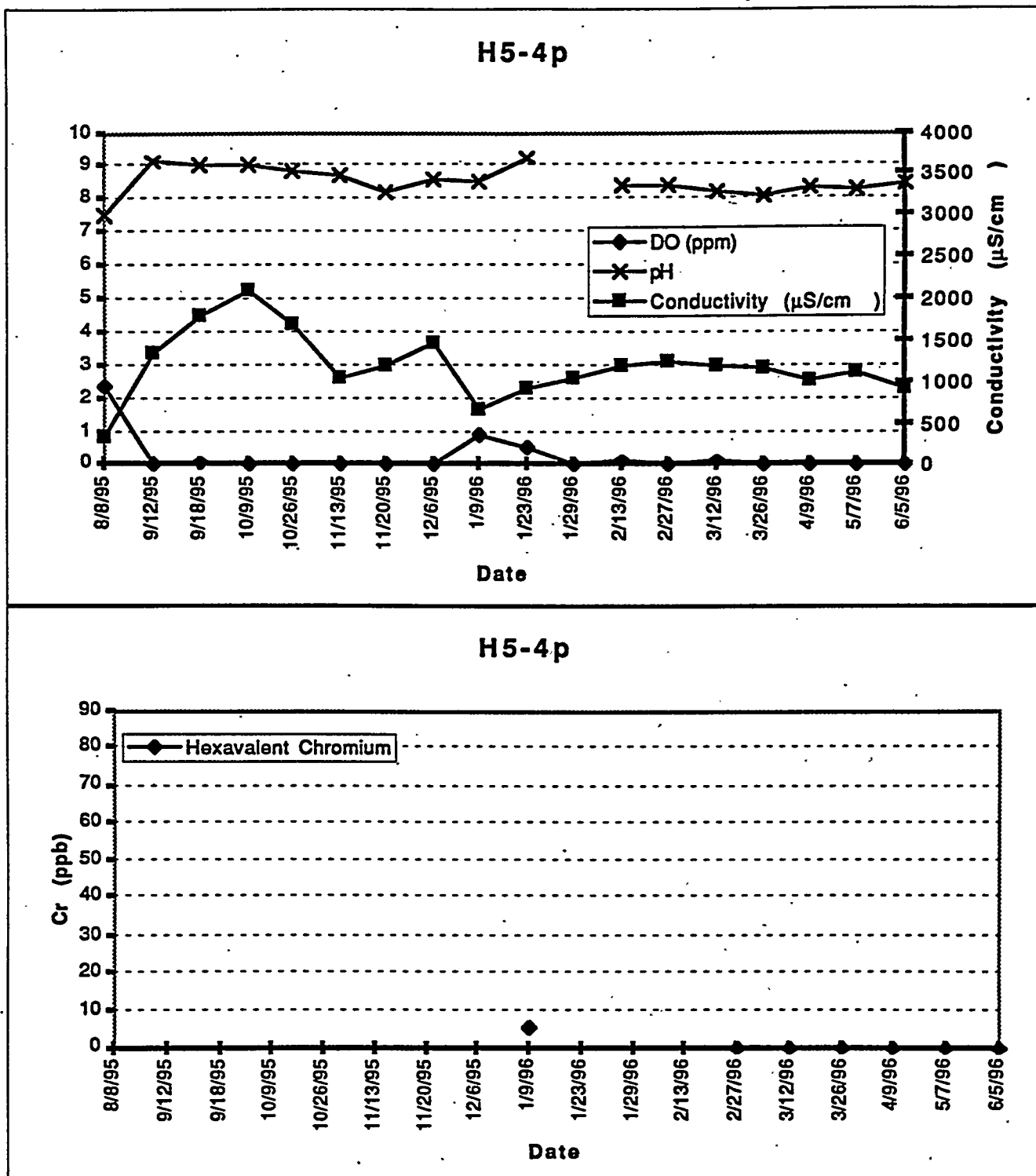


Figure H-3. Field measurements for Well H5-4p during post-experiment monitoring of 100-H area ISRM site.

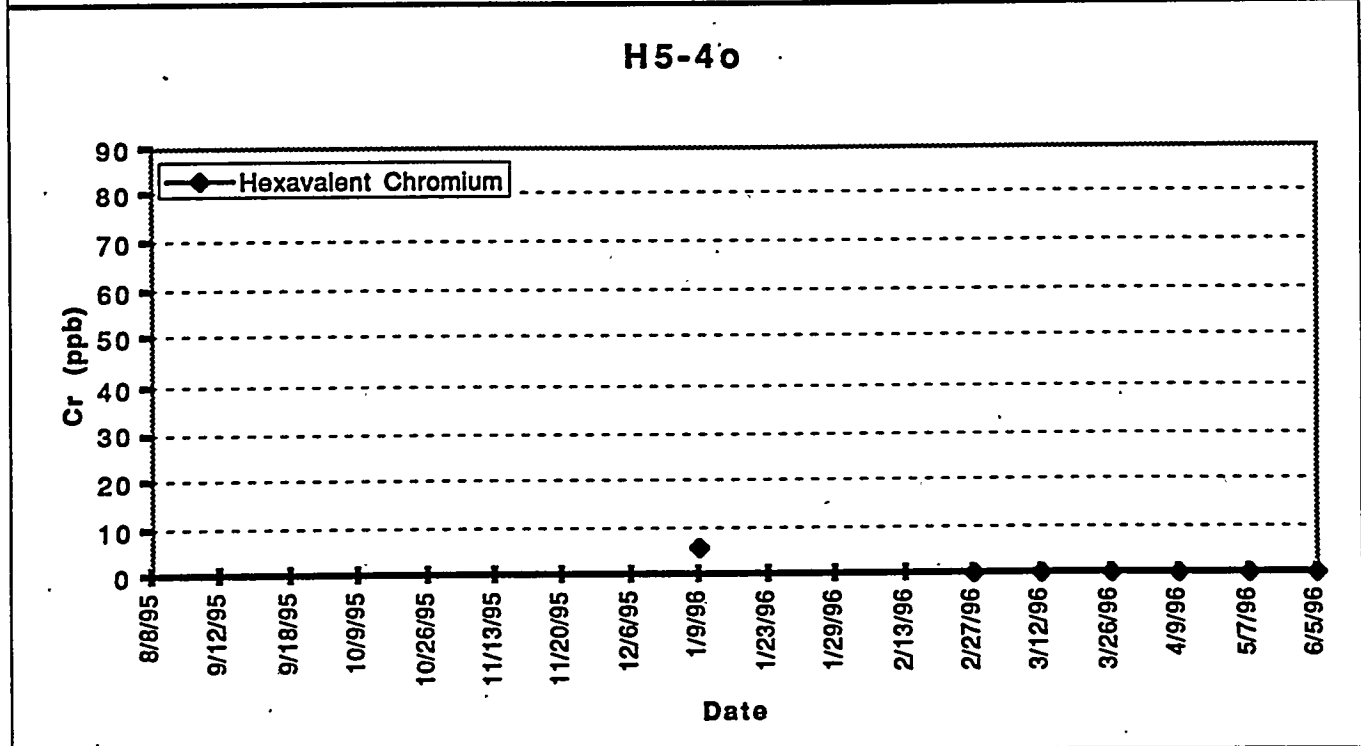
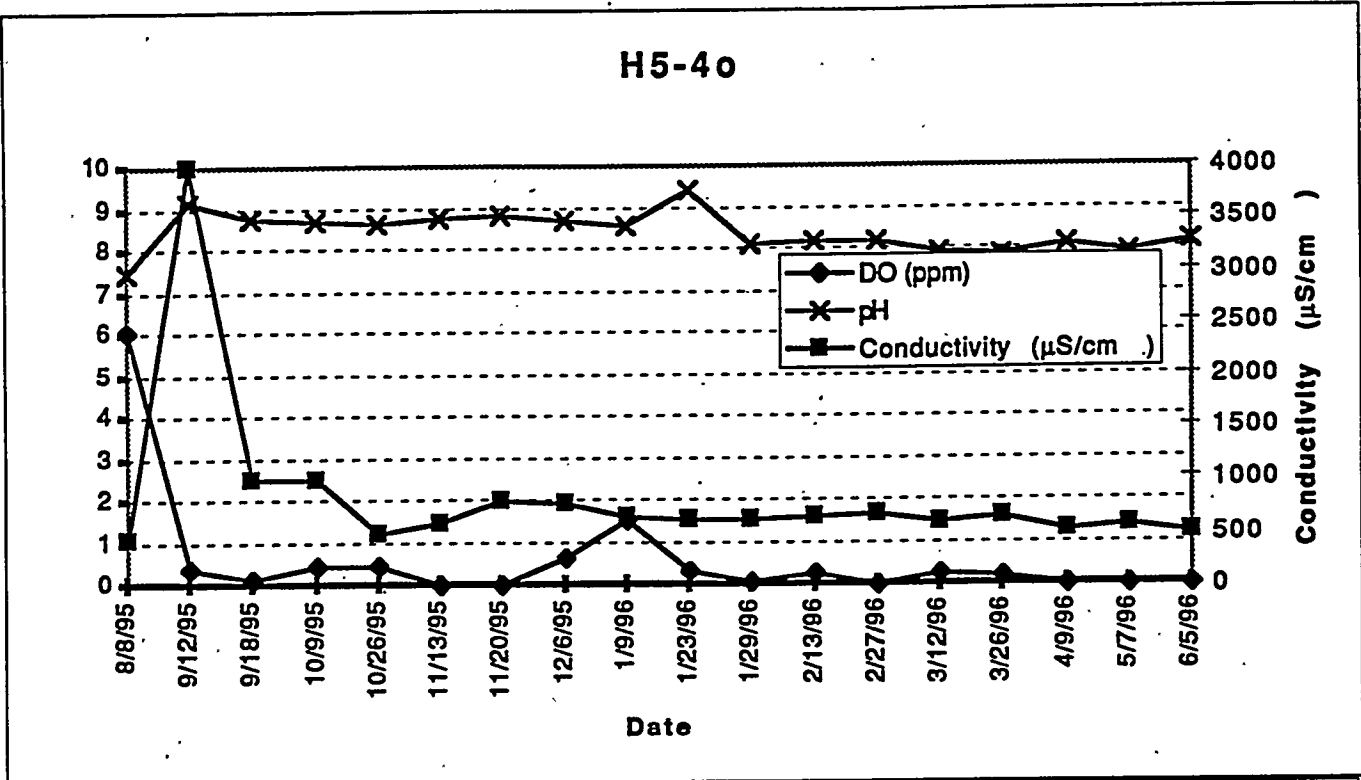


Figure H-4. Field measurements for Well H5-4o during post-experiment monitoring of 100-H area ISRM site.

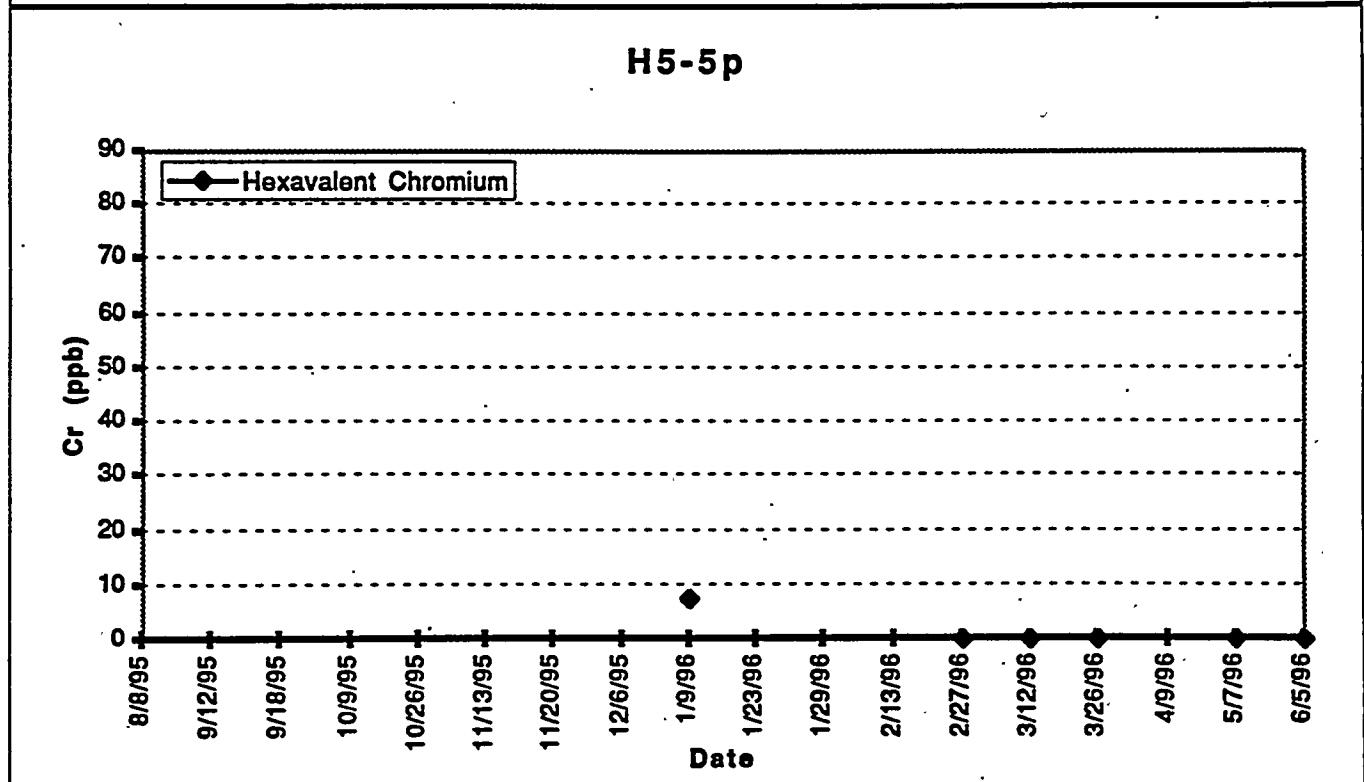
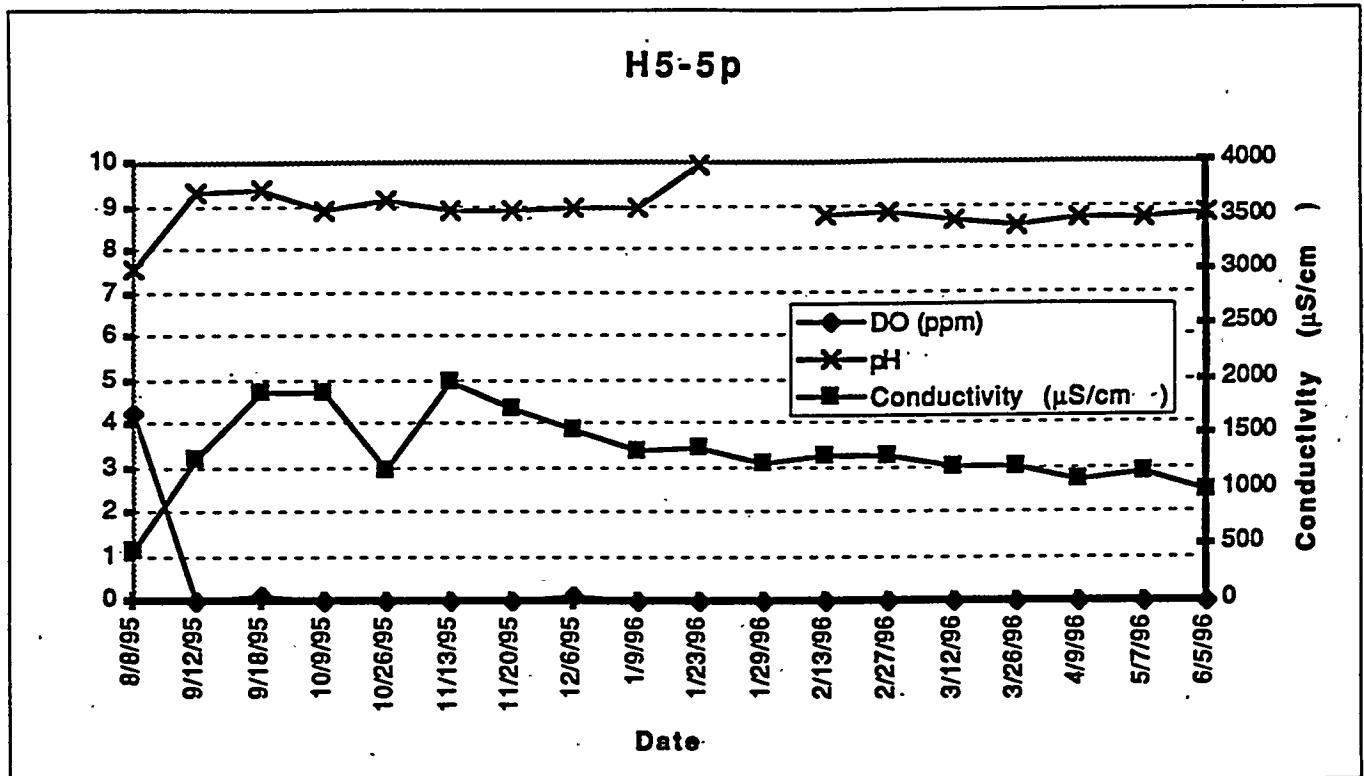
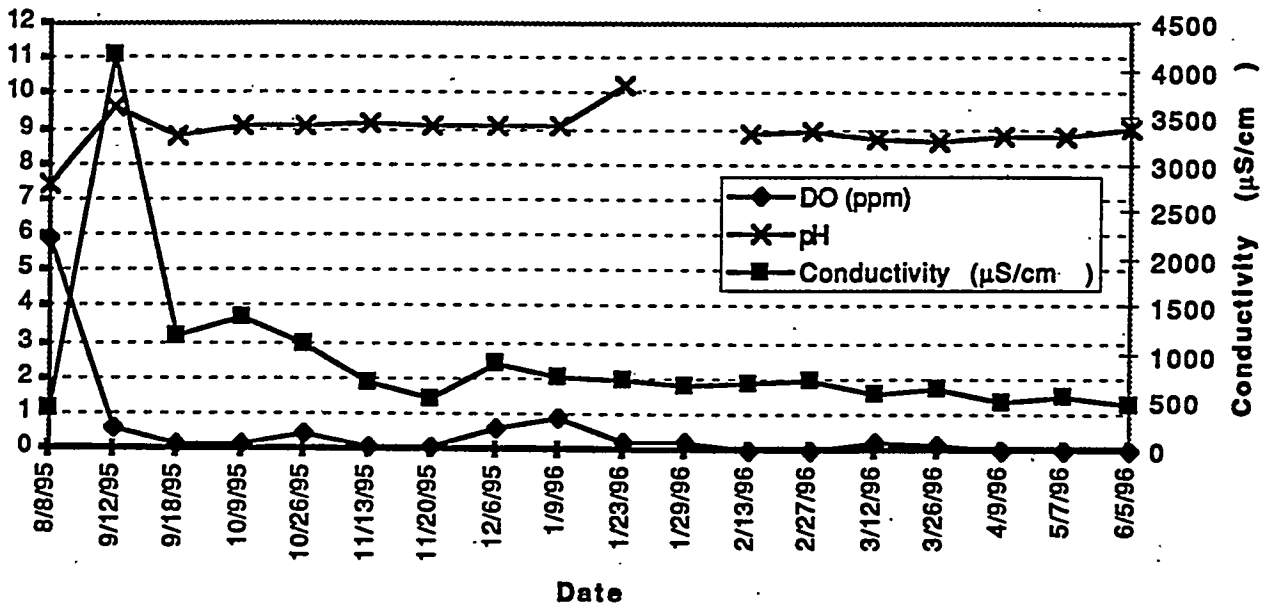


Figure H-5. Field Measurements for Well H5-5p during post-experiment monitoring of 100-H area ISRM site.

### H5-50



### H5-50

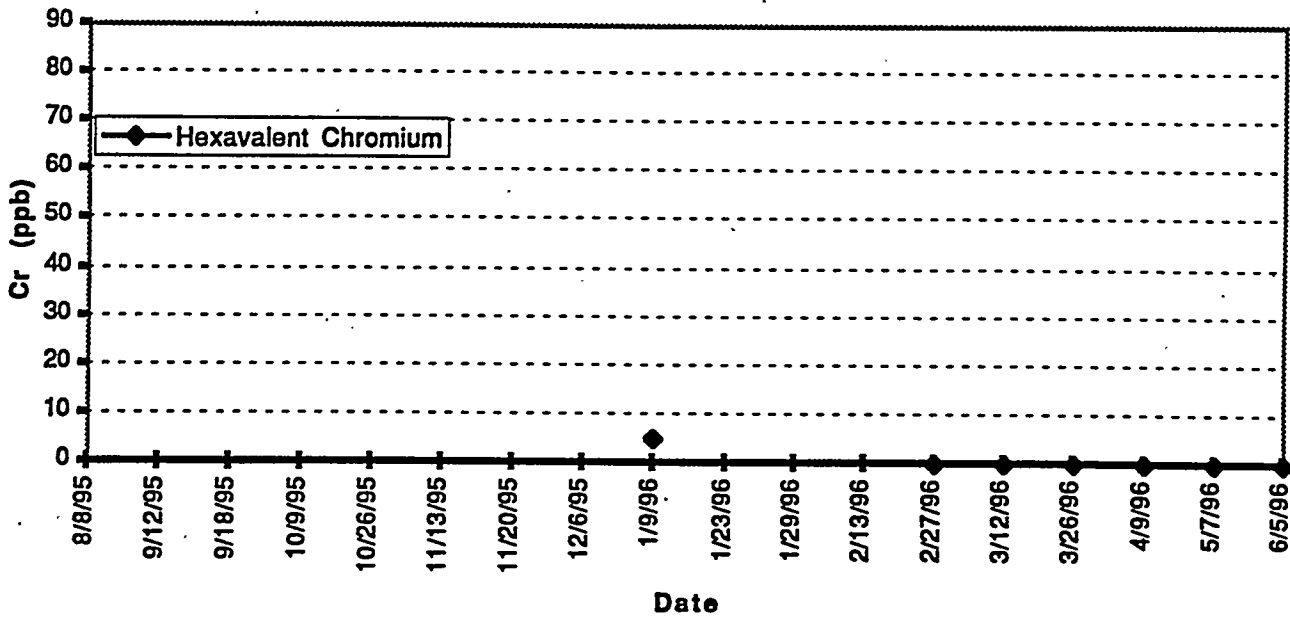


Figure H-6. Field Measurements for Well H5-50 during post-experiment monitoring of 100-H area ISRM site.

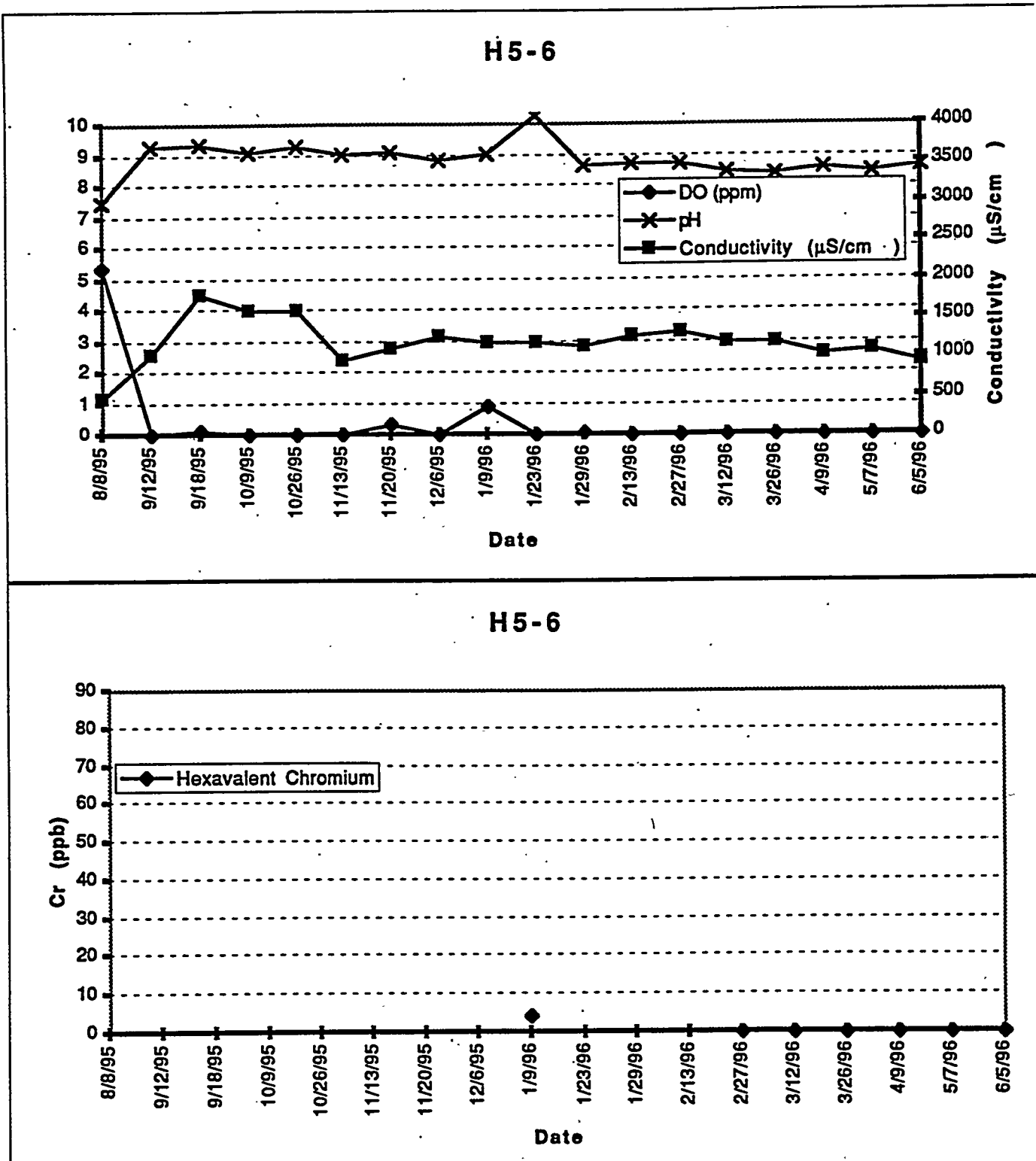
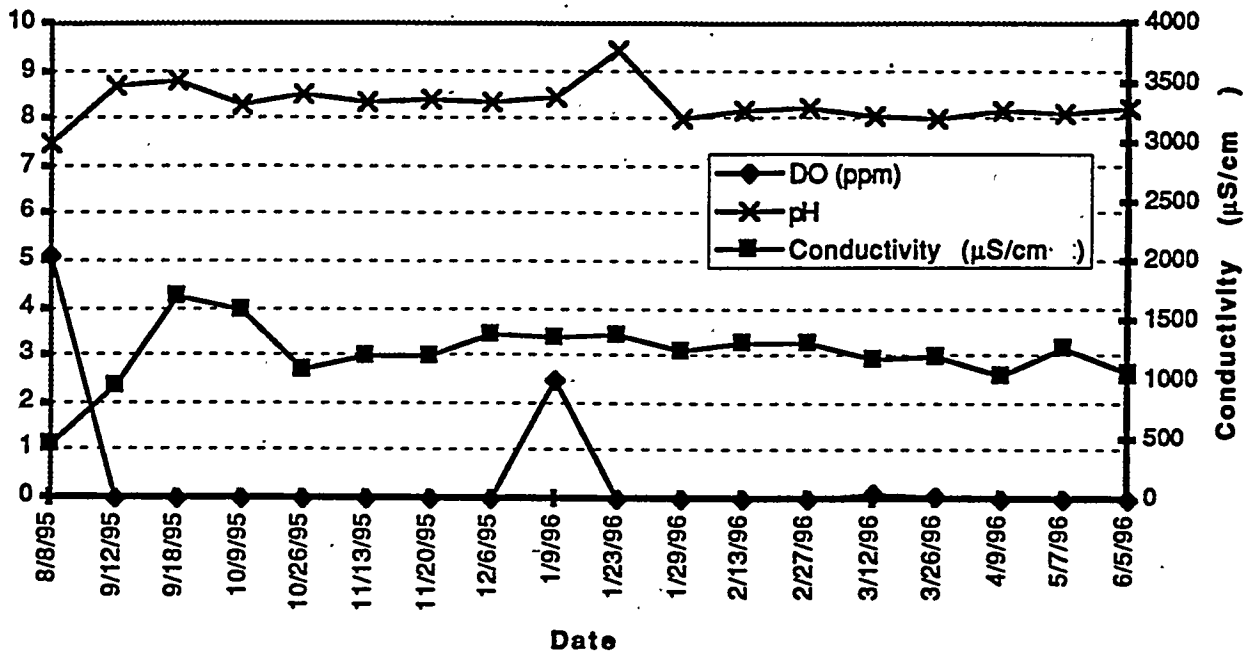


Figure H-7. Field Measurements for Well H5-6 during post-experiment monitoring of 100-H area ISRM site.

### H5-7



### H5-7

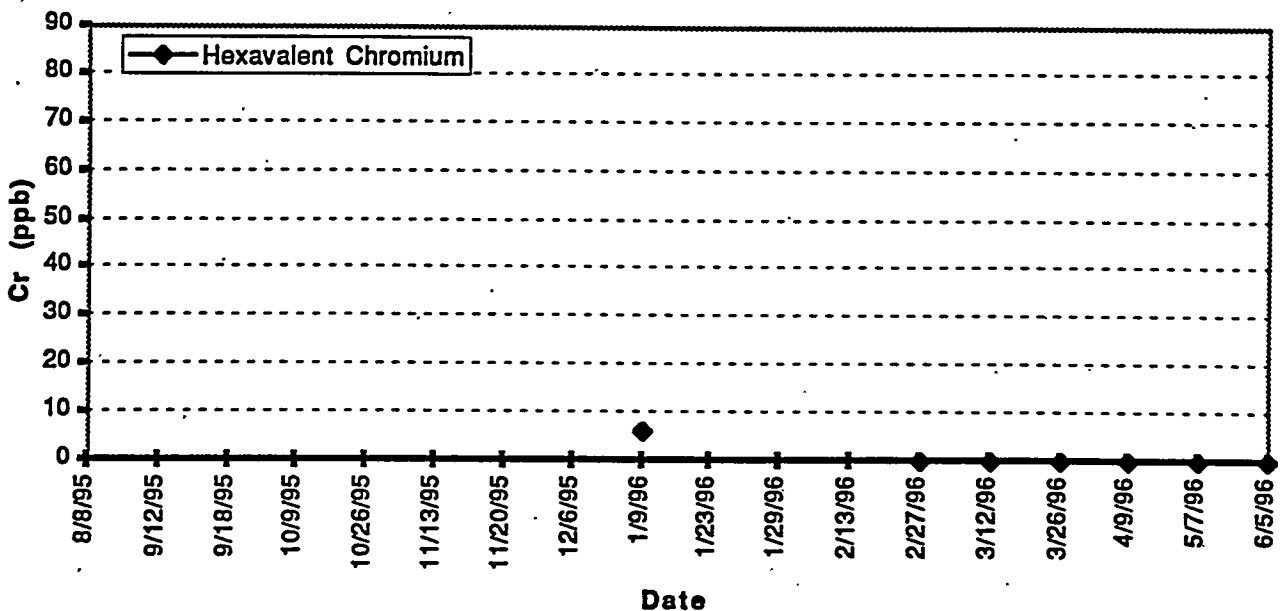


Figure H-8. Field Measurements for Well H5-7 during post-experiment monitoring of 100-H area ISRM site.

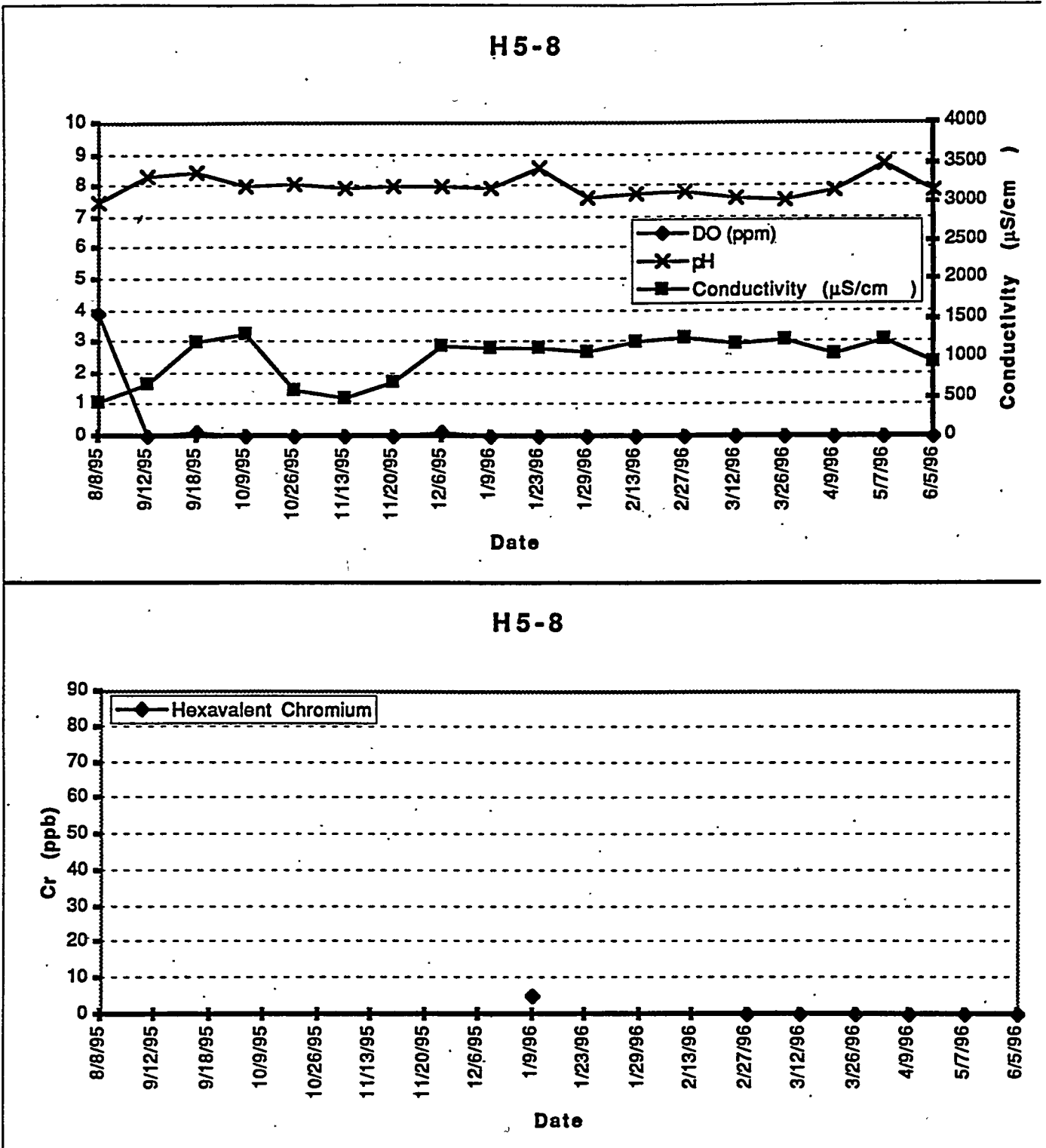
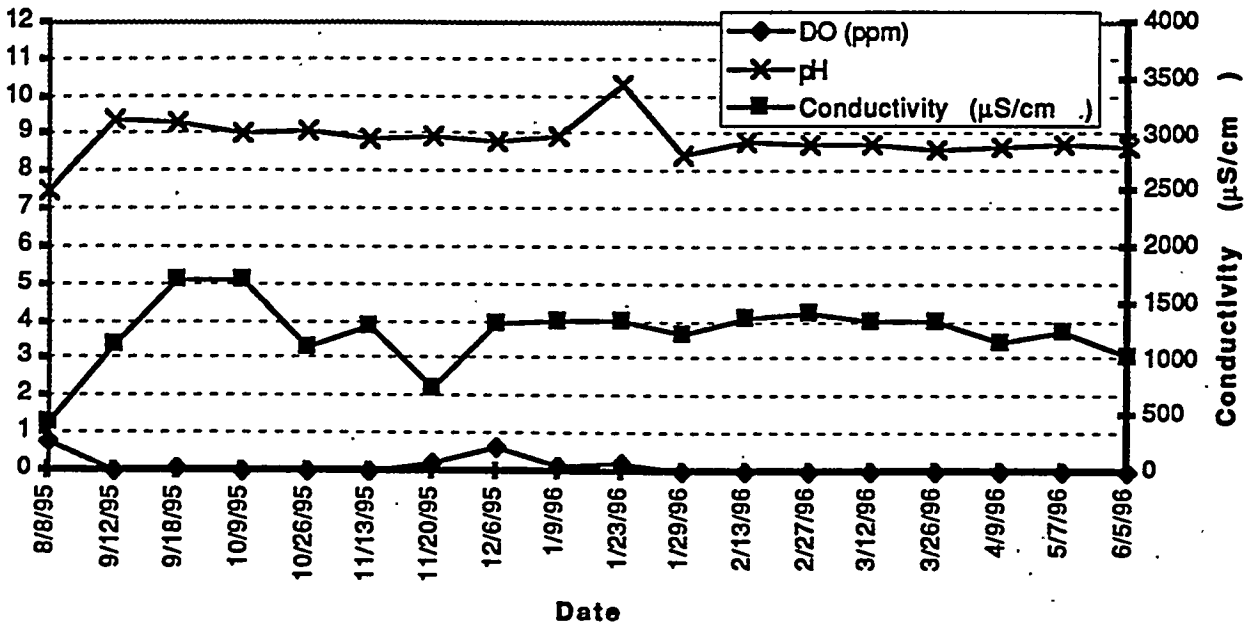


Figure H-9. Field Measurements for Well H5-8 during post-experiment monitoring of 100-H area ISRM site.

### H5-9



### H5-9

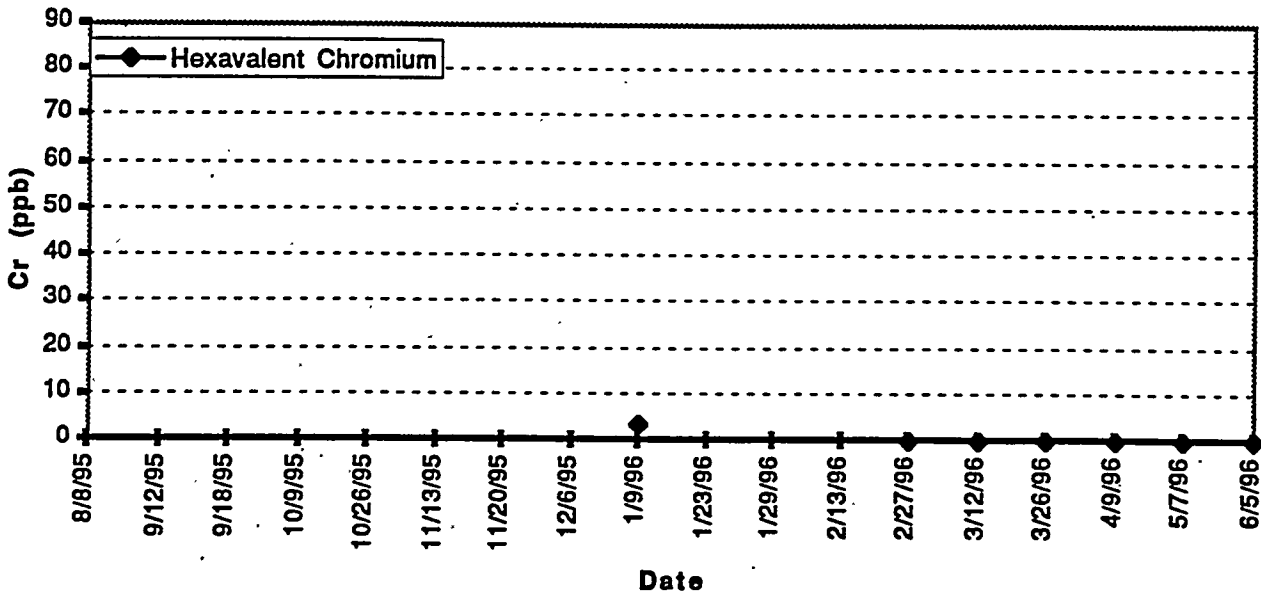


Figure H-10. Field Measurements for Well H5-9 during post-experiment monitoring of 100-H area ISRM site.

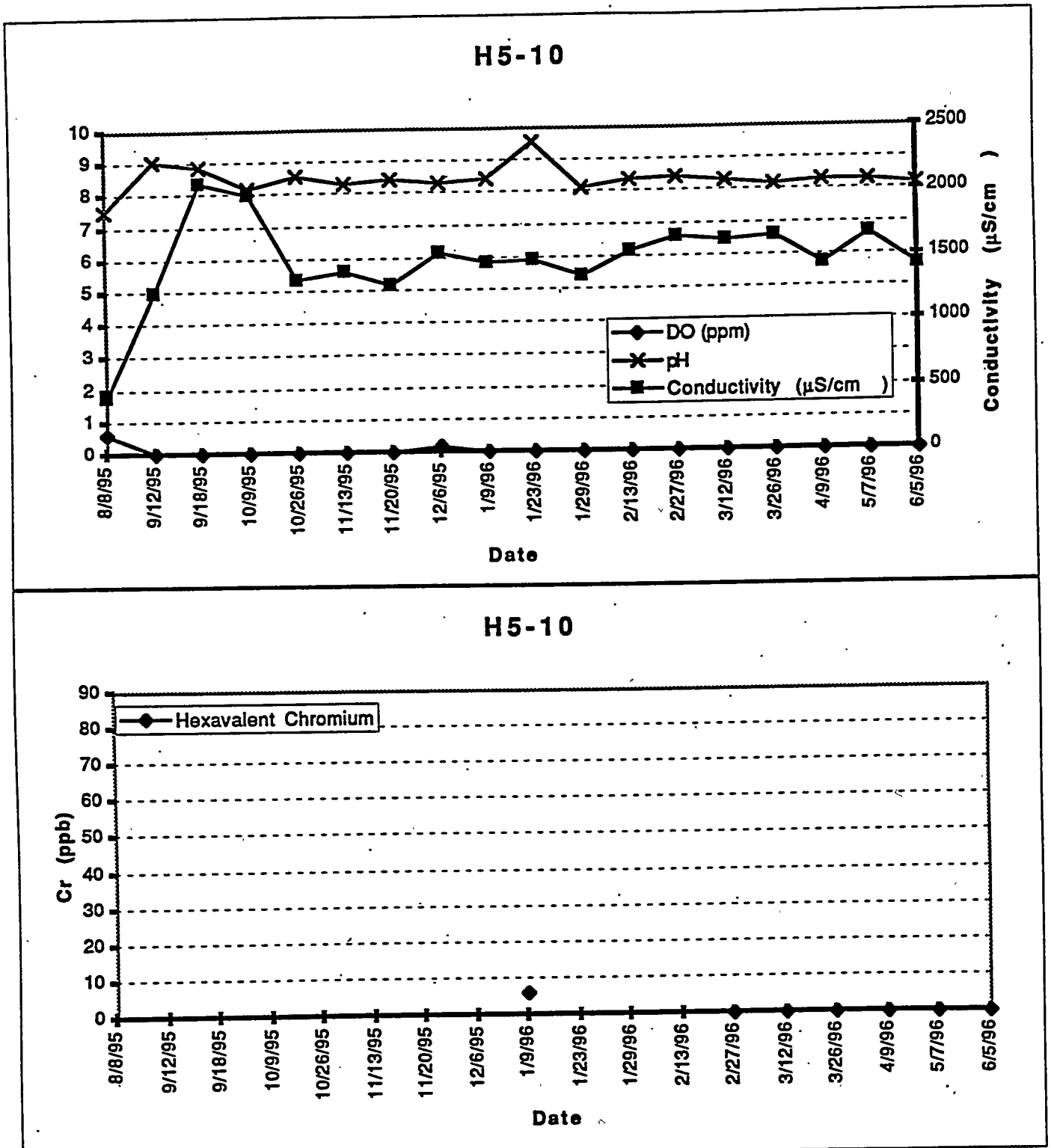
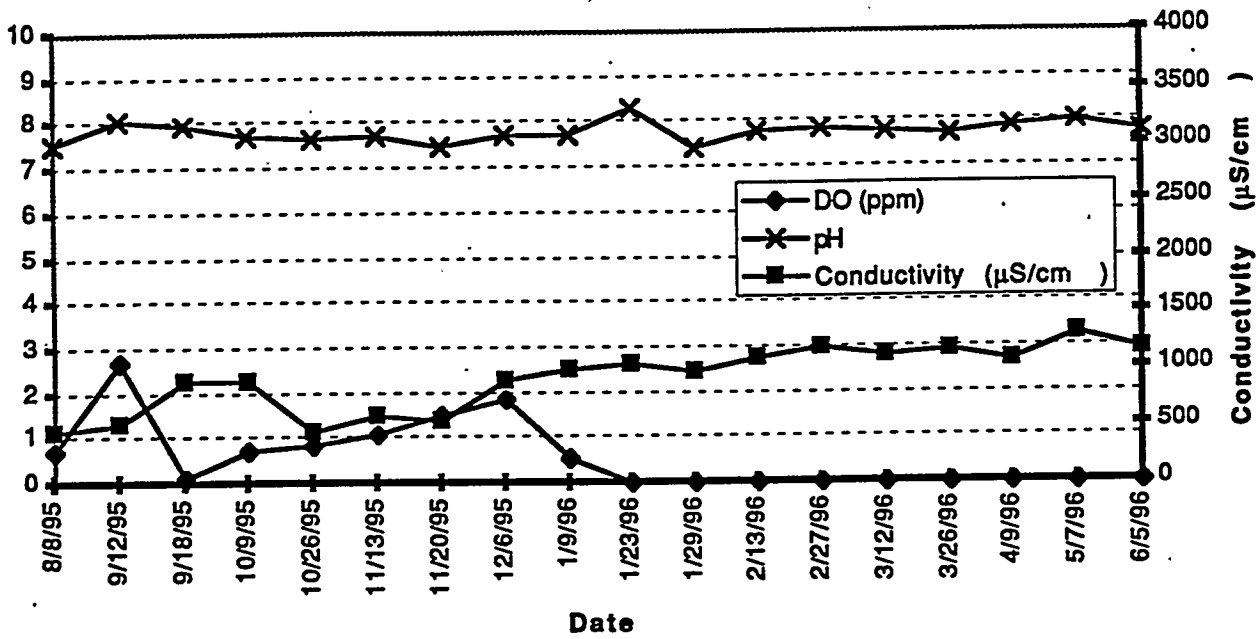


Figure H-11. Field Measurements for Well H5-10 during post-experiment monitoring of 100-H area ISRM site.

### H5-11



### H5-11

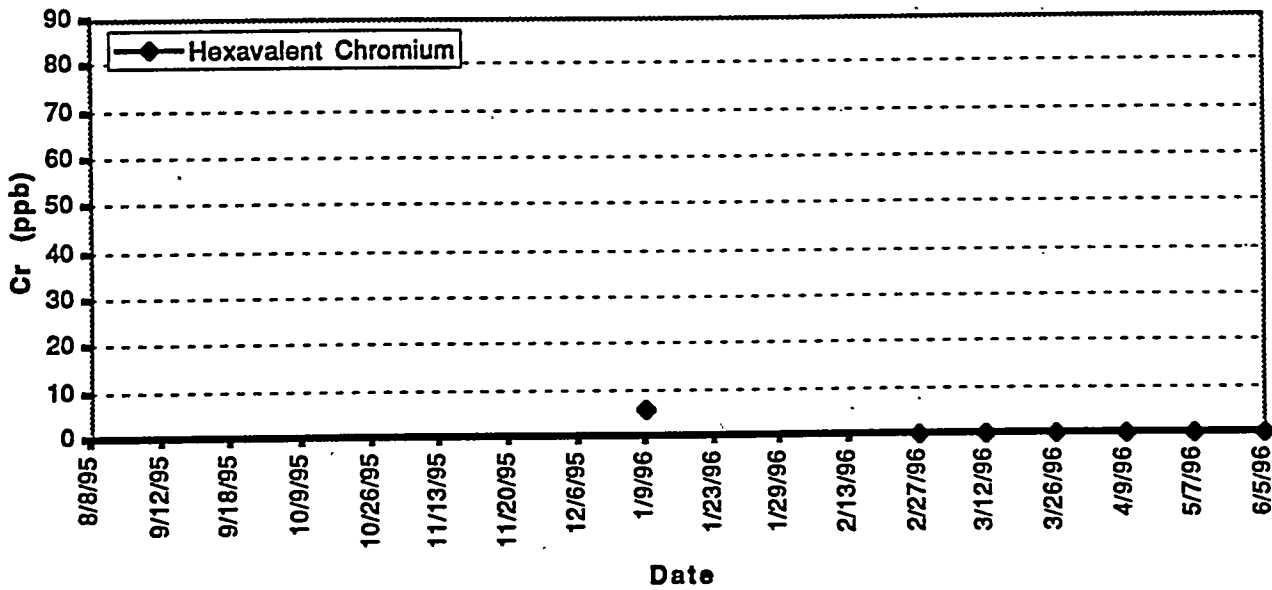


Figure H-12. Field Measurements for Well H5-11 during post-experiment monitoring of 100-H area ISRM site.

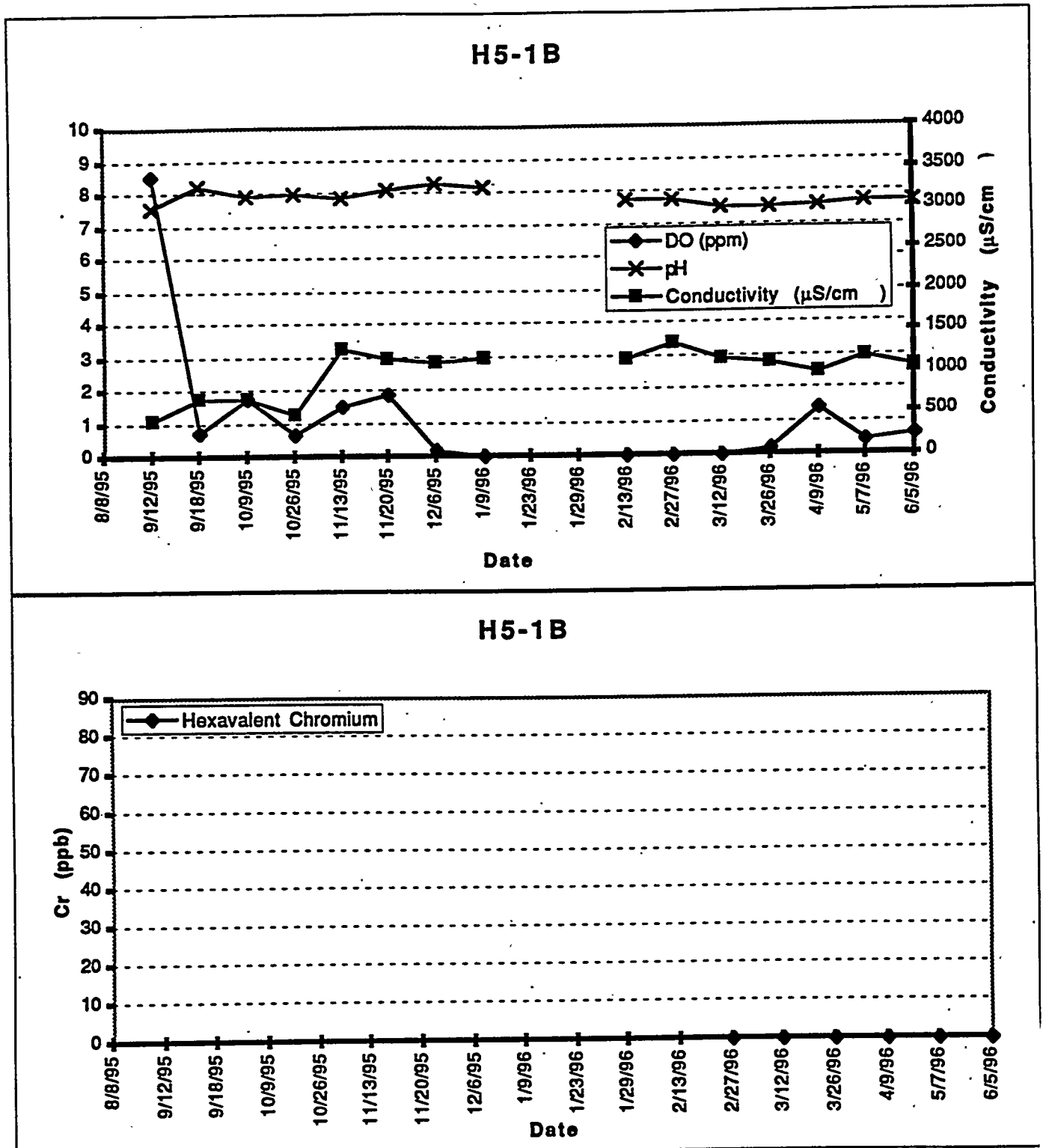
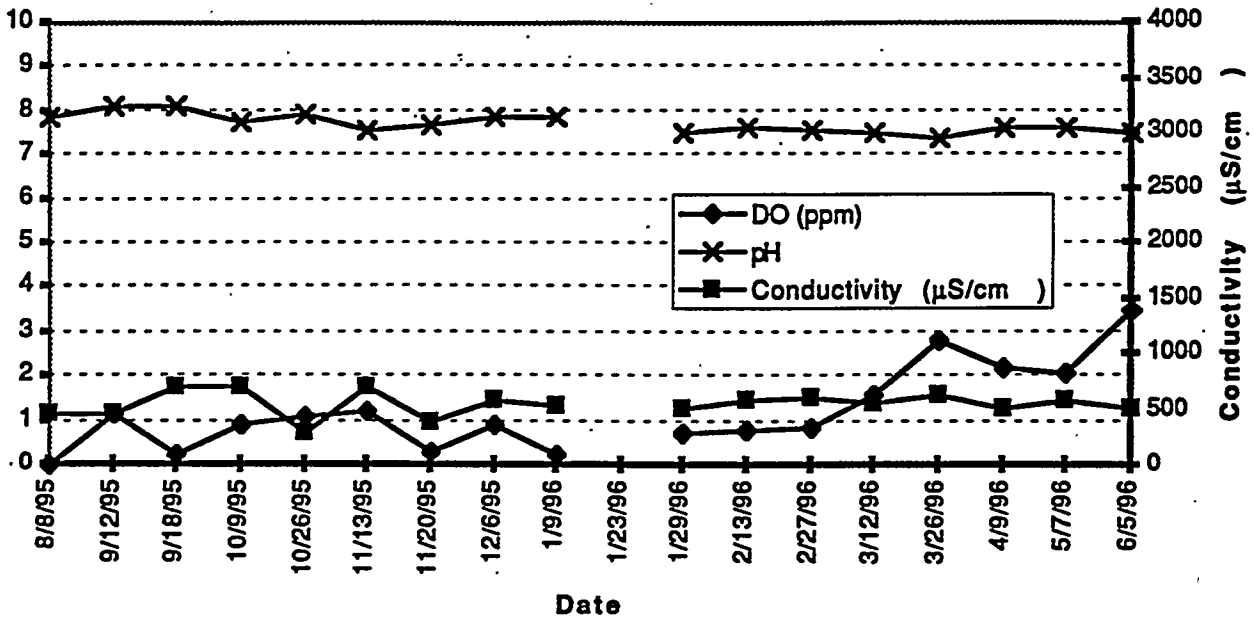


Figure H-13. Field Measurements for Well H5-1B during post-experiment monitoring of 100-H area ISRM site.

### H5-12



### H5-12

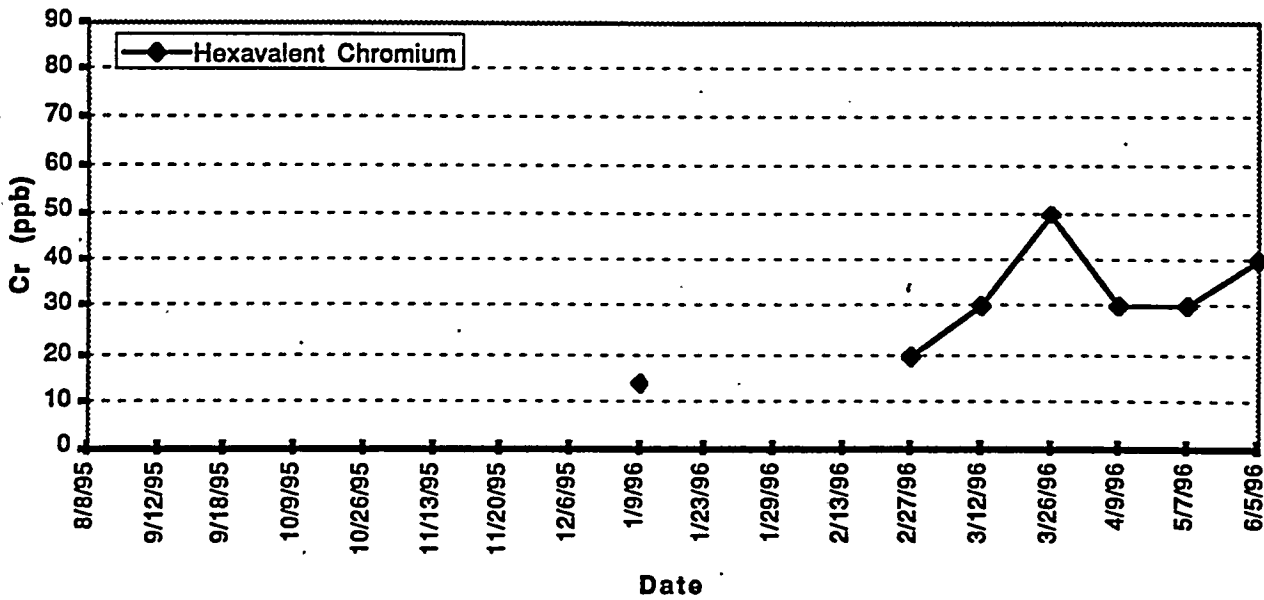


Figure H-14. Field Measurements for Well H5-12 during post-experiment monitoring of 100-H area ISRM site.

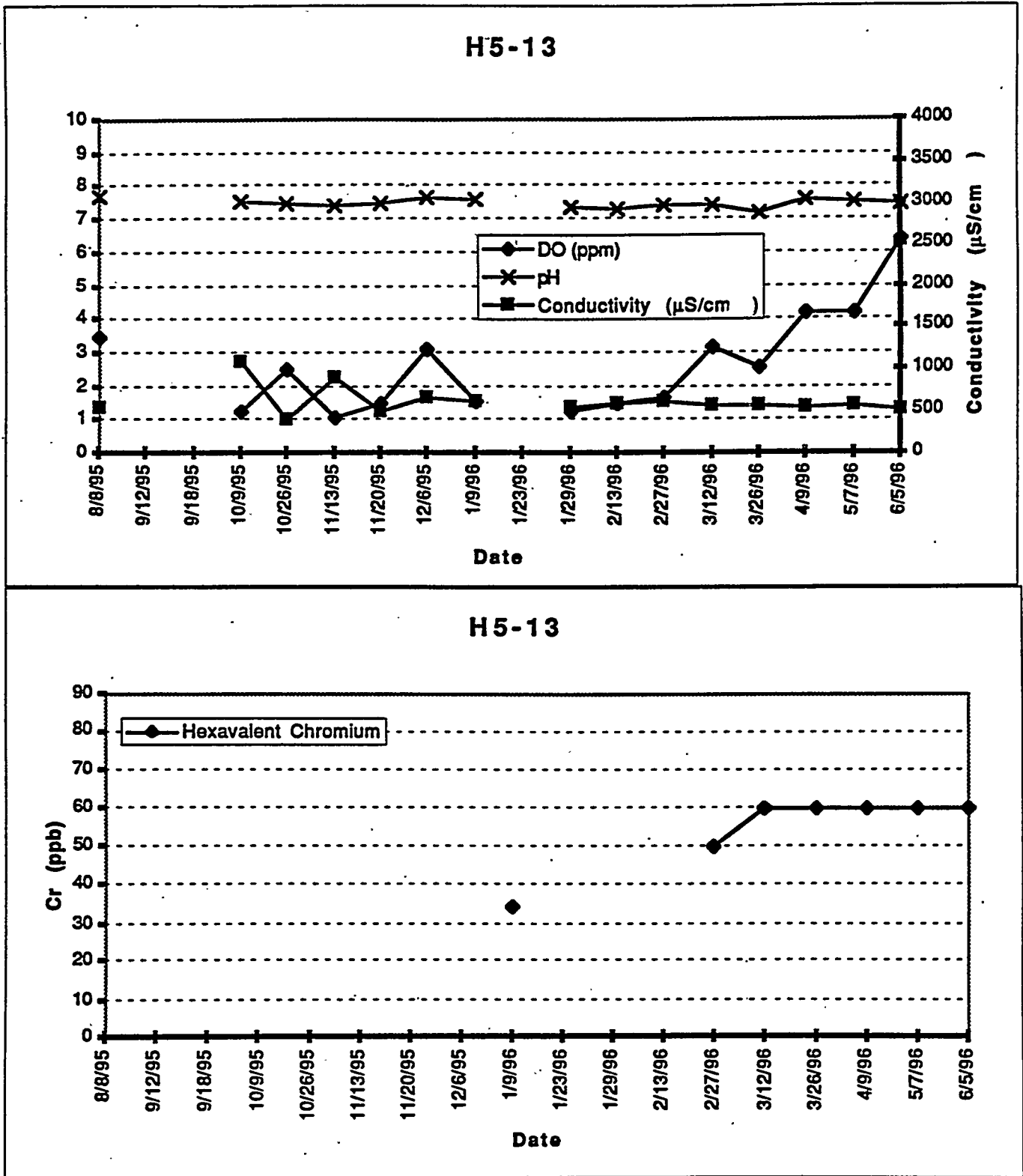
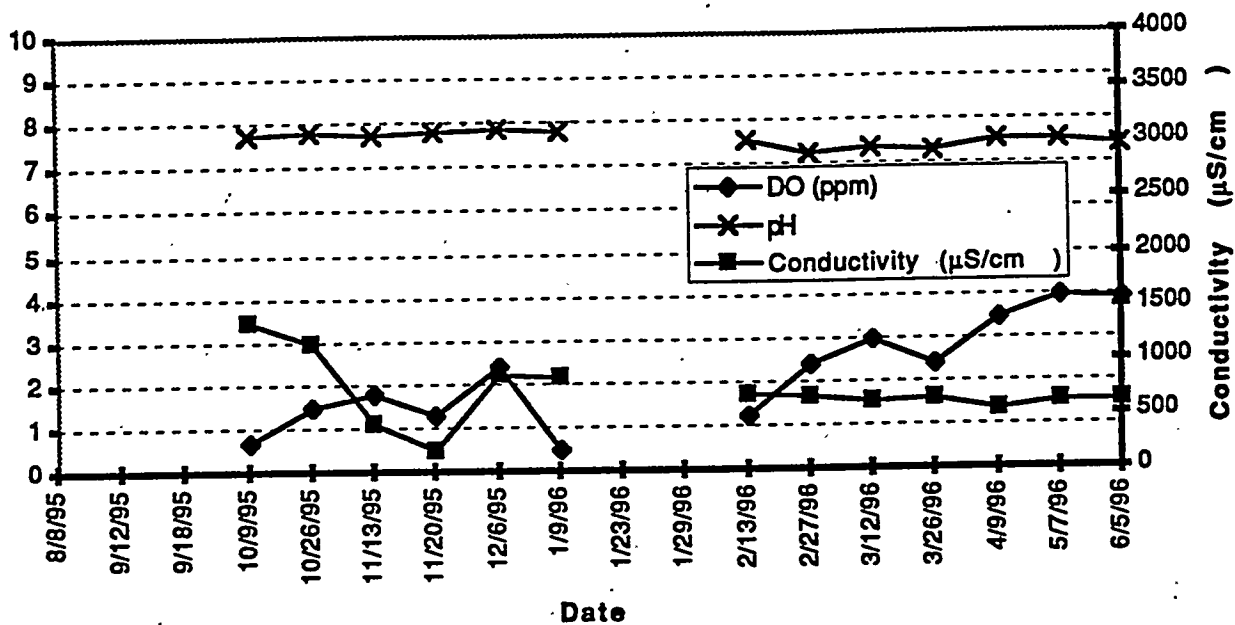


Figure H-15. Field Measurements for Well H5-13 during post-experiment monitoring of 100-H area ISRM site.

### H5-14



### H5-14

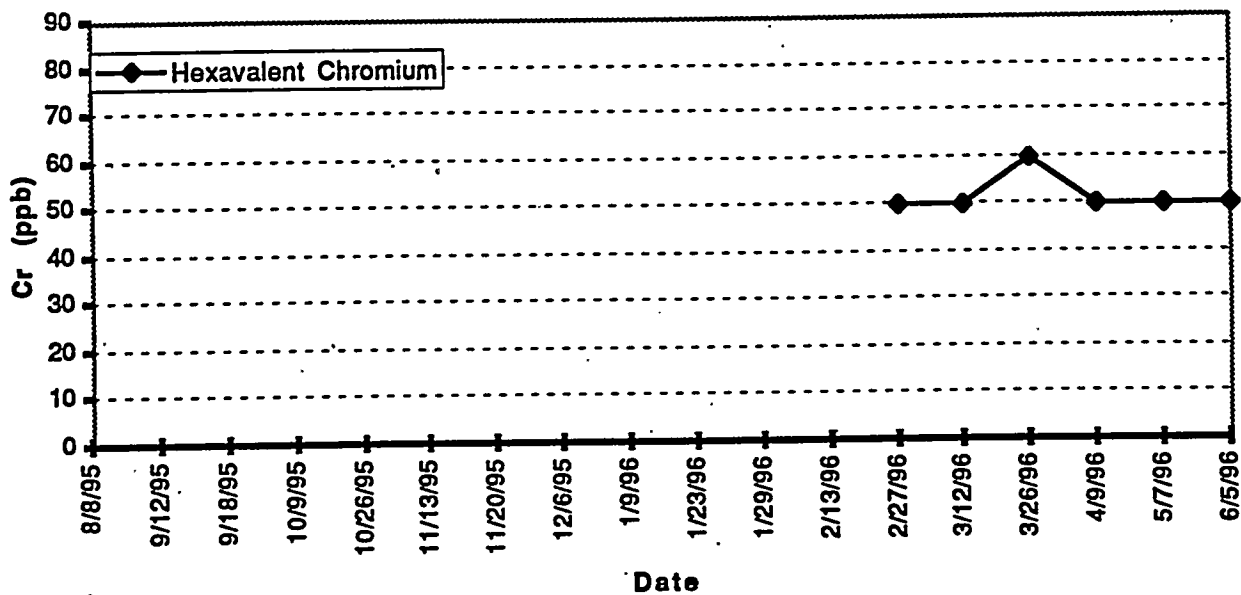


Figure H-16. Field Measurements for Well H5-14 during post-experiment monitoring of 100-H area ISRM site.

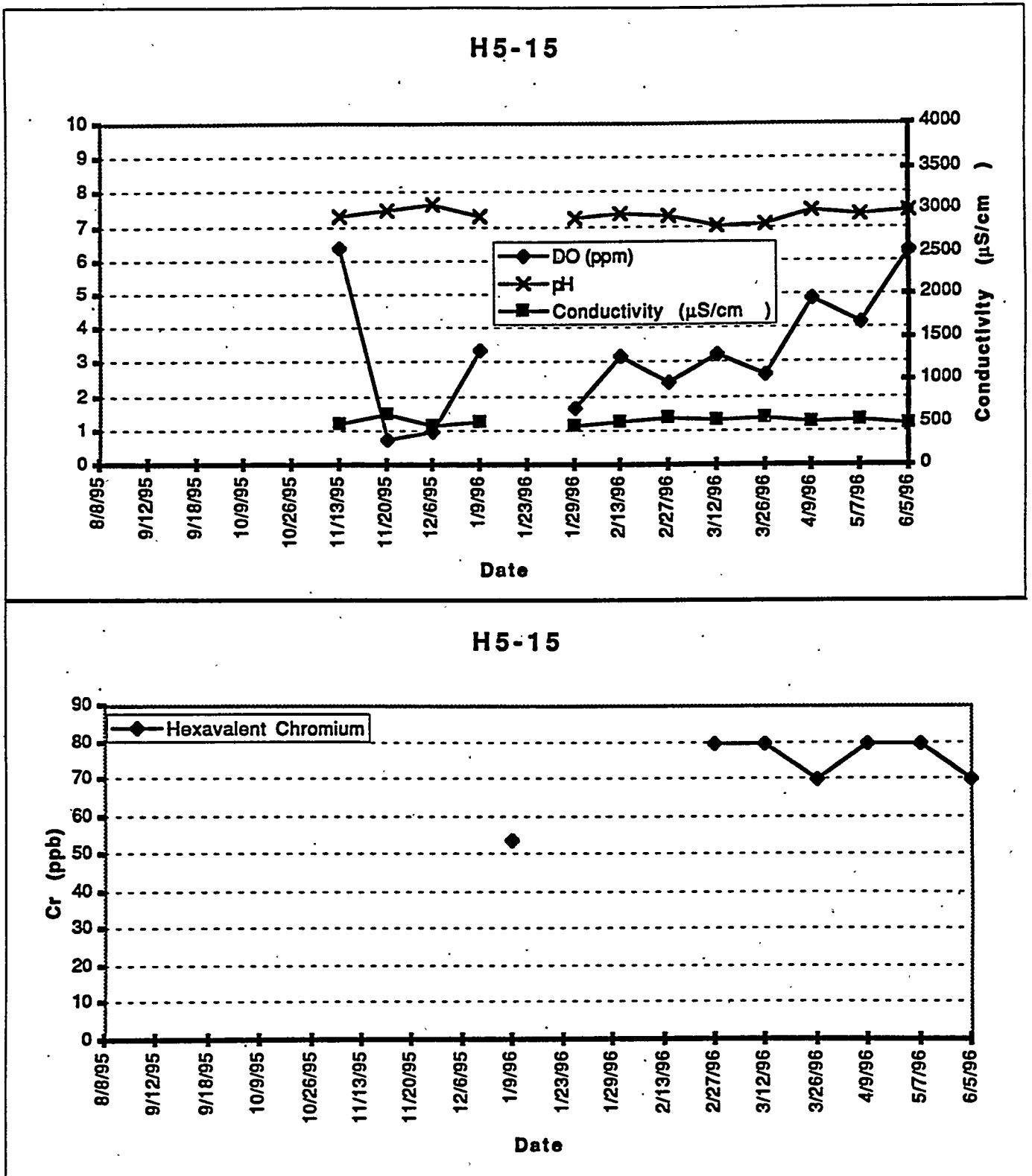
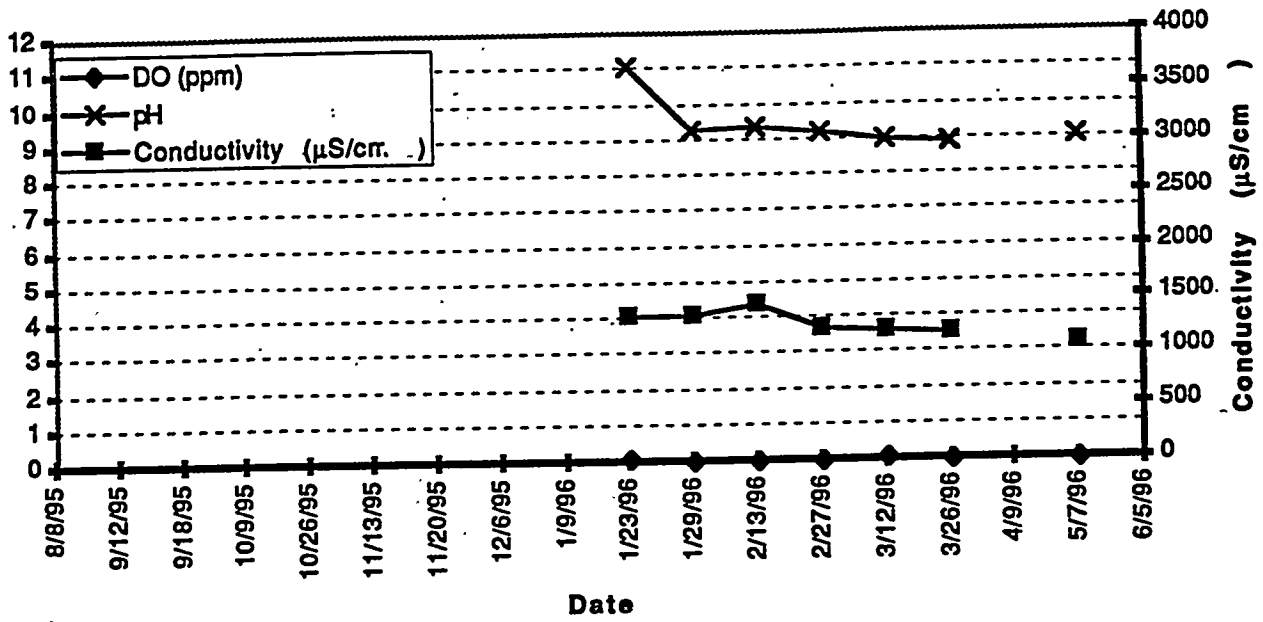


Figure H-17. Field Measurements for Well H5-15 during post-experiment monitoring of 100-H area ISRM site.

### H5-2



### H5-2

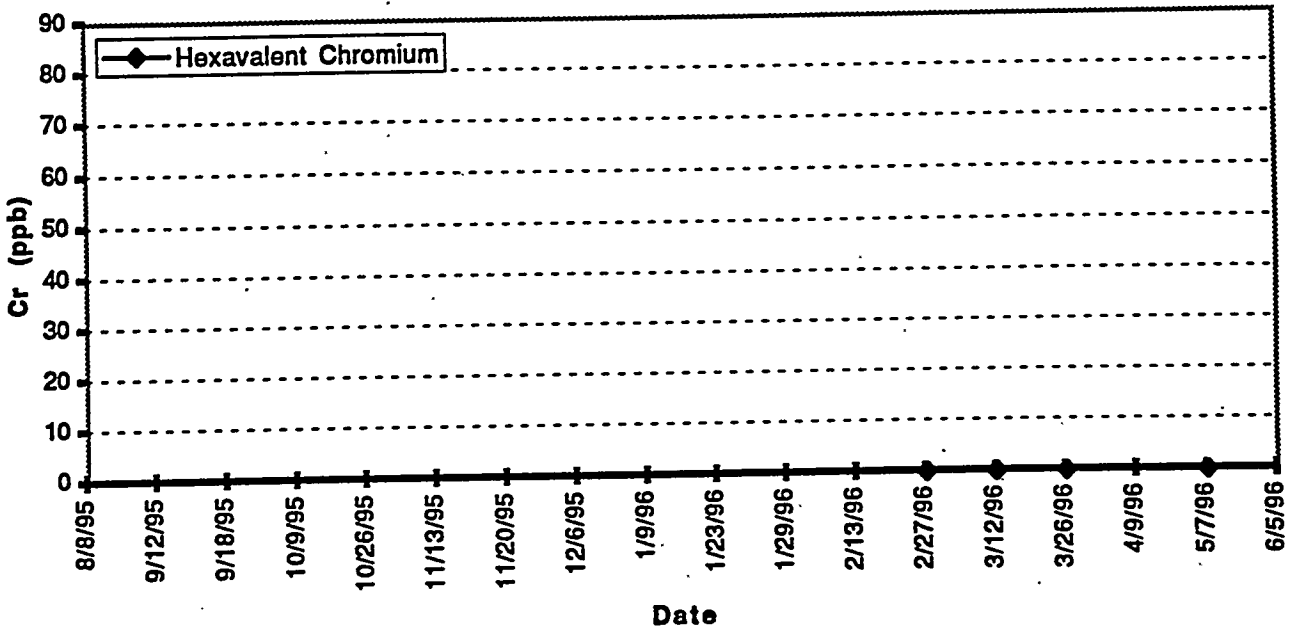


Figure H-18. Field Measurements for Well H5-2 during post-experiment monitoring of 100-H area ISRM site.

## Distribution

<u>No. Of Copies</u>	<u>No. Of Copies</u>
<b>OFFSITE</b>	
Dave Biancasino, EM-54 U.S. Department of Energy Office of Science and Technology Cloverleaf Building 2400 Century Blvd. Germantown, MD 20874	Donna L. Powaukee Nez Perce Tribe ERWM Manager P.O. Box 365 Lapwai, ID 83540-0365
Grover Chamberlain, EM-54 U.S. Department of Energy Office of Science and Technology Cloverleaf Building 2400 Century Blvd. Germantown, MD 20874	Philip Washer, DOE-SR U.S. Department of Energy Savannah River Operations Office RFD #1, Bldg. 703A, Rm E208 North P.O. Box A Aiken, SC 29802
Bob Cook Yakama Indian Nation P.O. Box 151 Toppenish, WA 98984	F. J. Wobber U.S. Department of Energy Office of Health and Envir. Research Germantown, MD 20874-1290
Paul Danielson Nez Perce Tribe ERWM P.O. Box 365 Lapwai, ID 83540-0365	James A. Wright, DOE-SR U.S. Department of Energy Savannah River Operations Office RFD #1, Bldg. 703A, Rm E208 North P.O. Box A Aiken, SC 29802
Tom Engle, HAB Department of Civil Engineering University of Washington Seattle, WA 98185	<b>ONSITE</b>
Stuart Harris Confederated Tribes of the Umatilla Indian Reservation P.O. Box 638 Pendleton, OR 97801	7 <b>DOE Richland Operations Office</b>
Jim Paulson, DOE-CH U.S. Department of Energy Chicago Operations Office Environmental Programs 9800 South Cass Ave. Argon, IL 60439	J. A. Frey J. P. Hanson R. M. Rosselli K. M. Thompson A. C. Tortoso M. C. Vargas D. M. Wanek
Jim M. Phelan, SNL Sandia National Laboratory Eubank SE Albuquerque, NM 87185-5800	6 <b>Bechtel Hanford, Inc.</b>
	M. P. Connelly G. C. Henckle V. M. Johnson A. J. Knepp J. D. Ludowise T. E. Moody

**No. Of  
Copies**

**No. Of  
Copies**

4 **U. S. Environmental Protection Agency**

P. R. Beaver  
D. A. Faulk  
L. E. Gadbois  
D. R. Sherwood

4 **Washington Department of Ecology**

D. N. Goswami  
M. A. Selby  
W. W. Soper  
N. H. Uziemblo

97 **Pacific Northwest National Laboratory**

J. E. Amonette  
C. L. Blair  
K. J. Cantrell  
C. R. Cole (5)  
J. L. Devary  
P. E. Dresel  
R. M. Ecker  
J. S. Fruchter (50)

T. J. Gilmore  
Y. A. Gorby  
D. I. Kaplan  
S. P. Luttrell  
W. J. Martin  
D. R. Newcomer  
K. B. Olsen  
M. E. Peterson  
S. C. Slate  
F. A. Spane  
G. P. Streile  
J. E. Szecsody  
S. S. Teel  
P. D. Thorne  
C. K. Thornhill  
E. C. Thornton  
V. R. Vermeul (5)  
W. D. Webber  
R. E. Wildung  
M. D. Williams (5)  
M. S. Witkowski  
S. B. Yabusaki  
Publishing Coordination  
Technical Report Files (5)

K1-06